

**The Chemistry of Boryl Amidinates and
Luminescent Properties of Symmetrically and
Unsymmetrically Substituted Diboranes(4)**

Dissertation

Zur Erlangung des Grades des Doktors der
Naturwissenschaften der Naturwissenschaftlich-
Technischen Fakultät der Universität des Saarlandes

von

M. Sc. Yvonne Kaiser

Saarbrücken

2021

Tag des Kolloquiums: 28.09.2021

Dekan: Prof. Dr. Jörn Walter

Berichterstatter: Prof. Dr. David Scheschkewitz

Prof. Dr. Dominik Munz

Vorsitz: Prof. Dr. Johann Jauch

Akademischer Mitarbeiter: Dr. Bernd Morgenstern

The present dissertation was prepared in the time between October 2016 and June 2021 at the Institute for General and Inorganic Chemistry of the Faculty of Natural Science and Engineering at the Saarland University under the supervision of Prof. Dr. David Scheschkewitz.

Die vorliegende Dissertation wurde in der Zeit zwischen Oktober 2016 und Juni 2021 am Institut für Allgemeine und Anorganische Chemie der Naturwissenschaftlich-Technischen Fakultät an der Universität des Saarlandes unter der Aufsicht von Prof. Dr. David Scheschkewitz erstellt.

Abstract

The intrinsic electron deficiency in organoboron compounds offers the synthetic chemist a wide range of possibilities. The present dissertation focused on two areas: (1) The chemistry of boryl amidinates was further developed and (2) novel unsymmetrically substituted diboranes(4) were prepared and investigated for their optoelectronic properties.

With one exception, the prepared selection of boryl benzamidinates adopt the typical *N,N*-chelating form. Attempts to synthesize amidinate-stabilized borylenes for the first time were carried out. Furthermore, the reactivity of the boryl benzamidinates towards bases/ nucleophiles was investigated. A benzazaborole was isolated in the process. In addition, the phenyl ring of the only open-chain derivative was dearomatized by nucleophilic attack of organometallic reagents.

In the second part, a large number of substituted diboranes(4) were synthesized and structurally characterized. Spectroscopic investigations showed that for 1,2-bis(dimethylamino)diboranes(4) an unsymmetrical substitution with electron-donating and -withdrawing groups is crucial in order to induce fluorescence. The substitution of the 1,4-diaza-2,3-diborinanes at their boron centers leads to a modified skeletal structure. Finally, the attachment of 4-(dimethylamino)phenyl to 1,2-diduryldiboranes(4) leads to extraordinary Stokes shifts in non-polar solvents.

Zusammenfassung

Der intrinsische Elektronenmangel in Organoborverbindungen bietet dem synthetischen Chemiker eine Vielzahl von Möglichkeiten. Die vorliegende Dissertation konzentrierte sich auf zwei Gebiete: (1) Die Chemie der Borylamidinate wurde weiterentwickelt und (2) neuartige unsymmetrisch substituierte Diborane(4) wurden hergestellt und auf ihre optoelektronischen Eigenschaften untersucht.

Mit einer Ausnahme nimmt die präparierte Auswahl an Borylbenzamidinen die typische *N,N*-chelatisierende Form an. Es wurden Versuche zur erstmaligen Synthese von amidinatstabilisierten Borylenen unternommen. Weiterhin wurde die Reaktivität der Borylbenzamidinate gegenüber Basen/ Nucleophilen untersucht. Dabei wurde ein Benzazaborol isoliert. Außerdem wurde der Phenylring des einzigen offenkettigen Derivats durch nucleophilen Angriff von metallorganischen Reagenzien dearomatisiert.

Im zweiten Teil wurde eine große Anzahl von substituierten Diboranen(4) synthetisiert und strukturell charakterisiert. Spektroskopische Untersuchungen zeigten, dass für 1,2-Bis(dimethylamino)diborane(4) eine unsymmetrische Substitution mit elektronendonierenden und -ziehenden Gruppen entscheidend ist, um Fluoreszenz zu induzieren. Die Substitution der 1,4-Diaza-2,3-Diborinane an ihren Bor-Zentren führt zu einer veränderten Gerüststruktur. Schließlich führt die Substitution mit 4-(Dimethylamino)phenyl an 1,2-Diduryldiborane(4) zu außergewöhnlichen Stokes-Verschiebungen in unpolaren Lösungsmitteln.

Publications

This thesis has been published in parts in:

- Y. Kaiser, A. Grandjean, V. Huch, M. Zimmer, G. Jung, D. Scheschkewitz: "Luminescent Symmetrically and Unsymmetrically Substituted Diboranes(4)" *Z. anorg. allg. Chem.* **2020**, 646(13), 816-827.

Other publications:

- L. Klemmer, Y. Kaiser, V. Huch, M. Zimmer, D. Scheschkewitz: "Persistent Digermenes with Acyl- and α -Chlorosilyl Functionalities" *Chem. Eur. J.* **2019**, 25(52), 12187-12195.
- D. Nieder, L. Klemmer, Y. Kaiser, V. Huch, D. Scheschkewitz: "Isolation and Reactivity of a Digerma Analogue of Vinylolithiums: a Lithium Digermenide" *Organometallics* **2018**, 37, 632-635.

Danksagung

An erster Stelle möchte ich **Prof. Dr. David Scheschkewitz** für das entgegengebrachte Vertrauen und die Chance bedanken die facettenreiche Borchemie im Laufe meiner Promotion zu erkunden und im Arbeitskreis zu etablieren. Außerdem möchte ich mich bei ihm für seine stetige Ermutigung bedanken bei Tagungen, Konferenzen oder Workshops meine Forschung zu präsentieren und sie mit Externen zu diskutieren.

Vielen Dank an **Prof. Dr. Dominik Munz** für das Erstellen des Zweitgutachtens.

Außerdem möchte ich **Prof. Dr. Gregor Jung** für die erfolgreiche Kooperation und hilfreiche Diskussionen im Zusammenhang damit danken.

Ein besonderer Dank gilt **Dr. Carsten Präsang**, der mir den Weg zur Borchemie gezeigt hat und bei sämtlichen wissenschaftlichen Fragen während meiner Promotion zur Stelle war.

Danke auch an **Dr. Diego Andrada** dafür, dass er mir immer ein Ansprechpartner in Sachen theoretischer Chemie war, **und seiner gesamten Gruppe** für eine gute Zusammenarbeit und die freundliche Atmosphäre.

Ein großes Dankeschön geht auch an die Menschen, mit denen ich schon eine super Zeit im Studium verbracht habe und die im Laufe der Promotion immer wichtiger für mich geworden sind: Danke **Sascha** für deinen Optimismus, immer freundliche Worte und unser letztes gemeinsames Meisterwerk eines "Protokolls". Danke **Lukas**, du warst ein unvergesslicher Bench-Nachbar mit einem Ohr für fachliche und persönliche Probleme und großem Unterhaltungsfaktor. **Thomas**, danke dir vielmals für klasse Zusammenarbeit bei außergewöhnlichen Fragestellungen und beim Retten aussterbender Vereine, stets gute Laune und ein Auge für das Wesentliche, wie z.B. ein *Gerüst*. Und danke **Yannic** für exzellente musikalische Begleitung im Labor, sowohl vom Band als auch live, hilfreiche Ratschläge bei Syntheseproblemen und gute Gesellschaft auf Schweizer Ski-Pisten.

Ein großer Dank geht an **David N.**, der zusammen mit **Philipp** und dem "Digermenid" mich in meinem Vertiefungspraktikum damals für den AK Scheschkewitz begeistern konnte. Danke euch beiden für aufrichtiges Interesse

an meiner Forschung, auch nachdem ihr die Uni verlassen habt, und super Tipps, wo immer ihr helfen konntet.

Von Herzen möchte ich mich bei **Bianca** bedanken. Nicht nur für herausragende Unterstützung in bürokratischen Fragen und superlustigen Kaffee-Klatsch, sondern auch dafür, dass sie in diversen Situationen zu meiner persönlichen Mrs. Miyagi geworden ist.

Danke vielmals an alle ehemaligen und aktuellen Mitglieder des Arbeitskreises, der Glasbläserei und der Werkstatt **Dr. Andreas Rammo, Dr. Anukul Jana, Dr. Hui Zhao, Dr. Cem B. Yildiz, Dr. Harinath Adimulam, Nadine Poitiers, Marc Hunsicker, Anna-Lena Thömmes, Daniel Mühlhausen, Luisa Giarrana, Philipp Grewelinger, Andreas Kell, Marcel Lambert, Dibya J. Barman, Lena Pesch, Andreas Adolf, Britta Schreiber, Eveline Altmeyer** und **Sylvia Beetz** und besonders **Dr. Kinga Leszczyńska** und **Dr. Paresh K. Majhi**, von deren Expertise ich immens profitieren konnte, für die gute Zusammenarbeit und freundliche Arbeitsatmosphäre.

Dankeschön auch an meine Vertiefer **Anna Heib** und **Oliver Andler** für große Lernbereitschaft und Freude an den bearbeiteten Forschungsgebieten.

Ein großes Dankeschön an **Dr. Volker Huch** und **Dr. Bernd Morgenstern** für die Durchführung der Kristallstrukturanalysen, an **Dr. Michael Zimmer** für die Unterstützung in Sachen NMR-Spektroskopie und an **Susanne Harling** für die CHN-Analytik.

Von ganzem Herzen bedanke ich mich bei meinem Felsen in der Brandung, **Patrick**. Ich liebe dich für deine Geduld und die enorme Rückendeckung während der gesamten Zeit.

Vielen lieben Dank auch an die **Engel für Chrissi**, meine **Wiltinger Katzen**, die Mädels vom **FC Kommlingen** und die **Affentennis reloaded Leute** für den perfekten Ausgleich zum Promotionsleben.

Zu guter Letzt geht ein riesengroßes Dankeschön an meine **komplette Familie** (Jessi, Mama, Papa, Omas, Opa, Godi, Petty, Stefan, Doris, Cousinen und Cousins und deren Familien bzw. Anhänge) für immer offene Ohren und einen felsenfesten Glauben an mich.

Content

List of Abbreviations	XXVI
List of Figures.....	XXVIII
List of Schemes.....	XLII
List of Tables	L
Preface.....	1
1. Introduction.....	3
1.1 Basics of ^{11}B NMR Spectroscopy	3
1.2 Boryl amidinates and guanidates.....	5
1.3 Group 13 element(I) heterocycles with β -diketiminato-, 1,2-diamido organyl- and amidinato-/guanidinato- ligands	15
1.4 Bis(dimethylamino)diboranes(4), tetraorganyldiboranes(4) and six- membered diaza-heterocycles with diborane(4)-motif	18
2. Aims and Scope	31
3. Results and Discussion	33
3.1. Synthesis of various boron benzamidinate complexes	33
3.1.1 Synthesis of trimethylsilyl- <i>N,N'</i> -bis(2,6-diisopropyl-phenyl) benzamidinate 103	33
3.1.2 Attempts to synthesize dihaloboryl- <i>N,N'</i> -bis(2,6-diisopropyl-phenyl) benzamidinate 104a,b	35
3.1.3 Synthesis of dichloroboryl- <i>N,N'</i> -bis(2,6-diisopropylphenyl) benzamidinate 104a	40
3.1.4 Synthesis of <i>N,N'</i> -di- ^t butyl-dichloroboryl benzamidinate 119	41
3.1.5 Synthesis of dichloroboryl- <i>N,N'</i> -bis(2,6-diisopropylphenyl) 4- (dimethylamino)benzamidinate 121	42
3.1.6 Synthesis of dichloroboryl- <i>N,N'</i> -bis(2,6-diisopropylphenyl) penta- fluorobenzamidinate 124	44

3.1.7 Synthesis of chlorophenylboryl- <i>N,N'</i> -bis(2,6-diisopropyl-phenyl) benzamidinate 126	45
3.1.8 Synthesis of chlorocyclohexylboryl- <i>N,N'</i> -bis(2,6-diisopropylphenyl) benzamidinate 128	46
3.1.9 Synthesis of chlorodimethylaminoboryl- <i>N,N'</i> -bis(2,6-diisopropyl-phenyl) benzamidinate 130	48
3.1.10 Synthesis of <i>N,N'</i> -di- <i>t</i> -butyl-chlorodimethylaminoboryl benzamidinate 131	49
3.2. Structural comparison of the solid-state structures of various boron benzamidinates.....	51
3.3. Reduction attempts of dihaloboryl- <i>N,N'</i> -bis(2,6-diisopropylphenyl) benzamidinates 104a,b	55
3.4. Reactivity of boryl benzamidinates.....	58
3.4.1 Reactivity of benzamidinate 104a towards NHCs.....	58
3.4.2. Attempted NHC abstraction from ^{<i>i</i>Pr₂Me₂} NHC coordinated benzazaborol-3-imine 136	64
3.4.3 Reactivity of further boron benzamidinate complexes towards NHCs.....	69
3.4.4. Reactivity of boron benzamidinates towards metalorganic reagents.....	72
3.4.5 Reactivity of diazaboretidine 145 - attempted exchange of NMe ₂ with Cl.....	76
3.5 Concluding Remarks.....	79
3.6. Syntheses and spectroscopic studies of diboranes(4).....	81
3.6.1 Syntheses and spectroscopic studies of 1,2-bis(dimethylamino)-diboranes(4).....	81
3.6.2 Syntheses and spectroscopic studies of 1,4-diaza-2,3-diborinanes.....	103
3.6.3 Syntheses and spectroscopic studies of 1,2-diduryldiboranes(4).....	131
4. Conclusion and Outlook.....	145
5. Experimental Section.....	153
5.1. General.....	153

5.1.1 Experimental conditions	153
5.1.2 Solvent purification	153
5.1.3 Analytical methods	153
5.2. Starting Materials	154
5.2.1 General Starting materials.....	154
5.2.2 Synthesis of (E)-N,N'-bis(2,6-diisopropylphenyl)benzimidamide 105 ^[286]	155
5.2.3 Synthesis of lithium (E)-(2,6-diisopropylphenyl)((2,6- diisopropylphenyl)imino)(phenyl)methyl)amide 102 ^[287]	156
5.2.4 Synthesis of ^{iPr} 2Me2NHC 135 ^[281]	157
5.2.5 Synthesis of bromodurene 195	157
5.2.6 Synthesis of dichlorocyclohexyl borane 127 ^[288]	158
5.2.7 Synthesis of tris(dimethylamino)borane 200	159
5.2.8 Synthesis of Dichloro(dimethylamino)borane 129	159
5.2.9 Synthesis of Chlorobis(dimethylamino)borane 167 ^[289]	160
5.2.10 Synthesis of tetrakis(dimethylamino)diborane(4) 53 ^[289]	160
5.2.11 Synthesis of 1,2-dichloro-1,2-bis(dimethylamino) diborane(4) 54a ^[93- 95,289]	161
5.2.12 Synthesis of isolated monolithiated compounds.....	162
5.2.13 2-(Ethoxycarbonylamino-phenyl)-carbamic acid ethyl ester 212 ^[291]	165
5.2.14 Synthesis of <i>N,N</i> -dimethyl-1,2-diaminobenzene 213 ^[291]	165
5.2.15 Synthesis of <i>N,N</i> -dilithium dimethyl-1,2-diaminobenzene 165 ^[292]	166
5.2.16 Synthesis of 1,2-diduryl-1,2-bis(dimethylamino)diborane(4) 55k ^[98,104]	167
5.2.17 Synthesis of 1,2-diduryl-1,2-dimethoxydiborane(4) 65b ^[98,104]	168
5.2.18 Synthesis of 1,2-dihalo-1,2-diduryldiboranes(4) 64e,f ^[98,104]	168
5.3. Synthesis of various boryl benzamidinates	170

5.3.1 Synthesis of (E)- <i>N,N</i> -bis(2,6-diisopropylphenyl)- <i>N</i> -(trimethylsilyl)benzimidamide 103 ^[193]	170
5.3.2 Attempts to synthesize (E)- <i>N</i> -(dihaloboryl)- <i>N,N'</i> -bis(2,6-diisopropylphenyl)benzimidamide 104a,b ^[27,30,33,34,37]	171
5.3.3 Synthesis of (E)- <i>N</i> -(dichloroboryl)- <i>N,N'</i> -bis(2,6-diisopropylphenyl)-benzimidamide 104a	174
5.3.4 Synthesis of (E)- <i>N,N'</i> -di- <i>tert</i> -butyl- <i>N</i> -(dichloro-boryl)benzimidamide 119	175
5.3.5 Synthesis of (E)- <i>N</i> -(dichloroboryl)- <i>N,N'</i> -bis(2,6-diisopropylphenyl)-4-(dimethylamino)benzimidamide 121	176
5.3.6 Synthesis of (E)- <i>N</i> -(dichloroboryl)- <i>N,N'</i> -bis(2,6-diisopropylphenyl)-2,3,4,5,6-pentafluorobenzimidamide 124	178
5.3.7 Synthesis of (E)- <i>N</i> -(chloro(phenyl)boryl)- <i>N,N'</i> -bis(2,6-diisopropylphenyl)benzimidamide 126	180
5.3.8 Synthesis of (E)- <i>N</i> -(chloro(cyclohexyl)boryl)- <i>N,N</i> -bis(2,6-diisopropylphenyl)benzimidamide 128	181
5.3.9 Synthesis of (E)- <i>N</i> -(chloro(dimethylamino)boryl)- <i>N,N'</i> -bis(2,6-diisopropylphenyl)benzimidamide 130	182
5.3.10 Synthesis of (E)- <i>N,N'</i> -di- <i>tert</i> -butyl- <i>N</i> -(chloro(dimethylamino)-boryl)benzimidamide 131	183
5.4. Reduction attempts of (E)- <i>N</i> -(dihaloboryl)- <i>N,N'</i> -bis(2,6-diisopropylphenyl)benzimidamide 104a,b	184
5.5. Reactivity of boryl benzamidates towards NHCs	188
5.5.1 Reactivity of (E)- <i>N</i> -(dichloroboryl)- <i>N,N'</i> -bis(2,6-diisopropylphenyl)-benzimidamide 104a towards NHCs	188
5.5.2 Attempted NHC abstraction from ^{iPr₂Me₂} NHC coordinated (E)-1-chloro- <i>N,N</i> -bis(2,6-diisopropylphenyl)-1,2-dihydro-3H-benzo[<i>c</i>][1,2]azaborol-3-imine 136	191
5.5.3 Reactivity of further boryl benzamidate complexes towards NHCs	193
5.6. Reactivity of boryl benzamidates towards metalorganic reagents.....	196

5.6.1 Reactivity of (E)- <i>N</i> -(dichloroboryl)- <i>N,N'</i> -bis(2,6-diisopropylphenyl)-benzimidamide 104a towards metalorganic reagents	196
5.6.2 Reactivity of (E)- <i>N</i> -(chloro(cyclohexyl)boryl)- <i>N,N'</i> -bis(2,6-diisopropylphenyl)benzimidamide 128 towards metalorganic reagents.....	196
5.6.3 Synthesis of 1,3-bis(2,6-diisopropylphenyl)-4-(4-isopropylcyclohexa-2,5-dien-1-ylidene)- <i>N,N</i> -dimethyl-1,3,2-diazaboretidin-2-amine 145	197
5.6.4 Reactivity of (E)- <i>N</i> -(chloro(dimethylamino)boryl)- <i>N,N'</i> -bis(2,6-diisopropylphenyl)benzimidamide 130 towards metalorganic reagents ..	198
5.6.5 Reactivity of Diazaboretidine 145 - Attempted Exchange of NMe ₂ with Cl.....	201
5.7. Synthesis of 1,2-bis(dimethylamino) diboranes(4)	202
5.7.1 Synthesis of 2-chloro-1,2-bis(dimethylamino)-1-para- <i>N,N</i> -dimethylaniline diborane(4) 156	202
5.7.2 Synthesis of 1,2-bis(dimethylamino)-1,2-bis(para- <i>N,N</i> -dimethylaniline) diborane(4) 157	203
5.7.3 Isolation of 1,1-bis(dimethylamino)-2,2-bis(para- <i>N,N</i> -dimethylaniline) diborane(4) 158	204
5.7.4 Synthesis of 1,2-bis(dimethylamino)-1-para- <i>N,N</i> -dimethylaniline-2-pentafluorophenyl diborane(4) 161	205
5.7.5 Reactivity of 2-chloro-1,2-bis(dimethylamino)-1-para- <i>N,N</i> -dimethylaniline diborane(4) 156 towards 4-cyanophenyl lithium and 4-nitrophenyl lithium	206
5.8. Synthesis of diazadiborinanes	207
5.8.1 Synthesis of 1,4-dimethyl-2,3-bis(dimethylamino)-1,2,3,4-tetrahydrobenzo[e][1,4,2,3]diazadiborinane 166	207
5.8.2 Synthesis of 2,3-bis(para- <i>N,N</i> -dimethylaniline)-1,4-dimethyl-1,2,3,4-tetrahydrobenzo[e][1,4,2,3]diazadiborinane 169	208
5.8.3 Synthesis of 2,3-bis(pentafluorophenyl)-1,4-dimethyl-1,2,3,4-tetrahydrobenzo[e][1,4,2,3]diazadiborinane 170	210
5.8.4 Synthesis of 1,4-dimethyl-2-dimethylamino-3-para- <i>N,N</i> -dimethylaniline-1,2,3,4-tetrahydrobenzo[e][1,4,2,3]diazadiborinane 172	211

5.8.5 Reactivity of 1,4-dimethyl-2-dimethylamino-3-chloro-1,2,3,4-tetrahydrobenzo[e][1,4,2,3]diazadiborinane 171 towards various extended or electron-rich aromatic systems	213
5.8.6 Synthesis of 2-chloro-1,4-dimethyl-3-para- <i>N,N</i> -dimethylaniline-1,2,3,4-tetrahydrobenzo[e][1,4,2,3]diazadiborinane 180	216
5.8.7 Synthesis of 1,4-dimethyl-3-para- <i>N,N</i> -dimethylaniline-2-pentafluorophenyl-1,2,3,4-tetrahydrobenzo[e][1,4,2,3]diazadiborinane 181	218
5.8.8 Synthesis of 4-(1,4-dimethyl-3-(4-nitrophenoxy)-3,4-dihydrobenzo[e][1,4,2,3]diazadiborin-2(1H)-yl)- <i>N,N</i> -dimethylaniline 183	219
5.9. Synthesis of 1,2-diduryl diboranes(4).....	221
5.9.1 Synthesis of 1-chloro-2-dimethylamino-1,2-(2,3,5,6-tetramethylphenyl) diborane(4) 185	221
5.9.2 Synthesis of 2-dimethylamino-1-para- <i>N,N</i> -dimethylaniline-1,2-(2,3,5,6-tetramethylphenyl) diborane(4) 186	222
5.9.3 Synthesis of 2-chloro-1-para- <i>N,N</i> -dimethylaniline-1,2-(2,3,5,6-tetramethylphenyl) diborane(4) 187	223
5.9.4 Synthesis of 1,2-para- <i>N,N</i> -dimethylaniline-1,2-(2,3,5,6-tetramethylphenyl) diborane(4) 188	224
5.9.5 Attempted Synthesis of 1-para- <i>N,N</i> -dimethylaniline-2-pentafluorophenyl-1,2-(2,3,5,6-tetramethylphenyl) diborane(4) 189	225
5.9.6 Synthesis of 2-chloro-1-pentafluorophenyl-1,2-(2,3,5,6-tetramethylphenyl) diborane(4) 190	226
6. Literature	227
7. Appendix	247
7.1 Overview of numbered compounds	247
7.2 ¹¹ B NMR signals of diboranes(4)	268
7.3 Crude product ¹ H NMR spectra of reactions between 91 and various aryl lithium compounds.....	272

7.4 UV-vis Spectra and ϵ determination	276
7.4.1 2-chloro-1,2-bis(dimethylamino)-1-para- <i>N,N</i> -dimethylaniline diborane(4) 156	276
7.4.2 1,2-bis(dimethylamino)-1,2-bis(para- <i>N,N</i> -dimethylaniline) diborane(4) 157	277
7.4.3 1,2-bis(dimethylamino)-1-para- <i>N,N</i> -dimethylaniline-2- pentafluorophenyl diborane(4) 161	278
7.4.4 1,4-dimethyl-2,3-bis(dimethylamino)-1,2,3,4-tetrahydrobenzo[e]- [1,4,2,3]diazadiborinane 166	279
7.4.5 2,3-bis(para- <i>N,N</i> -dimethylaniline)-1,4-dimethyl-1,2,3,4-tetrahydro- benzo[e][1,4,2,3]diazadiborinane 169	281
7.4.6 2,3-bis(pentafluorophenyl)-1,4-dimethyl-1,2,3,4-tetrahydrobenzo[e]- [1,4,2,3]diazadiborinane 170	283
7.4.7 1,4-dimethyl-2-dimethylamino-3-para- <i>N,N</i> -dimethylaniline-1,2,3,4- tetrahydrobenzo[e][1,4,2,3]diazadiborinane 172	286
7.4.8 2-chloro-1,4-dimethyl-3-para- <i>N,N</i> -dimethylaniline-1,2,3,4-tetrahydro- benzo[e][1,4,2,3]diazadiborinane 180	288
7.4.9 1,4-dimethyl-3-para- <i>N,N</i> -dimethylaniline-2-pentafluorophenyl-1,2,3,4- tetrahydrobenzo[e][1,4,2,3]diazadiborinane 181	290
7.4.10 4-(1,4-dimethyl-3-(4-nitrophenoxy)-3,4-dihydrobenzo[e]- [1,4,2,3]diazadiborin-2(1H)-yl)- <i>N,N</i> -dimethylaniline 183	292
7.4.11 1-chloro-2-dimethylamino-1,2-(2,3,5,6-tetramethylphenyl) diborane(4) 185	294
7.4.12 2-dimethylamino-1-para- <i>N,N</i> -dimethylaniline-1,2-(2,3,5,6-tetramethyl- phenyl) diborane(4) 186	295
7.4.13 2-chloro-1-para- <i>N,N</i> -dimethylaniline-1,2-(2,3,5,6-tetramethylphenyl) diborane(4) 187	297
7.4.14 1,2-para- <i>N,N</i> -dimethylaniline-1,2-(2,3,5,6-tetramethylphenyl) diborane(4) 188	298
7.5 Crystal data and structure refinement	300

7.5.1 (E)- <i>N,N'</i> -bis(2,6-diisopropylphenyl)- <i>N</i> -(trimethylsilyl)benzimidamide 103	300
7.5.2 (E)- <i>N</i> -(dichloroboryl)- <i>N,N'</i> -bis(2,6-diisopropylphenyl)-benzimidamide 104a	301
7.5.3 (E)- <i>N,N'</i> -di- <i>tert</i> -butyl- <i>N</i> -(dichloro-boryl)benzimidamide 119	302
7.5.4 (E)- <i>N</i> -(dichloroboryl)- <i>N,N'</i> -bis(2,6-diisopropylphenyl)-2,3,4,5,6- pentafluorobenzimidamide 124	303
7.5.5 (E)- <i>N</i> -(chloro(phenyl)boryl)- <i>N,N'</i> -bis(2,6-diisopropyl- phenyl)benzimidamide 126	304
7.5.6 (E)- <i>N</i> -(chloro(cyclohexyl)boryl)- <i>N,N'</i> -bis(2,6-diisopropylphenyl)- benzimidamide 128	305
7.5.7. (E)- <i>N</i> -(chloro(dimethylamino)boryl)- <i>N,N'</i> -bis(2,6-diisopropylphenyl)- benzimidamide 130	306
7.5.8 (E)- <i>N,N'</i> -di- <i>tert</i> -butyl- <i>N</i> -(chloro(dimethylamino)-boryl)benzimidamide 131	307
7.5.9 Benzazaborole 136	308
7.5.10 Diazaboretidine 145	309
7.5.11 2-chloro-1,2-bis(dimethylamino)-1- <i>para-N,N</i> -dimethylaniline diborane(4) 156	310
7.5.12 1,2-bis(dimethylamino)-1,2-bis(<i>para-N,N</i> -dimethylaniline) diborane(4) 157	311
7.5.13 1,1-bis(dimethylamino)-2,2-bis(<i>para-N,N</i> -dimethyl-aniline) diborane(4) 158	312
7.5.14 1,2-bis(dimethylamino)-1- <i>para-N,N</i> -dimethylaniline-2-pentafluor- phenyl diborane(4) 161	313
7.5.15 1,4-dimethyl-2,3-bis(dimethylamino)-1,2,3,4-tetrahydrobenzo[e]- [1,4,2,3]diazadiborinane 166	314
7.5.16 2,3-bis(<i>para-N,N</i> -dimethylaniline)-1,4-dimethyl-1,2,3,4-tetrahydro- benzo[e][1,4,2,3]diazadiborinane 169	315

7.5.17 2,3-bis(pentafluorophenyl)-1,4-dimethyl-1,2,3,4-tetrahydrobenzo[e]-[1,4,2,3]diazadiborinane 170	316
7.5.18 1,4-dimethyl-2-dimethylamino-3-para- <i>N,N</i> -dimethylaniline-1,2,3,4-tetrahydrobenzo[e][1,4,2,3]diazadiborinane 172	317
7.5.19 2-chloro-1,4-dimethyl-3-para- <i>N,N</i> -dimethylaniline-1,2,3,4-tetrahydrobenzo[e][1,4,2,3]diazadiborinane 180	319
7.5.20 1,4-dimethyl-3-para- <i>N,N</i> -dimethylaniline-2-pentafluorophenyl-1,2,3,4-tetrahydrobenzo[e][1,4,2,3]diazadiborinane 181	320
7.5.21 4-(1,4-dimethyl-3-(4-nitrophenoxy)-3,4-dihydrobenzo[e]-[1,4,2,3]diazadiborin-2(1H)-yl)- <i>N,N</i> -dimethylaniline 183	321
7.5.22 1-chloro-2-dimethylamino-1,2-(2,3,5,6-tetramethylphenyl)diborane(4) 185	323
7.5.23 2-chloro-1- <i>para-N,N</i> -dimethylaniline-1,2-(2,3,5,6-tetramethylphenyl)diborane(4) 187	324

List of Abbreviations

A	Ampere
Å	Angstrom
Alk	alkyl
An	9-anthracenyl
Ar	aryl
Ar ^f	pentafluorophenyl or 3,5-bis(trifluoromethyl)phenyl
ⁿ Bu	<i>n</i> -butyl
ⁿ BuLi	<i>n</i> -butyllithium
^t Bu	<i>tert</i> -butyl
C	Celsius
CAAC	cyclic (alkyl)(amino)carbene
CAAC ^{Me}	1-Dip-3,3,5,5-tetramethyl-pyrrolidin-2-ylidene
cat	catecholato
Cp	cyclopentadienyl
Cy	cyclohexyl
CV	Cyclic Voltammetry
DCM	dichloromethane
Dep	2,6-diethylphenyl
DFT	Density Functional Theory
diglyme	bis(2-methoxyethyl) ether
Dip	2,6-diisopropylphenyl
DMAP	4-dimethylaminopyridine
dme	dimethoxyethane
dmf	<i>N,N</i> -dimethylformamide
Dur	duryl = 2,3,5,6-tetramethylphenyl
EPR or ESR	electron paramagnetic resonance (EPR) or electron spin resonance (ESR)
eq	equivalents
Et	ethyl
Fc	ferrocenyl
flu	9-fluorenyl
FT	Fourier Transformation
h	hour
HOMO	Highest Occupied Molecular Orbital
Hz	Hertz
IDip	1,3-Dip-imidazol-2-ylidene
liPr	1,3-diisopropylimidazol-2-ylidene
IMe	1,3-dimethylimidazol-2-ylidene
IMes	1,3-Mes-imidazol-2-ylidene

ind	indenyl
iPr	isopropyl
IR	infrared
K	Kelvin
LDA	lithium diisopropylamide
LUMO	Lowest Unoccupied Molecular Orbital
Me	methyl
Mes	mesityl = 2,4,6-trimethylphenyl
Mes*	2,4,6-tri- <i>tert</i> -butylphenyl
MO	Molecular Orbital
NHC	<i>N</i> -heterocyclic carbene
iPr ₂ Me ₂ NHC	1,3-diisopropyl-4,5-dimethyl-imidazol-2-ylidene
Me ₄ NHC	1,3,4,5-tetramethyl-imidazol-2-ylidene
NMR	Nuclear Magnetic Resonance
Npht	naphthyl
Nrb	<i>exo</i> -2-norbornyl = bicyclo[2.2.1]-2-heptyl
octaflu	1,1,4,4,7,7,10,10-octamethyldicyclohexyl-9-fluorenyl
OLED	organic light-emitting diode
OTf	trifluoromethanesulfonate
Ph	phenyl
ppm	Parts per million
rt	room temperature
SIMes	1,3-Mes-imidazolidin-2-ylidene
thf	tetrahydrofuran
Tip	2,4,6-triisopropylphenyl
TMS	Trimethylsilyl = SiMe ₃ (in the context of NMR spectroscopy: tetramethylsilyl = SiMe ₄)
tol	toluene
<i>o</i> -tol	<i>ortho</i> -tolyl = 2-methylphenyl
Tos	Tosylate = <i>p</i> -toluenesulfonate
triglyme	triethylene glycol dimethyl ether
UV	Ultraviolet
V	Volt
Vis	Visible
VT	variable temperature

List of Figures

Figure 1. Reported boryl amidinate complexes.	5
Figure 2. Reported structurally characterized boron guanidate complexes.	6
Figure 3. Literature-known diboron complexes of binucleating bis(amidinate) ligands.	8
Figure 4. The deployed boryl guanidates 2i , 10c,d and 18 for the reactivity studies towards isocyanides, carbonmonoxide, benzaldehyde and carbondioxide.	9
Figure 5. Insertion-products 19a,b , 20e-f and 21a,b of isonitriles into the B-N bonds of boryl guanidates 2i , 10c,d and 18 and de-insertion equilibrium of 20e,f	10
Figure 6. Isolated product 22a of guanidate 10c with CO and equilibrium between guanidate 18 and 22b under CO atmosphere.	10
Figure 7. Guanidate and amidinate stabilized group 13 element(I) structures. 41a : R = NCy ₂ ; 41b : R = 2,6-dimethylpiperidine; 42a : R = ^t Bu; 42b : R = NCy ₂ ; 42c : R = NiPr ₂ ; 42d : R = 2,6-dimethylpiperidine.	15
Figure 8. Group 13 element NHC analogues.	16
Figure 9. Isolated group 13 element (I) structures stabilized by β-diketiminato ligands.	16
Figure 10. Isolated boron(I) β-diketiminato structure in an iron coordination sphere 51 and the calculated structures 52a (X = CMe) and 52b (X = N).	17
Figure 11. Targeted symmetrically (Ar = Ar') and unsymmetrically (Ar ≠ Ar') substituted Diboranes(4) with 1,2-bis(dimethylamino)- (IV), 1,4-diaza-2,3-diborinane- (V) and 1,2-bisduryl- (VI) substitution pattern.	32
Figure 12. Molecular Structure of 103 in the solid state (ellipsoids at 50% probability, hydrogen atoms and second molecule of the asymmetric unit omitted for clarity). Selected bond lengths [Å] and angles [°]: Si1-N3 1.786(2), N3-C35 1.392(3), N4-C35 1.285(3), C35-C36 1.501(4), C35-N3-Si1 115.7(2), N4-C35-N3 115.6(2).	34
Figure 13. ¹ H NMR spectrum of trimethylsilylbenzamidine 103	35

Figure 14. ¹ H NMR spectrum of dibromoboryl benzamidinate 104b . Ratio of integrated Dip-isopropyl-CH signals of 104b :side products 86:14.....	37
Figure 15. ¹ H NMR spectrum of partly decomposed 104a (marked with “\$”) to proposed rearrangement product 116 (marked with “+”), and doubly protonated ligand (marked with “#”).....	39
Figure 16. ¹ H NMR spectrum of dichloroboryl benzamidinate 104a . Ratio of integrated Dip-isopropyl-CH signals of 104a :side products 88:12. Rearrangement product 116 (marked with “+”), and doubly protonated ligand (marked with “#”).	41
Figure 17. ¹ H NMR spectrum of dichloroboryl benzamidinate 121 and rearrangement product 122 . Ratio of integrated Ar-aniline-CH signals of 121 :proposed rearrangement product 122 55:45. 121 marked with “\$” and proposed rearrangement product 122 marked with “+”.	43
Figure 18. ¹¹ B NMR spectrum of dichloroboryl benzamidinate 121 and rearrangement product 122	44
Figure 19. ¹ H NMR spectrum of chlorophenylboryl benzamidinate 126 . Doubly protonated ligand as minor side product is marked with “*”).....	46
Figure 20. ¹ H NMR spectrum of chlorocyclohexylboryl benzamidinate 128	47
Figure 21. ¹ H NMR spectrum of chlorodimethylaminoboryl benzamidinate 130	49
Figure 22. Molecular structures of boryl benzamidinates 104a , 119 , 124 , 126 , 128 and 131 . For detailed information see next page.	52
Figure 22 continued. Top left: Molecular Structure of 104a in the solid state (ellipsoids at 50% probability, hydrogen atoms omitted for clarity, asymmetric unit doubled). Selected bond lengths [Å] and angles [°]: Cl1-B1 1.81(1), N1-B1 1.59(2), N1-C1 1.34(1), C1-C2 1.42(2), C1-N1-B1 85.9(7), N1-B1-N1’ 84(1), N1-C1-N1’ 104(1). Top right: Molecular Structure of 119 in the solid state (ellipsoids at 50% probability, hydrogen atoms omitted for clarity, asymmetric unit doubled). Selected bond lengths [Å] and angles [°]: Cl1-B1 1.8364(8), N1-B1 1.561(1), N1-C1 1.336(1), C1-C2 1.478(2), C1-N1-B1 87.73(6), N1-B1-N1’ 83.04(8), N1-C1-N1’ 101.5(1). Middle left: Molecular Structure of 124 in the solid state (ellipsoids at 50% probability, hydrogen atoms and co-crystallized	

dichloromethane omitted for clarity). Selected bond lengths [Å] and angles [°]: Cl1-B1 1.811(2), Cl2-B1 1.818(2), N1-B1 1.588(2), N2-B1 1.585(3), N1-C1 1.330(2), N2-C1 1.332(2), C1-C14 1.469(2), C1-N1-B1 87.4(1), C1-N2-B1 87.5(1), N1-B1-N2 82.0(1), N1-C1-N2 103.0(2). **Middle right:** Molecular Structure of **126** in the solid state (ellipsoids at 50% probability, hydrogen atoms, co-crystallized dichloromethane and second molecule in the asymmetric unit omitted for clarity). Selected bond lengths [Å] and angles [°]: Cl1-B1 1.847(2), C32-B1 1.592(3), N1-B1 1.604(3), N2-B1 1.620(3), N1-C1 1.343(2), N2-C1 1.332(2), C1-C2 1.471(3), C1-N1-B1 88.6(2), C1-N2-B1 88.3(2), N1-B1-N2 80.6(1), N1-C1-N2 102.4(2). **Bottom left:** Molecular Structure of **128** in the solid state (ellipsoids at 50% probability, hydrogen atoms and co-crystallized toluene omitted for clarity). Selected bond lengths [Å] and angles [°]: Cl1-B1 1.868(2), C8-B1 1.586(2), N1-B1 1.611(2), N2-B1 1.595(2), N1-C1 1.329(2), N2-C1 1.344(2), C1-C2 1.467(2), C1-N1-B1 88.50(9), C1-N2-B1 88.66(9), N1-B1-N2 80.79(9), N1-C1-N2 102.1(1). **Bottom right:** . Molecular Structure of **131** in the solid state (ellipsoids at 50% probability, hydrogen atoms and disorder of one ^tbutyl-group omitted for clarity). Selected bond lengths [Å] and angles [°]: Cl1-B1 1.870(2), N3-B1 1.440(2), N2-B1 1.646(2), N1-B1 1.576(2), N1-C1 1.339(2), N2-C1 1.320(2), C1-C2 1.483(2), C1-N1-B1 90.0(1), N1-B1-N2 80.0(1), N1-C1-N2 102.4(1), C1-N2-B1 87.7(1). 53

Figure 23. Molecular Structure of **130** in the solid state (ellipsoids at 50% probability, hydrogen atoms omitted for clarity). Selected bond lengths [Å] and angles [°]: Cl1-B1 1.8067(1), N3-B1 1.383(2), N2-B1 1.464(2), N1-C25 1.280(1), N2-C25 1.400(1), C25-C26 1.501(2), C25-N2-B1 125.64(9), N1-C25-N2 118.07(9), N2-B1-N3 126.9(1)..... 54

Figure 24. Considered structures and their calculated singlet-triplet-gaps at the BP86+D3(BJ)/def2-SVP level of theory..... 57

Figure 25. Comparison of spectra of **104a** with remaining impurities (bottom) and after addition of 2.2 eq. ⁱPr₂Me₂NHC **135** (top)..... 59

Figure 26. ¹H NMR spectrum of the Imidazolium-salt-byproduct (iPr₂Me₂NHC•HCl). 60

Figure 27. ¹H NMR spectrum of benzazaborole **136**. 61

Figure 28. Molecular Structure of 136 in the solid state (ellipsoids at 50% probability, hydrogen atoms and co-crystallized benzene omitted for clarity). Selected bond lengths [Å] and angles [°]: Cl1-B1 1.943(3), C20-B1 1.660(4), N1-B1 1.533(3), N1-C7 1.383(3), N2-C7 1.287(3), C7-N1-B1 113.0(2), N1-C7-N2 121.5(2), C7-N2-C _{Dip} 120.9(2), N1-B1-C _{Ph} 100.0(2), N1-B1-C20 114.9(2), C20-B1-Cl1 106.3(2).	62
Figure 29. ¹ H NMR spectrum of the reaction between benzazaborole 136 and triphenylborane (140).	65
Figure 30. ¹¹ B NMR spectrum of the reaction between benzazaborole 136 and triphenylborane (140).	66
Figure 31. ¹ H NMR spectrum of the reaction between benzazaborole 136 and perfluorinated triphenylborane (143).	67
Figure 32. ¹¹ B NMR spectrum of the reaction between benzazaborole 136 and perfluorinated triphenylborane (143).	68
Figure 33. ¹⁹ F NMR spectrum of the reaction between benzazaborole 136 and perfluorinated triphenylborane (143).	68
Figure 34. ¹¹ B NMR spectrum of the reaction mixture after stirring 5 days at room temperature in benzene with c = 0.02 M.	71
Figure 35. Molecular Structure of 145 in the solid state (ellipsoids at 50% probability, hydrogen atoms omitted for clarity). Selected bond lengths [Å] and angles [°]: N3-B1 1.385(1), N1-B1 1.460(1), N2-B1 1.464(1), N1-C1 1.417(1), N2-C1 1.421(1), C1-C2 1.357(1), N3-B1-N1 134.88(9), N3-B1-N2 135.21(9), N2-B1-N1 89.91(7), B1-N2-C1 88.11(7), B1-N1-C1 88.42(7), N2-C1-N1 93.47(7).....	74
Figure 36. ¹¹ B NMR spectrum of the reaction between diazaboretidine 145 and BCl ₃ after warming to room temperature.	77
Figure 37. ¹¹ B NMR spectrum of the reaction between diazaboretidine 145 and BCl ₃ after storage overnight at 5°C.	78
Figure 38. ¹ H NMR spectrum of the crude 156	83
Figure 39. Molecular structure of 156 in the solid state (ellipsoids at 50% probability, hydrogen atoms and chlorine disorder omitted for clarity). Selected bond lengths [Å] and angles [°]: B1-B2 1.702(2), B1-N1 1.395(1), B2-N2	

1.386(1), B1-C5 1.577(1), B2-C11 1.829(1), C8-N3 1.384(1), $\Sigma \angle$ B1 360.0, $\Sigma \angle$ B2 360.0, $\Sigma \angle$ N1 360.0, $\Sigma \angle$ N2 360.0, $\Sigma \angle$ N3 355.9, angle between B coord. Planes 89.2(2).	84
Figure 40. Absorption (blue), excitation (red) and emission (black) spectra of 1,2-bis(dimethylamino) diborane(4) 156 in hexane (5 μ M).	85
Figure 41. UV/Vis spectra of a 5 μ M solution of 156 in hexane under the influence of air (violet to orange) and one UV/Vis spectrum of a hydrolyzed sample of 156 (red) in hexane. 1 : decreasing absorption band at 286 nm/ consumption of diborane(4) 66 ; 2 : increasing absorption band at 324 nm/ accumulation of the intermediate species; 3 : decreasing absorption band at 324 nm/ consumption of the intermediate species; 4 : increasing absorption band at 280 nm/ formation of the hydrolysis product.	86
Figure 42. ^{11}B NMR of a hydrolyzed sample of diborane(4) 156 .	87
Figure 43. ^1H NMR of a hydrolyzed sample of diborane(4) 156 .	87
Figure 44. Cyclic voltammogram of 156 in dichloromethane ($c = 3$ mM), with a platinum working electrode, a platinum counter electrode, a silver quasi reference electrode, scan rate at 100 mV s^{-1} and $\text{Bu}_4\text{N}^+\text{PF}_6^-$ ($c = 0.1$ M) as conductive salt.	89
Figure 45. Cyclic voltammogram of 156 in thf ($c = 3$ mM), with a platinum working electrode, a platinum counter electrode, a silver quasi reference electrode, scan rate at 100 mV s^{-1} and $\text{Bu}_4\text{N}^+\text{PF}_6^-$ ($c = 0.1$ M) as conductive salt.	89
Figure 46. ^1H NMR spectrum of the crude product of 157 .	90
Figure 47. Molecular structure of 157 in the solid state (ellipsoids at 50% probability, hydrogen atoms omitted for clarity). Selected bond lengths [\AA] and angles [$^\circ$]: B1-B2 1.716(3), B1-N1 1.399(3), B2-N3 1.405(3), B1-C1 1.585(3), B2-C12 1.576(3), C4-N2 1.384(3), C15-N4 1.400(3), $\Sigma \angle$ B1 359.9, $\Sigma \angle$ B2 360.0, $\Sigma \angle$ N1 359.9, $\Sigma \angle$ N3 360.0, $\Sigma \angle$ N2 359.5, $\Sigma \angle$ N4 350.1, angle between B coord. planes 83.8(1).	92
Figure 48. Absorption (blue), excitation (red) and emission (black) spectra of 1,2-bis(dimethylamino) diborane(4) 157 in hexane (5 μ M).	93

- Figure 49.** UV/Vis spectra of a 5 μM solution of **157** in hexane exposed to air (violet to red). **1**: increasing absorption band at 334 nm/ accumulation of the intermediate species; **2**: decreasing absorption band at 334 nm/ consumption of the intermediate species; **3**: increasing absorption band at 277 nm/ formation of suspected hydrolysis product. 94
- Figure 50.** Cyclic voltammogram of **157** in dichloromethane ($c = 3 \text{ mM}$), with a platinum working electrode, a platinum counter electrode, a silver quasi reference electrode, scan rate at 100 mV s^{-1} and $\text{Bu}_4\text{N}^+\text{PF}_6^-$ ($c = 0.1 \text{ M}$) as conductive salt..... 95
- Figure 51.** Cyclic voltammograms of **157** in dichloromethane ($c = 3 \text{ mM}$), with a platinum working electrode, a platinum counter electrode, a silver quasi reference electrode, scan rate at 100 mV s^{-1} and $\text{Bu}_4\text{N}^+\text{PF}_6^-$ ($c = 0.1 \text{ M}$) as conductive salt..... 95
- Figure 52.** Molecular structure of **158** in the solid state (ellipsoids at 50% probability, hydrogen atoms omitted for clarity). Selected bond lengths [\AA] and angles [$^\circ$]: B1-B2 1.722(2), B1-C1 1.560(2), B1-C9 1.559(2), B2-N3 1.433(2), B2-N4 1.423(2), C4-N1 1.381(2), C12-N2 1.372(2), $\Sigma \nabla \text{ B1}$ 359.85, $\Sigma \nabla \text{ B2}$ 360.0, $\Sigma \nabla \text{ N1}$ 353.14, $\Sigma \nabla \text{ N2}$ 359.71, $\Sigma \nabla \text{ N3}$ 359.33, $\Sigma \nabla \text{ N4}$ 359.7, angle between B coord. Planes 78.7(1). 97
- Figure 53.** Molecular structure of **161** in the solid state (ellipsoids at 50% probability, hydrogen atoms and co-crystallized α -difluoro-benzene omitted for clarity). Selected bond lengths [\AA] and angles [$^\circ$]: B1-B2 1.713(1), B1-N1 1.399(1), B1-C1 1.572(1), B2-N2 1.387(1), B2-C11 1.602(1), C4-N3 1.389(1), $\Sigma \nabla \text{ B1}$ 360.0, $\Sigma \nabla \text{ B2}$ 360.0, $\Sigma \nabla \text{ N1}$ 360.0, $\Sigma \nabla \text{ N2}$ 360.0, $\Sigma \nabla \text{ N3}$ 353.6, angle between B coord. Planes 85.58(7). 99
- Figure 54.** Absorption (blue), excitation (red) and emission (black) spectra of 1,2-bis(dimethyl-amino) diborane(4) **161** in hexane/ diethylether(5%). 100
- Figure 55.** ^{11}B NMR spectrum of the crude product of *p*-benzonitrile substituted diborane(4) **162**. 101
- Figure 56.** ^{11}B NMR spectrum of the crude product of *p*-nitrophenyl substituted diborane(4) **163**. 102

Figure 57. Literature known cyclic diazadiboron compounds by Norman and Russell. ^[139] 91a : R = H; 93 : R = Me; 92a : R = H; 164 : R = Me.....	103
Figure 58. Molecular structure of 166 in the solid state (ellipsoids at 50% probability, hydrogen atoms omitted for clarity). Selected bond lengths [Å] and angles [°]: B1-B2 1.687(2), B1-N1 1.411(2), B1-N3 1.458(2), B2-N2 1.414(2), B2-N4 1.453(2), $\Sigma \nabla$ B1 359.8, $\Sigma \nabla$ B2 359.6, $\Sigma \nabla$ N1 360.0, $\Sigma \nabla$ N2 360.0, largest deviation from the best plane through the atoms of the 1,4-diaza-2,3-diborinane heterocycle for B1: 0.262(1) Å.	105
Figure 59. Absorption (blue), excitation (red) and emission (black) spectra of diazadiborinane 166 in hexane.....	106
Figure 60. Structure and luminescent features of newly synthesized diborinane 166 in comparison to Norman and Russel's extended fused system 93	106
Figure 61. ¹ H NMR spectrum of the crude product of 169	108
Figure 62. Molecular structure of 169 in the solid state (ellipsoids at 50% probability, hydrogen atoms and second molecule in the asymmetric unit omitted for clarity). Selected bond lengths [Å] and angles [°]: B1-B2 1.687(4), B1-N1 1.428(3), B1-C9 1.571(3), B2-N2 1.416(3), B2-C17 1.572(4), N3-C12 1.377(3), N4-C20 1.383(3), $\Sigma \nabla$ B1 359.9, $\Sigma \nabla$ B2 360.0, $\Sigma \nabla$ N1 360.0, $\Sigma \nabla$ N2 359.9, $\Sigma \nabla$ N3 360.0, $\Sigma \nabla$ N4 359.8, largest deviation from the best plane through the atoms of the 1,4-diaza-2,3-diborinane heterocycle for N1: 0.055(2) Å.....	109
Figure 63. Absorption (blue), excitation (red) and emission (black) spectra of diazadiborinane 169 in hexane/ diethylether (5%).	110
Figure 64. Absorption (blue), excitation (red) and emission (black) spectra of the unknown decomposition species in a solution of 169 in hexane/ diethylether(5%).	111
Figure 65. UV/Vis spectra of a 5 μM solution of 169 in diglyme under the influence of air (violet to red) and excitation band of a desomposed sample (black) in diglyme.	111
Figure 66. Excitation spectra (left) and emission spectra (right) of the decomposed species in the solution of 169 in hexane/ diethylether (5%) (black) and in diglyme after exposition to air overnight (red).	112

Figure 67. Molecular Structure of 170 in the solid state (ellipsoids at 50% probability, hydrogen atoms and cocrystallized toluene omitted for clarity). Selected bond lengths [Å] and angles [°]: B1-B2 1.663(2), B1-N2 1.396(2), B1-C9 1.590(2), B2-N1 1.401(2), B2-C14 1.587(2), $\Sigma \nabla$ B1 360.0, $\Sigma \nabla$ B2 360.0, $\Sigma \nabla$ N1 360.0, $\Sigma \nabla$ N2 360.0, largest deviation from the best plane through the atoms of the 1,4-diaza-2,3-diborinane heterocycle for C1: 0.026(1) Å.	113
Figure 68. ¹ H NMR spectrum of the crude product of diborinane 172 . (172 is marked with “#”)	115
Figure 69. Molecular Structure of 172 in the solid state (ellipsoids at 50% probability, hydrogen atoms omitted for clarity). Selected bond lengths [Å] and angles [°]: B1-B2 1.686(3), B1-N1 1.423(3), B1-C9 1.584(3), B2-N2 1.449(3), B2-N3 1.421(3), N4-C12 1.412(2), $\Sigma \nabla$ B1 360.0, $\Sigma \nabla$ B2 359.9, $\Sigma \nabla$ N1 360.0, $\Sigma \nabla$ N2 360.0, $\Sigma \nabla$ N3 359.0, $\Sigma \nabla$ N4 348.2, largest deviation from the best plane through the atoms of the 1,4-diaza-2,3-diborinane heterocycle for B2: 0.132(1) Å.....	116
Figure 70. Absorption (blue), excitation (red) and emission (black) spectra of diazadiborinane 172 in hexane.....	117
Figure 71. ¹ H NMR spectrum of YK181 . Selected resonances of anticipated product 173 marked and integrated.....	118
Figure 72. ¹¹ B NMR spectrum of YK181 . Selected resonances of anticipated product 173 at 46.5 and 31.8 ppm.....	119
Figure 73. ¹ H NMR of the crude product of 180 (only resonances of 180 are marked and integrated).	121
Figure 74. Molecular structure of 180 in the solid state (ellipsoids at 50% probability, hydrogen atoms omitted for clarity). Selected bond lengths [Å] and angles [°]: B1-B2 1.663(2), B1-N1 1.410(2), B1-C9 1.570(2), B2-N2 1.400(2), B2-C1 1.794(2), N3-C12 1.380(2), $\Sigma \nabla$ B1 360.0, $\Sigma \nabla$ B2 359.9, $\Sigma \nabla$ N1 360.0, $\Sigma \nabla$ N2 360.0, $\Sigma \nabla$ N3 359.9, largest deviation from the best plane through the atoms of the 1,4-diaza-2,3-diborinane heterocycle for N2: 0.034(1) Å.	123
Figure 75. UV/Vis spectra of a 5 μM solution of 180 in diglyme under the influence of air (violet to red) and excitation band of a desomposed sample (black) in diglyme.	124

Figure 76. Excitation spectra (left) and emission spectra (right) of the decomposed species in the solution of 180 in hexane/ diethylether (5%) (black) and in diglyme after exposition to air overnight (red).....	124
Figure 77. Molecular structure of 181 in the solid state (ellipsoids at 50% probability, hydrogen atoms omitted for clarity). Selected bond lengths [Å] and angles [°]: B1-B2 1.676(2), B1-N1 1.422(1), B1-C9 1.571(1), B2-N2 1.402(1), B2-C17 1.595(1), N3-C12 1.404(1), $\Sigma \nabla$ B1 360.0, $\Sigma \nabla$ B2 360.0, $\Sigma \nabla$ N1 360.0, $\Sigma \nabla$ N2 360.0, $\Sigma \nabla$ N3 348.5, largest deviation from the best plane through the atoms of the 1,4-diaza-2,3-diborinane heterocycle for B1: 0.052(1) Å.	126
Figure 78. Absorption (blue), excitation (red) and emission (black) spectra of diazadiborinane 181 in hexane.....	127
Figure 79. UV/Vis spectra of a 5 μ M solution of 181 in diglyme under the influence of air (violet to red) and excitation band of a decomposed sample (black) in diglyme.	128
Figure 80. Excitation spectra (left) and emission spectra (right) of the decomposed species in the solution of 181 in hexane (black) and in diglyme after exposition to air overnight (red).....	128
Figure 81. Molecular Structure of 183 in the solid state (ellipsoids at 50% probability, hydrogen atoms omitted for clarity). Selected bond lengths [Å] and angles [°]: B1-B2 1.684(2), B1-N1 1.413(1), B1-C9 1.575(1), B2-N2 1.419(1), B2-O1 1.399(1), N3-C12 1.394(1), O1-C17 1.363(1), C20-N4 1.457(1), $\Sigma \nabla$ B1 360.0, $\Sigma \nabla$ B2 360.0, $\Sigma \nabla$ N1 360.0, $\Sigma \nabla$ N2 360.0, $\Sigma \nabla$ N3 351.8, $\Sigma \nabla$ N4 360.0, largest deviation from the best plane through the atoms of the 1,4-diaza-2,3-diborinane heterocycle for N1: 0.028(1) Å.	130
Figure 82. Molecular structure of 185 in the solid state (ellipsoids at 50% probability, hydrogen atoms and second molecule in the asymmetric unit omitted for clarity). Selected bond lengths [Å] and angles [°]: B1-B2 1.704(2), B1-N1 1.388(2), B2-C11 1.791(2), B1-C1 1.589(2), B2-C11 1.568(2), $\Sigma \nabla$ B1 360.0, $\Sigma \nabla$ B2 359.4, $\Sigma \nabla$ N1 360.0, angle between B coord. Planes 63.1(1).	132
Figure 83. ^1H NMR spectrum of diduryldiborane(4) 186	133
Figure 84. Absorption (blue), excitation (red) and emission (black) spectra of diduryldiborane(4) 186 in hexane.	134

Figure 85. Molecular structure of 187 in the solid state (ellipsoids at 50% probability, hydrogen atoms and second molecule in the asymmetric unit omitted for clarity). Selected bond lengths [Å] and angles [°]: B1-B2 1.690(3), B1-C11 1.800(2), B1-C1 1.573(3), B2-C11 1.531(3), B2-C19 1.592(3), C14-N1 1.365(2), Σ \angle B1 360.0, Σ \angle B2 359.4, Σ \angle N1 358.7, angle between B coord. Planes 64.3(1).....	136
Figure 86. Absorption (blue), excitation (red) and emission (black) spectra of diduryldiborane(4) 187 in hexane.....	137
Figure 87. ^{11}B NMR spectrum of diduryldiborane(4) 188 at 343K.....	138
Figure 88. ^1H NMR spectrum of diduryldiborane(4) 188	139
Figure 89. Absorption (blue), excitation (red) and emission (black) spectra of diduryldiborane(4) 188 in hexane.....	140
Figure 90. ^1H NMR spectrum of diduryldiborane(4) 190	142
Figure 91. ^{19}F NMR spectrum of diduryldiborane(4) 190	143
Figure 92. ^1H NMR spectrum of YK181 . Selected resonances of anticipated product 93 marked and integrated.....	272
Figure 93. ^1H NMR spectrum of YK173 . Selected resonances of anticipated product 94 marked and integrated.....	273
Figure 94. ^1H NMR spectrum of YK174 . Selected resonances of anticipated product 95 marked and integrated.....	273
Figure 95. ^1H NMR spectrum of YK172 . Selected resonances of anticipated product 96 marked and integrated.....	274
Figure 96. ^1H NMR spectrum of YK176 . Selected resonances of anticipated product 97 marked and integrated.....	274
Figure 97. ^1H NMR spectrum of YK184 . Selected resonances of anticipated product 98 marked and integrated.....	275
Figure 98. ^1H NMR spectrum of YK182 . Selected resonances of anticipated product 99 marked and integrated.....	275
Figure 99. UV/Vis spectra of 1,2-bis(dimethylamino) diborane(4) 156 in hexane at different concentrations (0.7 mM – 1 mM).....	276

Figure 100. Determination of ϵ ($13200 \text{ M}^{-1} \text{ cm}^{-1}$) by linear regression of absorbance ($\lambda = 282 \text{ nm}$) of 156 against concentration.	276
Figure 101. UV/Vis spectra of 1,2-bis(dimethylamino) diborane(4) 157 in hexane at different concentrations (0.6 mM – 0.9 mM).	277
Figure 102. Determination of ϵ ($34900 \text{ M}^{-1} \text{ cm}^{-1}$) by linear regression of absorbance ($\lambda = 281 \text{ nm}$) of 157 against concentration.	277
Figure 103. UV/Vis spectra of 1,2-bis(dimethylamino) diborane(4) 161 in diethylether at different concentrations (0.4 mM – 1 mM).	278
Figure 104. Determination of ϵ ($17300 \text{ M}^{-1} \text{ cm}^{-1}$) by linear regression of absorbance ($\lambda = 286 \text{ nm}$) of 161 against concentration.	278
Figure 105. UV/Vis spectra of cyclic 1,4-diaza-2,3-diborinane 166 in hexane at different concentrations (0.6 mM – 0.9 mM).	279
Figure 106. Determination of ϵ ($11800 \text{ M}^{-1} \text{ cm}^{-1}$) by linear regression of absorbance ($\lambda = 314 \text{ nm}$) of 166 against concentration.	279
Figure 107. Determination of ϵ ($12100 \text{ M}^{-1} \text{ cm}^{-1}$) by linear regression of absorbance ($\lambda = 308 \text{ nm}$) of 166 against concentration.	280
Figure 108. Determination of ϵ ($9840 \text{ M}^{-1} \text{ cm}^{-1}$) by linear regression of absorbance ($\lambda = 272 \text{ nm}$) of 166 against concentration.	280
Figure 109. Determination of ϵ ($34900 \text{ M}^{-1} \text{ cm}^{-1}$) by linear regression of absorbance ($\lambda = 234 \text{ nm}$) of 166 against concentration.	281
Figure 110. UV/Vis spectra of cyclic 1,4-diaza-2,3-diborinane 169 in diethylether at different concentrations (0.4 mM – 1 mM).	281
Figure 111. Determination of ϵ ($35500 \text{ M}^{-1} \text{ cm}^{-1}$) by linear regression of absorbance ($\lambda = 342 \text{ nm}$) of 169 against concentration.	282
Figure 112. Determination of ϵ ($34700 \text{ M}^{-1} \text{ cm}^{-1}$) by linear regression of absorbance ($\lambda = 261 \text{ nm}$) of 169 against concentration.	282
Figure 113. Determination of ϵ ($27300 \text{ M}^{-1} \text{ cm}^{-1}$) by linear regression of absorbance ($\lambda = 232 \text{ nm}$) of 169 against concentration.	283
Figure 114. UV/Vis spectra of cyclic 1,4-diaza-2,3-diborinane 170 in diethylether at different concentrations (0.4 mM – 0.7 mM).	283

Figure 115. Determination of ϵ ($15800 \text{ M}^{-1} \text{ cm}^{-1}$) by linear regression of absorbance ($\lambda = 327 \text{ nm}$) of 170 against concentration.	284
Figure 116. Determination of ϵ ($14800 \text{ M}^{-1} \text{ cm}^{-1}$) by linear regression of absorbance ($\lambda = 315 \text{ nm}$) of 170 against concentration.	284
Figure 117. Determination of ϵ ($24900 \text{ M}^{-1} \text{ cm}^{-1}$) by linear regression of absorbance ($\lambda = 243 \text{ nm}$) of 170 against concentration.	285
Figure 118. Determination of ϵ ($35000 \text{ M}^{-1} \text{ cm}^{-1}$) by linear regression of absorbance ($\lambda = 216 \text{ nm}$) of 170 against concentration.	285
Figure 119. UV/Vis spectra of cyclic 1,4-diaza-2,3-diborinane 172 in hexane at different concentrations (0.4 mM – 0.7 mM).	286
Figure 120. Determination of ϵ ($15800 \text{ M}^{-1} \text{ cm}^{-1}$) by linear regression of absorbance ($\lambda = 327 \text{ nm}$) of 172 against concentration.	286
Figure 121. Determination of ϵ ($14800 \text{ M}^{-1} \text{ cm}^{-1}$) by linear regression of absorbance ($\lambda = 315 \text{ nm}$) of 172 against concentration.	287
Figure 122. Determination of ϵ ($24900 \text{ M}^{-1} \text{ cm}^{-1}$) by linear regression of absorbance ($\lambda = 243 \text{ nm}$) of 172 against concentration.	287
Figure 123. Determination of ϵ ($35000 \text{ M}^{-1} \text{ cm}^{-1}$) by linear regression of absorbance ($\lambda = 216 \text{ nm}$) of 172 against concentration.	288
Figure 124. UV/Vis spectra of cyclic 1,4-diaza-2,3-diborinane 180 in diethylether at different concentrations (0.4 mM – 1 mM).	288
Figure 125. Determination of ϵ ($21200 \text{ M}^{-1} \text{ cm}^{-1}$) by linear regression of absorbance ($\lambda = 334 \text{ nm}$) of 180 against concentration.	289
Figure 126. Determination of ϵ ($18700 \text{ M}^{-1} \text{ cm}^{-1}$) by linear regression of absorbance ($\lambda = 255 \text{ nm}$) of 180 against concentration.	289
Figure 127. Determination of ϵ ($18900 \text{ M}^{-1} \text{ cm}^{-1}$) by linear regression of absorbance ($\lambda = 232 \text{ nm}$) of 180 against concentration.	290
Figure 128. UV/Vis spectra of cyclic 1,4-diaza-2,3-diborinane 181 in hexane at different concentrations (0.4 mM – 1 mM).	290

Figure 129. Determination of ϵ ($16900 \text{ M}^{-1} \text{ cm}^{-1}$) by linear regression of absorbance ($\lambda = 349 \text{ nm}$) of 181 against concentration.	291
Figure 130. Determination of ϵ ($15000 \text{ M}^{-1} \text{ cm}^{-1}$) by linear regression of absorbance ($\lambda = 313 \text{ nm}$) of 181 against concentration.	291
Figure 131. Determination of ϵ ($21000 \text{ M}^{-1} \text{ cm}^{-1}$) by linear regression of absorbance ($\lambda = 263 \text{ nm}$) of 181 against concentration.	292
Figure 132. UV/Vis spectra of cyclic 1,4-diaza-2,3-diborinane 183 in diethylether at different concentrations (0.4 mM – 1 mM).	292
Figure 133. Determination of ϵ ($25100 \text{ M}^{-1} \text{ cm}^{-1}$) by linear regression of absorbance ($\lambda = 316 \text{ nm}$) of 183 against concentration.	293
Figure 134. Determination of ϵ ($20700 \text{ M}^{-1} \text{ cm}^{-1}$) by linear regression of absorbance ($\lambda = 259 \text{ nm}$) of 183 against concentration.	293
Figure 135. Determination of ϵ ($26200 \text{ M}^{-1} \text{ cm}^{-1}$) by linear regression of absorbance ($\lambda = 232 \text{ nm}$) of 183 against concentration.	294
Figure 136. UV/Vis spectra of 1,2-diduryl diborane(4) 185 in hexane at different concentrations (0.4 mM – 1 mM).	294
Figure 137. Determination of ϵ ($3380 \text{ M}^{-1} \text{ cm}^{-1}$) by linear regression of absorbance ($\lambda = 313 \text{ nm}$) of 185 against concentration.	295
Figure 138. UV/Vis spectra of 1,2-diduryl diborane(4) 186 in hexane at different concentrations (0.2 mM – 0.8 mM).	295
Figure 139. Determination of ϵ ($44000 \text{ M}^{-1} \text{ cm}^{-1}$) by linear regression of absorbance ($\lambda = 337 \text{ nm}$) of 186 against concentration.	296
Figure 140. Determination of ϵ ($15800 \text{ M}^{-1} \text{ cm}^{-1}$) by linear regression of absorbance ($\lambda = 242 \text{ nm}$) of 186 against concentration.	296
Figure 141. UV/Vis spectra of 1,2-diduryl diborane(4) 187 in hexane at different concentrations (0.2 mM – 0.8 mM).	297
Figure 142. Determination of ϵ ($33800 \text{ M}^{-1} \text{ cm}^{-1}$) by linear regression of absorbance ($\lambda = 347 \text{ nm}$) of 187 against concentration.	297
Figure 143. UV/Vis spectra of 1,2-diduryl diborane(4) 188 in hexane at different concentrations (0.2 mM – 0.8 mM).	298

Figure 144. Determination of ϵ ($48200 \text{ M}^{-1} \text{ cm}^{-1}$) by linear regression of absorbance ($\lambda = 341 \text{ nm}$) of 188 against concentration.	298
Figure 145. Determination of ϵ ($13900 \text{ M}^{-1} \text{ cm}^{-1}$) by linear regression of absorbance ($\lambda = 279 \text{ nm}$) of 188 against concentration.	299
Figure 146. Determination of ϵ ($17100 \text{ M}^{-1} \text{ cm}^{-1}$) by linear regression of absorbance ($\lambda = 244 \text{ nm}$) of 188 against concentration.	299

List of Schemes

Scheme 1. Synthesis of boryl amidinates and guanidates.....	6
Scheme 2. Synthesis of boryl amidinates and guanidates by carbodiimide insertion.....	7
Scheme 3. Further syntheses of boryl amidinates and guanidates.....	8
Scheme 4. Reactivity of boryl amidinate complexes 6a (R = iPr) and 6b (R = ^t Bu) towards small molecules.	9
Scheme 5. Reactivity of boryl guanidates 2i (a), 10c (b) Ar = Ph- <i>p</i> - ^t Bu and 18 (c) Ar = Ph- <i>p</i> -Me towards benzaldehyde plus equilibrium between boryl guanidate 18 and 27 under CO ₂ atmosphere (d) Ar = Ph- <i>p</i> - ^t Bu.	11
Scheme 6. Reactivity of boryl amidinate 1d towards Yamashita's boryl anion 28 yielding 29	12
Scheme 7. Halogenide abstraction from boryl guanidate 2p and boryl formamidinate 5a (R = NiPr ₂ , X = Br) and 5b (R = Ph, X = Cl). 31a : R = NiPr ₂ ; 31b : R = Ph.	12
Scheme 8. (a): Synthesis of boryl amidinate cations 32a (R = Cy) and 32b (R = iPr) from borane 33 and carbodiimides 34a (R = Cy) and 34b (R = iPr), respectively. (b): Synthesis of the mixed amidinate and guanidate stabilized cation 36 from the borylium cation 35 which is prepared by reaction of borane 33 and silver trifluoromethanesulfonate.....	13
Scheme 9. Reactions of cationic aminoborylene iron complexes 37a (R = Cy) and 37b (R = iPr) with dicyclohexylcarbodiimide to 39a (R = Cy) and 39b (R = iPr).....	14
Scheme 10. Synthesis of 1,2-dimethyl(amino)-1,2-dihalo diboranes(4) 54a (X = Cl) and 54b (X = Br) from tetrakis(dimethylamino)diborane(4) 53 with HCl (Y = H) or trihaloborane (Y = X ₂ B).....	18
Scheme 11. Halide substitution on diboranes(4) 54a and 54b with aryl and/or alkyl metals (RM = ⁿ BuLi, ^t BuLi, allylMgCl, PhLi, MesLi, indLi, NphtLi, CpNa, fluLi TipLi, octafluLi, AnLi, DurLi, 4- ^t butyl-2,6-dimethylphenyl lithium, 2,5-di- ^t butylphenyl lithium) to yield the symmetrically substituted diboranes(4) 55a : R = ⁿ Bu, 55b : R = ^t Bu, 55c : R = allyl, 55d : R = Ph, 55e : Mes, 55f : R = 1-ind, 55g : R	

= Cp, **55h**: R = flu, **55i**: R = Tip, **55j**: R = An, **55k**: R = Dur, **55l**: R = 4-^tbutyl-2,6-dimethylphenyl, **55m**: R = 2,5-di-^tbutylphenyl, and unsymmetrically substituted diboranes(4) **56a**: R = ^tBu, X = Cl, **56b**: R = allyl, X = Cl, **56c**: R = Mes, X = Br, **56d**: R = 1-ind, X = Cl, **56e**: R = ^tBu, X = Br, **56f**: R = Cp, X = Br, **56g**: R = flu, X = Br, **56h**: R = octaflu, X = Br, and **57a**: R = ^tBu, R' = Ph, **57b**: R = ^tBu, R' = Npht, **57c**: R = flu, R' = Cp, **57d**: R = octaflu, R' = Cp, **57e**: R = Mes, R' = Ph, as well as arylene bridged unsymmetrically substituted diboranes(4) **58a**: R = R' = H, **58b**: R = Me, R' = H, **58c**: R = R' = Me, and **59a**: R = R' = H, **59b**: R = Me, R' = H, **59c**: R = R' = Me..... 19

Scheme 12. Synthesis of 1,2-bis(dimethylamino)-1,2-bis(aryloxy) diborane(4) **60** and conversion with lithiumorganyls to 1,2-bis(dimethylamino)-1,2-diorganyl diboranes(4) **55a**: R = ⁿBu, **55h**: R = flu and **61**: R = CC-Ph. 19

Scheme 13. Synthesis of diboranes(4) **55a**: R = ⁿBu, **55d**: R = Ph and **63**: R = Et by reductive coupling (M = Na or K) of chloroboranes **62a**: R = ⁿBu, **62b**: R = Ph or **62c**: R = Et..... 20

Scheme 14. Conversion of dimethylamino-groups in 1,2-disubstituted diboranes(4) **55b,e,k-m** into methoxy- (**65a-d**) or halide-groups (**64a-g**).^[96-98,104] **64a**: R = ^tBu, X = Cl; **64b**: R = ^tBu, X = Br; **64c**: R = Mes, X = Cl, **64d**: R = Mes, X = Br; **64e**: R = Dur, X = Cl; **64f**: R = Dur, X = Br; **64g**: R = 4-^tbutyl-2,6-dimethylphenyl, X = Cl; **64h**: R = 2,5-di-^tbutylphenyl, X = Cl; **65a**: R = Mes; **65b**: R = Dur; **65c**: R = 4-^tbutyl-2,6-dimethylphenyl; **65d**: R = 2,5-di-^tbutylphenyl. ... 20

Scheme 15. Synthesis of donor-free symmetrically substituted diboranes(4) **68** and unsymmetrically substituted diboranes(4) **70a-d** via methoxy diboranes(4) **67a,b** and **69a-c** from tetramethoxy diborane(4) **66** plus the synthesis of tetra-*o*-tolyl-diborane(4) **71** from bis(catecholato) diborane(4) **72**. 21

Scheme 16. Synthesis of pentafluorophenyl-substituted diboranes(4) **73a,b** from borane **74** and tris(pentafluorophenyl) borane forming borole **76**, which is subsequently reacted with acetylenes to intermediate **77a,b** that under thermal treatment are arranged to diboranes(4) **73a,b**. **77a & 73a**: R = ⁿPr; **77b & 73b**: R = Ph. 22

Scheme 17. Rearrangements of 1,2-substitution patterns on diboranes(4) **54a**, **64c**: Ar = Mes, **64e**: Ar = Dur, **64d**: Ar = Mes, X = Br, **80**: Ar = Mes, X = I, to 1,1-substitution on diboranes(4) **78**, **79a**: Ar = Mes, **79b**: Ar = Dur and **81a**: Ar =

Mes, X = Cl, L = SIMes, **81b**: Ar = Mes, X = Br, L = PEt₃, **81c**: Ar = Mes, X = Br, L = PCy₂Me, **81d**: Ar = Mes, X = Cl, L = PEt₃, **81e**: Ar = Mes, X = I, L = PEt₃, **81f**: Ar = Mes, X = Cl, L = PCy₂Me, **81g**: Ar = Mes, X = I, L = PCy₂Me, **81h**: Ar = Mes, X = Br, L = SIMes, **81i**: Ar = Mes, X = Cl, L = IDip, **81j**: Ar = Mes, X = Cl, L = CAAC^{Me}, **81k**: Ar = Mes, X = Br, L = CAAC^{Me}, **81l**: Ar = Dur, X = Cl, L = CAAC^{Me}, **81m**: Ar = Dur, X = Br, L = CAAC^{Me}. 23

Scheme 18. Synthesis of 1,4-diaza-2,3-diborinane species **83a-j** from according diboranes(4) **54a**, **64c**, **82** and polycyclic species **84a-d** from diborane(4) **53**. 24

Scheme 19. Synthesis of unsaturated 1,4-diaza-2,3-diborinane species **85a-f**, **87**, **88a,b** from according diboranes(4) **54a**, **64c,e**. **54a**: R = NMe₂, X = Cl; **64c**: R = Mes, X = Cl; **64e**: R = Dur, X = Cl; **85a**: R = NMe₂, R' = 2,4-dimethylphenyl; **85b**: R = NMe₂, R' = Mes; **85c**: R = NMe₂, R' = 2,6-dimethylphenyl; **85d**: R = NMe₂, R' = *p*-tolyl; **85e**: R = Mes, R' = *p*-tolyl; **85f**: R = Dur, R' = *p*-tolyl; **85g**: R = NMe₂, R' = *t*Bu; **88a**: R' = Mes; **88b**: R' = 2,6-dimethylphenyl. 25

Scheme 20. Reactivity of **83c** (saturated backbone) and **85b-d** (unsaturated backbone) towards BH₃-SMe₂, HCl/Et₂O, BBr₃ or BI₃ and comproportioning reaction between dimethylamino derivatives **83c/85b-d** and according hydrogen/halide derivatives **89a-h** to the mixed species **90a-g**. 26

Scheme 21. Synthesis of polycyclic 1,4-diaza-2,3-diborinanes **91a-c** and diazaboroles **92a,b** (as side products) from diborane(4) **53**. Isolated ratio **91a:92a** = 73:27, **91b:92b** = 81:19. 26

Scheme 22. Synthesis of *N*-methylated 1,4-diaza-2,3-diborinane **93** from **91a** and subsequent conversion to the radical species **94**. 27

Scheme 23. Oxidation of diborenes **95a-d** to monoradical cations **96a-d** with BAr^f₄⁻ (Ar^f = 3,5-(CF₃)₂-Ph) or borole radical-anion **[97]^{•-}** as counterpart. 28

Scheme 24. Reduction of diboranes(4) **55d**, **65a**, **70d**, **71**, **100a-d** to monoradical-anions **98a-f** or diborane(4) dianions **99a-c**. 28

Scheme 25. Proposed synthesis of boryl amidinate structures **I** (Ar = aryl, R = alkyl or aryl, X = halogen, alkyl, aryl or amine) from amidinate ligands **II** (Ar = aryl, R = alkyl or aryl, [M] = lithium, trimethylsilyl) and di- or tri-haloboranes (BX₃

= BCl ₃ , BBr ₃ , BCl ₂ R, R = alkyl, aryl, amine) and possible reduction to boron(I) structure III or reaction with nucleophiles and bases.....	31
Scheme 26. Synthesis of trimethylsilylbenzamidinium 103	33
Scheme 27. Reactivity of trimethylsilylbenzamidinium 103 towards trihaloboranes (BCl ₃ and BBr ₃).....	36
Scheme 28. Synthesis of dichloroboryl benzamidinate 104a from carbodiimine 101 and phenyllithium <i>via</i> lithium benzamidinate 102	36
Scheme 29. Synthesis of dihaloboryl benzamidinates 104 from benzamidinium 105 <i>via</i> lithium benzamidinate 102	39
Scheme 30. Bürger's observed rearrangement (a) and proposed rearrangement pathway (b) plus proposed analogous rearrangement pathway of 104a to 116 and its mesomeric forms (c).	38
Scheme 31. Synthesis of dichloroboryl benzamidinate 104a from isolated lithium benzamidinate 102 and possible rearrangement product 116	41
Scheme 32. Synthesis of dichloroboryl benzamidinate 119 from carbodiimine 117 <i>via</i> lithium amidinate 118	42
Scheme 33. Synthesis of dichloroboryl benzamidinate 121	42
Scheme 34. Synthesis of dichloroboryl benzamidinate 124	45
Scheme 35. Synthesis of chlorophenylboryl benzamidinate 126	46
Scheme 36. Synthesis of chlorocyclohexylboryl benzamidinate 128	47
Scheme 37. Synthesis of chlorodimethylaminoboryl benzamidinate 130	48
Scheme 38. Synthesis of chlorodimethylaminoboryl benzamidinate 131	50
Scheme 39. Reduction attempts of dichloroboryl benzamidinate 104a,b to aimed at structure 132	55
Scheme 40. Synthesis and proposed formation mechanism of benzazaborole 136	63
Scheme 41. Attempted reaction of dichloroboryl benzamidinate 104a with Me ⁴ NHC.....	64
Scheme 42. Reaction of benzazaborole 136 with triphenylborane 140	64

Scheme 43. Reaction between benzazaborole 136 and perfluorinated triphenylborane (143).	69
Scheme 44. Reactivity of benzamidinates 119 (R = ^t Bu, X _a = X _b = Cl) and 128 (R = Dip, X _a = Cl, X _b = cyclohexyl) towards ^{iPr} 2Me ₂ NHC 135	70
Scheme 45. Reactivity of chlorophenylboryl benzamidinate 126 towards ^{iPr} 2Me ₂ NHC 135	70
Scheme 46. Reactivity of benzamidinates 119 (R = ^t Bu, X _a = X _b = Cl) and 128 (R = Dip, X _a = Cl, X _b = cyclo-hexyl) towards ^{Me} 4NHC 139	71
Scheme 47. Reactivity of benzamidinates 104a (X _a = X _b = Cl) and 128 (X _a = Cl, X _b = cyclo-hexyl) towards metalorganic reagents.	72
Scheme 48. Synthesis and proposed mechanism of diazaboretidine 145	73
Scheme 49. Reactivity of naphthyl- and phenyl-oxazolines towards organolithium reagents.	75
Scheme 50. Reactivity of chlorodimethylaminoboryl benzamidine 30 towards various metalorganic reagents. R-M = nBuLi, KHMDS, (Tip) ₂ Si=SiTipLi	76
Scheme 51. Reaction between diazaboretidine 145 and BCl ₃	77
Scheme 52. Reported boryl benzamidinates 104a : Ar = Ph, R = Dip, X = Y = Cl, ; 104b : Ar = Ph, R = Dip, X = Y = Br, 119 : Ar = Ph, R = ^t Bu, X = Y = Cl, 121 : Ar = Ph-NMe ₂ , R = Dip, X = Y = Cl, 124 : Ar = C ₆ F ₅ , R = Dip, X = Y = Cl, 126 : Ar = Ph, R = Dip, X = Cl, Y = Ph, 128 : Ar = Ph, R = Dip, X = Cl, Y = cyclohexyl, 130 , 131 : Ar = Ph, R = ^t Bu, X = Cl, Y = NMe ₂ and rearrangement products 116 : R' = H and 122 : R' = NMe ₂	79
Scheme 53. Reported reactivity of boryl benzamidinate 104a towards ^{iPr} 2Me ₂ NHC to yield 136 and reported reactivity of boryl benzamidinate 130 towards metalorganic reagents to yield isolated 145 : R = iPr and observed 152 : R = ⁿ butyl, 153 : N(SiMe ₃) ₂ and 154 : R = Si(Tip)=SiTip ₂	80
Scheme 54. Synthesis of diborane(4) 156	83
Scheme 55. Synthesis of diborane(4) 157	90
Scheme 56. Reaction of 1,2-dichloro diborane(4) 54a with an excess of 4-dimethylaminophenyl lithium (155) to the 1,1-isomer 158 and the 1,2-isomer 157	96

Scheme 57. Synthesis of unsymmetrically substituted diborane(4) 161 .	98
Scheme 58. Synthesis of acceptor substituted diboranes(4) 162 (R = CN) and 163 (R = NO ₂).	101
Scheme 59. Synthesis of diazadiborinane 166 .	104
Scheme 60. Synthesis of bis(aminophenyl) substituted diazadiborinane 169 .	107
Scheme 61. Synthesis of bis(pentafluorophenyl)-substituted diazadiborinane 170 .	112
Scheme 62. Synthesis of unsymmetrically substituted diazadiborinane 172 .	114
Scheme 63. Reactivity of diazadiborinane 171 towards various aromatic lithium organyls.	118
Scheme 64. Synthesis of unsymmetrically substituted chloro-diazadiborinane 180 .	121
Scheme 65. Synthesis of unsymmetrically substituted diazadiborinane 181 .	125
Scheme 66. Synthesis of 4-nitrophenoxy substituted diazadiborinane 183 .	129
Scheme 67. Synthesis of diduryldiborane(4) 185 .	131
Scheme 68. Synthesis of aminophenyl-substituted dimethylaminodiduryldiborane(4) 186 .	133
Scheme 69. Synthesis of aminophenyl substituted chloro-diduryldiborane(4) 187 .	135
Scheme 70. Synthesis of symmetrically substituted bis(aminophenyl)-diduryldiborane(4) 188 .	138
Scheme 71. Attempted reaction of aminophenyl substituted chloro-diduryldiborane(4) 187 with pentafluorophenyl lithium (160).	141
Scheme 72. Synthesis of pentafluorophenyl substituted chloro-1,2-diduryldiborane(4) 190 .	142
Scheme 73. Synthesis and isolation of boryl benzamidates in the closed form (104a,b , 119 , 124 , 126 , 128 and 131) and open chained form (130) from either lithium amidinate 102 or 123 plus the isolated product 136 from the reaction	

between 104a and 2 ^{iPr} 2Me ₂ NHC and the isolated product 145 from the reaction between open chained boryl amidinate 130 and iPrMgCl.	145
Scheme 74. Suggested rearrangement pathway of 104a to 116 , which was mostly observed after storage of 104a in concentrated solution.....	146
Scheme 75. By DFT-calculations suggested guanidate borylene 134 retrosynthesis proposition <i>via</i> 215 and 216 plus previously reported 217	147
Scheme 76. Suggested rearomatization of 154 to form 218	148
Scheme 77. Synthesized and structurally characterized substituted 1,2-bis(dimethylamino)-diboranes(4), 156 , 157 and 161 , 1,1-isomer 158 , benzo fused cyclic 1,4-diaza-2,3-diborinanes 166 , 169 , 170 , 172 , 181 and 183 as well as 1,2-diduryl-diboranes(4) 185 to 188	149

List of Tables

Table 1. ^{11}B NMR chemical shifts of tricoordinate (BX_3) and tetracoordinate (BX_4) boron atoms.	4
Table 2. Multinuclear NMR resonances of isolated diazaboretidine 145 and spectroscopically observed diazaboretidines 152 , 153 and 154	76
Table 3. ^{11}B NMR resonances of reaction mixtures of unsymmetrically with various aryls substituted diazadiborinanes 173 to 179	120
Table 4. Spectroscopic data for synthesized diboranes(4). Wavelengths λ [nm], wavenumbers ν [cm^{-1}] and extinction coefficients ϵ [$\text{L mol}^{-1} \text{cm}^{-1}$].....	151
Table 5. Numbered compounds (introduction).	247
Table 6. Numbered Compounds (Results and Discussion, Conclusion and Outlook, Experimental Section)	260
Table 7. Reviewed diboranes(4) and their ^{11}B NMR chemical shifts.....	268

Preface

Boron constitutes about 0.001% by weight of Earth's crust and occurs mainly in the form of borate minerals. The majority of mined borate ores undergo refinement into boric acid or sodium tetraborate before further processing.^[1-3] The isolation of elemental boron was first accomplished by Joseph-Louis Gay-Lussac and Louis Jacques Thenard and independently by Sir Humphry Davy in 1808 by heating boron oxide with potassium metal.^[1] Manufacturing of pure boron is not necessary for most purposes and its elemental form is only rarely used in applications such as doping of semiconductors or in its amorphous form as boron fibers in some high strength materials.^[4,5] In contrast, boron containing compounds are of great importance in diverse fields: Boron oxide is added to fiberglass to increase its strength or as a fluxing agent to facilitate processing,^[6] and in borosilicate glass to lower the coefficient of thermal expansion.^[7] Boron's deployment in metallurgy (metal borides)^[8] and ceramics (boron carbide and nitride)^[9,10] is also dedicated to improving the hardness and toughness of the materials. Together with the use of boron compounds in detergents and fertilizers, these applications account for three-quarters of the world consumption of borates.^[2,3] In emerging areas of research organoboranes gain more and more attention. They have been established as reactive intermediates in organic chemistry, with the Nobel prize winning hydroboration probably as the most prominent example.^[11-13] Especially the metallomimetic chemistry of selected compounds, often accompanied by the possibility of small molecule activation, contributes to the significance of this research, as it impacts the production of value added fine chemicals or fuel synthesis.^[14-17] Other energy-related processes, for example hydrogen production and storage and production of electrolyte materials, benefit immensely from employment of boron-containing compounds. Also remarkable is the variety of examples of boron-based fluorescent emitters in OLED materials for the conversion of electrical energy to light.^[16,17] All in all, boronchemistry has a multitude of possible applications and remains a field worth investigating.

1. Introduction

Boron's unique electronic structure directly effects its diverse molecular chemistry. The intrinsic electron deficiency enables tricoordinate boron to act as electrophile/ Lewis-acid. Conversion with nucleophiles lead to anionic structures with completely different properties.^[18] It is also the unique electronic properties that enable 3-center-2-electron bonding in for example diborane(6) and polyhedral borane clusters.^[19]

In the following literature review two areas of boron research are addressed: Firstly, boron compounds with *N,N*-chelating ligands and in this context group 13 element(I) structures stabilized by bidentate nitrogen ligands and secondly, the synthesis of known diboranes(4). As it is the most frequent applied analytic tool in boron chemistry, the principles of ¹¹B NMR spectroscopy are presented in advance.

1.1 Basics of ¹¹B NMR Spectroscopy

Except from ¹H and ¹³C as most popular nuclei for NMR measurements, ¹¹B NMR spectroscopy contributed immensely to the development of today's very rich boron chemistry. With an abundance of 80.4%, a nuclear spin of $I = 3/2$ and a factor 3 larger magnetic moment ¹¹B is superior to the ¹⁰B isotope (abundance: 19.6%, $I = 3$), which can also be measured by NMR spectroscopy. Both display large quadrupole moments, that increase line widths of the resulting spectra. However, ¹¹B is with a one order of magnitude smaller quadrupole moment in advantage here as well.^[20-22]

The chemical shift is probably of most informative value when analyzing an ¹¹B NMR spectrum and is most commonly referenced to BF₃·OEt₂. Chemical shifts for boron nuclei with the coordination numbers three and four, the former being more deshielded, show vast differences provided that the same substituents are compared (Table 1). This comes with the advantage that equilibria between boranes as Lewis acids and diverse Lewis-bases can easily be monitored with ¹¹B NMR spectroscopy. The electronic properties of the substituent also play an important role. The deshielding in three-coordinate boron compounds can be

1. Introduction

lowered by substituents with a free electron pair allowing for p- π -interaction between the free electron pair and the vacant orbital at the boron center. Considering Table 1 the following order of increasing p- π -interaction can be deduced: B < alkyl < C=C \leq Ph < I < Br < Cl < NR₂ < OR < F. Substituents without free electron pair such as the alkyl-group can lower the deshielding of the boron nucleus by hyperconjugation. This is demonstrated by comparison of the chemical shifts of triethylborane (86.6 ppm) with the more deshielded tetra(ethyl)diborane(4) (105.5 ppm).^[23] This comparison is appropriate in the way that diboranes(4) can be regarded as tricoordinate boron nuclei which are only influenced by two substituents. The resonances of the diboranes(4) discussed in this thesis range from 30 ppm to 104 ppm (see Table 7, Section 7.2) reflecting the substituent effects described above.

Table 1. ¹¹B NMR chemical shifts of tricoordinate (BX₃) and tetracoordinate (BX₄⁻) boron atoms.^[23]

X	$\delta(\text{BX}_3)$ [ppm]	$\delta(\text{BX}_4^-)$ [ppm]
CH ₃	86.2	-20.2
C ₂ H ₅	86.6	-17.5
ⁿ C ₃ H ₇	86.6	-17.5
ⁿ C ₄ H ₉	86.5	-17.6
CH=CH ₂	56.4	-16.1
C ₆ H ₅	68.0	-6.7
I	-7.9	-127.5
Br	38.7	-23.8
Cl	46.5	6.7
F	10.0	-1.6
NHMe	24.6	0.2
OMe	18.3	2.7

1.2 Boryl amidinates and guanidates

Amidinate and guanidate ligands share the same NCN-binding site of the general formula $[\text{RC}(\text{NR}')_2]^-$. As opposed to the isolobal carboxylate group $[\text{RCO}_2]^-$, the additional substituents at the nitrogen (R') atoms allow for modification of the steric and electronic properties of these ligands. Depending on whether a nitrogen or a carbon is attached to the center-carbon, the ligands are named amidinates (carbon) or guanidates (nitrogen). The first boron guanidates were observed IR-spectroscopically by Lappert in 1966.^[24] Isolation of the first boron amidinate structure **1a** (Figure 1) was then reported by Dehnicke^[25] and the first isolated guanidates **2a-e** were described by Bürger^[26] (Figure 2). In the meantime, a whole variety of four-membered boron *N*-heterocycles have been synthesized exploiting the facile tunability of those ligands (**1b-i**, **3a-g**, **4**, **5a,b**, **6a,b**, **7**, **8**, **9a,b**, Figure 1, **2f-r**, **10a-d**, Figure 2).^[25-45] Almost all of them adopt the *N,N*-chelating, closed ring structure, except for the Dip-formamidinate complexes **5a,b** (Figure 1), which adopt an open-chained form.

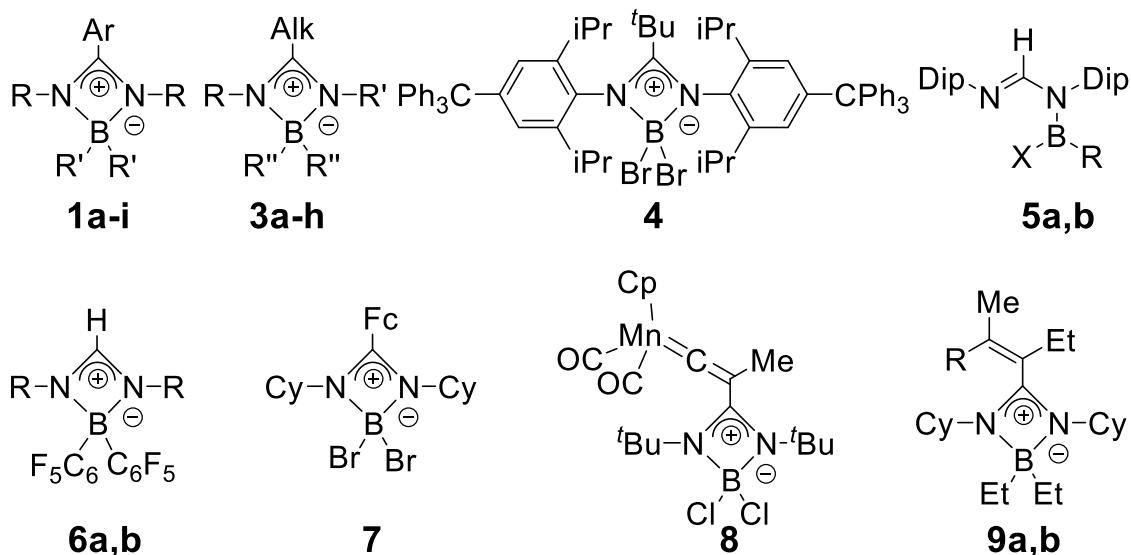


Figure 1. Reported boryl amidinate complexes.^[25,29-35,38-41,43,44] **1a:** Ar = Ph, R = SiMe₃, R' = Br; **1b:** Ar = Ph, R = SiMe₃, R' = Cl; **1c:** Ar = Ph, R = Cy, R' = Cl; **1d:** Ar = Ph, R = iPr, R' = Br; **1e:** Ar = C₆F₅, R = ^tBu, R' = C₆F₅; **1f:** Ar = C₆F₅, R = iPr, R' = C₆F₅; **1g:** Ar = C₆F₅, R = SiMe₃, R' = C₆F₅; **1h:** Ar = C₆F₅, R = Dip, R' = C₆F₅; **1i:** Ar = Mes*, R = Cy, R' = Cl; **3a:** Alk = Me, R = R' = Cy, BR''₂ = BCl₂; **3b:** Alk = Me, R = R' = iPr, BR''₂ = BCl₂; **3c:** Alk = Me, R = Dip, R' = C₆F₅, BR''₂ = B(C₆F₅)₂; **3d:** Alk = Me, R = Dip, R' = *p*-Ph-CN, BR''₂ = B(C₆F₅)₂; **3e:** Alk = ⁿBu, R = R' = ^tBu, BR''₂ = BCIPh; **3f:** Alk = ⁿBu, R = R' = Cy, BR''₂ = BCIPh; **3g:** Alk = ^tBu, R = R' = Cy, BR''₂ = BCIPh; **3h:** Alk = ^tBu, R = R' = 2,6-diisopropyl-4-tritylphenyl, BR''₂ = BB₂; **5a:** R = NiPr₂, X = Br; **5b:** R = Ph, X = Cl; **6a:** R = iPr; **6b:** R = ^tBu; **9a:** R = Me; **9b:** R = SnMe₃. (Dip = 2,6-iPr₂C₆H₃, Cy = cyclohexyl, Cp = cyclopentadienyl, Mes* = 2,4,6-^tBu₃C₆H₂)

1. Introduction

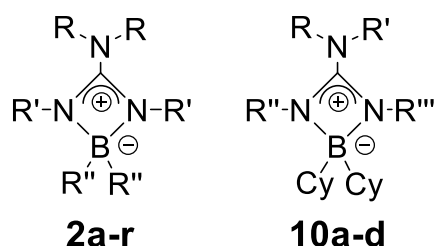
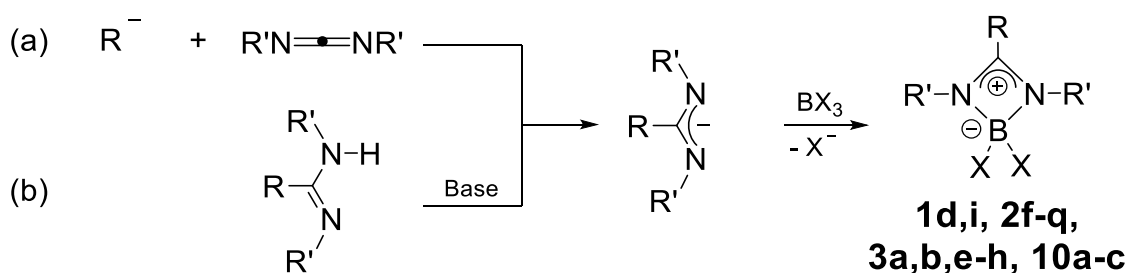


Figure 2. Reported structurally characterized boron guanidate complexes.^[26-28,34,36,37,42,45] **2 a:** R = Me, R' = iPr, R'' = CF₃; **2b:** R = Me, R' = Cy, R'' = CF₃; **2c:** R = Me, R' = Ph, R'' = CF₃; **2d:** R = Me, R' = *p*-Tol, R'' = CF₃; **2e:** R = Me, R' = *p*-MeO-Ph, R'' = CF₃; **2f:** R = Me, R' = Dip, R'' = Br; **2g:** R = Me, R' = iPr, R'' = Nrb; **2h:** R = Me, R' = Cy, R'' = Nrb; **2i:** R = Me, R' = iPr, R'' = Cy; **2j:** R = Me, R' = Cy, R'' = Cy; **2k:** R = Me, R' = Dip, R'' = Cy; **2l:** R = Ph, R' = Mes, R'' = Cl; **2m:** R = Ph, R' = Dip, R'' = Cl; **2n:** R = SiMe₃, R' = Cy, R'' = Cl; **2o:** R = iPr, R' = Dip, R'' = Br; **2p:** R = Cy, R' = Dip, R'' = Br; **2q:** R = iPr, R' = Cy, R'' = Cl; **2r:** R = Cy, R' = Cy, R'' = Cl; **10a:** R = iPr, R' = H, R'' = iPr, R''' = Ph; **10b:** R = iPr, R' = H, R'' = iPr, R''' = *p*-Tol; **10c:** R = iPr, R' = H, R'' = iPr, R''' = *p*-^tBu-C₆H₄; **10d:** R = iPr, R' = BCy₂, R'' = iPr, R''' = *p*-^tBu-C₆H₄. (Cy = cyclohexyl, Nrb = *exo*-2-norbornyl = bicyclo[2.2.1]-2-heptyl, Dip = 2,6-*i*Pr₂C₆H₃, Mes = 2,4,6-*t*-Me₃C₆H₂)

The majority of these boron(III) complexes have been synthesized by salt metathesis from alkali metal precursors (Scheme 1), which in turn can either be prepared by addition of organo-metal-bonds to carbodiimides (Scheme 1a) or by N-H-deprotonation of the corresponding neutral ligands (Scheme 1b).^[27,28,30,33,34,37,39,42-44] Instead of metal salts, trimethylsilyl halides can also be eliminated by reacting the corresponding *N*-silylated ligand with boron trihalides yielding the anticipated structural motifs, for example **1a,b** and **5a,b** (Figure 1).^[25,33,35]

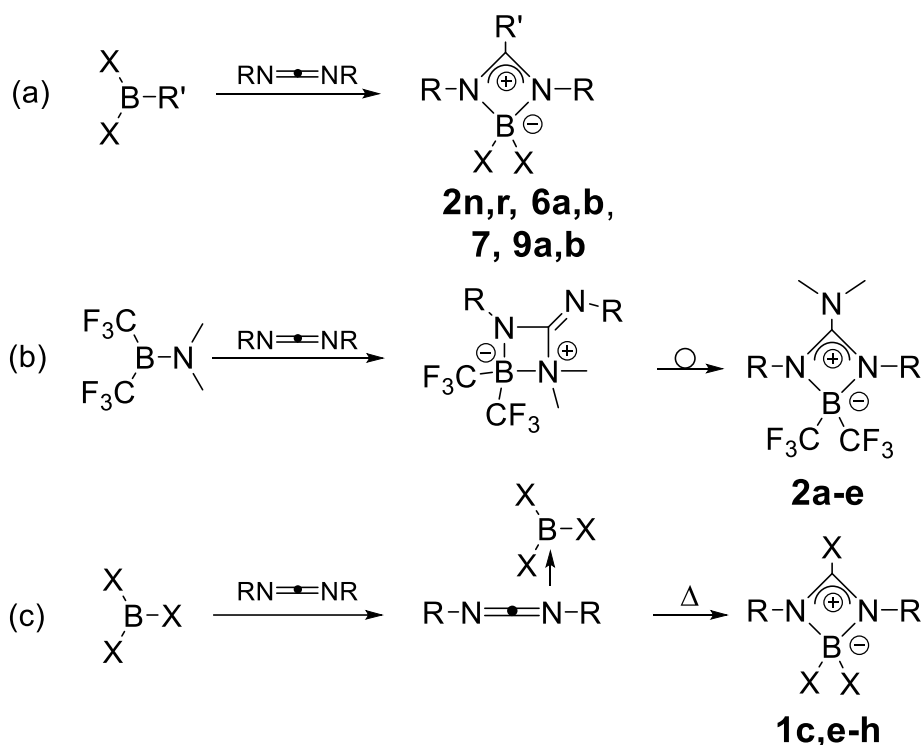


Scheme 1. Synthesis of boryl amidinates and guanidates.^[27,28,30,33,34,37,39,42-44] (a): R = Mes*, R' = Cy; BX₃ = BCl₃ (**1i**); R = Me, M = Li, R' = Cy; BX₃ = BCl₃ (**3a**); R = Me, R' = iPr; BX₃ = BCl₃ (**3b**); R = ⁿBu, R' = ^tBu; BX₃ = BCl₂Ph (**3e**); R = ⁿBu, R' = Cy; BX₃ = BPhCl₂ (**3f**); R = ^tBu, R' = Cy; BX₃ = BPhCl₂ (**3g**); R = NMe₂, R' = Dip; BX₃ = BBr₃ (**2f**); R = NMe₂, R' = iPr, BX₃ = BCINrb₂ (**2g**); R = NMe₂, R' = Cy; BX₃ = BCINrb₂ (**2h**); R = NMe₂, R' = iPr; BX₃ = BCiCy₂ (**2i**); R = NMe₂, R' = Cy; BX₃ = CiBCy₂ (**2j**); R = NMe₂, R' = Dip; BX₃ = BCiCy₂ (**2k**); R = NPh₂, R' = Mes; BX₃ = BCl₃ (**2l**); R = NPh₂, R' = Dip; BX₃ = BCl₃ (**2m**); R = N(SiMe₃)₂, R' = Cy; BX₃ = BCl₃ (**2n**). (b): R = Ph, R' = iPr; BX₃ = BBr₃ (**1d**); R = ^tBu, R' = 2,6-*i*Pr₂-4-CPh₃C₆H₂, BX₃ = BBr₃ (**3h**); R = NiPr₂, R' = Dip; BX₃ = BBr₃ (**2o**); R = NCy₂, R' = Dip; BX₃ = BBr₃ (**2p**); R = NiPr₂, R' = Cy; BX₃ = BCl₃ (**2q**); R = N(*i*Pr)H, =NR' = =NPh, -NR' = -NiPr; BX₃ = BCiCy₂ (**10a**); R = N(*i*Pr)H, =NR' = =N(*p*-Tol), -NR' = -NiPr; BX₃ = BCiCy₂ (**10b**); M = Li, R = N(*i*Pr)H, =NR' = =N(*p*-^tBu-Ph), -NR' = -NiPr; BX₃ = BCiCy₂ (**10c**). (Mes* = 2,4,6-^tBu₃C₆H₂, Mes = 2,4,6-*t*-Me₃C₆H₂, Nrb = *exo*-2-norbornyl = bicyclo[2.2.1]-2-heptyl, Cy = cyclohexyl)

Additionally, four-membered boron(III) *N*-heterocycles can be realized by direct addition of B-R bonds to carbodiimides (Scheme 2a)^[31,33,34,36,38], which can also

1. Introduction

be a reversible reaction under specific circumstances^[42]. In some cases, spectroscopic evidence provided mechanistic insights. The first step of the reaction between carbodiimides and bis(trifluoro)dimethylamino borane is a [2+2] cycloaddition between one of the C=N bonds and the formal B=N double bond followed by rearrangement to the boryl guanidate complexes **2a-e** (Scheme 2b).^[26] In case of haloboranes, the Lewis acid-base adducts of carbodiimides and different boranes have been isolated and characterized by x-ray structural analysis as intermediates, which upon heating rearrange to boryl amidinates **1c,e-h** by migration of one of the substituents (Scheme 2c).^[32,41] As a net result, both mechanisms constitute additions of B-R bonds to one of the C=N bonds of carbodiimides, as mentioned above.

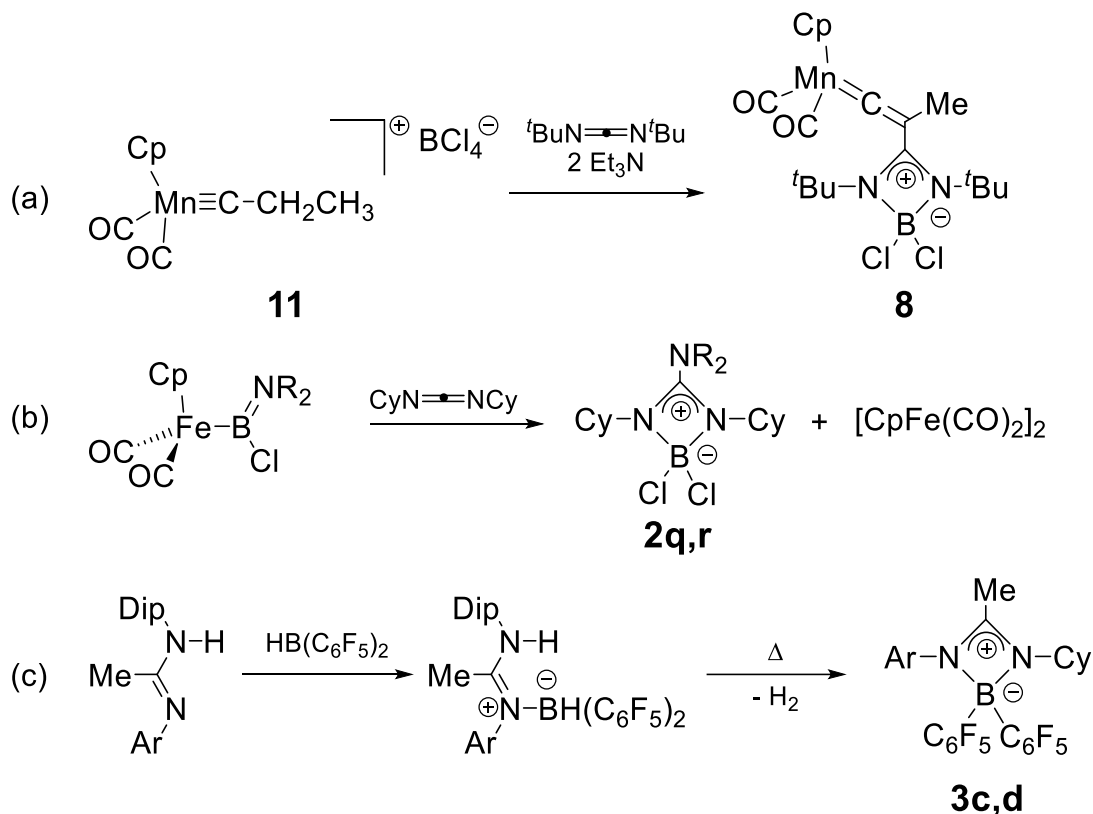


Scheme 2. Synthesis of boryl amidinates and guanidates by carbodiimide insertion. ^[26,31-34,36,38,41] (a): R' = H, X = C₆F₅, R = iPr (**6a**); R' = H, X = C₆F₅, R = ^tBu (**6b**); R' = Fc, X = Br, R = Cy (**7**); R' = 2-methylpent-2-en-3-yl, R = Cy, X = Et (**9a**); R' = 2-trimethylstannylpent-2-en-3-yl, R = Cy, X = Et (**9b**); R' = N(SiMe₃)₂, X = Cl, R = Cy (**2n**); R' = NCy₂, X = Cl, R = Cy (**2r**). (b): R = iPr, (**2a**); R = Cy (**2b**); R = Ph (**2c**); R = *p*-Tol (**2d**); R = *p*-MeO-Ph (**2e**). (c) BX₃ = BCl₂Ph, R = Cy (**1c**), BX₃ = B(C₆F₅)₃, R = ^tBu (**1e**); BX₃ = B(C₆F₅)₃, R = iPr (**1f**); BX₃ = B(C₆F₅)₃, R = SiMe₃ (**1g**); BX₃ = B(C₆F₅)₃, R = Dip (**1h**). (Cy = cyclohexyl, Fc = ferrocenyl)

Apart from those general syntheses for boryl guanidates and amidinates, a few alternative protocols have been reported. One of the first amidinate structures, namely **8**, was synthesized from the cationic manganese complex **11** in which BCl₄⁻ acts as the counterion and boron source (Scheme 3a).^[29] Reaction of iron-boryl complexes with a carbodiimide yields the boryl guanidate complexes

1. Introduction

2q,r (Scheme 3b).^[36] H₂ release from the Lewis acid-base adduct between an amidine and Pier's borane results in amidinates **3c,d** (Scheme 3c).^[40]



Scheme 3. Further syntheses of boryl amidinates and guanidates. ^[29,36,40] (b): R = *i*Pr (**2q**); R = Cy (**2r**). (c): Ar = C₆F₅ (**3c**); Ar = *p*-Ph-CN (**3d**). (Cp = cyclopentadienyl, Cy = cyclohexyl, Dip = 2,6-*i*Pr₂C₆H₃)

Diboron complexes of binucleating bis(amidinate) ligands are accessible with the aforementioned methods, namely salt metathesis and TMSCl elimination (**12a-d**, **13**, Figure 3).^[46]

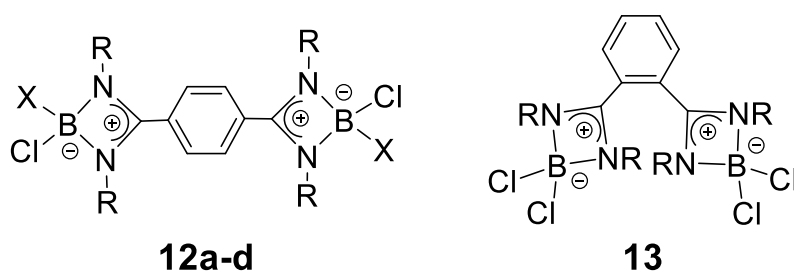
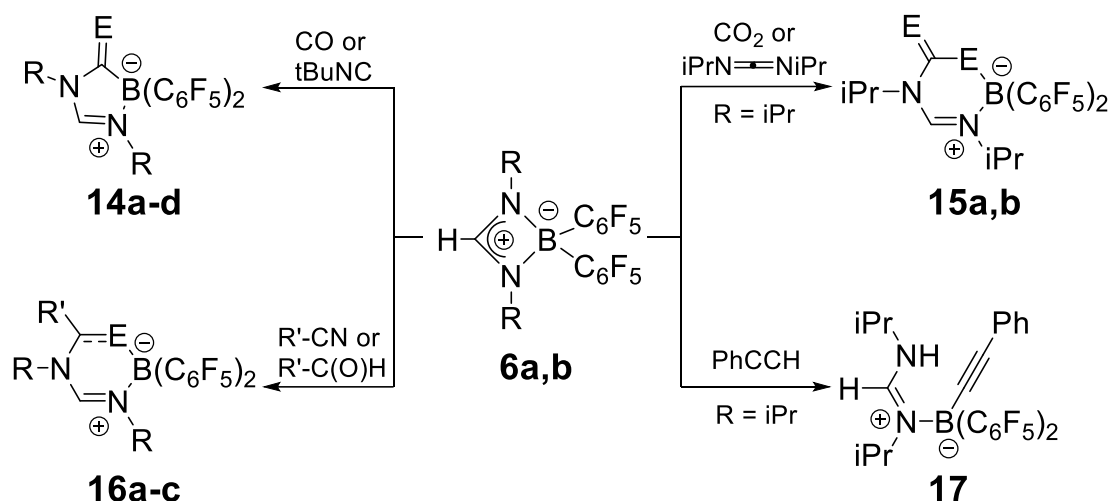


Figure 3. Literature-known diboron complexes of binucleating bis(amidinate) ligands.^[46] **12a**: X = Cl, R = SiMe₃; **12b**: X = Ph, R = SiMe₃; **12c**: X = Cl, R = Cy; **12d**: X = Ph, R = Cy; **13**: R = SiMe₃. (Cy = cyclohexyl)

The strain of the four-membered BN₂C cycles of boryl amidinates and guanidates leads to facile ring opening or expansion by various small molecules. The reactivity of boryl amidinates **6a** and **6b**, for instance, is shown

1. Introduction

in Scheme 4. They react with tert-butyl isocyanide and carbon monoxide under insertion into a B-N-bond to yield the five-membered rings **14a-d**. Diisopropylcarbodiimide, carbon dioxide, acetonitrile and benzaldehyde also insert into the B-N-bond under formation of the six-membered rings **15a,b** and **16a-c**. Phenylacetylene reacts *via* C-H-addition across the B-N-bond to the open chained structure **17**.^[38]



Scheme 4. Reactivity of boryl amidinate complexes **6a** (R = iPr) and **6b** (R = *t*Bu) towards small molecules.^[38] **14a**: R = iPr, E = O; **14b**: R = *t*Bu, E = O; **14c**: R = iPr, E = N*t*Bu; **14d**: R = *t*Bu, E = N*t*Bu; **15a**: E = O; **15b**: E = NiPr; **16a**: saturated C-E bond, R = iPr, R' = Ph, E = O; **16b**: saturated C-E bond, R = *t*Bu, R' = Ph, E = O; **16c**: C-E double bond, R = iPr, R' = Me, E = N.

A few years later the regioselectivity of carbon monoxide-, isocyanide-, benzaldehyde- and carbon dioxide-insertions into the B-N bonds of unsymmetrically substituted boryl guanidates was examined. Proof-of-principle reactions were also carried out with a symmetrically substituted boryl guanidate **2i**.^[45] All the deployed boryl guanidates **2i**, **10c,d** and **18** are shown in Figure 4.

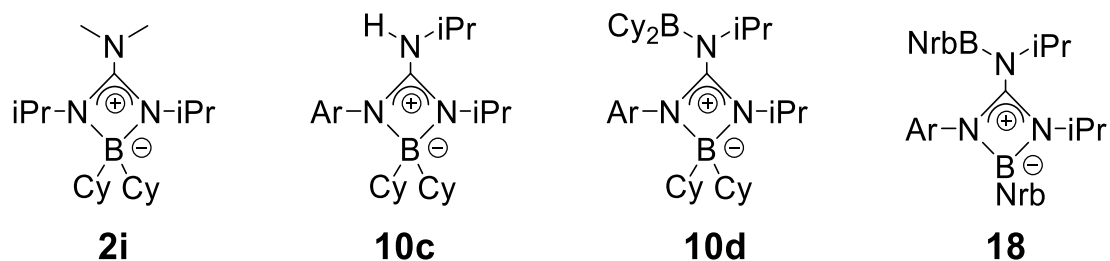


Figure 4. The deployed boryl guanidates **2i**, **10c,d** and **18** for the reactivity studies towards isocyanides, carbon monoxide, benzaldehyde and carbon dioxide.^[45] **10c**: Ar = Ph-*p*-*t*Bu, **10d**: Ar = Ph-*p*-*t*Bu, **18**: Ar = Ph-*p*-Me (Cy = cyclohexyl, Nrb = *exo*-2-norbornyl = bicyclo[2.2.1]-2-heptyl)

Aromatic isonitriles insert into the B-N bond to form **19a,b**, **20a-f** and **21a,b**, as already observed for amidinates.^[38] In the cases of unsymmetrically substituted boryl guanidates the insertion is mostly observed into the B-N(iPr) bond (**20a-f**),

1. Introduction

except when the choice is between B-N(iPr) and B-N(Ph-*p*-^tBu). In some of these cases, insertions into either of the B-N bonds are observed (**20a,b** and **21a,b**, Figure 5). Besides, it was also reported that the derivatives **20e,f** are in a temperature-dependent equilibrium with the de-insertion products.^[45]

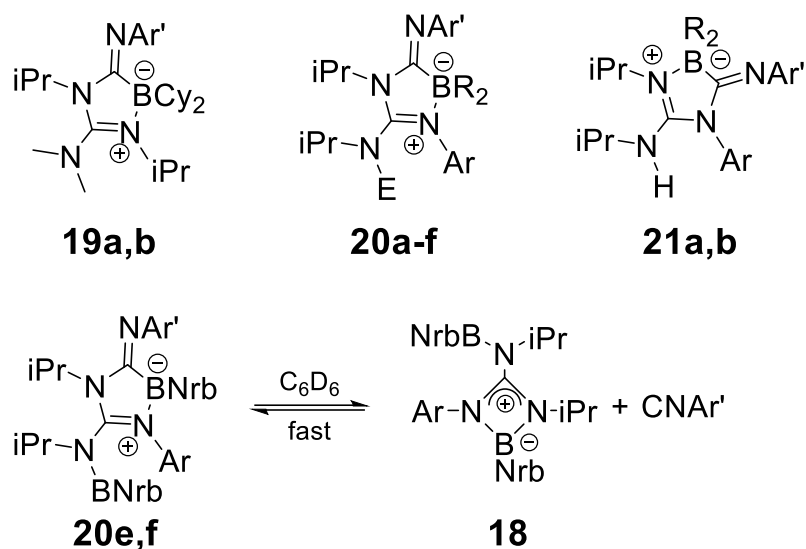


Figure 5. Insertion-products **19a,b**, **20e-f** and **21a,b** of isonitriles into the B-N bonds of boryl guanidates **2i**, **10c,d** and **18** and de-insertion equilibrium of **20e,f**.^[45] **19a**: Ar' = 2,6-Me₂-Ph; **19b**: Ar' = 4-OMe-Ph; **20a**: Ar' = 2,6-Me₂-Ph, BR₂ = BCy₂, Ar = Ph-*p*-^tBu, E = H; **20b**: Ar' = 4-OMe-Ph, BR₂ = BCy₂, Ar = Ph-*p*-^tBu, E = H; **20c**: Ar' = 2,6-Me₂-Ph, BR₂ = BCy₂, Ar = Ph-*p*-^tBu, E = BCy₂; **20d**: Ar' = 4-OMe-Ph, BR₂ = BCy₂, Ar = Ph-*p*-^tBu, E = BCy₂; **20e**: Ar' = 2,6-Me₂-Ph, BR₂ = BNrb, Ar = Ph-*p*-Me, E = BNrb; **20f**: Ar' = 4-OMe-Ph, BR₂ = BNrb, Ar = Ph-*p*-Me, E = BNrb; **21a**: Ar' = 2,6-Me₂-Ph, BR₂ = BCy₂, Ar = Ph-*p*-^tBu, E = H; **21b**: Ar' = 4-OMe-Ph, BR₂ = BCy₂, Ar = Ph-*p*-^tBu, E = H; **18**: Ar = Ph-*p*-Me; CNAr' = CN-Ph-2,6-Me₂; CNAr' = CN-Ph-*p*-OMe (Cy = cyclohexyl, Nrb = *exo*-2-norbornyl = bicyclo[2.2.1]-2-heptyl)

The reactions of **2i** and **10c,d** with carbon monoxide were rather inconclusive and only **22a** could be isolated in moderate yields (Figure 6). The reaction between **18** and carbon monoxide resulted in an equilibrium with **22b**, but is clearly shifted to the educt side.^[45]

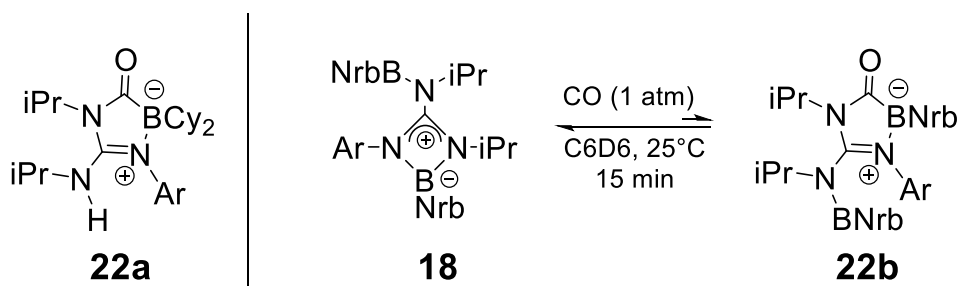
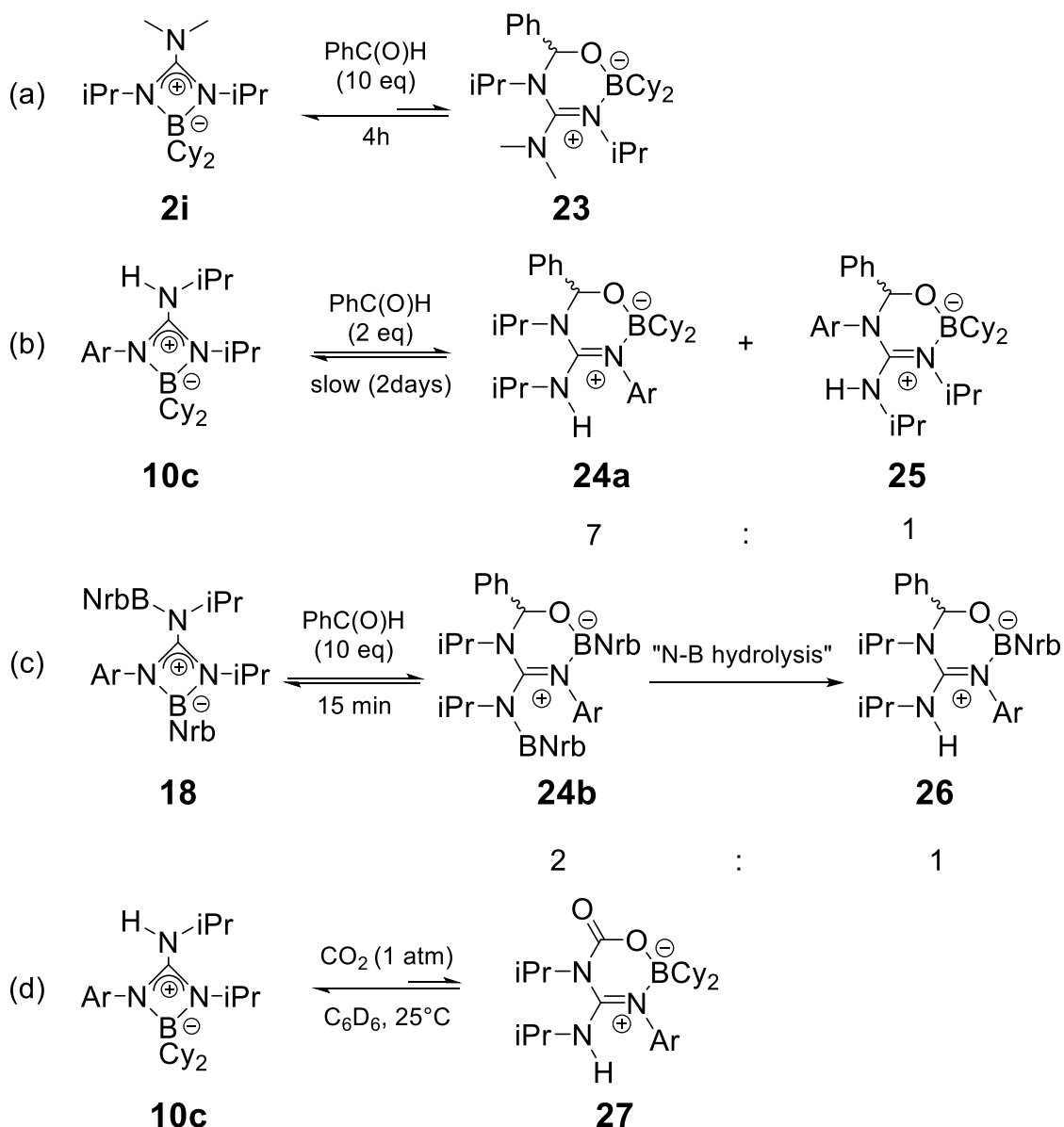


Figure 6. Isolated product **22a** of guanidate **10c** with CO and equilibrium between guanidate **18** and **22b** under CO atmosphere.^[45] **22a**: Ar = Ph-*p*-^tBu; **18**: Ar = Ph-*p*-Me; **22b**: Ar = Ph-*p*-Me (Cy = cyclohexyl, Nrb = *exo*-2-norbornyl = bicyclo[2.2.1]-2-heptyl)

Several more equilibria were observed with **2i**, **10c**, **18** and benzaldehyde and with **10c** and carbon dioxide (Scheme 5). With unsymmetrically substituted

1. Introduction

guanidates **10c** and **18**, the insertion into the B-N(iPr) bond proved to be preferable in these cases, as well (Scheme 5b,c). As observed before, in the reaction of benzaldehyde with guanidate **10c** both regio-isomers were observed, but the majority showed insertion into the B-N(iPr) bond (Scheme 5b). In the reactions that involved CO₂ only with **10c** an insertion product (**27**) was detected in equilibrium with the de-insertion products (Scheme 5d). No CO₂-insertion product could be isolated.^[45]

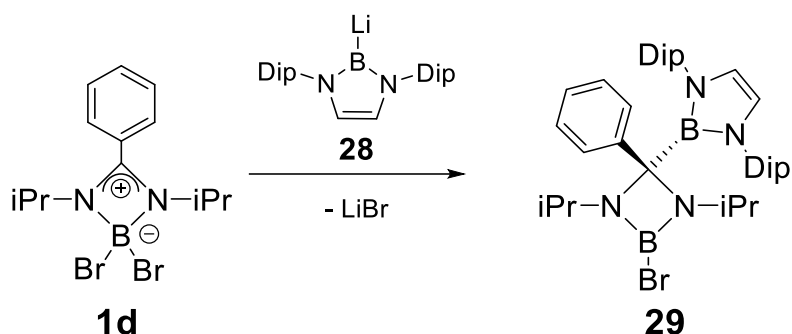


Scheme 5. Reactivity of boryl guanidates **2i** (a), **10c** (b) Ar = Ph-*p*-Bu and **18** (c) Ar = Ph-*p*-Me towards benzaldehyde plus equilibrium between boryl guanidate **18** and **27** under CO₂ atmosphere (d) Ar = Ph-*p*-Bu.^[45] (Cy = cyclohexyl, Nrb = *exo*-2-norbornyl = bicyclo[2.2.1]-2-heptyl)

So far there has only been one report of a reaction of either boryl amidinates or guanidates with an anionic nucleophile. Boryl benzamidinate **1d** was reacted

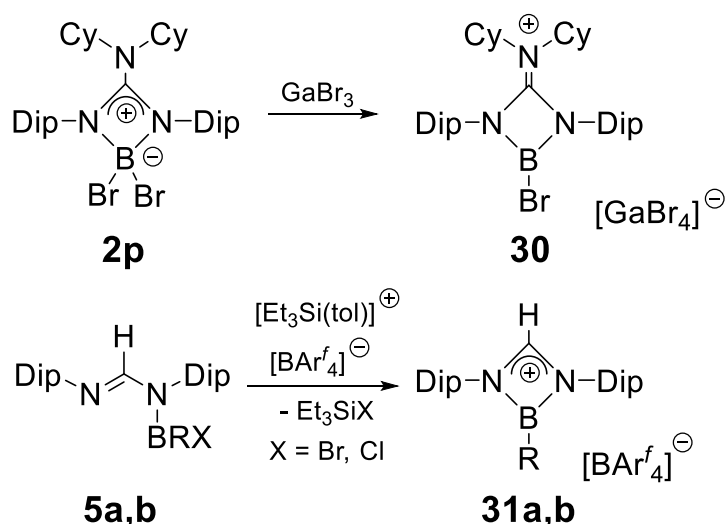
1. Introduction

with Yamashita's boryl anion **28**, which attacks the imine carbon center to give **29** (Scheme 6).^[43,44]



Scheme 6. Reactivity of boryl amidinate **1d** towards Yamashita's boryl anion **28** yielding **29**.^[43,44]

Boryl amidinates and guanidates with residual halide groups have been deployed as starting material for cationic structures as well (**30**, **31a,b**, Scheme 7). The abstraction of a bromide from **2p** by gallium tribromide led to the isolation of the guanidinium ion **30** with the concomitantly formed tetrabromogallate as counter anion.^[28] The abstraction of a bromide or a chloride from the open-chained formamidinates **5a** or **5b** is possible with the triethylsilylium cation. The resulting structures **31a,b** include the perfluorinated tetraphenylborate as non-coordinating counter anion (Scheme 7).^[35]

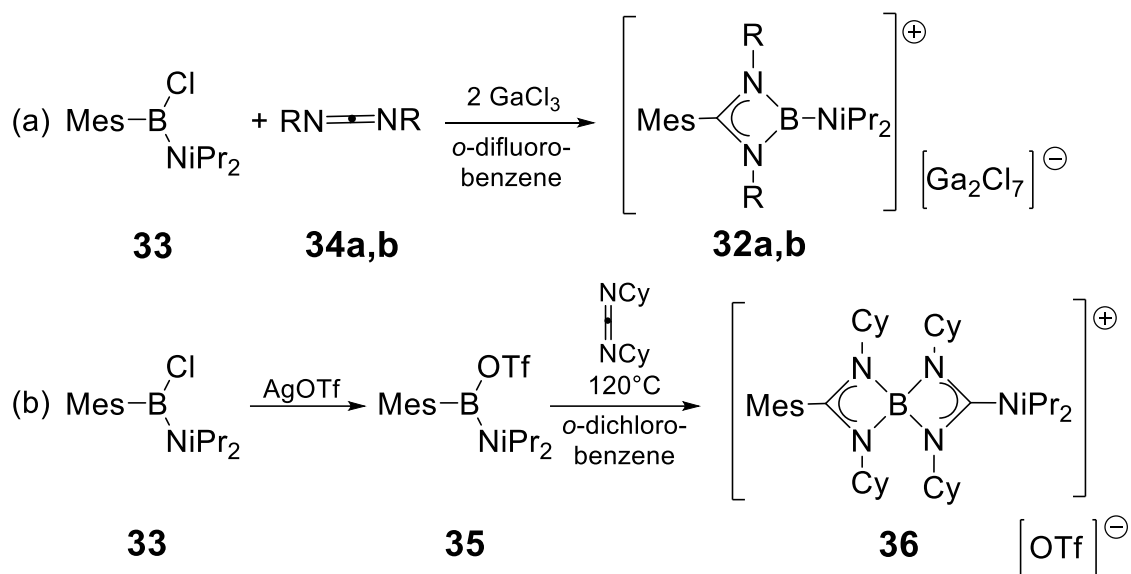


Scheme 7. Halogenide abstraction from boryl guanidate **2p** and boryl formamidinate **5a** (R = NiPr_2 , X = Br) and **5b** (R = Ph, X = Cl). **31a**: R = NiPr_2 ; **31b**: R = Ph.^[28,35] (Cy = cyclohexyl, Dip = 2,6- $\text{iPr}_2\text{C}_6\text{H}_3$, BAr_4^- = tetrakis(pentafluorophenyl)borate)

Recently, the one-pot preparation of the cationic amidinate structures **32a,b** by the reaction of chlorodiisopropylmesitylborane **33**, carbodiimides **34a,b** and two equivalents gallium trichloride was reported. The same study described the

1. Introduction

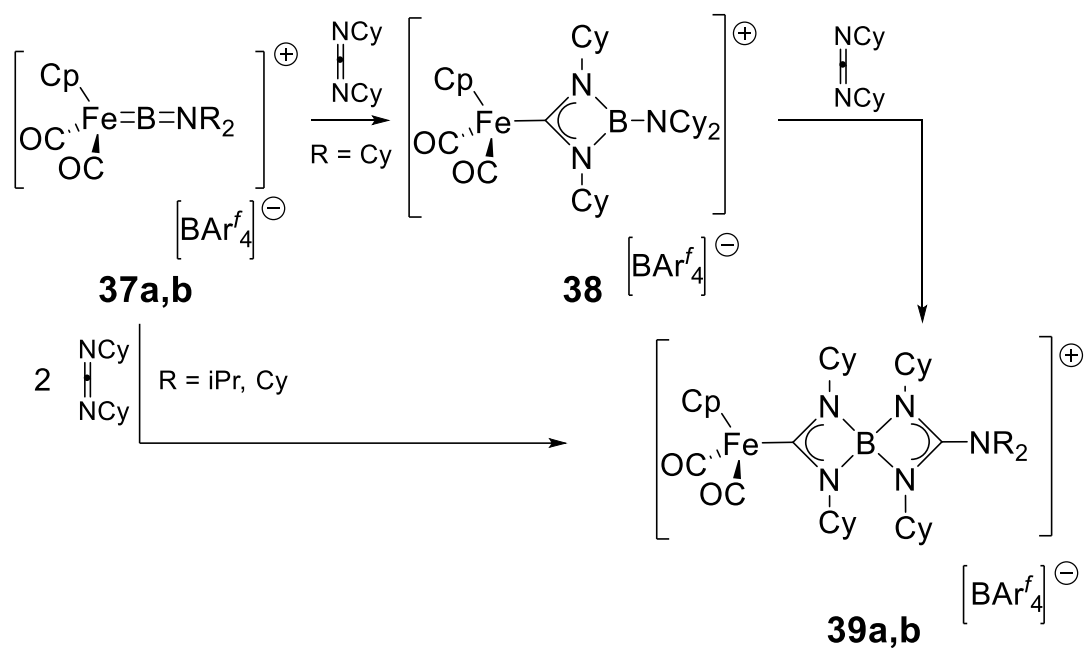
synthesis of a borylium cation as a contact ion pair **35**, which was subsequently treated with dicyclohexylcarbodiimide to form the mixed amidinate- and guanidate-stabilized cation **36**.^[47]



Scheme 8. (a): Synthesis of boryl amidinate cations **32a** (R = Cy) and **32b** (R = iPr) from borane **33** and carbodiimides **34a** (R = Cy) and **34b** (R = iPr), respectively. (b): Synthesis of the mixed amidinate and guanidate stabilized cation **36** from the borylium cation **35** which is prepared by reaction of borane **33** and silver trifluoromethanesulfonate.^[47] (Mes = 2,4,6-Me₃C₆H₂, Cy = cyclohexyl, OTf = trifluoromethanesulfonate)

Earlier reports demonstrated that similar cationic structures can be obtained from cationic iron borylene complexes **37a,b**. The addition of one equivalent of dicyclohexylcarbodiimide to the borylene complex **37a** yields the cationic boryl amidinate **38**, which can be transformed to the mixed boryl amidinate/guanidate **39a** by addition of a second equivalent of dicyclohexylcarbodiimide.^[36] The same product class can also be prepared by direct addition of two equivalents dicyclohexylcarbodiimide to the iron borylene complexes **37a** or **37b**, respectively, leading to **39a** or **39b**.^[48,49]

1. Introduction



Scheme 9. Reactions of cationic aminoborylene iron complexes **37a** (R = Cy) and **37b** (R = iPr) with dicyclohexylcarbodiimide to **39a** (R = Cy) and **39b** (R = iPr).^[36,48,49] (Cp = cyclopentadienyl, Cy = cyclohexyl, Ar^f = pentafluorophenyl)

1.3 Group 13 element(I) heterocycles with β -diketiminato-, 1,2-diamido organyl- and amidinato-/guanidinato- ligands

The isolation of NHCs had an immense impact on numerous fields of chemistry.^[50-55] Analogues with different ring sizes or different low valent atoms and therefore other properties are thus an attractive target. Especially Group 13 elements with their intrinsic electron deficiency are of interest.^[56]

Only a few attempts to reduce guanidate boron dihalides (see Section 1.2) have been reported so far, but boron(I) amidinate or guanidate complexes remain elusive.^[27,28] Theoretical considerations reveal small singlet-triplet gaps (6-10 kcal mol⁻¹) of these boron (I) structures suggesting considerable reactivity and hence instability impeding their isolation.^[27,57] Consequently, attempts to synthesize Group 13 element(I) species with amidinate or guanidate ligands were up to now only successful in the cases of the heavier elements. For gallium(I) (**40**), indium(I) (**41a**) and thallium(I) (**42b**) the same guanidate ligand provided sufficient stability for isolation.^[58] Further guanidate or amidinate indium(I) and thallium(I) species have been reported since (**41b,c**, **42a,c,d**, Figure 7).^[59,60] It is noteworthy that one of the indium(I) complexes (**31c**) and all of the thallium complexes **42a-d** do not adopt the typical *N,N*-chelating coordination mode, but exhibit *N*-aryl coordination instead.

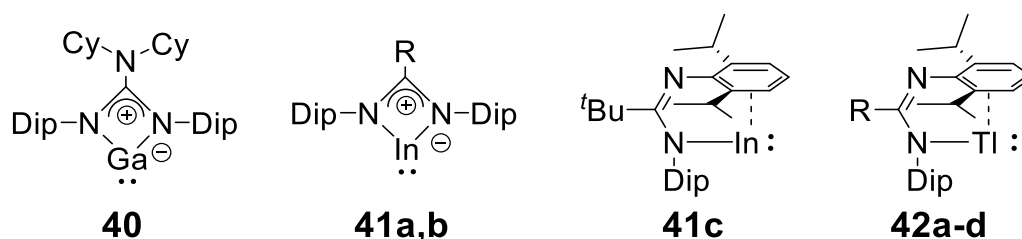


Figure 7. Guanidate and amidinate stabilized group 13 element(I) structures. **41a**: R = NCy₂; **41b**: R = 2,6-dimethylpiperidine; **42a**: R = ^tBu; **42b**: R = NCy₂; **42c**: R = NiPr₂; **42d**: R = 2,6-dimethylpiperidine.^[58-60] (Cy = cyclohexyl, Dip = 2,6-iPr₂C₆H₃).

The Arduengo-type NHC analogues of Group 13 are rarely described. Recently the first neutral five-membered cyclic triel(I) carbenoids have been isolated as **43a-c** (Figure 8).^[61] Several boryl(I)-lithium salts **44a-f**, which still represent the only isolated boron-NHC-analogues^[62-66] and anionic gallium(I) five-membered *N*-heterocycles (**45a-d**, **46**, Figure 8) have been described in the literature previously.^[67-73] As for aluminium, no monomeric five membered *N*-heterocycles have been isolated.

1. Introduction

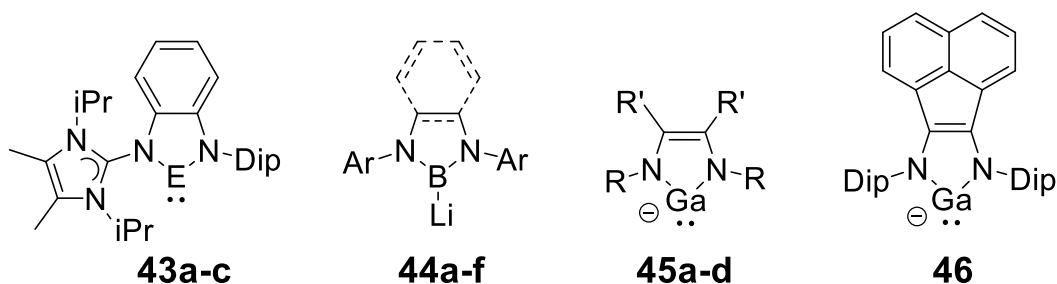


Figure 8. Group 13 element NHC analogues. **43a**: E = Ga; **43b**: E = In; **43c**: E = Tl; **44a**: saturated backbone, Ar = Dip; **44b**: saturated backbone, Ar = Mes; **44c**: unsaturated backbone, Ar = Dip; **44d**: unsaturated backbone, Ar = Mes; **44e**: phenyl fused backbone, Ar = Dip; **44f**: phenyl fused backbone, Ar = Mes; **45a**: R = ^tBu, R' = H; **45b**: R = Dip, R' = H; **45c**: R = Dip, R' = Me; **45d**: R = 2,6-(di-4-tert-butylphenyl)phenyl, R' = Me.^[61-73] (Dip = 2,6-iPr₂C₆H₃, Mes = 2,4,6-Me₃C₆H₂)

A variety of six-membered element(I) heterocycles has also been realized. The monomeric β -diketiminato complexes with aluminum(I) (**47a,b**)^[74-77], gallium(I) (**48**)^[78], indium(I) (**49a-c**)^[79-82] and thallium(I) (**50a-e**)^[82-85] have been isolated (Figure 9).

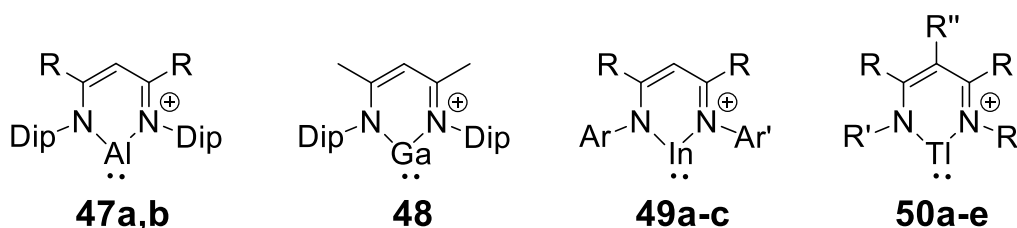


Figure 9. Isolated group 13 element (I) structures stabilized by β -diketiminato ligands. **47a**: R = Me; **47b**: R = ^tBu; **49a**: R = Me, Ar = Ar' = Dip; **49b**: R = Me, Ar = Dip, Ar' = 2-methoxyphenyl; **49c**: R = CF₃, Ar = Ar' = Dip; **50a**: R = Me, R' = 2,6-dimethylphenyl, R'' = H; **50b**: R = Ph, R' = SiMe₃, R'' = H; **50c**: R = H, R' = Dip, R'' = Ph; **50d**: R = Me, R' = Dip, R'' = H; **50e**: R = Me, R' = 2,6-difluorophenyl, R'' = H.^[74-85] (Dip = 2,6-iPr₂C₆H₃)

The corresponding boron compound was predicted to feature a small singlet-triplet gap^[86,87] and by now, has only been trapped in the coordination sphere of Cp*Fe(CO)₂^[88] (**51**, Figure 10). Recent theoretical investigations suggest that with an appropriate ligand design as in **52a,b** (Figure 10) the isolation of a boron(I) embedded into a *N,N*-chelating six-membered ring structure might be possible.^[89]

1. Introduction

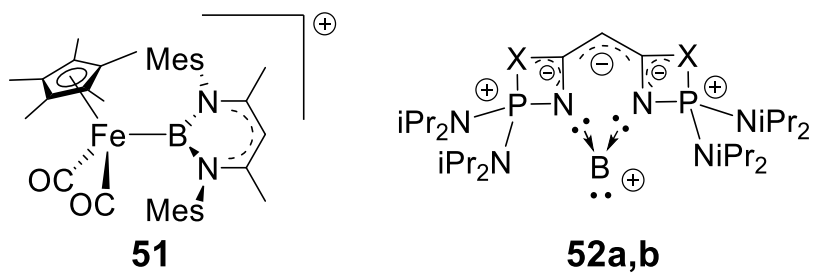
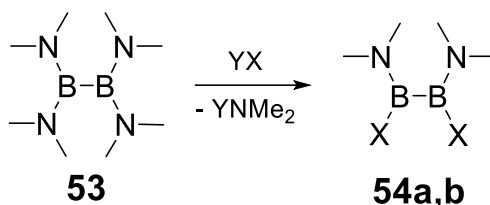


Figure 10. Isolated boron(I) β -diketiminato structure in an iron coordination sphere **51** and the calculated structures **52a** (X = CMe) and **52b** (X = N).^[88,89] (Mes = 2,4,6- Me₃C₆H₂)

1.4 Bis(dimethylamino)diboranes(4), tetraorganyldiboranes(4) and six-membered diaza-heterocycles with diborane(4)-motif

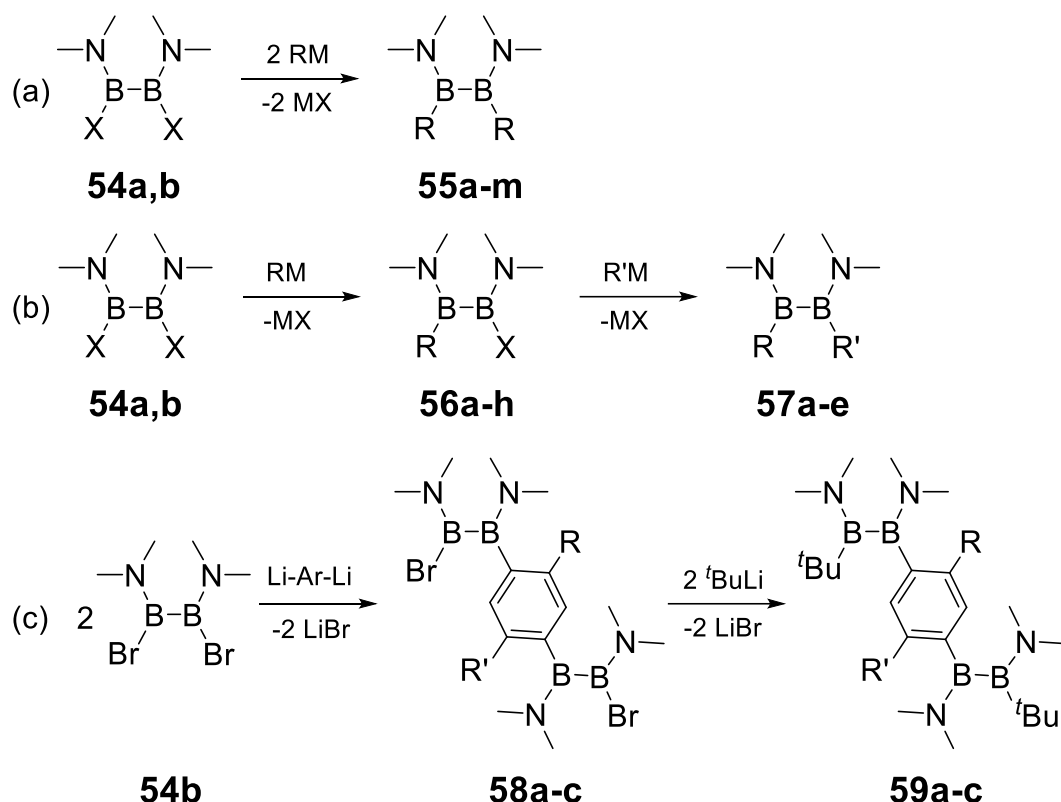
Diboranes(4) were discovered in 1925^[19,90] making available a versatile and extremely useful class of reagents. In particular, the isolation of the remarkably stable tetrakis(dimethylamino)diborane(4) **53** (already observed by Urry *et al.* in 1954^[91]) by Brotherton and co-workers in 1960^[92] opened up a wide range of synthetic possibilities. For example, the treatment of tetrakis(dimethylamino)diborane(4) with HCl^[93] or BX₃ (X = Cl, Br)^[94,95] yields the mixed 1,2-bis(dimethylamino)-1,2-dihalo-diboranes(4) providing a better leaving group at each boron atom.



Scheme 10. Synthesis of 1,2-dimethyl(amino)-1,2-dihalo diboranes(4) **54a** (X = Cl) and **54b** (X = Br) from tetrakis(dimethylamino)diborane(4) **53** with HCl (Y = H) or trihaloborane (Y = X₂B).^[93-95]

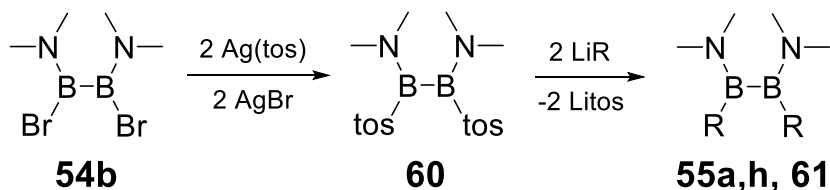
By reaction of diborane(4) 1,2-dihalides **54a,b** with aryl and/or alkyl metal compounds various symmetrically (**55a-j**) and unsymmetrically (**56a-h**, **57a-d**) substituted 1,2-bis(dimethylamino)diboranes(4) have been synthesized (Scheme 11a,b).^[93,95-111] This route represents the most popular for 1,2-disubstituted 1,2-bis(dimethylamino)diboranes(4). In addition arylene-bridged, unsymmetrically substituted diboranes(4) **58a-c** and **59a-c** have been realized this way (Scheme 11c).^[105,112,113]

1. Introduction



Scheme 11. Halide substitution on diboranes(4) **54a** and **54b** with aryl and/or alkyl metals (RM = ⁿBuLi, ^tBuLi, allylMgCl, PhLi, MesLi, indLi, NphLi, CpNa, fluLi TipLi, octafluLi, AnLi, DurLi, 4-^tbutyl-2,6-dimethylphenyl lithium, 2,5-di-^tbutylphenyl lithium) to yield the symmetrically substituted diboranes(4) **55a**: R = ⁿBu, **55b**: R = ^tBu, **55c**: R = allyl, **55d**: R = Ph, **55e**: Mes, **55f**: R = 1-ind, **55g**: R = Cp, **55h**: R = flu, **55i**: R = Tip, **55j**: R = An, **55k**: R = Dur, **55l**: R = 4-^tbutyl-2,6-dimethylphenyl, **55m**: R = 2,5-di-^tbutylphenyl, and unsymmetrically substituted diboranes(4) **56a**: R = ^tBu, X = Cl, **56b**: R = allyl, X = Cl, **56c**: R = Mes, X = Br, **56d**: R = 1-ind, X = Cl, **56e**: R = ^tBu, X = Br, **56f**: R = Cp, X = Br, **56g**: R = flu, X = Br, **56h**: R = octaflu, X = Br, and **57a**: R = ^tBu, R' = Ph, **57b**: R = ^tBu, R' = Nph, **57c**: R = flu, R' = Cp, **57d**: R = octaflu, R' = Cp, **57e**: R = Mes, R' = Ph, as well as arylene bridged unsymmetrically substituted diboranes(4) **58a**: R = R' = H, **58b**: R = Me, R' = H, **58c**: R = R' = Me, and **59a**: R = R' = H, **59b**: R = Me, R' = H, **59c**: R = R' = Me.^[93,95-113] (ind = indenyl, Cp = cyclopentadienyl, flu = 9-fluorenyl, Tip = 2,4,6-triisopropylphenyl, octaflu = 1,1,4,4,7,7,10,10-octamethyldicyclohexyl-9-fluorenyl, An = 9-anthracenyl, Nph = naphthyl, Dur = 2,3,5,6-tetramethylphenyl)

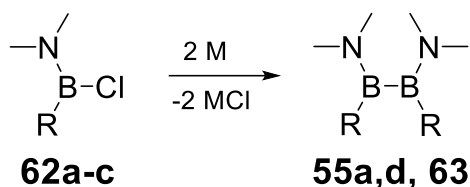
Furthermore, the synthesis of 1,2-bis(dimethylamino)-1,2-tosyldiboranes(4) **60** and its use as electrophilic substrate with the tosyl substituent as alternative leaving group has been demonstrated. The reaction of **60** with lithiumorganyls lead to the symmetrically substituted diboranes(4) **55a,h**, **61** (Scheme 12).^[114]



Scheme 12. Synthesis of 1,2-bis(dimethylamino)-1,2-bistosylato diborane(4) **60** and conversion with lithiumorganyls to 1,2-bis(dimethylamino)-1,2-diorganyl diboranes(4) **55a**: R = ⁿBu, **55h**: R = flu and **61**: R = CC-Ph.^[114] (tos = *p*-toluenesulfonate, flu = 9-fluorenyl)

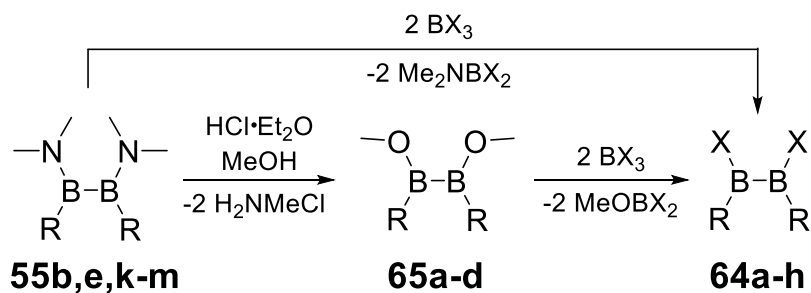
1. Introduction

Another possibility of synthesizing diboranes(4) with a 1,2 substitution pattern is by reductive coupling of the corresponding amino-chloro-organyl boranes **62a-c** with alkali metals (M = Na or K, Scheme 13). This has been employed for the synthesis of **55a,d** and **63**.^[115,116]



Scheme 13. Synthesis of diboranes(4) **55a**: R = ⁿBu, **55d**: R = Ph and **63**: R = Et by reductive coupling (M = Na or K) of chloroboranes **62a**: R = ⁿBu, **62b**: R = Ph or **62c**: R = Et.^[115,116]

Transformation of the remaining amino into chloro groups provides synthetic access to donor-free diboranes(4), meaning substituents without a free electron pair adjacent to the electron-deficient boron atoms. Conversion from 1,2-bisdimethylaminodiboranes(4) **55b,e,k-m** to 1,2-dihalodiboranes(4) **64a-g** can either be realized by directly using BX₃ (BX₃ = BCl₃, MeBBR₂) to yield **64a,b**^[96,97] or first turning the dimethylamino-groups into methoxy groups by treatment with MeOH in the presence of HCl (diboranes(4) **65a-d**), then subsequently reacting them with BX₃ (BX₃ = BCl₃, BBr₃) to 1,2-dihalo-diboranes(4) **64c-g** (Scheme 14).^[98,104]

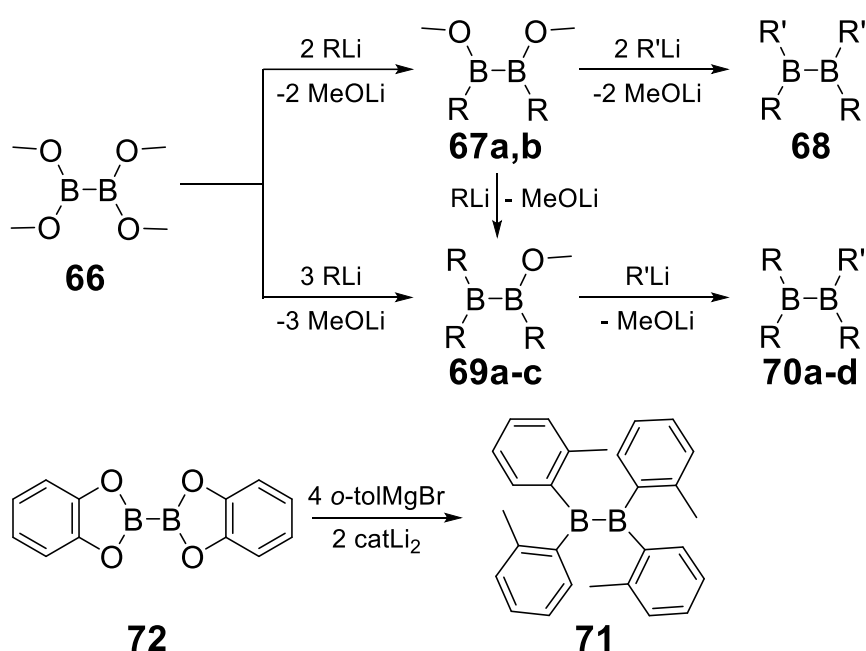


Scheme 14. Conversion of dimethylamino-groups in 1,2-disubstituted diboranes(4) **55b,e,k-m** into methoxy- (**65a-d**) or halide-groups (**64a-g**).^[96-98,104] **64a**: R = ^tBu, X = Cl; **64b**: R = ^tBu, X = Br; **64c**: R = Mes, X = Cl, **64d**: R = Mes, X = Br; **64e**: R = Dur, X = Cl; **64f**: R = Dur, X = Br; **64g**: R = 4-^tbutyl-2,6-dimethylphenyl, X = Cl; **64h**: R = 2,5-di-^tbutylphenyl, X = Cl; **65a**: R = Mes; **65b**: R = Dur; **65c**: R = 4-^tbutyl-2,6-dimethylphenyl; **65d**: R = 2,5-di-^tbutylphenyl. (Mes = 2,4,6-Me₃C₆H₂; Dur = 2,3,5,6-Me₄C₆H)

However, tetrasubstituted donor free diboranes(4) have mostly been accessed by reaction of organolithium compounds with precursors featuring alkoxy- or aryloxy leaving groups. Reaction of tetramethoxydiborane(4) **66** with two equivalents of organolithium compounds yields 1,2-disubstituted 1,2-dimethoxy diboranes **67a,b**, which can be transformed with another organolithium

1. Introduction

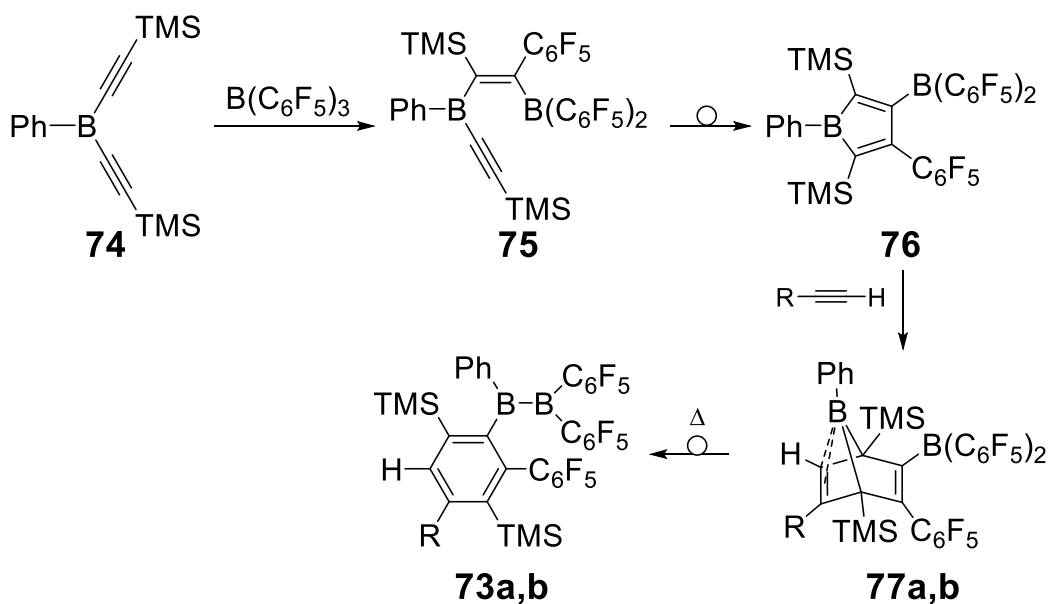
compound to the mixed symmetrically tetrasubstituted diborane(4) **68** (Scheme 15). Conversion of either **66** or **67a,b** with the according number of equivalents of organolithium compounds yields trisubstituted methoxy-diboranes(4) **69a-c**. By reacting **69a,b** with a different organometallic reagent the unsymmetrically tetrasubstituted diboranes(4) **70a-d** can be isolated (Scheme 15). Notably, sterically demanding groups, i.e. ^tbutyl or mesityl groups, can only be attached three times to a diborane(4).^[96,97,102,117-121] In contrast, tetra(*ortho*-tolyl) diborane(4) **71** was directly synthesized from dicatecholato diborane(4) **72** with the corresponding Grignard reagent (*o*-tolMgBr) (Scheme 15)^[122]



Scheme 15. Synthesis of donor-free symmetrically substituted diboranes(4) **68** and unsymmetrically substituted diboranes(4) **70a-d** via methoxy diboranes(4) **67a,b** and **69a-c** from tetramethoxy diborane(4) **66** plus the synthesis of tetra-*o*-tolyl-diborane(4) **71** from bis(catecholato) diborane(4) **72**.^[96,97,102,117-122] **67a**: R = ^tBu; **67b**: R = Mes; **68**: R = ^tBu, R' = CH₂^tBu; **69a**: R = ^tBu; **69b**: R = Mes; **69c**: R = 2,6-Mes₂-Ph; **70a**: R = ^tBu, R' = CH₂^tBu; **70b**: R = ^tBu, R' = Me; **70c**: R = Mes, R' = CH₂SiMe₃; **70d**: R = Mes, R' = Ph. (cat = catecholato, Mes = 2,4,6-Me₃C₆H₂)

The pentafluorophenyl-substituted diboranes(4) **73a,b** were synthesized by a different approach. First, bis(acetylene)-phenyl borane **74** was reacted with tris(pentafluorophenyl)borane to diborylalkene **75**, which rearranges at room temperature to borole **76**. Conversion with phenylacetylene or propylacetylene leads to intermediates **77a,b** which finally rearrange to the pentafluorophenyl-substituted diboranes(4) **73a,b** at 60°C.^[123,124]

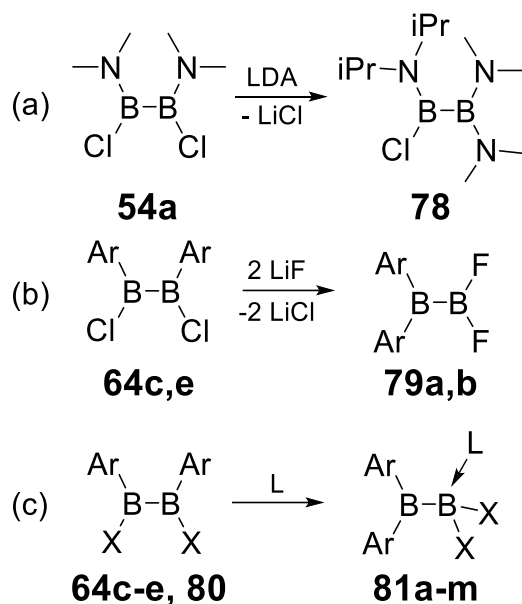
1. Introduction



Scheme 16. Synthesis of pentafluorophenyl-substituted diboranes(4) **73a,b** from borane **74** and tris(pentafluorophenyl) borane forming borole **76**, which is subsequently reacted with acetylenes to intermediate **77a,b** that under thermal treatment are arranged to diboranes(4) **73a,b**. **77a** & **73a**: R = *n*Pr; **77b** & **73b**: R = Ph.^[123,124] (TMS = trimethylsilyl)

Occasionally, the substitution pattern of diboranes(4) changes from 1,2- to 1,1 substitution during a nucleophilic attack. The reaction of diborane(4) **54a** with lithium diisopropylamide, for instance, results in 1,1-bis(dimethylamino) diborane(4) **78**, instead of the expected 1,2-derivative (Scheme 17a).^[125] Similar behavior was also reported for the transhalogenation of 1,2-bisaryl-1,2-dichlorodiboranes(4) **64c,e** with lithium fluoride leading to **79a,b** as isolated products (Scheme 17b).^[126,127] In addition, it has been reported that treatment of 1,2-bisaryl-1,2-dihalodiboranes(4) **64c-e** and **80** with a variety of bases yields the corresponding Lewis-base adducts of 1,1-bisaryl-2,2-dihalodiboranes(4) **81a-m** either as main or as side products.^[128-132]

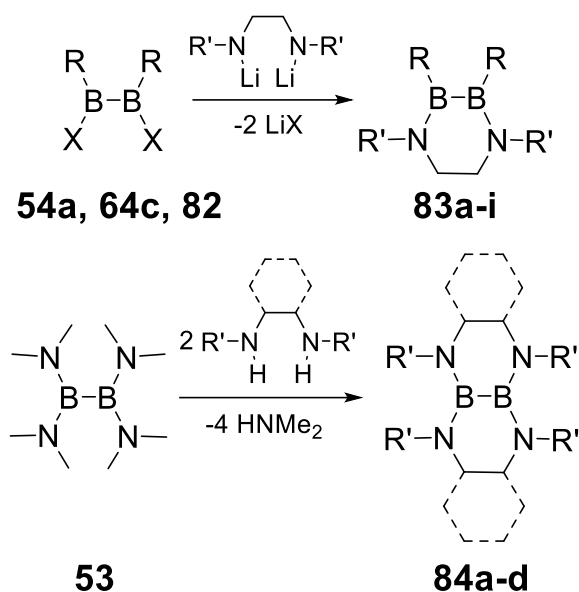
1. Introduction



Scheme 17. Rearrangements of 1,2-substitution patterns on diboranes(4) **54a**, **64c**: Ar = Mes, **64e**: Ar = Dur, **64d**: Ar = Mes, X = Br, **80**: Ar = Mes, X = I, to 1,1-substitution on diboranes(4) **78**, **79a**: Ar = Mes, **79b**: Ar = Dur and **81a**: Ar = Mes, X = Cl, L = SIMes, **81b**: Ar = Mes, X = Br, L = PEt₃, **81c**: Ar = Mes, X = Br, L = PCy₂Me, **81d**: Ar = Mes, X = Cl, L = PEt₃, **81e**: Ar = Mes, X = I, L = PEt₃, **81f**: Ar = Mes, X = Cl, L = PCy₂Me, **81g**: Ar = Mes, X = I, L = PCy₂Me, **81h**: Ar = Mes, X = Br, L = SIMes, **81i**: Ar = Mes, X = Cl, L = IDip, **81j**: Ar = Mes, X = Cl, L = CAAC^{Me}, **81k**: Ar = Mes, X = Br, L = CAAC^{Me}, **81l**: Ar = Dur, X = Cl, L = CAAC^{Me}, **81m**: Ar = Dur, X = Br, L = CAAC^{Me}.^[125-132] (LDA = lithium diisopropylamide, Mes = 2,4,6-Me₃C₆H₂, Dur = 2,3,5,6-tetramethylphenyl, SIMes = 1,3-Mes-imidazolidin-2-ylidene, IDip = 1,3-Dip-imidazol-2-ylidene, CAAC^{Me} = 1-Dip-3,3,5,5-tetramethyl-pyrrolidin-2-ylidene)

Diaza-heterocycles with diborane(4)-moiety, namely 1,4-diaza-2,3-diborinanes, have been scarcely reported because the 1,1-isomers with 1,3,2-diazaborole moieties are thermodynamically favored.^[133] The group of Nöth were the first to selectively synthesize cyclic 1,4-diaza-2,3-diborinanes **83a** and **83b** by reaction of the dianion of *N,N'*-dimethyl-ethylenediamine with 1,2-dichlorodiboranes(4) **54a** and **82** (Scheme 18).^[133] Later, more cyclic 1,4-diaza-2,3-diborinane species with saturated backbone **83c-i** were synthesized in analogous fashion (Scheme 18).^[134,135] Furthermore, transamination reactions of diborane(4) **53** with *N,N*-dimethyl-1,2-organyldiamines yielded the fused B-N-cycles **84a-d** (Scheme 18).^[134,136]

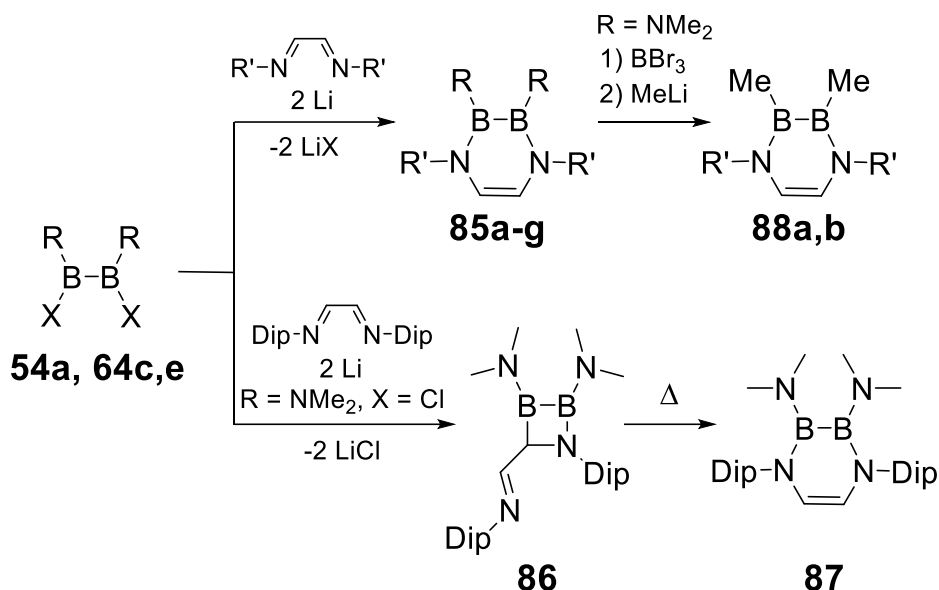
1. Introduction



Scheme 18. Synthesis of 1,4-diaza-2,3-diborinane species **83a-j** from according diboranes(4) **54a**, **64c**, **82** and polycyclic species **84a-d** from diborane(4) **53**.^[133-136] **54a**: R = NMe₂, X = Cl; **64c**: R = Mes, X = Cl; **82**: R = NEt₂, X = Br; **83a**: R = NMe₂, R' = Me; **83b**: R = NEt₂, R' = Me; **83c**: R = NMe₂, R' = Mes; **83d**: R = NMe₂, R' = Dip; **83e**: R = NMe₂, R' = 2,6-dimethylphenyl; **83f**: R = NMe₂, R' = 2,4-dimethylphenyl; **83g**: R = NMe₂, R' = benzyl; **83h**: R = NMe₂, R' = *p*-tolyl; **83i**: R = Mes, R' = *p*-tolyl; **84a**: R' = 2,6-dimethylphenyl; **84b**: R' = 2,4-dimethylphenyl; **84c**: R' = *p*-tolyl; **84d**: cyclohexyl-backbone, R' = H. (Mes = 2,4,6- Me₃C₆H₂)

When 1,2-dichlorodiboranes(4) **54a** and **64c,e** are reacted with doubly reduced 1,4-diazabutadienes the 1,4-diaza-2,3-diborinane species with unsaturated backbones **85a-g** are obtained (Scheme 19).^[135,137,138] In the case of the *N,N'*-Dip-1,4-diazabutadiene-ligand the intermediate **86** was formed, which subsequently rearranges to the 1,4-diaza-2,3-diborinane **87** (Scheme 19).^[138] Also, the dimethylamino groups in **85b,c** could be exchanged for bromo substituents followed by addition of methyl lithium to obtain the dimethylated 1,4-diaza-2,3-diborinanes **88a,b** (Scheme 19).^[138]

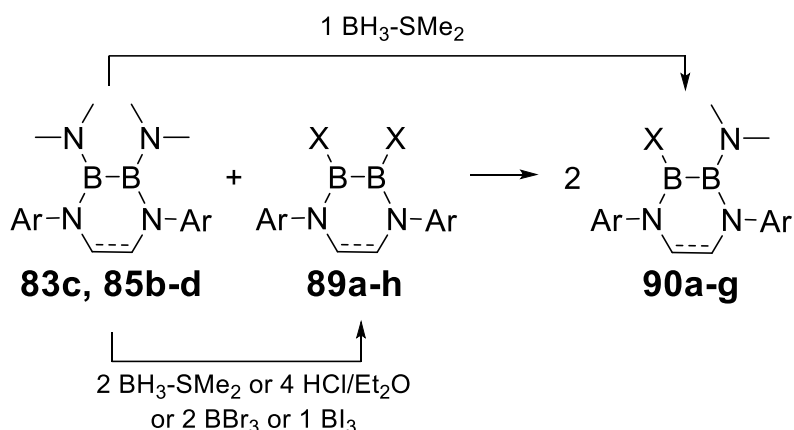
1. Introduction



Scheme 19. Synthesis of unsaturated 1,4-diaza-2,3-diborinane species **85a-f**, **87**, **88a,b** from according diboranes(4) **54a**, **64c,e**. **54a**: R = NMe₂, X = Cl; **64c**: R = Mes, X = Cl; **64e**: R = Dur, X = Cl; **85a**: R = NMe₂, R' = 2,4-dimethylphenyl; **85b**: R = NMe₂, R' = Mes; **85c**: R = NMe₂, R' = 2,6-dimethylphenyl; **85d**: R = NMe₂, R' = *p*-tolyl; **85e**: R = Mes, R' = *p*-tolyl; **85f**: R = Dur, R' = *p*-tolyl; **85g**: R = NMe₂, R' = *t*Bu; **88a**: R' = Mes; **88b**: R' = 2,6-dimethylphenyl.^[135,137,138] (Mes = 2,4,6-Me₃C₆H₂, Dur = 2,3,5,6-tetramethylphenyl, Dip = 2,6-*i*Pr₂C₆H₃)

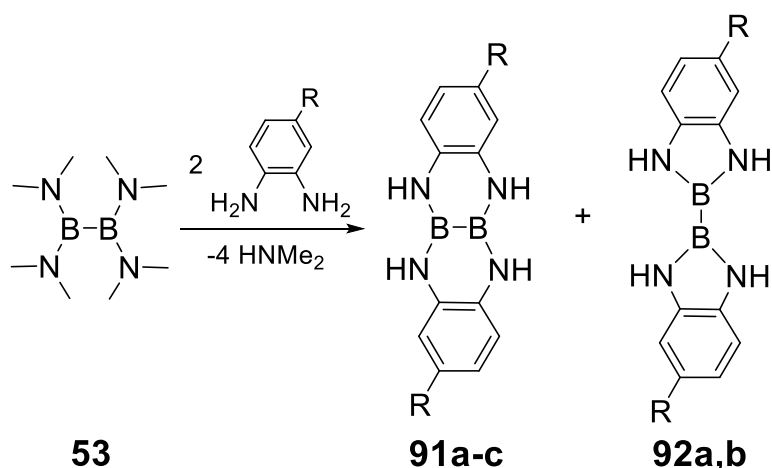
The exchange of the dimethylamino groups at the boron atoms in 1,4-diaza-2,3-diborinanes by hydride or halides was achieved with a variety of reagents (Scheme 20): two equivalents of BH₃·SMe₂ exchange both dimethylamino groups in **83c** for hydrogen atoms forming **89a** and by using only one equivalent of BH₃·SMe₂ even the unsymmetrical 1,4-diaza-2,3-diborinane **90a** was obtained. Furthermore, the 1,4-diaza-2,3-diborinanes **85b-d** were transformed into the chloro derivatives **89b,e,g** with four equivalents of ethereal HCl, whereas two equivalents BBr₃ were used to produce the bromo-species **89c,f,h**. One example of an iodo substituted 1,4-diaza-2,3-diborinane **89d** was synthesized by Braunschweig. Mixing of the dimethylamino-substituted heterocycles with the corresponding 1,2-dihydride or dihalide derivative, respectively, in a 1:1 stoichiometric ratio results in comproportionation to the unsymmetrically substituted 1,4-diaza-2,3-diborinanes **90a-g**.^[135,138]

1. Introduction



Scheme 20. Reactivity of **83c** (saturated backbone) and **85b-d** (unsaturated backbone) towards BH₃-SMe₂, HCl/Et₂O, BBr₃ or BI₃ and comproportioning reaction between dimethylamino derivatives **83c/85b-d** and according hydrogen/halide derivatives **89a-h** to the mixed species **90a-g**. **83c**: R = NMe₂, R' = Mes; **85b**: R = NMe₂, R' = Mes; **85c**: R = NMe₂, R' = 2,6-dimethylphenyl; **85d**: R = NMe₂, R' = *p*-tolyl; **89a**: Ar = Mes, X = H; **89b**: Ar = Mes, X = Cl; **89c**: Ar = Mes, X = Br; **89d**: Ar = Mes, X = I; **89e**: Ar = 2,6-dimethylphenyl, X = Cl; **89f**: Ar = 2,6-dimethylphenyl, X = Br; **89g**: Ar = *p*-tolyl, X = Cl; **89h**: Ar = *p*-tolyl, X = Br; **90a**: Ar = Mes, X = H; **90b**: Ar = Mes, X = Cl; **90c**: Ar = Mes, X = Br; **90d**: Ar = 2,6-dimethylphenyl, X = Cl; **90e**: Ar = 2,6-dimethylphenyl, X = Br; **90f**: Ar = *p*-tolyl, X = Cl; **90g**: Ar = *p*-tolyl, X = Br.^[135,138] (Mes = 2,4,6-Me₃C₆H₂)

Polycyclic derivatives were mostly prepared by transamination as in the example already shown above (**84d**, Scheme 18) Treatment of **53** with two equivalents of phenylene diamine derivatives mainly results in the polycyclic isomers **91a-c** (Scheme 21). For R = H, Me the formation of terminally substituted **92a,b** as side products was also observed.^[136,139]

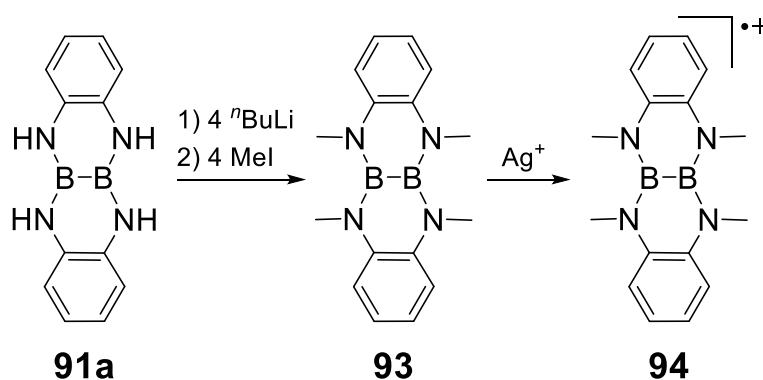


Scheme 21. Synthesis of polycyclic 1,4-diaza-2,3-diborinanes **91a-c** and diazaboroles **92a,b** (as side products) from diborane(4) **53**. Isolated ratio **91a:92a** = 73:27, **91b:92b** = 81:19. **91a**: R = H; **92a**: R = H; **91b**: R = Me; **92b**: R = Me; **91c**: R = ^tBu.^[136,139]

It has been reported that the nitrogen centers in **91a** and **92a** can be deprotonated by an appropriate base (ⁿBuLi). The obtained tetraanions can be reacted with electrophiles to yield *N*-substituted 1,4-diaza-2,3-diborinanes.

1. Introduction

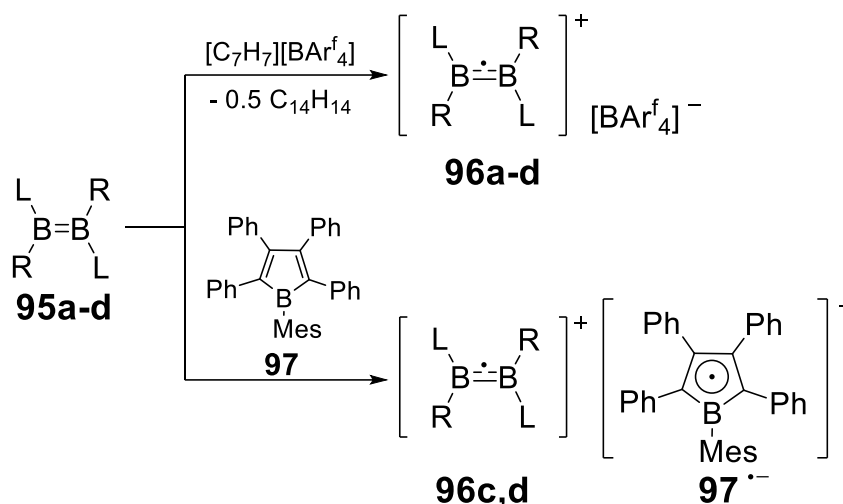
Following this synthetic procedure, *N*-methyl substituted **93** was isolated (Scheme 22). The *N*-methyl derivative of **91a**, namely **93**, and the *N*-methyl derivative of **92a** show fluorescence in a variety of solvents - a property that at the time had been reported for the first time for diborane(4) motifs. In addition, the 1,4-diaza-2,3-diborinane-species **93** ($\lambda_{\text{max,Em}} = 386 \text{ nm}$ in CH_2Cl_2) shows bathochromically shifted emission spectra compared to its diaza-borole isomer ($\lambda_{\text{max,Em}} = 334 \text{ nm}$ in CH_2Cl_2). These structures are sensitive to oxidation, as observed by cyclic voltametric measurements. This was finally confirmed by the formation of the radical cation **94** by treatment with a silver salt and its subsequent isolation (Scheme 22). EPR spectroscopy confirmed the radical structure.^[136,139,140]



Scheme 22. Synthesis of *N*-methylated 1,4-diaza-2,3-diborinane **93** from **91a** and subsequent conversion to the radical species **94**.^[136,139,140]

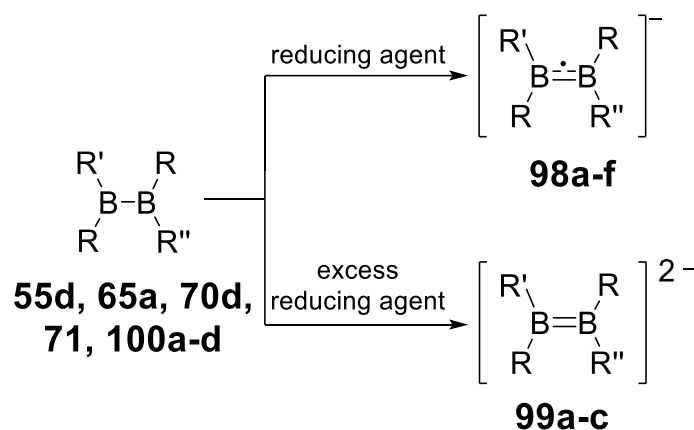
More radical-cationic diborane compounds were accessible from oxidation of neutral diborenes (Scheme 23). The group of Braunschweig examined the diborenes **95a-d** with cyclic voltametric measurements, which display at least one oxidation event for each diborene. On a preparative scale, the tropylium cation was used for the synthesis and subsequent isolation of the diboron radical cations **96a-d**. EPR spectra confirmed the presence of boron-centered radicals. Later, they found borole **97** also to be an appropriate oxidation agent making available the boron centered radical-cation radical-anion pairs **[96c][97] $^{\cdot-}$** and **[96d][97] $^{\cdot-}$** . The degeneration of the bond order to 1.5 during the oxidation step generally leads to a lengthening of the B-B distance in the solid-state structures of the radical cations compared to the corresponding diborenes.^[141-146]

1. Introduction



Scheme 23. Oxidation of diborenes **95a-d** to monoradical cations **96a-d** with BARf_4^- ($\text{Ar}^f = 3,5\text{-}(\text{CF}_3)_2\text{-Ph}$) or borole radical-anion **[97] \cdot^-** as counterpart.^[141-146] **95a**: R = Dur, L = IMe; **95b**: R = Mes, L = PEt_3 ; **95c**: R = iPr, L = liPr; **95d**: R = 4,4-dimethylpent-2-en-2-yl, L = liPr; **96a**: R = Dur, L = IMe; **96b**: R = Mes, L = PEt_3 ; **96c**: R = iPr, L = liPr; **96d**: R = 4,4-dimethylpent-2-en-2-yl, L = liPr. (Mes = 2,4,6- $\text{Me}_3\text{C}_6\text{H}_2$, Dur = 2,3,5,6-tetramethylphenyl, IMe = 1,3-dimethylimidazol-2-ylidene, liPr = 1,3-diisopropylimidazol-2-ylidene)

The formal bond order of 1.5 between two boron atoms is also accessible by one electron reduction of diboranes(4).^[19,147-154] Diboranes(4) **55d**, **65a**, **70d**, **71** und **100a-d** have been turned into monoradical anionic (**98a-f**) or dianionic (**99a-c**) species by reduction with Na/K alloy, lithium (powder), potassium graphite or magnesium with a catalytic amount of anthracene in ethereal solvents (Scheme 24).^[100-102,117,121,155-161] All monoradical-anions **98a-f** have been characterized by EPR spectroscopy.^[121,155-159]



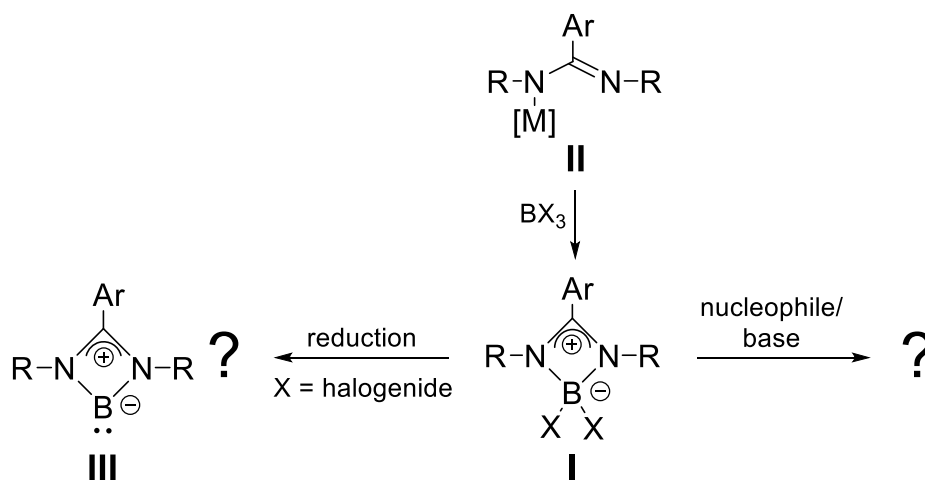
Scheme 24. Reduction of diboranes(4) **55d**, **65a**, **70d**, **71**, **100a-d** to monoradical-anions **98a-f** or diborane(4) dianions **99a-c**.^[100-102,117,121,155-161] **55d**: R = NMe_2 , R' = R'' = Ph; **65a**: R = OMe, R' = R'' = Mes; **70d**: R = R' = Mes, R'' = Ph; **71**: R = R' = R'' = o-tol; **100a**: R = R' = R'' = $\text{CH}_2\text{C}(\text{CH}_3)$; **100b**: R = R' = R'' = $\text{CH}_2\text{C}(\text{CD}_3)$; **100c**: R = R' = R'' = C(CH₃); **100d**: RR'B = pinB, R = R'' = Mes; **98a**: R = R' = R'' = $\text{CH}_2\text{C}(\text{CH}_3)$; **98b**: R = R' = R'' = $\text{CH}_2\text{C}(\text{CD}_3)$; **98c**: R = R' = R'' = C(CH₃); **98d**: R = OMe, R' = R'' = Mes; **98e**: R = R' = Mes, R'' = Ph; **98f**: RR'B = pinB, R = R'' = Mes; **99a**: R = R' = Mes, R'' = Ph; **99b**: R = NMe_2 , R' = R'' = Ph; **99c**: R = R' = R'' = o-tol.

1. Introduction

For a more complete review about the synthetic possibilities of diboranes(4), which would go beyond the scope of this work, see Marder and coworkers.^[19]

2. Aims and Scope

As outlined in the second chapter of the introduction, a wide collection of boryl amidinates and guanidates have already been reported (Figure 1, Figure 2).^[24-45] Their reactivity towards nucleophiles and bases is rarely studied apart from the reaction between boryl benzamidinate **1d** and Yamashita's boryl anion **18**, which shows a C-centered as opposed to the anticipated B-centered attack.^[43,44] The search for a four-membered cyclic NHC-analogue of boron, which would probably provide access to a different kind of coordination chemistry, is also ongoing. Hence, the first part of this work is focused on the synthesis and reactivity of boryl amidinate complexes. In this context the variability of substituents at the core structure **I** should be exploited by altering the aromatic group at the carbon atom (Ar), the substituents attached to the nitrogen atoms (R) and the substituents at the boron center (X, Scheme 25). This will be attempted by reacting different amidinate ligands **II** with different di- or tri-haloboranes (BX₃) and subsequently comparing the structural features of the resulting boryl amidinates **I** with each other and with literature-known compounds. Those complexes of type **I** should be reacted with compounds acting as nucleophiles or bases such as NHCs and metalorganic reagents to generalize their electrophilic properties. Additionally, the dihaloboryl amidinates **I** with X = halogen should be applied in reduction attempts to isolate the to date elusive NHC analogue of type **III**.



Scheme 25. Proposed synthesis of boryl amidinate structures **I** (Ar = aryl, R = alkyl or aryl, X = halogen, alkyl, aryl or amine) from amidinate ligands **II** (Ar = aryl, R = alkyl or aryl, [M] = lithium, trimethylsilyl) and di- or tri-haloboranes (BX₃ = BCl₃, BBr₃, BCl₂R, R = alkyl, aryl, amine) and possible reduction to boron(I) structure **III** or reaction with nucleophiles and bases.

2. Aims and Scope

The second part of this work was concerned with diboranes(4) and their optoelectronic properties. Organoborane functionalities have become popular in OLED materials, profiting from the electron withdrawing effect of the electron deficient boron atom.^[162-189] However, there is a lack of information on the luminescent properties of diboranes(4) except for one report on a polycyclic benzo fused 1,4-diaza-2,3-diborinane derivative **82**, which contains a central diborane(4) moiety.^[136] Thus, the synthesis of symmetrically and unsymmetrically substituted diborane(4) compounds and their optoelectronic characterization was the second major objective of this work. In addition, the effect on luminescence of an electron-donating substituent at one boron atom and at the same time an electron-withdrawing substituent at the other boron atom should be investigated. Starting from tetrakis(dimethylamino) diborane(4) the synthesis of 1,2-bis(aryl)-1,2-bis(dimethylamino) diboranes(4) **IV** was going to be approached first, then the exchange of substituents on the cyclic derivatives **V**. The tetraaryl diboranes(4) **VI** were considered highly interesting objects of study as they do not possess amino groups attached to the boron atoms (Figure 11). The aryl groups in all derivatives (**IV**, **V**, **VI**) are either the same ($Ar = Ar'$) forming symmetrically substituted diboranes(4) or distinct as one electron-donating and one electron-withdrawing substituent ($Ar \neq Ar'$). A comparative study of the fluorescent properties of the synthesized diboranes(4) of types **IV**, **V** and **VI** in solution was going to be performed to systematically gather information on their optoelectronic properties and possibly rationalize structure-characteristic-relationships.

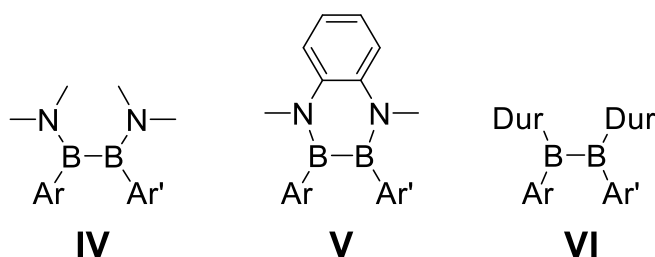


Figure 11. Targeted symmetrically ($Ar = Ar'$) and unsymmetrically ($Ar \neq Ar'$) substituted Diboranes(4) with 1,2-bis(dimethylamino)- (**IV**), 1,4-diaza-2,3-diborinane- (**V**) and 1,2-bisduryl- (**VI**) substitution pattern.

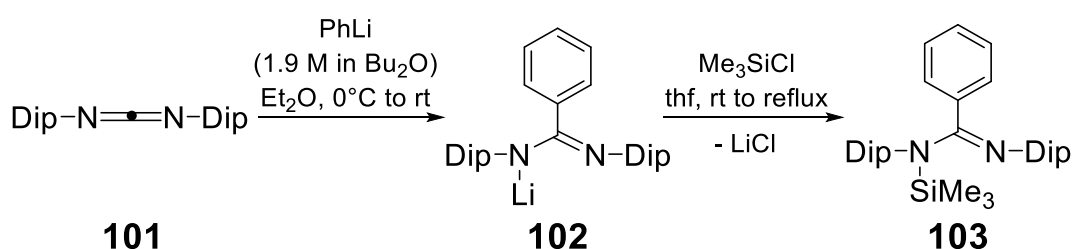
3. Results and Discussion

3.1. Synthesis of various boron benzamidinate complexes

The coordination chemistry of π -electron rich amidinato ligands has been studied intensively during the last decades. In main group chemistry, these ligands are predominantly used to stabilize lower oxidation states,^[56] but various saturated main group element complexes have been synthesized as well. First applications begin to emerge: dialkyl aluminum amidinates, for instance, are active catalysts in ethylene and lactone polymerization.^[190-192] The reactivity of the lighter analogues, namely boron amidinates, is relatively unexplored. Thus, the synthesis, characterization and reactivity studies of various boron benzamidinates is reported herein.

3.1.1 Synthesis of trimethylsilyl-*N,N'*-bis(2,6-diisopropyl-phenyl) benzamidinate **103**

The most common synthetic approaches towards main group element amidinato complexes are salt metathesis reactions and trimethylsilyl halide elimination from a suitable precursor. Thus, trimethylsilyl-benzamidine **103** was prepared as precursor for boryl benzamidinates following the procedure reported by Coles (Scheme 26).^[193]



Scheme 26. Synthesis of trimethylsilylbenzamidine **103**.^[193] (Dip = 2,6-iPr₂C₆H₃)

Crystallization from hexane afforded single crystals suitable for x-ray diffraction analysis (Figure 12) in overall 65% yield. In contrast to NH-amidines, which tend to tautomerize and isomerize, trimethylsilylated amidine scaffolds such as **103** are more stable and geometrically constrained in the *E-syn* configuration due to steric effects.^[193,194] No delocalization was found as indicated by the considerable bond length difference $\Delta_{\text{CN}} = d_{\text{C-N}}(1.392 \text{ \AA}) - d_{\text{C=N}}(1.285 \text{ \AA})$ of

3. Results and Discussion

0.107 Å. A rather large NCN-angle of $115.6(2)^\circ$ is a manifestation of the steric bulk of the groups attached to the amidine core, which is also apparent from the ^1H NMR spectrum (Figure 13): the resonances of the Dip- $\text{CH}(\text{CH}_3)_2$ group (1.11 ppm) and of the $\text{Si}(\text{CH}_3)_3$ group (0.57 ppm) are broadened probably due to hindered rotation.

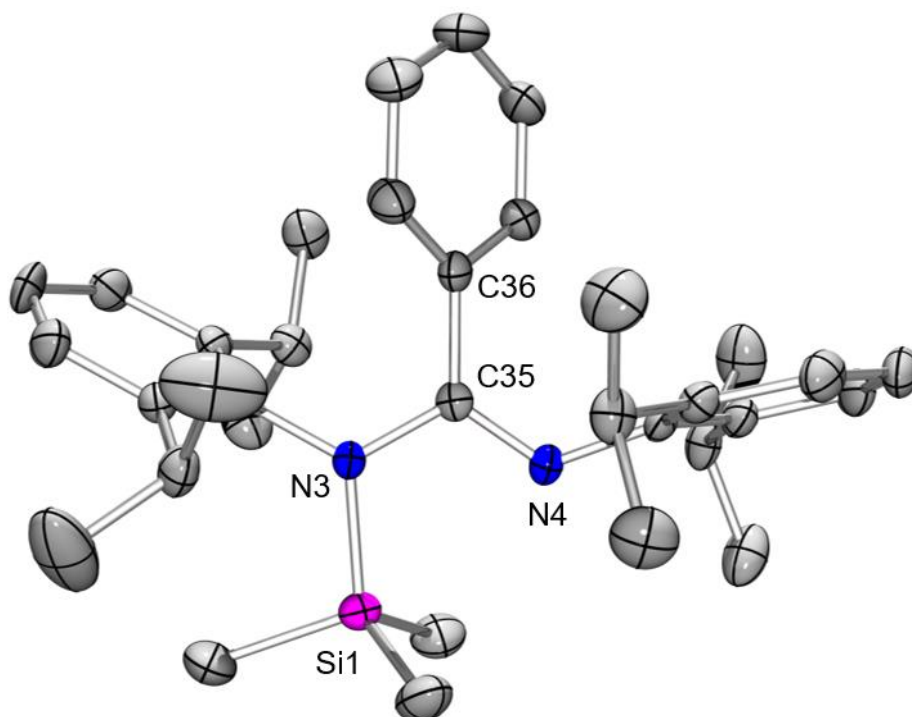


Figure 12. Molecular Structure of **103** in the solid state (ellipsoids at 50% probability, hydrogen atoms and second molecule of the asymmetric unit omitted for clarity). Selected bond lengths [Å] and angles [°]: Si1-N3 1.786(2), N3-C35 1.392(3), N4-C35 1.285(3), C35-C36 1.501(4), C35-N3-Si1 115.7(2), N4-C35-N3 115.6(2).

3. Results and Discussion

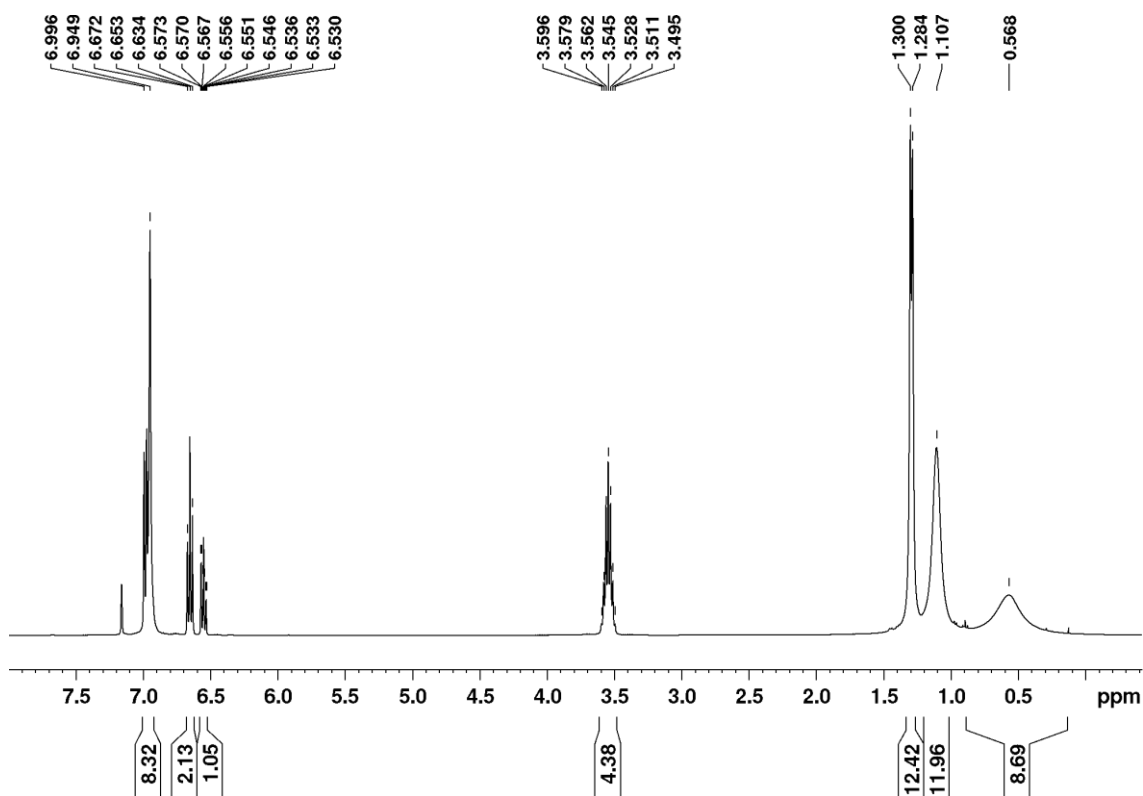
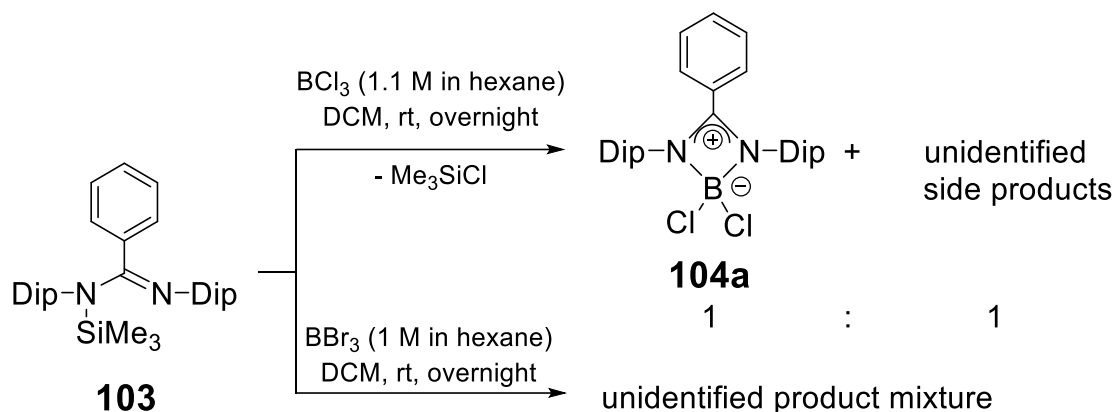


Figure 13. ¹H NMR spectrum of trimethylsilylbenzamidinium **103**.

3.1.2 Attempts to synthesize dihaloboryl-*N,N'*-bis(2,6-diisopropyl-phenyl) benzamidinate **104a,b**

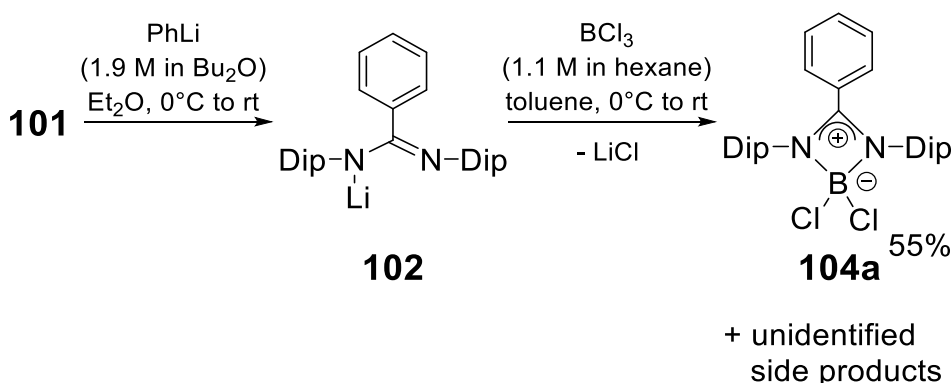
Several approaches to synthesize dihaloboryl benzamidinate complexes **104a,b** were tested. For one, the reaction between trimethylsilyl amidine **103** and borontrihalides (Scheme 27) was examined, following the procedure published by A. H. Cowley.^[46] Stirring with an excess of BX₃ (X = Cl, Br) overnight yielded a mixture of products in both cases, but only with BCl₃ the desired amidinate **104a** could be detected NMR spectroscopically and identified retrospectively by comparison with NMR spectra of the isolated **104a** (see Section 3.1.3). The ¹¹B NMR resonance of the main product (9.3 ppm) is located in the typical range for dichloroboryl benzamidinate complexes.^[33,46] The ratio of the integrated isopropyl methyne signals in the ¹H NMR spectrum indicated that about 50% of the mixture consists of **104a** provided that all species of the mixture have the amidine backbone in common.

3. Results and Discussion



Scheme 27. Reactivity of trimethylsilylbenzamidinium **103** towards trihaloboranes (BCl_3 and BBr_3).^[46] (Dip = 2,6-*i*Pr₂C₆H₃)

Since the first approach did not yield satisfying results, synthesis of **104a** was attempted from carbodiimine **101** by addition of phenyl lithium and subsequent reaction with BCl_3 (Scheme 28) following protocols by A. H. Cowley^[33,34] or H. Braunschweig^[37]. The intermediate **102** was washed with hexane for purification. After BCl_3 addition the reaction mixture was filtered from DCM. A ¹H NMR spectrum of the filtrate strongly suggested that 55% of the product mixture is **104a**. This is also reflected in the ¹¹B NMR spectrum with the main resonance (**104a**) at 9.3 ppm (see above) and the side product at 6.3 ppm. Both resonances strongly suggest a tetracoordinated boron species, although the one of the minor component at 6.3 ppm could not be assigned yet.

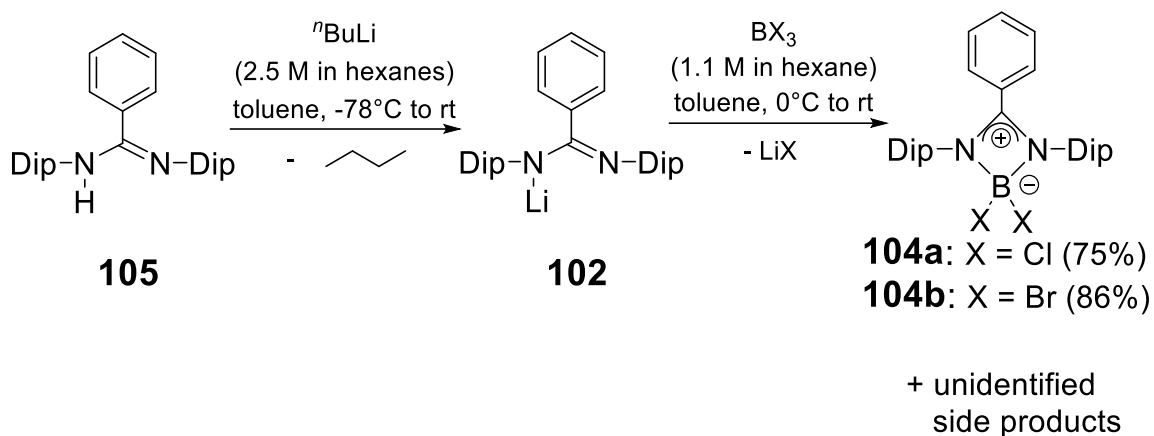


Scheme 28. Synthesis of dichloroboryl benzamidinate **104a** from carbodiimine **101** and phenyllithium *via* lithium benzamidinate **102**.^{[33],[34],[37]} (Dip = 2,6-*i*Pr₂C₆H₃)

The third approach to synthesize **104** was to deprotonate amidine **105** following the procedure established by Westerhausen^[195] and react the previously generated amidinate **102** with the corresponding boron trihalide (Scheme 29). The reaction mixture with BCl_3 was filtered and all volatiles were removed. The residue was washed with hexane. ¹H NMR analysis revealed an enhanced

3. Results and Discussion

selectivity of 75% apart from other yet unidentified side products. As the ^{11}B NMR spectrum seems to indicate a higher selectivity of 87% (determined by integration of ^{11}B resonances), minor side products without boron are contained in the crude mixture. The reaction mixture with BBr_3 was treated analogously. In this case both integration of ^1H (Figure 14) and ^{11}B NMR spectrum suggest 86% selectivity (integration of the isopropyl CH -signals).



Scheme 29. Synthesis of dihaloboryl benzamidinates **104** from benzamidine **105** via lithium benzamidinate **102**.^[195] (Dip = 2,6- $i\text{Pr}_2\text{C}_6\text{H}_3$)

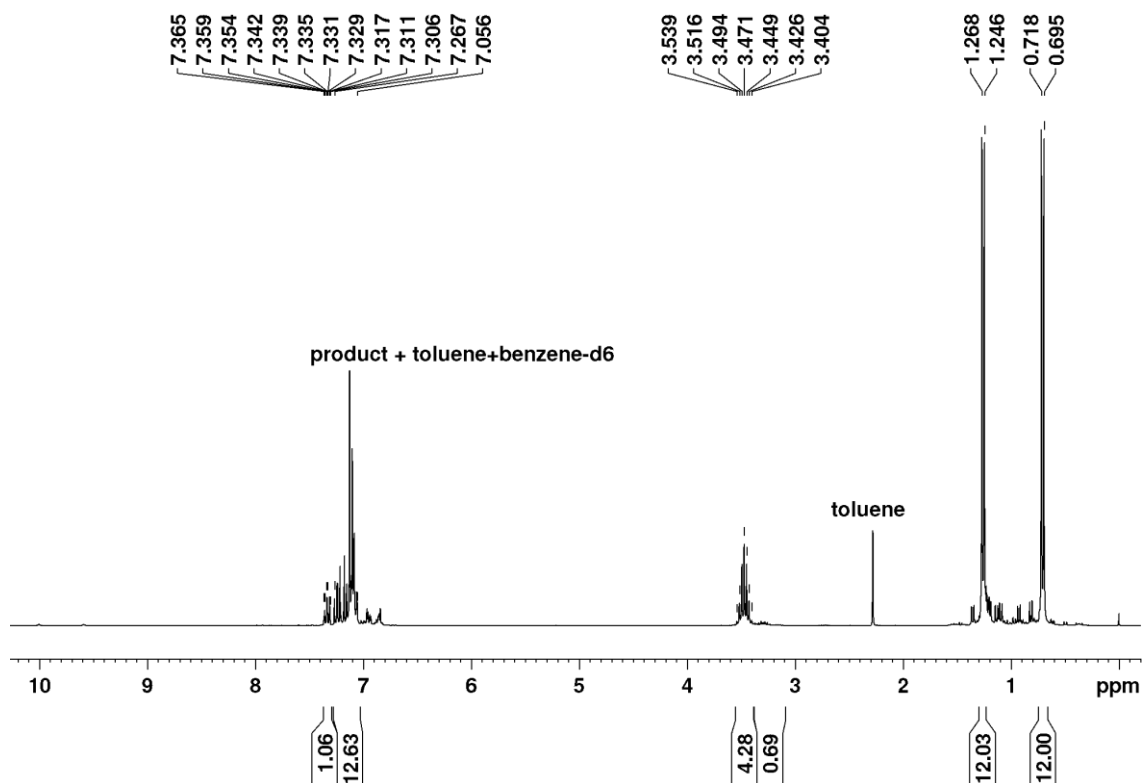


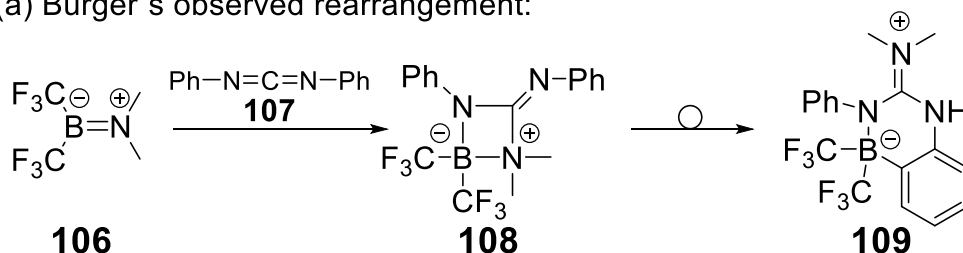
Figure 14. ^1H NMR spectrum of dibromoboryl benzamidinate **104b**. Ratio of integrated Dip-isopropyl- CH signals of **104b**:side products 86:14. (Dip = 2,6- $i\text{Pr}_2\text{C}_6\text{H}_3$)

In general, amidinato ligands are known for adopting various coordination modes.^[58,59,196-199] Additionally, Bürger reported on a rearrangement pathway of

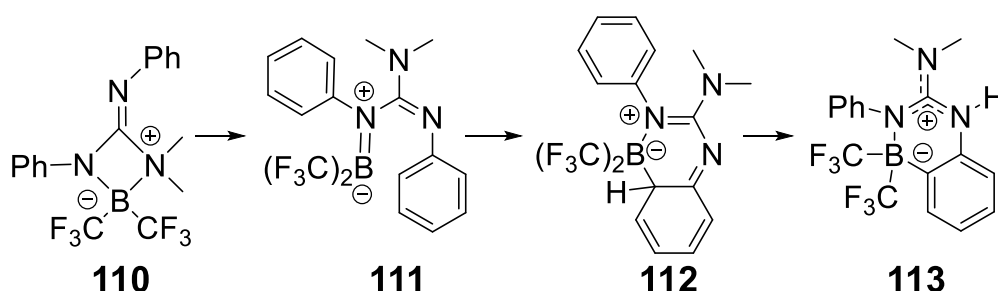
3. Results and Discussion

a boryl guanidate (Scheme 30),^[26] which might take place in an analogous form (Scheme 30) in case of the above and the following boron amidinates as well. Since the *ortho*-positions of the N-aryl substituents are blocked in case of **104a**, in contrast to Bürger's complex, an attack on the backbone phenyl group is assumed. Especially in concentrated solutions, equilibrium between the ring form **104a** and the open-chained form **114** in favor of **104a** is suspected. The right conformation **114'** then can undergo an electrophilic aromatic substitution reaction *via* σ -complex **115** yielding decomposition product **116**.

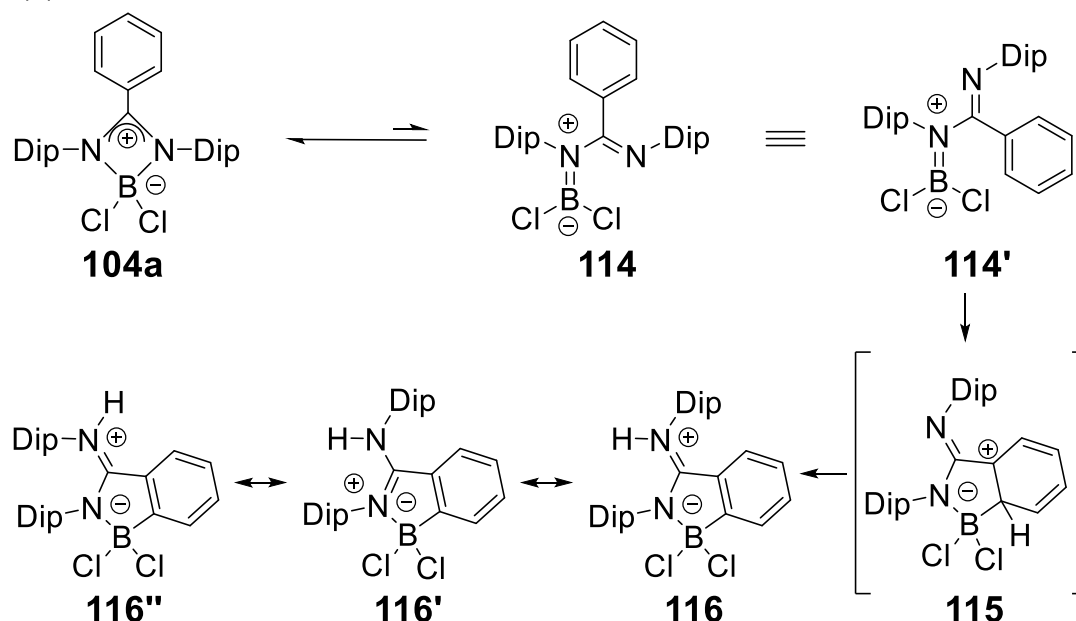
(a) Bürger's observed rearrangement:



(b) Bürger's proposed rearrangement pathway:



(c) transfer to this work:



Scheme 30. Bürger's observed rearrangement (a) and proposed rearrangement pathway (b)^[26] plus proposed analogous rearrangement pathway of **104a** to **116** and its mesomeric forms (c).^[26]

3. Results and Discussion

While keeping a solution of **104a** in benzene at 70°C for 13 days increases the amount of rearrangement/ decomposition products by 10%, one week in saturated solution at room temperature increases the amount by 35% possibly because of intensified intermolecular interactions. A ^1H NMR spectrum of a partly decomposed **104a** sample shows two new species with similar intensity (Figure 15).

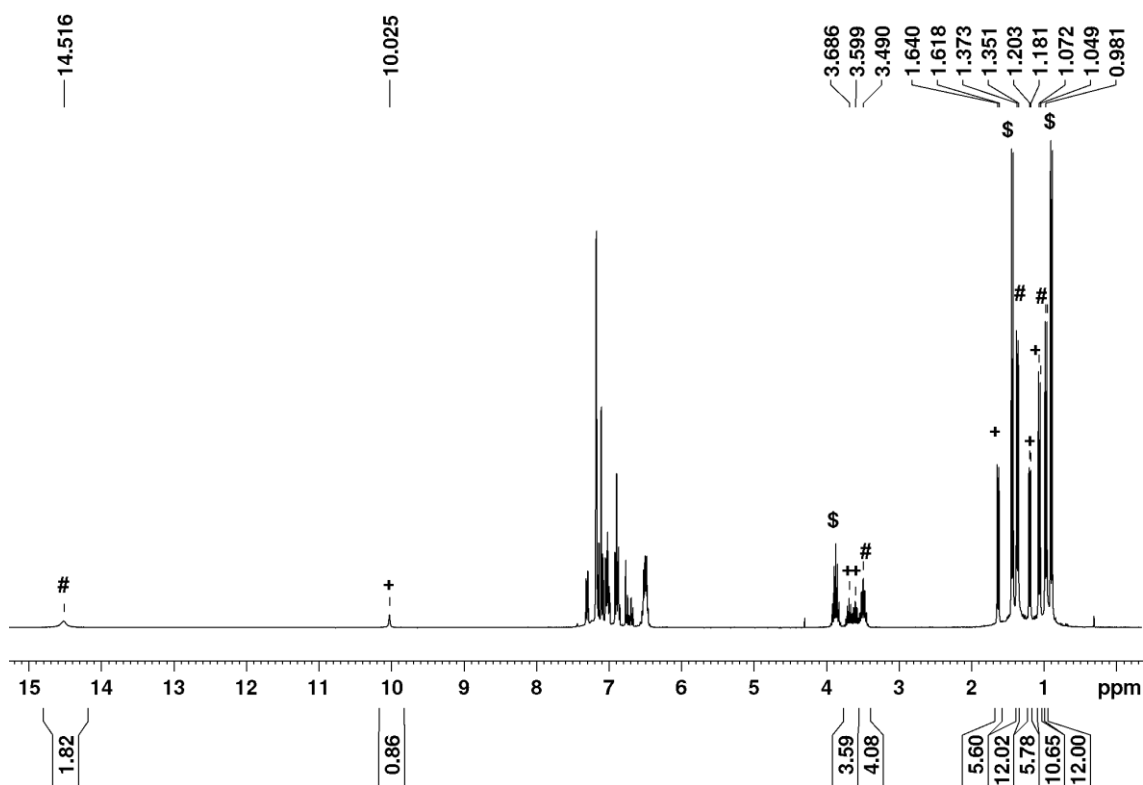


Figure 15. ^1H NMR spectrum of partly decomposed **104a** (marked with “\$”) to proposed rearrangement product **116** (marked with “+”), and doubly protonated ligand (marked with “#”).

One component in this mixture (marked with “+”) has lower symmetry than benzamidinate **104a** indicated by the doubled number of isopropyl- CH group signals at 3.69 ppm and 3.60 ppm (both sept, each 2H) and isopropyl- CH_3 group signals at 1.63 ppm, 1.19 ppm and 1.06 ppm (each d, altogether 24H). Additionally, a singlet at 10.03 ppm for one iminium proton is detected. Considering all these hints, the proposed rearrangement product **116** is suggested as species “+”. Another characteristic iminium signal at 14.52 ppm is observed, which could be attributed to the species (marked with “#”) that gives rise to one septet at 3.49 ppm (4H) for isopropyl- CH groups and two doublets at 1.36 ppm and 0.97 ppm (altogether 24H) for isopropyl- CH_3 groups. The second component shows two iminium protons per ligand-unit and no boron signal in the ^{11}B NMR spectrum which leads to the conclusion that “#” is a decomposition

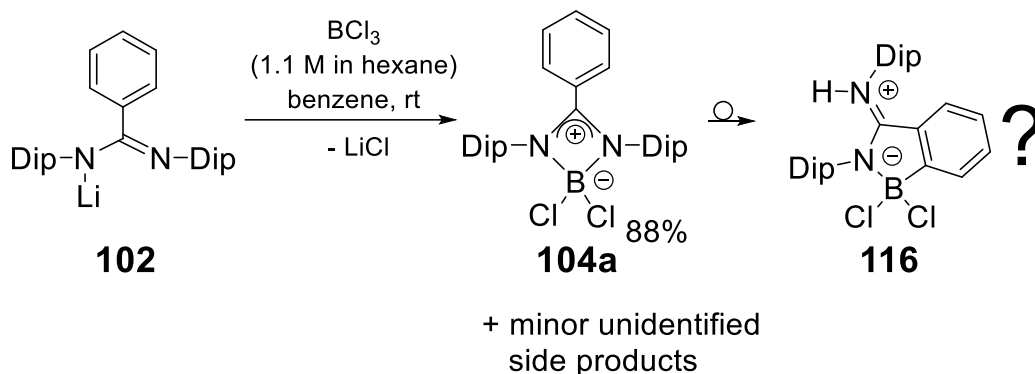
3. Results and Discussion

product with a doubly protonated ligand. VT-NMR of **104a** showed no change in ratio of the components at elevated temperature (333 K) indicating that dynamic processes, for example interchanging coordination modes, can be neglected in diluted solutions. For the dibromoboryl benzamidinate **104b** a similar composition of rearranged or decomposed species is observed.

3.1.3 Synthesis of dichloroboryl-*N,N'*-bis(2,6-diisopropylphenyl) benzamidinate **104a**

Finally, the synthesis with the best results turned out to be from the isolated and washed amidinate **102**, which was suspended in benzene and reacted with BCl₃ solution in hexane at room temperature. After stirring for 30 minutes the reaction mixture was filtered and all solvents and volatiles were distilled off in vacuum. Washing three times with hexane afforded dichloroboryl benzamidinate **104a** in 88% purity (determined by integration of the CH(CH₃) signals in the ¹H NMR spectrum (Figure 16). The ¹¹B NMR spectrum supports a higher selectivity of 95% (determined by integration of ¹¹B resonances 9.9 ppm for the main product and 7.0 ppm for the rearrangement product **116**), suggesting that one or more boron-free components are present in the mixture. Unfortunately, the purity of the product could not be increased by crystallization since further decomposition (see Section 3.1.2) was observed after storage in concentrated solution. In solution and in the ambient atmosphere, dichloroboryl benzamidinate **104a** undergoes rapid and unselective oxidation. In the solid state, it tolerates short periods of exposure to air and moisture but decomposes overnight. Under argon, no decomposition is observed even upon prolonged heating above the melting point (mp. 198-203°C).

3. Results and Discussion



Scheme 31. Synthesis of dichloroboryl benzamidinate **104a** from isolated lithium benzamidinate **102** and possible rearrangement product **116**. (Dip = 2,6- $\text{iPr}_2\text{C}_6\text{H}_3$)

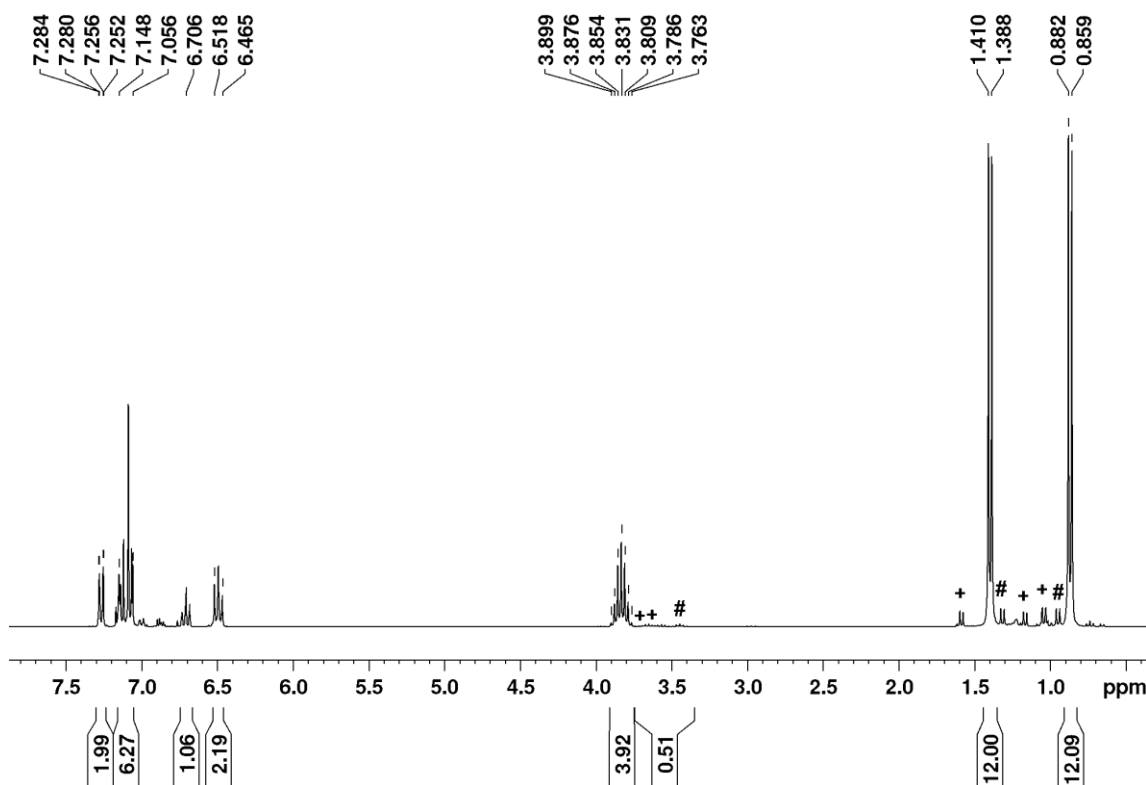


Figure 16. ^1H NMR spectrum of dichloroboryl benzamidinate **104a**. Ratio of integrated Dip-isopropyl- CH signals of **104a**:side products 88:12. Rearrangement product **116** (marked with "+"), and doubly protonated ligand (marked with "#"). (Dip = 2,6- $\text{iPr}_2\text{C}_6\text{H}_3$)

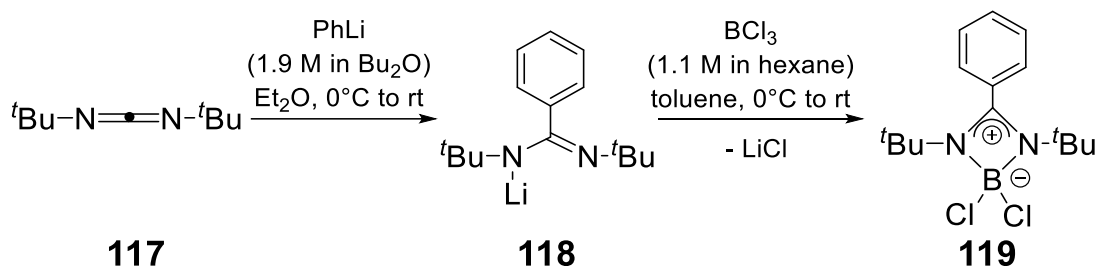
3.1.4 Synthesis of *N,N'*-di- t -butyl-dichloroboryl benzamidinate **119**

In order to examine the influence of the substituents at nitrogen on the amidinate scaffold, t -butyl groups were chosen instead of Dip groups due to their stronger inductive electron-donating effect.

In a first step carbodiimine **117** was reacted with phenyl lithium to form lithium benzamidinate **118**, which after the removal of solvents and volatiles was used without further purification. The reaction with BCl_3 solution in hexane (1.1 M)

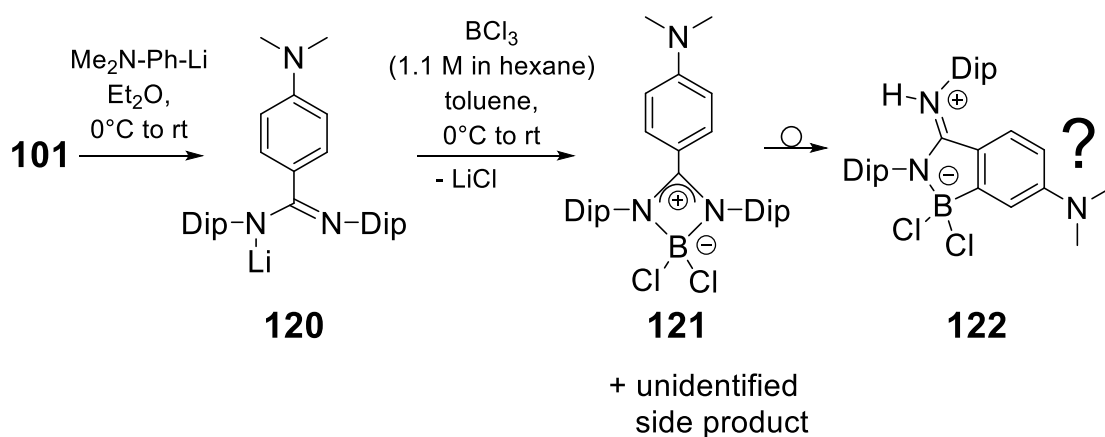
3. Results and Discussion

was carried out in toluene at 0°C. Filtration from toluene and evaporation of the solvent afforded benzamidinate **119** in 52% crystalline yield at -26°C (Scheme 32.). NMR spectroscopic investigations confirmed the purity of the compound with a single ¹¹B NMR resonance at 6.1 ppm in the typical range. Unlike in the cases of **104a,b**, no selectivity issues were encountered indicating that the ^tbutyl groups thermodynamically stabilize the four-membered ring in comparison to the previously applied Dip-substituents.



Scheme 32. Synthesis of dichloroboryl benzamidinate **119** from carbodiimine **117** via lithium amidinate **118**.

3.1.5 Synthesis of dichloroboryl-*N,N'*-bis(2,6-diisopropylphenyl) 4-(dimethylamino)benzamidinate **121**



Scheme 33. Synthesis of dichloroboryl benzamidinate **121**. (Dip = 2,6- iPr₂C₆H₃)

In order to vary the electronic nature of the phenyl-ring an electron-donating group in *para*-position was introduced. To this end, carbodiimine **101** was reacted with 4-(dimethylamino)phenyllithium at 0°C to give amidinate **120** (Scheme 33). Only 57% of the carbodiimine were converted after warming to room temperature, so the crude product was washed to obtain pure amidinate **120** in 29% yield. A solution of BCl₃ in hexane was added to a suspension of **120** in toluene and at 0°C (Scheme 33). After stirring two hours at room

3. Results and Discussion

temperature, a mixture of products consisting of 55% of the desired dichloroboryl amidinate **121** was obtained. The main impurity showed a similar ^1H NMR-spectroscopic pattern (Figure 17) as described above for **104a** and its suspected rearrangement product **116**. A considerable higher amount of rearrangement product (**122**) suggests that the more electron-donating group may facilitate the ring-opening as the first step of the rearrangement process. The ^{11}B NMR spectrum (Figure 18) shows one main product at 9.8 ppm (assigned to **121**) and two additional resonances at 7.2 ppm (assumed rearrangement product **122**) and 2.3 ppm (unidentified, minor side product). Purification by crystallization remained unsuccessful, hence the planned investigation of the reactivity of **121** was not pursued any further.

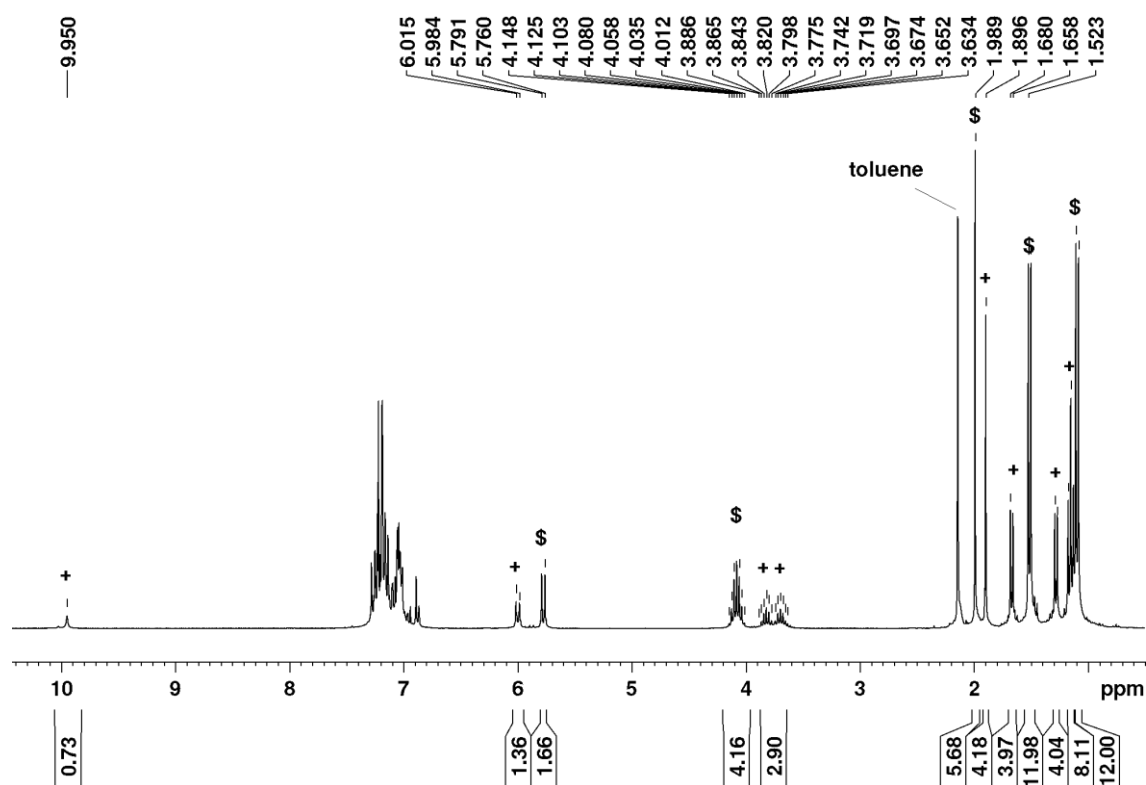


Figure 17. ^1H NMR spectrum of dichloroboryl benzamidinate **121** and rearrangement product **122**. Ratio of integrated Ar-aniline-CH signals of **121**:proposed rearrangement product **122** 55:45. **121** marked with "\$" and proposed rearrangement product **122** marked with "+".

3. Results and Discussion

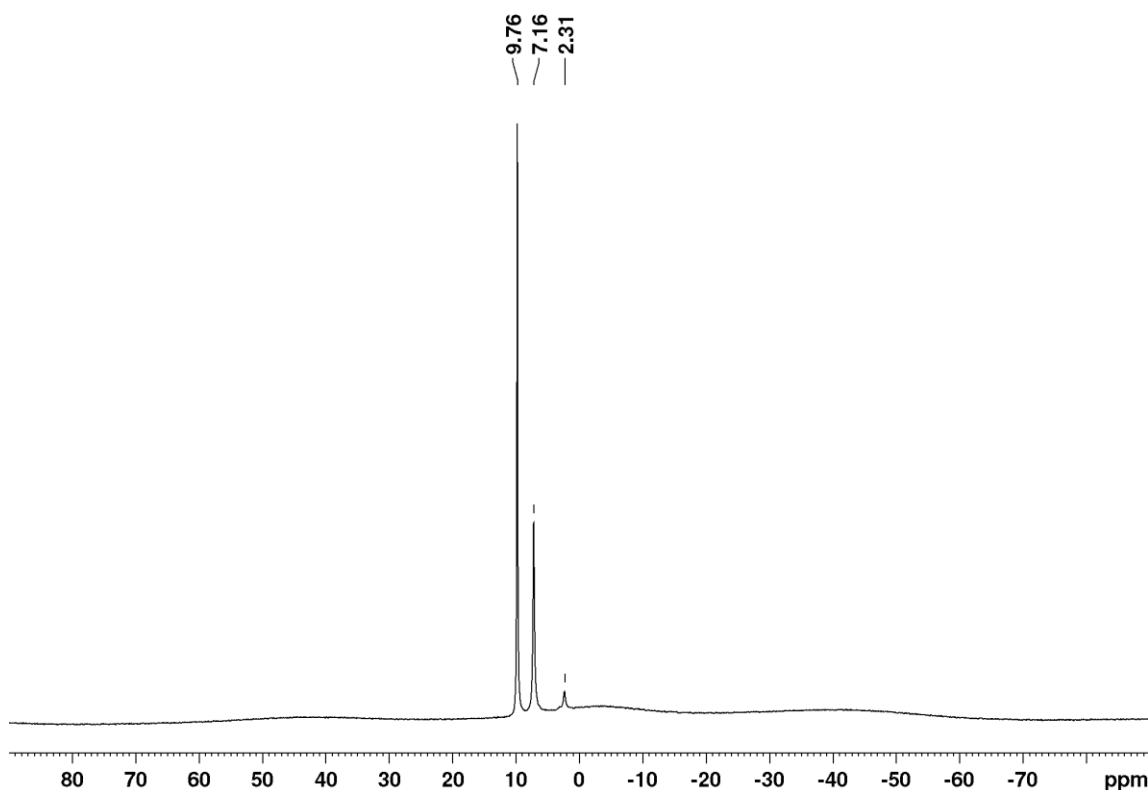


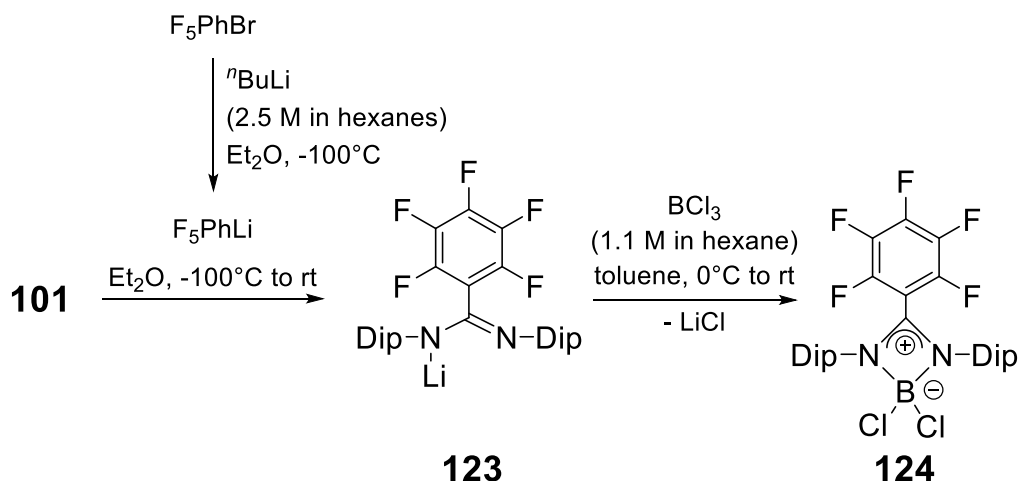
Figure 18. ¹¹B NMR spectrum of dichloroboryl benzamidinate **121** and rearrangement product **122**.

3.1.6 Synthesis of dichloroboryl-*N,N'*-bis(2,6-diisopropylphenyl) pentafluorobenzamidinate **124**

On the basis of the hypothesis that electron-donating groups in *para*-position facilitate the rearrangement of the benzamidinate core, the pentafluorophenyl group as σ -electron-withdrawing, but π -electron-donating substituent was anticipated to confer higher resilience. Following previously established procedures, the reaction between carbodiimine **101** and pentafluorophenyl lithium at low temperatures yielded amidinate **124** quantitatively (determined by multinuclear NMR spectroscopy). The conversion with BCl₃ in hexane or toluene at 0°C afforded **124** (Scheme 34) with high selectivity of 95% (as determined by ¹H and ¹¹B NMR spectroscopy). An ¹¹B NMR resonance at 10.8 ppm is in line with both isolated dichloroboryl benzamidinates **104a** and **119** above. Signals in the ¹⁹F NMR spectrum at -134.32 ppm, -143.15 ppm and -157.66 ppm display the typical pattern for a pentafluorophenyl-group. Finally, the isolation of **124** as single crystals from concentrated dichloromethane solution allowed for x-ray diffraction analysis and confirmed the anticipated

3. Results and Discussion

structure (see Section 3.2). In solution and in the ambient atmosphere, dichloroboryl benzamidinate **124** undergoes rapid and unselective oxidation. In the solid state, it tolerates short periods of exposure to air and moisture but decomposes overnight. Under argon, no decomposition is observed upon prolonged heating above the melting point (mp. >200°C).



Scheme 34. Synthesis of dichloroboryl benzamidinate **124**. (Dip = 2,6- $i\text{Pr}_2\text{C}_6\text{H}_3$)

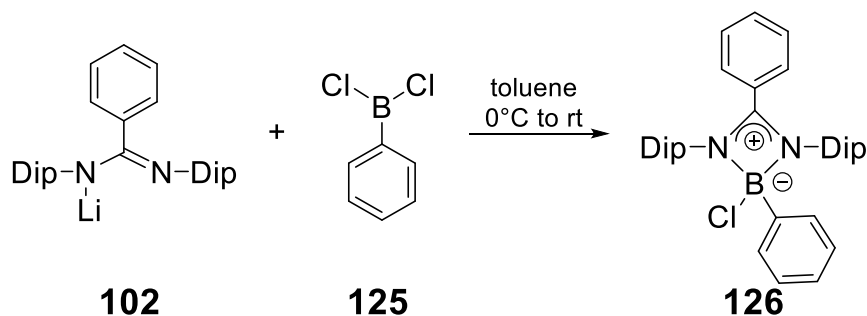
3.1.7 Synthesis of chlorophenylboryl-*N,N'*-bis(2,6-diisopropyl-phenyl) benzamidinate **126**

Another possible point of modification of the amidinato scaffold is the boron center. The effect of asymmetric substitution (one aromatic rest and one chlorine) at boron was thus explored. It was decided to follow literature and introduce the modified substituent at an early stage with the borane starting material.^[34,46] The previously isolated lithium amidinate **102** was suspended in toluene and one equivalent of neat dichlorophenyl borane **125** was added (Scheme 35). After crystallization from toluene, benzamidinate **126** was isolated in 42% yield.

The ^{11}B NMR resonance at 12.6 ppm is slightly downfield shifted compared to the boron benzamidinates described above. The signal is broadened as a consequence of the lower symmetry as typically observed for multipolar nuclei. The ^1H NMR spectrum (Figure 19) shows extensive broadening of the Dip- $\text{CH}(\text{CH}_3)_2$ (3.84 ppm) and one of the Dip- $\text{CH}(\text{CH}_3)_2$ (1.25 ppm) signals, presumably due to hindered rotation caused by steric congestion. The doubly protonated ligand is detected as a minor side product even after crystallization

3. Results and Discussion

(5% by integration of the Dip-CH(CH₃)₂ signals, Figure 19). Reactivity studies were performed without further purification (see Section 3.4).



Scheme 35. Synthesis of chlorophenylboryl benzamidinate **126**. (Dip = 2,6- iPr₂C₆H₃)

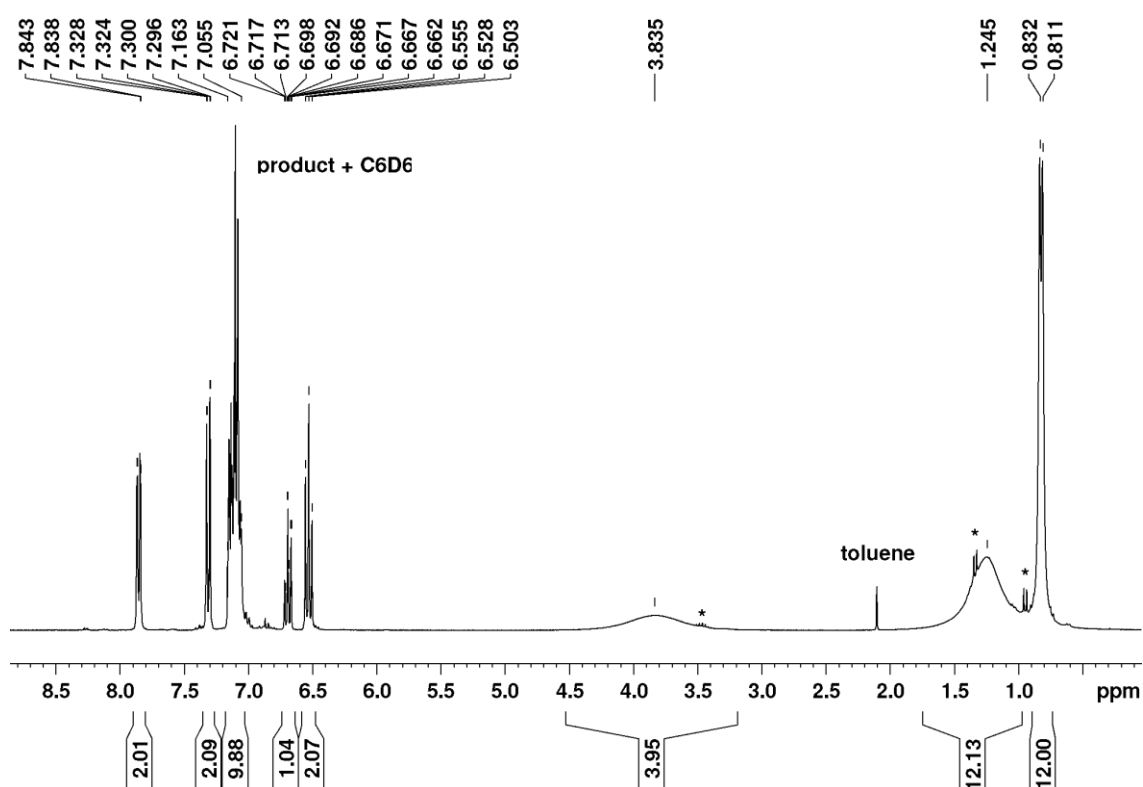


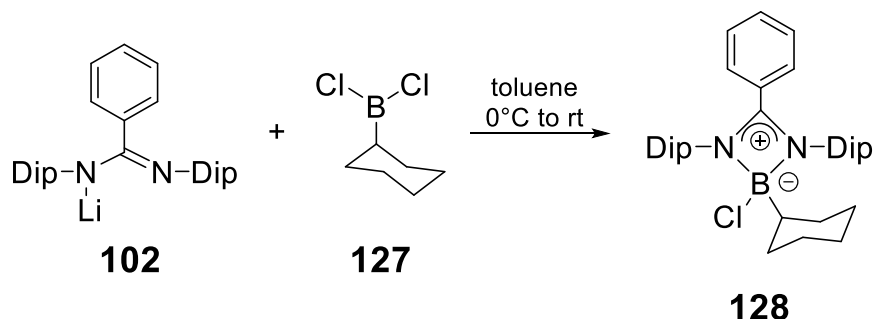
Figure 19. ¹H NMR spectrum of chlorophenylboryl benzamidinate **126**. Doubly protonated ligand as minor side product is marked with “*”.

3.1.8 Synthesis of chlorocyclohexylboryl-*N,N*-bis(2,6-diisopropylphenyl) benzamidinate **128**

The influence of an aliphatic substituent at boron was of interest as well. In analogy to the protocol described above (Section 3.1.7), the isolated amidinate **102** was suspended in toluene and neat dichlorocyclohexyl borane **127** was added at 0°C (Scheme 36). After crystallization from toluene, benzamidinate **128** was isolated in 51% yield. In solution and in the ambient atmosphere,

3. Results and Discussion

chlorocyclohexyl benzamidinate **128** undergoes rapid and unselective oxidation. In the solid state, it tolerates short periods of exposure to air and moisture but decomposes overnight. Under argon, no decomposition is observed upon prolonged heating above the melting point (mp. 208-215°C).



Scheme 36. Synthesis of chlorocyclohexylboryl benzamidinate **128**. (Dip = 2,6-*i*Pr₂C₆H₃)

The ¹¹B NMR resonance at 14.0 ppm is slightly more downfield-shifted compared to other boron benzamidinates reported in this thesis due to reduced π -donation at the boron center and broadened as a consequence of its lower symmetry (see also Section 3.1.7). As in case of **126**, the ¹H NMR spectrum (Figure 20) shows pronounced broadening of the Dip-CH(CH₃)₂ (3.85 ppm), cyclohexyl (1.70-1.62 ppm, 1.33 ppm) and one of the Dip-CH(CH₃)₂ (1.42 ppm) signals due to steric congestion.

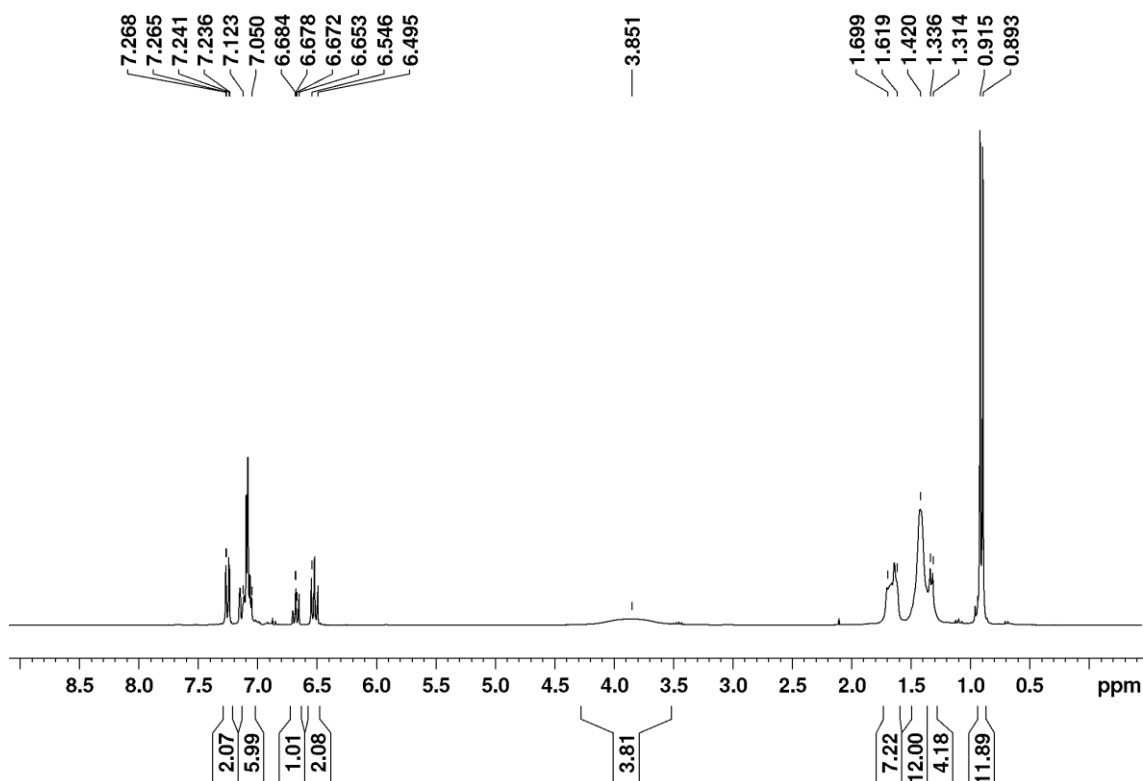
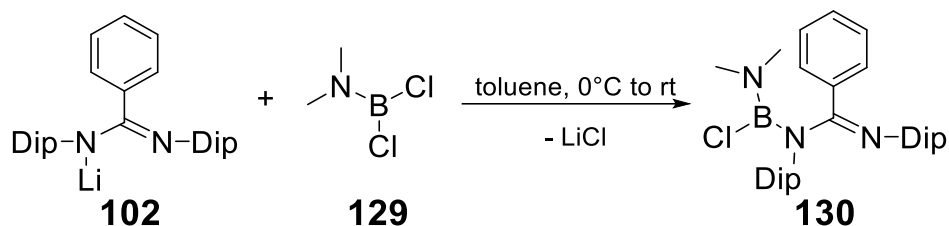


Figure 20. ¹H NMR spectrum of chlorocyclohexylboryl benzamidinate **128**.

3. Results and Discussion

3.1.9 Synthesis of chlorodimethylaminoboryl-*N,N'*-bis(2,6-diisopropylphenyl) benzamidinate **130**



Scheme 37. Synthesis of chlorodimethylaminoboryl benzamidinate **130**. (Dip = 2,6- $i\text{Pr}_2\text{C}_6\text{H}_3$)

In order to probe the effect of increased electron density at the boron center, a dimethylamino group was attached. In analogy to the other procedures (Sections 3.1.7 & 3.1.8), the isolated amidinate **102** was suspended in toluene and neat Me_2NBCl_2 **129** was added at 0°C (Scheme 37). Crystallization from hexane afforded benzamidinate **130** in 70% yield. All signals in the ^1H NMR spectrum (Figure 21) are broadened but show a similar signal distribution as the benzamidinates described in preceding sections. The ^{11}B NMR, however, with a broad resonance at 29.4 ppm suggested a tricoordinate aminoborane without the typical amidinate BN_2C ring structure, which could be confirmed by x-ray diffraction analysis (Section 3.2). Open-chained structures of boryl formamidinates have been reported before and the dynamics of the solvent dependent equilibrium with the closed form of a boryl guanidate has also been studied.^[35,45] In solution and in the ambient atmosphere, chlorodimethylaminoboryl benzamidinate **130** undergoes rapid and unselective oxidation. In the solid state, it tolerates short periods of exposure to air and moisture but decomposes overnight. Under argon, however, no decomposition is observed upon prolonged heating above the melting point (mp. 137-141°C).

3. Results and Discussion

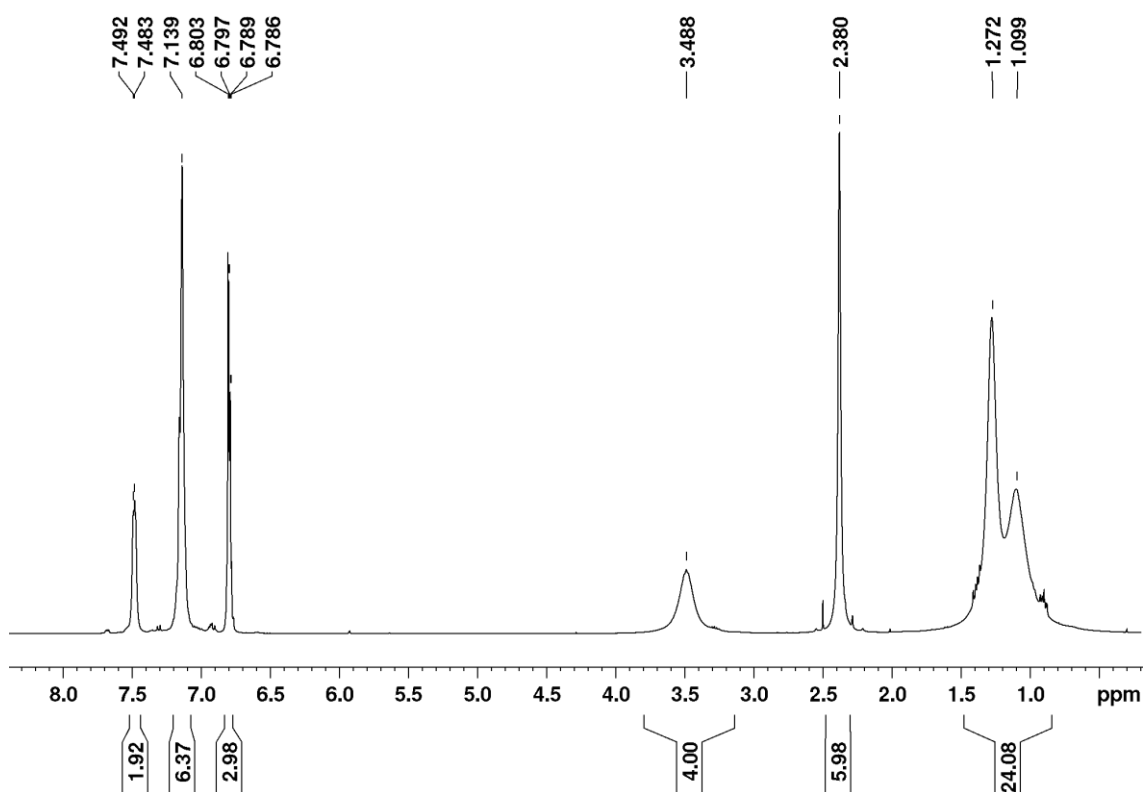


Figure 21. ^1H NMR spectrum of chlorodimethylaminoboryl benzamidinate **130**.

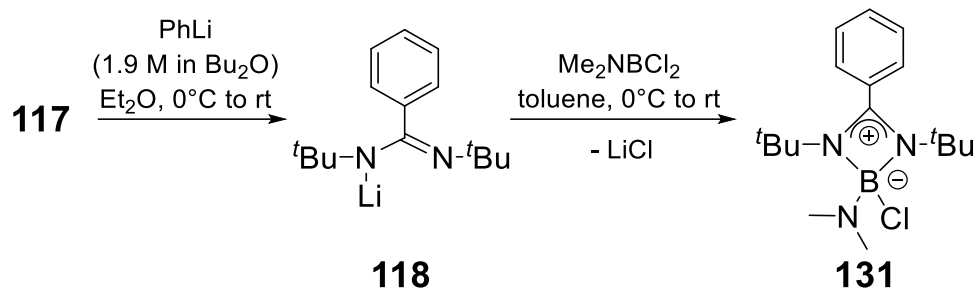
3.1.10 Synthesis of *N,N'*-di-*t*-butyl-chlorodimethylaminoboryl benzamidinate **131**

Since the presence of a dimethylamino group at boron had a marked influence on the complexation behaviour in **130** in comparison to the other *N*-Dip substituted boryl benzamidinates, the analogous *N*-*t*-butyl substituted amidinato derivative was also of interest, although the dichloro derivatives **104a** and **119** showed no major structural differences.

In a first step carbodiimine **117** was reacted with phenyl lithium to yield lithium benzamidinate **118**, which after removal of solvents and volatiles was used without further purification. The reaction with dichloro(dimethylamino)borane in toluene at 0°C , filtration from hexane and evaporation of the solvent afforded benzamidinate **131** in 15% crystalline yield at 5°C (Scheme 38). The NMR spectroscopic investigations showed one ^{11}B NMR resonance at 8.2 ppm in the typical range for a four-coordinate boron center as most of the other benzamidinate complexes discussed previously. Hence, in this case the formation of an BN_2C ring is assumed in contrast to the open-chained form of

3. Results and Discussion

130. This interpretation is in line with the well-established fact^[200] that the *t*-butyl groups increase the donor ability of the amidine-N atoms significantly.



Scheme 38. Synthesis of chlorodimethylaminoboryl benzamidinate **131**.

3.2. Structural comparison of the solid-state structures of various boron benzamidinates

The isolated and crystallized benzamidinates **104a**, **119**, **124**, **126**, **128** and **131** all feature the typical allylic coordination mode in the solid state (Figure 22). Single crystals suitable for x-ray diffraction analysis were grown either from a concentrated dichloromethane solution (**104a**, **119**, **124**, **126**), a concentrated toluene solution (**128**) or a concentrated hexane solution (**131**). The endocyclic B-N bond lengths for **104a**, **119** and **124** (1.561(1) Å-1.59(2) Å) are in the typical range, whereas benzamidinates with increased steric bulk around the boron center (**126**, **128**, **131**) show slightly elongated endocyclic B-N distances between 1.604(3) Å and 1.646(2) Å. However, C-N distances between 1.320(2) Å and 1.334(2) Å are comparable to previously reported boron benzamidinates.^[33,38,41,46] Note that **104a** and **119** are highly symmetric. Consequently, the endocyclic B-N and C-N bond lengths are the same, hence demonstrating the delocalization of the CN-double bond over the NCN-scaffold. The latter is also indicated for the other cyclic benzamidinates by small C-N bond length differences of $\Delta_{\text{CN}} = d_{\text{C-N}}(1.332 \text{ \AA}) - d_{\text{C=N}}(1.330 \text{ \AA}) = 0.002 \text{ \AA}$ for **124**, $\Delta_{\text{CN}} = d_{\text{C-N}}(1.343 \text{ \AA}) - d_{\text{C=N}}(1.332 \text{ \AA}) = 0.011 \text{ \AA}$ for **126**, $\Delta_{\text{CN}} = d_{\text{C-N}}(1.344 \text{ \AA}) - d_{\text{C=N}}(1.329 \text{ \AA}) = 0.015 \text{ \AA}$ for **128** and $\Delta_{\text{CN}} = d_{\text{C-N}}(1.339 \text{ \AA}) - d_{\text{C=N}}(1.320 \text{ \AA}) = 0.019 \text{ \AA}$ for **131**. The C1-C2 (1.42(2) Å) bond in **104a** is slightly shorter by 0.042-0.057 Å than those reported, hinting at possible π -interaction between the two delocalized systems, whereas the remaining benzamidinates **119**, **124**, **126**, **128** and **131** show C-C distances (from 1.467(2) Å to 1.483(2) Å) in the typical range.^[33,38,41,46] The N-C-N (101.5(1)°-104(1)°) and N-B-N (80.0(1)°-84(1)°) angles are also in the typical range for such four-membered BN₂C rings.^[33,38,41,46] The sum of endocyclic angles of the ring add up to $\approx 360^\circ$ in all cases, confirming perfect planarity. Although most of the benzamidinate complexes published so far show an orthogonal arrangement of the phenyl ring to the BN₂C-ring, the angle between the two planes in **104a** is only 36.7°, in **124** 45.6°, in **126** 35.6° and in **128** even 24.0° providing support for a certain π -interaction between the phenyl ring and the amidinate core structure. In contrast, *N*-butyl substituted benzamidinates **119** (angle between planes: 81.9°) and **131** (angle between planes: 88.2°) show a nearly orthogonal setup.

3. Results and Discussion

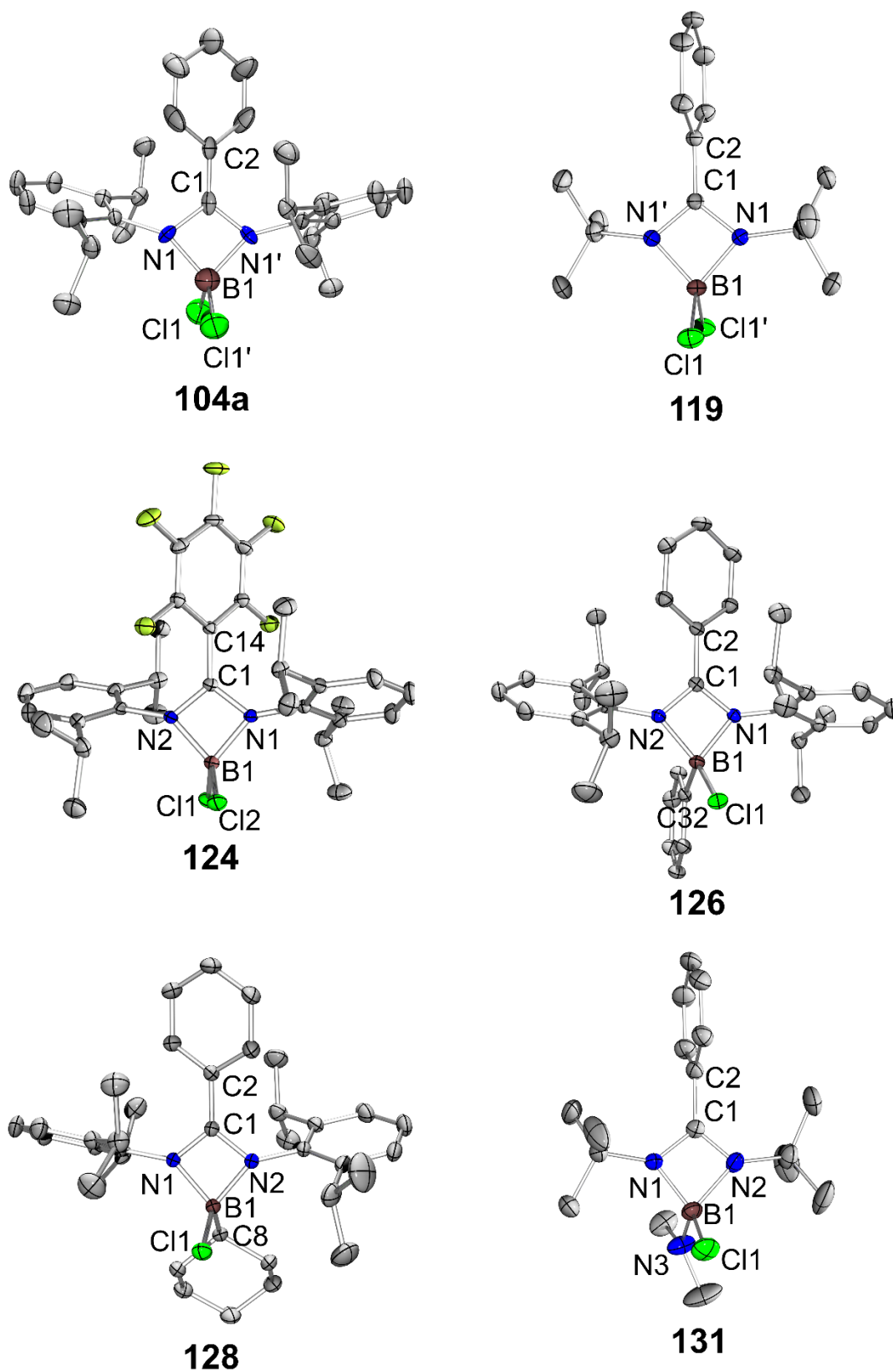


Figure 22. Molecular structures of boryl benzamidates **104a**, **119**, **124**, **126**, **128** and **131**. For detailed information see next page.

3. Results and Discussion

Figure 22 continued. Top left: Molecular Structure of **104a** in the solid state (ellipsoids at 50% probability, hydrogen atoms omitted for clarity, asymmetric unit doubled). Selected bond lengths [Å] and angles [°]: C11-B1 1.81(1), N1-B1 1.59(2), N1-C1 1.34(1), C1-C2 1.42(2), C1-N1-B1 85.9(7), N1-B1-N1' 84(1), N1-C1-N1' 104(1). **Top right:** Molecular Structure of **119** in the solid state (ellipsoids at 50% probability, hydrogen atoms omitted for clarity, asymmetric unit doubled). Selected bond lengths [Å] and angles [°]: C11-B1 1.8364(8), N1-B1 1.561(1), N1-C1 1.336(1), C1-C2 1.478(2), C1-N1-B1 87.73(6), N1-B1-N1' 83.04(8), N1-C1-N1' 101.5(1). **Middle left:** Molecular Structure of **124** in the solid state (ellipsoids at 50% probability, hydrogen atoms and co-crystallized dichloromethane omitted for clarity). Selected bond lengths [Å] and angles [°]: C11-B1 1.811(2), C12-B1 1.818(2), N1-B1 1.588(2), N2-B1 1.585(3), N1-C1 1.330(2), N2-C1 1.332(2), C1-C14 1.469(2), C1-N1-B1 87.4(1), C1-N2-B1 87.5(1), N1-B1-N2 82.0(1), N1-C1-N2 103.0(2). **Middle right:** Molecular Structure of **126** in the solid state (ellipsoids at 50% probability, hydrogen atoms, co-crystallized dichloromethane and second molecule in the asymmetric unit omitted for clarity). Selected bond lengths [Å] and angles [°]: C11-B1 1.847(2), C32-B1 1.592(3), N1-B1 1.604(3), N2-B1 1.620(3), N1-C1 1.343(2), N2-C1 1.332(2), C1-C2 1.471(3), C1-N1-B1 88.6(2), C1-N2-B1 88.3(2), N1-B1-N2 80.6(1), N1-C1-N2 102.4(2). **Bottom left:** Molecular Structure of **128** in the solid state (ellipsoids at 50% probability, hydrogen atoms and co-crystallized toluene omitted for clarity). Selected bond lengths [Å] and angles [°]: C11-B1 1.868(2), C8-B1 1.586(2), N1-B1 1.611(2), N2-B1 1.595(2), N1-C1 1.329(2), N2-C1 1.344(2), C1-C2 1.467(2), C1-N1-B1 88.50(9), C1-N2-B1 88.66(9), N1-B1-N2 80.79(9), N1-C1-N2 102.1(1). **Bottom right:** . Molecular Structure of **131** in the solid state (ellipsoids at 50% probability, hydrogen atoms and disorder of one ^tbutyl-group omitted for clarity). Selected bond lengths [Å] and angles [°]: C11-B1 1.870(2), N3-B1 1.440(2), N2-B1 1.646(2), N1-B1 1.576(2), N1-C1 1.339(2), N2-C1 1.320(2), C1-C2 1.483(2), C1-N1-B1 90.0(1), N1-B1-N2 80.0(1), N1-C1-N2 102.4(1), C1-N2-B1 87.7(1).

In contrast to above mentioned boron benzamidinates, single crystal x-ray analysis confirmed an open chained form of benzamidine **130** (Figure 23). The C25-N1 distance (1.280(1) Å) is significantly shorter than the C25-N2 distance (1.400(1) Å) indicating a double bond between C25 and N1 and a single bond between C25 and N2. The bond length difference ($\Delta_{CN} = d(C-N) - d(C=N)$) of 0.1201 Å is even slightly larger than in trimethylsilyl amidine **103**, consequently no delocalization of the double bond is assumed. The B-N3 distance (1.383(2) Å) is 0.080 Å shorter than the B-N2 distance indicating a more pronounced π -donation from N3 than from N2. The C25-C26 bond length (1.501(2) Å) and the N-C-N angle (118.07(9)°) are in the same range as in trimethyl benzamidine **103**. All in all, **130** and **103** show the same bonding situation, except for the arrangement of the Dip group around the C-N-single bond in the solid state.

3. Results and Discussion

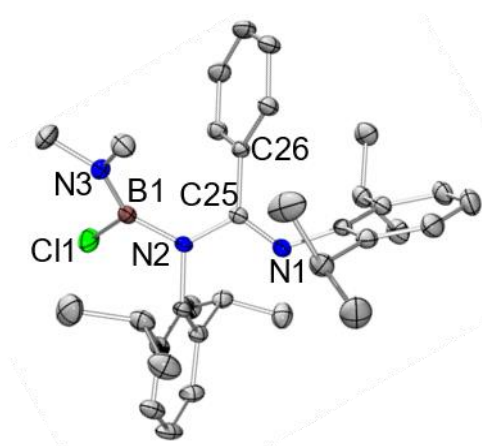
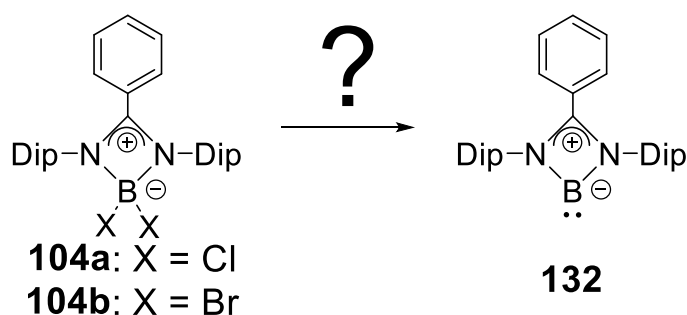


Figure 23. Molecular Structure of **130** in the solid state (ellipsoids at 50% probability, hydrogen atoms omitted for clarity). Selected bond lengths [Å] and angles [°]: Cl1-B1 1.8067(1), N3-B1 1.383(2), N2-B1 1.464(2), N1-C25 1.280(1), N2-C25 1.400(1), C25-C26 1.501(2), C25-N2-B1 125.64(9), N1-C25-N2 118.07(9), N2-B1-N3 126.9(1).

3.3. Reduction attempts of dihaloboryl-*N,N'*-bis(2,6-diisopropylphenyl) benzamidinates **104a,b**

Group 13 element(I) *N*-heterocycles are of considerable interest due to their unique structural properties. The donor-free parent species feature two perpendicular vacant p-orbitals and at the same time a lone pair of electrons at the triel center leading to ambiphilic properties, comparable to those of the more common tetrylenes.^[56] Amidinate and related ligands stabilize this bonding situation by σ -donation into one of the empty p-orbitals and π -donation into the other. While four-membered heterocycles containing gallium(I), indium(I) and thallium(I) have successfully been stabilized by either guanidate or amidinate ligands, the analogous aluminum and boron ring systems remain elusive.^[56] Attempts to synthesize said boron(I) heterocycles have been made in the past, but remained unsuccessful so far.^[27,28,39] With the dihaloboryl benzamidinates **104a,b** in hand, several reduction attempts to species such as **132** were performed.



Scheme 39. Reduction attempts of dichloroboryl benzamidinate **104a,b** to aimed at structure **132**. (Dip = 2,6- *i*Pr₂C₆H₃)

A variety of reducing agents were applied to both dibromo- and dichloroboryl benzamidinate **104a,b**. The Jones magnesium(I) reagent $\{[(\text{DipNacnac})\text{Mg}]_2\}$ ^[201] as mild reductant did not react with the starting material **104a** even after stirring overnight. Similarly, the stoichiometric use of disodium tetracarbonylferrate (Collman's reagent) in an attempt to trap the emerging boron(I) species in the coordination sphere of an Fe-center did not lead to full conversion in a number of solvents: stirring in toluene for 1h at room temperature lead to no conversion at all, so that dme was added to facilitate electron transfer. After 4 days at room temperature in a toluene/dme-mixture, 75% conversion to a mixture of products (according to isopropyl-*CH* resonances in the ¹H NMR spectrum) was reached.

3. Results and Discussion

Another experiment in thf at room temperature was stirred for 8 days, which lead to 90% conversion (according to isopropyl-CH resonances in the ^1H NMR spectrum). No ^{11}B NMR resonance was detected for the product, which could be taken as an indication for either radical components or the presence of an equilibrium mixture. The application of stoichiometric amounts of lithium powder with catalytic amounts of naphthalene in dme or stoichiometric amounts of lithium naphthalenide solution in dme to benzamidinate **104a,b** only resulted in partial conversion to a mixture of products as indicated by ^1H NMR spectroscopy. Potassium graphite (4 eq.) or a large excess of lithium powder in combination with stoichiometric or catalytic amounts of naphthalene led to full conversion to a mixture of unidentified products.

A possible reason for the difficulties to achieve a uniform conversion could be the lack of stability of the targeted boron(I) heterocycle due to the small singlet-triplet-gap predicted for borylenes such as **132**.^[27,202] As carbene-analogues are well known to be stabilized by coordination of an external base such as $i\text{Pr}_2\text{Me}_2\text{NHC}$, the reaction was repeated in the presence of one equivalent of this NHC using an excess of lithium powder and stoichiometric amounts of naphthalene. In these cases, an unidentified mixture of products had formed as well. Any attempt to stabilize the emerging boron(I) species remained thus unsuccessful.

Considering the results described above, curiosity arose whether other structurally related ligands would be more suitable to stabilize the desired boron(I) species. DFT calculations at the BP86+D3(BJ)/def2-SVP level of theory were performed to gather information on the singlet-triplet gaps. In Figure 24 the considered structures are shown including the calculated singlet-triplet-gaps. According to these theoretical results, a guanidate ligand as in **133** would be superior to the amidinate ligand as in **132**. The largest singlet-triplet gap (27.4 kcal mol $^{-1}$) was calculated for the anionic structure **134** suggesting its isolation as a viable task for future investigations.

3. Results and Discussion

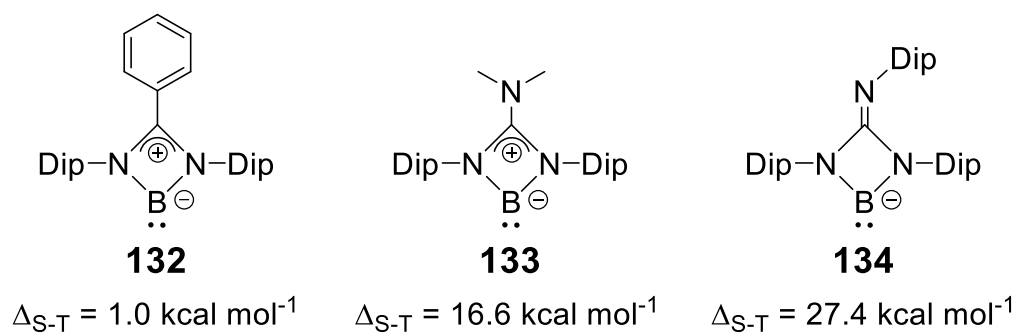


Figure 24. Considered structures and their calculated singlet-triplet-gaps at the BP86+D3(BJ)/def2-SVP level of theory. (Dip = 2,6- $i\text{Pr}_2\text{C}_6\text{H}_3$)

3.4. Reactivity of boryl benzamidates

3.4.1 Reactivity of benzamidate **104a** towards NHCs

N-heterocyclic carbenes (NHCs) as strong bases and nucleophiles are known to stabilize otherwise highly reactive cationic species to such an extent that the dissociation even of comparatively nucleophilic anions such as chloride is prompted.^[55] Dihaloboryl benzamidate complexes have so far not been studied in this regard. The closest approach was reported by Jones and Aldridge with the reaction of Yamashita's boryllithium reagent (thf)₂Li-{B(NDipCH)₂}^[62,65] **28**, which is isoelectronic to an NHC, towards dibromoboryl benzamidate **1d**. In this case, a nucleophilic attack at the imine carbon occurs with subsequent elimination of lithium bromide to yield **29** (see Section 1.2, Scheme 6).^[43,44]

Since some attempts to reduce dichloroboryl benzamidate complex **104a,b** to the corresponding boron(I) species (see Section 3.3) involved the addition of an *N*-heterocyclic carbene for potential stabilization of the targeted borylene **132**, the reactivity of **104a,b** towards NHCs needed to be tested beforehand. As a first result we observed that remaining impurities in **104a** react with ⁱPr₂Me₂NHC **135** instantly and precipitate leaving pure **104a** and excess NHC **135** in C₆D₆-solution (Figure 25).

3. Results and Discussion

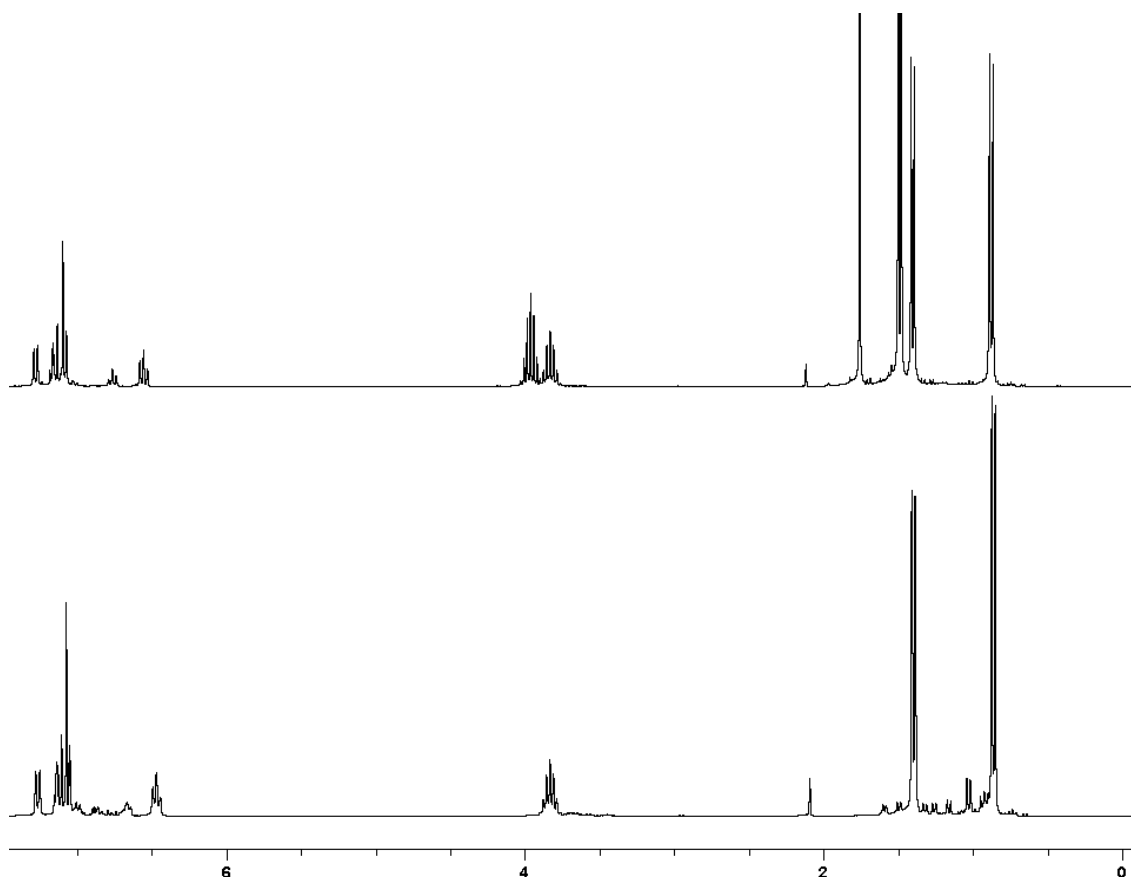


Figure 25. Comparison of spectra of **104a** with remaining impurities (bottom) and after addition of 2.2 eq. $i\text{Pr}_2\text{Me}_2\text{NHC}$ **135** (top).

After filtration, the reaction mixture was stirred for two days at room temperature leading to partial conversion to a uniform product according to NMR spectroscopy. In order to increase the reaction rate, elevated temperatures (70°C) were applied resulting in full conversion after eight days provided two equivalents of NHC were applied initially. Previous experiments showed that the application of only one equivalent NHC leads only to 50% conversion although all the NHC is consumed. Consequently, two equivalents of NHC **135** were required for full conversion. Additionally, precipitation was observed in the course of the reaction. The precipitate was washed with benzene and dissolved in CDCl_3 to be identified by ^1H NMR spectroscopy as the imidazolium-salt-byproduct ($i\text{Pr}_2\text{Me}_2\text{NHC}\cdot\text{HCl}$) due to HCl elimination in the course of the reaction.

3. Results and Discussion

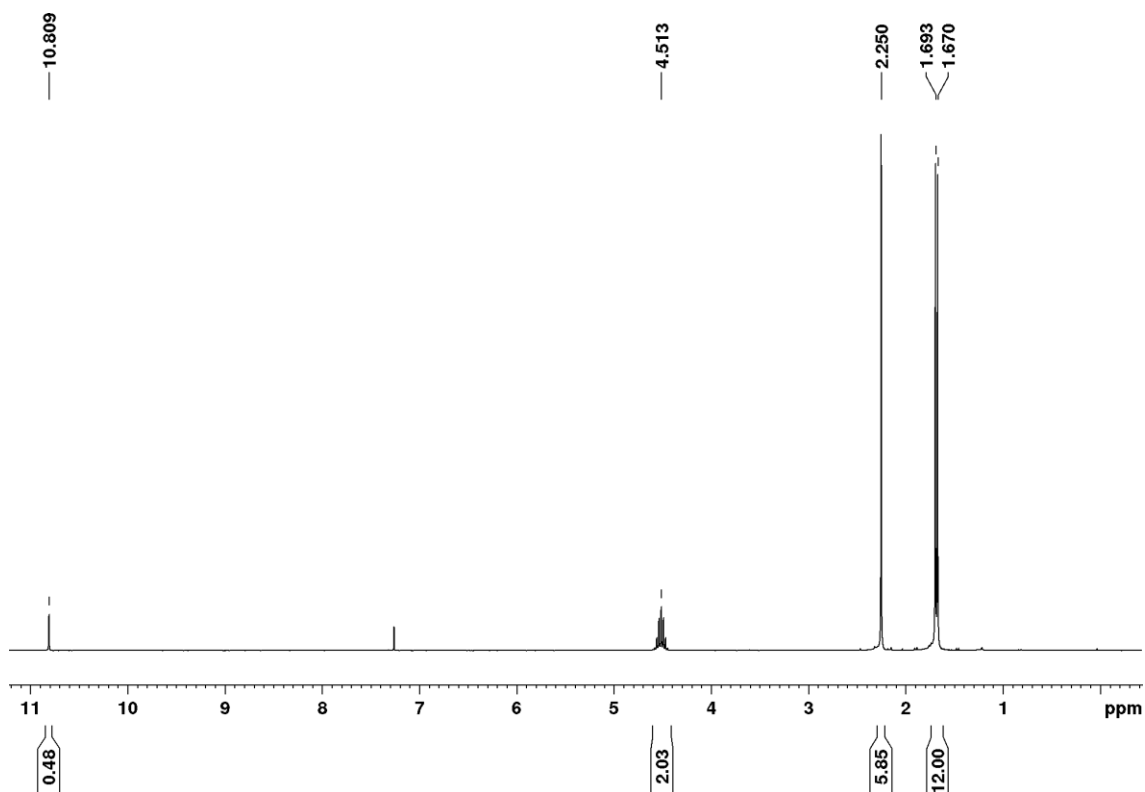


Figure 26. ¹H NMR spectrum of the Imidazolium-salt-byproduct (iPr₂Me₂NHC•HCl).

The ¹H NMR spectrum of the main product (Figure 27) shows six iPr-CH resonances of equal intensity in the range between 5.5 ppm and 3.0 ppm suggesting an asymmetric product with two chemically inequivalent Dip groups and one molecule of iPr₂Me₂NHC. The broad ¹¹B NMR resonance at 1.5 ppm suggests a tetracoordinate boron center and a signal at 161.5 ppm in the ¹³C NMR spectrum is in line with the presence of a datively bonded NHC.

3. Results and Discussion

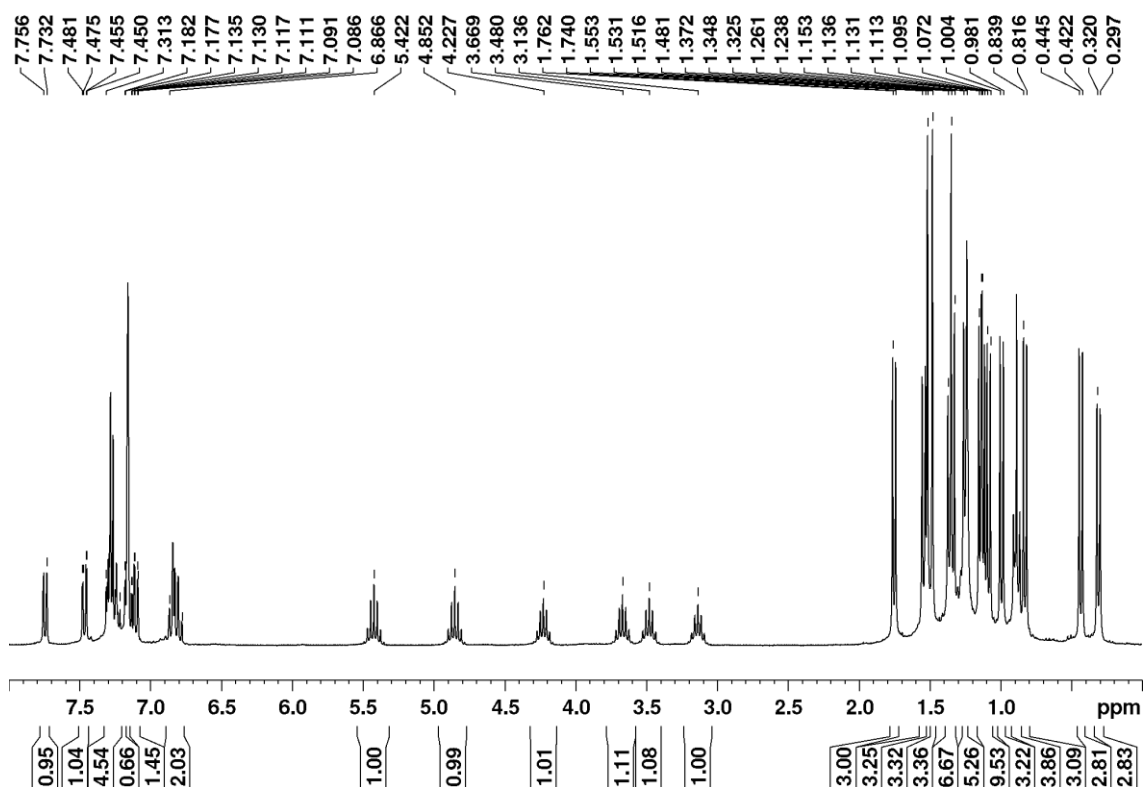


Figure 27. ^1H NMR spectrum of benzazaborole **136**.

The crude mixture was extracted with benzene and washed with hexane twice, affording a clean product in moderate yield (41%). Single crystals were grown from a concentrated benzene solution layered with hexane. X-ray diffraction analysis revealed the constitution of benzazaborole **136** (Scheme 40, Figure 28) exhibiting a similar structural motif as the postulated rearrangement product **116** (Section 3.1.2). The bond distance between the carbenic carbon atom and the boron center is at 1.660(4) Å slightly longer than in the corresponding $\text{BCl}_3\text{-NHC}$ complex (1.644 Å)^[203] hinting at a slightly weaker coordination. The B-Cl bond is significantly elongated as well (1.943(3) Å) compared to those of the $\text{BCl}_3\text{-NHC}$ complex (1.873 Å). Structurally related benzazaboroles were reported by Dostal with B-N bond lengths between 1.403 Å and 1.431 Å. In contrast to **136**, the boron center in Dostal's compounds is tricoordinate.^[204,205] Expectedly, the B-N distance in **136** is elongated (1.533(3) Å) due to tetra-coordination of the boron atom, which excludes any B-N π -interaction.

3. Results and Discussion

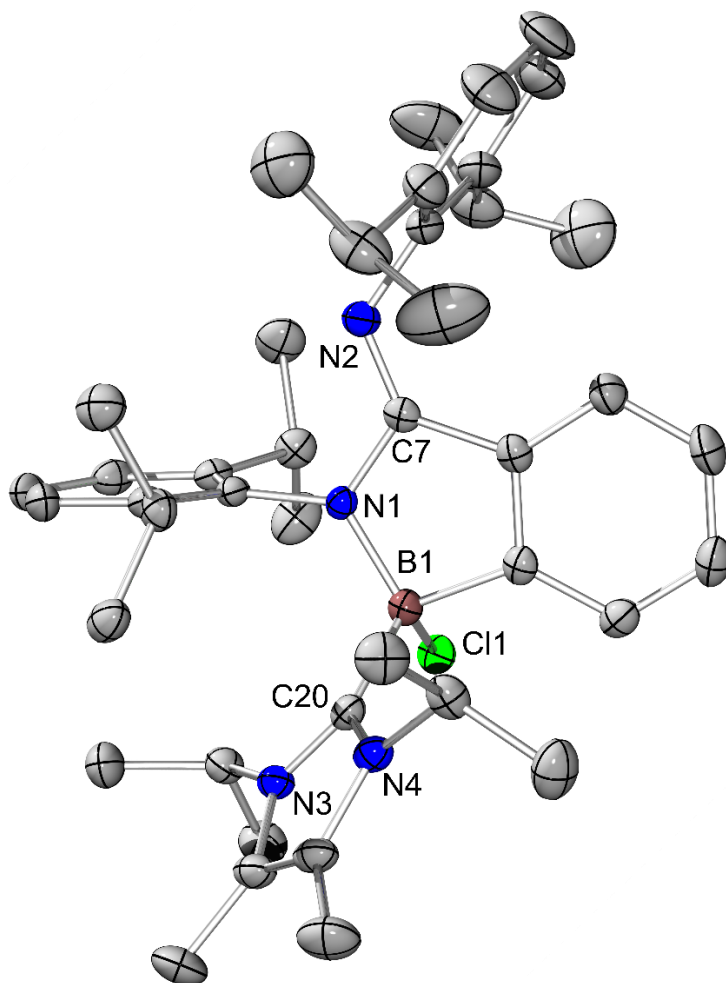
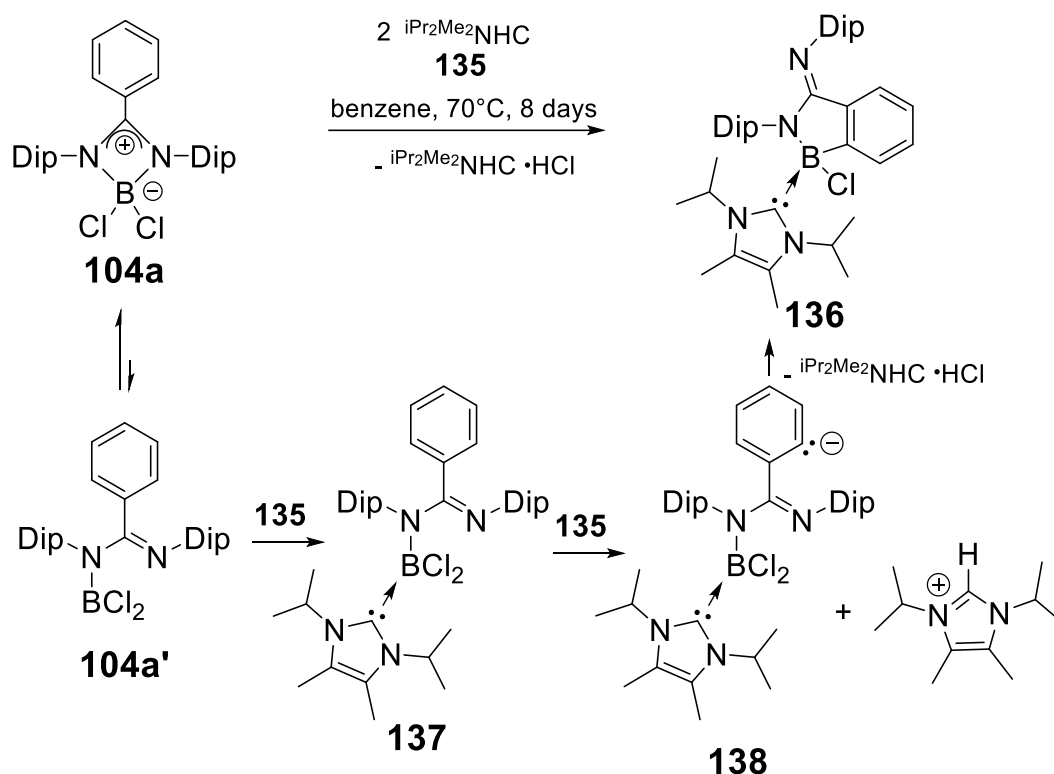


Figure 28. Molecular Structure of **136** in the solid state (ellipsoids at 50% probability, hydrogen atoms and co-crystallized benzene omitted for clarity). Selected bond lengths [Å] and angles [°]: Cl1-B1 1.943(3), C20-B1 1.660(4), N1-B1 1.533(3), N1-C7 1.383(3), N2-C7 1.287(3), C7-N1-B1 113.0(2), N1-C7-N2 121.5(2), C7-N2-C_{Dip} 120.9(2), N1-B1-C_{Ph} 100.0(2), N1-B1-C20 114.9(2), C20-B1-Cl1 106.3(2).

The proposed reaction mechanism is shown in Scheme 40. Although the sequence of events remains unclear at this point, it can be assumed that the closed form **104a** and the open chained form **104a'** are in equilibrium, which is shifted mostly to **104a**. This process could be the rate limiting step. Next, one equivalent of NHC **135** as a strong nucleophile coordinates to the boron center of **104a'** thus removing the latter from the equilibrium to give **137** as first intermediate. The second equivalent of NHC presumably acts as a base and as such deprotonates the phenyl-ring of **137** in *ortho*-position. The newly generated carbanionic center in the second intermediate **138** plausibly attacks the boron center. Finally, the elimination of chloride would result in the isolated product **136**. Further CH-activations in analogous benzamidinate-positions are only known from thermal rearrangement of a bis-silylene^[206] or a Palladium-complex^[207]. In solution and in the ambient atmosphere, benzazaborole **136**

3. Results and Discussion

undergoes rapid and unselective oxidation. In the solid state, it tolerates short periods of exposure to air and moisture but decomposes overnight. Under argon, decomposition is observed upon prolonged heating above the melting point (mp. >220°C).



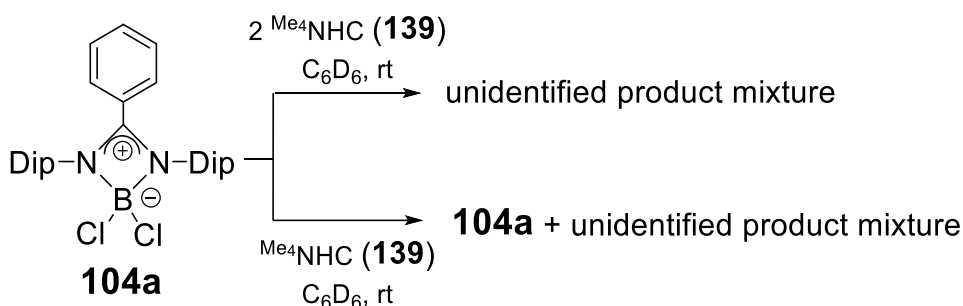
Scheme 40. Synthesis and proposed formation mechanism of benzazaborole **136**. (Dip = 2,6- $i\text{Pr}_2\text{C}_6\text{H}_3$)

Due to steric hindrance the reaction is slow even at 70°C. To reduce the reaction time the use of toluene as solvent was attempted in order allow for higher reaction temperatures. Unfortunately, side products were observed when heating the reaction mixture at 100°C for four days.

As an alternative, decreasing the steric bulk of the NHC could speed up the reaction. Therefore, in an NMR scale reaction boron benzamidinate **104a** was dissolved in C_6D_6 and added to two equivalents of Me_4NHC **139** (Scheme 41). The reaction was monitored by ^1H and ^{11}B NMR spectroscopy. After 10 minutes the ^1H NMR spectrum started to show an unselective conversion to a mixture of products. ^{11}B NMR shows one sharp signal at 9.9 ppm (starting material), one broad signal at 4.7 ppm and one very broad signal at -0.1 ppm. Overnight, **104a** is nearly fully consumed and converted to a complex mixture of unidentified products (^1H NMR spectrum). The ^{11}B NMR showed one very broad

3. Results and Discussion

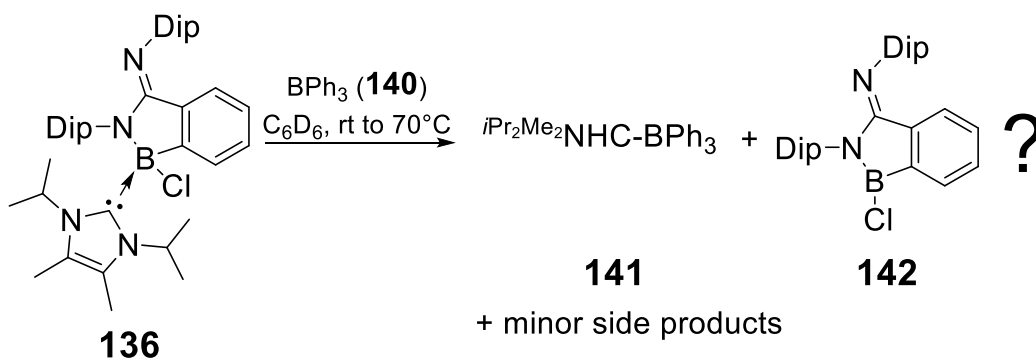
resonance at 0.0 ppm, representing the mixture of products observed in the ^1H NMR spectrum, and some residual starting material (9.9 ppm). The use of only one equivalent Me_4NHC results in a similar mixture, except for a higher amount of starting material **104a** remaining (Scheme 41).



Scheme 41. Attempted reaction of dichloroboryl benzamidinate **104a** with Me_4NHC . (Dip = 2,6- $i\text{Pr}_2\text{C}_6\text{H}_3$)

3.4.2. Attempted NHC abstraction from $i\text{Pr}_2\text{Me}_2\text{NHC}$ coordinated benzazaborol-3-imine **136**

Based on the presence of a nitrogen atom directly adjacent to the electron-deficient boron center of benzazaborole **136** we hypothesized that the coordination of the NHC may not be necessary for the stability of the molecule and be therefore only loosely bonded. Stronger Lewis acids, e.g. triphenylborane or its perfluorinated version, are known to act as NHC scavenger in such situations shifting any equilibrium towards the NHC-free substrate under concomitant formation of the corresponding NHC-triarylborane complex.^[208-212]



Scheme 42. Reaction of benzazaborole **136** with triphenylborane **140**. (Dip = 2,6- $i\text{Pr}_2\text{C}_6\text{H}_3$)

In an NMR scale reaction, the attempted NHC abstraction with BPh_3 in C_6D_6 (Scheme 42) did not proceed at room temperature, whereas heating at 70°C for

3. Results and Discussion

one day resulted in a mostly uniform product mixture according to the ^1H NMR spectrum (Figure 29). Disregarding the overlapping aryl resonances, a characteristic septet at 5.02 ppm (2H), the singlet at 1.52 ppm (6H) and the doublet at 0.69 ppm (12H) were assigned to NHC-borane complex **141**.^[208] Hence, the remaining signals in the alkyl region (3.21, 3.14 (each sept, altogether 4H), 1.28, 1.26 (each d, altogether 12H,), 1.06, 0.99 (each d, each 6H) are attributed to **142**. In the ^{11}B NMR spectrum (Figure 30) a relatively sharp resonance at -8.1 ppm, as reported for the NHC-borane complex **141**^[208], supports the hypothesis that the targeted NHC-borane complex **141** was formed.^[208-212] Additionally three broad resonances were detected. One of the two more downfield shifted signals (57.5 ppm, 43.6 ppm) would be attributed to the product of type **142** (Scheme 42). The existence of an equilibrium cannot be excluded based on the present data. The chemical shift of 0.6 ppm hints at a tetracoordinated, yet unidentified, boron species. For final peak assignment, the reaction needs to be repeated in a bigger scale and the product purified.

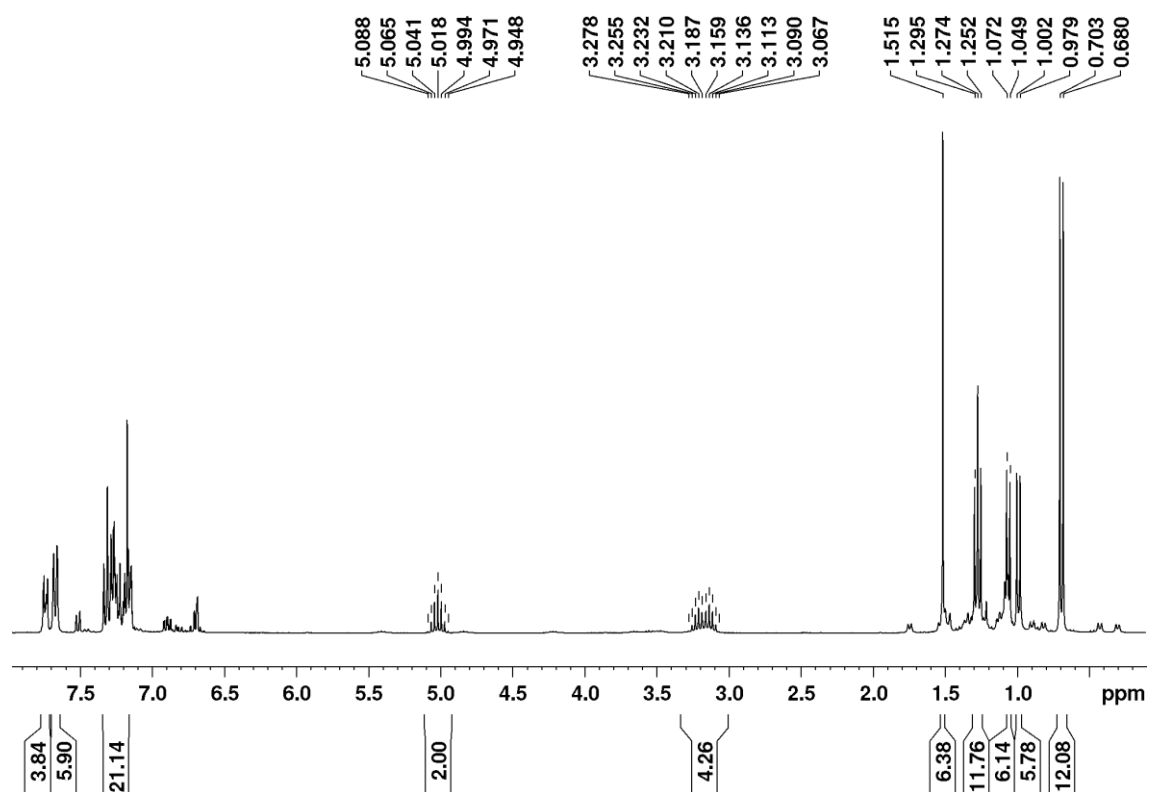


Figure 29. ^1H NMR spectrum of the reaction between benzazaborole **136** and triphenylborane (**140**).

3. Results and Discussion

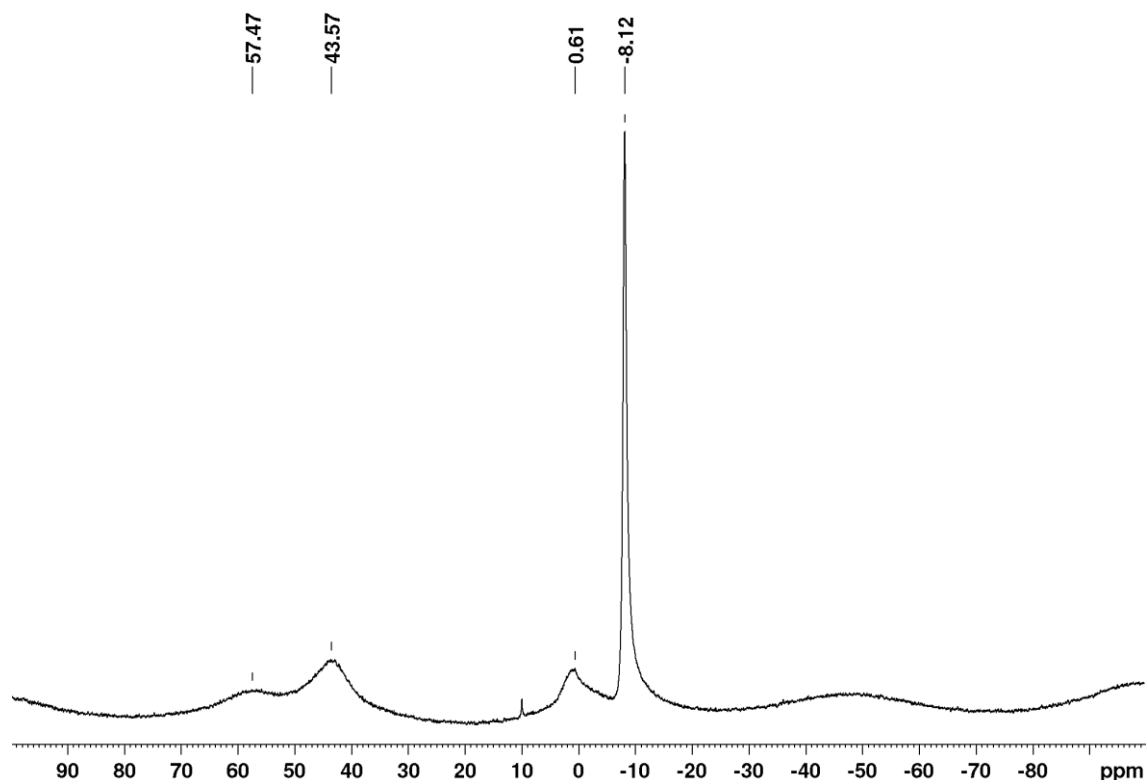


Figure 30. ^{11}B NMR spectrum of the reaction between benzazaborole **136** and triphenylborane (**140**).

As the reaction with triphenylborane required elevated temperatures, we tried the perfluorinated triphenylborane as a more reactive alternative. In an NMR scale reaction, both starting materials **136** and **143** were dissolved in C_6D_6 and an immediate, uniform reaction was observed NMR spectroscopically. The ^1H NMR spectrum (Figure 31) shows 10 aryl protons, one septet for coordinated $\text{NHC-CH}(\text{CH}_3)_2$ protons (4.16 ppm, 2H) and two septets for Dip- $\text{CH}(\text{CH}_3)_2$ protons (2.94 ppm, 2.85 ppm, altogether 4H). All remaining alkyl protons add up to 42 which fits perfectly to a species similar to the starting material **136**. In fact, the distribution of ^1H NMR signals resembles the one of the reaction mixture with BPh_3 (Figure 29).

3. Results and Discussion

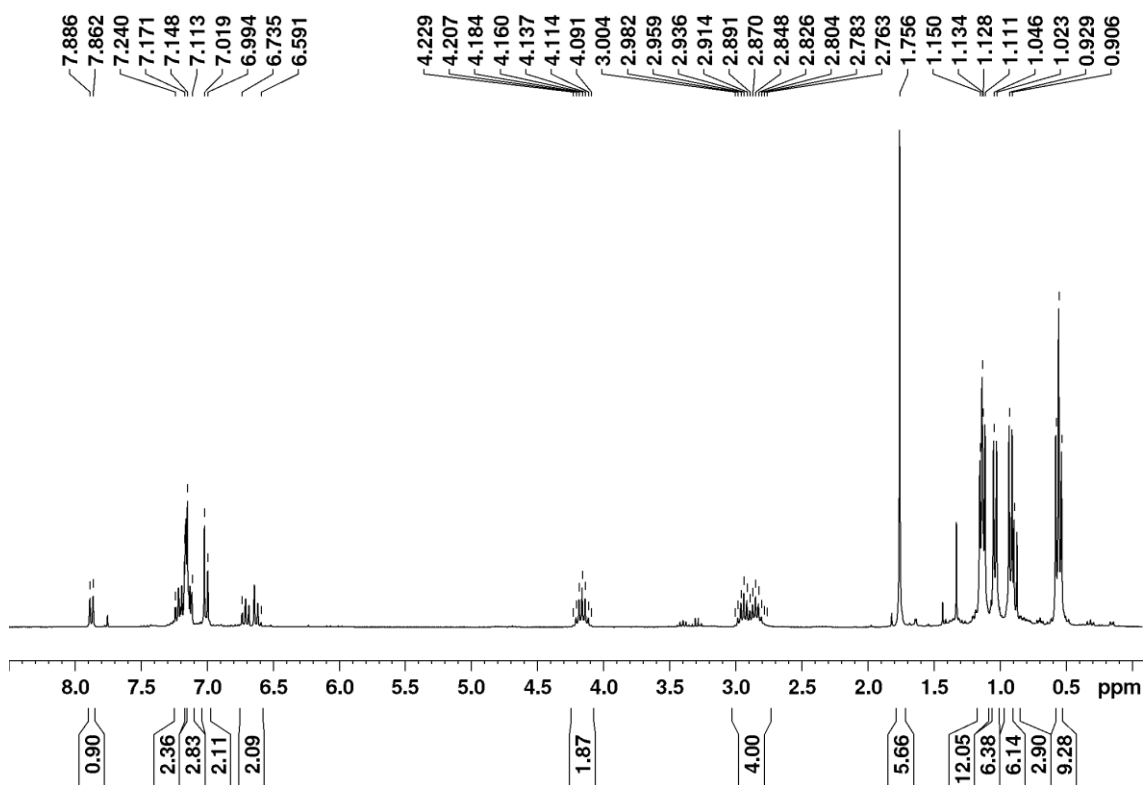


Figure 31. ^1H NMR spectrum of the reaction between benzazaborole **136** and perfluorinated triphenylborane (**143**).

The ^{11}B NMR spectrum (Figure 32), however, shows the expected sharp signal of the NHC-borane complex (-16.5 ppm^[213]) only as minor component in the reaction mixture. One major, very broad resonance at -2.9 ppm and one additional sharp signal at 10.0 ppm (unidentified side product) of much lower intensity is identified. Hence both boron centers in the main product must be represented by the broad resonance at -2.9 ppm and therefore be tetracoordinate. The ^{19}F NMR spectrum (Figure 33) shows mainly the three resonances at -131.48 ppm, -160.75 ppm and -166.16 ppm in the required 2:1:2 ratio.

3. Results and Discussion

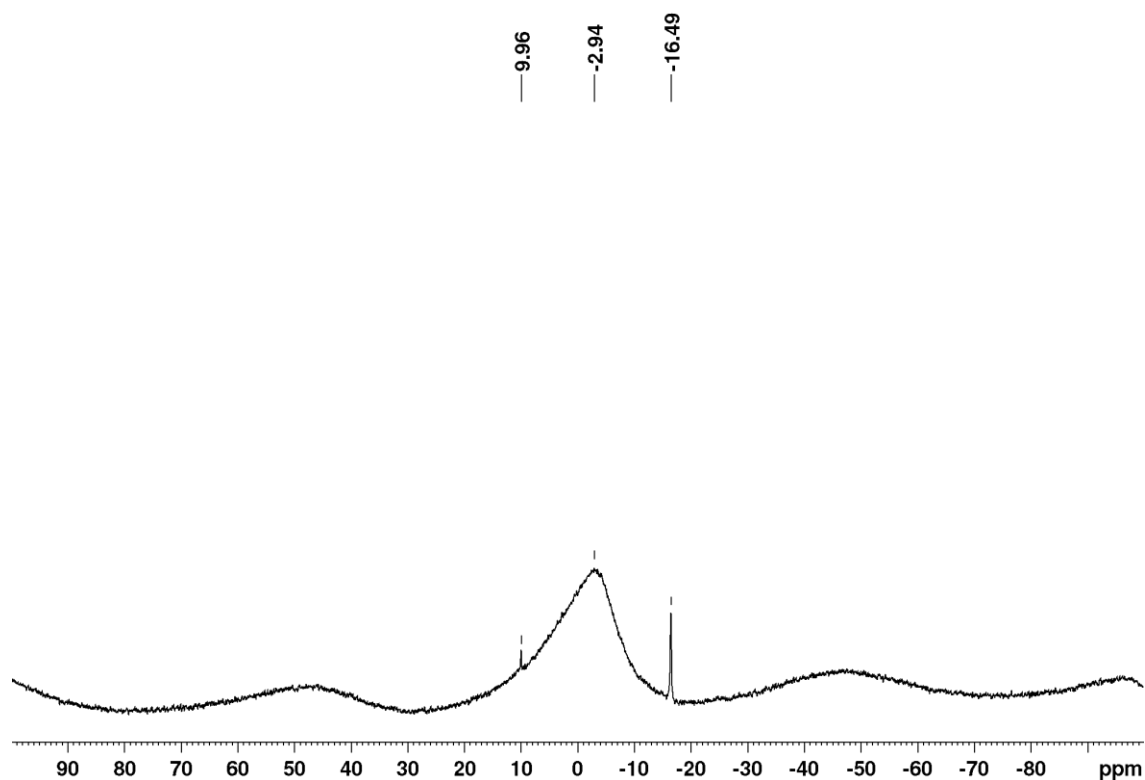


Figure 32. ^{11}B NMR spectrum of the reaction between benzazaborole **136** and perfluorinated triphenylborane (**143**).

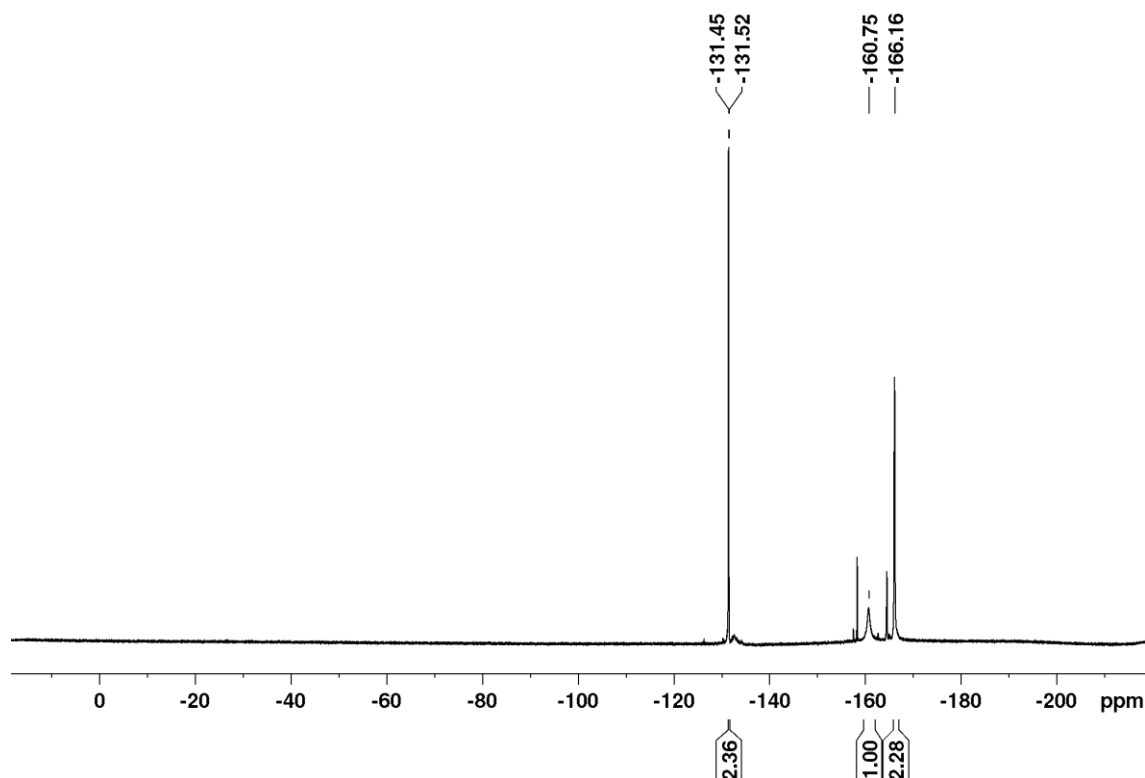
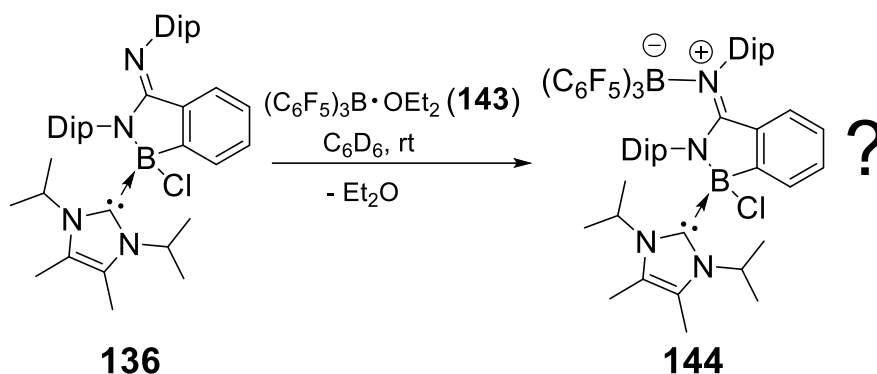


Figure 33. ^{19}F NMR spectrum of the reaction between benzazaborole **136** and perfluorinated triphenylborane (**143**).

On the basis of the available data, the imine coordinated $\text{B}(\text{C}_6\text{F}_5)_3$ **144** (Scheme 43) is a plausible constitution for the product. The backbone of **136** is still intact

3. Results and Discussion

according to the ^1H NMR spectrum and both boron centers appear to be tetracoordinate. Given that only little $\text{NHC-B}(\text{C}_6\text{F}_5)_3$ complex appears to have been formed, according to the ^{11}B NMR spectrum, the double donor-acceptor complex **144** is the simplest remaining explanation.



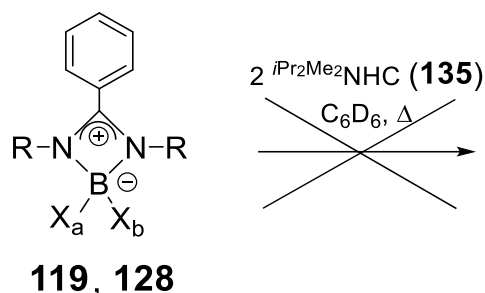
Scheme 43. Reaction between benzazaborole **136** and perfluorinated triphenylborane (**143**). (Dip = 2,6- $i\text{Pr}_2\text{C}_6\text{H}_3$)

3.4.3 Reactivity of further boron benzamidate complexes towards NHCs

To examine whether the discovered reaction pathways of benzamidate **104a** with *N*-heterocyclic carbenes (Section 3.4.1) are of general relevance, a selection of benzamidate complexes with other substituents were reacted with NHCs.

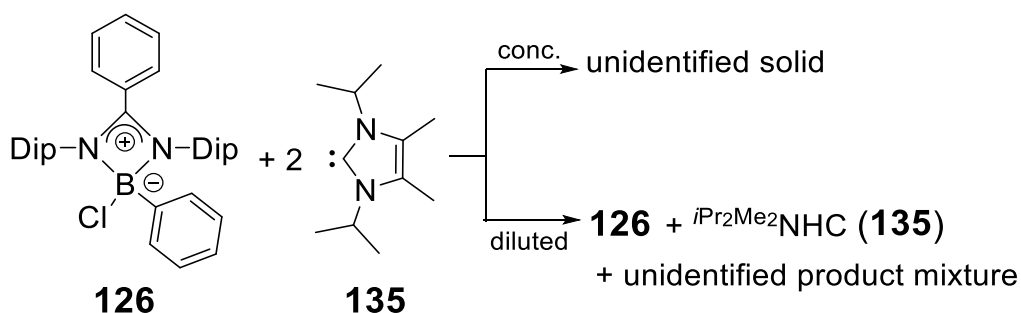
Boryl benzamidates **119** and **128** do not react with the sterically demanding $i\text{Pr}_2\text{Me}_2\text{NHC}$ at all, not even at elevated temperatures (Scheme 44). The reason in case of **119** is probably thermodynamic in nature, since the steric bulk is reduced compared to **104a** which does react with $i\text{Pr}_2\text{Me}_2\text{NHC}$ to benzazaborole **136** (see Section 3.4.1). In contrast, the reaction of **128** with $i\text{Pr}_2\text{Me}_2\text{NHC}$ is most likely kinetically inhibited because of significantly increased steric bulk compared to **104a** due to the presence of a cyclohexyl substituent at boron in addition to Dip groups at the nitrogen centers.

3. Results and Discussion



Scheme 44. Reactivity of benzamidinates **119** (R = ^tBu, X_a = X_b = Cl) and **128** (R = Dip, X_a = Cl, X_b = cyclohexyl) towards ⁱPr₂Me₂NHC **135**. (Dip = 2,6- ⁱPr₂C₆H₃)

The treatment of chlorophenylboryl benzamidinate **126** with one equivalent of ⁱPr₂Me₂NHC **135** (Scheme 45) in relatively concentrated C₆D₆-solution (0.2 M) results in an insoluble solid overnight, which was not further characterized. In an attempt to reduce solubility issues the reaction was carried out in a more diluted benzene solution (Scheme 45, 0.02 M). Even after 5 days at room temperature, however, the starting materials remain the major component detected in the ¹H NMR spectrum (**135**:**126** = 2:1) alongside minor unidentified products. Although the observed ¹¹B NMR signals at 12.6 ppm, 4.3 ppm and -4.5 ppm are likely due to tetracoordinate boron centers (Figure 34), the ¹H NMR is not in line with a benzazaborole structure analogous to **136**, since no signals are detected in the range (4.5 - 5.5 ppm) for the the low field shifted ⁱPr-CH signals of the coordinated NHC.



Scheme 45. Reactivity of chlorophenylboryl benzamidinate **126** towards ⁱPr₂Me₂NHC **135**. (Dip = 2,6- ⁱPr₂C₆H₃)

3. Results and Discussion

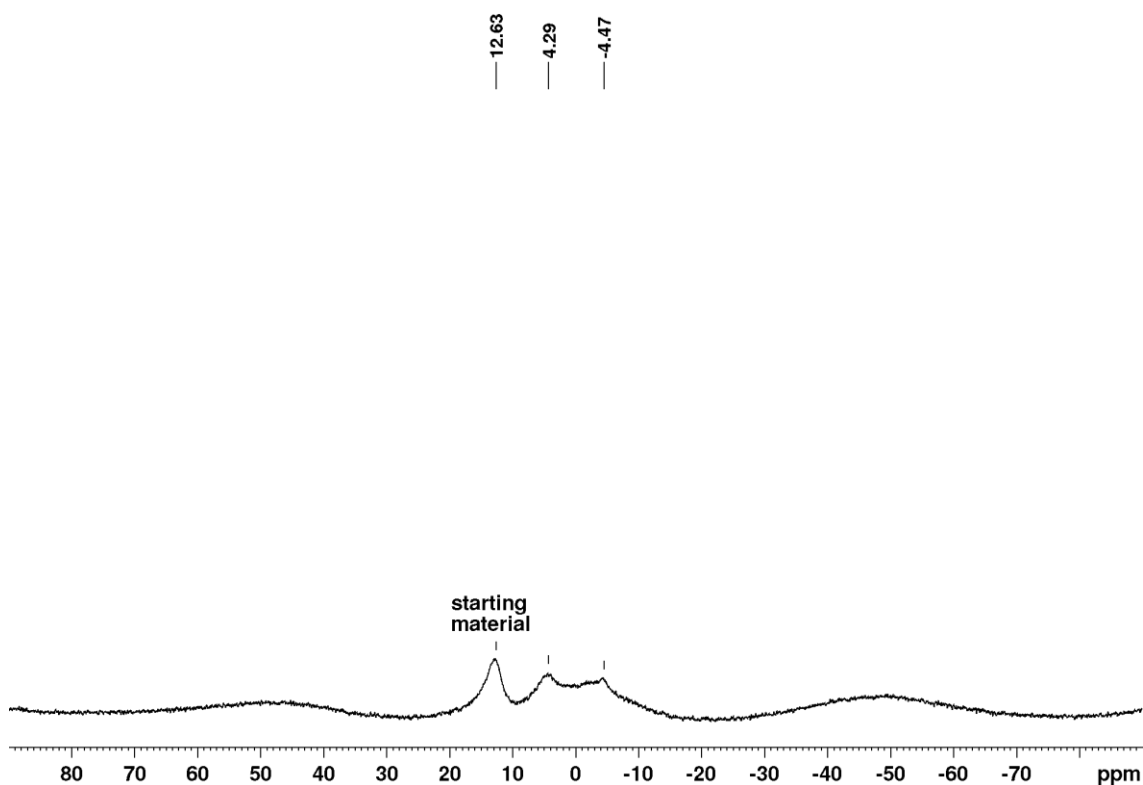
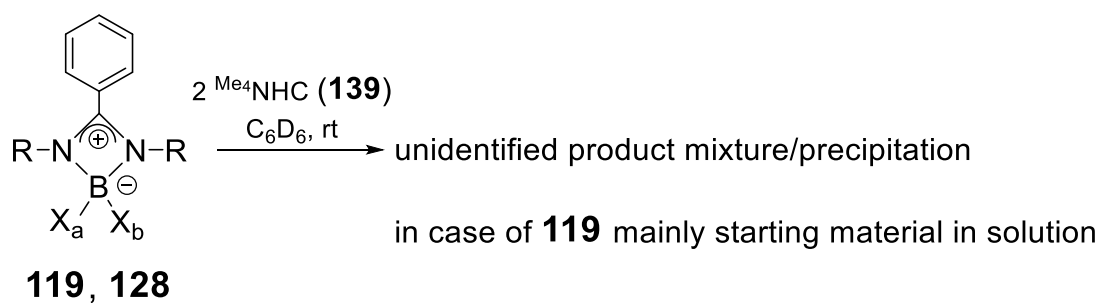


Figure 34. ^{11}B NMR spectrum of the reaction mixture after stirring 5 days at room temperature in benzene with $c = 0.02$ M.

In order to reduce kinetic hindrance by steric repulsion, **119** and **128** were reacted with the smaller Me_4NHC **139** (Scheme 46). Heavy precipitation of an insoluble solid was observed in both cases. The filtrate of the reaction of **119** was analyzed by ^1H and ^{11}B NMR spectroscopy showing mainly the starting material benzamidinate **119**.

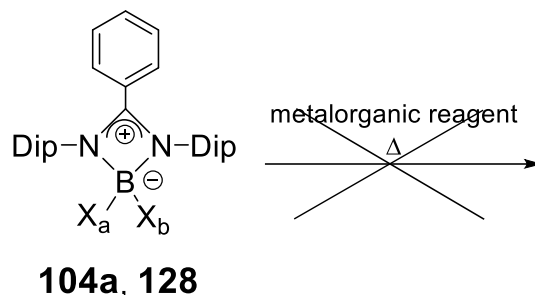


Scheme 46. Reactivity of benzamidinates **119** ($\text{R} = \text{tBu}$, $\text{X}_a = \text{X}_b = \text{Cl}$) and **128** ($\text{R} = \text{Dip}$, $\text{X}_a = \text{Cl}$, $\text{X}_b = \text{cyclo-hexyl}$) towards Me_4NHC **139**. ($\text{Dip} = 2,6\text{-iPr}_2\text{C}_6\text{H}_3$)

3. Results and Discussion

3.4.4. Reactivity of boron benzamidates towards metalorganic reagents

Since the reaction of benzamidinate complex **104a** with NHC to benzazaborole **136** (see Section 3.4.1) involves a deprotonation step, the question arose whether a similar transformation could also be effected by the reaction of strong anionic bases with the boron benzamidinate complexes.

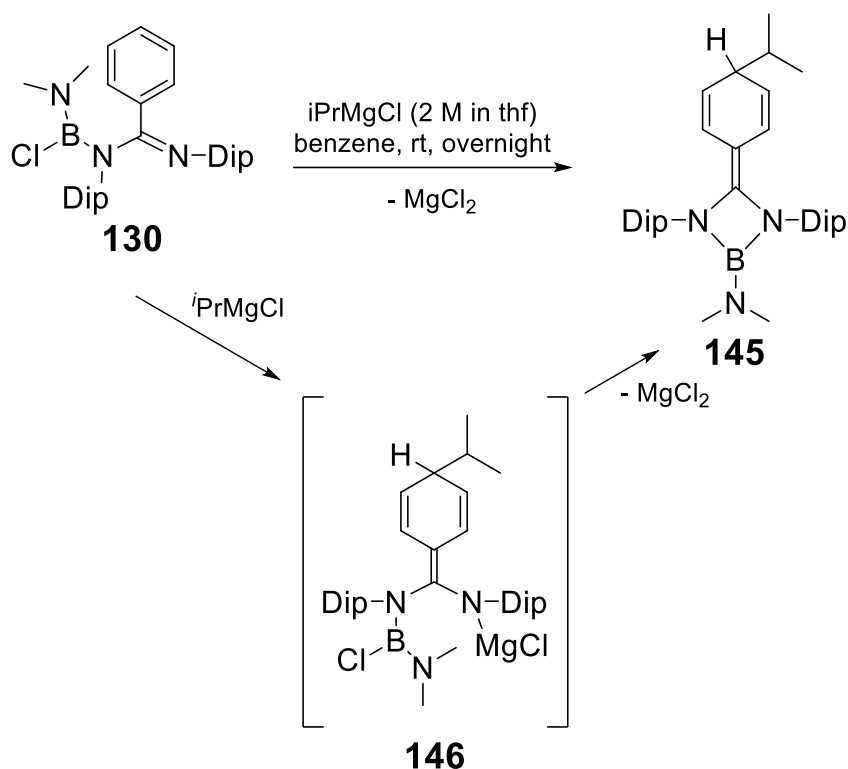


Scheme 47. Reactivity of benzamidates **104a** ($X_a = X_b = \text{Cl}$) and **128** ($X_a = \text{Cl}$, $X_b = \text{cyclohexyl}$) towards metalorganic reagents. (Dip = 2,6- $i\text{Pr}_2\text{C}_6\text{H}_3$)

Benzamidates **104a** and **128** were treated in an NMR scale reaction in C_6D_6 at room temperature with the following metalorganic reagents: $i\text{PrMgCl}$ (2 M solution in thf), $n\text{BuLi}$ (2.5 M solution in hexanes, only **104a**) and $\text{KN}(\text{SiMe}_3)_2$ (Scheme 47). In neither case any reaction could be observed by multinuclear NMR spectroscopy. Even elevated temperatures (60-70°C) could not invoke reactions between benzamidates **104a** and **128** and the metalorganic reagents.

In contrast, the amino-chloro-boryl benzamidinate complex **130** readily reacts with $i\text{PrMgCl}$ in a benzene/thf mixture, albeit not to the anticipated benzazaborole structure. Full conversion is reached overnight, and the formation of a uniform product was observed (Scheme 48).

3. Results and Discussion



Scheme 48. Synthesis and proposed mechanism of diazaboretidine **145**. (Dip = 2,6- $i\text{Pr}_2\text{C}_6\text{H}_3$)

The resonance in the ^{11}B NMR spectrum at 24.7 ppm indicates a tricoordinate aminoborane. In the ^1H NMR spectrum only six resonances are observed in the aromatic region, which are attributed to the Dip substituents without exception. Apparently, the phenyl ring underwent dearomatization and indeed two doublets at 5.93 and 4.90 ppm, each corresponding to two vinylic hydrogen atoms, support a cyclohexadiene structure. The doublet at 0.79 ppm with an integration of six protons strongly suggests that the isopropyl group had been incorporated into the product. Crystallization from a concentrated hexane solution at 0°C afforded single crystals in 23% yield. X-ray diffraction analysis confirmed the quinoidic structure **145** (Figure 35). The endocyclic B-N distances (N1-B1 1.460(1) Å, N2-B1 1.464(1) Å) are longer than those in the four membered ring **29** (1.410 Å, 1.412 Å) isolated by Jones and Aldridge.^{[43],[44]} The exocyclic B-N bond length (1.385(1) Å) is similar to that in Bertrand's four membered NHC (1.370 Å).^[35] The C1-C2-distance (1.357(1) Å) is shortened in comparison to the corresponding bond in the precursor molecule **130** (1.501(2) Å) confirming a substantial double bond character due to π -backdonation of the nitrogen lone pair into the vacant p-orbital at the boron center.

3. Results and Discussion

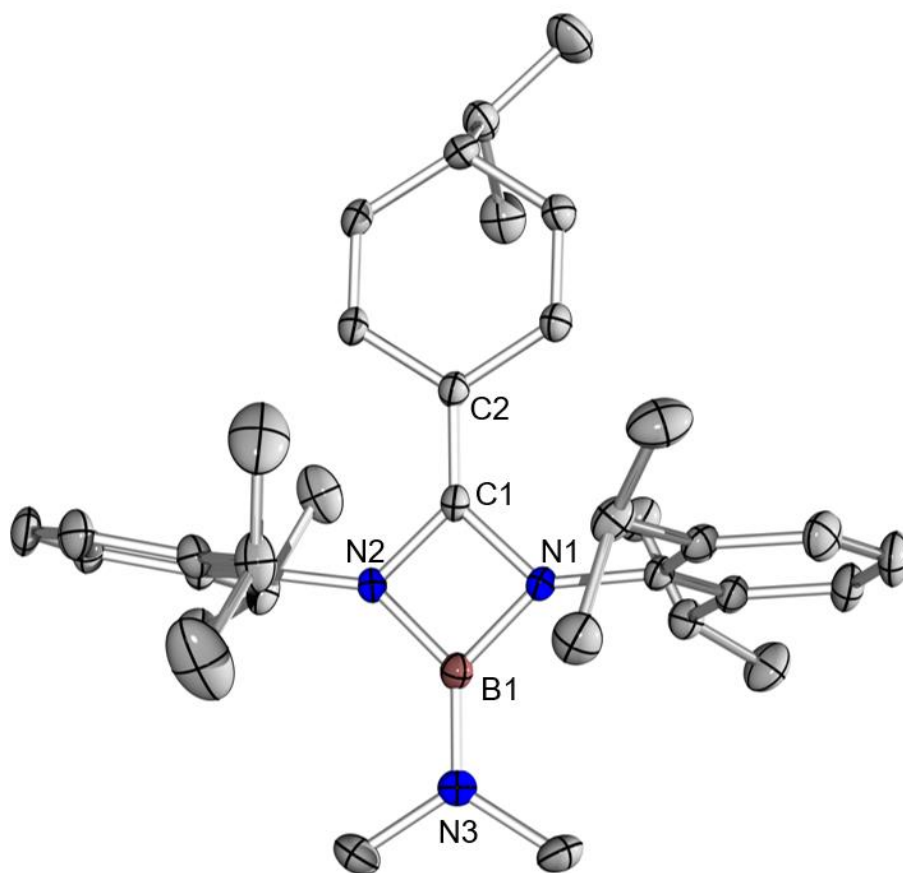
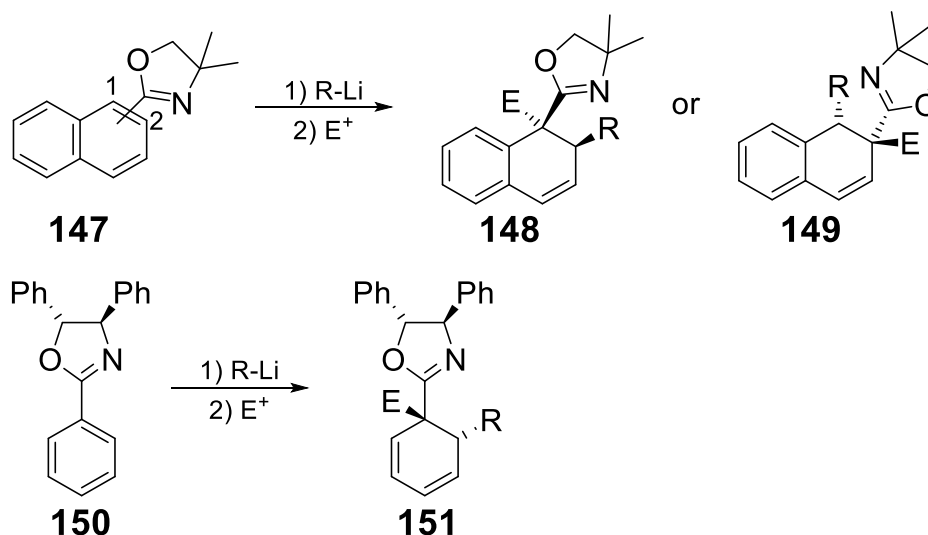


Figure 35. Molecular Structure of **145** in the solid state (ellipsoids at 50% probability, hydrogen atoms omitted for clarity). Selected bond lengths [Å] and angles [°]: N3-B1 1.385(1), N1-B1 1.460(1), N2-B1 1.464(1), N1-C1 1.417(1), N2-C1 1.421(1), C1-C2 1.357(1), N3-B1-N1 134.88(9), N3-B1-N2 135.21(9), N2-B1-N1 89.91(7), B1-N2-C1 88.11(7), B1-N1-C1 88.42(7), N2-C1-N1 93.47(7).

The reactivity of boron benzamidinates as electrophiles is generally not well explored, except for one example provided by Jones and Aldridge.^[43,44] Considering that the starting material **130** offers one other obvious electrophilic center at the chloroborane part, the nucleophilic dearomatization is somewhat surprising. However, this kind of reaction is widely known for naphthyl- and phenyl-oxazolines (Scheme 49), which are structurally similar to the amidine moiety in **130**.^[214-218]

3. Results and Discussion

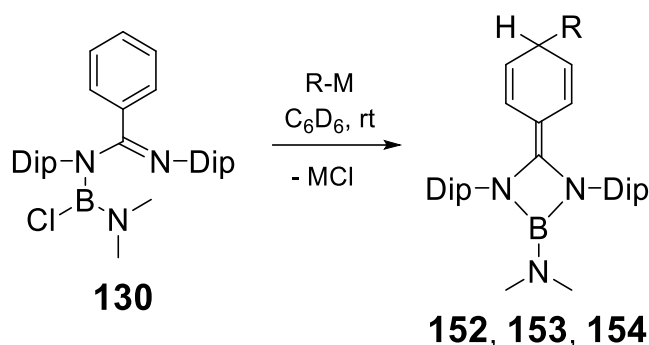


Scheme 49. Reactivity of naphthyl- and phenyl-oxazolines towards organolithium reagents.^[214,218]

The first reaction step is likely a 1,6-addition of the iso-propyl magnesium chloride resulting in intermediate **146** (Scheme 48). In contrast to the more prominent 1,4-addition^[214-218], the observed 1,6-addition is probably preferred due to steric hindrance at the *o*-phenyl-positions. The next logical step would be the nucleophilic attack of the amide nitrogen at the boron center followed by MgCl₂ elimination and formation of diazaboretidine **145**. In solution and in the ambient atmosphere, diazaboretidine **145** undergoes rapid and unselective oxidation. In the solid state, it tolerates exposure to air and moisture overnight. Under argon, no decomposition is observed upon prolonged heating above the melting point (mp. 145-147°C).

The reactivity of other metalorganic reagents, *i.e.* *n*-butyl lithium, potassium hexamethyldisilazide and lithium disilene^[219,220] towards **130**, was investigated in NMR scale reactions. ¹¹B and especially ¹H NMR spectra with the characteristic cyclohexadiene signals between 5.88 ppm and 4.81 ppm (Table 2) strongly suggest the formation of the analogous structural motifs **152**, **153**, **154** (Scheme 50). The crude product of the reaction between **130** and lithium disilene shows ²⁹Si NMR resonances at 75.9 ppm and 57.0 ppm, indicating the presence of an uncompromised Si=Si double bond in the product.^[219,220] The addition of ⁱPr₂Me₂NHC **135** to the reaction mixture of **130** with KHMDS in an attempt to modify the reactivity had no effect.

3. Results and Discussion



Scheme 50. Reactivity of chlorodimethylaminoboryl benzamidine **30** towards various metalorganic reagents. R-M = *n*BuLi, KHMDS, (Tip)₂Si=SiTipLi; **152**: R = *n*Butyl; **153**: R = N(SiMe₃)₂; **154**: R = Si(Tip)=Si(Tip)₂ (Dip = 2,6- *i*Pr₂C₆H₃, Tip = 2,4,6- *i*Pr₃C₆H₃)

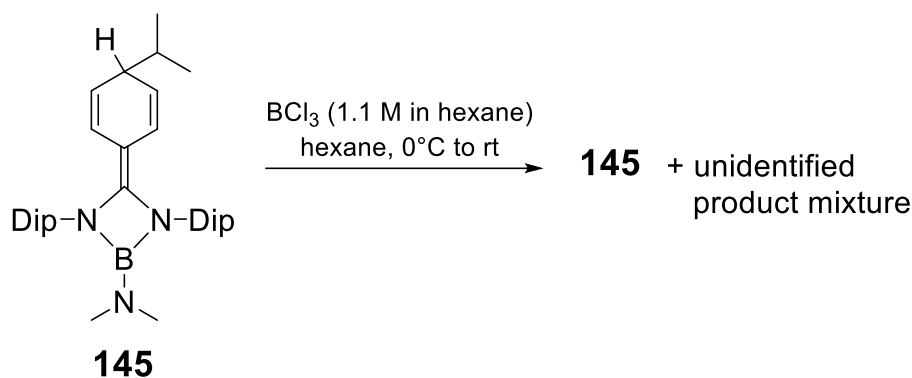
Table 2. Multinuclear NMR resonances of isolated diazaboretidine **145** and spectroscopically observed diazaboretidines **152**, **153** and **154**.

	¹ H NMR cyclohexadiene resonances [ppm]	¹¹ B NMR resonances [ppm]
145	5.93 (dd), 4.90 (dd)	24.7
152	5.88 (dd), 4.96 (dd)	24.6
153	5.74 (dd), 4.81 (dd)	24.9
154	5.58 (dd), 5.23 (dd)	26.7

3.4.5 Reactivity of diazaboretidine **145** - attempted exchange of NMe₂ with Cl

The NMe₂-group at the boron center is rather unreactive. Therefore, this boron center is unsuitable to transfer the whole structural motif to nucleophiles. It is well known that in a comproportionating reaction with half an equivalent of BCl₃ an NMe₂-group can be replaced by a chloro group thus generating an electrophilic, site at the boron center.^[92,221,222] Accordingly, diazaboretidine **145** was dissolved in hexane, cooled to 0°C and 0.5 equivalents of BCl₃ solution in hexane was added dropwise *via* syringe (Scheme 51).

3. Results and Discussion



Scheme 51. Reaction between diazaboretidine **145** and BCl_3 . (Dip = 2,6- $\text{iPr}_2\text{C}_6\text{H}_3$)

After warming to room temperature and removal of solvents in vacuum and other volatile components, ^{11}B NMR spectroscopic analysis of the reaction mixture (Figure 36) showed starting material (24.8 ppm) and several tetracoordinated boron species (9.9 ppm, 8.5 ppm, 7.0 ppm, 2.8 ppm (br s)).

Storage at 5°C overnight in C_6D_6 resulted in the consumption of starting material and only one broad resonance with low intensity in the ^{11}B NMR spectrum (Figure 37), meaning that the reaction was not finished yet, when the first NMR spectra were recorded. Thus, reaction time probably needs to be extended.

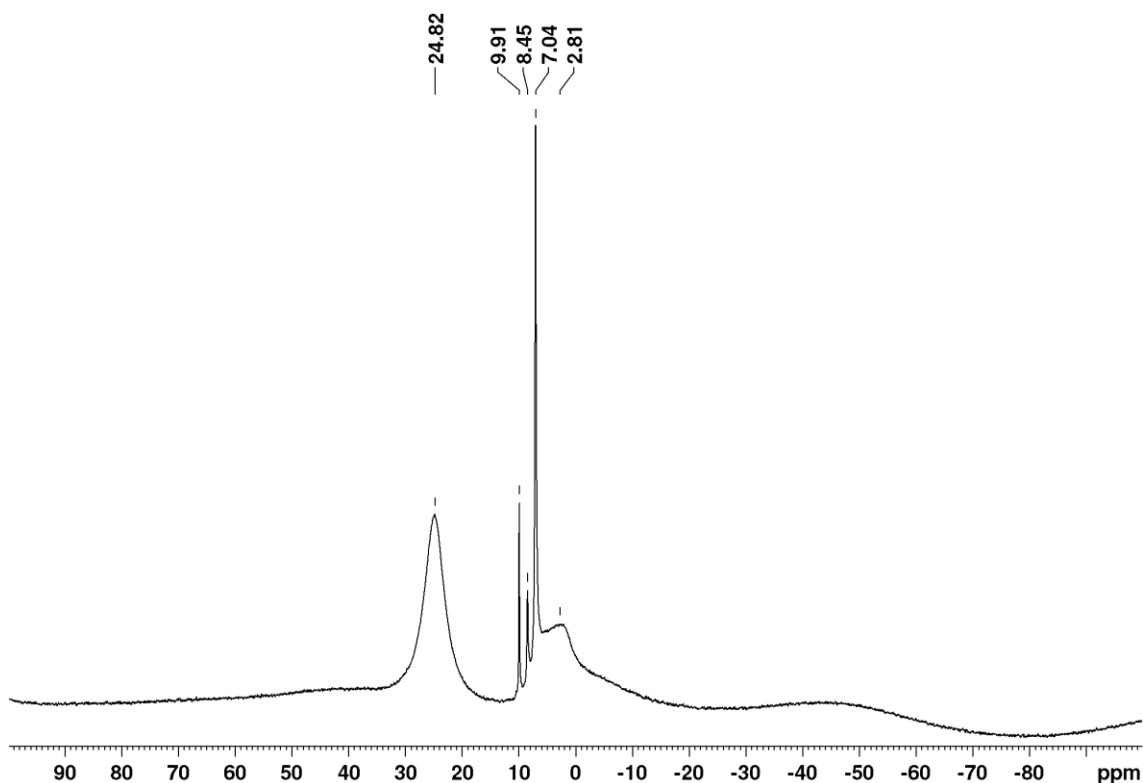


Figure 36. ^{11}B NMR spectrum of the reaction between diazaboretidine **145** and BCl_3 after warming to room temperature.

3. Results and Discussion

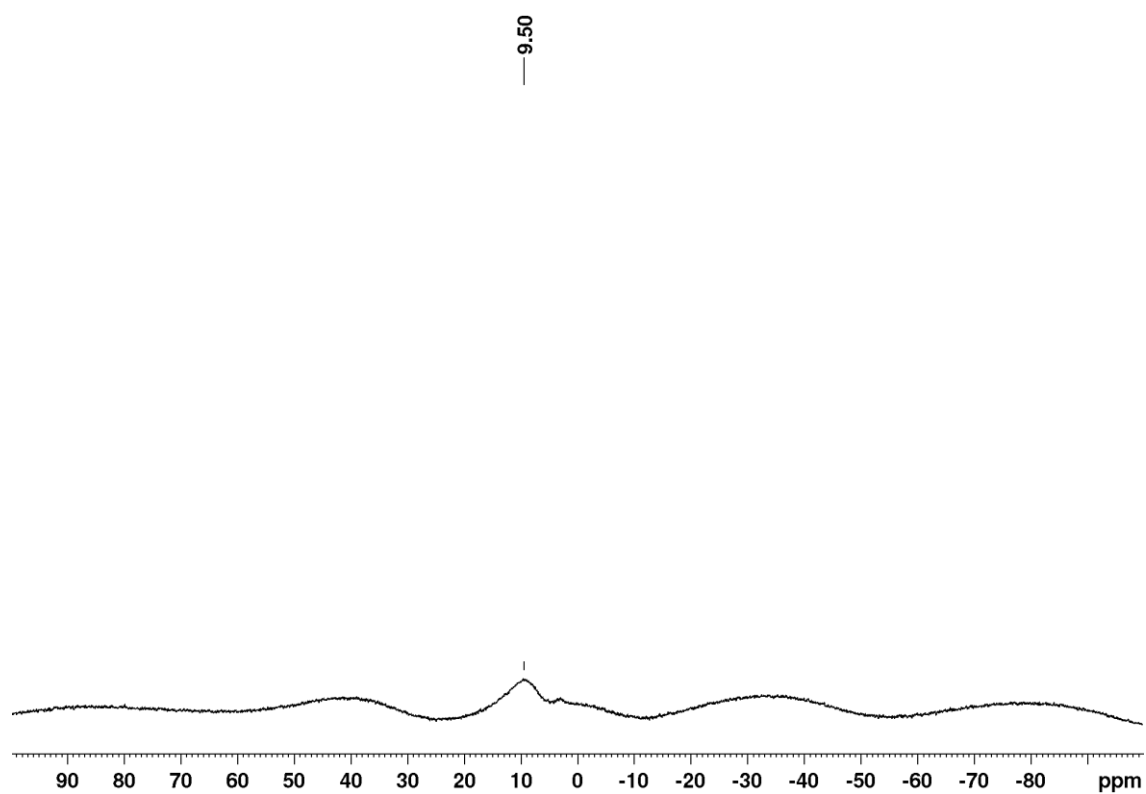
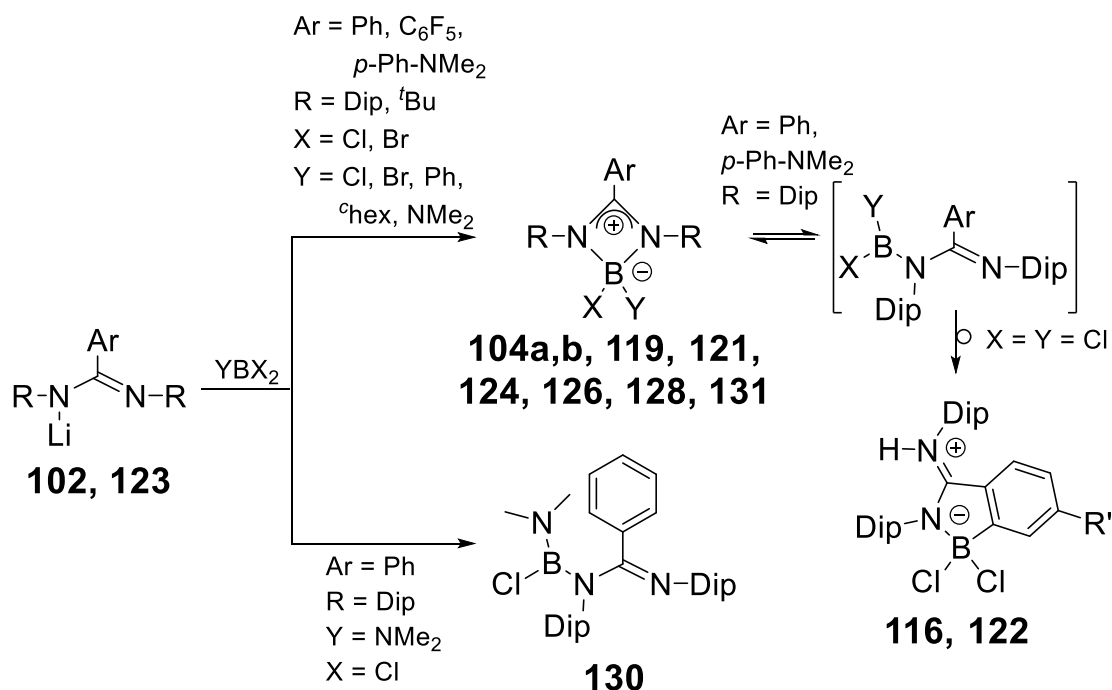


Figure 37. ^{11}B NMR spectrum of the reaction between diazaboretidine **145** and BCl_3 after storage overnight at 5°C .

3.5 Concluding Remarks

In summary, in this part of the PhD thesis the synthesis and reactivity of boryl amidinates was reported. They were routinely generated by salt metatheses of lithium amidinates and haloboranes. A great benefit of this synthetic strategy is the easy variation of ancillary substituents of the ligand system. The ligand-combination of *N*-Dip substituted chloro-dimethylamino-boryl benzamidinate leads to the isolation of the open chained derivative **130**, in stark contrast to the *N,N*-chelating form adopted by the other boryl amidinates **104a**, **119**, **124**, **126**, **128** and **131** (Scheme 52). Boryl benzamidinates **104b** and **121** as well as benzazaboroles **116** and **122**, which were postulated as rearrangement products of **104a** and **121**, respectively, could only be detected NMR spectroscopically (Scheme 52).

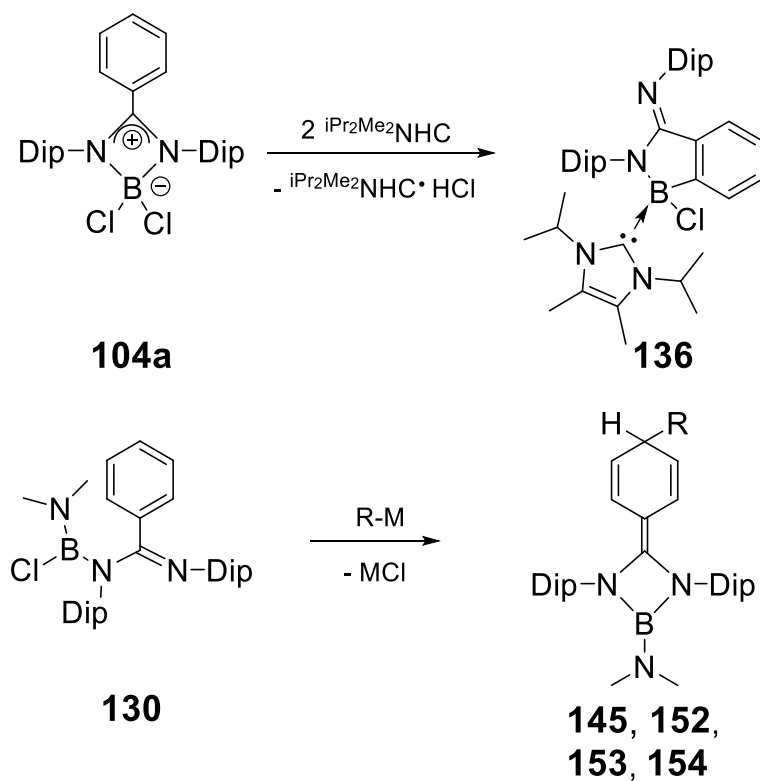


Scheme 52. Reported boryl benzamidinates **104a**: Ar = Ph, R = Dip, X = Y = Cl, ; **104b**: Ar = Ph, R = Dip, X = Y = Br, **119**: Ar = Ph, R = ^tBu, X = Y = Cl, **121**: Ar = Ph-NMe₂, R = Dip, X = Y = Cl, **124**: Ar = C₆F₅, R = Dip, X = Y = Cl, **126**: Ar = Ph, R = Dip, X = Cl, Y = Ph, **128**: Ar = Ph, R = Dip, X = Cl, Y = cyclohexyl, **130**, **131**: Ar = Ph, R = ^tBu, X = Cl, Y = NMe₂ and rearrangement products **116**: R' = H and **122**: R' = NMe₂. (Dip = 2,6- *i*Pr₂C₆H₃)

While several attempts to reduce (*E*)-*N*-(dihaloboryl)-*N,N'*-bis(2,6-diisopropylphenyl)-benzimidamides **104a,b** did not afford the targeted amidinate stabilized borylene, the reaction of **104a** with two equivalents of ^{*i*}Pr₂Me₂NHC yielded another benzazaborole, **136** (Scheme 53). Reactions of the synthesized boryl amidinates with anionic nucleophiles lead to dearomatization of the phenyl

3. Results and Discussion

ring only in case of the open-chained **130**. The thus isolated diazaboretidine **145** was fully characterized and further derivatives **152-154** were detected NMR spectroscopically (Scheme 53).



Scheme 53. Reported reactivity of boryl benzamidinate **104a** towards $i\text{Pr}_2\text{Me}_2\text{NHC}$ to yield **136** and reported reactivity of boryl benzamidinate **130** towards metalorganic reagents to yield isolated **145**: $\text{R} = \text{iPr}$ and observed **152**: $\text{R} = \textit{n}$ butyl, **153**: $\text{N}(\text{SiMe}_3)_2$ and **154**: $\text{R} = \text{Si}(\text{Tip})=\text{SiTip}_2$. (Dip = 2,6-diisopropylphenyl, Tip = 2,4,6-triisopropylphenyl)

3.6. Syntheses and spectroscopic studies of diboranes(4)

The luminescence of three-coordinate arylmonoboranes has been thoroughly investigated leading to numerous applications^[223-230], e.g. as anion sensors^[231-234], in bioimaging^[235-239], or as OLED materials^[16,17,162-170]. The boron center with its formally vacant p_z -orbital mostly acts as π -acceptor. In particular the BMe₂-group is frequently applied due to its strong electron-accepting properties combined with relative inertness towards oxygen and moisture due to steric congestion.^[171-189] Through introduction of appropriate donors, e.g. amino substituents,^[240] mediated by a suitable π -conjugated linking unit,^[184,187,241-248] the HOMO-LUMO gap can be narrowed, in some cases down to energy values corresponding to transitions in the near-IR.^[249-254] Even simple donor substituents such as 4-*N,N*-dimethylaniline lead to a red-shift of the longest wavelength absorption and emission bands.^[171,178] In addition, the HOMO-LUMO gap is further affected by increasing the inherent electron-deficiency at the boron center by incorporation of electron-withdrawing substituents.^[243,255,256] Notably, diboranes(4) have rarely been investigated in this regard.

The effect of donor-acceptor substitution (i.e. electron-rich and electron-poor substituents in the same molecular entity) to the boron centers of simple 1,2-bis(dimethylamino)diboranes(4), modified cyclic 1,4-diaza-2,3-diborinane derivatives and donor-free 1,2-diduryldiboranes(4) was examined in this PhD thesis.

3.6.1 Syntheses and spectroscopic studies of 1,2-bis(dimethylamino)-diboranes(4)

Diboranes(4) were discovered as early as 1925^[19,90] making available a versatile and extremely useful class of reagents. In particular, the isolation of the remarkably stable tetrakis(dimethylamino)diborane(4) (already observed by Urry *et al.* in 1954^[91]) by Brotherton and co-workers in 1960^[92] opened up a wide range of synthetic possibilities. For example, the treatment of tetrakis(dimethylamino)diborane(4) with HCl^[93] or BX₃ (X = Cl, Br)^[94,95] yields the mixed 1,2-bis(dimethylamino)-1,2-dihalo-diboranes(4), which can subsequently be converted to various 1,2-diorganyl-1,2-

3. Results and Discussion

bis(dimethylamino)diboranes(4) by reaction with aryl and/or alkyl lithium compounds.^[19,95,105,108,110,111] Transformation of the amino into chloro groups^[98,104] and subsequent treatment with two further equivalents of organolithium reagents provides access to donor-free tetraaryldiboranes(4) (see Section 1.4).^[120,122-124]

Based on literature-reported procedures for analogous substitution reactions the introduction of one 4-(dimethylamino)phenyl substituent to 1,2-dichloro-1,2-bis(dimethylamino)-diborane(4) **54a** was envisaged.^[93-95,257] 4-(Dimethylamino)phenyllithium (**155**) was prepared from 4-bromo-*N,N*-dimethylaniline and *n*BuLi in diethylether at low temperatures according to a modified literature procedure^[258] and isolated by filtration from hexane and washing with hexane prior to use. Reaction of dichlorodiborane(4) **54a** with an ethereal solution of the phenyllithium derivative **155** at -78°C afforded primarily diborane(4) **156** (Scheme 54) as indicated by the ^1H NMR spectrum (Figure 38). Subsequently **156** was isolated as bright yellow crystals in acceptable yield (46%). The ^{11}B NMR spectrum of purified **156** shows one broad signal at 43.9 ppm within the expected range for 1,2-bis(dimethylamino)diboranes(4).^[19] Considering the symmetry of the anticipated product^[95,257], two signals would be expected for **156**, which are probably too close in chemical shift to be resolved. The presence of five ^1H NMR signals between 2.88 and 2.77 ppm in the dimethylamino region with relative intensities corresponding to 18H atoms altogether, however, unambiguously proves that only monosubstitution has occurred. The signal at 2.87 ppm is of double the intensity than the four others suggesting chemically equivalent methyl groups and thus free rotation of one of the amino groups. This signal is assigned to the phenylogous NMe_2 group as its π -donation is expected to be weaker than in the cases of the directly boron-bonded NMe_2 groups. Diborane(4) **156** is sensitive to air and moisture in solution and the solid state.

3. Results and Discussion

($\Sigma \alpha = 355.9^\circ$), presumably as a consequence of the comparatively weaker donor ability due to the phenylogous extension confirming the conclusions from the ^1H NMR data. Moreover, the angle between the phenyl-ring plane normal and the B-B bonding axis amounts to 43.53° which shows significant deviation from the ideal 90° . The N3-C8 distance of $1.384(1)$ Å demonstrates as well that π -donation of the phenyl-bonded NMe_2 group is of smaller importance than in, for instance, $p\text{-Me}_2\text{N}(\text{C}_6\text{H}_4)\text{BMes}_2$ as characterized by Marder *et al.*^[178] in which the phenylene-bonded NMe_2 group as the strongest donor in the molecule is coordinated in a trigonal planar fashion and the N-C distance is accordingly shorter (1.368 Å).

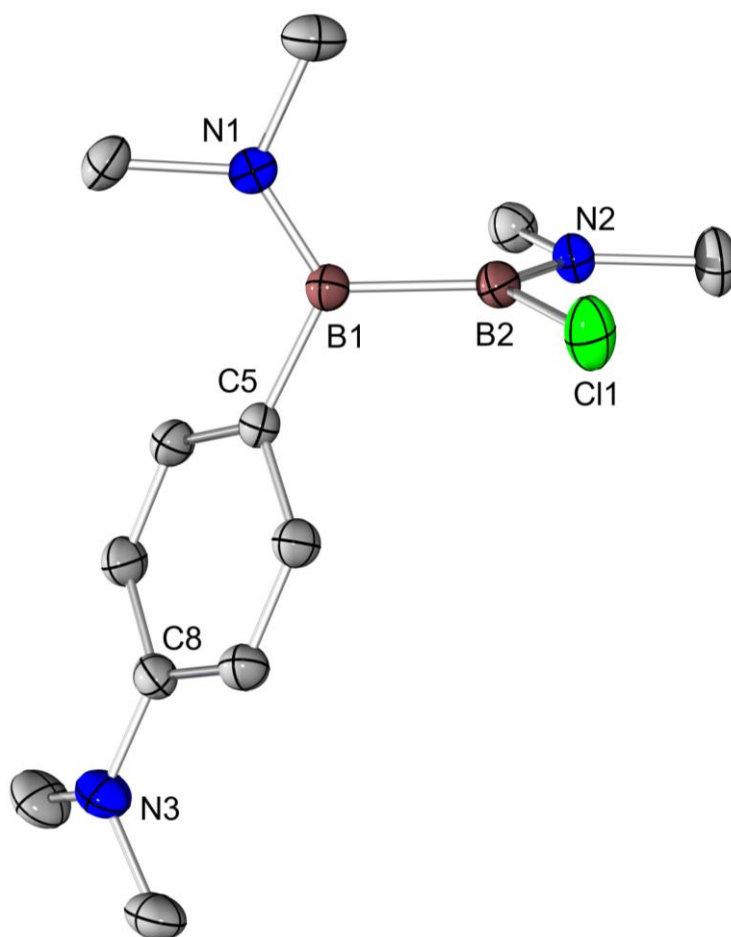


Figure 39. Molecular structure of **156** in the solid state (ellipsoids at 50% probability, hydrogen atoms and chlorine disorder omitted for clarity). Selected bond lengths [Å] and angles [°]: B1-B2 $1.702(2)$, B1-N1 $1.395(1)$, B2-N2 $1.386(1)$, B1-C5 $1.577(1)$, B2-Cl1 $1.829(1)$, C8-N3 $1.384(1)$, $\Sigma \angle$ B1 360.0 , $\Sigma \angle$ B2 360.0 , $\Sigma \angle$ N1 360.0 , $\Sigma \angle$ N2 360.0 , $\Sigma \angle$ N3 355.9 , angle between B coord. Planes $89.2(2)$.

UV/Vis spectroscopic studies of a solution of diborane(4) **156** ($c = 0.7$ to 1 mM) in hexane shows one absorption band maximum at 282 nm with an extinction coefficient of $\epsilon = 13200$ $\text{M}^{-1} \text{cm}^{-1}$. The absorption spectrum at $c = 5$ μM in

3. Results and Discussion

preparation for fluorescence measurements (Figure 40), however, showed two maxima, one at 284 nm similar to the one before and one at 320 nm. Fluorescence was detected only upon excitation of the second band, (Figure 40) with a maximum at 359 nm and a quantum yield of >95% (determined by Ulbricht sphere).

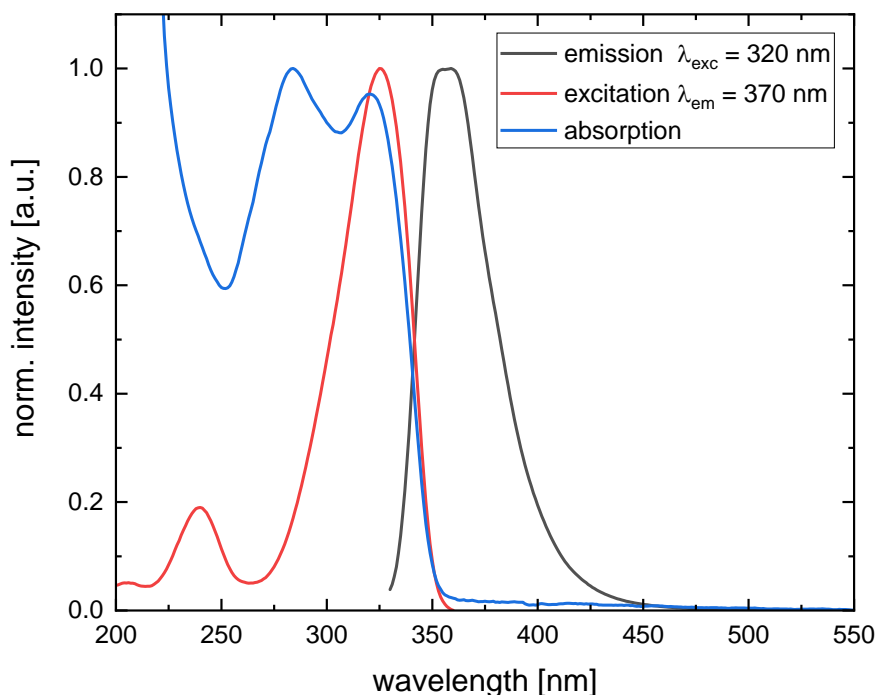


Figure 40. Absorption (blue), excitation (red) and emission (black) spectra of 1,2-bis(dimethylamino) diborane(4) **156** in hexane (5 μ M).

Investigation of the influence of air on the absorption spectrum revealed that the band at 320 nm represents an unknown intermediate on the way to an equally unknown hydrolysis product mixture. Figure 41 shows the changes in the UV spectrum of a 5 μ M hexane solution in a 10 mm cuvette at first under argon (violet), then exposed to air in a timespan up to 130 minutes (orange). Starting with an absorption band at 286 nm, an intermediate species is detected with an absorption band maximum at 324 nm. This intermediate then is converted to another species with an absorption band maximum at 280 nm, which fits perfectly to the absorption band found for a deliberately hydrolyzed sample of **156** (red).

3. Results and Discussion

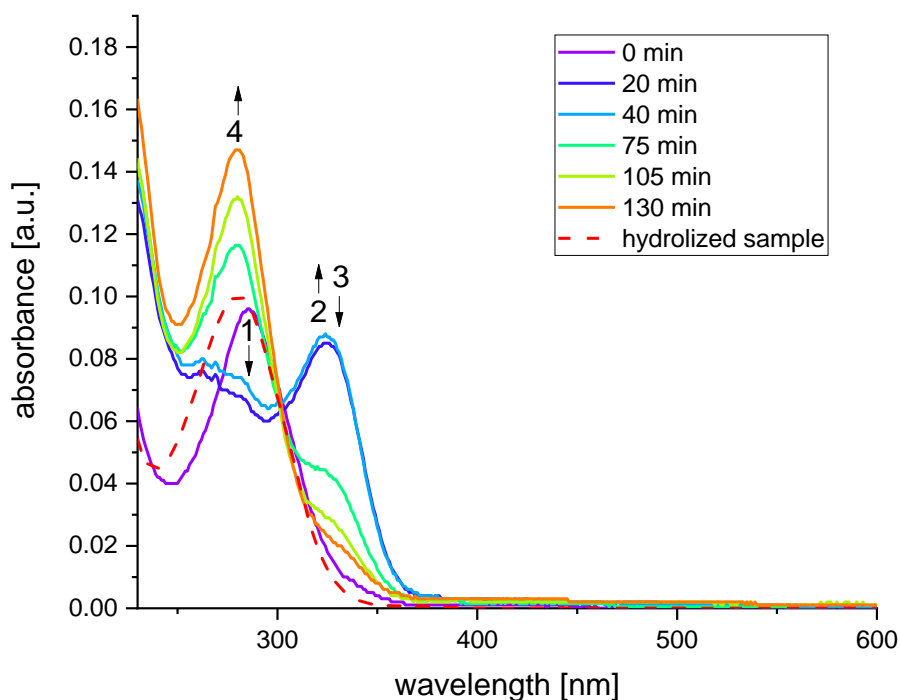


Figure 41. UV/Vis spectra of a 5 μM solution of **156** in hexane under the influence of air (violet to orange) and one UV/Vis spectrum of a hydrolyzed sample of **156** (red) in hexane. **1**: decreasing absorption band at 286 nm/ consumption of diborane(**4**) **66**; **2**: increasing absorption band at 324 nm/ accumulation of the intermediate species; **3**: decreasing absorption band at 324 nm/ consumption of the intermediate species; **4**: increasing absorption band at 280 nm/ formation of the hydrolysis product.

Hydrolysis of **156** was carried out in hexane with one equivalent of degassed water under argon atmosphere in the presence of triethylamine to capture the liberated HCl. The reaction mixture was stirred overnight. Subsequently all volatiles were removed and filtration from benzene was followed by drying *in vacuo*. Analysis of an NMR sample revealed a uniform product formation with ^{11}B NMR resonances at 48.8 ppm and 36.7 ppm in the typical range for amino-, or oxy-substituted diboranes and a minor side product with a signal at 0.7 ppm in the typical range for tetracoordinated boron species (Figure 42). Evaluation of the ^1H NMR did not lead to an unambiguous structure determination. Typical doublets at 7.59 ppm and 6.79 ppm in the ratio 1:1 and an integration of 2H each strongly suggest the retention of the *para*-dimethylamino group in the product. Singlets at 2.94 ppm, 2.90 ppm, 2.78 ppm, 2.59 ppm and 2.02 ppm (br) with an integration of altogether 30H suggests the presence of five dimethylamino-groups per aniline-group. Since no product was isolated, the possibility exists, that some of those signals belong to the side product already observed in the ^{11}B NMR spectrum. In conclusion, a structure proposal cannot be made at this point.

3. Results and Discussion

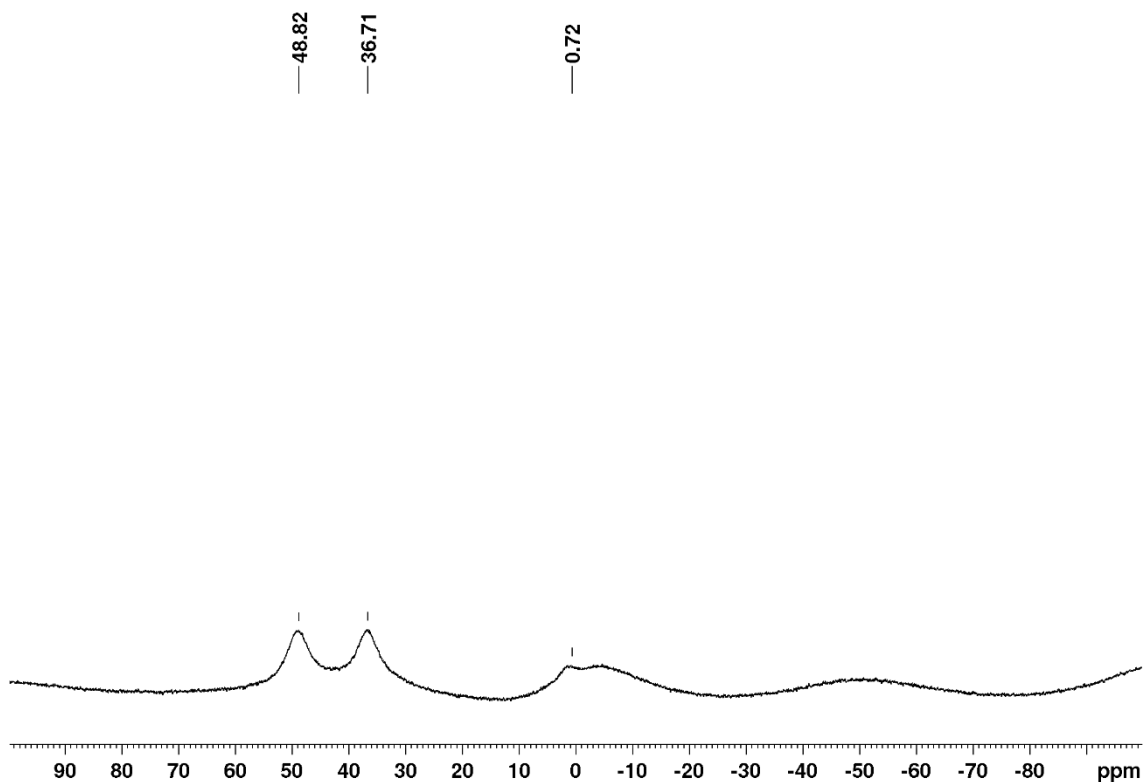


Figure 42. ^{11}B NMR of a hydrolyzed sample of diborane(4) **156**.

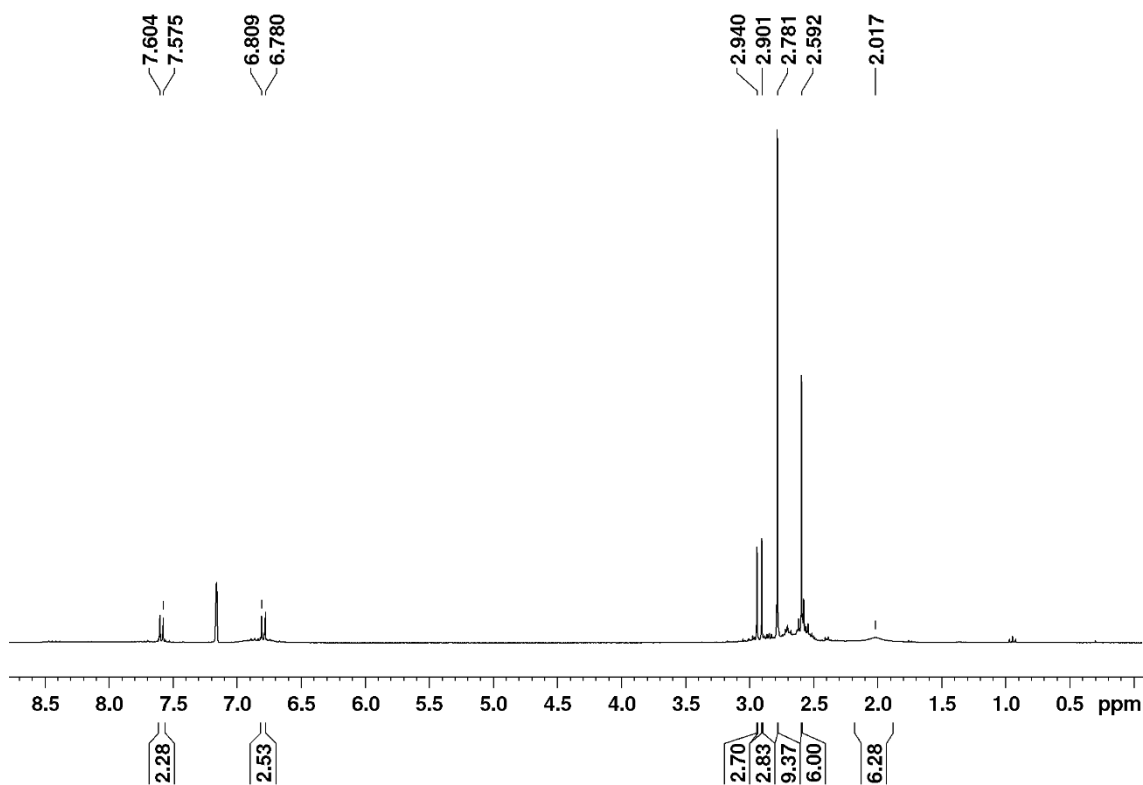


Figure 43. ^1H NMR of a hydrolyzed sample of diborane(4) **156**.

To gain insight into the decomposition modes of **156**, cyclic voltametric measurements were performed with a platinum working electrode, a platinum counter electrode, a silver quasi-reference electrode, $\text{Bu}_4\text{N}^+\text{PF}_6^-$ ($c = 0.1 \text{ M}$) as

3. Results and Discussion

conductive salt and ferrocene ($c = 0.3 \text{ mM}$) as external reference. Since oxidative decomposition of **156** was suspected, the cyclic voltammetric measurements focused on comparably high potentials. Dry dichloromethane was chosen as solvent because of its wide positive range. Figure 44 shows the cyclic voltammogram, which was recorded without ferrocene for clarity reasons. Presence of oxygen in the measuring solution can be excluded as the first reduction step of the oxygen reduction reaction (ORR) is reported at -0.79 V in dichloromethane and no reduction wave was observed in Figure 44.^[259] For **156** two oxidation steps are detected: one at 0.56 V and one at 1.43 V , whereby only the first seems to be quasi-reversible under the conditions of the measurement. Clearly, in both cases the electron transfer is followed by an irreversible homogeneous chemical reaction, probably due to the use of dichloromethane. Indeed, in thf the first oxidation step shows reversibility (Figure 45), but the second one is outside the measuring window. Since *N,N*-dimethylaniline (DMA) is known to exhibit an oxidation wave at 0.76 V vs. SCE (standard calomel electrode) in acetonitrile^[260] it is likely that the *N,N*-dimethylaminophenyl moiety in **156** is oxidized in the voltametric process. It has even been shown by rapid scan cyclic voltammetry that this oxidation can be reversible, as observed for **156** (Figure 45), when the scan rate is faster than the dimerization reaction of $\text{DMA}^{\bullet+}$ to tetramethylbenzidine.^[260,261] In contrast to the investigations in this thesis, reduction is mostly observed for aryl-/pinacolato-diboranes(4). Yamashita reports on cyclic voltammetric measurements in thf with one reduction step for the diboranes(4) *o*-tol₂B-Bo-tol₂ (-2.1 V vs. $\text{Cp}_2\text{Fe}/\text{Cp}_2\text{Fe}^+$)^[122] and pinB-BMes₂ (-2.5 V vs. $\text{Cp}_2\text{Fe}/\text{Cp}_2\text{Fe}^+$)^[159]. Because of these far negative potentials and the fact that B₂pin₂ does not show a reduction potential within the measuring window of thf^[159] it can be expected that the reduction potential of **156** lies outside of the applied measuring window.

3. Results and Discussion

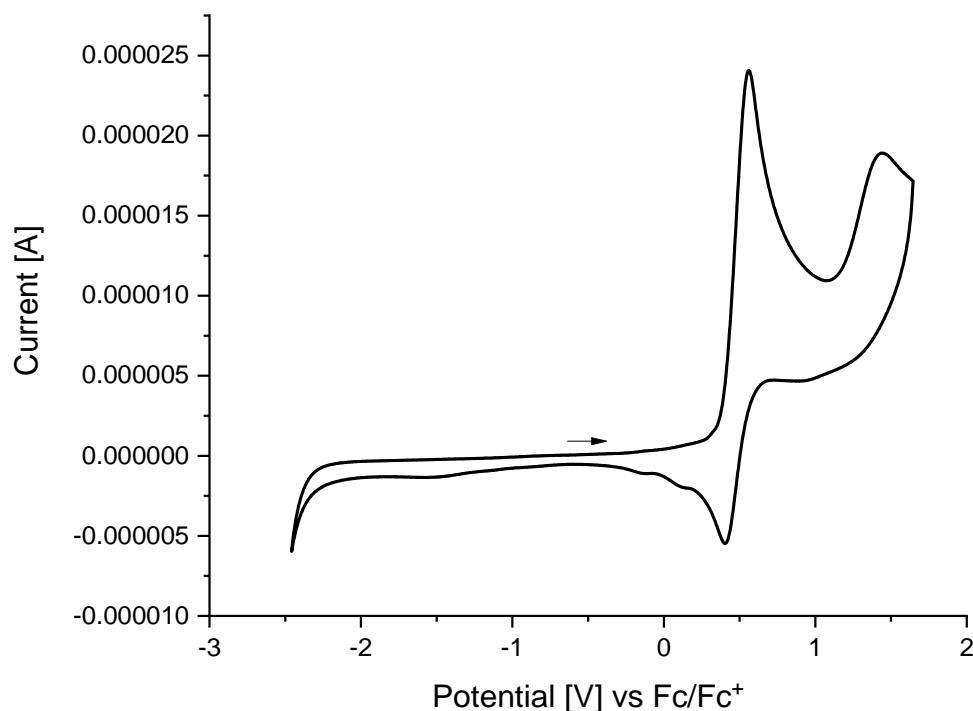


Figure 44. Cyclic voltammogram of **156** in dichloromethane ($c = 3 \text{ mM}$), with a platinum working electrode, a platinum counter electrode, a silver quasi reference electrode, scan rate at 100 mV s^{-1} and $\text{Bu}_4\text{N}^+\text{PF}_6^-$ ($c = 0.1 \text{ M}$) as conductive salt.

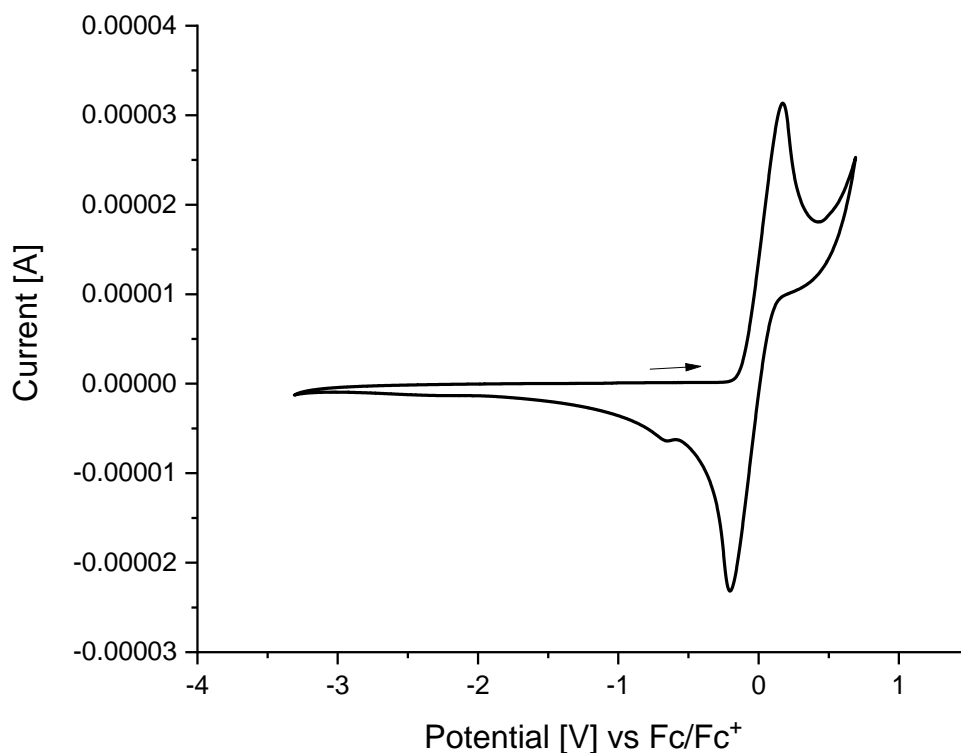
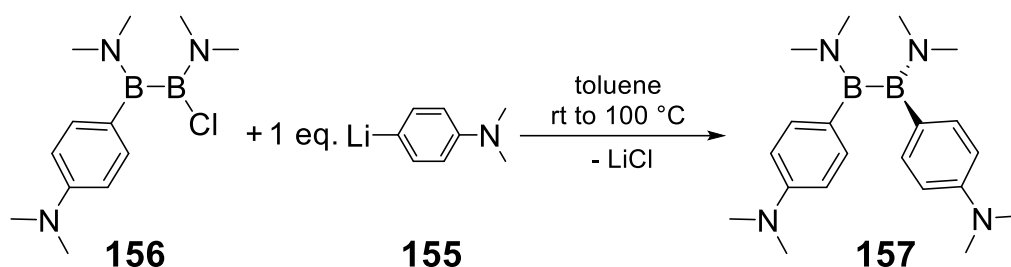


Figure 45. Cyclic voltammogram of **156** in thf ($c = 3 \text{ mM}$), with a platinum working electrode, a platinum counter electrode, a silver quasi reference electrode, scan rate at 100 mV s^{-1} and $\text{Bu}_4\text{N}^+\text{PF}_6^-$ ($c = 0.1 \text{ M}$) as conductive salt.

The symmetric 1,2-bis(dimethylamino)diborane(4) **157** was synthesized by reaction with an additional equivalent of 4-(dimethylamino)phenyllithium to previously isolated monosubstituted diborane(4) **156** in diethylether at low

3. Results and Discussion

temperatures. After warming to room temperature, the solvent was exchanged for toluene and subsequent heating of the mixture to 100°C for one hour completed the reaction. Symmetrically substituted diborane(4) **157** was predominantly obtained, as demonstrated by ¹H NMR spectrum (Figure 46) and isolated as yellow crystals in moderate yields (32%) (Scheme 55). The ¹¹B NMR spectrum of isolated **157** shows one broad signal at 49.4 ppm within the expected range for 1,2-bis(dimethylamino)-diboranes(4).^[95,108,110,111,257] Conversely, attempts to prepare **157** selectively from **54a** remained unsuccessful (*vide infra*). Diborane(4) **157** is sensitive to air and moisture in solution, but stable at least overnight in the solid state.



Scheme 55. Synthesis of diborane(4) **157**.

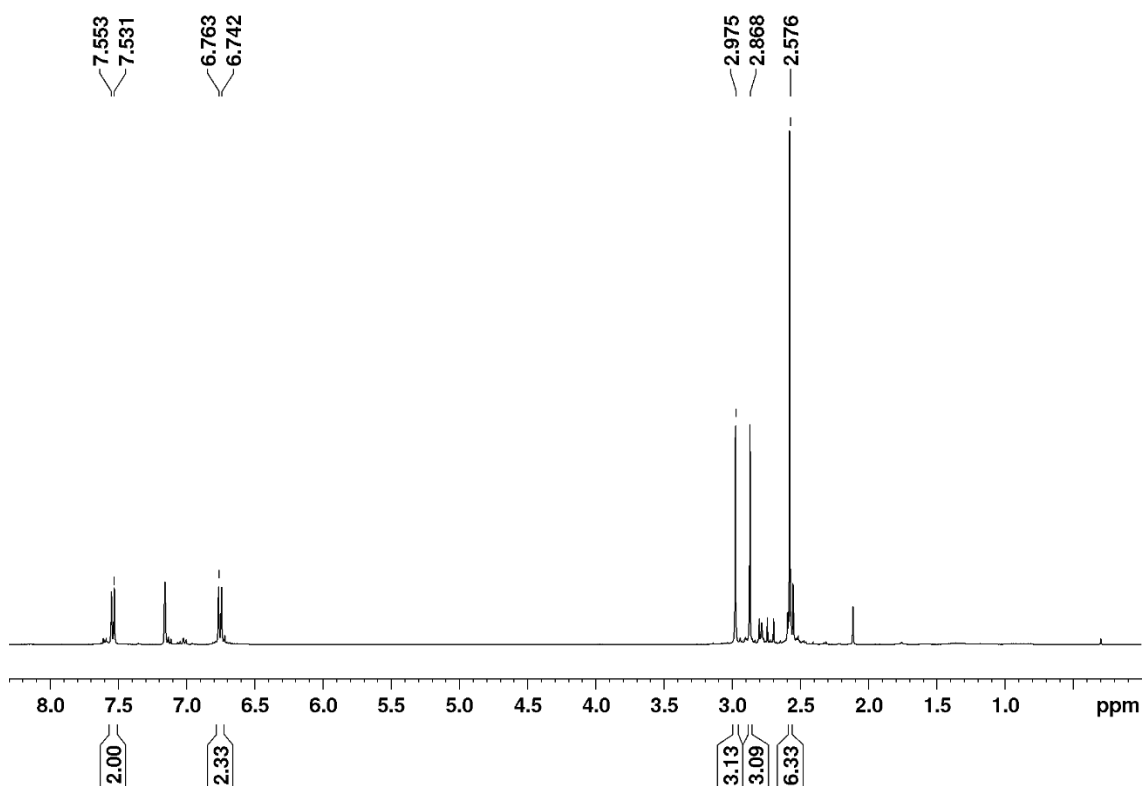


Figure 46. ¹H NMR spectrum of the crude product of **157**.

X-ray diffraction analysis allowed for the determination of the molecular structure of **157** in the solid state (Figure 47). The B-B bond length in **157**

3. Results and Discussion

(1.716(3) Å) is similar to the one found for **156** and thus in line with literature reported 1,2-bis(dimethylamino) diboranes(4).^[95] As found for **156**, the B-planes are coordinated in a trigonal-planar fashion ($\Sigma\angle(B) \approx 360^\circ$) and the B-coordination planes are almost perpendicular ($83.8(1)^\circ$). The B-N bond lengths of 1.399(3) Å and 1.405(3) Å are in the typical range^[95,108,110,111,257] and the planar coordination environments of the NMe₂ nitrogen atoms demonstrate the expected B-N double bond character.^[95,108,110,111,257] The seeming trigonal-planar coordination environment of one of the N atoms of the phenyl-bonded NMe₂ groups ($\Sigma\angle N2 = 359.5^\circ$) is likely an artifact of the insufficient modelling of a positional disorder at N2. In any case, the nitrogen center of the other *para*-dimethylamino group is pyramidalized to a certain extent ($\Sigma\angle N4 = 350.1^\circ$). Irrespective of the degree of pyramidalization at the nitrogen atoms, the N-C_{phenyl} distances are of comparable size (1.384(3) Å, 1.400(3) Å) demonstrating that π -donation of the *para*-NMe₂ group is of smaller importance and thus comparable to the situation in **156** as discussed in the previous section. In addition, both angles between the phenyl ring-plane normal and the B-B bonding axis deviate considerably from the ideal 90° (36.34° (N2-Ph)/ 60.4° (N4-Ph)) underscoring the assumption of a rather weak π -electron donation through the phenyl ring, if any.

3. Results and Discussion

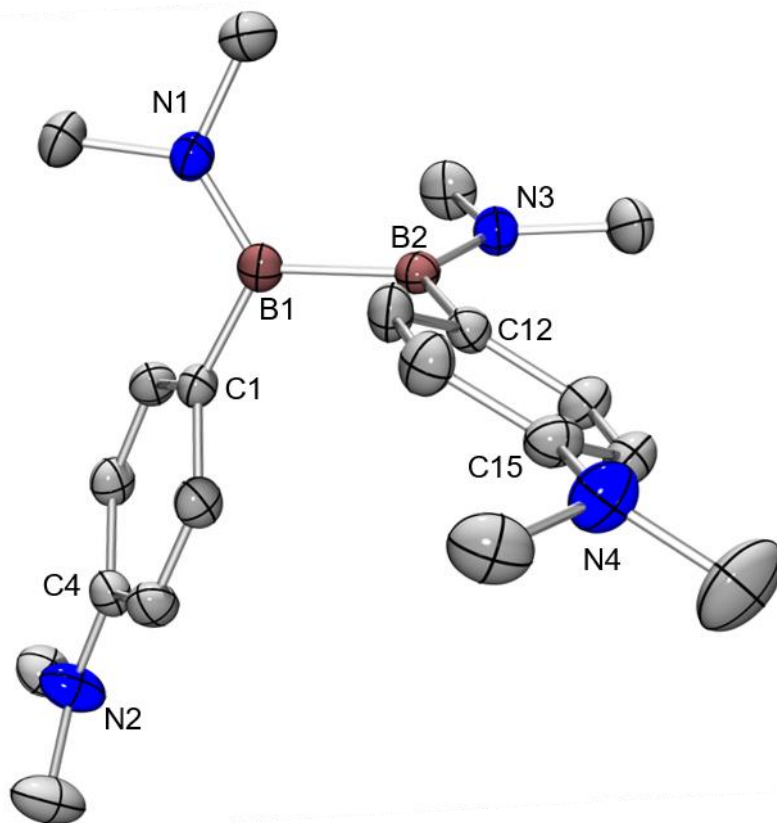


Figure 47. Molecular structure of **157** in the solid state (ellipsoids at 50% probability, hydrogen atoms omitted for clarity). Selected bond lengths [Å] and angles [°]: B1-B2 1.716(3), B1-N1 1.399(3), B2-N3 1.405(3), B1-C1 1.585(3), B2-C12 1.576(3), C4-N2 1.384(3), C15-N4 1.400(3), $\Sigma \angle$ B1 359.9, $\Sigma \angle$ B2 360.0, $\Sigma \angle$ N1 359.9, $\Sigma \angle$ N3 360.0, $\Sigma \angle$ N2 359.5, $\Sigma \angle$ N4 350.1, angle between B coord. planes 83.8(1).

UV/Vis spectroscopy of a hexane solution of diborane(4) **157** ($c = 0.6$ to 0.9 mM) shows one absorption band maximum at 281 nm with an extinction coefficient of $\epsilon = 34900 \text{ M}^{-1} \text{ cm}^{-1}$. The absorption spectrum at $c = 5 \mu\text{M}$ in preparation for fluorescence measurements (Figure 48), however, showed three maxima, one at 286 nm corresponding the one at higher concentrations, one at 296 nm and one at 334 nm with lower intensity. Only after excitation of the last two fluorescence was detected (Figure 48) with maxima at 330 nm and 384 nm and quantum yields of $<5\%$ and $13\% \pm 5\%$ (determined by Ulbricht sphere), respectively.

3. Results and Discussion

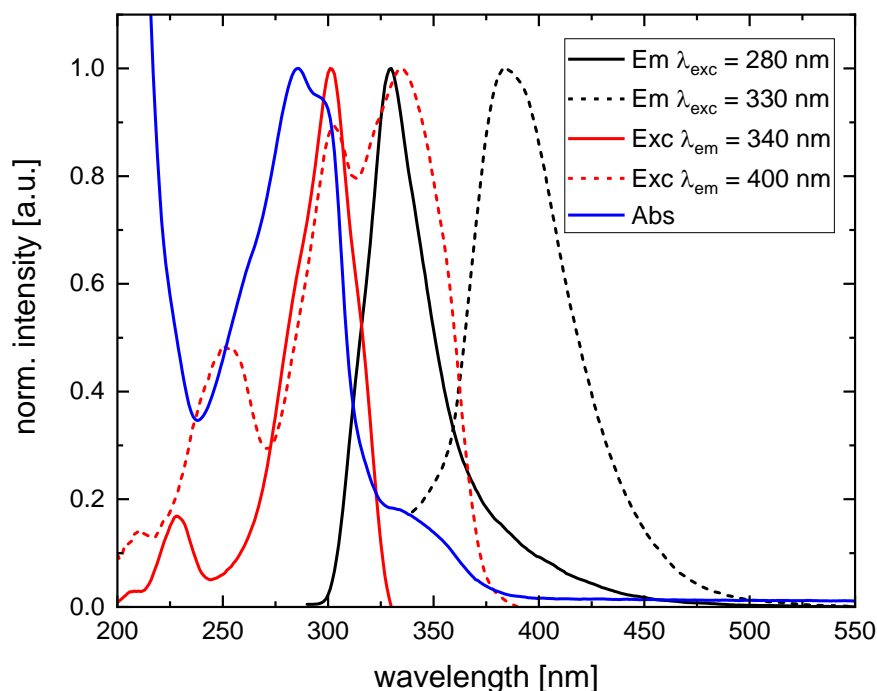


Figure 48. Absorption (blue), excitation (red) and emission (black) spectra of 1,2-bis(dimethylamino) diborane(4) **157** in hexane (5 μ M).

Exposure to air and monitoring of the changes in the UV/Vis spectra were more ambiguous than in case of diborane(4) **156**. Figure 49 shows the changes in the UV spectrum of a 5 μ M hexane solution of **157** in a 10 mm cuvette at first under argon (violet), then exposed to air for a timespan of up to 180 minutes (red). In this case, the longest wavelength absorption at 334 nm seems to be intermediate in nature as well since its intensity first increases slightly, then decreases again in relation to the main absorption band. The absorption band at 296 nm (Figure 48) was not observed in this experiment. Both fluorescent species, however, do not emerge from the band at 281 nm observed in the absorption spectrum at higher concentration and therefore it is assumed that in analogy to **156**, the fluorescence results from species formed through contamination with air and/or moisture.

3. Results and Discussion

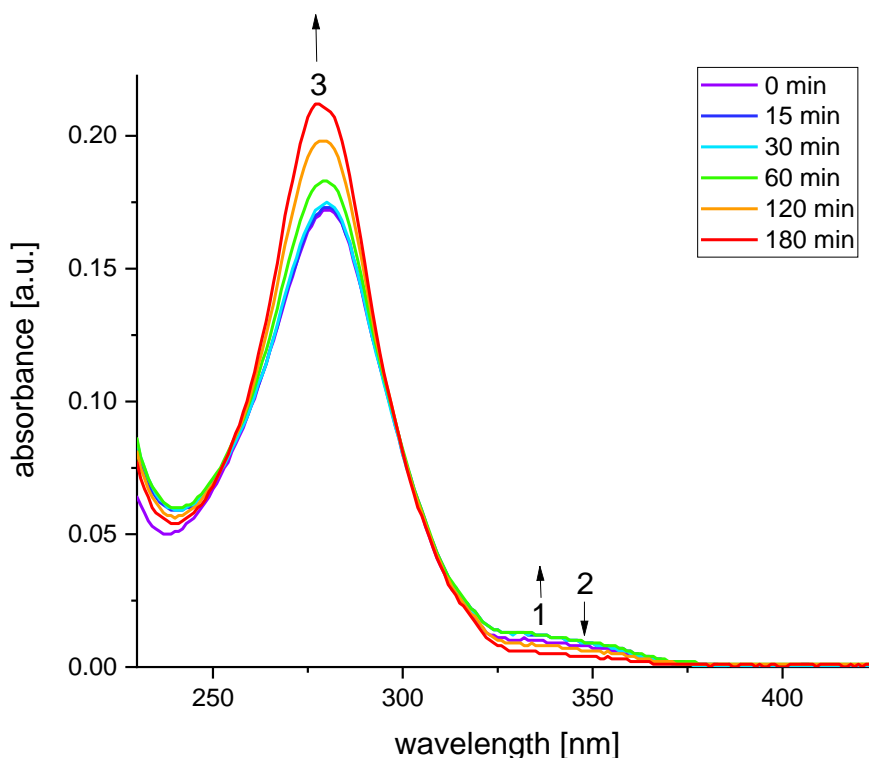


Figure 49. UV/Vis spectra of a 5 µM solution of **157** in hexane exposed to air (violet to red). **1**: increasing absorption band at 334 nm/ accumulation of the intermediate species; **2**: decreasing absorption band at 334 nm/ consumption of the intermediate species; **3**: increasing absorption band at 277 nm/ formation of suspected hydrolysis product.

Cyclic voltammetry was performed with a platinum working electrode, a platinum counter electrode, a silver quasi-reference electrode, $\text{Bu}_4\text{N}^+\text{PF}_6^-$ ($c = 0.1 \text{ M}$) as conductive salt and ferrocene ($c = 0.3 \text{ mM}$) as external reference. To gather more information about the decomposition modes of diborane(4) **157**. Since oxidative decomposition of **157** was suspected, the cyclic voltammetric measurements focused on comparably high potentials. Because of its wide positive range dry dichloromethane was chosen as solvent, although the stability of any oxidized or reduced species would probably have benefitted from the donor-stabilization by thf. Figure 50 shows the cyclic voltammogram, which was recorded without ferrocene for clarity reasons. Two irreversible oxidation steps at 0.37 V and at 0.58 V are detected for **157**. Both electron transfers are followed by a chemical reaction and the resulting species are partially reduced again (also irreversibly). By narrowing the scan window from -2.5 V to 1.5 V (Figure 50) to -2.5 V to 0.5 V a voltammogram with only one oxidation step at 0.37 V and one reduction step at -1.21 V (Figure 51) is recorded. With a scan window of -2.5 V to -0.6 V neither oxidation nor reduction is detected (Figure 51). This leads to the conclusion that the reduction

3. Results and Discussion

step at 0.08 V results from the species produced by the oxidation at 0.58 V and the reduction step at -1.21 V results from the species produced by the oxidation at 0.37 V. As discussed previously, diboranes(4) are rather known for their reducibility^[122,159], so that only the *N,N*-dimethylaminophenyl groups in analogy to **156** are suspected to be oxidized^[260,261] here, as well. However, a cyclic voltammogram in chemical less reactive solvents as thf or acetonitrile would provide more information about the electrochemical behavior of **157**.

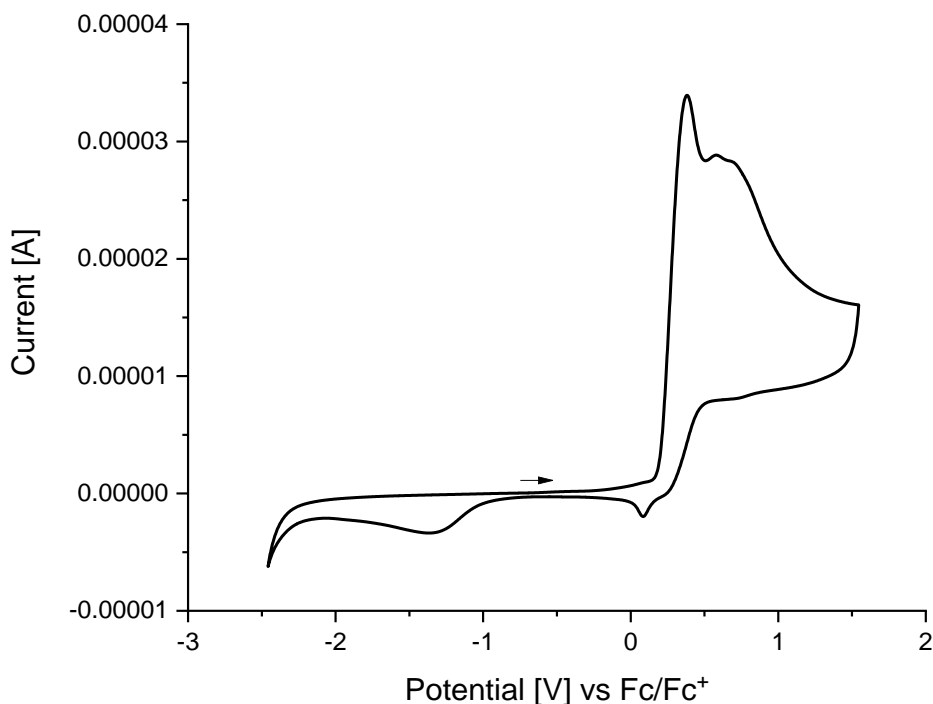


Figure 50. Cyclic voltammogram of **157** in dichloromethane ($c = 3 \text{ mM}$), with a platinum working electrode, a platinum counter electrode, a silver quasi reference electrode, scan rate at 100 mV s^{-1} and $\text{Bu}_4\text{N}^+\text{PF}_6^-$ ($c = 0.1 \text{ M}$) as conductive salt.

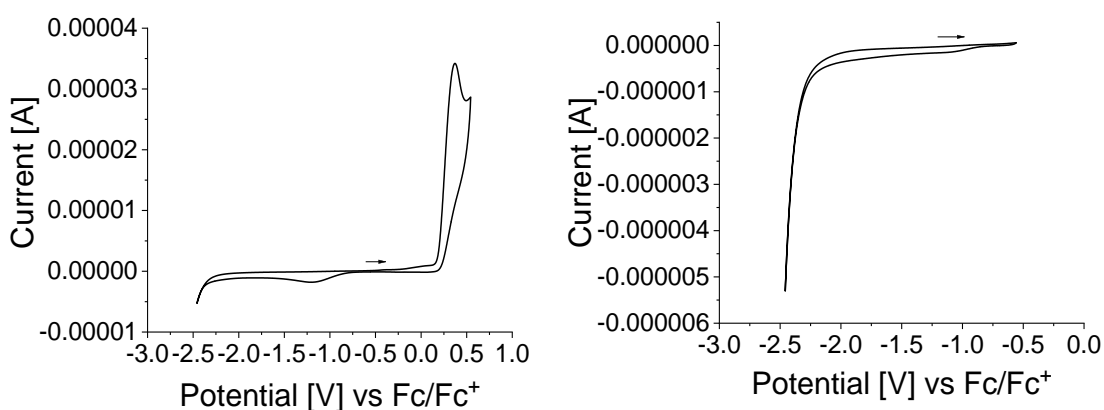
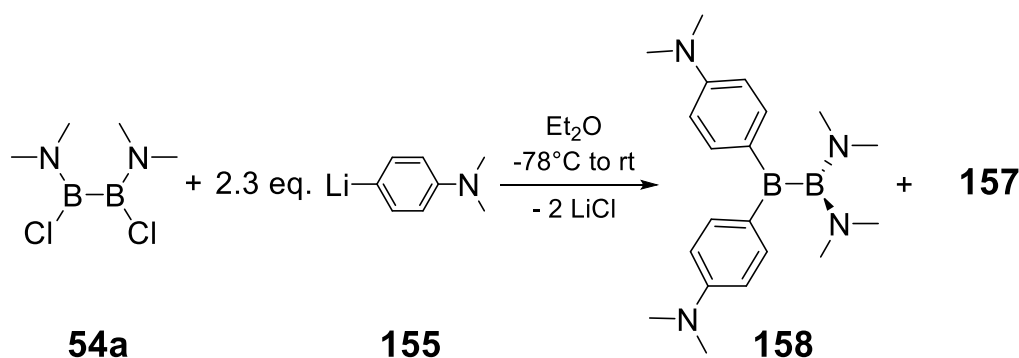


Figure 51. Cyclic voltammograms of **157** in dichloromethane ($c = 3 \text{ mM}$), with a platinum working electrode, a platinum counter electrode, a silver quasi reference electrode, scan rate at 100 mV s^{-1} and $\text{Bu}_4\text{N}^+\text{PF}_6^-$ ($c = 0.1 \text{ M}$) as conductive salt.

3. Results and Discussion

In an attempt to synthesize **157** directly without intermittent isolation of monosubstituted **156**, 2.3 equivalents of 4-(dimethylamino)phenyllithium dissolved in diethylether were added dropwise to the precooled (-78°C) solution of 1,2-dichlorodiborane(4) **54a** solution. After warming to room temperature solvents and volatile components were distilled off in vacuum. Filtration from hexane gave a yellow solution from which yellow crystals of 1,1-diaryl-2,2-bis(dimethylamino)diborane(4) **158** were obtained at 5°C (Scheme 56). The ^{11}B NMR spectrum of the dissolved crystals shows one broad signal at 79.0 ppm in the range for aryl-substituted diboranes(4)^[120,122-124] and one broad signal at 38.4 ppm within the expected range for dimethylamino-substituted diboranes(4).^[95,108,110,111,257] NMR spectroscopic analysis of the mother liquor showed only the 1,2-isomer **157** remaining in solution, indicating that the 1,1-isomer **158** is only a side product and crystallized from the solution quantitatively. Such substituent rearrangements of diboranes(4) were already reported several times (see Section 1.4).^[125-132,262]



Scheme 56. Reaction of 1,2-dichloro diborane(4) **54a** with an excess of 4-dimethylaminophenyl lithium (**155**) to the 1,1-isomer **158** and the 1,2-isomer **157**.

The molecular structure of **158** is shown in Figure 52. The B-B bond length ($1.722(2) \text{ \AA}$) is similar to the one in the 1,2-isomer **157** ($1.716(3) \text{ \AA}$). The sum of angles around both B atoms ($\Sigma \alpha = 360^{\circ}$) indicates trigonal planar coordination environments. The angle between B-coordination planes ($78.7(1)^{\circ}$) is a bit smaller than in the 1,2-isomer **157**. The B-N bond lengths of $1.433(2) \text{ \AA}$ and $1.423(2) \text{ \AA}$ are elongated compared to **157**. As both amino groups are bonded to the same boron atom less π -electron donation from each of them is needed. The planar coordination environments of the NMe_2 nitrogen atoms demonstrate nonetheless a significant B-N double bond character as usual for this class of compounds.^[95,108,110,111,257] Like in **157** one of the N atoms of the phenyl-bonded

3. Results and Discussion

NMe₂ groups is coordinated in a trigonal planar fashion ($\Sigma \angle N2 = 359.7^\circ$), the other one is pyramidalized to a certain extent ($\Sigma \angle N1 = 353.1^\circ$). The N-C_{para} distance at the pyramidalized nitrogen N1 (1.381(2) Å) is in the same range as the ones in **157**, but the bond length between the trigonal planar coordinated nitrogen N2 and the phenyl-carbon (1.372(2) Å) is slightly shorter and consequently closer to the one in *p*-Me₂N(C₆H₄)BMes₂ as characterized by Marder *et al.*^[178]. Nonetheless, the angle between the normal of the phenyl-ring-plane bonded to the pyramidalized nitrogen (N1) and the B-B binding axis is unexpectedly closer to 90°, namely 83.43°, than the other one (69.55°), leading to the conclusion that N2 may increase electron density in the phenyl ring, but all in all the interaction with the boron center B1 is in both cases negligible.

Unfortunately, problems with the reproducibility of the isolation of this side product prevented further characterization of **158**.

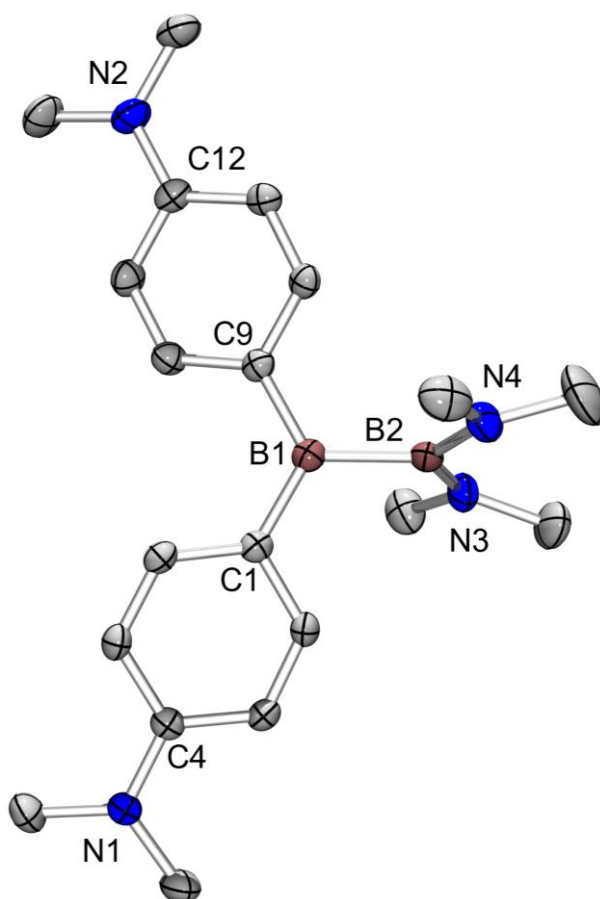
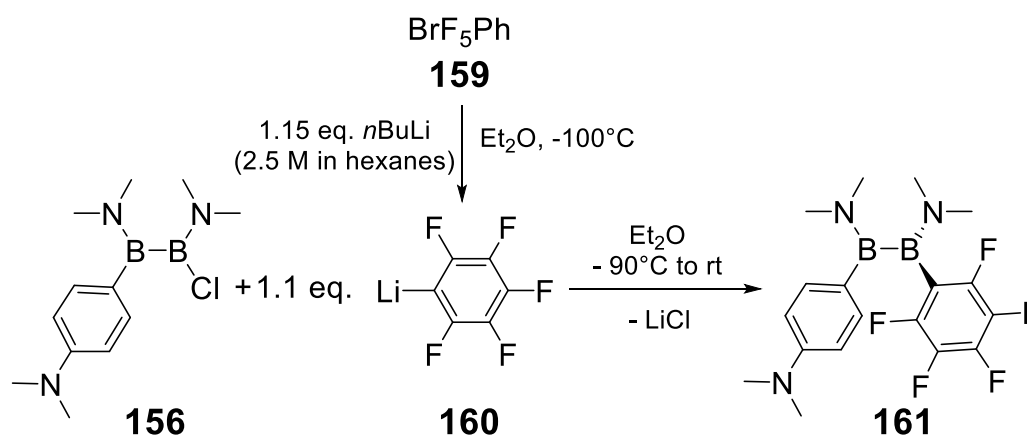


Figure 52. Molecular structure of **158** in the solid state (ellipsoids at 50% probability, hydrogen atoms omitted for clarity). Selected bond lengths [Å] and angles [°]: B1-B2 1.722(2), B1-C1 1.560(2), B1-C9 1.559(2), B2-N3 1.433(2), B2-N4 1.423(2), C4-N1 1.381(2), C12-N2 1.372(2), $\Sigma \angle B1$ 359.85, $\Sigma \angle B2$ 360.0, $\Sigma \angle N1$ 353.14, $\Sigma \angle N2$ 359.71, $\Sigma \angle N3$ 359.33, $\Sigma \angle N4$ 359.7, angle between B coord. Planes 78.7(1).

3. Results and Discussion

The next goal was to introduce an electron-withdrawing substituent. Thus, the pentafluorophenyl group was incorporated by the reaction of **156** in diethylether at low temperatures with previously generated pentafluorophenyllithium.^[263] Addition of a precooled solution of **156** in diethylether at -90°C is crucial for the stability of the anion. After warming to room temperature multinuclear NMR spectroscopy indicated quantitative formation of **156** (Scheme 57). Subsequent standard workup afforded diborane(4) **161** as colorless crystals in acceptable yield (52%). The ^{11}B NMR spectrum of **161** shows one broad signal at 45.8 ppm in the expected range for 1,2-bis(dimethylamino)diboranes(4).^[95,108,110,111,257] Diborane(4) **161** is sensitive to air and moisture in solution, but stable overnight in the solid state.



Scheme 57. Synthesis of unsymmetrically substituted diborane(4) **161**.

Single crystals could be grown from a concentrated *o*-difluorobenzene solution at -26°C and the molecular structure is shown in Figure 53. The B-B bond length in **161** (1.713(1) Å) is similar to those found in other diboranes(4) reported in this PhD thesis and therefore in the typical range.^[95] The sum of angles around the B atoms ($\Sigma\alpha = 360^{\circ}$) indicates trigonal-planar coordination environments, which are nearly orthogonal to each other (angle between B-coordination planes $85.58(7)^{\circ}$). The B-N bond lengths of 1.399(1) Å and 1.387(1) Å are also in the typical range^[95,108,110,111,257] and the planar coordination environments of the NMe_2 nitrogen atoms demonstrate the significant B-N double bond character, as usual for this class of compounds.^[95,108,110,111,257] In contrast, the N atom of the phenyl-bonded NMe_2 group is slightly pyramidalized ($\Sigma\alpha = 353.6^{\circ}$). Additionally, the N3-C4 distance of 1.389(1) Å demonstrates that π -donation of the phenyl-bonded NMe_2 group

3. Results and Discussion

is, as in the similar structural motifs above, of smaller importance. This is supported by an angle between the phenyl-ring-plane normal and B-B bonding axis of 56.92°.

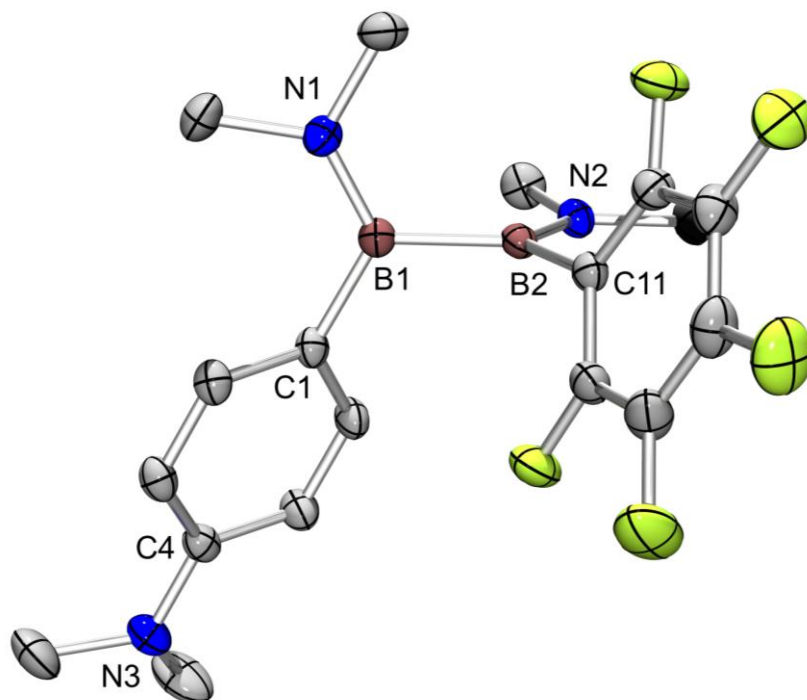


Figure 53. Molecular structure of **161** in the solid state (ellipsoids at 50% probability, hydrogen atoms and co-crystallized *o*-difluoro-benzene omitted for clarity). Selected bond lengths [Å] and angles [°]: B1-B2 1.713(1), B1-N1 1.399(1), B1-C1 1.572(1), B2-N2 1.387(1), B2-C11 1.602(1), C4-N3 1.389(1), $\Sigma \angle$ B1 360.0, $\Sigma \angle$ B2 360.0, $\Sigma \angle$ N1 360.0, $\Sigma \angle$ N2 360.0, $\Sigma \angle$ N3 353.6, angle between B coord. Planes 85.58(7).

In the UV-vis spectrum of **161** in diethylether ($c = 0.4\text{--}1\text{ mM}$), an absorption band at 287 nm was detected with an extinction coefficient ϵ of $17300\text{ M}^{-1}\text{ cm}^{-1}$. Remarkably, **161** turned out to be the only 1,2-bis(dimethylamino)diborane(4) studied in this work which showed fluorescence in hexane solution with 5% diethylether ($c = 5\text{ }\mu\text{M}$, $\lambda_{\text{em,max}} = 335\text{ nm}$, $\lambda_{\text{exc,max}} = 290\text{ nm}$, Figure 54), albeit with a poor quantum yield of below 5%. Fluorescence measurements were carried out in hexane with 5% diethylether, because of the low solubility of **161** in hexane, meaning that **161** was dissolved in diethylether to give a concentration of 1 mM and then the solution was diluted with hexane down to 5 μM .

3. Results and Discussion

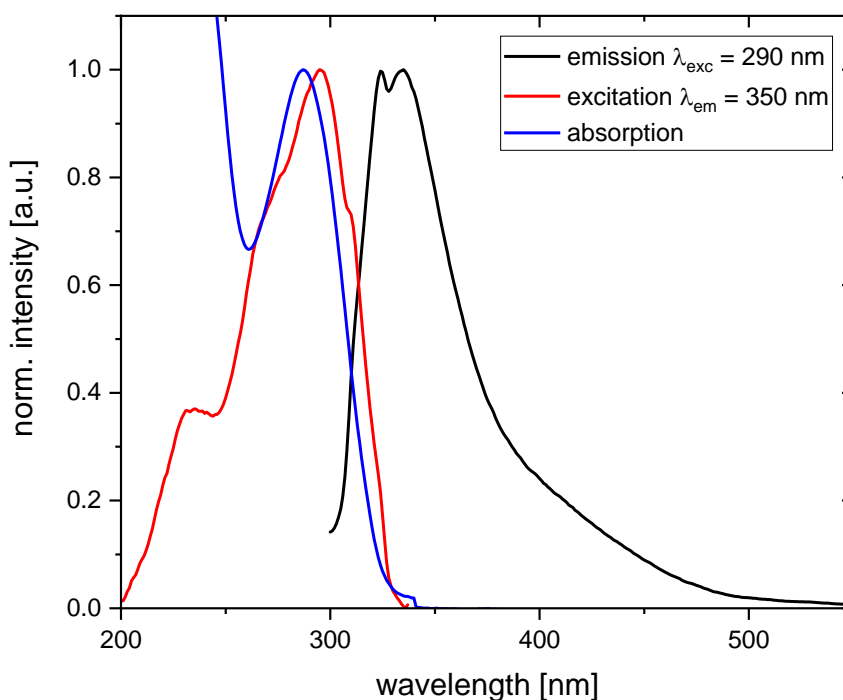
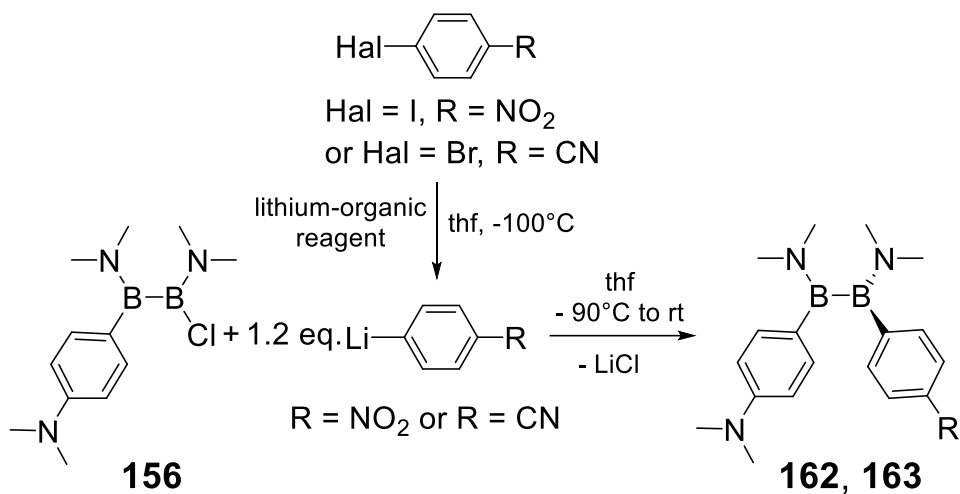


Figure 54. Absorption (blue), excitation (red) and emission (black) spectra of 1,2-bis(dimethylamino) diborane(4) **161** in hexane/ diethylether(5%).

The pentafluorophenyl substituent has σ -electron withdrawing, but π -electron donating properties. The question arose whether a σ - and π -withdrawing substituent could be attached as well in order to realize a 1,2- π -donor/acceptor substitution pattern in a 1,2-bis(dimethylamino)diborane(4). The reactivity of diborane(4) **156** towards 4-cyanophenyllithium and 4-nitrophenyllithium was thus investigated. The lithiumorganic reagents were generated and subsequently treated with the substrate in the cold due to their thermal instability.^[264,265] The addition of a precooled diborane(4) **156** solution to the cooled anion solution is followed by stirring in the cooling bath for 30 minutes and warming up to room temperature. All solvents and volatiles were removed and an NMR sample was analyzed. In both cases the ^{11}B NMR spectra (Figure 55/ Figure 56) suggest the formation of the targeted diboranes(4) **162**/**163** (Scheme 58) with a broad signal at 36.4 ppm for the 4-dimethylaminophenyl substituted boron in both spectra and one slightly downfield shifted broad signal at 47.6 ppm for the 4-cyanophenyl-substituted boron center of **162** (Figure 55) and at 48.6 ppm for the 4-nitrophenyl-substituted boron of **163**. Additionally, an unidentified, tetracoordinated species with a signal at 1.6 ppm could be observed in the ^{11}B NMR spectrum of the

3. Results and Discussion

reaction with 4-nitrophenyllithium (Figure 56). Unfortunately, attempts to isolate either **162** or **163** remained unsuccessful.



Scheme 58. Synthesis of acceptor substituted diboranes(4) **162** (R = CN) and **163** (R = NO₂).

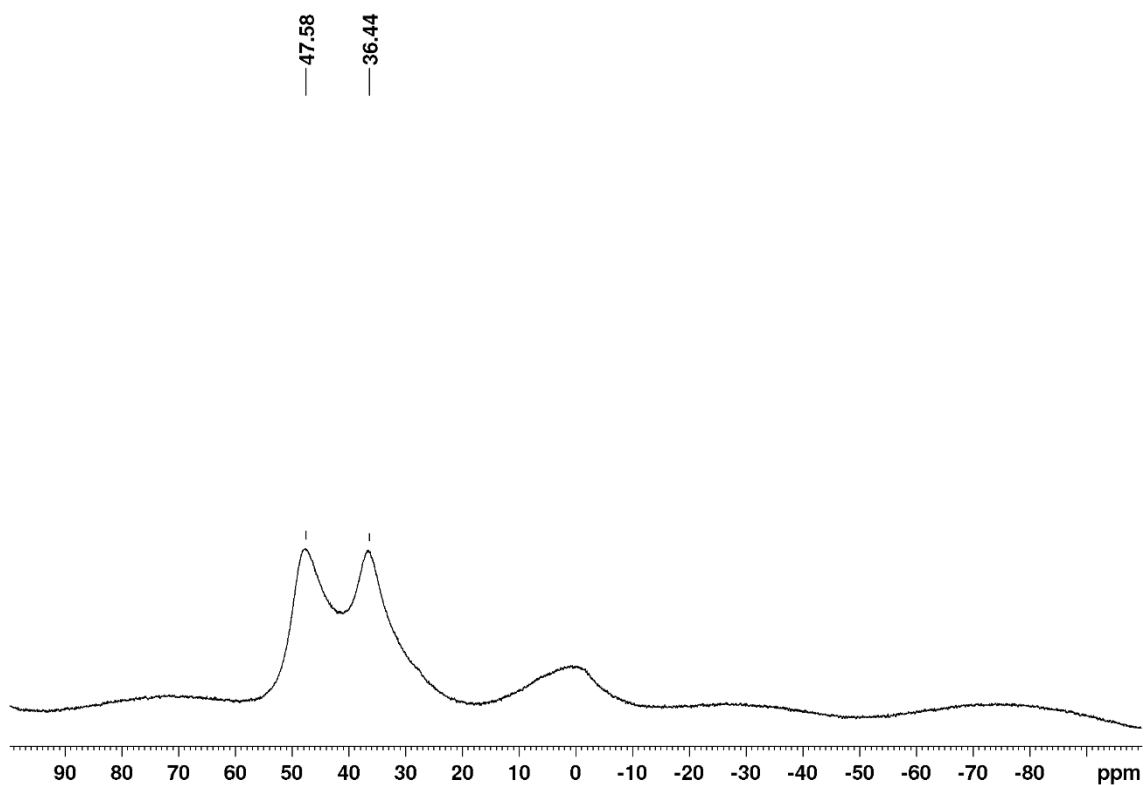


Figure 55. ¹¹B NMR spectrum of the crude product of *p*-benzonitrile substituted diborane(4) **162**.

3. Results and Discussion

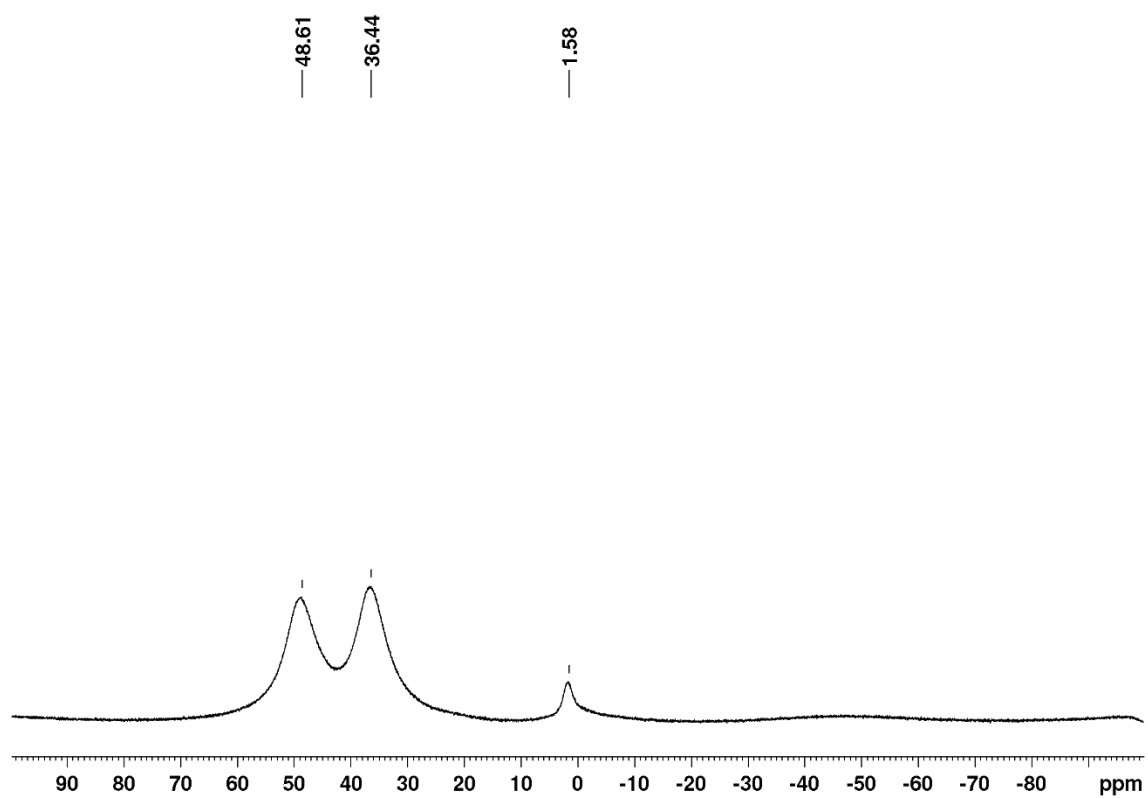


Figure 56. ^{11}B NMR spectrum of the crude product of *p*-nitrophenyl substituted diborane(4) **163**.

3.6.2 Syntheses and spectroscopic studies of 1,4-diaza-2,3-diborinanes

Cyclic 1,4-diaza-2,3-diborinanes have been scarcely reported because their 1,1-isomers with 1,3,2-diazaborole moieties are thermodynamically favored.^[133] The group of Nöth were the first to selectively synthesize a cyclic 1,4-diaza-2,3-diborinane.^[133] Further cyclic 1,4-diaza-2,3-diborinane species were synthesized by Şahin and the Braunschweig group.^[134,135,137,138] Norman and Russel isolated both possible isomers **91a** and **92a** from the reaction between *o*-phenylenediamine and tetrakis(dimethylamino)diborane(4) *via* transamination (Figure 57).^[139] For a more extensive literature review see Section 1.4. With R = Me (**93**, **164**, Figure 57) at the nitrogen atoms, Norman and Russel found both isomers to be fluorescent.^[136] While diazaboroles are known to be fluorescent,^[266-271] 1,4-diaza-2,3-diborinane derivatives have not been intensely investigated in this regard. Based on the observation of fluorescence for the diazadiborinane **93**, in this work one *o*-diaminophenyl ligand was attached to the diborane(4) moiety to functionalize the luminescent skeleton at the boron centers comparable to above discussed 1,2-bis(dimethylamino)diboranes(4). The low concentrations needed for fluorescence measurements are prone to decomposition even at small amounts of air contamination. In addition, Norman and Russel demonstrated with the isolation of the corresponding radical structure of **93** the tendency of these structural motifs to be oxidized.^[140] Consequently, the behavior in UV/Vis experiments after exposition to air was studied for selected diazadiborinanes.

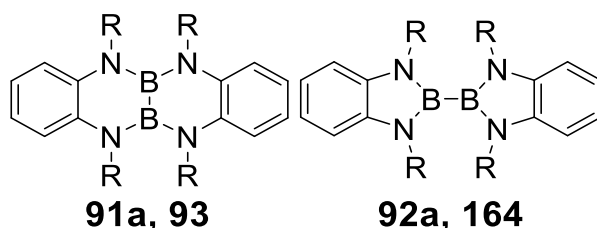
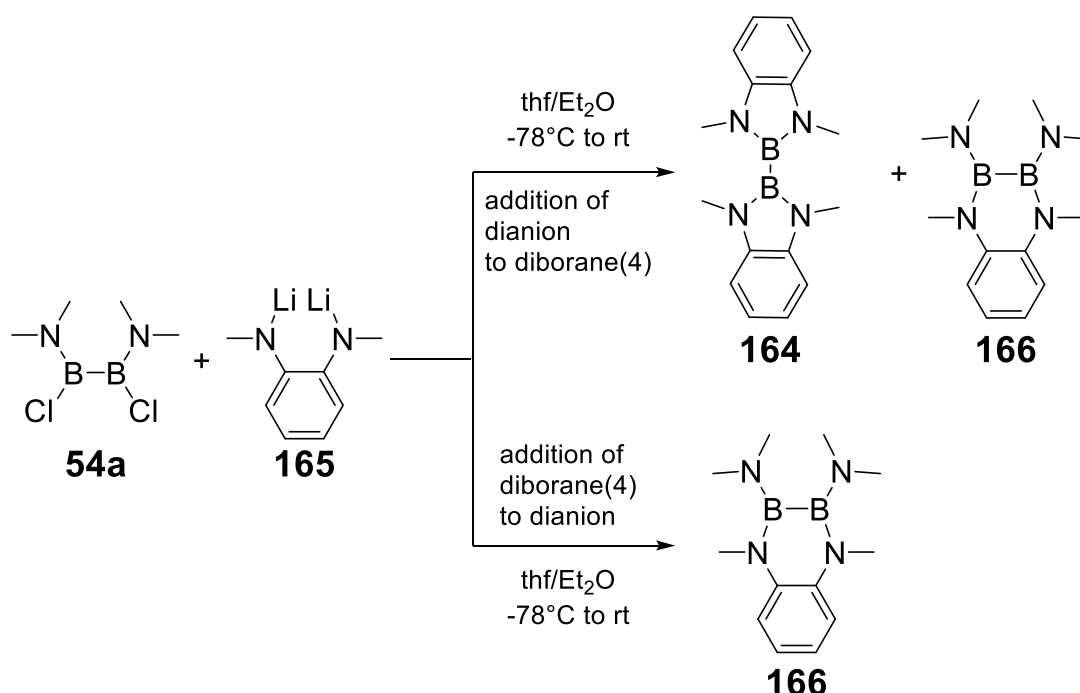


Figure 57. Literature known cyclic diazadiboron compounds by Norman and Russell.^[139] **91a**: R = H; **93**: R = Me; **92a**: R = H; **164**: R = Me

In the first step the *o*-diaminophenyl ligand needed to be introduced. When applying the established literature procedure^[133-135,137,138] by adding the dianion thf-solution dropwise to the precooled (-78°C) ethereal solution of the diborane(4), the formation of the 1,1-diazaborole-isomer **164**^[136] was observed NMR spectroscopically in considerable amounts (**164**:**166** = 35:65 determined

3. Results and Discussion

by ^1H NMR, Scheme 59). Finally, diborinane **166** was prepared selectively by dissolution of dianion **165** in thf, cooling to -78°C and dropwise addition of the solution of diborane(4) **54a** in diethylether (Scheme 59), but isolation of **166** could only be achieved in 43% yield. The ^{11}B NMR spectrum of **166** shows one signal at 33.7 ppm in the expected range for these cyclic 1,4-diaza-2,3-diborinanes.^[140] In solution as well as in the solid state and in the ambient atmosphere, compound **166** undergoes rapid and unselective oxidation. Under argon, no decomposition is observed upon prolonged heating above the melting point (mp. $135\text{-}138^\circ\text{C}$).



Scheme 59. Synthesis of diazadiborinane **166**.^[136]

Single crystals were obtained from a concentrated hexane solution at 5°C . The solid-state structure is shown in Figure 58. The B-B bond length ($1.687(2)$ Å) is slightly shorter than in the 1,2-bis(dimethylamino)diboranes(4) above (Section 3.6.1), in accordance with the bond lengths observed in the 1,4-diaza-2,3-diborinane prepared by Braunschweig (1.673 Å)^[138]. Monocycles with a saturated endocyclic C-C unit reported by Braunschweig (1.699 Å)^[138] and Şahin (1.710 Å - 1.725 Å)^[134] have slightly longer B-B bonds, whereas the B-B bond in the bicyclic 1,4-diaza-2,3-diborinane reported by Norman and Russell (**93**: 1.650 Å)^[140] is shorter. The sums of angles around the boron and endocyclic nitrogen atoms in the cyclic 1,4-diaza-2,3-diborinane **166** confirm trigonal planar coordination geometries ($\Sigma \angle \approx 360^\circ$). The largest deviation from

3. Results and Discussion

the best plane through the atoms of the 1,4-diaza-2,3-diborinane heterocycle with 0.262(1) Å is observed for B1. Şahin explained the deviation from planarity in analogous compounds by steric interactions between the substituents.^[134,137] In addition, the strong π -donor properties of the exocyclic NMe₂ group might suppress the formation of endocyclic B-N π -bonds, an assumption that finds support in the comparison of the B-N bond lengths. The exocyclic B-NMe₂ bonds in **166** (1.411(2) Å, 1.414(2) Å), though slightly elongated compared to the B-NMe₂ bond lengths in the 1,2-bis(dimethylamino)diboranes(4) in Section 3.6.1, show close to planar arrangement of the according B- and N-coordination planes (13.1(1)°, 19.9(1)°), indicating a pronounced B-N double bond character. The endocyclic B-N bond lengths (B1-N3 1.458(2) Å, B2-N4 1.453(2) Å) are longer than the exocyclic ones suggesting weaker π -electron contribution in the latter case.

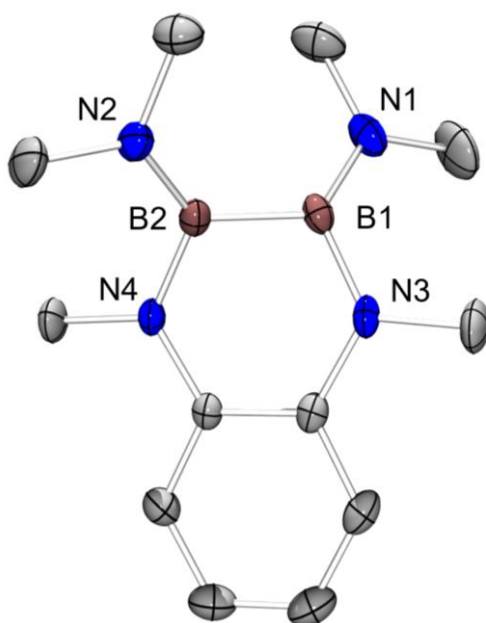


Figure 58. Molecular structure of **166** in the solid state (ellipsoids at 50% probability, hydrogen atoms omitted for clarity). Selected bond lengths [Å] and angles [°]: B1-B2 1.687(2), B1-N1 1.411(2), B1-N3 1.458(2), B2-N2 1.414(2), B2-N4 1.453(2), $\Sigma \sphericalangle$ B1 359.8, $\Sigma \sphericalangle$ B2 359.6, $\Sigma \sphericalangle$ N1 360.0, $\Sigma \sphericalangle$ N2 360.0, largest deviation from the best plane through the atoms of the 1,4-diaza-2,3-diborinane heterocycle for B1: 0.262(1) Å.

UV/Vis spectroscopy of a solution of diborinane **166** in hexane ($c = 0.6$ - 0.9 mM) showed multiple absorption band maxima at 314 nm ($\epsilon = 11800$ M⁻¹ cm⁻¹), 308 nm ($\epsilon = 12100$ M⁻¹ cm⁻¹), 272 nm ($\epsilon = 9840$ M⁻¹ cm⁻¹) and 234 nm ($\epsilon = 34900$ M⁻¹ cm⁻¹). The absorption spectrum at $c = 5$ μ M in preparation for fluorescence measurements (Figure 59) is in

3. Results and Discussion

accordance with that obtained at higher concentrations. Upon excitation of the longest wavelength absorption band ($\lambda_{\max} = 297 \text{ nm}/ 303 \text{ nm}$), fluorescence was detected (Figure 59) with a maximum at 325 nm and a quantum yield of $55 \pm 5\%$ (determined by Ulbricht sphere). Compared to Norman and Russell's bicyclic 1,4-diaza-2,3-diborinane isomer **93**^[136] (Figure 60) emission of cyclic 1,4-diaza-2,3-diborinane **166** is hypsochromically shifted, probably due to the absence of one half of the fused cyclic system.

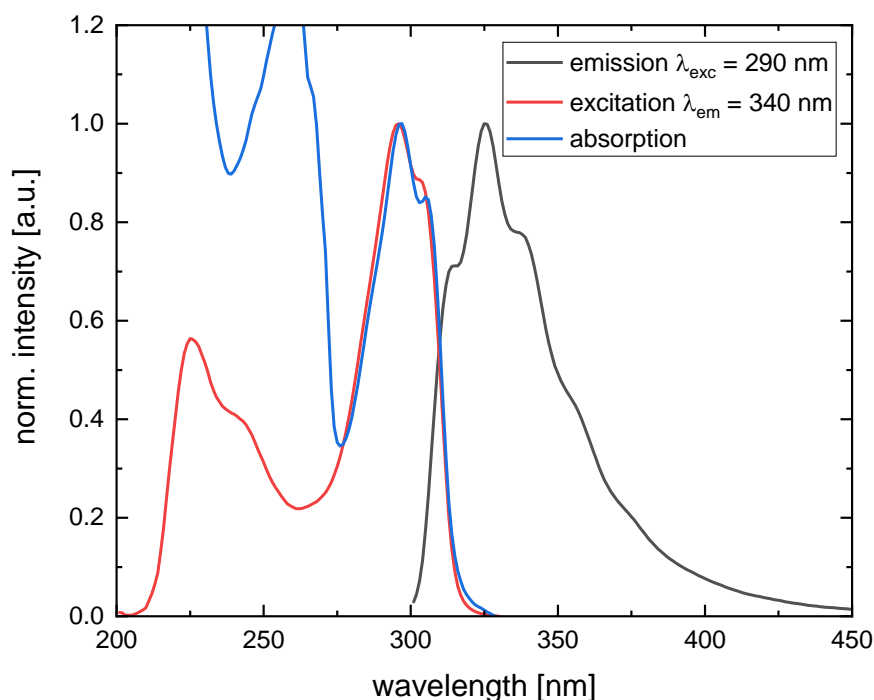


Figure 59. Absorption (blue), excitation (red) and emission (black) spectra of diazadiborinane **166** in hexane.

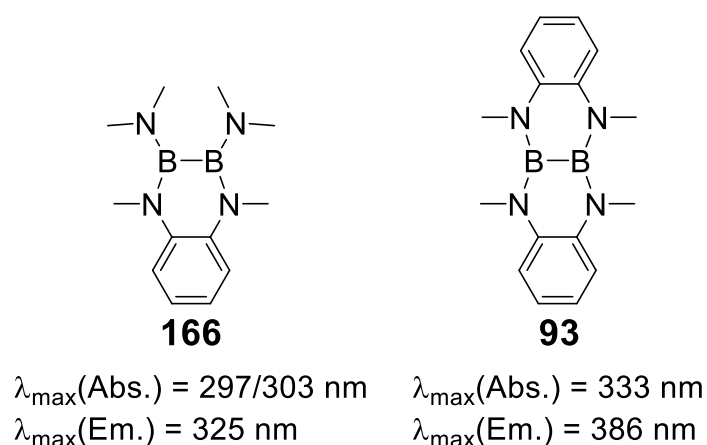
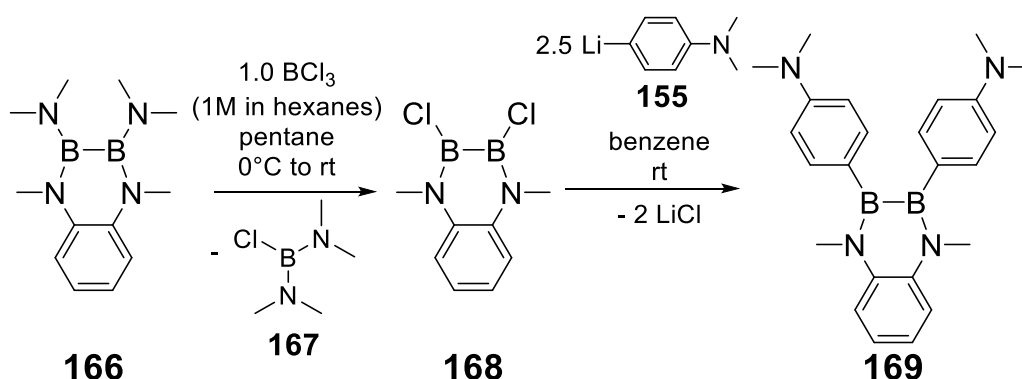


Figure 60. Structure and luminescent features of newly synthesized diborinane **166** in comparison to Norman and Russell's extended fused system **93**.^[136]

In a first attempt to functionalize the diazadiborinane rings, the same substituent was going to be attached to each boron center in order to minimize selectivity.

3. Results and Discussion

Therefore, both dimethylamino groups in **166** should be replaced by two chlorine atoms to enhance the electrophilicity of the boron centers. In the case of **166**, cleaving off the *o*-phenylenediamine-ligand during the reaction is conceivable. Nonetheless, as the Braunschweig group demonstrated, the dimethylamino groups in diazadiborinanes can be exchanged by halogens.^[138] Indeed, treatment of **166** in hexane at 0°C using 1 equivalent of BCl₃ solution (1.1 M in hexane) yields the anticipated structure **168** quantitatively (Scheme 60) after removal of all volatiles *in vacuo*. The ¹H NMR spectrum only displays resonances of the *o*-phenylenediamine ligand and only one signal for N-bonded methyl groups in the expected integrated ratio. In line with the dichlorinated 1,4-diaza-2,3-diborinane **168**, only one signal in the ¹¹B NMR spectrum is observed at 40.0 ppm. The chlorinated diborinane **168** was thus used without further purification: it reacts in a salt metathesis with two equivalents of 4-dimethylaminophenyllithium at room temperature in benzene to give the bis(4-dimethylaminophenyl)-substituted **169** selectively (Scheme 60), as indicated by ¹H NMR spectrum (Figure 61).



Scheme 60. Synthesis of bis(aminophenyl) substituted diazadiborinane **169**.^[138]

3. Results and Discussion

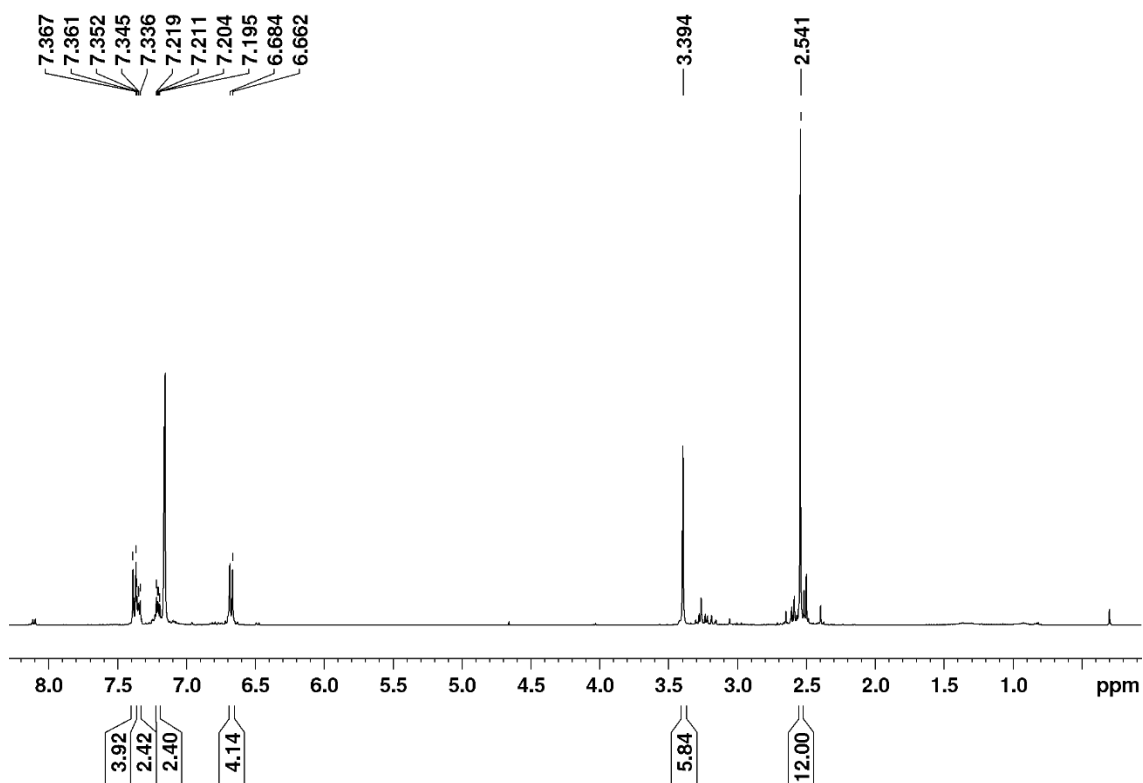


Figure 61. ^1H NMR spectrum of the crude product of **169**.

Diazadiborinane **169** was purified by crystallization from a mixture of toluene and hexane at room temperature and was isolated as yellow crystals only in mediocre yield (21%). ^{11}B NMR spectrum of the crystalline **169** shows one broad signal (46.4 ppm) in the same range as the starting material **168**. In solution and in the ambient atmosphere, diazadiborinane **169** undergoes rapid and unselective oxidation. In the solid state, it tolerates exposure to air and moisture overnight. Under argon, unselective decomposition is observed upon prolonged heating above the melting point (mp. 180-182°C).

Single crystal x-ray determination afforded the molecular structure of **169**, which is shown in Figure 62. The B-B-bond length and the sum of angles around the boron and endocyclic nitrogen atoms compare well to those in **166**. The largest deviation from the best plane through the atoms of the 1,4-diaza-2,3-diborinane heterocycle with 0.055(2) Å is observed for N1. Compared to **166** the endocyclic B-N bond lengths in **169** (1.428(3) Å, 1.416(3) Å) are shorter, due to increased endocyclic B-N- π -bond interaction. The coordination environment of the aminophenyl nitrogen atoms is trigonal planar ($\Sigma \angle \approx 360^\circ$). This circumstance provides a hint at π -donor contribution of the *para*-dimethylaminophenyl group in **169**. The N-C_{phenyl} bond lengths, however, are in the same range as those in

3. Results and Discussion

1,2-bis(dimethylamino)diboranes(4) (Section 3.6.1) and the angles between the *para*-dimethylaminophenyl ring-plane normals and the B-B bonding axis deviate from ideal 90° (44.0°/ 60.0°), so that donor effects of the *para*-NMe₂-phenyl group are probably weak in this case as well.

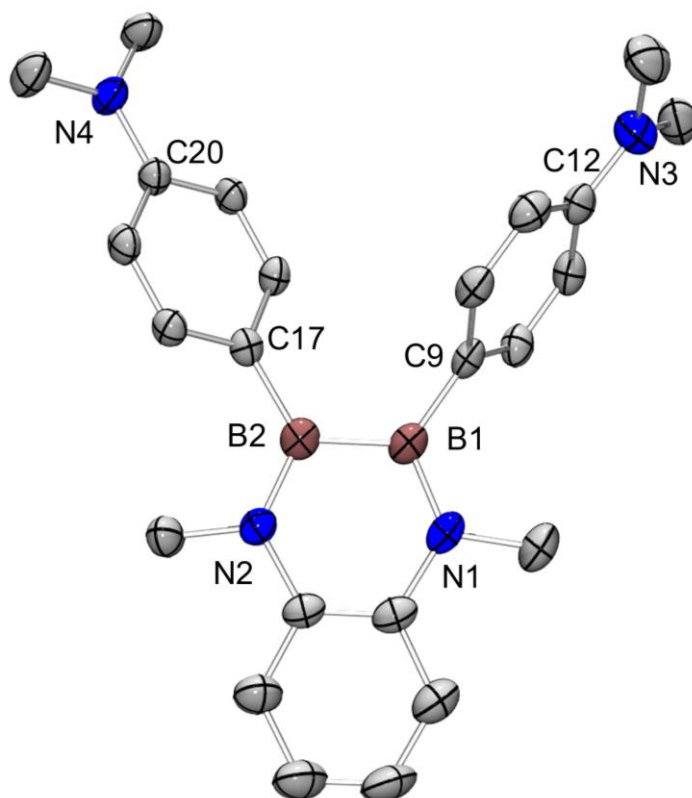


Figure 62. Molecular structure of **169** in the solid state (ellipsoids at 50% probability, hydrogen atoms and second molecule in the asymmetric unit omitted for clarity). Selected bond lengths [Å] and angles [°]: B1-B2 1.687(4), B1-N1 1.428(3), B1-C9 1.571(3), B2-N2 1.416(3), B2-C17 1.572(4), N3-C12 1.377(3), N4-C20 1.383(3), $\Sigma \angle$ B1 359.9, $\Sigma \angle$ B2 360.0, $\Sigma \angle$ N1 360.0, $\Sigma \angle$ N2 359.9, $\Sigma \angle$ N3 360.0, $\Sigma \angle$ N4 359.8, largest deviation from the best plane through the atoms of the 1,4-diaza-2,3-diborinane heterocycle for N1: 0.055(2) Å.

UV/Vis spectroscopic studies of the diborinane **169** in diethylether solution ($c = 0.4$ to 1 mM) shows multiple absorption band maxima at 342 nm ($\epsilon = 35500$ M⁻¹ cm⁻¹), 261 nm ($\epsilon = 34700$ M⁻¹ cm⁻¹) and 232 nm ($\epsilon = 27300$ M⁻¹ cm⁻¹), which correlates with the absorption spectrum at $c = 5$ μ M (in hexane with 5‰ diethylether) in preparation for fluorescence measurements (Figure 63). Additionally, the longest wavelength absorption band perfectly fits the excitation band ($\lambda_{\text{max}} = 341$ nm). The emission band is split into two maxima at $\lambda_{\text{em,max}} = 473$ nm and $\lambda_{\text{em,max}} = 511$ nm presumably due to vibronic coupling (Figure 63). The quantum yield was determined to $17 \pm 5\%$ in an Ulbricht sphere. The presence of two aminophenyl substituents results in a

3. Results and Discussion

bathochromic shift compared to Norman and Russell's cyclic 1,4-diaza-2,3-diborinane isomer.^[136]

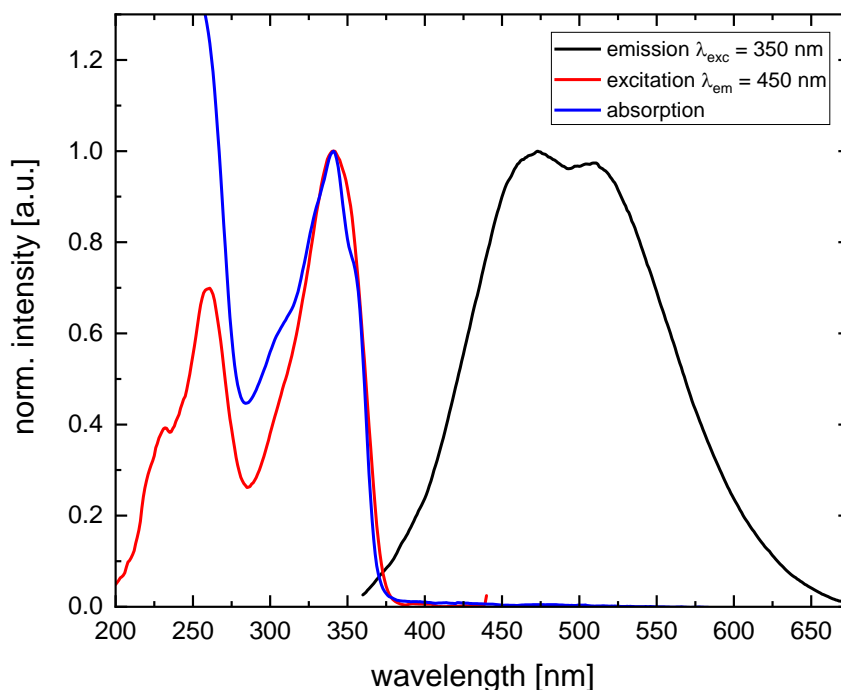


Figure 63. Absorption (blue), excitation (red) and emission (black) spectra of diazadiborinane **169** in hexane/ diethylether (5%).

Additional excitation that is hypsochromically shifted compared to the longest wavelength absorption was observed for **169** during routine measurements (Figure 64). A sample was tested for air sensitivity at low concentration in diglyme to avoid evaporation of the solvent while the cuvette was kept open. Figure 65 shows the time resolved change of the absorption spectrum of **169** under argon (violet) up until exposition to air overnight (red). The excitation spectrum of the decomposed sample (black, Figure 65) fits perfectly to the band at 304 nm emerging upon exposition to air. The use of diglyme instead of hexane resulted in a slight bathochromic shift of the spectra (Figure 66).

3. Results and Discussion

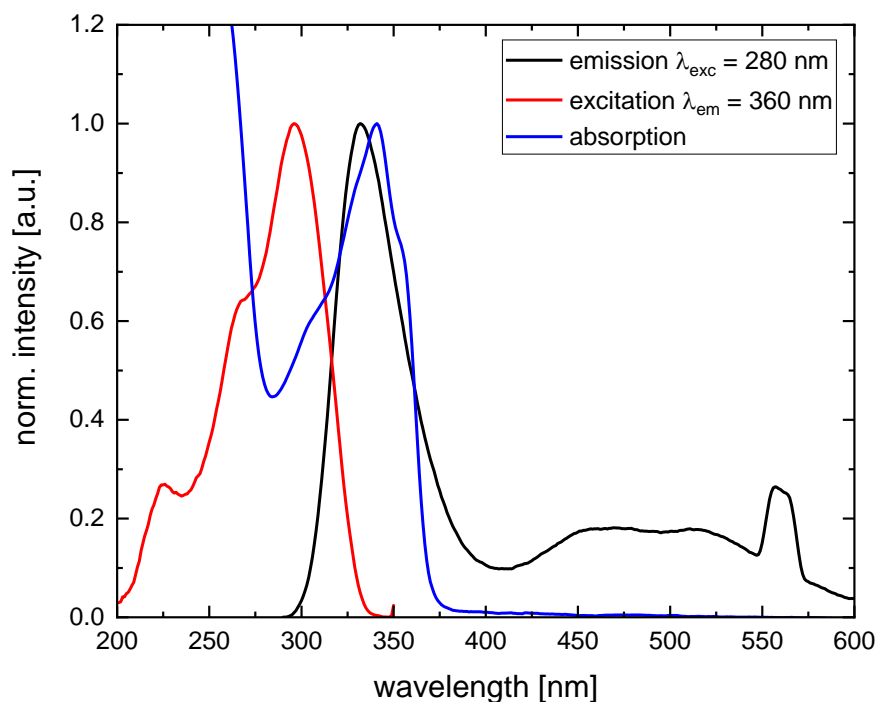


Figure 64. Absorption (blue), excitation (red) and emission (black) spectra of the unknown decomposition species in a solution of **169** in hexane/ diethylether(5%).

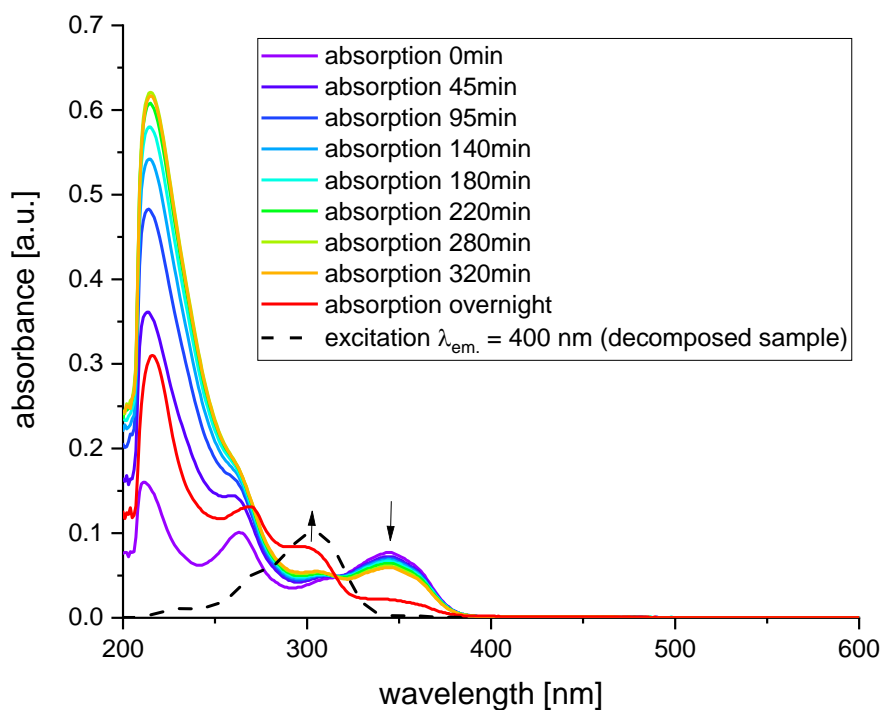


Figure 65. UV/Vis spectra of a 5 μM solution of **169** in diglyme under the influence of air (violet to red) and excitation band of a desomposed sample (black) in diglyme.

3. Results and Discussion

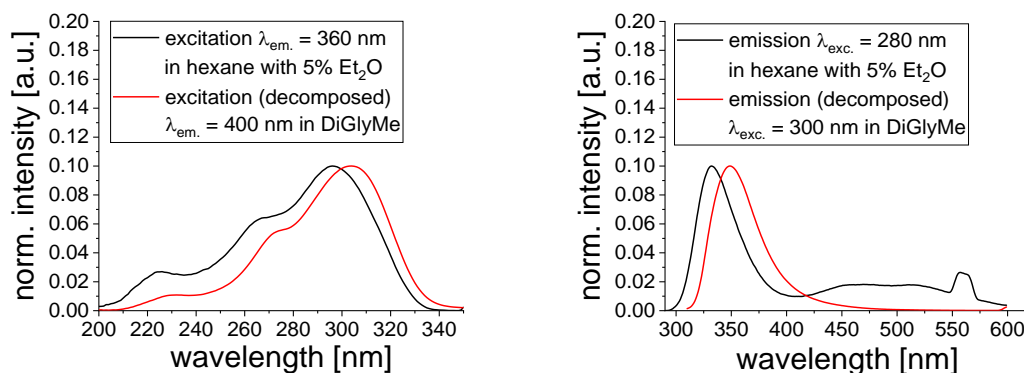
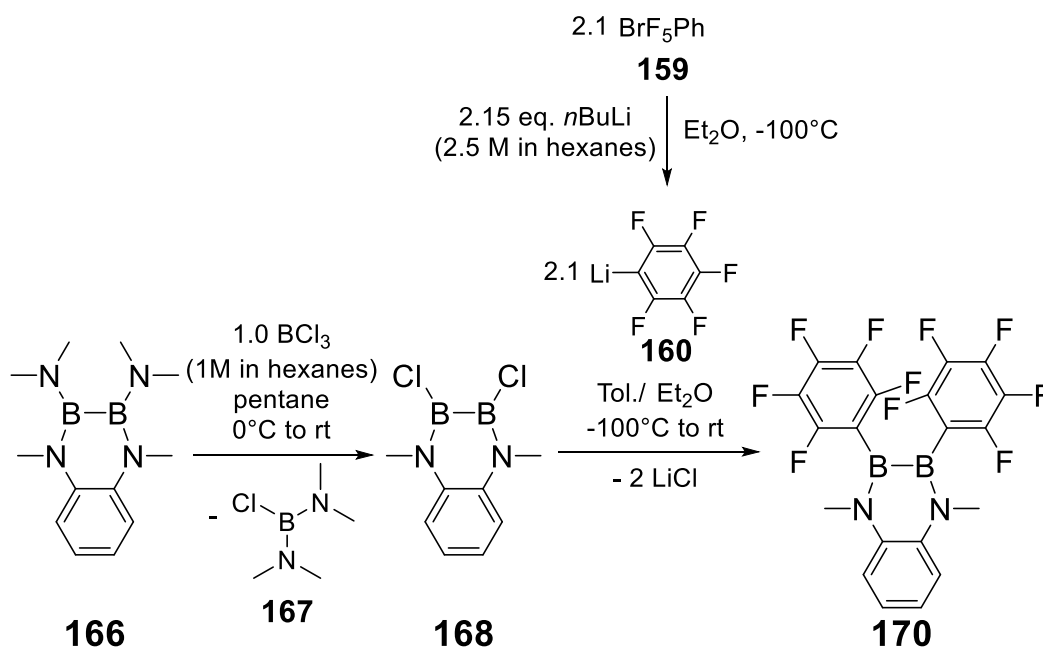


Figure 66. Excitation spectra (left) and emission spectra (right) of the decomposed species in the solution of **169** in hexane/ diethylether (5%) (black) and in diglyme after exposition to air overnight (red).

To test whether the pentafluorophenyl group could be attached to the diazadiborinane skeleton, an analogous procedure as described for the introduction of two aminophenyl substituents was followed. In a salt metathesis with two equivalents of the previously generated anion **160** and the dichlorodiazadiborinane **168** the bis(pentafluorophenyl)-substituted diborinane **170** was synthesized quantitatively (indicated by multinuclear NMR spectra of the crude product) and isolated as colorless crystals in mediocre yield by crystallization from toluene (26%) (Scheme 61). The ^{11}B NMR spectrum shows one broad signal (42.2 ppm) in the same range as cyclic 1,4-diaza-2,3-diborinanes **168** and **169**.



Scheme 61. Synthesis of bis(pentafluorophenyl)-substituted diazadiborinane **170**.

3. Results and Discussion

Single crystals were obtained from a toluene solution at room temperature. The molecular structure (Figure 67) shows the same features as **166** and **169** regarding the B-B-bond length and sum of angles around the boron and endocyclic nitrogen atoms. The largest deviation from the best plane through the atoms of the 1,4-diaza-2,3-diborinane heterocycle with 0.026(1) Å is observed for C1. The rather small deviation from planarity hints at pronounced endocyclic B-N-double bond character. Indeed, the endocyclic B-N bond lengths in **170** (1.396(2) Å, 1.401(2) Å) are even shorter than in **169**, due the increased endocyclic B-N- π -bond interaction. Expectedly, the pentafluorophenyl substituent is a far less efficient π -donor than from the *p*-dimethylaminophenyl substituent.

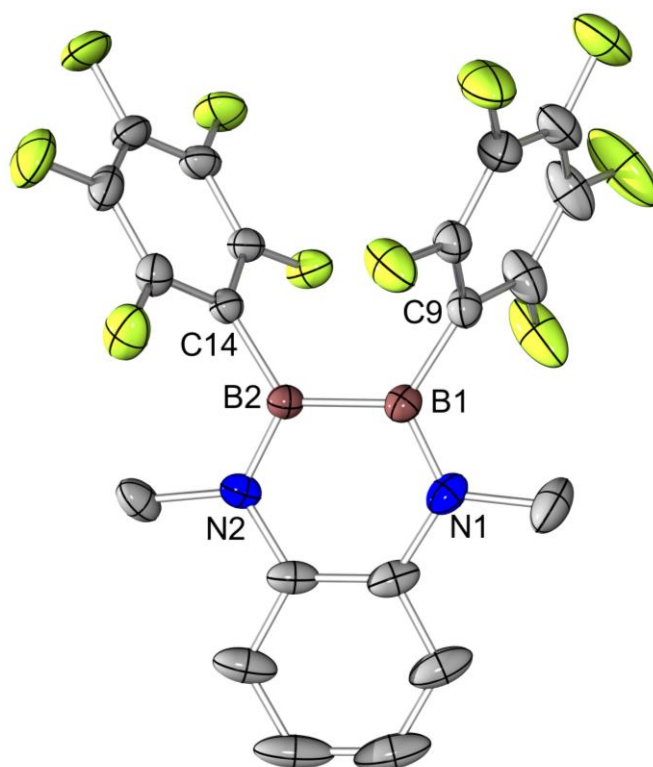


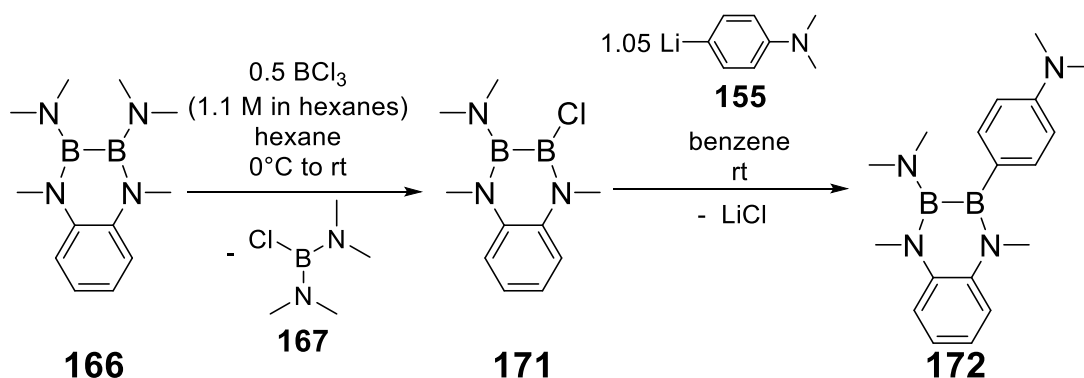
Figure 67. Molecular Structure of **170** in the solid state (ellipsoids at 50% probability, hydrogen atoms and cocrystallized toluene omitted for clarity). Selected bond lengths [Å] and angles [°]: B1-B2 1.663(2), B1-N2 1.396(2), B1-C9 1.590(2), B2-N1 1.401(2), B2-C14 1.587(2), Σ \sphericalangle B1 360.0, Σ \sphericalangle B2 360.0, Σ \sphericalangle N1 360.0, Σ \sphericalangle N2 360.0, largest deviation from the best plane through the atoms of the 1,4-diaza-2,3-diborinane heterocycle for C1: 0.026(1) Å.

In terms of photophysical properties, only the absorption spectra were examined for **170**, because no emission of light was observed when exposing **170** towards UV light (365 nm or 254 nm, respectively). The diborinane solution in diethylether ($c = 0.3$ -1 mM) shows multiple absorption bands at 317 nm ($\epsilon = 18300 \text{ M}^{-1} \text{ cm}^{-1}$), 254 nm ($\epsilon = 13800 \text{ M}^{-1} \text{ cm}^{-1}$) and 231 nm

3. Results and Discussion

($\epsilon = 25000 \text{ M}^{-1} \text{ cm}^{-1}$). The two absorption bands at longer wavelengths are hypsochromically shifted compared to **169**, which indicates less delocalization of electrons in the case of **170**.

Next, unsymmetrically substituted diborinanes were targeted. As a first step, in analogy to the synthesis of **168**, one of the two dimethylamino groups in **166** should be exchanged by one chlorine atom. Apart from the already discussed potential problem of cleaving off the *o*-phenylene diamine ligand during the reaction, it is also not self-evident that selective exchange of one dimethylamino group by a chlorine is achievable. Notwithstanding, the anticipated diborinane **171** in hexane at 0°C is selectively formed upon treatment of **166** with 0.5 equivalents of BCl_3 solution (1.1 M in hexane, Scheme 62). The chlorinated diborane **171** was dissolved in hexane and dried *in vacuo* twice to completely remove residual bis(dimethylamine)chloroborane (**167**) resulting in spectroscopically pure product. The ^{11}B NMR spectrum of **171** shows only two signals at 40.2 ppm and 31.8 ppm, which was therefore used without further purification. The subsequent reaction with 4-(dimethylamino)phenyllithium affords **172** as main product as indicated by ^1H (Figure 68) and ^{11}B NMR spectroscopy. It was isolated as yellow crystals in moderate yields by crystallization from hexane (31%) (Scheme 62). The ^{11}B NMR spectrum of the isolated diborinane **172** shows two signals in a 1:1 ratio at 47.2 ppm and 34.0 ppm, similar to those of **171**. The product is sensitive to air and moisture in the solid state and in solution.



Scheme 62. Synthesis of unsymmetrically substituted diazadiborinane **172**.

3. Results and Discussion

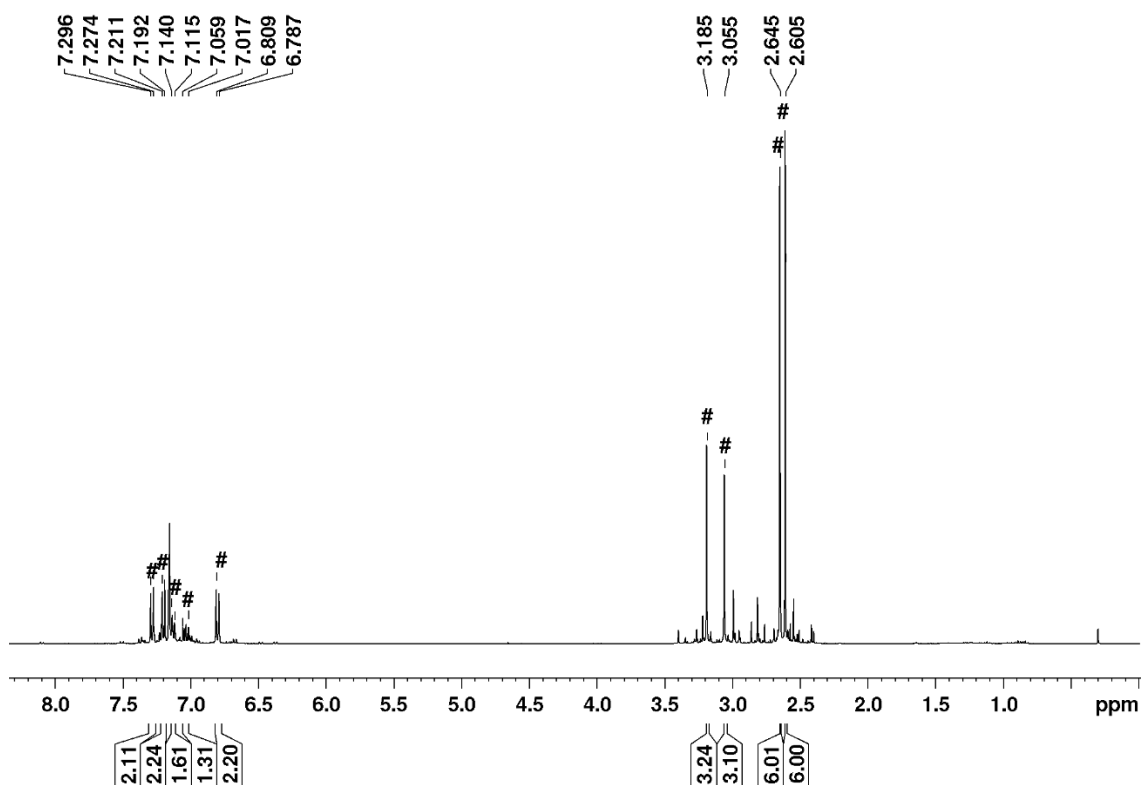


Figure 68. ^1H NMR spectrum of the crude product of diborinane **172**. (**172** is marked with “#”)

Single crystals were obtained from a concentrated hexane solution at 5°C . The solid-state structure (Figure 69) reveals similar structural parameters for the B-B bond length and sum of angles around the boron and endocyclic nitrogen atoms as in diborinanes **166**, **169**, **170** described in previous sections. The largest deviation from the best plane through the atoms of the 1,4-diaza-2,3-diborinane heterocycle with $0.132(1)$ Å is observed for B2. The deviation from planarity lies between the one of **166** and **169**, demonstrating a correlation between the number of directly boron attached NMe_2 groups and the planarity of the CNBBNC-ring. Şahin had explained the deviation from planarity in analogous compounds by steric interactions between the substituents.^[137] As discussed before, the strong π -donor properties of the exocyclic NMe_2 group might suppress the formation of endocyclic B-N π bonds. The B2-N2 bond length ($1.449(3)$ Å) is marginally longer than the other endocyclic B1-N1 bond ($1.423(3)$ Å), substantiating this hypothesis. The *para*-dimethylamino nitrogen atom of **172** shows pyramidalized coordination with $\Sigma\varphi = 348.2^\circ$ and a longer N4-C12 bond length ($1.412(2)$ Å) than those in **169**, but in the same range as in the 1,2-bis(dimethylamino)diboranes(4) (see Section 3.6.1), so that donor effects of the *para*- NMe_2 group are most likely weak, which is also reflected in

3. Results and Discussion

the angle between the aminophenyl ring-plane normal and the B-B binding axis of 38.83°.

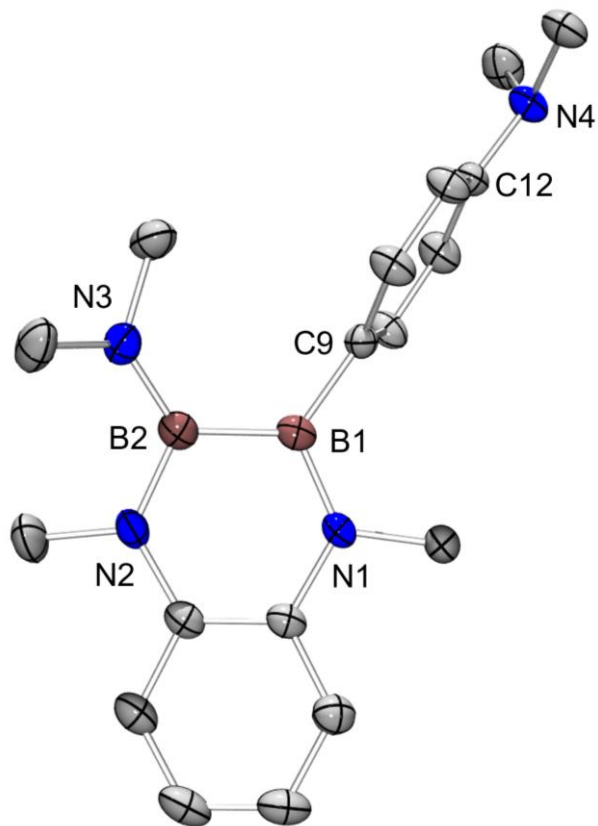


Figure 69. Molecular Structure of **172** in the solid state (ellipsoids at 50% probability, hydrogen atoms omitted for clarity). Selected bond lengths [Å] and angles [°]: B1-B2 1.686(3), B1-N1 1.423(3), B1-C9 1.584(3), B2-N2 1.449(3), B2-N3 1.421(3), N4-C12 1.412(2), $\Sigma \angle$ B1 360.0, $\Sigma \angle$ B2 359.9, $\Sigma \angle$ N1 360.0, $\Sigma \angle$ N2 360.0, $\Sigma \angle$ N3 359.0, $\Sigma \angle$ N4 348.2, largest deviation from the best plane through the atoms of the 1,4-diaza-2,3-diborinane heterocycle for B2: 0.132(1) Å.

A solution of diborinane **172** in hexane ($c = 0.4\text{-}0.7$ mM) shows multiple absorption band maxima at 327 nm ($\epsilon = 158100$ M⁻¹ cm⁻¹), 315 nm ($\epsilon = 14840$ M⁻¹ cm⁻¹), 243 nm ($\epsilon = 24880$ M⁻¹ cm⁻¹) and 216 nm ($\epsilon = 34980$ M⁻¹ cm⁻¹). Identical absorption bands are observed at lower concentrations of **172** ($c = 5$ μM) in preparation for fluorescence measurements (Figure 70). In addition, the longest wavelength absorption band fits the excitation band ($\lambda_{\text{max}} = 313$ nm) perfectly. Emission was detected with a maximum at 355 nm and a quantum yield of $48 \pm 5\%$ (determined by Ulbricht sphere). On the one hand the presence of only one aminophenyl substituent results in a hypsochromic shift compared to the doubly aminophenyl-substituted diborinane **169** and also compared to Norman and Russell's bicyclic 1,4-diaza-2,3-diborinane isomer^[136] due to a smaller conjugated system, but on the other

3. Results and Discussion

hand a bathochromic shift in emission is observed when compared to starting diborinane **166**, which is indicative of the expansion of the conjugated system.

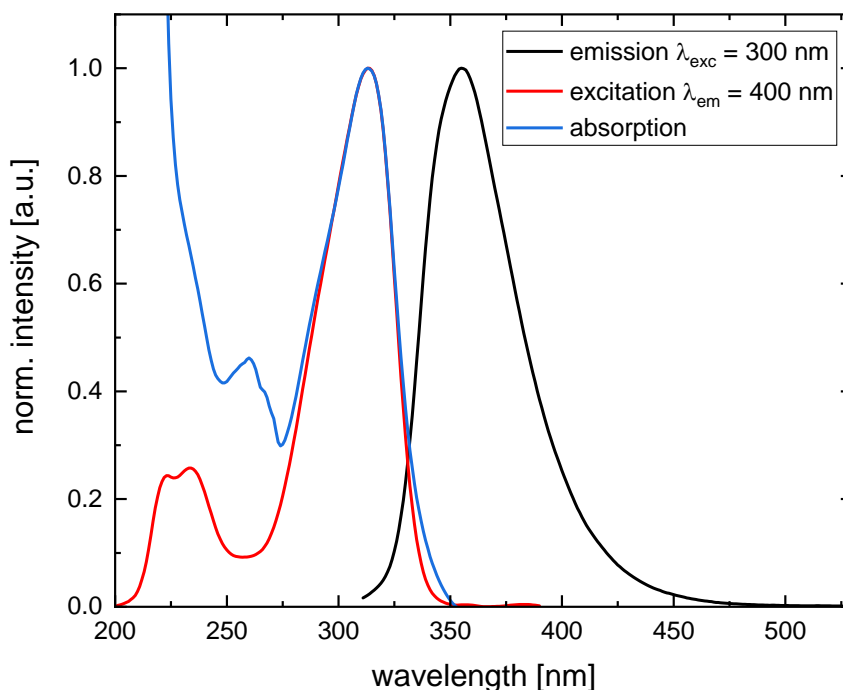
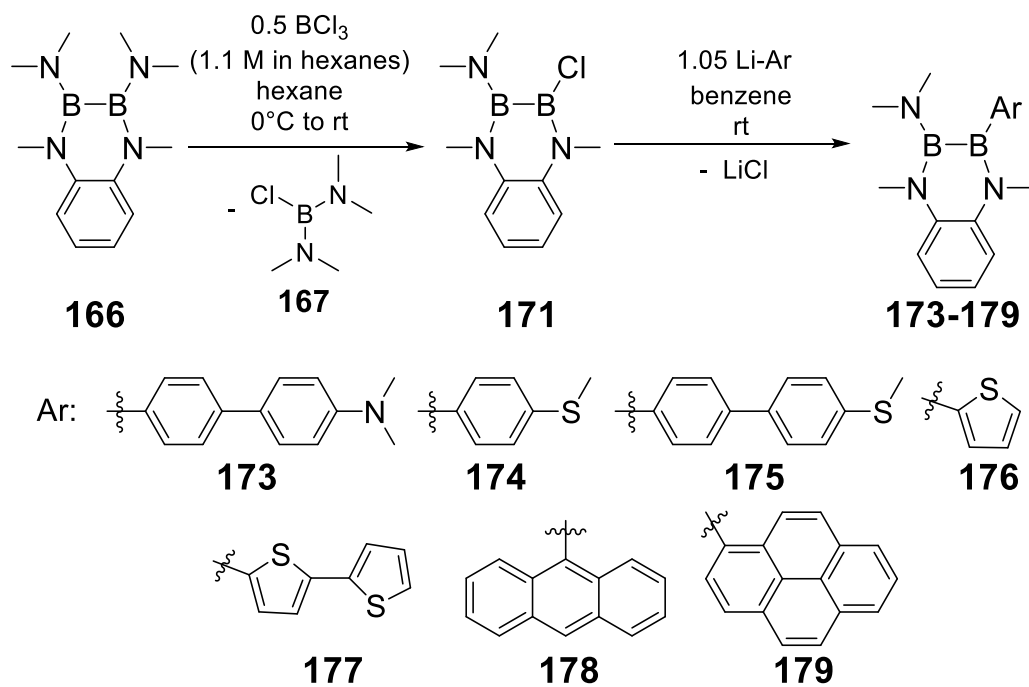


Figure 70. Absorption (blue), excitation (red) and emission (black) spectra of diazadiborinane **172** in hexane.

Since diborinane **172** exhibits fluorescence with acceptable quantum yield, other substituents were considered to induce a bathochromic shift of the excitation and emission bands. Following the procedure described above, the starting chloro diborinane **171** was synthesized through replacement of one dimethylamino group in **166** by a chloro substituent with 0.5 equivalents of BCl_3 solution (Scheme 63) Subsequent reaction with the appropriate aryllithium species (either isolated or generated just before use, Scheme 63) yielded the anticipated structures suggested by ^{11}B NMR resonances and selected ^1H NMR resonances (Table 3), which compare well to the one of diborinane **172**. While ^{11}B NMR spectra confirm selective formation of the anticipated structures **173** to **179**, in the case of **173** (^1H NMR and ^{11}B NMR spectra displayed as representatives in Figure 71 and Figure 72) a minor unidentified side product was observed as well. The ^1H NMR spectra (see Section 7.3), however, suggest that although the anticipated structures are formed as main products, a considerable number of sometimes apparently boron-free side products are formed as well. Isolation of the compounds was therefore not pursued.

3. Results and Discussion



Scheme 63. Reactivity of diazadiborinane 171 towards various aromatic lithium organyls.

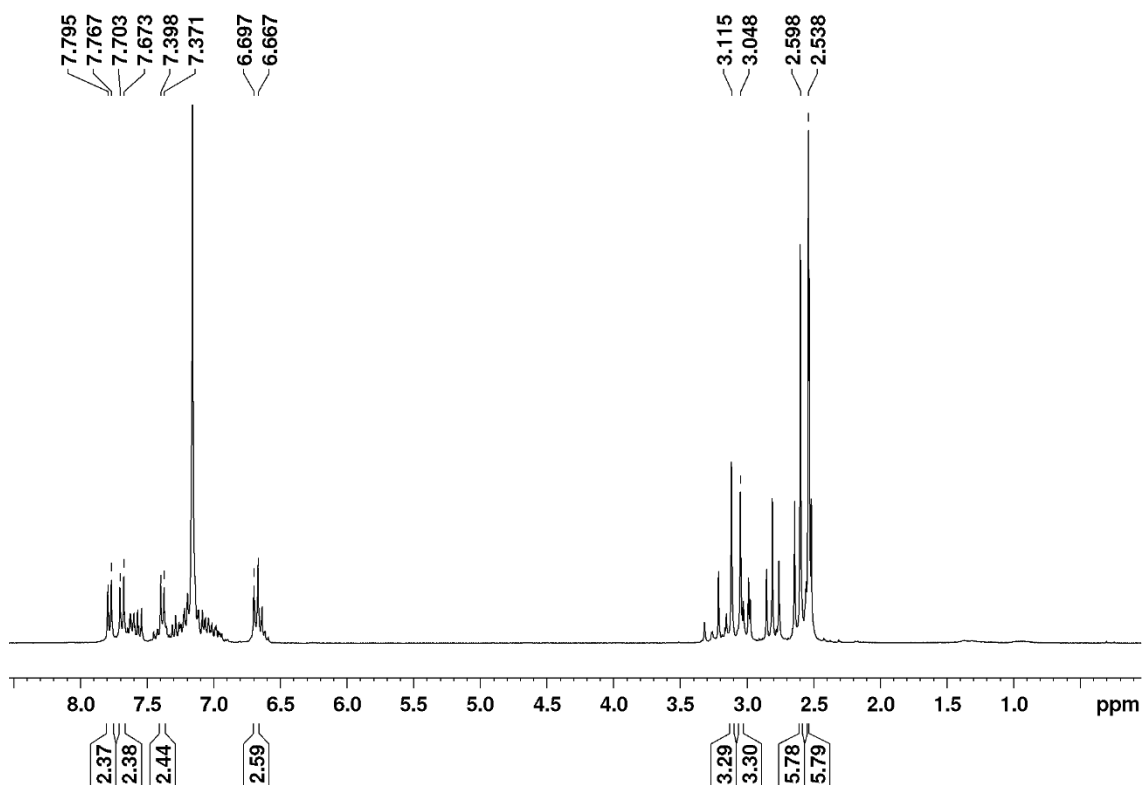


Figure 71. ¹H NMR spectrum of YK181. Selected resonances of anticipated product 173 marked and integrated.

3. Results and Discussion

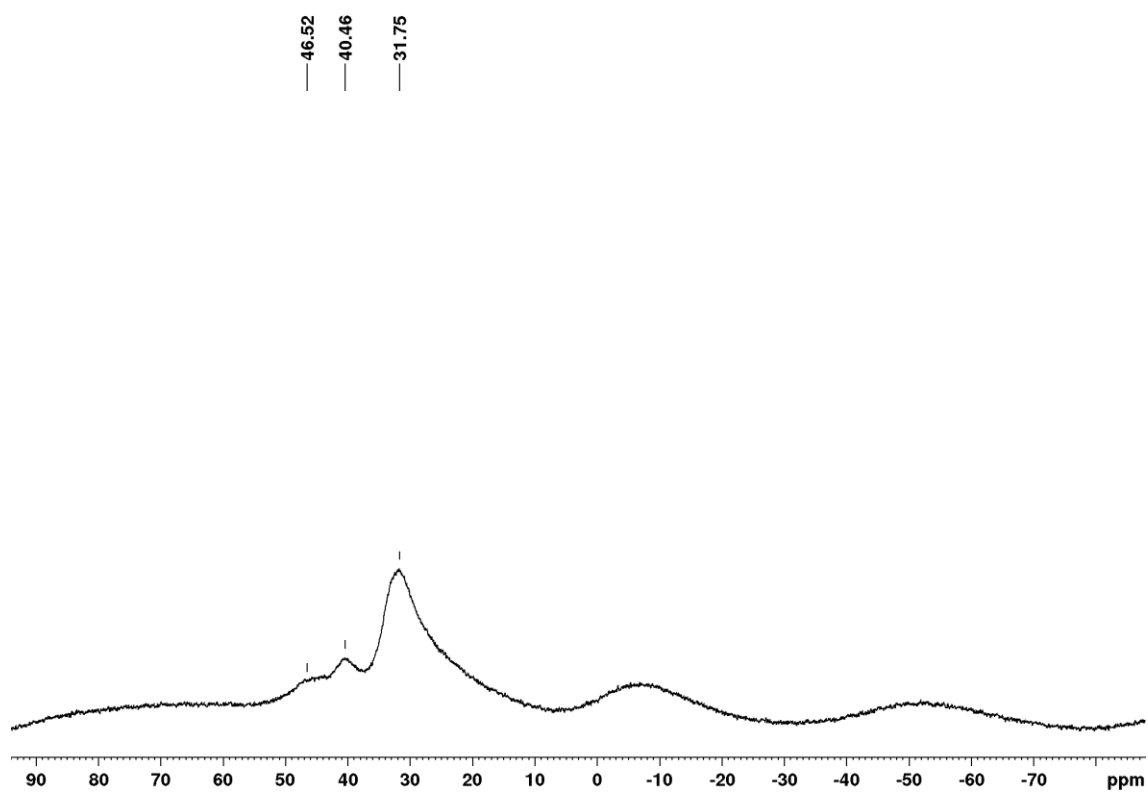


Figure 72. ^{11}B NMR spectrum of YK181. Selected resonances of anticipated product **173** at 46.5 and 31.8 ppm.

3. Results and Discussion

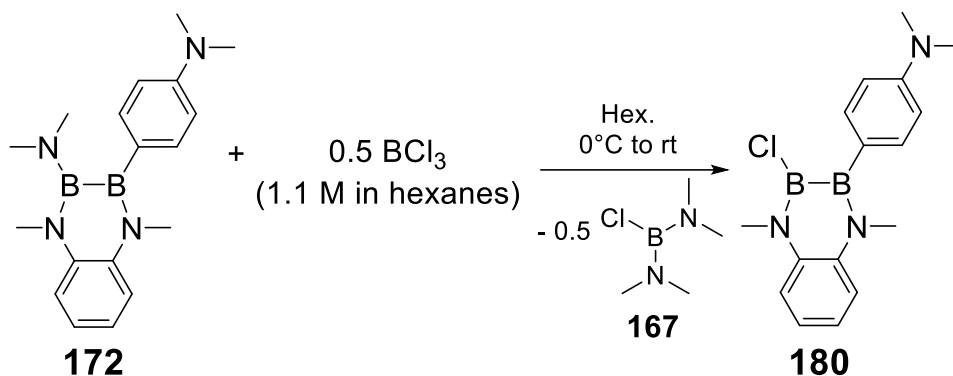
Table 3. ^{11}B NMR resonances of reaction mixtures of unsymmetrically with various aryls substituted diazadiborinanes **173** to **179**.

Anticipated structure	^{11}B NMR resonances [ppm]	Selected ^1H NMR resonances [ppm]
173	46.5 (very br s), 40.5 (br, s, minor unidentified side product), 31.8 (br, s)	3.11, 3.05 (each s, each 3H, B-NCH ₃), 2.60 (s, 6H, Ar-NCH ₃)
174	48.7 (br s), 33.5 (br, s)	3.02, 3.02 (each s, altogether 6H, B-NCH ₃), 2.54 (s, 6H, Ar-NCH ₃)
175	48.6 (br s), 34.7 (br, s)	3.07, 3.05 (each s, each 3H, B-NCH ₃), 2.58 (s, 6H, Ar-NCH ₃)
176	46.2 (br s), 33.5 (br, s)	3.09, 2.96 (each s, each 3H, B-NCH ₃), 2.55 (s, 6H, Ar-NCH ₃)
177	45.6 (br s), 33.8 (br, s)	3.12, 2.95 (each s, each 3H, B-NCH ₃), 2.58 (s, 6H, Ar-NCH ₃)
178	47.1 (br s), 33.0 (br, s)	3.07, 2.90 (each s, each 3H, B-NCH ₃), 2.18 (s, 6H, Ar-NCH ₃)
179	46.9 (br s), 33.2 (br, s)	3.10, 2.98 (each s, each 3H, B-NCH ₃), 2.33 (s, 6H, Ar-NCH ₃)

To be able to attach an additional organic substituent at the second boron center, the boron-bonded dimethylamino group of **172** was exchanged for a chloro substituent. Following the procedure established for the synthesis of **171**, treatment of **172** with 0.5 equivalents of BCl₃ solution (1.1 M in hexane) yielded **180** as the main product as evident from ^1H NMR spectroscopy (Scheme 64, Figure 73). Colorless crystals of **180** were isolated in moderate yield by crystallization from a mixture of toluene and hexane (42%). The ^{11}B NMR spectrum of **180** shows a single broad signal at 43.2 ppm in the expected

3. Results and Discussion

range.^[134,135,137,138] As in the case of **156**, the expected two signals are probably too close in chemical shift to be resolved. In solution as well as in the solid state and in the ambient atmosphere, diborinane **180** undergoes rapid and unselective oxidation. Under argon, no decomposition is observed upon prolonged heating above the melting point (mp. 115-120°C).



Scheme 64. Synthesis of unsymmetrically substituted chloro-diazadiborinane **180**.

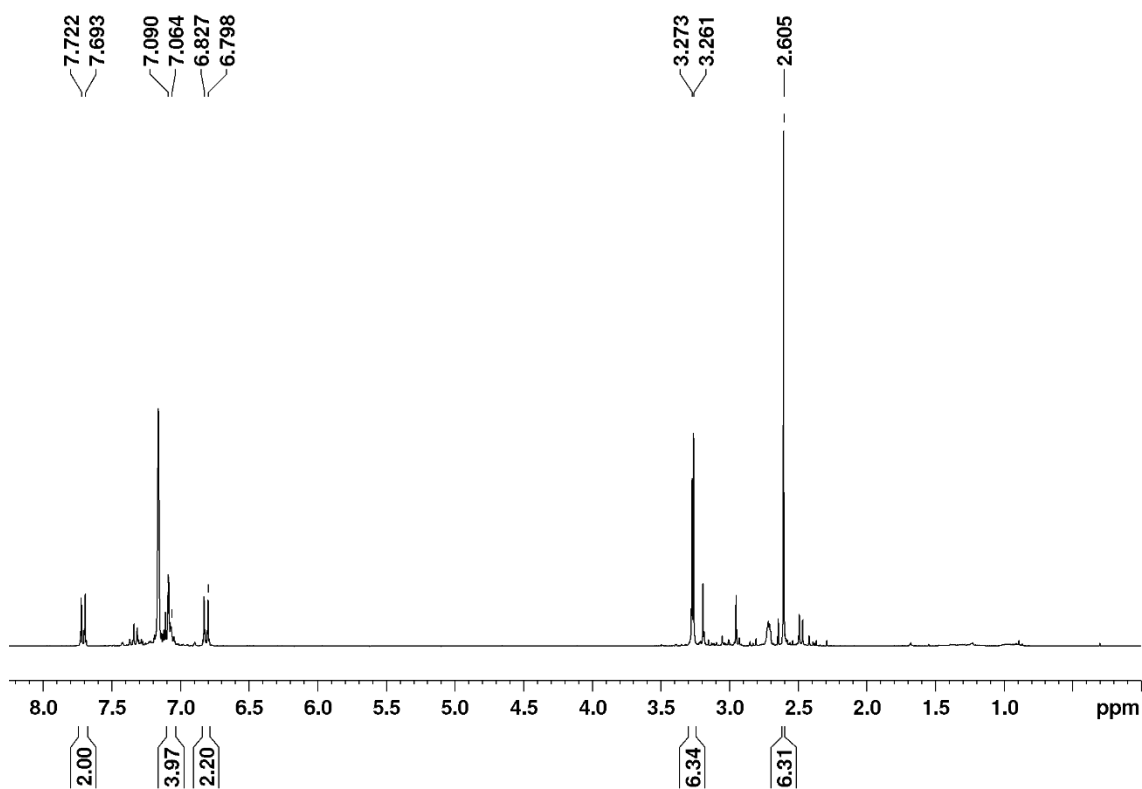


Figure 73. ¹H NMR of the crude product of **180** (only resonances of **180** are marked and integrated).

Single crystals could be obtained from a mixture of toluene and hexane solution at room temperature. The molecular structure is shown in Figure 74. The B-B bond length (1.663(2) Å) is shorter than in the 1,2-bis(dimethylamino)diboranes (Section 3.6.1) and, in contrast to the other diborinane structures described

3. Results and Discussion

above, even slightly shorter than the bond lengths observed in the 1,4-diaza-2,3-diborinines prepared by Braunschweig (1.673 Å)^[135], most likely due to lowered steric interaction of the substituents. The sum of angles around the boron and endocyclic nitrogen atoms in cyclic 1,4-diaza-2,3-diborinane **180**, in line with the other 1,4-diaza-2,3-diborinanes show trigonal planar coordination geometries ($\Sigma \angle \approx 360^\circ$). The largest deviation from the best plane through the atoms of the 1,4-diaza-2,3-diborinane heterocycle with 0.034(1) Å is observed for N2. The deviation from planarity is quite small suggesting pronounced endocyclic B-N π -bond interaction. Compared to **166** and **172** the endocyclic B-N bond lengths in **180** (1.410(2) Å, 1.400(2) Å) are shorter, supporting increased endocyclic B-N- π -bond interaction. The coordination environment of the aminophenyl nitrogen atom in **180** is almost perfectly trigonal planar ($\Sigma \angle = 359.9^\circ$). This circumstance provides a hint at π -donor contribution of the *para*-NMe₂-phenyl group. The N-C_{phenyl} bond length of **180**, however, is in the same range as those in 1,2-bis(dimethylamino)diboranes(4) (Section 3.6.1) and the angle between the aminophenyl ring-plane normal and the B-B binding axis amounts to 35.60°, so that donor effects of the NMe₂-aniline group are likely weak as well.

3. Results and Discussion

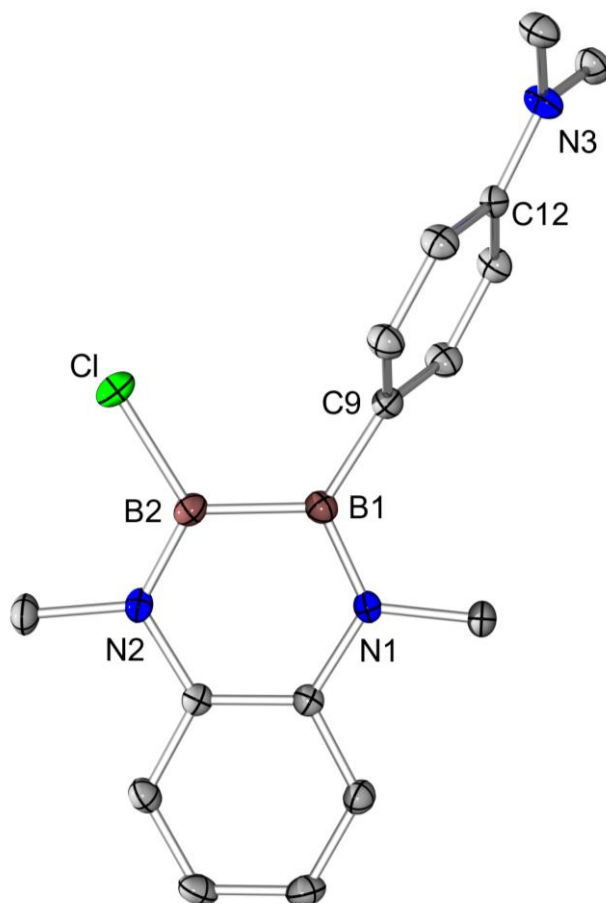


Figure 74. Molecular structure of **180** in the solid state (ellipsoids at 50% probability, hydrogen atoms omitted for clarity). Selected bond lengths [Å] and angles [°]: B1-B2 1.663(2), B1-N1 1.410(2), B1-C9 1.570(2), B2-N2 1.400(2), B2-Cl 1.794(2), N3-C12 1.380(2), $\Sigma \angle$ B1 360.0, $\Sigma \angle$ B2 359.9, $\Sigma \angle$ N1 360.0, $\Sigma \angle$ N2 360.0, $\Sigma \angle$ N3 359.9, largest deviation from the best plane through the atoms of the 1,4-diaza-2,3-diborinane heterocycle for N2: 0.034(1) Å.

Diborinane **180** shows absorption maxima in diethylether ($c = 0.4\text{-}1\text{ mM}$) at 334 nm ($\epsilon = 21200\text{ M}^{-1}\text{ cm}^{-1}$), 255 nm ($\epsilon = 18700\text{ M}^{-1}\text{ cm}^{-1}$) and 232 nm ($\epsilon = 18900\text{ M}^{-1}\text{ cm}^{-1}$). In contrast to **172**, no emission was detected for excitement at the longest wavelength absorption suggesting that the B-bonded chloro substituent quenches the fluorescence. In the case of **180**, sensitivity towards air was tested in diglyme. Decomposition was observed by absorption spectroscopy (Figure 75) and as in the case of **169** a fluorescent species emerged, which was already detected in a sample of **180** in hexane with 5% diethylether solution ($c = 5\text{ }\mu\text{M}$). Here as well, a bathochromic shift of the emission and excitation spectra could be observed when the experiments were carried out in diglyme (Figure 76).

3. Results and Discussion

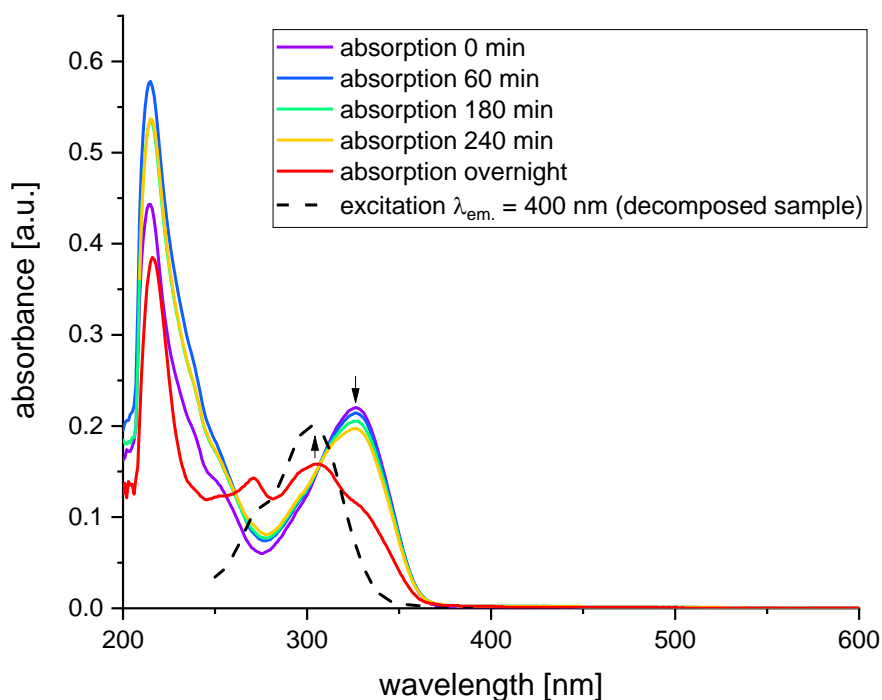


Figure 75. UV/vis spectra of a 5 μM solution of **180** in diglyme under the influence of air (violet to red) and excitation band of a desomposed sample (black) in diglyme.

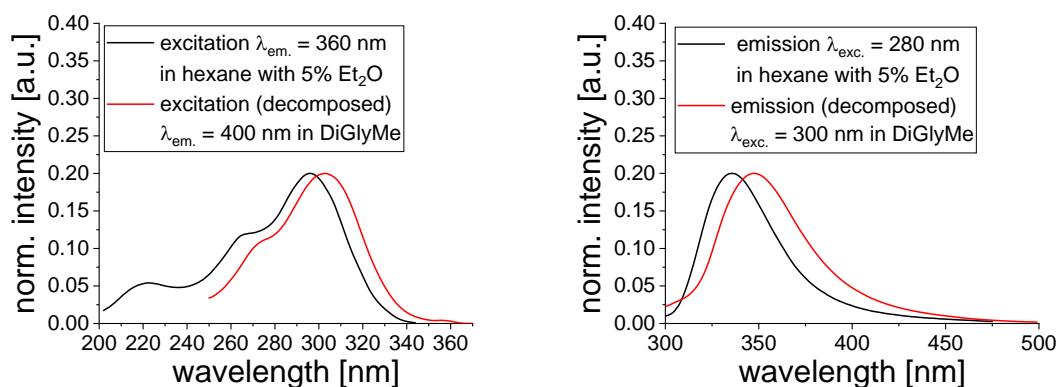
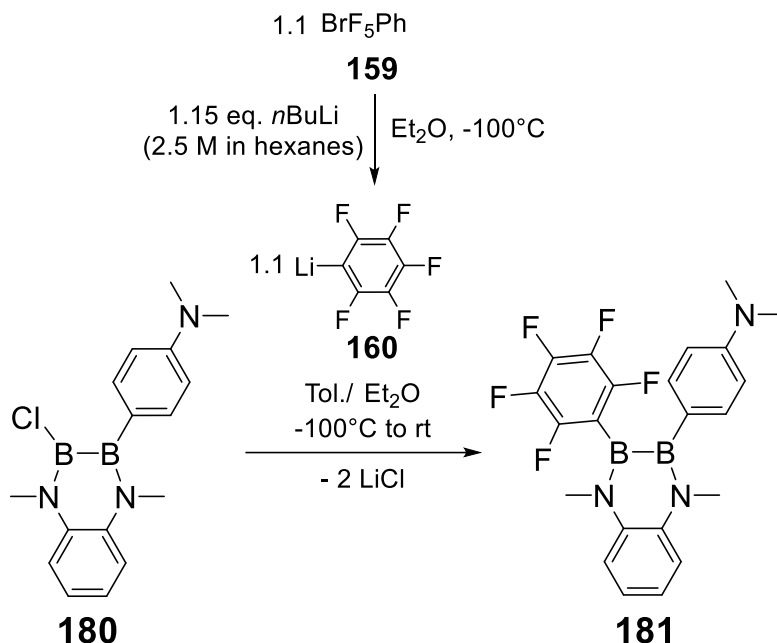


Figure 76. Excitation spectra (left) and emission spectra (right) of the decomposed species in the solution of **180** in hexane/ diethylether (5%) (black) and in diglyme after exposition to air overnight (red).

Diborinane **180** was then employed in a salt metathesis reaction with a selected aryllithium reagent to give an unsymmetrically substituted diaryl diborinane. Previously generated pentafluorophenyllithium^[263] was reacted with **180** in a mixture of toluene and diethylether at -100°C to selectively yield the unsymmetrically substituted cyclic diazadiborinane **181** in acceptable yields (49%) as a colorless powder (Scheme 65). The ^{11}B NMR spectrum shows one broad signal at 45.3 ppm in the same range as **180**. Again, the expected two signals are presumably too close in chemical shift to be resolved. In solution and in the ambient atmosphere, **181** undergoes rapid and unselective oxidation. In the solid state, it tolerates exposure to air and moisture overnight. Under

3. Results and Discussion

argon, no decomposition is observed upon prolonged heating above the melting point (mp. 131-135°C).



Scheme 65. Synthesis of unsymmetrically substituted diazadiborinane **181**.

Single crystals were obtained from a hexane solution at room temperature. The molecular structure is shown in Figure 77. The B-B bond length (1.676(2) Å) is in the same range as the previously discussed 1,4-diaza-2,3-diborinanes in this thesis and trigonal planar coordination environment is adopted around the boron and endocyclic nitrogen atoms, too. The largest deviation from the best plane through the atoms of the 1,4-diaza-2,3-diborinane heterocycle with 0.052(1) Å is observed for B1. The deviation from planarity is rather small hinting at pronounced endocyclic B-N- π -bond interaction, which is supported by shorter endocyclic B-N bond lengths in **181** (1.422(1) Å, 1.402(1) Å) compared to **166** and **172**. The coordination environment of the aminophenyl nitrogen atom in **181** is pyramidalized ($\Sigma \angle = 348.5^\circ$) and the N-C_{phenyl} bond length, is in the same range as those in 1,2-bis(dimethylamino)diboranes(4) in Section 3.6.1. Furthermore, an angle between the aminophenyl ring plane normal and the B-B binding axis of 50.03° is observed, so that donor effects of the NMe₂-aniline group are most likely weak as well.

3. Results and Discussion

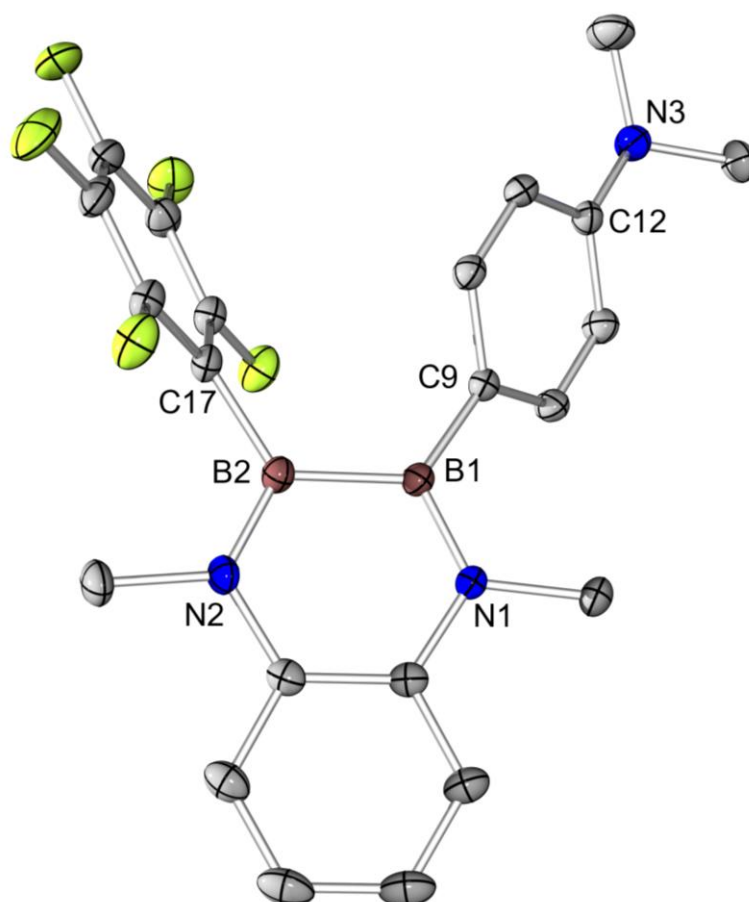


Figure 77. Molecular structure of **181** in the solid state (ellipsoids at 50% probability, hydrogen atoms omitted for clarity). Selected bond lengths [Å] and angles [°]: B1-B2 1.676(2), B1-N1 1.422(1), B1-C9 1.571(1), B2-N2 1.402(1), B2-C17 1.595(1), N3-C12 1.404(1), Σ \angle B1 360.0, Σ \angle B2 360.0, Σ \angle N1 360.0, Σ \angle N2 360.0, Σ \angle N3 348.5, largest deviation from the best plane through the atoms of the 1,4-diaza-2,3-diborinane heterocycle for B1: 0.052(1) Å.

The diborinane **181** solution in hexane ($c = 0.4$ - 1 mM) shows multiple UV-vis absorption band maxima at 349 nm ($\epsilon = 16900$ M⁻¹ cm⁻¹), 313 nm ($\epsilon = 15000$ M⁻¹ cm⁻¹) and 263 nm ($\epsilon = 21000$ M⁻¹ cm⁻¹) identical with the absorption spectrum at $c = 5$ μ M in preparation for fluorescence measurements. Pentafluorophenyl-substituted diborinane **181** is almost equally excited at three distinct maxima at $\lambda_{exc,max} = 266$ nm, $\lambda_{exc,max} = 300$ nm and $\lambda_{exc,max} = 350$ nm but exhibits only one emission maximum at $\lambda_{em,max} = 406$ nm in accordance with Kasha's rule (Figure 78).^[272] Quantum yield is determined by Ulbricht Sphere and amounts in this case to poor $7 \pm 5\%$. The second aryl substituent leads to a bathochromic shift in emission in comparison to **172** probably due to extension of the conjugated system but is not as bathochromically shifted as **169** with two aminophenyl groups indicating a less pronounced delocalization of electrons in **181**.

3. Results and Discussion

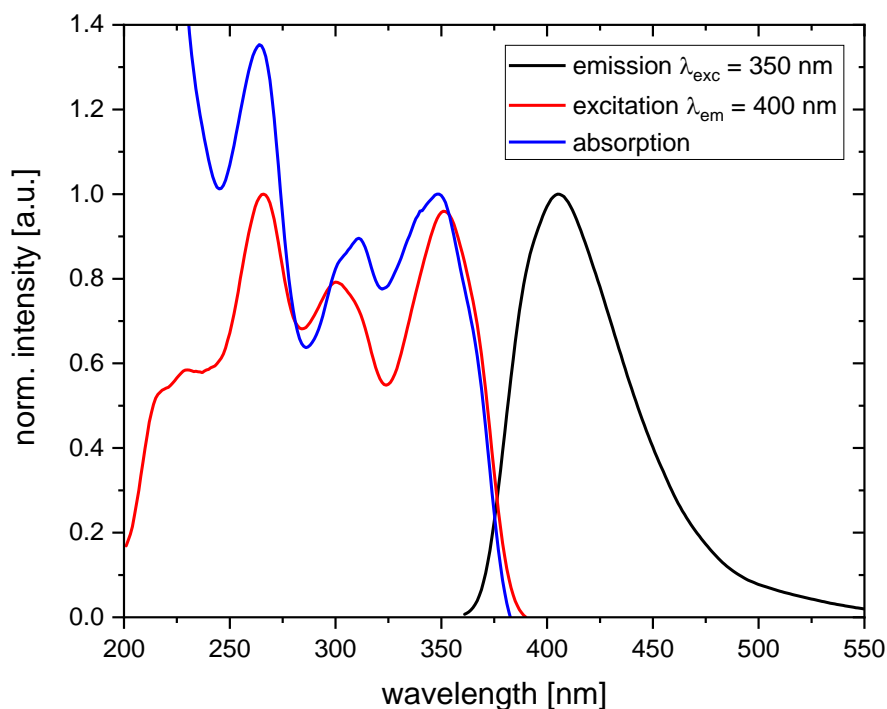


Figure 78. Absorption (blue), excitation (red) and emission (black) spectra of diazadiborinane **181** in hexane.

In the case of **181** the sensitivity towards air was studied in diglyme and analogous behavior to the cases of **169** and **180** was found. The longest wavelength absorption band loses intensity and a band at smaller wavelength emerges after exposition to air (Figure 79). The emerging species is also showing fluorescence and was observed before in a hexane solution of **181**. Due to overlaps of the excitation bands of **181** and the decomposed species both are excited in the freshly prepared hexane solution (black, Figure 80). Here, as well, a bathochromic shift was observed upon change of the solvent from hexane to diglyme (Figure 80).

3. Results and Discussion

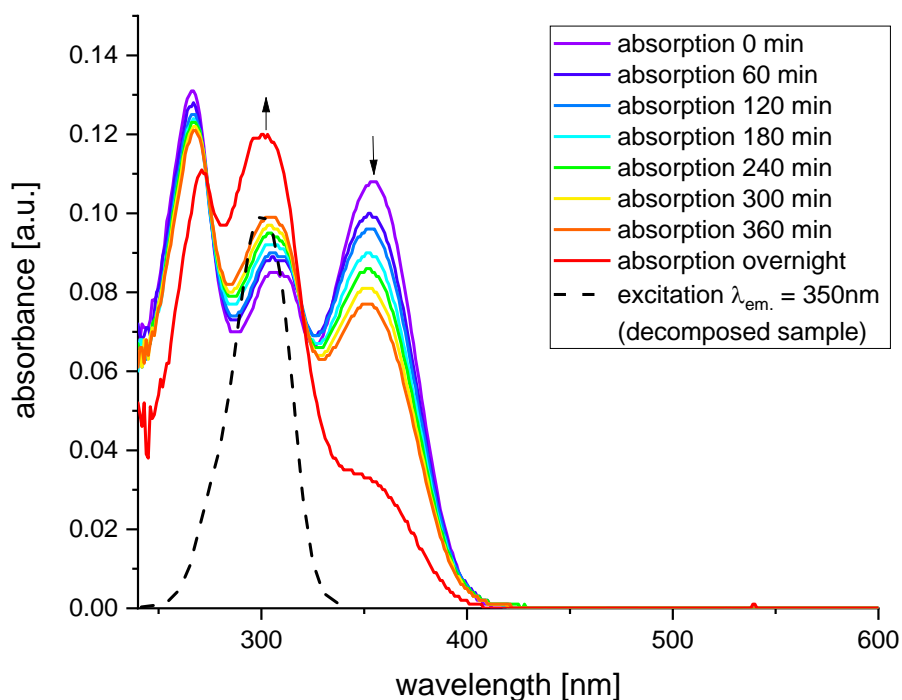


Figure 79. UV/vis spectra of a 5 μM solution of **181** in diglyme under the influence of air (violet to red) and excitation band of a desomposed sample (black) in diglyme.

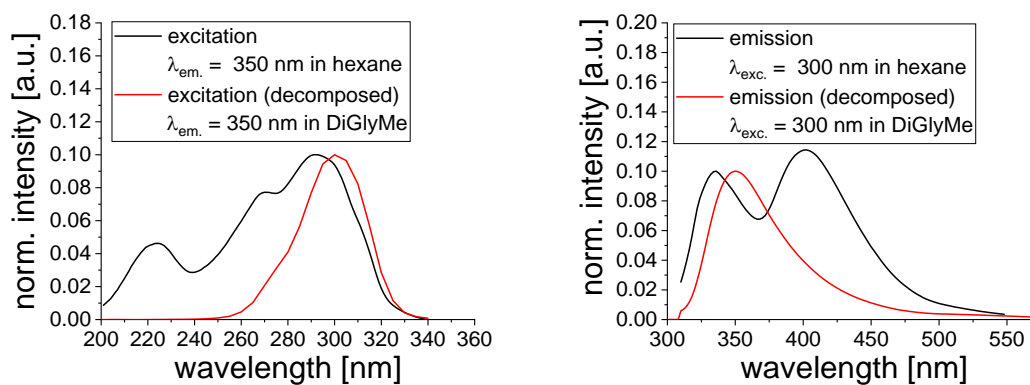
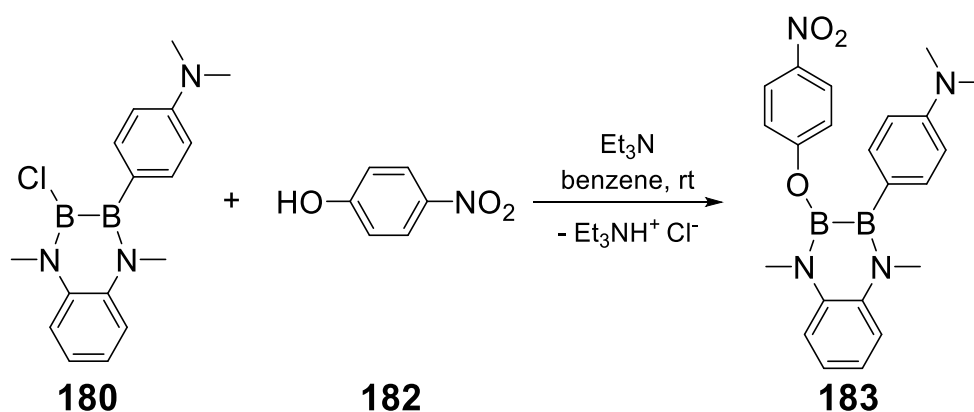


Figure 80. Excitation spectra (left) and emission spectra (right) of the decomposed species in the solution of **181** in hexane (black) and in diglyme after exposition to air overnight (red).

3. Results and Discussion

In the next step, a more electron withdrawing aryl substituent, *p*-nitrophenyl for example, should replace pentafluorophenyl. Considering its anion is hard to generate and very labile, the stability of the diborane moiety towards the nitro-group was tested, by choosing *p*-nitrophenol in a first attempt to react with **180** under HCl elimination. Therefore, 1,4-diaza-2,3-diborinane **180** and *p*-nitrophenol were separately dissolved and suspended in benzene, respectively. Triethylamine, as reagent to capture the eliminated HCl, was added to the diborinane solution, which afterwards is transferred *via cannula* to the nitrophenol suspension. Stirring for 1.5 hours selectively yields the desired nitrophenol substituted diborane **183** (Scheme 66).



Scheme 66. Synthesis of 4-nitrophenoxy substituted diazadiborinane **183**.

Single crystals were obtained in an NMR-tube from a C₆D₆-solution. **183** crystallizes in two different space groups (*P* $\bar{1}$ and *C*2/*c*). The molecular structure of the monoclinic system (*C*2/*c*) is discussed and shown in Figure 81, because of better structure refinement parameters (R indices). The B-B bond length (1.684(2) Å) is in the typical range^[135] and trigonal planar coordination geometries ($\Sigma \angle \approx 360^\circ$) are found around the boron and endocyclic nitrogen atoms. The largest deviation from the best plane through the atoms of the 1,4-diaza-2,3-diborinane heterocycle with 0.028(1) Å is observed for N1. The deviation from planarity is rather small, hinting at pronounced endocyclic B-N-double bond character. In addition, when compared to **166** and **172** the endocyclic B-N bond lengths in **183** (1.413(1) Å, 1.419(1) Å) are shorter, due to increased endocyclic B-N- π -bond interaction, as observed for the other diborinanes without direct attachment of one NMe₂-group (**169**, **170**, **180**, **181**) to the boron center. The coordination environment of N3 in **183** is pyramidalized

3. Results and Discussion

($\Sigma \tau = 351.8^\circ$) and the N-C_{phenyl} bond length, is in the same range as those in 1,2-bis(dimethylamino) diboranes(4) of Section 3.6.1 so that donor effects of the *para*-NMe₂ group are most likely weak in this case as well. This is in line with an angle between the phenyl ring-plane normal and the B-B binding axis of 36.14°.

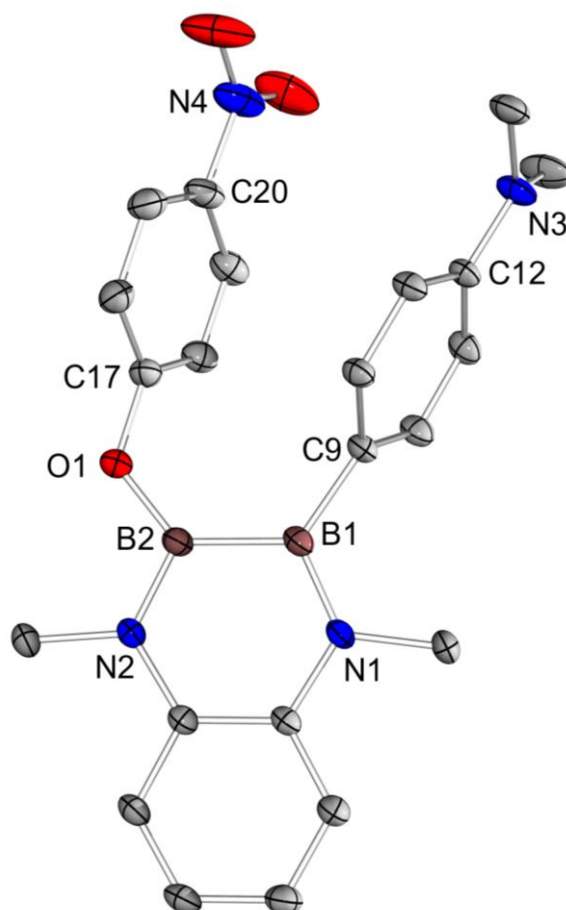


Figure 81. Molecular Structure of **183** in the solid state (ellipsoids at 50% probability, hydrogen atoms omitted for clarity). Selected bond lengths [Å] and angles [°]: B1-B2 1.684(2), B1-N1 1.413(1), B1-C9 1.575(1), B2-N2 1.419(1), B2-O1 1.399(1), N3-C12 1.394(1), O1-C17 1.363(1), C20-N4 1.457(1), $\Sigma \tau$ B1 360.0, $\Sigma \tau$ B2 360.0, $\Sigma \tau$ N1 360.0, $\Sigma \tau$ N2 360.0, $\Sigma \tau$ N3 351.8, $\Sigma \tau$ N4 360.0, largest deviation from the best plane through the atoms of the 1,4-diaza-2,3-diborinane heterocycle for N1: 0.028(1) Å.

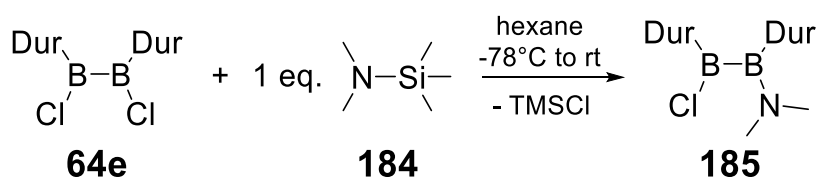
In terms of photophysical properties only absorption was examined. Diborinane **183** solution in diethylether ($c = 0.4$ - 1 mM) shows multiple absorption bands at 316 nm ($\epsilon = 25100$ M⁻¹ cm⁻¹), 259 nm ($\epsilon = 20700$ M⁻¹ cm⁻¹) and 232 nm ($\epsilon = 26200$ M⁻¹ cm⁻¹). The two absorption bands at longer wavelengths are hypsochromically shifted compared to the ones of **169** and **181**, which indicates a lower degree of electron delocalization in the case of **183**.

3. Results and Discussion

3.6.3 Syntheses and spectroscopic studies of 1,2-diduryldiboranes(4)

A lot of reported fluorescent monoboranes do not contain directly attached amino groups but mostly bulky aryl substituents for kinetic stabilization (for example BMe_2 ^[171-189]). Hence, the properties of symmetrically and unsymmetrically substituted 1,2-diaryl diboranes(4) in comparison to the analogously substituted 1,2-bis(dimethylamino)diboranes(4) were to be investigated. The bulky aryl ligand 2,3,5,6-tetramethylphenyl (from here on: duryl) was chosen.

1,2-Dichloro-1,2-diduryldiborane(4) (**64e**) was synthesized according to the literature procedure.^[98,104] For selective unsymmetrical substitution, protection of one reactive site by reaction of **64e** with $\text{Me}_3\text{SiNMe}_2$ in hexane at -78°C following modified literature procedure was performed,^[273] which afforded **185** in very good yields (83%) as a colorless solid (Scheme 67). The ^{11}B NMR spectrum shows a very broad peak at 88.0 ppm for the chloro-substituted boron atom, as expected^[98,104], and one broad signal at 47.2 ppm for the amino-substituted, also in the expected range.^[95,108,110,111,257] The monochlorinated dimethylamino-1,2-diduryldiborane(4) **185** shows a weak absorption band at 313 nm ($\epsilon = 3380 \text{ M}^{-1} \text{ cm}^{-1}$) in hexane ($c = 0.4\text{-}1 \text{ mM}$), but almost no emission. Air and moisture sensitivity of **185** was observed for the solid state and in solution.



Scheme 67. Synthesis of diduryldiborane(4) **185**.^[98,104,273] (Dur = 2,3,5,6-tetramethylphenyl)

As a representative example of the dimethylamino-substituted 1,2-diduryldiboranes(4) reported in this thesis the solid state structure of **185** was determined (Figure 82). Single crystals were grown from hexane solution at room temperature. The B-B bond length (1.704(2) Å) is slightly longer than those in the cyclic 1,4-diaza-2,3-diborinanes above and hence in the range of bis(dimethylamino)diborane(4) B-B bonds, but compares well to those of $\text{Me}_2\text{BBMe}_2\text{Ph}$ (1.706 Å^[120]) and the equally unsymmetric diborane(4) reported by Erker (1.714 Å^[123,124]). The diduryldiborane(4) **185** shows planar coordination

3. Results and Discussion

geometry around the boron centers ($\Sigma \angle = 360^\circ/359.4^\circ$). Moreover, the coordination geometry around the NMe₂ group is planar and the B-N bond length is similar to those in the bis(dimethylamino)diboranes(4) described in Section 3.6.1, leading to the conclusion that the same bonding situation between boron and nitrogen can be assumed. The angle between the coordination planes at the boron atoms is smaller ($63.1(1)^\circ$) than in bis(dimethylamino)diboranes(4) in Section 3.6.1. The B-C_{Dur} distances ($1.589(2)$ Å / $1.568(2)$ Å) are in the usual range for B-aryl bonds.^[95,108]

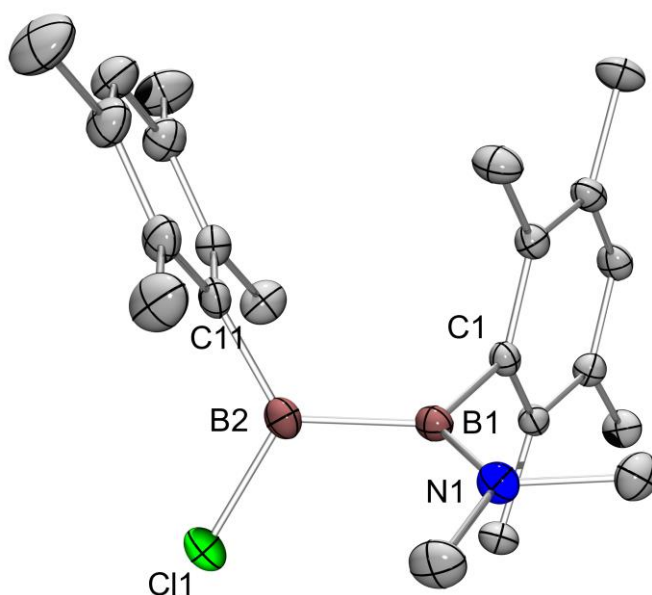
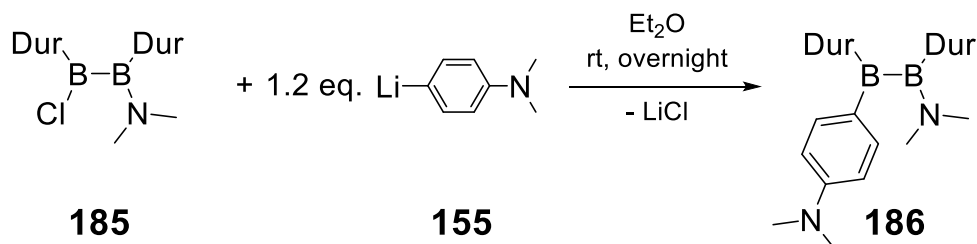


Figure 82. Molecular structure of **185** in the solid state (ellipsoids at 50% probability, hydrogen atoms and second molecule in the asymmetric unit omitted for clarity). Selected bond lengths [Å] and angles [°]: B1-B2 1.704(2), B1-N1 1.388(2), B2-Cl1 1.791(2), B1-C1 1.589(2), B2-C11 1.568(2), $\Sigma \angle$ B1 360.0, $\Sigma \angle$ B2 359.4, $\Sigma \angle$ N1 360.0, angle between B coord. Planes $63.1(1)$.

For the incorporation of the donor substituent, the monochlorinated diborane(4) precursor **185** and 4-(dimethylamino)phenyllithium were mixed in solid form, diethylether was added and the reaction mixture stirred overnight. Diborane(4) **186** was quantitatively obtained, as indicated by NMR spectroscopic analysis of the crude product, and isolated by filtration and precipitation from hexane in acceptable yield (51%) (Scheme 68). The ¹¹B NMR spectrum exhibits the anticipated two broad signals, one at 87.1 ppm attributed to the 4-(dimethylamino)phenyl-substituted and the second at 53.2 ppm for the amino-substituted boron center. The chemical shifts are comparable to the signals of **185**. Additionally, the ¹H NMR spectrum (Figure 83) shows the expected number of resonances, which strongly suggests the formation of **186**. Exposure

3. Results and Discussion

to ambient air revealed stability under these conditions at least for several days in the solid state as well as in solution.



Scheme 68. Synthesis of aminophenyl-substituted dimethylaminodiduryldiborane(4) **186**. (Dur = 2,3,5,6-tetramethylphenyl)

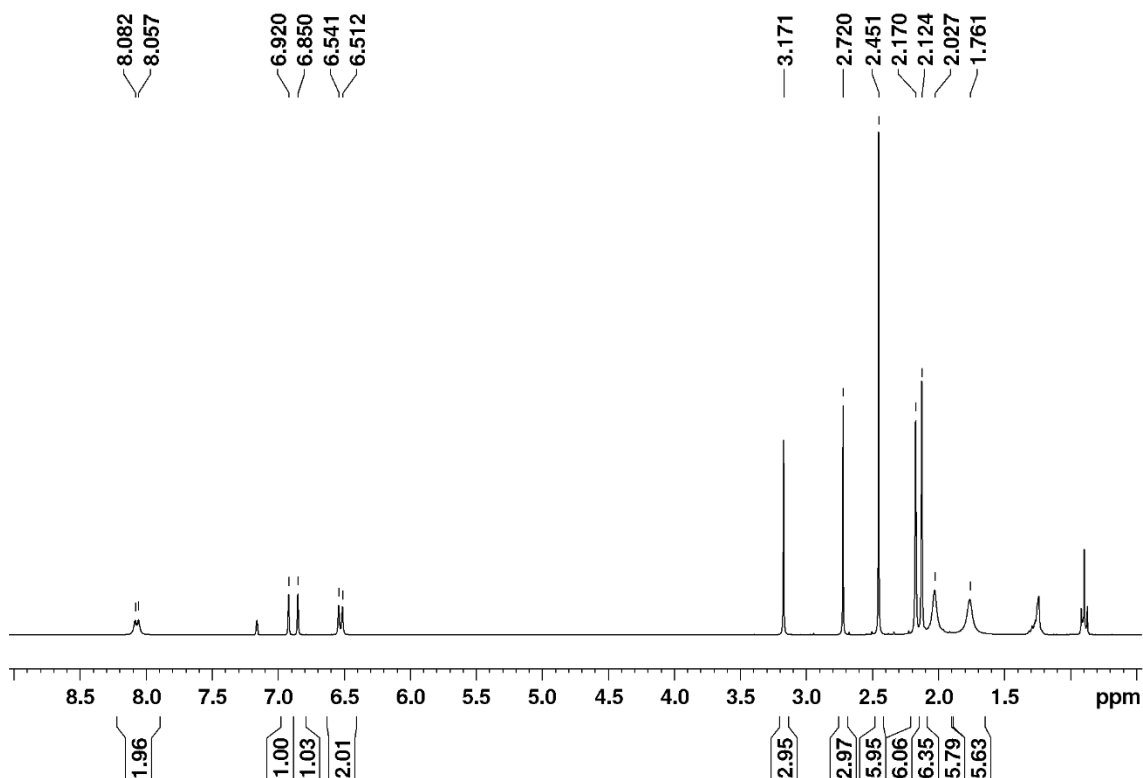


Figure 83. ^1H NMR spectrum of diduryldiborane(4) **186**.

UV-vis spectroscopic studies show one minor absorption band at 242 nm ($\epsilon = 1580 \text{ M}^{-1} \text{ cm}^{-1}$) and one distinct absorption band at 337 nm ($\epsilon = 44000 \text{ M}^{-1} \text{ cm}^{-1}$). The longest wavelength absorption of the related dimethylaminophenyl-substituted dimesitylmonoborane is reported in the same range^[171,178] indicating that the absorbing system in both compounds is the aminophenylboron moiety. Another parallel is that fluorescence can be detected for both compounds in nonpolar solvent when exciting the longest wavelength absorption which correlates perfectly with the excitation band maximum (Figure 84). Diborane(4) **186** exhibits the emission band maximum at 430 nm (Figure 84) in hexane solution ($c = 2.5 \mu\text{M}$) resulting in a Stokes shift of 93 nm

3. Results and Discussion

(6418 cm^{-1}) which is much more pronounced than that reported for dimethylaminophenyl-substituted dimesityl-monoborane (33 nm (2636 cm^{-1})^[171], 14 nm (1075 cm^{-1})^[178]) in nonpolar solvent (cyclohexane). The quantum yield in the case of **186** is unfortunately below 5%.

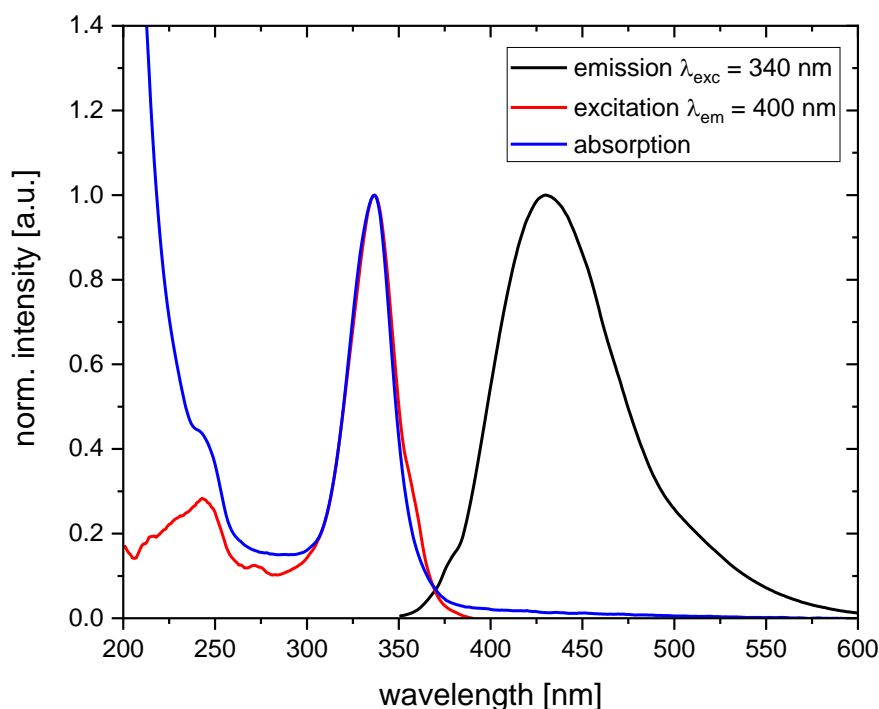


Figure 84. Absorption (blue), excitation (red) and emission (black) spectra of diduryldiborane(4) **186** in hexane.

The next goal was to synthesize diboranes(4) without direct amino stabilization. The unsymmetrically substituted diborane(4) **187** was synthesized from 1,2-dichlorodiborane(4) **64e** by reaction with one equivalent of 4-(dimethylamino)phenyllithium and isolated as yellow amorphous solid in 45% yield (Scheme 69). In order to increase selectivity, a temperature of -78°C had to be maintained during the synthesis. The ^{11}B NMR spectrum shows one very broad signal at 81.1 ppm. In contrast to the amino-substituted analogue **186**, the chloro-derivative **187** is sensitive towards air and moisture in solid state and in solution, which can be attributed to the reactive B-Cl bond.

3. Results and Discussion

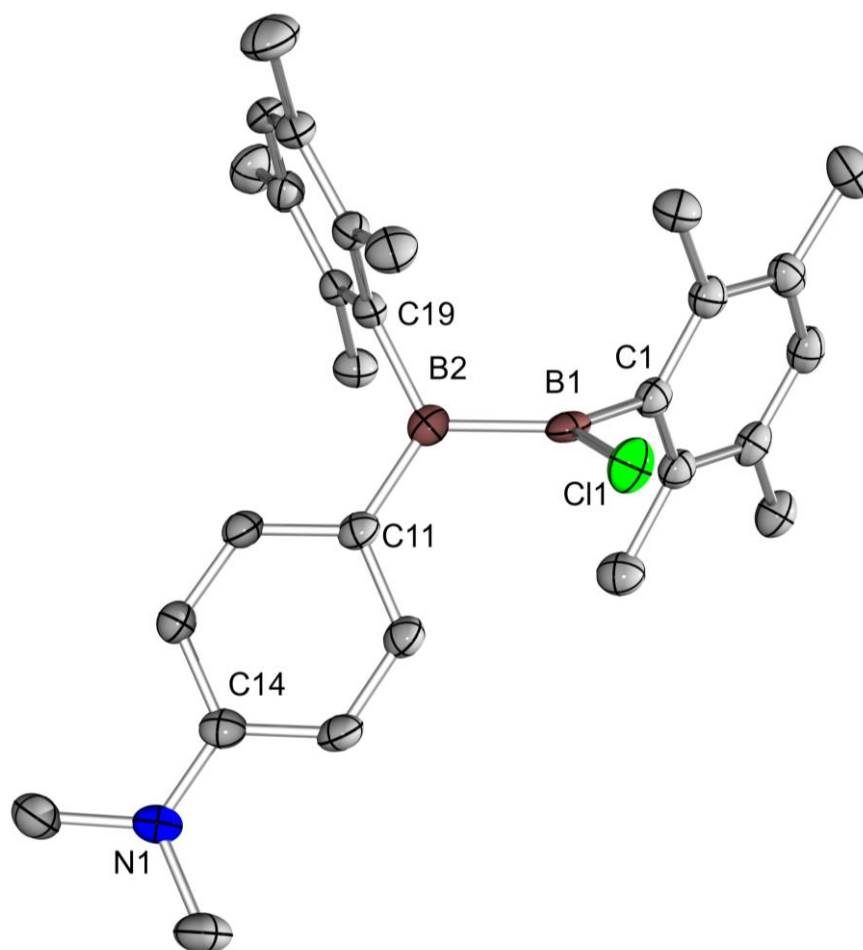


Figure 85. Molecular structure of **187** in the solid state (ellipsoids at 50% probability, hydrogen atoms and second molecule in the asymmetric unit omitted for clarity). Selected bond lengths [Å] and angles [°]: B1-B2 1.690(3), B1-C1 1.800(2), B1-C1 1.573(3), B2-C11 1.531(3), B2-C19 1.592(3), C14-N1 1.365(2), $\Sigma \angle$ B1 360.0, $\Sigma \angle$ B2 359.4, $\Sigma \angle$ N1 358.7, angle between B coord. Planes 64.3(1).

Diborane(4) **187** exhibits an absorption maximum at 347 nm ($\epsilon = 33800 \text{ M}^{-1} \text{ cm}^{-1}$) in hexane solution ($c = 0.2\text{-}0.8 \text{ mM}$) in the same range as the dimethylamino substituted diborane(4) **186** hinting at the aminophenylboron-moiety as the main absorbing unit, here as well. Thus expectedly, fluorescence (Figure 86) could be invoked in hexane solution ($c = 2.5 \text{ }\mu\text{M}$) with an excitation maximum at 339 nm, supporting the aminophenylboron unit as fluorescence origin, and an emission maximum at 520 nm which results in an even more pronounced Stokes shift (181 nm, 10268 cm^{-1}) than for **186**. Quantum yield in this case amounts to $14 \pm 5\%$, approaching that of the dimethylaminophenyl substituted dimesityl-monoborane (42%) in cyclohexane^[171]. Unfortunately, **187** turned out to be photolabile and decomposes to unknown species upon irradiation.

3. Results and Discussion

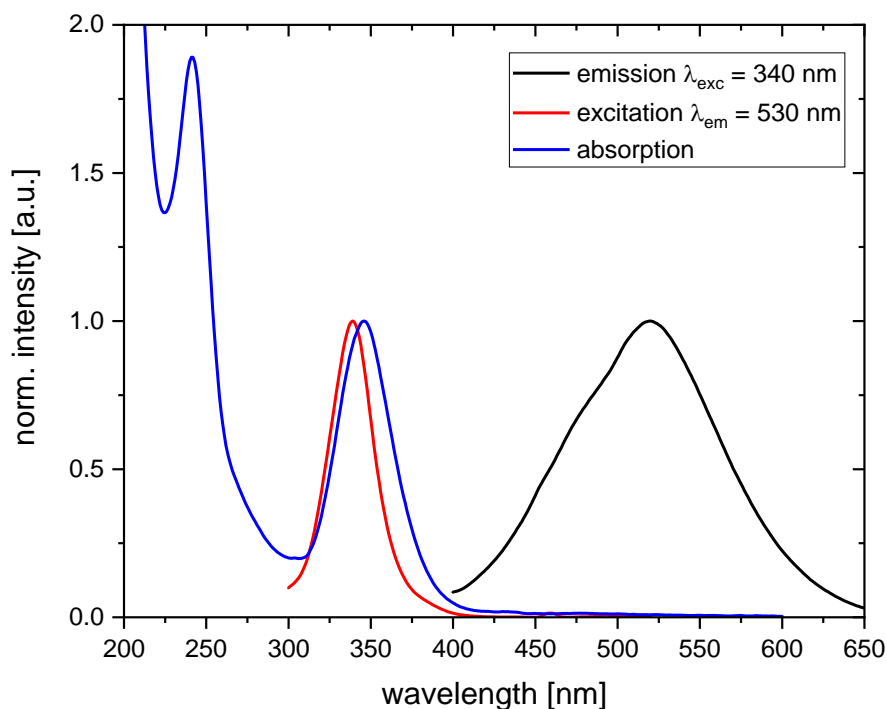
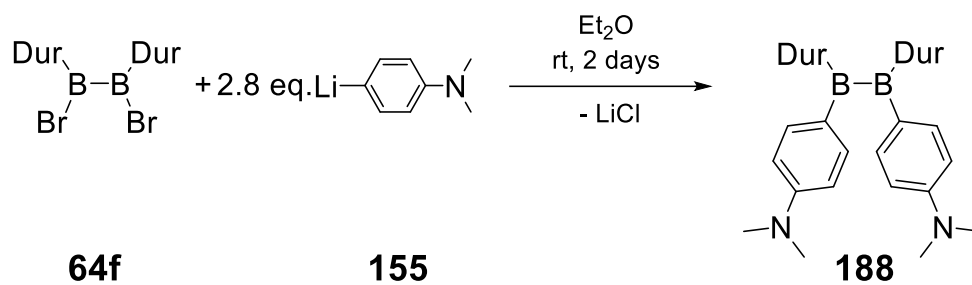


Figure 86. Absorption (blue), excitation (red) and emission (black) spectra of diduryldiborane(4) **187** in hexane.

In order to investigate the properties of a doubly aminophenyl substituted 1,2-diduryldiborane(4), **188** was synthesized directly from 1,2-dibromodiborane(4) **64f** by reaction at room temperature with two equivalents of 4-(dimethylamino)phenyllithium in diethylether for two days. While NMR spectroscopic analysis of the crude product shows the formation of one compound selectively in the ^1H and ^{11}B NMR spectra, its isolation as yellow microcrystalline solid could only be achieved with poor yield (19%) (Scheme 70). Long reaction times indicate a sterically hindered position at the boron center. No ^{11}B NMR signal could be observed at room temperature. At 343 K, however, sufficient sharpening occurred to give rise to a clearly distinguishable, nevertheless still broad signal at 87.1 ppm (Figure 87). Additionally, the ^1H NMR spectrum (Figure 88) shows the anticipated resonances, which strongly suggests the formation of **188**, as planned. Stability for days towards air and moisture in the solid state and in solution was discovered for **188**.

3. Results and Discussion



Scheme 70. Synthesis of symmetrically substituted bis(aminophenyl)-diduryldiborane(4) **188**. (Dur = 2,3,5,6-tetramethylphenyl)

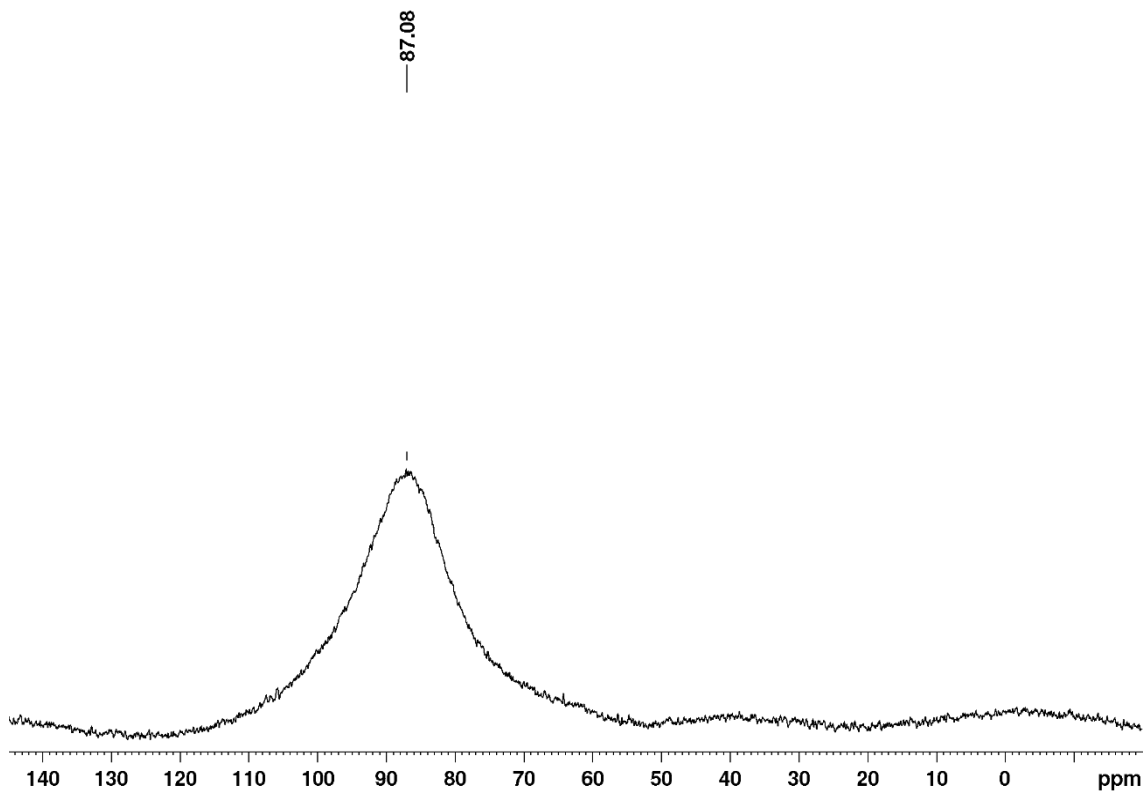


Figure 87. ¹¹B NMR spectrum of diduryldiborane(4) **188** at 343K.

3. Results and Discussion

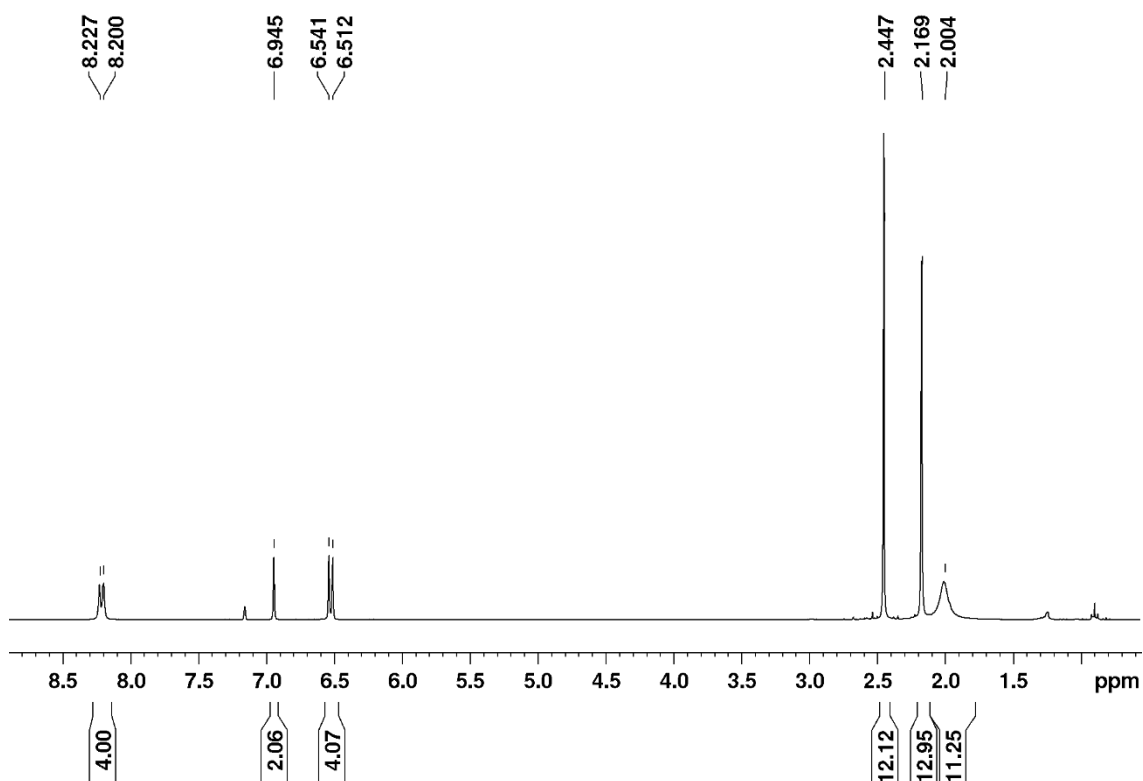


Figure 88. ^1H NMR spectrum of diduryldiborane(4) **188**.

Diborane(4) **188** exhibits two minor absorption maxima at 244 nm ($\epsilon = 17100 \text{ M}^{-1} \text{ cm}^{-1}$) and 279 nm ($\epsilon = 13900 \text{ M}^{-1} \text{ cm}^{-1}$) and one intense absorption maximum at 341 nm ($\epsilon = 48200 \text{ M}^{-1} \text{ cm}^{-1}$) in hexane solution ($c = 0.2\text{-}0.8 \text{ mM}$) in the same range as the dimethylamino substituted diborane(4) **186** and chlorodiduryldiborane(4) **187** suggesting as in the other cases the aminophenylboron-moieties as the main absorbing units. As anticipated, fluorescence (Figure 89) could be invoked in hexane solution ($c = 2.5 \text{ }\mu\text{M}$) with an excitation maximum at 341 nm, supporting the aminophenylboron unit as fluorescence source, and emission maxima at 474 nm and 558 nm both originating from the same excitation band suggesting either vibronic coupling or excitation to a higher state with a significant delay of non-radiative decay to the S_1 state (i.e. a violation of Kasha's rule^[272]). Due to the high stability of **188** under air, it is at least very unlikely that impurities or decomposition products are responsible for the second emission. This results in immense Stokes shifts (133 nm, 8229 cm^{-1} / 217 nm, 11404 cm^{-1}). Large Stokes shifts suggest a pronounced geometric distortion in the excited state and intramolecular charge-transfer (ICT), as known for the related dimethylaminophenyl-substituted dimesitylborane^[171] In the case of **188** the second emission band could even occur from a twisted ICT state, although this

3. Results and Discussion

is normally stabilized only by polar solvents.^[274] Quantum yield in this case amounts to $20 \pm 5\%$, approaching that of the dimethylaminophenyl substituted dimesityl-monoborane (42%) in cyclohexane^[171]. Unfortunately, **188** turned out to be photolabile and decomposes to unknown species upon irradiation.

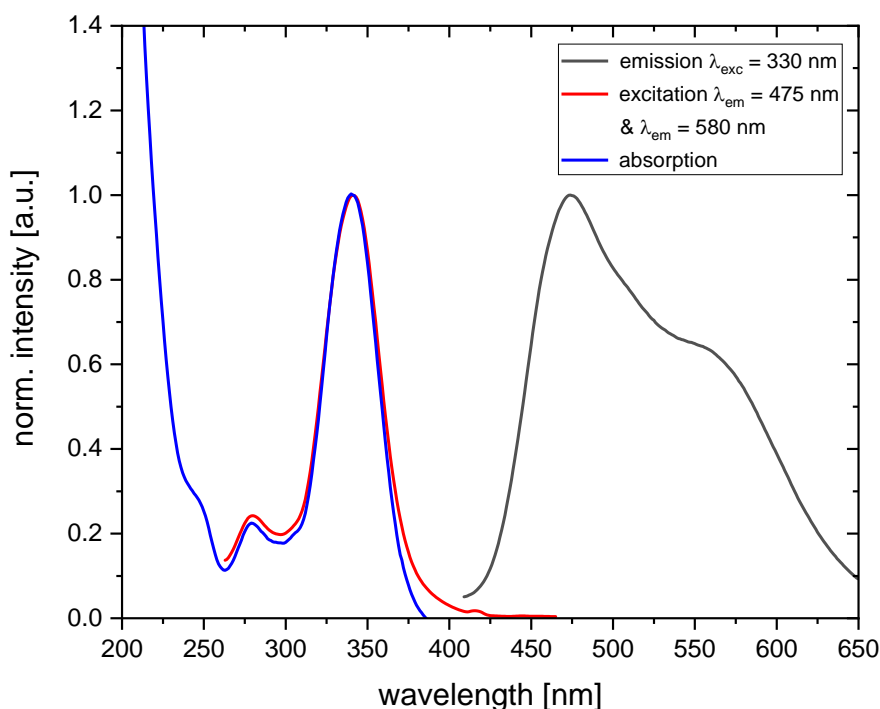
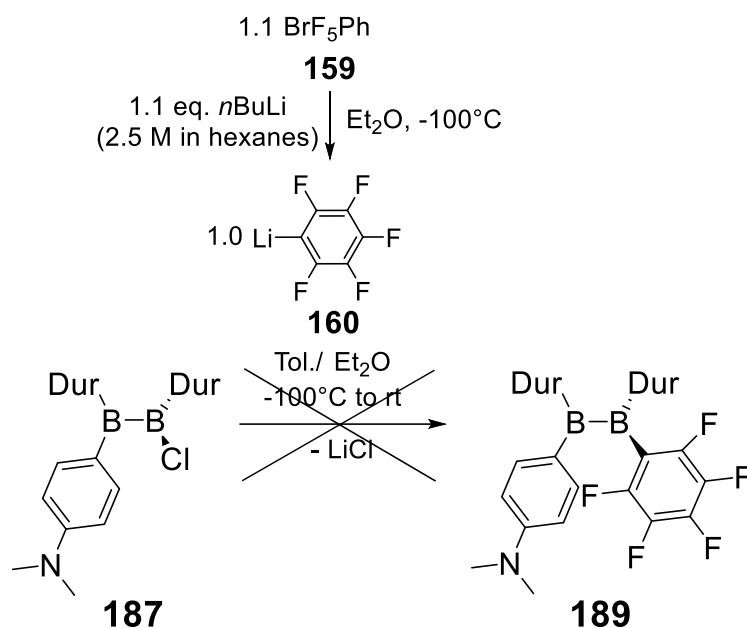


Figure 89. Absorption (blue), excitation (red) and emission (black) spectra of diduryldiborane(4) **188** in hexane.

In analogy to **161** and **181**, a 4-dimethylaminophenyl and pentafluorophenyl substituted diduryldiborane(4) **189** was aimed at (Scheme 71). In the attempted reaction of **187** in toluene with pentafluorophenyllithium in diethylether at -78°C , however, only decomposition of the anion and unreacted **187** was observed NMR spectroscopically after warming to room temperature. The addition of a second substituent to **187** requires longer reaction times at room temperature as previously observed during the synthesis of **188** (see above). Pentafluorophenyllithium, however, is unstable at room temperature leading to decomposition before appreciable conversion to the targeted product had taken place.

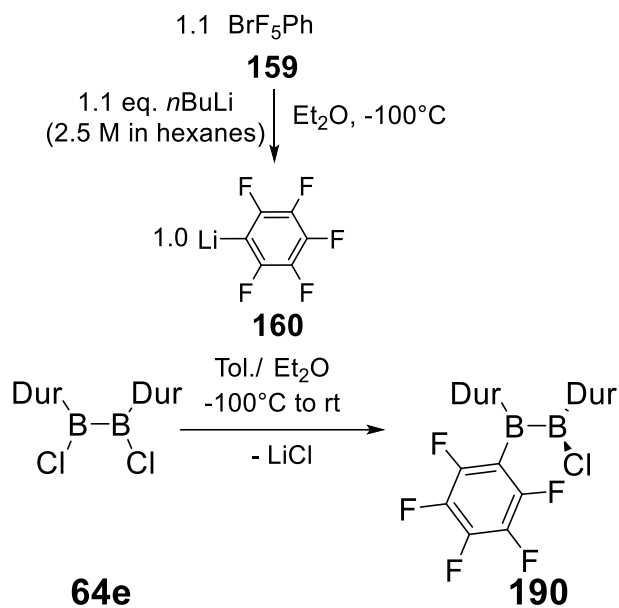
3. Results and Discussion



Scheme 71. Attempted reaction of aminophenyl substituted chloro-diduryldiborane(4) **187** with pentafluorophenyl lithium (**160**). (Dur = 2,3,5,6-tetramethylphenyl)

In order to circumvent the stability problem with pentafluorophenyllithium at room temperature, the pentafluorophenyl substituent should be attached first, which might allow for longer reaction times in the second substitution reaction. Therefore, pentafluorophenyllithium was reacted with 1,2-dichloro diborane(4) **64e** at low temperatures (Scheme 72). After warming to room temperature, solvent and volatile components were removed, followed by filtration from hexane. NMR spectroscopic analysis of the filtrate strongly suggested the selective formation of **190** with the typical duryl-signals at 6.84 ppm, 6.82 ppm (each s, altogether 2H, DurH) and 2.00 ppm, 1.98 ppm, 1.90 ppm, 1.88 ppm (each s, each 6H, Dur-CH₃) in the ¹H NMR spectrum (Figure 90), the typical signals for a pentafluorophenyl-group at -120.2 to -120.4 ppm (m, 2F, F₅Ph-*o*F), -142.5 ppm (tt, ³J_{F-F} = 21.1 Hz, ⁴J_{F-F} = 8.1 Hz, F₅Ph-*p*E), -160.7 to 160.9 (m, 2F, F₅Ph-*m*E) in the ¹⁹F NMR spectrum (Figure 91) and a broad signal in the ¹¹B NMR spectrum at 87.7 ppm. Due to time constraints towards the end of this PhD project, **190** has not yet been fully characterized or reacted with 4-dimethylaminophenyllithium.

3. Results and Discussion



Scheme 72. Synthesis of pentafluorophenyl substituted chloro-1,2-diduryldiborane(4) **190**. (Dur = 2,3,5,6-tetramethylphenyl)

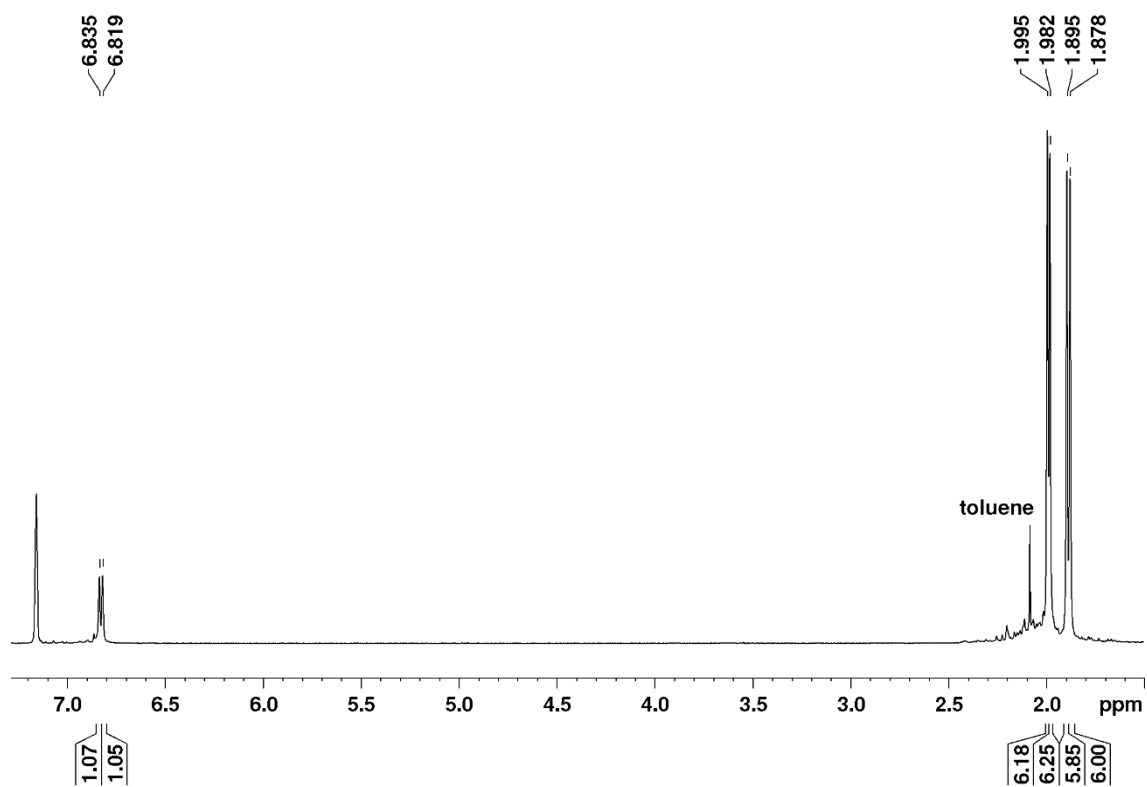


Figure 90. ¹H NMR spectrum of diduryldiborane(4) **190**.

3. Results and Discussion

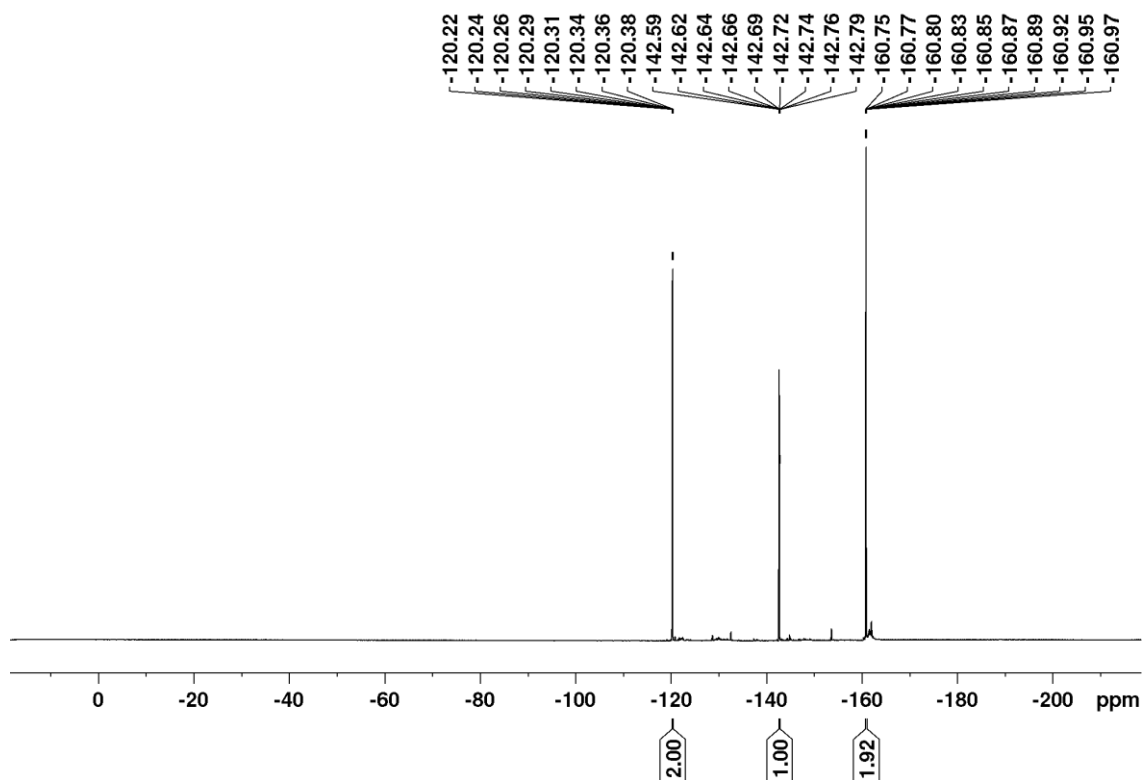
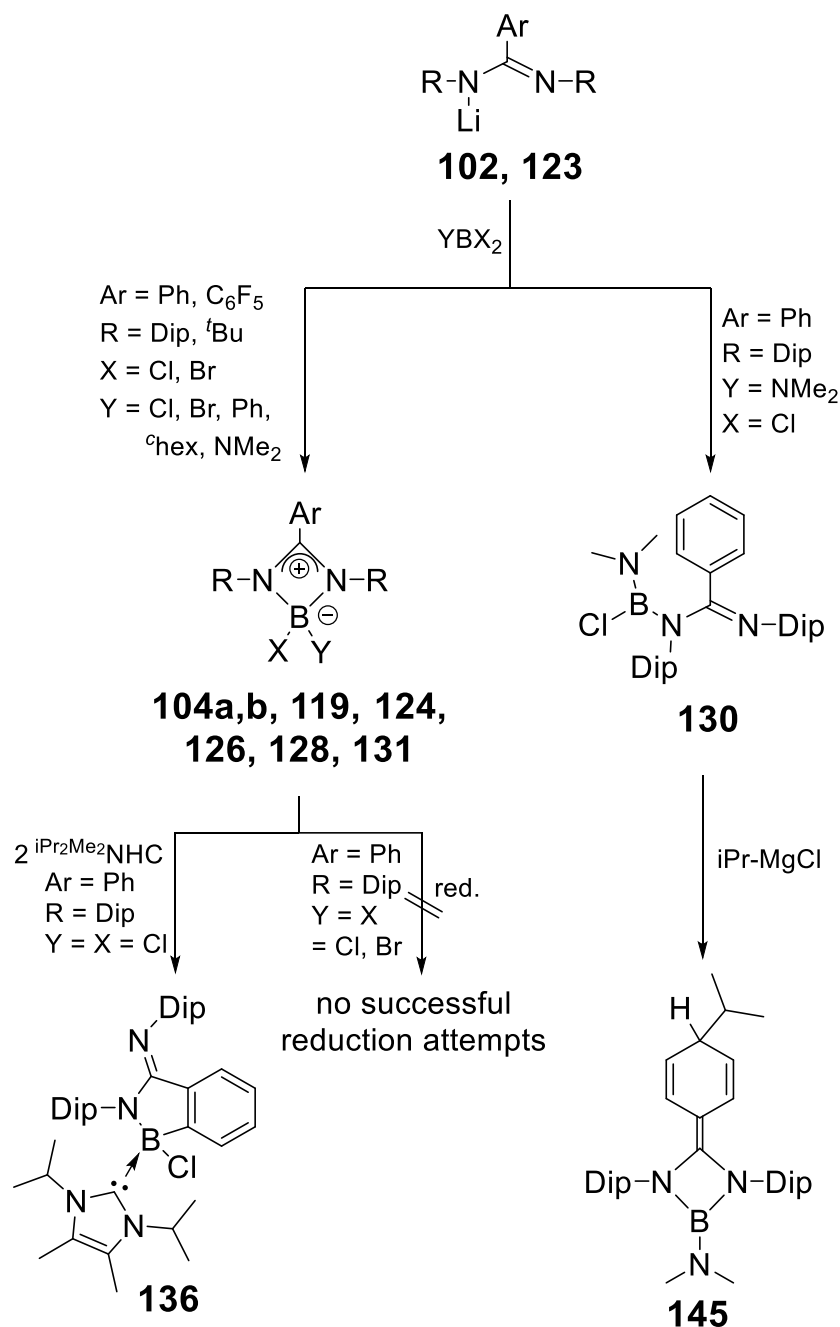


Figure 91. ^{19}F NMR spectrum of diduryldiborane(4) **190**.

4. Conclusion and Outlook



Scheme 73. Synthesis and isolation of boryl benzamidinates in the closed form (**104a,b, 119, 124, 126, 128** and **131**) and open chained form (**130**) from either lithium amidinate **102** or **123** plus the isolated product **136** from the reaction between **104a** and 2 ⁱPr₂Me₂NHC and the isolated product **145** from the reaction between open chained boryl amidinate **130** and ⁱPrMgCl. **102**: Ar = Ph, R = Dip; **123**: Ar = C₆F₅; **104a**: Ar = Ph, R = Dip, X = Y = Cl; **104b**: Ar = Ph, R = Dip, X = Y = Br; **119**: Ar = Ph, R = ^tBu, X = Y = Cl; **124**: Ar = C₆F₅, R = Dip, X = Y = Cl; **126**: Ar = Ph, R = Dip, X = Cl, Y = Ph; **128**: Ar = Ph, R = Dip, X = Cl, Y = cyclohexyl; **131**: Ar = Ph, R = ^tBu, X = Cl, Y = NMe₂. (Dip = 2,6- ⁱPr₂C₆H₃)

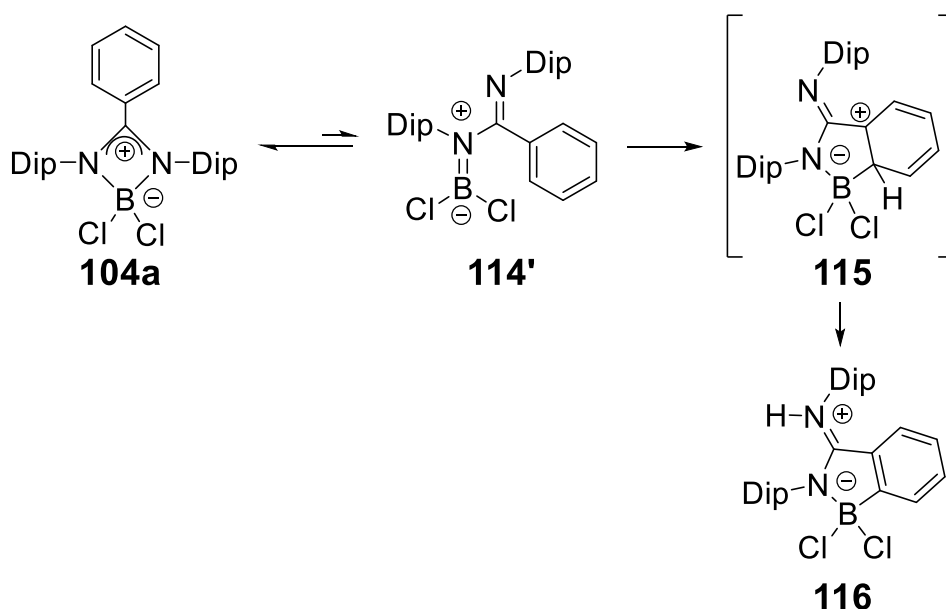
Emerging applications of saturated main group element amidinate complexes, for example dialkyl aluminium amidinates,^[190-192] rose the question about the synthetic possibilities of their lighter analogues, namely boryl amidinates. A

4. Conclusion and Outlook

large collection of boryl amidinates and guanidates has been synthesized so far, but their reactivity remains rather unexplored. [24-45]

Thus, in one part of this PhD thesis a number of new boryl benzamidinate complexes **104a and b**, **119**, **124**, **126**, **128**, **130**, **131** have been synthesized by applying the established synthetic method of reacting lithium amidinates **102** or **123** with chloroboranes ($\text{YBX}_2 = \text{BCl}_3, \text{BBr}_3, \text{PhBCl}_2, \text{cyclohexylBCl}_2, \text{Me}_2\text{NBCl}_2$, Scheme 73).^[195] Their reactivity in reduction reactions and towards bases/nucleophiles was investigated.

Most of the newly synthesized and characterized boryl amidinates take on the anticipated *N,N*-chelating form (**104a and b**, **119**, **124**, **126**, **128**, **131**). In the cases of the *N*-Dip substituted amidinates, isolation of the corresponding boryl amidinates has been more difficult, especially in the case of **104a**, because of rearrangement in concentrated solution, most likely due to the steric bulk and therefore a more constrained four-membered ring. A rearrangement pathway as displayed in Scheme 74 was suggested with benzazaborole **116** as major rearrangement product by considering literature^[26] and, in retrospect, the isolation of a similar structural motif **136** during this PhD studies (Scheme 73).

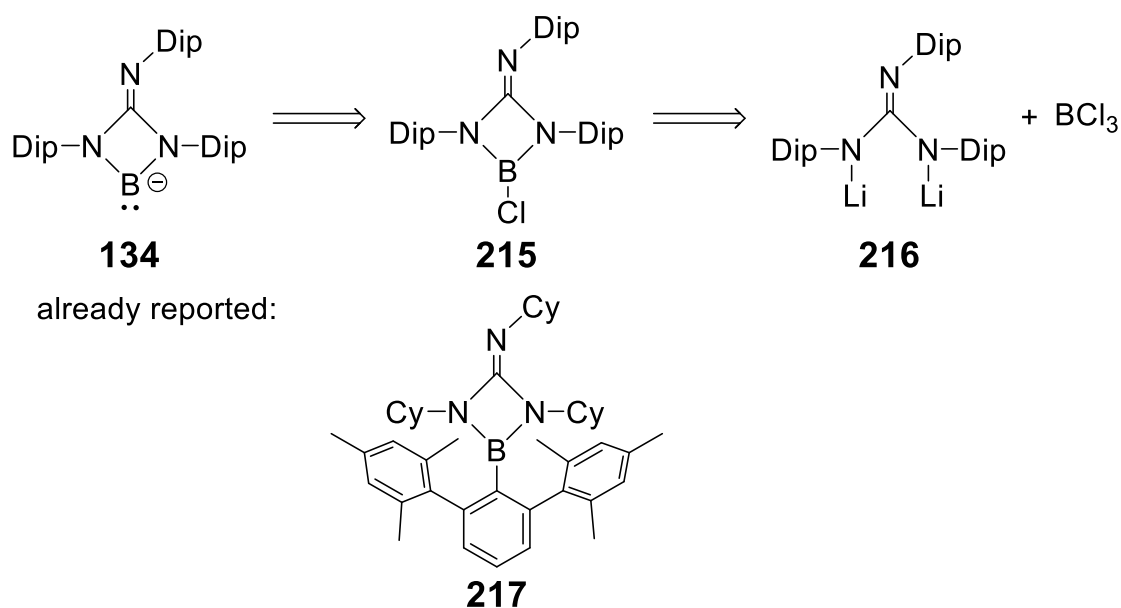


Scheme 74. Suggested rearrangement pathway of **104a** to **116**, which was mostly observed after storage of **104a** in concentrated solution.

Previous attempts to synthesize amidinate or guanidate stabilized borylenes failed. [27,28,39] Attempts to reduce dihaloboryl amidinates **104a,b** with various reducing agents did not succeed either. While the Dip groups probably provide

4. Conclusion and Outlook

the required kinetic stabilization, DFT calculations suggested that our chosen ligand-system does not induce a large enough singlet-triplet gap to force a singlet state amidinate-borylene. As CAACs are known to provide stability for radical structures,^[275] future reduction attempts should be performed in their presence. Another possibility would be to alter the ligand system. Our DFT studies suggest that a guanidate ligand would be preferred to increase the singlet-triplet gap and that a ligand attachment with the imine function in the backbone enlarges the singlet-triplet gap even more. This would result in the anionic borylene structure **134** (Scheme 75). The suitable precursor **215** could be synthesized following literature procedures to prepare the dianionic ligand **216** and react it with borontrichloride.^[276,277] A similar structure has already been reported (**217**, Scheme 75)^[278,279] but steric protection would be lowered in **215**, so that intermolecular coordination could be a problem in this case.

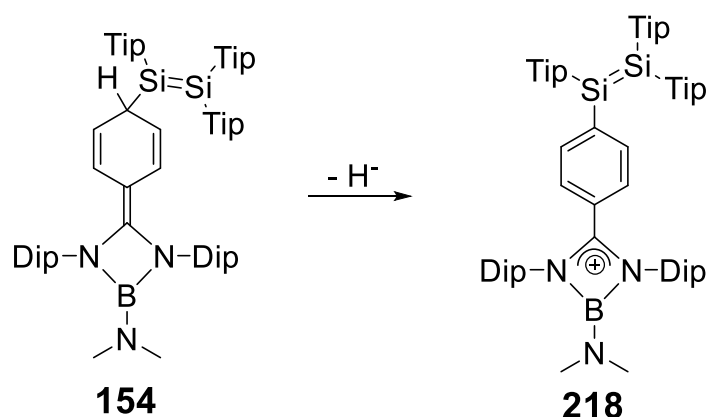


Scheme 75. By DFT-calculations suggested guanidate borylene **134** retrosynthesis proposition via **215** and **216** plus previously reported **217**.^[278,279]

By altering the substituents on the boryl group we found an exception for the usually adopted *N,N*-chelating mode: dimethylaminoboryl amidinate **130** adopts an open chained form in solid state, which was confirmed by x-ray diffraction analysis, as well as in solution, which was indicated by ^{11}B NMR spectroscopy. This leads to a difference in reactivity towards nucleophiles/ bases. Where no reaction was observed for the closed form boryl amidinates **104a** and **128**, various metal organic reagents perform nucleophilic attacks on the phenyl ring of the dimethylaminoboryl benzamidinate **130** thereby dearomatizing the latter

4. Conclusion and Outlook

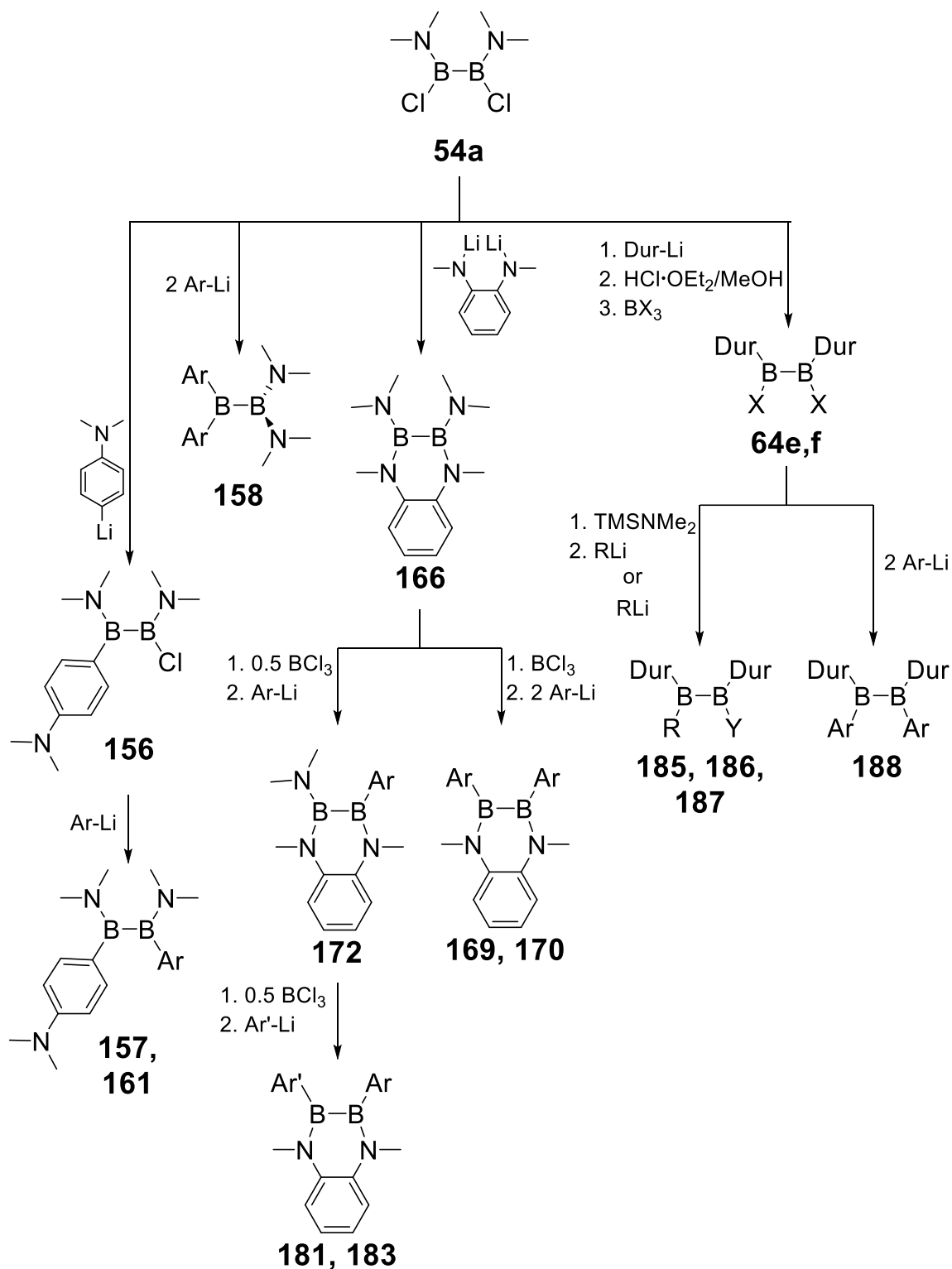
and subsequent metalchloride elimination leads to a quinoidic structure. **145** (Scheme 73) was isolated and structurally characterized as representative. Several others, among them **154** (Scheme 76), were observed NMR-spectroscopically. In future experiments, the exchange of the dimethylamino group at the boron center could be pursued to be able to attach various substituents at this end of the interesting structural motif. The spectroscopically observed structures, especially the disilyl substituted derivative **154**, should be isolated and characterized as it represents an interesting target for further investigations. For example, rearomatization could be attempted by hydride abstraction to form the cationic structure **218** (Scheme 76). The disilyl moiety attached to the phenyl ring and an electron deficient substituent in *para*-position could result in interesting optoelectronic properties, as has in principle previously been observed for aryl substituted disilenes in our group.^[280]



Scheme 76. Suggested rearomatization of **154** to form **218**.

Three-coordinate boron compounds, especially arylmonoboranes, are widely known for their luminescent properties,^[223-230] but diboranes(4) have rarely been investigated in this regard. Therefore, a systematic study with different diborane(4) skeletal structures was performed as second part of this PhD project.

4. Conclusion and Outlook



Scheme 77. Synthesized and structurally characterized substituted 1,2-bis(dimethylamino)-diboranes(4), **156**, **157** and **161**, 1,1-isomer **158**, benzo fused cyclic 1,4-diaza-2,3-diborinanes **166**, **169**, **170**, **172**, **181** and **183** as well as 1,2-diduryl-diboranes(4) **185** to **188**. **64e**: X = Cl; **64f**: X = Br; **157**: Ar = Ph-NMe₂; **158**: Ar = Ph-NMe₂; **161**: Ar = C₆F₅; **169**: Ar = Ph-NMe₂; **170**: Ar = C₆F₅; **172**: Ar = Ph-NMe₂; **181**: Ar = Ph-NMe₂, Ar' = C₆F₅; **183**: Ar = Ph-NMe₂, Ar' = O-Ph-NO₂; **185**: R = NMe₂, Y = Cl; **186**: R = Ph-NMe₂, Y = NMe₂; **187**: R = Ph-NMe₂, Y = Cl; **188**: Ar = Ph-NMe₂.

The isolation and structural characterization of substituted 1,2-bis(dimethylamino)diboranes(4), **156**, **157** and **161**, benzo fused cyclic

4. Conclusion and Outlook

1,4-diaza-2,3-diborinanes **166**, **169**, **170**, **172**, **181** and **183** as well as 1,2-diduryl-diboranes(4) **185** to **188** was reported (Scheme 77). When **54a** is reacted with excess of *p*-*N,N*-dimethylaminophenyllithium partial rearrangement to the 1,1-isomer **158** was observed, which could be isolated in small quantities and characterized by x-ray diffraction analysis and NMR spectroscopy. Cyclic voltametric measurements of **156** and **157** showed the sensitivity of the *p*-Ph-NMe₂-moiety towards oxidation. Rapid decomposition of 1,4-diaza-2,3-diborinanes **169**, **180** and **181**, which was observed in UV-Vis measurements, also hint at sensitivity towards oxidation. In future endeavours, a comprehensive cyclic voltammetry-study should be performed for all the isolated diboranes(4) and subsequently, chemical oxidation should be investigated.

Spectroscopic studies (Table 4) showed that in principle fluorescence can be invoked in 1,2-bis(dimethylamino)diboranes(4) by unsymmetrical substitution with electron donating and withdrawing groups at the boron centers, i.e. diborane(4) **161**. Substitution on the cyclic 1,4-diaza-2,3-diborinane boron center mostly modified the electronic constitution of the skeletal structure (**166**, **169**, **170**, **172**, **180**, **181**, **183**). Finally, substitution on 1,2-diduryl-diboranes(4) with 4-dimethylaminophenyl groups (**186-188**) gave partly extraordinary Stokes shifts in nonpolar solvent, whereby **187** and **188** are photolabile. A major aspect of future investigations should be to examine the origin of these exceptional Stokes shifts. ESR measurements under irradiation of **187** and **188** could elucidate the reason behind their photo-instability. Additionally, substituents should be varied and extended π -systems could be attached to further explore the possibilities of luminescent diboranes(4).

4. Conclusion and Outlook

Table 4. Spectroscopic data for synthesized diboranes(4). Wavelengths λ [nm], wavenumbers ν [cm^{-1}] and extinction coefficients ϵ [$\text{L mol}^{-1} \text{cm}^{-1}$]

	$\lambda_{\text{abs,max}}$ (ϵ)	$\lambda_{\text{exc,max}}$	$\lambda_{\text{em,max}}$	$\Delta\lambda$ ($\Delta\nu$)	Φ_{fl}
156	282 (13200)	-	-	-	-
157	281 (34900)	-	-	-	-
161	287 (17300)	290	335	45 (4632)	< 5%
166	234 (34900) 272 (9840) 308 (12100) 314 (11800)	297/303	325	28 (2901)/ 22 (2234)	55 \pm 5%
169	232 (27300) 261 (34700) 342 (35500)	341	473/511	132 (8184)/ 170 (9756)	17 \pm 5%
170	231 (25000) 254 (13800) 317 (18300)	-	-	-	-
172	216 (35000) 243 (24900) 315 (14800) 327 (15800)	313	355	42 (3780)	48 \pm 5%
180	232 (18900) 255 (18700) 334 (21200)	-	-	-	-
181	263 (21000) 313 (15000) 349 (16900)	266/300/350	406	140 (12963)/ 106 (8703)/ 56 (3941)	7 \pm 5%
183	232 (26200) 259 (20700) 316 (25100)	-	-	-	-
185	313 (3380)	-	-	-	-
186	242 (15800) 337 (44000)	337	430	93 (6418)	< 5%
187	347 (33800)	339	520	181 (10268)	14 \pm 5%
188	244 (17100) 279 (13900) 341 (48200)	341	474/ 558	133 (8229)/ 217 (11404)	20 \pm 5%

5. Experimental Section

5.1. General

5.1.1 Experimental conditions

All manipulations, if not indicated otherwise, were carried out under a protective atmosphere of argon using standard Schlenk techniques or a glovebox. The protection gas used was Argon 5.0 supplied by Air Liquide and was used without further purification.

All glassware was cleaned in a KOH/ isopropanol bath, neutralized and kept in a drying oven at 120°C overnight prior to use. All setups were evacuated and purged with argon three times. The high vacuum was generated with a slide vane rotary vacuum pump RZ 6 from VakuumbRAND.

5.1.2 Solvent purification

Pentane, benzene and dimethoxyethane (dme) were refluxed with sodium/benzophenone and distilled prior to use. Methanol was dried over Mg and distilled prior to use. Dichloromethane, hexane, diethylether (Et₂O), tetrahydrofuran (thf) and toluene were taken directly from a solvent purification system (Innovative Technology PureSolv MD7). *o*-Difluorobenzene was refluxed over CaH₂ and distilled prior to use. C₆D₆ was refluxed over potassium and distilled prior to use. CDCl₃ was refluxed over P₄O₁₀ and distilled prior to use.

5.1.3 Analytical methods

NMR spectra were recorded at 300 K on a Bruker Avance III 300 (¹H: 300.13 MHz, ¹¹B: 96.29 MHz, ¹³C: 75.47 MHz, ¹⁹F: 282.40 MHz, ²⁹Si: 59.6 MHz) and a Bruker Avance III HD 400 (¹H: 400.13 MHz, ¹¹B: 128.38 MHz, ¹³C: 100.61 MHz, ²⁹Si: 79.5 MHz). Chemical shifts are reported relative to SiMe₄, BF₃-OEt₂ or CFC₃. ¹H and ¹³C NMR spectra were referenced to the peaks of the residual protons of deuterated solvents or the deuterated solvent itself (CDCl₃: δH: 7.26 ppm, δC: 77.16 ppm; C₆D₆: δH: 7.16 ppm, δC: 128.06 ppm;

5. Experimental Section

thf-d₈: δ H: 3.58 ppm, 1.72 ppm, δ C: 67.21 ppm, 25.31 ppm. All chemical shifts are reported in parts per million (ppm). Coupling constants are reported in Hertz (Hz). The multiplicity and shape of the observed signals are given as s = singlet, d = doublet, t = triplet, sept = septet, m = multiplet or convoluted signals, br = broad signal.

UV/Vis spectra were measured using a Shimadzu UV-2600 spectrometer in quartz cells with a path length of 1 mm.

Fluorescence spectra were measured using Jasco FP-6500 spectrofluorometer in quartz cells with a path length of 10 mm. The corresponding UV/Vis spectra were measured with a Jasco V-650 spectrometer. Quantum yields were measured using Hamamatsu Quantaurus-QY C11347-11.

Fourier-Transform IR spectra were acquired on a Bruker Vertex 70 spectrometer in attenuated total reflectance (ATR) mode.

Melting points were determined under argon in closed NMR tubes and are uncorrected. NMR spectra were run directly afterwards on a solution of the cooled down melt.

Elemental analysis was carried out on an elemental vario Micro Cube.

5.2. Starting Materials

5.2.1 General Starting materials

Commercially purchased chemicals:

- used without further purification:
di-^tbutyldiimine, bithiophene, *N,N*-dimethyltrimethylsilylamine, durene and lithium aluminumhydride were purchased from *abcr*, bromine and ethyl chloroformate were purchased from *Acros Organics*, benzoic acid, 2,6-diisopropylaniline, cyclohexene, 4-bromo-*N,N*-dimethylaniline, bromopentafluorobenzene, 4-bromobenzonitrile, 4-iodonitrobenzene, 9-bromoanthracene, 1-bromopyrene, *p*-nitrophenol and 4-bromothioanisole were purchased from *Alfa Aesar*, dimethylamine(g) was purchased from *GHC*, borontrichloride(g) was purchased from *Praxair*, ⁿbutyllithium solution in hexanes (2.5 M), borontrichloride and -tribromide solution in

5. Experimental Section

hexanes (1 M), phenyl lithium solution in dibutylether (1.9 M), disodium tetracarbonylferrate, isopropylmagnesiumchloride solution in thf (2 M), potassium hexamethyldisilazide, 2-bromothiophene and *o*-phenylenediamine were purchased from *Sigma Aldrich*, bis(2,6-diisopropylphenyl)-methanediimine, dichlorophenylborane and tributylsilane were purchased from *TCI*, triphenylborane was purchased from *VWR*.

- purified prior to use:

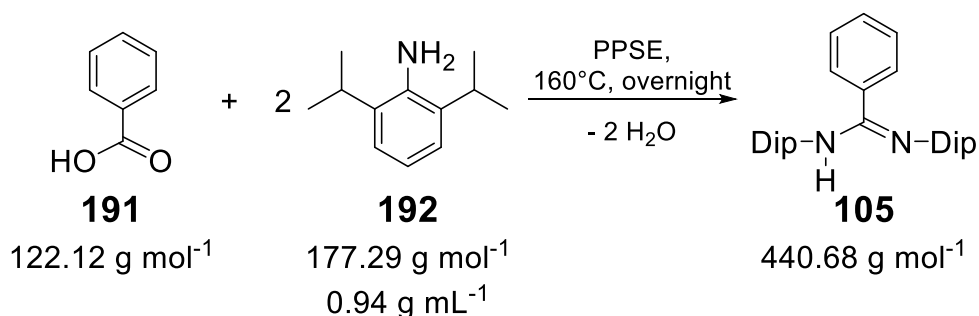
Trimethylsilylchloride was purchased from *Acros Organics* and distilled from Mg prior to use, triethylamine is purchased from *Acros Organics* and distilled prior to use, borontribromide was purchased from *Sigma Aldrich* and distilled from copper-wire prior to use.

Starting materials supplied by the group:

- Jones' Magnesium [$\{(\text{DipNacnac})\text{Mg}\}_2$]^[201], lithium powder, potassium graphite, 1,3-diisopropyl-4,5-dimethyl-1,3-dihydro-2H-imidazole-2-thione^[281], Me_4NHC ^[281], disilenide ($\text{Tip}_2\text{Si}=\text{SiTipLi-dme}_2$)^[219,220], $(\text{F}_5\text{C}_6)_3\text{B-OEt}_2$ ^{[282],[283]}, 4'-bromo-*N,N*-dimethyl-[1,1'-biphenyl]-4-amine^[284], 4'-bromo-[1,1'-biphenyl]-4-yl)(methyl)sulfane^[285].

5.2.2 Synthesis of (E)-*N,N'*-bis(2,6-diisopropylphenyl)benzimidamide

105^[286]



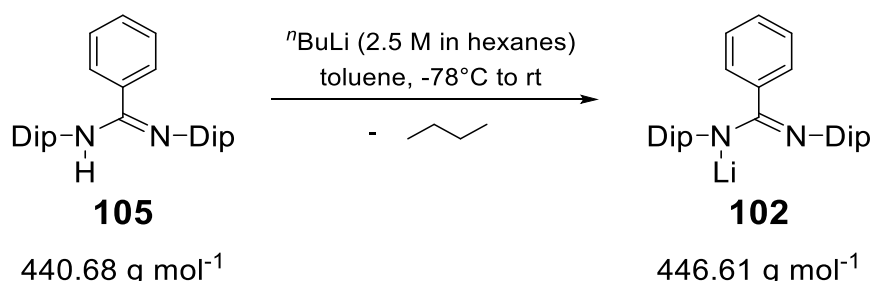
YK083_4: A 1L-Schlenk flask is charged with phosphorouspentoxide (evacuated with flask, 45.0 g, 159 mmol), dichloromethane (abs., 200 mL), and hexamethyldisiloxane (200 mL, 152 g, 0.936 mol). The reaction mixture is heated to reflux, which is maintained for two hours. Subsequently all volatile components are removed and the residue, PPSE (trimethylsilyl polyphosphate),

5. Experimental Section

is heated to 160°C. Benzoic Acid (9.00 g, 73.7 mmol, 1 eq.) and 2,6-diisopropylaniline (28.0 mL, 26.3 g, 148 mmol, 2.0 eq.) are added to the hot PPSE. The reaction mixture is heated overnight at 160°C and poured hot into a 1 M solution of NaOH (800 mL) stirring vigorously. The aqueous phase is extracted with dichloromethane (3x 400 mL, caution: exothermal dissolution). The combined organic phases are dried over MgSO₄ and the solvent is removed to yield the crude amidine. Filtration from hexane and concentration of the filtrate affords the pure amidine **105** (19.7 g, 60%) as colorless microcrystalline solid at 5°C.

¹H NMR (300.13 MHz, CDCl₃, 300 K, TMS): δ = 7.42–6.89 (m, 11H, Ar-CH), 5.72 (s, 1H, NH), 3.49 (bs) + 3.28 (sept, ³J = 6.8 Hz) (2H, Dip-CH(CH₃)₂), 3.19 (sept, ³J = 6.8 Hz) + 3.03 (bs) (2H, Dip-CH(CH₃)₂), 1.38 (d, ³J = 6.9 Hz) + 1.32 (bs) + 1.26 (d, ³J = 6.6 Hz) (12H, Dip-CH(CH₃)₂), 1.01 (d, ³J = 6.5 Hz) + 0.90 (d, ³J = 6.6 Hz) + 0.83 (bs) (12H, Dip-CH(CH₃)₂) ppm.

5.2.3 Synthesis of lithium (E)-(2,6-diisopropylphenyl)((2,6-diisopropylphenyl)imino)(phenyl)methyl)amide **102**^[287]



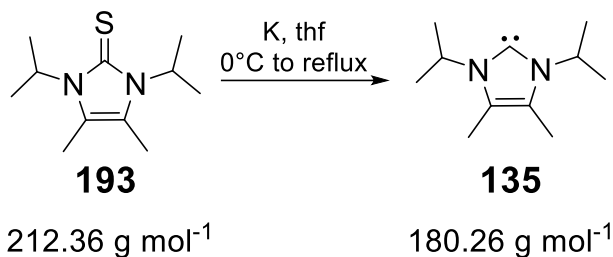
YK107: Benzamidine **105** (3.80 g, 8.62 mmol, 1 eq.) is dissolved in toluene (50 mL) and cooled to -78°C (isopropanol/ liquid nitrogen). ⁿButyl lithium solution in hexanes (2.37 M, 3.8 mL, 9.00 mmol, 1.05 eq.) is added dropwise *via* syringe. The reaction mixture is stirred in the cooling bath for 1 hour and is then allowed to reach room temperature. Stirring is continued for 1 hour. Removal of solvent and volatile components *in vacuo* is followed by washing with hexane (3x 10 mL). Thorough drying affords amidinate **102** (3.33 g, 87%) as a white powder.

¹H NMR (300.13 MHz, C₆D₆, 300 K, TMS): A few drops of *thf-d*₈ is added to increase solubility of the product in C₆D₆. δ = 7.19-7.13 (m, 6H, Ar-CH), 7.05-

5. Experimental Section

7.00 (m, 2H, Ar-CH), 6.87-6.75 (m, 3H, Ar-CH), 3.75 (sept, $^3J = 6.8$ Hz, 4H, Dip-CH(CH₃)₂), 1.29 (d, $^3J = 6.8$ Hz, 12H, Dip-CH(CH₃)₂), 1.07 (d, $^3J = 6.9$ Hz, 12H, Dip-CH(CH₃)₂) ppm. **⁷Li NMR** (116.64 MHz, C₆D₆, 300 K, Li⁺ aq): A few drops of thf-d₈ is added to increase solubility of the product in C₆D₆. $\delta = 1.74$ (s) ppm.

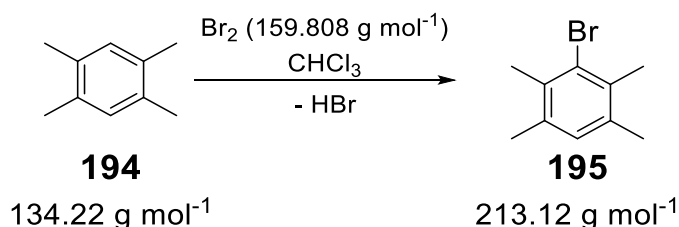
5.2.4 Synthesis of ⁱPr₂Me₂NHC **135**^[281]



YK127: A Schlenk-flask is charged with thione **193** (8.45 g, 39.8 mmol, 1 eq.) and evacuated (3x). Thf (ca 150 mL) is added and the reaction mixture is cooled to 0°C. Potassium (3.5 g, 89.5 mmol, 2.3 eq.) is cut in mineral oil, washed twice in hexane and added to the cooled reaction mixture, which is subsequently refluxed for 5 h. Cooling to rt is followed by filtration and removing all solvents and volatile components. The crude product is twice sublimed yielding NHC **135** as colorless solid (6.30 g, 87%).

¹H NMR (300.13 MHz, C₆D₆, 300 K, TMS): $\delta = 3.96$ (sept, $^3J = 6.6$ Hz, 2H, NCH(CH₃)₂), 1.74 (s, 6H, CH₃), 1.50 (d, $^3J = 6.6$ Hz, 12H) ppm.

5.2.5 Synthesis of bromodurene **195**



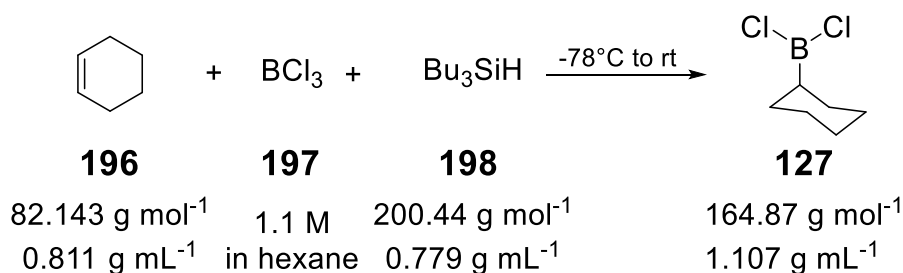
YK120: This reaction was not carried out under argon atmosphere. Durene (556 g, 4.14 mol) is dissolved in chloroform (ca. 1.5 L). The solution is filled in a 2 L-three-necked flask connected to a wash-bottle-setup filled with sodium hydroxide solution. Both are cooled in an ice bath. Bromine (223 mL, 695 g,

5. Experimental Section

4.35 mol) is added dropwise through an aluminum foil covered dropping funnel. The reaction mixture is stirred in the ice bath overnight, new ice is added and the reaction mixture is stirred for 3 days. Subsequently deionized water is added and stirred for 1 h. The phases were separated and the organic layer is washed twice with sodium hydroxide solution (2 M), deionized water, and saturated sodium chloride solution. All solvents and volatiles are removed under vacuum. Two times dry distillation affords 239 g bromodurene **195** (1.12 mol, 27%).

¹H NMR (400 MHz, CDCl₃, 300 K, TMS): δ = 2.30 (s, 6H, Dur-CH₃), 2.38 (s, 6H, Dur-CH₃), 6.91 (s, 1H, Dur-CH) ppm.

5.2.6 Synthesis of dichlorocyclohexyl borane **127**^[288]

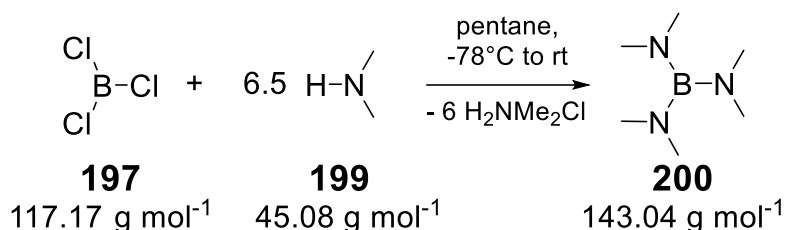


YK207: BCl₃ solution (1.1 M in hexane, 36.4 mL, 40.0 mmol, 1 eq.) is cooled to -78°C and cyclohexene (degassed, 4.0 mL, 40.0 mmol, 1 eq.) is added *via* syringe. The reaction mixture is stirred for 15 minutes at -78°C, then tributylsilane (10.3 mL, 40.0 mmol, 1.eq.) is added dropwise *via* syringe. The reaction mixture is slowly allowed to reach room temperature and is stirred 1 hour at room temperature. Solvent is removed carefully *in vacuo*. Distillation at 40 mbar afforded the desired dichlorocyclohexyl borane **127**.

¹¹B NMR (96.29 MHz, C₆D₆, 343 K, BF₃-Et₂O): δ = 63.3 (s) ppm.

5. Experimental Section

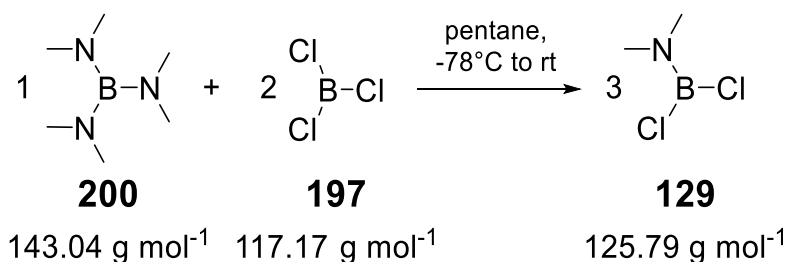
5.2.7 Synthesis of tris(dimethylamino)borane **200**



YK073: Pentane (750 mL) is filled in a 2 L-three necked flask equipped with a kpg-stirrer and is cooled to -78°C (isopropanol/ dry ice) for 30 minutes. Dimethylamine (750 mL, 11.3 mol) is condensed in the flask. BCl_3 (143 mL, 1.74 mol) is condensed in a cooled (-78°C) separate Schlenk tube. BCl_3 is transferred dropwise to the dimethylamine-solution by evaporating the BCl_3 in the Schlenk flask and letting it flow through a condenser. The reaction mixture is allowed to warm to room temperature overnight and is filtered through a Büchner funnel. Removal of solvent and volatile components is followed by distillation (50 mbar, 62°C) with Vigreux column yielding $\text{B}(\text{NMe}_2)_3$ **200** as colorless liquid (202 g, 41%).

$^1\text{H NMR}$ (300.13 MHz, C_6D_6 , 300 K, TMS): $\delta = 2.55$ (s, 18H, $\text{N}(\underline{\text{C}}\text{H}_3)_2$) ppm. $^{11}\text{B NMR}$ (96.29 MHz, C_6D_6 , 300 K, $\text{BF}_3\text{-Et}_2\text{O}$): $\delta = 27.6$ (s) ppm $^{13}\text{C NMR}$ (75.47 MHz, C_6D_6 , 300K, TMS): $\delta = 39.6$ (s, $\text{N}(\underline{\text{C}}\text{H}_3)_2$) ppm.

5.2.8 Synthesis of Dichloro(dimethylamino)borane **129**



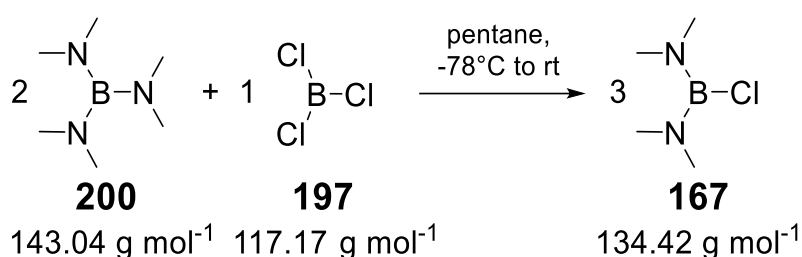
YK197: Tris(dimethylamino)borane **200** (27.8 g, 0.194 mol) is dissolved in pentane (100 mL). BCl_3 (32 mL, 0.388 mol) is condensed in a cooled (-78°C) separate Schlenk tube and subsequently condensed to the cooled (0°C) tris(dimethylamino)borane solution. The reaction mixture is allowed to reach room temperature and is stirred overnight. Removal of solvent and volatile components is followed by distillation (100 mbar, 47°C - 49°C) with Vigreux

5. Experimental Section

column yielding Cl_2BNMe_2 **129** as colorless liquid (26.1 g, 36%). (Loss of yield is attributed to low pressure (20 mbar) at the start of the distillation leading to condensed product in the cooling trap). The product solidifies as dimer and is stored as solid at rt.

$^1\text{H NMR}$ (300.13 MHz, C_6D_6 , 300 K, TMS): $\delta = 2.36$ (s, 6H, $\text{N}(\text{CH}_3)_2$) ppm. $^{11}\text{B NMR}$ (96.29 MHz, C_6D_6 , 300 K, $\text{BF}_3\text{-Et}_2\text{O}$): $\delta = 30.4$ (br s) ppm

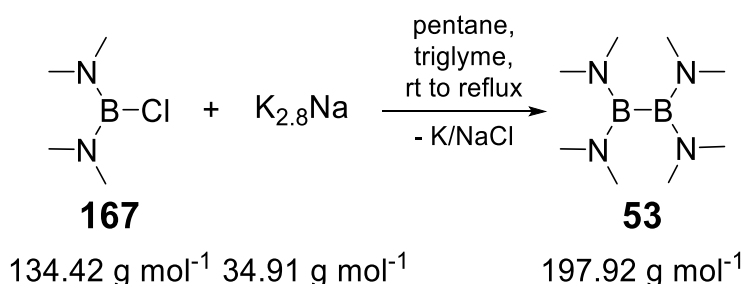
5.2.9 Synthesis of Chlorobis(dimethylamino)borane **167**^[289]



YK074: Tris(dimethylamino)borane **200** (202 g, 1.42 mol) is dissolved in pentane (100 mL). BCl_3 (58 mL, 0.71 mol) is condensed in a cooled (-78°C) separate Schlenk tube and subsequently condensed to the cooled (-78°C) tris(dimethylamino)borane solution. The reaction mixture is allowed to reach room temperature and is stirred overnight. Removal of solvent and volatile components is followed by distillation (25 mbar, 50°C) with Vigreux column yielding $\text{ClB}(\text{NMe}_2)_2$ **167** as colorless liquid (268 g, 93%).

$^1\text{H NMR}$ (300.13 MHz, C_6D_6 , 300 K, TMS): $\delta = 2.50$ (s, 12H, $\text{N}(\text{CH}_3)_2$) ppm. $^{11}\text{B NMR}$ (96.29 MHz, C_6D_6 , 300 K, $\text{BF}_3\text{-Et}_2\text{O}$): $\delta = 28.0$ (s) ppm $^{13}\text{C NMR}$ (75.47 MHz, C_6D_6 , 300K, TMS): $\delta = 39.9$ (s, $\text{N}(\text{CH}_3)_2$) ppm.

5.2.10 Synthesis of tetrakis(dimethylamino)diborane(**4**) **53**^[289]

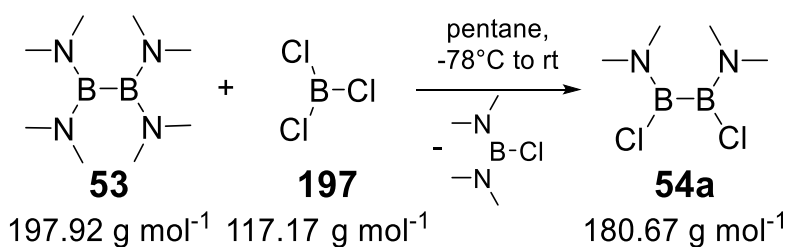


5. Experimental Section

YK082: Na/K_{2.8} alloy (43.3 g, 1.24 mol) is suspended in a 1:1 mixture of pentane and hexane (each 250 mL) and triglyme is added. First a 20 mL portion of Chloro(dimethylamino)borane **167** (147 mL, 0.93 mol) is added through a dropping funnel and when the reaction mixture starts warming up the rest of the borane is added dropwise. The reaction mixture is refluxed for five hours and stirred at room temperature overnight. The reaction mixture is filtered through a frit. Removal of solvent and volatile components is followed by distillation (main fraction: 11-16 mbar, 79-88°C) with Vigreux column yielding Tetrakis(dimethylamino) diborane(4) **53** as colorless liquid (87.3 g, 95%).

¹H NMR (300.13 MHz, CDCl₃, 300 K, TMS): δ = 2.66 (s, 24H, N(CH₃)₂) ppm.
¹¹B NMR (96.29 MHz, CDCl₃, 300 K, BF₃-Et₂O): δ = 36.9 (s) ppm
¹³C NMR (75.47 MHz, CDCl₃, 300K, TMS): δ = 41.3 (s, N(CH₃)₂) ppm.

5.2.11 Synthesis of 1,2-dichloro-1,2-bis(dimethylamino) diborane(4) **54a**^[93-95,289]



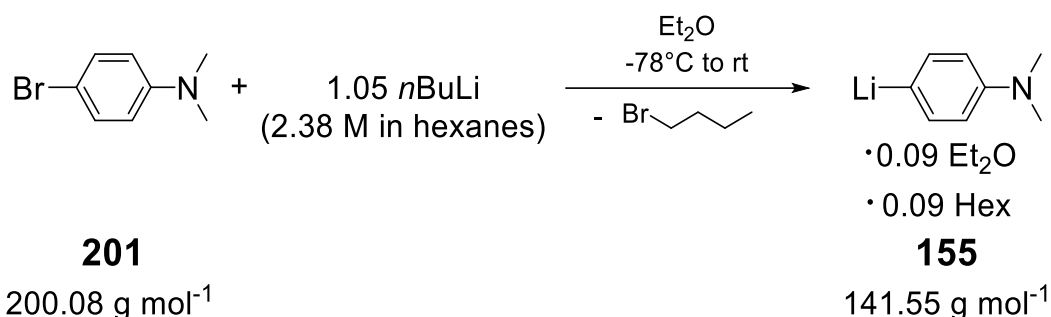
YK111: Tetrakis(dimethylamino) diborane(4) **53** (67.6 g, 0.342 mol) is dissolved in pentane (150 mL). BCl₃ (29 mL, 0.359 mol) is condensed in a cooled (-78°C) separate Schlenk tube and subsequently condensed to the cooled (-78°C) diborane(4) solution. The reaction mixture is allowed to reach room temperature and is stirred overnight. Removal of solvent and volatile components is followed by distillation (16 mbar, 82-85°C) with Vigreux column yielding 1,2-dichloro-1,2-bis(dimethylamino) diborane(4) **54a** as colorless liquid (53.2 g, 86%).

¹H NMR (300.13 MHz, CDCl₃, 300 K, TMS): δ = 2.86, 2.89 (each s, each 6H, N(CH₃)₂) ppm. **¹¹B NMR** (96.29 MHz, CDCl₃, 300 K, BF₃-Et₂O): δ = 37.6 (s) ppm

5. Experimental Section

5.2.12 Synthesis of isolated monolithiated compounds

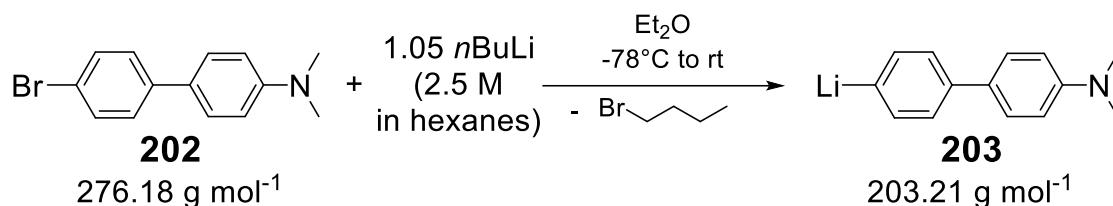
General procedure: The corresponding Bromoarene or -heterocycle (**201**, **202**, **204**, **206** or **208**) (1 eq.) is dissolved in diethyl ether (ca. 2 mL/mmol) and cooled to -78°C in a cooling bath (*iso*-propanol/ liquid nitrogen). *n*-Butyl lithium solution in hexanes (2.38 M, 1.04 eq.) is added dropwise through a dropping funnel. The reaction mixture is stirred in the cooling bath for 5 minutes and is then allowed to reach room temperature. Removal of solvent and volatile species *in vacuo* is followed by filtration from hexane. The residue is washed with hexane twice and dried *in vacuo*. The desired lithium compounds **155**, **203**, **205**, **207** and **209** are isolated and used without further purification.



Data for YK112_2^[258]: From 4-bromo-*N,N*-dimethylaniline (**201**) (9.20 g, 46.0 mmol), *n*-butyl lithium solution in hexanes (20.0 mL, 2.38 M, 47.6 mmol, 1.04 eq.). The desired (4-(dimethylamino)phenyl)lithium **155** is isolated with traces of hexane (8%) and diethyl ether (8%) (determined *via* ¹H NMR spectroscopy) in quantitative yield (6.27 g, 96%).

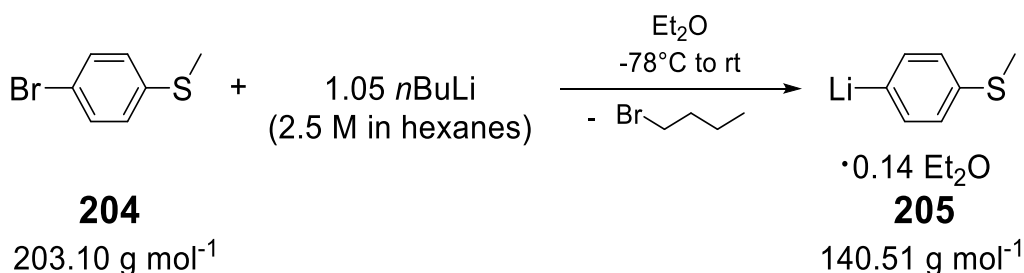
¹H NMR (300.13 MHz, C₆D₆, 300 K, TMS): *A few drops of thf-d₈ is added to increase solubility of the product in C₆D₆.* δ = 8.33 (d, ³J = 8.0 Hz, 2H, PhH), 6.96 (d, ³J = 8.1 Hz, 2H, PhH), 3.26 (q, ³J = 7.0 Hz, 0.8H, Et₂O-CH₂), 2.75 (s, 6H, Ph-N(CH₃)₂), 1.22 (bs, 0.8H, Hex-CH₂), 1.10 (t, ³J = 3.7 Hz, 0.6H, Et₂O-CH₃), 0.87 (t, ³J = 6.5 Hz, 0.6H, Hex-CH₃) ppm. **⁷Li NMR** (116.64 MHz, C₆D₆, 300 K, Li⁺ aq): *A few drops of thf-d₈ is added to increase solubility of the product in C₆D₆.* δ = 2.32 ppm.

5. Experimental Section



Data for YK180: From 4'-bromo-*N,N*-dimethyl[1,1'-biphenyl]-4-amine (**202**) (536 mg, 1.94 mmol), *n*butyl lithium solution in hexanes (0.82 mL, 2.5 M, 2.03 mmol, 1.05 eq.). The desired 4'-(dimethylamino)-[1,1'-biphenyl]4-yl lithium **203** is isolated in 79% yield (313 mg).

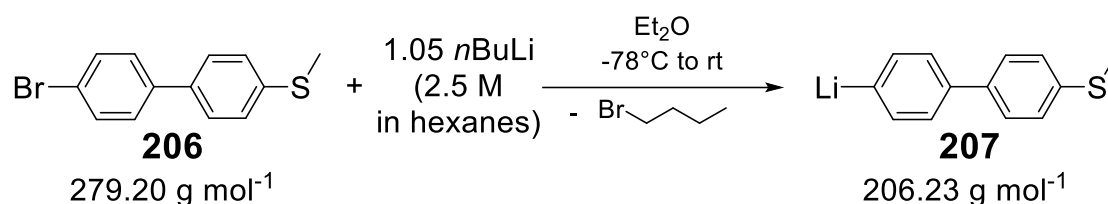
¹H NMR (300.13 MHz, thf-*d*₈, 300 K, TMS): δ = 7.76 (d, ³J = 7.6 Hz, 2H, Ar-CH), 7.23 (d, ³J = 8.9 Hz, 2H, Ar-CH), 6.94 (d, ³J = 7.6 Hz, 2H, Ar-CH), 6.55 (d, ³J = 8.9 Hz, 2H, Ar-CH), 2.72 (s, 6H, Ar-N(CH₃)₂) ppm. **⁷Li NMR** (116.64 MHz, thf-*d*₈, 300 K, Li⁺ aq): δ = 1.47 ppm.



Data for YK168^[290]: From 4-bromothioanisole (**204**) (1.06 g, 5.22 mmol), *n*butyl lithium solution in hexanes (2.2 mL, 2.5 M, 5.48 mmol, 1.05 eq.). The desired 4-lithiothioanisole **205** is isolated with traces of diethyl ether (14%) (determined via ¹H NMR spectroscopy) in 83% yield (610 mg).

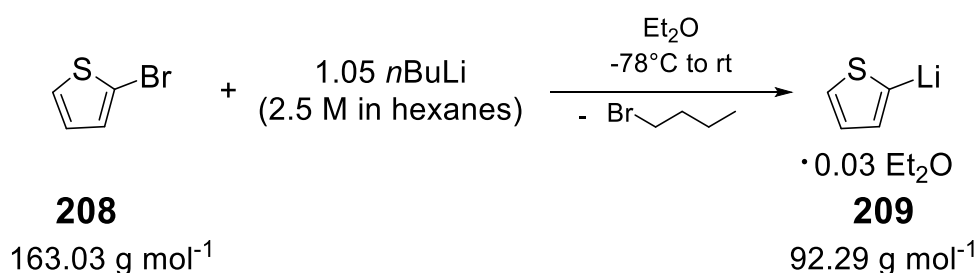
¹H NMR (300.13 MHz, C₆D₆, 300 K, TMS): A few drops of thf-*d*₈ is added to increase solubility of the product in C₆D₆. δ = 8.17 (d, ³J = 7.6 Hz, 2H, PhH), 7.39 (d, ³J = 7.5 Hz, 2H, PhH), 3.26 (q, ³J = 7.0 Hz, 0.3H, Et₂O-CH₂), 2.31 (s, 3H, Ph-SCH₃), 1.08 (t, ³J = 3.7 Hz, 0.5H, Et₂O-CH₃) ppm. **⁷Li NMR** (116.64 MHz, C₆D₆, 300 K, Li⁺ aq): A few drops of thf-*d*₈ is added to increase solubility of the product in C₆D₆. δ = 1.61 ppm.

5. Experimental Section



Data for YK169: From (4'-bromo-[1,1'-biphenyl]-4-yl)(methyl)sulfane (**206**) (730 mg, 2.62 mmol), *n*butyl lithium solution in hexanes (1.1 mL, 2.5 M, 2.75 mmol, 1.05 eq.). The desired (4'-(methylthio)-[1,1'-biphenyl]-4-yl)lithium **207** is isolated in 78% yield (422 mg).

¹H NMR (400.13 MHz, thf-d₈, 300 K, TMS): δ = 7.92 (d, ³J = 7.6 Hz, 2H, Ar-CH), 7.48 (d, ³J = 8.6 Hz, 2H, Ar-CH), 7.22 (d, ³J = 8.5 Hz, 2H, Ar-CH), 7.09 (d, ³J = 7.6 Hz, 2H, Ar-CH), 2.45 (s, 3H, Ar-SCH₃) ppm. **⁷Li NMR** (116.64 MHz, thf-d₈, 300 K, Li⁺ aq): δ = -0.64 ppm.

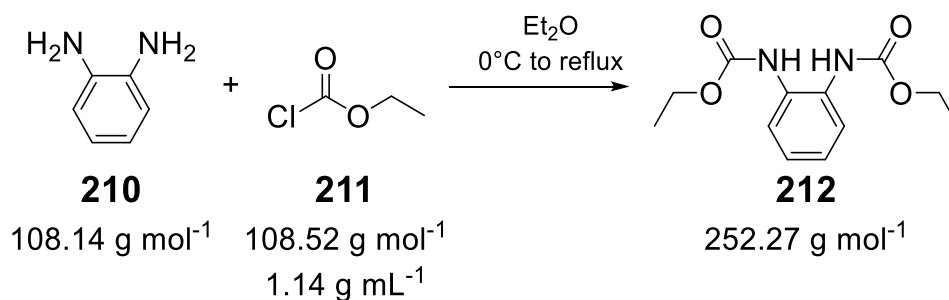


Data for YK170: From 2-bromothiophene (**208**) (0.48 mL, 4.96 mmol), *n*butyl lithium solution in hexanes (2.1 mL, 2.5 M, 5.21 mmol, 1.05 eq.). The desired 2-lithiothiophene **209** is isolated with traces of diethyl ether (3%) (determined *via* ¹H NMR spectroscopy) in 54% yield (246 mg).

¹H NMR (300.13 MHz, C₆D₆, 300 K, TMS): *A few drops of thf-d₈ is added to increase solubility of the product in C₆D₆.* δ = 8.05 (d, ³J = 4.1 Hz, 1H), 7.74 (d, ³J = 2.8 Hz, 1H), 7.65 (dd, ³J = 4.2, ³J = 4.2 Hz, 1H), 3.26 (q, ³J = 7.0 Hz, 0.1H, Et₂O-CH₂), 1.09 (t, ³J = 3.7 Hz, 0.2H, Et₂O-CH₃) ppm. **⁷Li NMR** (116.64 MHz, C₆D₆, 300 K, Li⁺ aq): *A few drops of thf-d₈ is added to increase solubility of the product in C₆D₆.* δ = 1.68 ppm.

5. Experimental Section

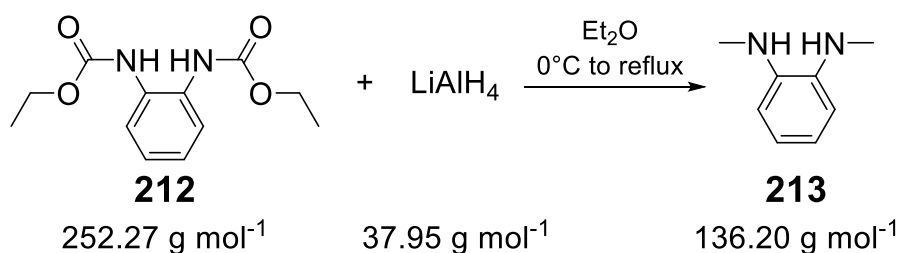
5.2.13 2-(Ethoxycarbonylamino-phenyl)-carbamic acid ethyl ester **212**^[291]



YK151_4: A solution of ethyl chloroformate (22.4 mL, 235 mmol) in toluene (88 mL) is added dropwise through a dropping funnel to a cold (0°C) solution of 1,2-diaminobenzene (25.4 g, 235 mmol) in toluene (300 mL) and a white precipitate is formed immediately. The reaction mixture is stirred at room temperature for 3 h, the precipitate is removed by filtration, and the toluene is removed under vacuum. The crude **212** is recrystallized from toluene at 5°C to give a solid in a final yield of 59% (17.6 g).

¹H NMR (300.13 MHz, CDCl₃, 300 K, TMS) δ : 7.47 (br s, 2H, Ar-CH), 7.15-7.10 (m, 2H, Ar-CH), 7.04 (br s, 2H, NH), 4.23 (q, ³J = 7.1 Hz, 4H, Et-CH₂), 1.31 (t, ³J = 7.1 Hz, 6H, Et-CH₃).

5.2.14 Synthesis of *N,N*-dimethyl-1,2-diaminobenzene **213**^[291]



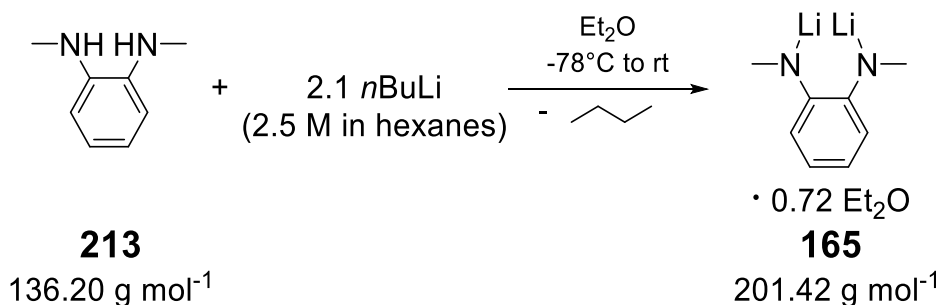
YK147_5: 2-(Ethoxycarbonylamino-phenyl)-carbamic acid ethyl ester **212** (16.8 g, 66.6 mmol) is dissolved in thf (ca. 160 mL), LiAlH₄ (7.6 g, 200 mmol) is suspended in thf (175 mL) and cooled to 0°C. The carbamic acid ethyl ester solution is added dropwise through a dropping funnel to the cooled LiAlH₄ suspension. The reaction mixture is stirred at 0°C for 1 h and at rt overnight. The reaction mixture is refluxed for 6 h. Subsequently the mixture was cooled to 0°C and then water (48 mL, slowly), NaOH 15% (48 mL) and water (144 mL) were added. The mixture was stirred overnight under argon atmosphere. The

5. Experimental Section

white precipitate was filtered off and extracted with warm thf, and the volatiles were removed under vacuum to give green oil that was acidified with HCl 10% (200 mL). The aqueous solution was washed three times with dichloromethane (3x 200 mL). The aqueous solution was basified with NaOH 10% (180 mL) and extracted three times with dichloromethane (3x 300 mL). The organic phase was dried over anhydrous MgSO₄ and the solvent was removed under vacuum to give redish solid of **213** in a final yield of 64% (5.85 g, 43.0 mmol).

¹H NMR (400.13 MHz, C₆D₆, 300 K, TMS) δ = 7.00-6.95 (m, 2H, Ar-CH), 6.63-6.59 (m, 2H, Ar-CH), 2.74 (br s, 2H, NH), 2.42 (s, 6H, NCH₃) ppm.

5.2.15 Synthesis of *N,N'*-dilithium dimethyl-1,2-diaminobenzene **165**^[292]

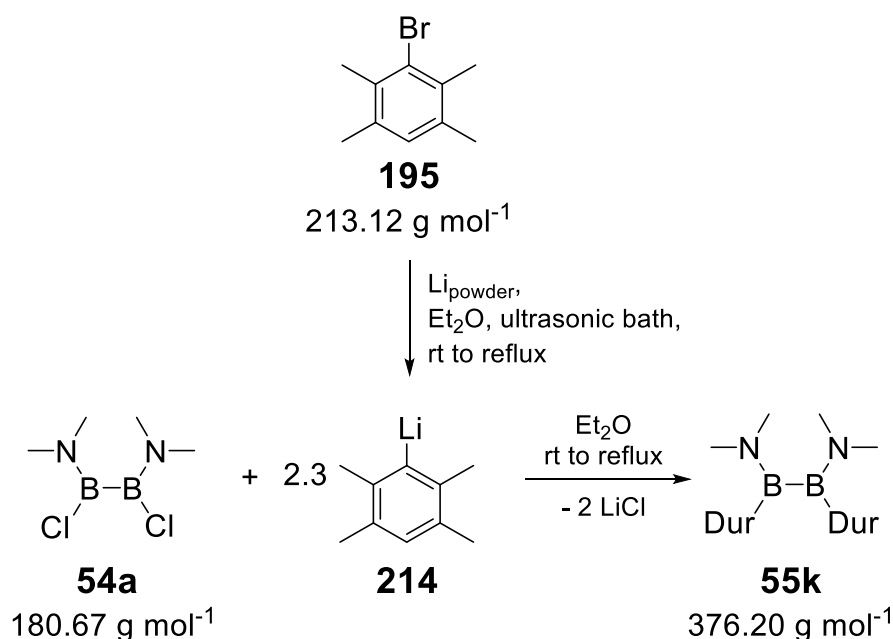


YK148_2: *N,N'*-dimethyl-1,2-diaminobenzene (**213**) (6.26 g, 46.0 mmol, 1 eq.) is dissolved in Et₂O (150 mL) and cooled in a -78°C cooling bath (*iso*-propanol/liquid nitrogen) for 30 minutes. ⁿButyl lithium solution in hexanes (39.0 mL, 2.5 M, 96.5 mmol, 2.1 eq.) is added dropwise *via* dropping funnel. The reaction mixture is stirred in the cooling bath for 10 minutes and is then allowed to reach room temperature. Removal of solvent and volatile species *in vacuo* is followed by filtration from hexane. The residue is washed with hexane twice and dried *in vacuo*. The desired *N,N'*-dilithium dimethyl-1,2-diaminobenzene **165** is isolated with 0.72 diethyl ether (determined *via* ¹H NMR spectroscopy) in quantitative yield.

¹H NMR (400.13 MHz, thf-d₈, 300K, TMS): δ = 5.94 - 5.90 (m, 2H, ArH), 5.48 - 5.44 (m, 2H, ArH), 3.38 (q, ³J = 7.0 Hz, 2.83H, Et₂O-CH₂ (coord.)), 2.75 (s, 6H, Ar-NCH₃), 1.11 (t, ³J = 7.0 Hz, 4.33H, Et₂O-CH₃) ppm. **⁷Li NMR** (116.64 MHz, thf-d₈, 300 K, Li⁺ aq): δ = -0.82 ppm.

5. Experimental Section

5.2.16 Synthesis of 1,2-diduryl-1,2-bis(dimethylamino)diborane(4) **55k**^[98,104]

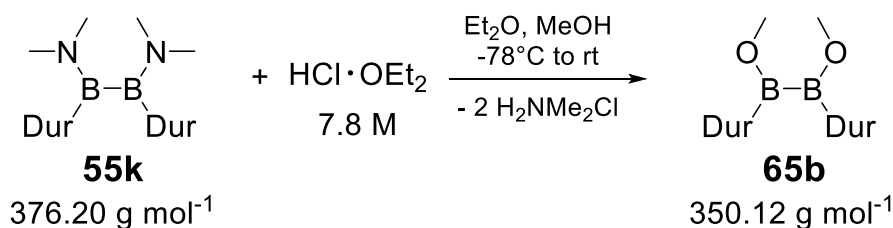


OA006: Lithium powder (5.70 g, 821 mmol) was suspended in diethyl ether (500 ml) at rt. The mixture was kept in an ultrasonic bath while a solution of 3-bromodurene **195** (50.0 g, 235 mmol) in diethyl ether (80 ml) was added dropwise over 45 min. The resulting suspension was kept in the ultrasonic bath, heated to reflux for 2 h and then cooled to rt. After the dropwise addition of 1,2-bis-(dimethylamino)-1,2-dichlorodiborane(4) **54a** (19.0 ml, 20.5 g, 104 mmol) over 20 min, the mixture was refluxed for 2 h, cooled to rt and stirred for 18 h. The suspension was filtered and the filtrate was concentrated under reduced pressure. Hexane was added to the residue and the resulting suspension was filtered. Removal of the solvent of the filtrate under reduced pressure gave a pale yellow solid that was recrystallized from 300 ml ethanol. After washing with ice-cold ethanol, 1,2-diduryl-1,2-bis-dimethylamino-diborane **55k** (33.1 g, 85 % yield) was obtained as colorless crystals.

¹H NMR (300 MHz, CDCl₃, 300 K, TMS): δ = 1.90 (s, 12H, Dur-CH₃), 2.23 (s, 12H, Dur-CH₃), 2.64 (s, 6H, N(CH₃)₂), 3.06 (s, 6H, N(CH₃)₂), 6.94 (s, 2 H, Dur-CH) ppm. **¹¹B NMR** (96 MHz, CDCl₃, 300 K, BF₃-OEt₂): δ = 50.8 ppm.

5. Experimental Section

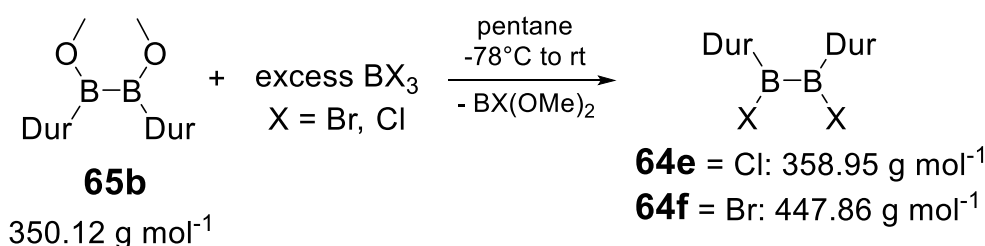
5.2.17 Synthesis of 1,2-diduryl-1,2-dimethoxydiborane(4) **65b**^[98,104]



OA009: Diborane **55k** (25.0 g, 66.5 mmol) was dissolved in diethyl ether (180 ml) and methanol (abs., 75 ml) and the solution was cooled to -78°C . HCl-Et₂O (7.8 M, 88 ml, 686 mmol) was added dropwise at -78°C over 30 min. After completion of the addition, the mixture was allowed to slowly warm to rt. Stirring was continued for 18 h and the solvent was removed under vacuum. Crude diborane **65b** was obtained as a colorless solid and divided into two equal parts for the conversion to the halogenated diboranes **64e** and **64f**.

¹H NMR (300 MHz, C₆D₆, 300 K, TMS): $\delta = 2.09$ (s, 12H, Dur-CH₃), 2.11 (s, 12H, Dur-CH₃), 3.50 (s, 6H, OCH₃), 6.85 (s, 2H, Dur-CH) ppm. **¹¹B NMR** (96 MHz, C₆D₆, 300 K, BF₃-OEt₂): $\delta = 59.0$ (s) ppm.

5.2.18 Synthesis of 1,2-dihalo-1,2-diduryldiboranes(4) **64e,f**^[98,104]



OA010: Boron trichloride (11.0 ml, 15.7 g, 134 mmol) was condensed at -78°C and added to a cooled (-78°C) suspension of crude diborane **65b** (33.3 mmol) in pentane (150 ml). The mixture was allowed to slowly warm to -10°C and was stored at -26°C overnight. After 18 h, the solvent and excess BCl₃ were removed under vacuum and pentane (150 ml) was added to the residue. Filtration of the resulting suspension led to a yellow filtrate which was concentrated under vacuum. Colorless crystals of dichlorodiborane **64e** (8.18 g, 68 % yield) were obtained by storing the solution at -26°C for several days.

5. Experimental Section

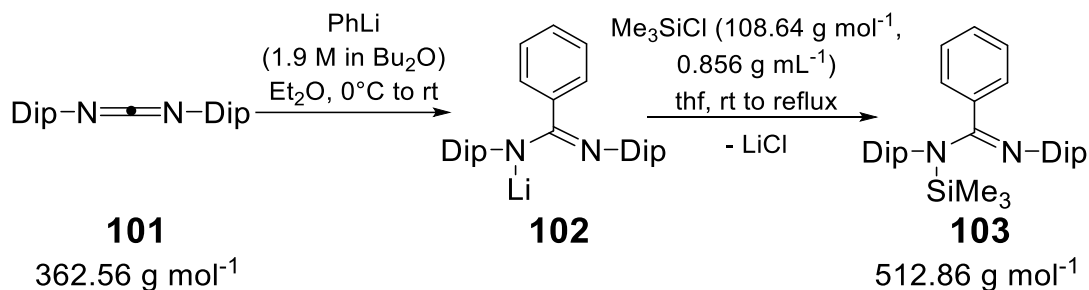
¹H NMR (300 MHz, C₆D₆, 300 K, TMS): δ = 1.95 (s, 12H, Dur-CH₃), 2.07 (s, 12H, Dur-CH₃), 6.80 (s, 2 H, Dur-CH) ppm. **¹¹B NMR** (96 MHz, C₆D₆, 300 K, BF₃-OEt₂): δ = 83.7 (s) ppm.

OA011: Boron tribromide (7.4 ml, 19.5 g, 77.6 mmol) was added to a cooled (−78°C) suspension of crude diborane **65b** (33.3 mmol) in pentane (150 ml). The mixture was allowed to slowly warm to −10 °C and was stored at −26 °C overnight. After 18 h, the solvent and excess BBr₃ were removed under vacuum and pentane (150 ml) was added to the residue. Filtration of the resulting suspension led to a yellow solution from which small yellow crystals were obtained after several minutes at rt. The mixture was stored at −26 °C for several days to complete crystallisation of dibromodiborane **64f** (7.51 g, 53 % yield).

¹H NMR (300 MHz, C₆D₆, 300 K, TMS): δ = 1.94 (s, 12H, Dur-CH₃), 2.11 (s, 12H, Dur-CH₃), 6.80 (s, 2 H, Dur-CH) ppm. **¹¹B NMR** (96 MHz, C₆D₆, 300 K, BF₃-OEt₂): δ = 86.6 (s) ppm.

5.3. Synthesis of various boryl benzamidinates

5.3.1 Synthesis of (E)-N,N-bis(2,6-diisopropylphenyl)-N-(trimethylsilyl)benzimidamide **103**^[193]

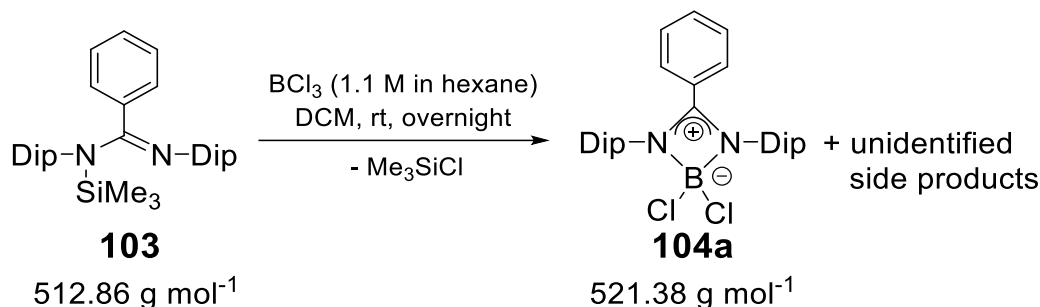


YK075_2: Bis(2,6-diisopropylphenyl)methanediimine (5.05 g, 13.9 mmol, 1 eq.) is dissolved in Et₂O (100 mL) and cooled to 0°C. Phenyl lithium solution in dibutyl ether (1.9 M, 8.0 mL, 15.2 mmol, 1.1 eq.) is added dropwise *via* syringe. The reaction mixture is allowed to reach room temperature. Stirring is continued for 1 hour. Removal of solvents *in vacuo* is followed by washing with hexane (80 mL) and thorough drying. The washed benzamidinate **102** is dissolved in thf (90 mL) and trimethylsilyl chloride (2 mL, 1.71 g, 15.7 mmol, 1.13 eq.) is added dropwise *via* syringe. The reaction mixture is refluxed for 2 hours. Removal of solvents and volatile species *in vacuo* is followed by filtration from hexane. Reducing the filtrate volume gives a colorless solution from which 4.62 g (3 batches, 65%) of silylamidinate **103** are obtained as colorless crystals.

¹H NMR (400.13 MHz, C₆D₆, 300 K, TMS): δ = 7.00-6.95 (m, 8H, Ar-CH), 6.65 (t, ³J = 7.4 Hz, 2H, Ph-CH), 6.55 (tt, ³J = 7.4 Hz, ⁴J = 1.2 Hz, 1H, Ph-CH), 3.55 (sept, ³J = 6.9 Hz, 4H, Dip-CH(CH₃)₂), 1.29 (d, ³J = 6.7 Hz, 12H, Dip-CH(CH₃)₂), 1.11 (bs, 12H, Dip-CH(CH₃)₂), 0.57 (bs, 9H, Si(CH₃)₃) ppm. **¹³C NMR**{¹H} (100.61 MHz, C₆D₆, 300 K, TMS): δ = 161.8 (s, N-CN), 147.1, 139.8 (each bs, each Dip-C_{quart.}), 133.9 (s, Ph-C_{quart.}), 129.1, 126.9 (each s, each Ph-CH), 123.7 (bs, Dip-CH), 28.6 (s, Dip-CH(CH₃)₂), 25.8 (s, Dip-CH(CH₃)), 23.4 (bs, Dip-CH(CH₃)), 1.8 (s, Si(CH₃)₃) ppm. **²⁹Si NMR** (79.50 MHz, C₆D₆, 300 K, TMS): δ = 4.2 ppm. **MP:** >200°C (stable). **IR** (powder): ν(C=N & C_{Ar}=C_{Ar}) = 1607, 1599, 1586, 1572 cm⁻¹. **Elemental Analysis:** C₃₄H₄₈N₂Si (512.86 g/mol); C 79.55 (calc. 79.63); H 9.27 (calc. 9.43), N 5.36 (calc. 5.46) %.

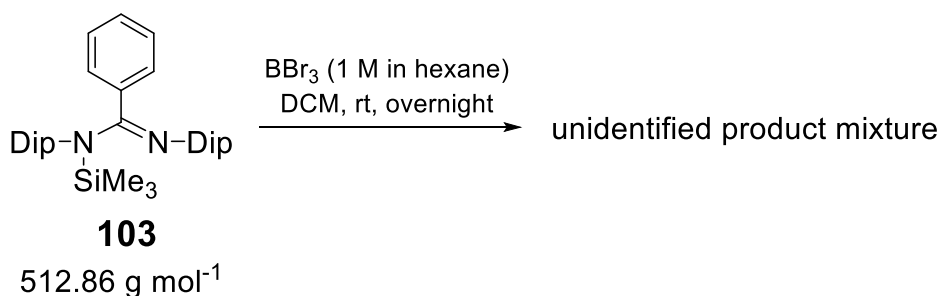
5. Experimental Section

5.3.2 Attempts to synthesize (E)-N-(dihaloboryl)-N,N'-bis(2,6-diisopropylphenyl)benzimidamide **104a,b**^[27,30,33,34,37]



YK079_3(Cl): Silylamidinate **103** (2.05 g, 4.00 mmol, 1 eq.) is dissolved in dichloromethane (30 mL) and an excess of BCl_3 solution (1M in hexanes, 27.0 mL, 27.0 mmol, 6.75 eq.) is added slowly at room temperature. The reaction mixture is stirred overnight. Removal of solvent and volatile components affords a white foam consisting of ca. 50% desired boron-amidinate-complex **104a** (determined *via* ^1H NMR spectroscopy). Purification by crystallization is not successful.

*Note: Analytical Data of the main product **104a** in Section 5.3.3.*

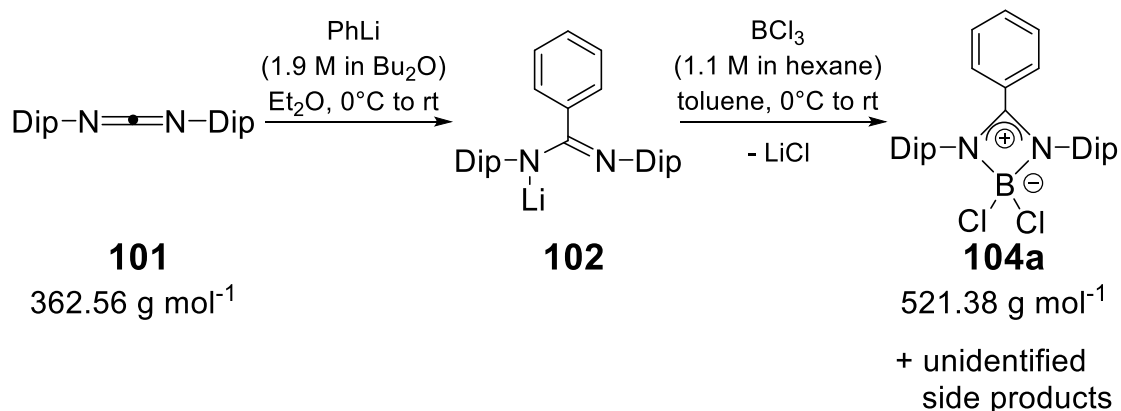


YK077_3(Br): The Schlenk flask is covered by aluminum foil to protect the reaction mixture from light. Silylamidinate **103** (274 mg, 0.534 mmol, 1 eq.) is dissolved in dichloromethane (5 mL) and an excess of BBr_3 solution (1M in hexanes, 4.3 mL, 4.30 mmol, 8.05 eq.) is added slowly at room temperature. The reaction mixture is stirred overnight. Removal of solvent and volatile components affords a purple colored slime covering a colorless foam. NMR spectroscopic analysis revealed the lack of desired **104b** and only an unidentified product mixture.

Note: ^1H NMR data were due to signal overlaps beyond interpretation.

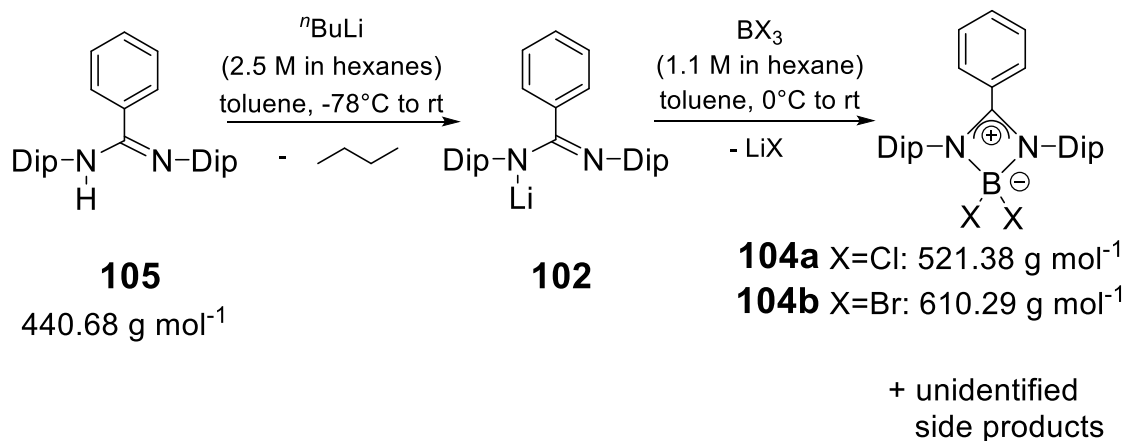
5. Experimental Section

¹¹B NMR (96.29 MHz, C₆D₆, 300 K, BF₃-Et₂O): δ = 1.3, 1.1, -10.7 ppm.



YK084(CI): Bis(2,6-diisopropylphenyl)methanediimine (**101**) (250 mg, 0.690 mmol, 1 eq.) is dissolved in Et₂O (5 mL) and cooled to 0°C. Phenyl lithium solution in dibutyl ether (1.9 M, 0.38 mL, 0.722 mmol, 1.05 eq.) is added dropwise *via* syringe. The reaction mixture is allowed to reach room temperature. Stirring is continued for 1 hour. Removal of solvents *in vacuo* is followed by washing with hexane (4 mL) and thorough drying. The intermediate **102** is suspended in toluene and BCl₃ solution (1M in hexanes, 0.83 mL, 0.830 mmol, 1.2 eq.) is added dropwise *via* syringe. Stirring is continued for 1 hour. Removal of solvent and volatile species *in vacuo* is followed by filtration from dichloromethane. ¹H NMR spectrum of the filtrate shows 55% of the desired boron-amidinate-complex **104a**.

Note: Analytical Data of the main product 104a in Section 5.3.3.



5. Experimental Section

YK086_2(Cl): Amidine **105** (2.07 g, 4.64 mmol, 1 eq.) is dissolved in toluene (30 mL) and cooled to -78°C (isopropanol/ liquid nitrogen). n -Butyl lithium solution in hexanes (2.37 M, 2.1 mL, 4.98 mmol, 1.07 eq.) is added dropwise *via* syringe. The reaction mixture is stirred in the cooling bath for 1 hour and then allowed to reach room temperature. Stirring is continued for 1 hour. The reaction mixture is cooled to 0°C and BCl_3 solution (1M in hexanes, 5.2 mL, 5.20 mmol, 1.1 eq.) is added. The reaction mixture is allowed to reach room temperature and stirring is continued for 30 minutes. Removal of solvent and volatile components is followed by filtration from toluene and washing with hexane. Thorough drying affords 705 mg amidinate complex **104a** as colorless powder containing ca. 15% impurities (determined *via* ^1H NMR spectroscopy).

Note: Analytical Data of the main product 104a in Section 5.3.3.

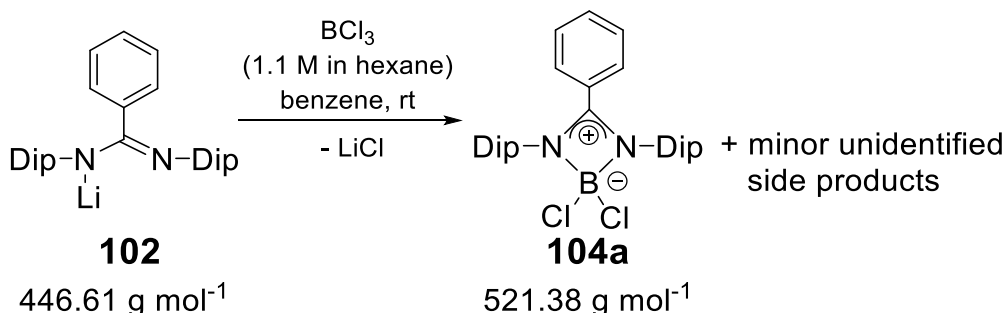
YK088(Br): Amidine **105** (1.92 g, 4.36 mmol, 1 eq.) is dissolved in toluene (50 mL) and cooled to -78°C (isopropanol/ liquid nitrogen). n -Butyl lithium solution in hexanes (2.5 M, 2.0 mL, 5.00 mmol, 1.15 eq.) is added dropwise *via* syringe. The reaction mixture is stirred in the cooling bath for 1 hour and is then allowed to reach room temperature. Stirring is continued for 1 hour. The Schlenk flask is covered with aluminum foil. The reaction mixture is cooled to 0°C and BBr_3 solution (1 M in hexanes, 5.5 mL, 5.50 mmol, 1.3 eq.) is added. The reaction mixture is allowed to reach room temperature and stirring is continued for 30 minutes. Removal of solvent and volatile components is followed by filtration from toluene. Thorough drying affords desired amidinate complex **104b** as colorless powder containing ca. 14% impurities (determined *via* ^1H NMR spectroscopy).

Note: The following NMR data is limited to signals of the main product 104b.

^1H NMR (300.13 MHz, C_6D_6 , 300 K, TMS): 7.34 (tt, $^3\text{J} = 7.2$ Hz, $^4\text{J} = 1.6$ Hz, 1H, Ph-CH), 7.27-7.06 (m, 13H, Ar-CH, tol-CH, C_6D_6 -H_x), 3.47 (sept, $^3\text{J} = 6.8$ Hz, 4H, Dip-CH(CH₃)₂), 1.26 (d, $^3\text{J} = 6.7$ Hz, 12H, Dip-CH(CH₃)₂), 0.71 (d, $^3\text{J} = 6.8$ Hz, 12H, Dip-CH(CH₃)₂) ppm. ^{11}B NMR (96.29 MHz, C_6D_6 , 343 K, $\text{BF}_3\text{-Et}_2\text{O}$): $\delta = 1.3$ (s) ppm.

5. Experimental Section

5.3.3 Synthesis of (E)-N-(dichloroboryl)-N,N'-bis(2,6-diisopropylphenyl)-benzimidamide **104a**



YK108_6: Previously isolated lithium amidinate **102** (1.01 g, 2.26 mmol, 1 eq.) is suspended in benzene (60 mL). BCl_3 solution (1.1 M in hexane, 2.2 mL, 2.42 mmol, 1.1 eq.) is added and stirring is continued for 30 minutes. Filtration is followed by removal of solvent and volatile components and washing with hexane (3x 10 mL). Thorough drying affords 480 mg (41%) amidinate complex **104a** as colorless powder containing ca. 12% unidentified impurities (determined *via* ^1H NMR spectrum). The product is used without further purification. Single crystals suitable for x-ray diffraction could be grown from a concentrated dichloromethane solution at 5°C.

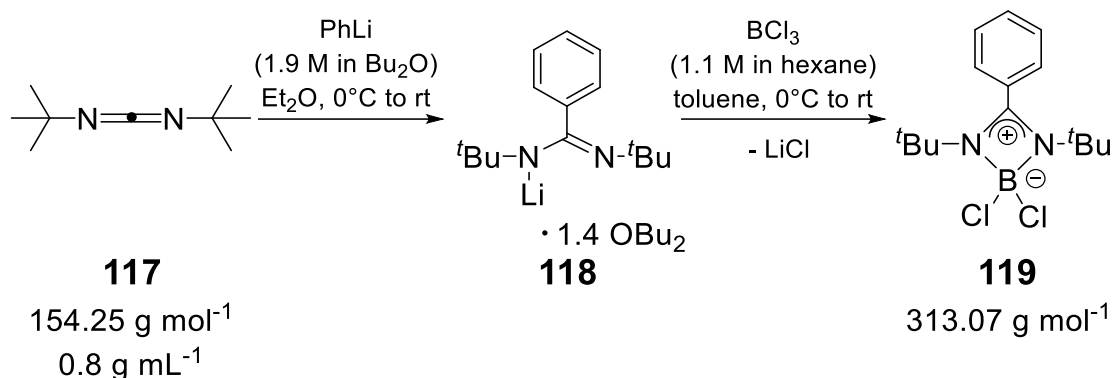
*Note: the following NMR data is limited to signals of the main product **104a**.*

^1H NMR (300.13 MHz, C_6D_6 , 300 K, TMS): δ = 7.27 (dd, 3J = 8.4 Hz, 4J = 1.2 Hz, 2H, Ph-CH), 7.15-7.06 (m, 6H, Ar-CH), 6.71 (tt, 3J = 7.5 Hz, 4J = 0.6 Hz, 1H, Ph-CH), 6.52-6.47 (m, 2H, Ph-CH), 3.83 (sept, 3J = 6.8 Hz, 4H, Dip-CH(CH₃)₂), 1.40 (d, 3J = 6.7 Hz, 12H, Dip-CH(CH₃)₂), 0.87 (d, 3J = 6.9 Hz, 12H, Dip-CH(CH₃)₂) ppm. **^{11}B NMR** (96.29 MHz, C_6D_6 , 343 K, $\text{BF}_3\text{-Et}_2\text{O}$): δ = 9.9 (s) ppm. **^{13}C NMR{ ^1H }** (100.61 MHz, C_6D_6 , 300 K, TMS): δ = 173.3 (br q, $J_{\text{C-B}}$ = 8.8 Hz, NCN), 146.7 (s, Dip-Ar-C_{quart}.N), 133.7 (Ph-CH), 133.2 (s, Dip-Ar-C_{quart}.), 130.6, 129.0 (each s, each Ph-CH), 128.8 (s, Dip-Ar-CH), 125.2 (br s, Ph-C_{quart}.), 125.0 (s, Dip-Ar-CH), 29.2 (s, Dip-CH(CH₃)₂), 25.7, 23.6 (each s, each Dip-CH(CH₃)₂) ppm. **Elemental Analysis:** C₃₁H₃₉BCl₂N₂ (521.38 g/mol); C 71.00 (calc. 71.41); H 7.44 (calc. 7.54), N 5.75 (calc. 5.37) %. **MP:** 198-203°C (stable).

5. Experimental Section

5.3.4 Synthesis of (E)-N,N'-di-tert-butyl-N-(dichloro-boryl)benzimidamide

119



YK216_2: Di-tert-butylmethanediimine (**117**) (1.5 mL, 7.78 mmol, 1 eq.) is dissolved in Et₂O (ca. 120 mL) and cooled to 0°C. Phenyl lithium solution in thf (1.9 M in Bu₂O, 4.2 mL, 7.98 mmol, 1.03 eq.) is added dropwise *via* syringe. The reaction mixture is stirred at 0°C for 10 minutes and is then allowed to reach room temperature. Removal of solvents and volatile components affords the intermediate lithium benzamidinate **118**, which is used without further purification.

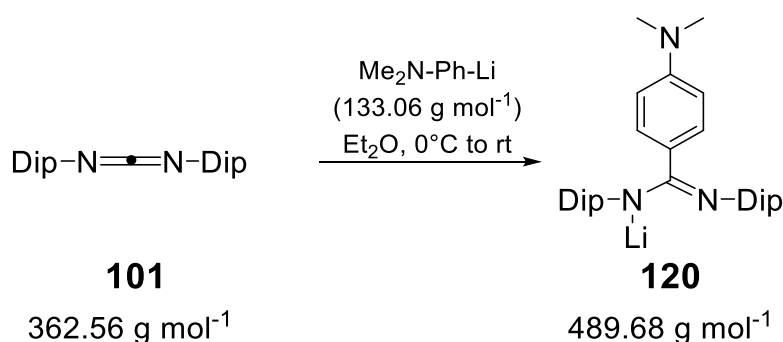
¹H NMR (300.13 MHz, C₆D₆, 300 K, TMS): A few drops of thf-d₈ is added to increase solubility of the product in C₆D₆. δ = 7.44 (br d, ³J = 7.2 Hz, 2H, Ph-CH), 7.18-7.08 (m, 3H, Ph-CH), 3.29 (t, ³J = 6.4 Hz, 2.9H, OBU-CH₂), 1.58-1.49 (m, 3.1H, OBU-CH₂), 1.44-1.31 (m, 3.4H, OBU-CH₂), 1.23 (s, 18H, ^tBu-CH₃), 0.88 (t, ³J = 7.3 Hz, 4.4H, OBU-CH₃) ppm. **⁷Li NMR** (116.64 MHz, C₆D₆, 300 K, Li⁺ aq): A few drops of thf-d₈ is added to increase solubility of the product in C₆D₆. δ = 1.6 (s) ppm.

YK218_2: Lithium benzamidinate **118** (7.78 mmol from YK216_2), is suspended in toluene (ca. 120 mL). The reaction mixture is cooled to 0°C and BCl₃ solution (1.1 M in hexanes, 7.8 mL, 8.56 mmol, 1.1 eq.) is added. The reaction mixture is allowed to reach room temperature. Removal of solvents and volatile components is followed by filtration from toluene. Reducing the filtrate volume gives a yellow solution from which 1.26 g (52%) of **119** are obtained as colorless crystals at -26°C. Single crystals suitable for x-ray diffraction could be grown from a concentrated dichloromethane solution at 5°C.

5. Experimental Section

^1H NMR (400.13 MHz, C_6D_6 , 300 K, TMS): $\delta = 6.97\text{--}6.83$ (m, 5H, Ph-CH), 1.19 (s, 18H, $^t\text{Bu-CH}_3$) ppm. **^{11}B NMR** (96.29 MHz, C_6D_6 , 343 K, $\text{BF}_3\text{-Et}_2\text{O}$): $\delta = 6.1$ (s) ppm. **^{13}C NMR{ ^1H }** (100.61 MHz, C_6D_6 , 300 K, TMS): $\delta = 174.2$ (q, $J_{\text{C-B}} = 8.3$ Hz, N-CN), 130.3 (q, $J_{\text{C-B}} = 7.1$ Hz, Ph- C_{quart}), 130.6, 128.4, 127.8 (each s, each Ph-CH), 54.6 (s, $^t\text{Bu-C(CH}_3)_3$), 30.6 (s, $^t\text{Bu-C(CH}_3)_3$) ppm. **Elemental Analysis:** $\text{C}_{15}\text{H}_{23}\text{BCl}_2\text{N}_2$ (313.07 g/mol); C 58.19 (calc. 57.55); H 7.51 (calc. 7.41), N 9.12 (calc. 8.95) %. **MP:** $>200^\circ\text{C}$ (stable).

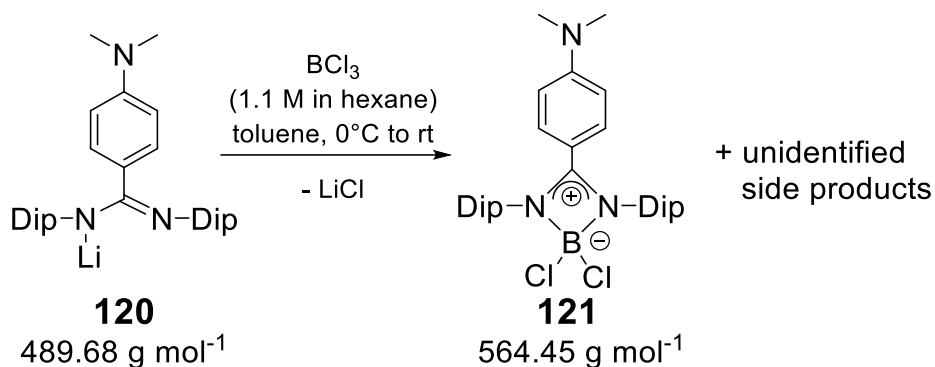
5.3.5 Synthesis of (E)-N-(dichloroboryl)-N,N'-bis(2,6-diisopropylphenyl)-4-(dimethylamino)benzimidamide **121**



YK135: Bis(2,6-diisopropylphenyl)methanediimine (**101**) (494 mg, 1.36 mmol, 1 eq.) is dissolved in Et_2O (5 mL) and cooled to 0°C . A solution of 4-(dimethylamino)phenyl lithium (161 mg, 1.21 mmol, 0.9 eq.) in Et_2O (5 mL) is added dropwise *via* syringe. The reaction mixture is allowed to reach room temperature. Stirring is continued for 30 minutes. Removal of solvents *in vacuo* is followed by washing with hexane and thorough drying. The targeted lithium amidinate **120** is isolated with 29% yield (193 mg) and used without further purification.

^1H NMR (300.13 MHz, C_6D_6 , 300 K, TMS): A few drops of *thf-d*₈ is added to increase solubility of the product in C_6D_6 . $\delta = 7.18$ (d, $^3J = 7.2$ Hz, 4H, Ar-CH), 7.13 (d, $^3J = 8.9$ Hz, 2H, aniline-Ar-CH), 7.04 (dd, $^3J = 8.2$ Hz, $^3J = 8.2$ Hz, 2H, Ar-CH), 6.21 (d, $^3J = 8.9$ Hz, 2H; aniline-Ar-CH) 3.83 (sept, $^3J = 6.9$ Hz, 4H, Dip-CH(CH₃)₂), 2.25 (s, 6H, N(CH₃)₂), 1.31 (d, $^3J = 6.9$ Hz, 12H, Dip-CH(CH₃)₂), 1.15 (d, $^3J = 6.9$ Hz, 12H, Dip-CH(CH₃)₂) ppm. **^7Li NMR** (116.64 MHz, C_6D_6 , 300 K, Li^+ aq): A few drops of *thf-d*₈ is added to increase solubility of the product in C_6D_6 . $\delta = 1.6$ (s) ppm.

5. Experimental Section



YK136: Previously synthesized lithium amidinate **120** (187 mg, 0.382 mmol, 1 eq.) is suspended in toluene (5 mL). The reaction mixture is cooled to 0°C and BCl_3 solution (1.1 M in hexanes, 0.4 mL, 0.44 mmol, 1.15 eq.) is added. The reaction mixture is allowed to reach room temperature and stirring is continued overnight. Solvent and volatile components are removed to afford a white powder consisting of 55% desired amidinate boron compound **121** (determined via ^1H NMR spectrum).

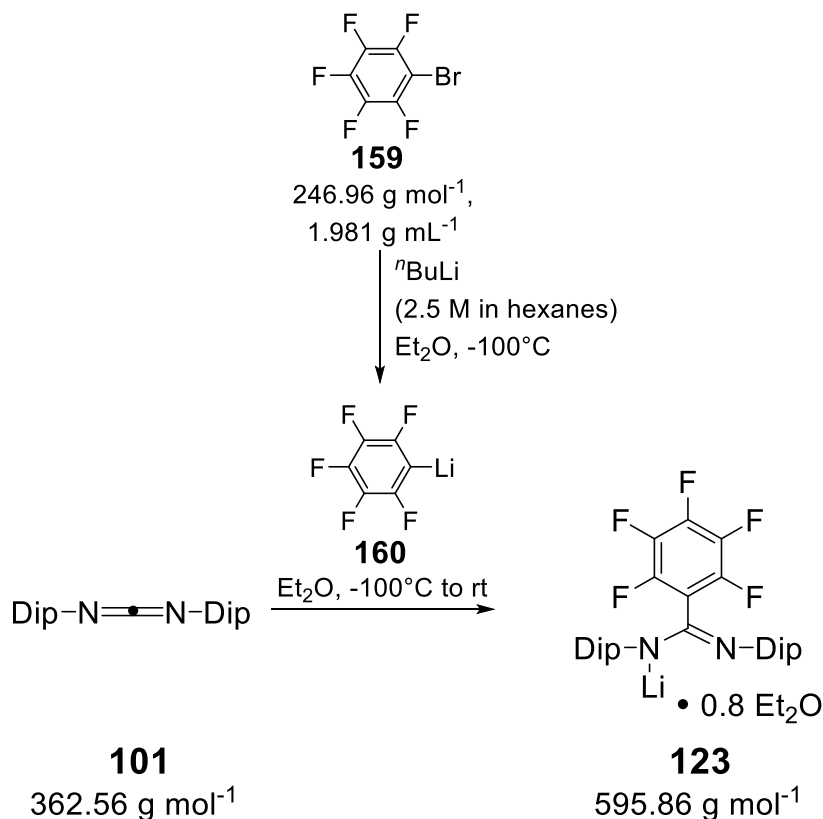
*Note: The following NMR data is limited to signals of the main product **121**.*

^1H NMR (300.13 MHz, C_6D_6 , 300 K, TMS): δ = 7.25-6.84 (m, integral not defined due to signal overlaps, Ar-CH), 5.75 (d, 3J = 9.2 Hz, 2H, aniline-Ar-CH), 4.05 (sept, 3J = 6.8 Hz, 4H, Dip-CH(CH₃)₂), 1.96 (s, 6H, N(CH₃)₂), 1.48 (d, 3J = 6.7 Hz, 12H, Dip-CH(CH₃)₂), 1.07 (d, 3J = 6.9 Hz, 12H, Dip-CH(CH₃)₂) ppm.

^{11}B NMR (96.29 MHz, C_6D_6 , 343 K, $\text{BF}_3\text{-Et}_2\text{O}$): δ = 9.78 (s) ppm.

5. Experimental Section

5.3.6 Synthesis of (E)-N-(dichloroboryl)-N,N'-bis(2,6-diisopropylphenyl)-2,3,4,5,6-pentafluorobenzimidamide **124**

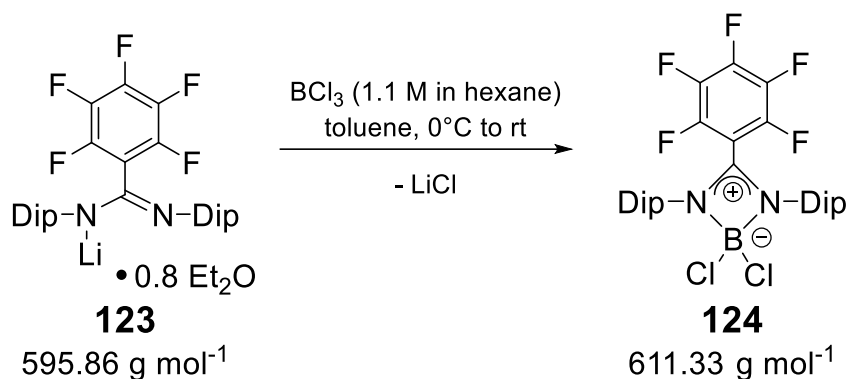


YK191: Bromopentafluorobenzene (degassed, 0.18 mL, 1.44 mmol, 1.04 eq.) is dissolved in Et₂O (5 mL) and cooled to -100°C (ethanol/ liquid nitrogen) before ⁿButyl lithium solution (2.5 M in hexanes, 0.61 mL, 1.53 mmol, 1.1 eq.) is added. Stirring is continued for 30 minutes at -100°C. Carbodiimine **101** (500 mg, 1.38 mmol, 1 eq.) is dissolved in Et₂O (9 mL) and cooled to -80°C (ethanol/ liquid nitrogen). The carbodiimine solution is transferred *via* cannula to the anion solution and the reaction mixture is allowed to warm slowly to 11°C. After stirring another 15 minutes at room temperature solvent and volatile species are removed *in vacuo*. The targeted lithium amidinate **123** coordinated by 0.8 eq. Et₂O is obtained in quantitative yield and used without further purification.

¹H NMR (300.13 MHz, C₆D₆, 300 K, TMS): A few drops of *thf-d₈* is added to increase solubility of the product in C₆D₆. δ = 7.02 (d, ³J = 7.0 Hz, 4H, Ar-CH), 6.90 (t, ³J = 6.9 Hz, 2H, Ar-CH), 3.63 (sept, ³J = 6.8 Hz, 4H, Dip-CH(CH₃)₂), 3.25 (q, ³J = 7.0 Hz, 3.25H, coord. Et₂O-CH₂), 1.17 (d, ³J = 6.9 Hz, 12H, Dip-CH(CH₃)₂), 1.11 (d, ³J = 6.4 Hz, 12H, Dip-CH(CH₃)₂), 1.08 (t, ³J = 6.6 Hz, 4.9H, coord. Et₂O-CH₃) ppm. **⁷Li NMR** (116.64 MHz, C₆D₆, 300 K, Li⁺ aq): A few drops

5. Experimental Section

of *thf-d₈* is added to increase solubility of the product in *C₆D₆*. $\delta = 1.5$ (s) ppm. **¹⁹F NMR** (282.40 MHz, *C₆D₆*, 300 K, *CFCl₃*): $\delta = -134.0$ (d, $^3J = 19$ Hz, 2F, *F₅Ph-oF*), $-156.83 - -157.03$ (m, 1F, *F₅Ph-pF*), $-163.69 - -163.85$ (m, 2F, *F₅Ph-mF*) ppm.



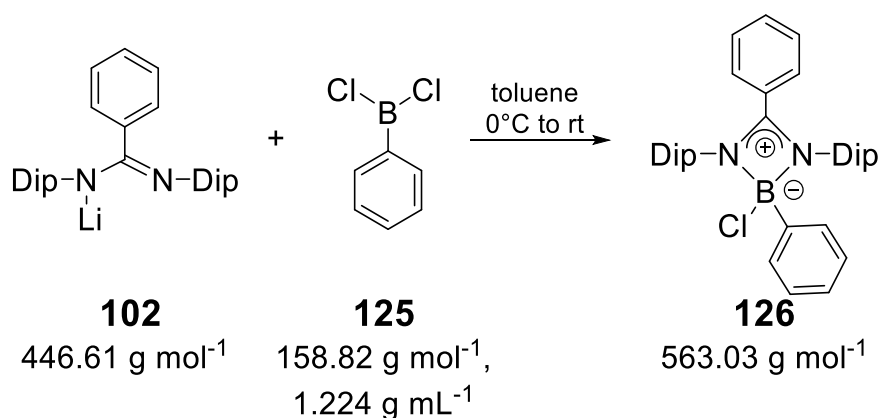
YK192: Previously isolated lithium amidinate **123** (674 mg, 1.13 mmol, 1 eq.) is suspended in hexane (15 mL). The reaction mixture is cooled to 0°C and *BCl₃* solution (1.1 M in hexanes, 1.08 mL, 1.19 mmol, 1.05 eq.) is added. The reaction mixture is allowed to reach room temperature and stirring is continued for 30 minutes. Removal of solvent and volatile components is followed by filtration from dichloromethane. Single crystals of amidinate **124** could be obtained from a concentrated dichloromethane solution at 5°C in 15% yield (105 mg).

¹H NMR (300.13 MHz, *C₆D₆*, 300 K, TMS): $\delta = 7.09\text{-}6.98$ (m, 6H, Ar-CH), 3.64 (sept, $^3J = 6.7$ Hz, 4H, Dip-CH(CH₃)₂), 1.39 (d, $^3J = 6.6$ Hz, 12H, Dip-CH(CH₃)₂), 0.99 (d, $^3J = 6.8$ Hz, 12H, Dip-CH(CH₃)₂) ppm. **¹¹B NMR** (96.29 MHz, *C₆D₆*, 343 K, *BF₃-Et₂O*): $\delta = 10.8$ (s) ppm. **¹⁹F NMR** (282.40 MHz, *C₆D₆*, 300 K, *CFCl₃*): $\delta = -134.32$ (dm, $^3J = 20$ Hz, 2F, *F₅Ph-oF*), -143.15 (tt, $^3J = 22$ Hz, $^4J = 6$ Hz, 1F, *F₅Ph-pF*), $-157.55 - -157.77$ (m, 2F, *F₅Ph-mF*) ppm. **¹³C NMR{¹H}** (75.47 MHz, *C₆D₆*, 300 K, TMS): $\delta = 163.5$ (br d, $J_{\text{C-B}} = 5.7$ Hz, NCN), 147.0 (s, Dip-Ar-Cquart.), 145.6 (dm, $J_{\text{C-F}} = 261.6$ Hz, Ph-CF), 142.8 (*the expected second doublet-signal could not be found*, Ph-CF), 138.2 (dm, $J_{\text{C-F}} = 259.7$ Hz, Ph-CF), 131.4 (s, Dip-Ar-Cquart.N), 129.2 (s, Dip-Ar-CH), 124.8 (s, Dip-Ar-CH), 102.2 (br s, *F₅Ph-Cquart.*), 29.1 (s, Dip-CH(CH₃)₂), 26.7, 23.5 (each s, each Dip-CH(CH₃)₂)

5. Experimental Section

ppm. **MP:** >200°C (stable). **Elemental Analysis:** C₃₁H₃₄BCl₂F₅N₂ (611.33 g/mol); C 58.46 (calc. 60.91); H 5.63 (calc. 5.61), N 4.43 (calc. 4.58) %.

5.3.7 Synthesis of (E)-N-(chloro(phenyl)boryl)-N,N'-bis(2,6-diisopropylphenyl)benzimidamide **126**

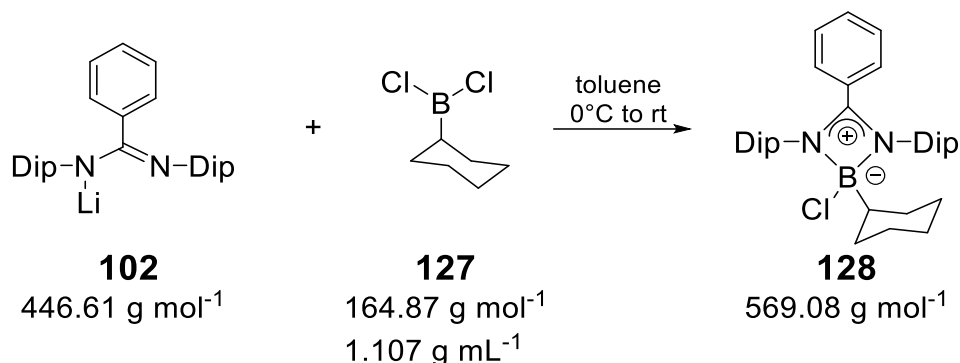


YK222: Previously isolated lithium amidinate **102** (471 mg, 1.06 mmol, 1 eq.) is suspended in toluene (20 mL) and cooled to 0°C. Dichlorophenyl borane (**125**) (0.15 mL, 1.16 mmol, 1.1 eq.) is added and stirring is continued for 30 minutes. The reaction mixture is allowed to reach room temperature. Removal of solvent and volatile components is followed by filtration from toluene. Single crystals of amidinate complex **126** are obtained from a concentrated toluene solution at 5°C in 42% yield (251 mg).

¹H NMR (300.13 MHz, C₆D₆, 300 K, TMS): δ = 7.86 (dd, ³J = 8.0 Hz, ⁴J = 1.8 Hz, 2H, Ph-CH), 7.32 (dd, ³J = 8.4 Hz, ⁴J = 1.3 Hz, 2H, Ph-CH), 7.16-7.06 (m, 10H, Ar-CH+C₆D₆-H_x), 6.69 (tt, ³J = 7.5 Hz, ⁴J = 1.3 Hz, 1H, Ph-CH), 6.53 (t, ³J = 8.0 Hz, 2H, Ph-CH), 3.84 (br s, 4H, Dip-CH(CH₃)₂), 1.25 (br s, 12H, Dip-CH(CH₃)), 0.82 (d, ³J = 6.5 Hz, 12H, Dip-CH(CH₃)) ppm. **¹¹B NMR** (96.29 MHz, C₆D₆, 343 K, BF₃-Et₂O): δ = 12.6 (br s) ppm. **¹³C NMR{¹H}** (100.61 MHz, C₆D₆, 300 K, TMS): δ = 172.2 (s, N-CN), 145.9 (br s, Dip-Ar-C_{quart.}), 134.9 (s, Ph-C_{quart.}), 132.8, 132.4, 130.2, 128.4 (each s, each Ph-CH), 127.8 (s, Dip-Ar-CH), 127.5 (s, Ph-CH), 127.1 (s, Dip-Ar-C_{quart.}), 126.3 (s, Ph-C_{quart.}), 124.7 (Dip-Ar-CH), 28.7 (s, Dip-CH(CH₃)₂), 25.2 (br s, Dip-CH(CH₃)₂), 23.4 (s, Dip-CH(CH₃)₂) ppm. **Elemental Analysis:** C₃₇H₄₄BClN₂ (563.03 g/mol); C 78.95 (calc. 78.93); H 7.86 (calc. 7.88), N 4.93 (calc. 4.98) %. **MP:** >200°C (stable).

5. Experimental Section

5.3.8 Synthesis of (E)-N-(chloro(cyclohexyl)boryl)-N,N'-bis(2,6-diisopropylphenyl)benzimidamide **128**

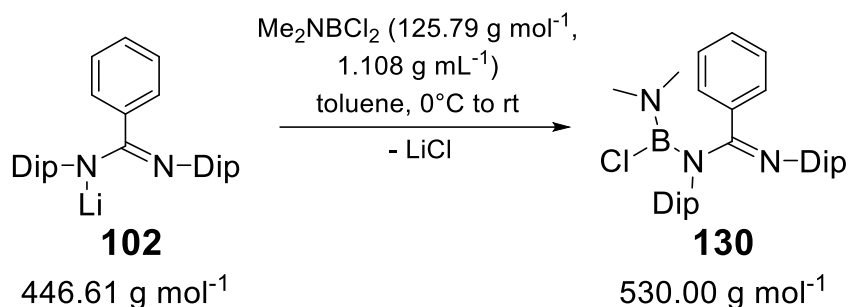


YK208_2: Previously isolated lithium amidinate **102** (812 mg, 1.82 mmol, 1 eq.) is suspended in toluene (50 mL) and cooled to 0°C. Dichlorocyclohexyl borane (**127**) (0.28 mL, 1.91 mmol, 1.05 eq.) is added and stirring is continued for 30 minutes. The reaction mixture is allowed to reach room temperature. Removal of solvent and volatile components is followed by filtration from toluene. Single crystals of benzamidinate complex **128** are obtained from a concentrated toluene solution at -26°C in 51% yield (523 mg).

¹H NMR (300.13 MHz, C₆D₆, 300 K, TMS): $\delta = 7.27\text{-}7.24$ (m, 2H, Ar-CH), 7.12-7.05 (m, 6H, Ar-CH), 6.68 (tt, $^3J = 7.5 \text{ Hz}$, $^4J = 1.7 \text{ Hz}$, 1H, Ar-CH), 6.55-6.50 (m, 2H, Ar-CH), 3.85 (br s, 4H, Dip-CH(CH₃)₂), 1.70-1.62 (m, 7H, $^{\text{c}}$ hexyl-CH), 1.42 (br s, 12H, Dip-CH(CH₃)₂), 1.33 (d, $^3J = 6.7 \text{ Hz}$, 4H, $^{\text{c}}$ hexyl-CH), 0.90 (d, $^3J = 6.8 \text{ Hz}$, 12H, Dip-CH(CH₃)₂) ppm. **¹¹B NMR** (96.29 MHz, C₆D₆, 343 K, BF₃-Et₂O): $\delta = 14.0$ (br s) ppm. **¹³C NMR{¹H}** (75.47 MHz, C₆D₆, 300 K, TMS): $\delta = 170.5$ (s, N-CN), 146.0, 136.0 (each s, each Ar-C_{quart.}), 132.6, 130.4, 128.5 (each s, each Ph-CH), 128.1 (s, Ar-CH), 126.4 (s, Ph-C_{quart.}), 124.9 (s, Ar-CH), 32.7 (br s, $^{\text{c}}$ Hex-CH-B), 29.2 (s, Dip-CH(CH₃)₂), 28.9, 28.1, 27.6 (each s, each $^{\text{c}}$ Hex-CH), 25.0, 24.0 (each s, each Dip-CH(CH₃)₂) ppm. **Elemental Analysis:** C₃₇H₅₀BClN₂ (569.08 g/mol); C 77.80 (calc. 78.09); H 8.62 (calc. 8.86), N 5.10 (calc. 4.92) %. **MP:** 208-215°C.

5. Experimental Section

5.3.9 Synthesis of (E)-N-(chloro(dimethylamino)boryl)-N,N'-bis(2,6-diisopropylphenyl)benzimidamide **130**

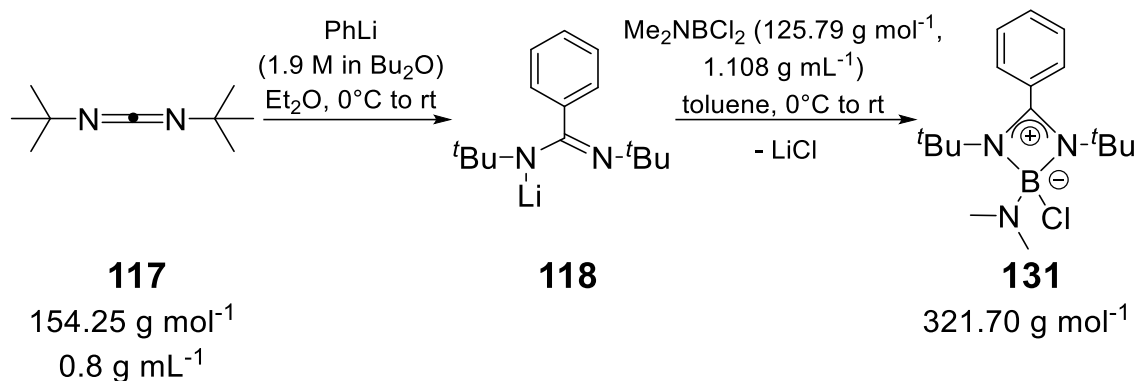


YK198_3: Previously isolated lithium amidinate **102** (971 mg, 2.17 mmol, 1 eq.) is suspended in toluene (40 mL). The reaction mixture is cooled to 0°C and dimethylaminodichloro borane (0.26 mL, 2.29 mmol, 1.06 eq.) is added. The reaction mixture is allowed to reach room temperature and stirring is continued for 30 minutes. Removal of solvent and volatile components is followed by filtration from hexane. Reducing the filtrate volume gives a pale yellow solution from which 801 mg (70%) of boryl amidinate **130** are obtained as colorless crystals at 5°C.

¹H NMR (400.13 MHz, C₆D₆, 300 K, TMS): δ = 7.49-7.48 (m, 2H, Ph-CH), 7.14 (s, 6H, Ar-CH), 6.80-6.79 (m, 3H, Ph-CH), 3.49 (bs, 4H, Dip-CH(CH₃)₂), 2.38 (s, 6H, N(CH₃)₂), 1.27, 1.10 (each bs, altogether 24H, Dip-CH(CH₃)₂) ppm. **¹¹B NMR** (128.29 MHz, C₆D₆, 343 K, BF₃-Et₂O): δ = 29.4 (bs) ppm. **¹³C NMR{¹H}** (100.61 MHz, C₆D₆, 300 K, TMS): δ = 157.7 (s, N-CN), 141.9 (br s, Dip-Ar-C_{quart.}), 134.8 (Ph-C_{quart.}), 130.2, 129.6, 127.8 (s, Ph-CH), 125.8 (br s, Dip-Ar-C_{quart.}), 124.3 (s, Dip-Ar-CH), 39.9 (s, N(CH₃)₂), 28.6 (br s, Dip-CH(CH₃)), 25.3, 24.1 (each s, each Dip-CH(CH₃)₂) ppm. **MP:** 137-141°C (stable). **IR** (powder): ν(C=N) = 1613 cm⁻¹. **Elemental Analysis:** C₃₃H₄₅BClN₃ (530.00 g/mol); C 74.51 (calc. 74.78); H 8.45 (calc. 8.56), N 7.97 (calc. 7.93) %.

5. Experimental Section

5.3.10 Synthesis of (E)-N,N'-di-tert-butyl-N-(chloro(dimethylamino)-boryl)benzimidamide **131**

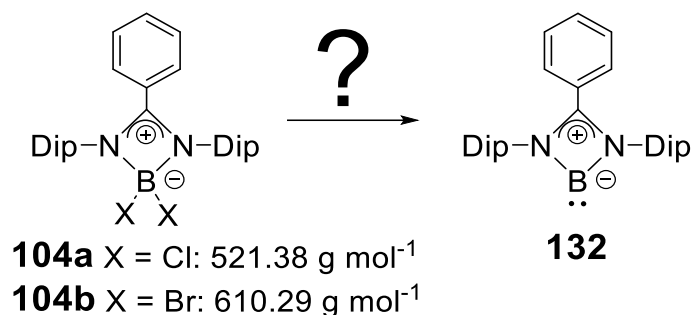


YK226: Di-tert-butylmethanediimine (**117**) (0.5 mL, 2.59 mmol, 1 eq.) is dissolved in Et₂O (ca. 30 mL) and cooled to 0°C. Phenyl lithium solution in thf (1.9 M in Bu₂O, 1.4 mL, 2.66 mmol, 1.03 eq.) is added dropwise *via* syringe. The reaction mixture is stirred at 0°C for 1 hour and is then allowed to reach room temperature. The reaction mixture is cooled to 0°C and dichlorodimethylamino borane is added dropwise *via* syringe. The reaction mixture is stirred at 0°C for 5 minutes and is then allowed to reach room temperature again. Removal of solvent is followed by filtration from hexane. Single crystals of benzamidinate complex **131** could be obtained from a concentrated hexane solution in poor yield (128 mg, 15%).

¹H NMR (300.13 MHz, C₆D₆, 300 K, TMS): 7.05-6.89 (m, 5H, Ph-CH), 2.79 (s, 6H, N(CH₃)₂), 1.14 (s, 18H, ^tBu-CH₃) ppm. **¹¹B NMR** (96.3 MHz, C₆D₆, 343 K, BF₃-Et₂O): δ = 8.3 (br s) ppm. **¹³C NMR{¹H}** (96.3 MHz, C₆D₆, 300 K, TMS): δ = 171.2 (s, N-CN), 132.5 (s, Ph-C_{quart.}), 129.7, 128.6, 128.2, 127.9 (each s, each Ph-CH), 52.2 (s, -N(CH₃)₂), 39.0 (s, -C(CH₃)₃), 30.8 (s, -C(CH₃)₃) ppm. **MP:** 98-101°C (stable). **Elemental Analysis:** C₁₇H₂₉BClN₃ (321.70 g/mol); C 63.01 (calc. 63.47); H 8.81 (calc. 9.09), N 12.89 (calc. 13.06) %.

5. Experimental Section

5.4. Reduction attempts of (E)-N-(dihaloboryl)-N,N'-bis(2,6-diisopropylphenyl)benzimidamide **104a,b**



YK110: Dichloroboryl benzamidinate **104a** (72 mg, 0.139 mmol, 1 eq.) and Jones Magnesium [$\{(\text{DipNacnac})\text{Mg}\}_2\text{]^{[201]}$ (100 mg, 0.140 mmol, 1 eq.) were separately suspended in Et₂O (each 1.5 mL) and cooled to -70°C. The reducing agent suspension is transferred to the benzamidinate suspension. The reaction mixture is allowed to reach room temperature and is stirred overnight. ¹¹B NMR analysis shows solely educt.

Note: ¹H NMR data were due to signal overlaps beyond interpretation.

¹¹B NMR (96.29 MHz, C₆D₆, 300 K, BF₃-Et₂O): δ = 10.0 (starting material) ppm.

YK093: Dibromoboryl benzamidinate **104b** (100 mg, 0.164 mmol, 1 eq.) is dissolved in toluene (1.4 mL) and disodium tetracarbonylferrate (56.7 mg, 0.164 mmol, 1 eq.) is suspended in toluene (2.4 mL) and cooled in an ice bath. The benzamidinate **104b** solution is added dropwise *via* syringe to the suspension. The reaction mixture is stirred for 15 min at 0°C and 40 min at room temperature. NMR analysis showed no reaction. Dme (2 mL) is added and the reaction mixture is stirred overnight. An NMR sample showed low conversion. After 5 days stirring at room temperature all volatiles are removed and the reaction mixture is filtered from toluene. Analysis of the extract showed a mixture of products in the ¹H NMR spectrum and no signal in the ¹¹B NMR spectrum.

Note: ¹H NMR data were due to signal broadening and overlaps beyond interpretation and no signal was detected in the ¹¹B NMR.

5. Experimental Section

YK096: Dibromoboryl benzamidine **104b** (200 mg, 0.328 mmol, 1 eq.) is dissolved in thf (10 mL) and disodium tetracarbonylferrat (250 mg, 0.723 mmol, 2.2 eq.) is suspended in thf (10 mL) and cooled to -78°C . The benzamidinat **104b** solution is added dropwise *via* syringe to the suspension. The reaction mixture is slowly warmed to room temperature overnight. An NMR sample showed low conversion. After 8 days stirring at room temperature all volatiles are removed and the reaction mixture is filtered from toluene. Analysis of the extract showed a mixture of products in the ^1H NMR spectrum and only educt signal in the ^{11}B NMR spectrum.

^{11}B NMR (96.29 MHz, C_6D_6 , 300 K, $\text{BF}_3\text{-Et}_2\text{O}$): $\delta = 1.9$ (s, starting material) ppm.

YK099: Dichloroboryl benzamidine **104a** (200 mg, 0.346 mmol, 1 eq.) is dissolved in thf (5 mL) and disodium tetracarbonylferrat (180 mg, 0.519 mmol, 1.5 eq.) is suspended in thf (15 mL) and both are cooled to -78°C . The benzamidinat **104a** solution is added *via cannula* to the suspension. The reaction mixture is slowly warmed to room temperature over 2 h. An NMR sample showed low conversion. After 3 days stirring at room temperature all volatiles are removed and the reaction mixture is filtered from toluene. Analysis of the extract showed a mixture of products in the ^1H NMR spectrum and only educt signal in the ^{11}B NMR spectrum.

Note: ^1H NMR data were due to signal broadening and overlaps beyond interpretation.

^{11}B NMR (96.29 MHz, C_6D_6 , 300 K, $\text{BF}_3\text{-Et}_2\text{O}$): $\delta = 10.0$ (s, starting material) ppm.

YK091: Dibromoboryl benzamidine **104b** (200 mg, 0.328 mmol, 1 eq.) and naphthalene (1.6 mg, 0.013 mmol, 0.04 eq.) are dissolved in dme. The solution and a flask charged with lithium powder (5.0 mg, 0.722 mmol, 2.2 eq.) are cooled to -78°C . The solution is cannulated to the lithium powder and is slowly allowed to warm to room temperature over 2 h and stirred overnight. Removal of solvents and volatiles is followed by filtration from toluene. NMR analysis of

5. Experimental Section

the extract showed a mixture of products and starting material in the ^1H NMR spectrum and only starting material in the ^{11}B NMR spectrum.

Note: ^1H NMR data were due to signal overlaps beyond interpretation.

^{11}B NMR (96.29 MHz, C_6D_6 , 300 K, $\text{BF}_3\text{-Et}_2\text{O}$): $\delta = 1.9$ (s, starting material) ppm.

YK095: Dibromoboryl benzamidinate **104b** (118 mg, 0.193 mmol, 1 eq.) is dissolved in dme (1 mL) and cooled to -78°C . An overnight prepared lithium naphthalenide solution (0.5 M) in dme (0.85 mL, 0.425 mmol, 2.2 eq.) is added dropwise *via* syringe. The reaction mixture is allowed to warm to room temperature. All solvents and volatiles are removed. NMR analysis showed a mixture of products in the ^1H NMR spectrum and only educt signal in the ^{11}B NMR spectrum.

Note: ^1H NMR data were due to signal broadening and overlaps beyond interpretation.

^{11}B NMR (96.29 MHz, C_6D_6 , 300 K, $\text{BF}_3\text{-Et}_2\text{O}$): $\delta = 10.0$ (s, starting material) ppm.

YK089: Dibromoboryl benzamidine **104b** (226 mg, 0.370 mmol, 1 eq.) and potassium graphite (199 mg, 1.47 mmol, 4.0 eq.) are mixed as solids and benzene (3 mL) is added while cooling the reaction mixture in an ice bath. Cooling is removed the reaction mixture is stirred at room temperature. No reaction is observed after 1 h, so dme (3 mL) is added. After 2 h the color turned brown-red and no starting material is detected by ^1H NMR spectroscopy. Removal of all solvents and volatiles is followed by filtration from toluene. NMR analysis of the extract showed a mixture of products in the ^1H NMR spectrum and one broad signal in the ^{11}B NMR spectrum.

Note: ^1H NMR data were due to signal overlaps beyond interpretation.

^{11}B NMR (96.29 MHz, C_6D_6 , 300 K, $\text{BF}_3\text{-Et}_2\text{O}$): $\delta = 1.4$ ppm.

5. Experimental Section

YK090: Dibromoboryl benzamidine **104b** (200 mg, 0.328 mmol, 1 eq.) and naphthalene (4.0 mg, 0.031 mmol, 0.1 eq.) are dissolved in dme. The solution and a flask charged with lithium powder (48.0 mg, 6.92 mmol, 21 eq.) are cooled to -78°C . The solution is cannulated to the lithium powder and is slowly allowed to warm to room temperature overnight. Removal of solvents and volatiles is followed by filtration from toluene. NMR analysis of the extract showed a mixture of products in the ^1H NMR spectrum and no signal in the ^{11}B NMR spectrum.

Note: ^1H NMR data were due to signal overlaps beyond interpretation and no signal was detected in the ^{11}B NMR.

YK097/101: Lithium powder (23 mg, 3.31 mmol, 10 eq./ 27 mg, 3.89 mmol, 10 eq.) and naphthalene (42.0 mg, 0.328 mmol, 1 eq./ 49.0 mg, 0.382 mmol, 1 eq.) were stirred overnight in dme (0.8 mL/ 1.5 mL). Dihaloboryl benzamidinate **104a,b** (each 200 mg, 0.328 mmol/0.384 mmol, 1 eq.) is dissolved in dme (2 mL/1.5 mL) and both solutions are cooled to -78°C . Benzamidinate **104a,b** solution is transferred *via cannula* to the reducing agent. The reaction mixture is slowly allowed to reach room temperature followed by removal of solvents and all volatiles. NMR analyses showed a mixture of products.

Note: ^1H NMR data were due to signal broadening and overlaps beyond interpretation.

^{11}B NMR (YK097) (96.29 MHz, C_6D_6 , 300 K, $\text{BF}_3\text{-Et}_2\text{O}$): $\delta = 32.3, -6.9, -14.9, -26.1$ ppm.

^{11}B NMR (YK101) (96.29 MHz, C_6D_6 , 300 K, $\text{BF}_3\text{-Et}_2\text{O}$): $\delta = 32.0, -9.6, -15.4, -26.8$ ppm.

YK103/104/105/103_2: Lithium powder (10 eq.) and naphthalene (1 eq.) were stirred overnight in dme (0.2 M). Dichloroboryl benzamidinate **104a** (1 eq.) and $i\text{Pr}_2\text{Me}_2\text{NHC}$ (1 eq.) were dissolved in dme (0.2 M) and filtered. Both solutions were cooled to -78°C . Benzamidinate **104a** solution is transferred *via cannula*

5. Experimental Section

to the reduction solution (for **YK105**: inverse). The reaction mixture is slowly allowed to reach room temperature. Removal of solvents and all volatiles is followed by filtration from toluene (for **YK105**: hexane).

Note: ^1H NMR data were due to signal overlaps beyond interpretation.

^{11}B NMR (YK103) (96.29 MHz, C_6D_6 , 300 K, $\text{BF}_3\text{-Et}_2\text{O}$): $\delta = 32.6, -3.5$ ppm.

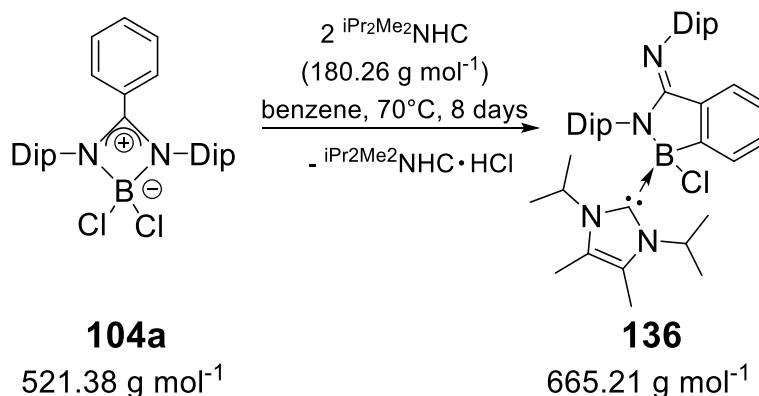
^{11}B NMR (YK103_2) (96.29 MHz, C_6D_6 , 300 K, $\text{BF}_3\text{-Et}_2\text{O}$): $\delta = -3.7$ ppm.

^{11}B NMR (YK104) (96.29 MHz, C_6D_6 , 300 K, $\text{BF}_3\text{-Et}_2\text{O}$): $\delta = 31.7, 10.9, -4.0$ ppm.

^{11}B NMR (YK105) (96.29 MHz, C_6D_6 , 300 K, $\text{BF}_3\text{-Et}_2\text{O}$): $\delta = 32.4, 13.1, -3.0$ ppm.

5.5. Reactivity of boryl benzamidates towards NHCs

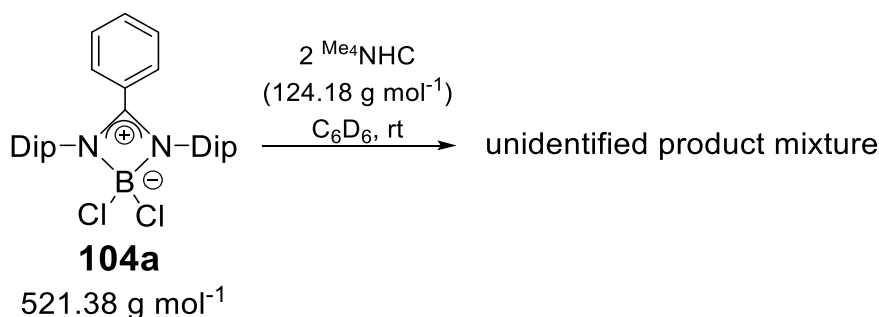
5.5.1 Reactivity of (E)-N-(dichloroboryl)-N,N'-bis(2,6-diisopropylphenyl)-benzimidamide **104a** towards NHCs



YK128_4/VAH-8: Borane amidinate complex **104a** (1.28 g, 2.46 mmol, 1 eq.) and NHC **135** (0.887 g, 4.92 mmol, 2 eq.) are mixed as solids and dissolved in benzene (20 mL). The reaction mixture is filtered and the filtrate is heated at 70°C for 8 days. Filtration is followed by removal of solvent and volatile components. The residue is washed with hexane twice to give benzazaborole **136** as brownish solid (0.666 g, 41%). Single Crystals suitable for x-ray diffraction are grown from a concentrated benzene solution layered with hexane at room temperature.

5. Experimental Section

$^1\text{H NMR}$ (300.13 MHz, C_6D_6 , 300 K, TMS): δ = 7.75 (d, ^3J = 7.3 Hz, 1H, Ar-CH), 7.47 (dd, ^3J = 7.7 Hz, ^4J = 1.7 Hz, 1H, Ar-CH), 7.31-7.22 (m, 4H, Ar-CH), 7.16 (dd, ^3J = 14.1 Hz, ^4J = 1.6 Hz, 1H, Ar-CH), 7.10 (dd, ^3J = 7.7 Hz, ^4J = 1.7 Hz, 1H, Ar-CH), 6.87-6.78 (m, 2H, Ar-CH), 5.42 (sept, ^3J = 7 Hz, 1H, NHC-CH(CH₃)₂), 4.85 (sept, ^3J = 6.9 Hz, 1H, NHC-CH(CH₃)₂), 4.23 (sept, ^3J = 6.6 Hz, 1H, Dip-CH(CH₃)₂), 3.67 (sept, ^3J = 6.8 Hz, 1H, Dip-CH(CH₃)₂), 3.48 (sept, ^3J = 6.8 Hz, 1H, Dip-CH(CH₃)₂), 3.14 (sept, ^3J = 6.7 Hz, 1H, Dip-CH(CH₃)₂), 1.75 (d, ^3J = 6.5 Hz, 3H, Dip-CH(CH₃)₂), 1.54 (d, ^3J = 6.8 Hz, 3H, Dip-CH(CH₃)₂), 1.52, 1.48 (each s, each 3H, each NHC-CH₃), 1.36 (d, ^3J = 7.0 Hz, 3H, Dip-CH(CH₃)₂), 1.34 (d, ^3J = 6.9 Hz, 3H, NHC-CH(CH₃)₂), 1.25 (d, ^3J = 6.8 Hz, 3H, Dip-CH(CH₃)₂), 1.14 (d, ^3J = 6.8 Hz, 3H, Dip-CH(CH₃)₂), 1.13 (d, ^3J = 6.8 Hz, 3H, Dip-CH(CH₃)₂), 1.08 (d, ^3J = 6.9 Hz, 3H, Dip-CH(CH₃)₂), 0.99 (d, ^3J = 7.0 Hz, 3H, NHC-CH(CH₃)₂), 0.83 (d, ^3J = 6.9 Hz, 3H, NHC-CH(CH₃)₂), 0.43 (d, ^3J = 7.1 Hz, 3H, NHC-CH(CH₃)₂), 0.31 (d, ^3J = 6.7 Hz, 3H, Dip-CH(CH₃)₂) ppm. **$^{11}\text{B NMR}$** (96.29 MHz, C_6D_6 , 300 K, $\text{BF}_3\text{-Et}_2\text{O}$): δ = 1.5 (br s) ppm. **$^{13}\text{C NMR}\{^1\text{H}\}$** (100.61 MHz, C_6D_6 , 300 K, TMS): δ = 161.5 (s, NHC-carbene-C), 150.8 (s, imine-C), 148.7, 147.2, 140.3, 139.4, 138.0, 135.2, 130.7, 129.2, 128.2, 128.0, 127.3, 127.3, 127.2 (each s, each Ar-C), 126.1 (s, NHC-C_{quart.}), 125.9 (s, Ar-C), 125.6 (s, NHC-C_{quart.}), 124.5, 123.9, 123.7, 122.5 (each s, each Ar-C), 53.4, 50.3 (each s, each NHC-CH(CH₃)₂), 29.2, 28.9, 28.0, 27.6 (each s, each Dip-CH(CH₃)₂), 27.5, 27.2, 27.0, 26.2, 25.1, 25.1, 24.2, 23.8 (each s, each Dip-CH(CH₃)), 22.5, 22.3, 20.1, 19.7 (each s, each NHC-CH(CH₃)₂), 10.2, 10.1 (each s, each NHC-CH₃) ppm. **IR** (powder): $\nu(\text{C}=\text{N})$ = 1616 cm^{-1} . **Elemental Analysis:** $\text{C}_{42}\text{H}_{58}\text{BClN}_4$ (665.21 g/mol); C 75.37 (calc. 75.83); H 8.63 (calc. 8.79), N 9.36 (calc. 8.42) %. **MP:** >220°C (partially stable).

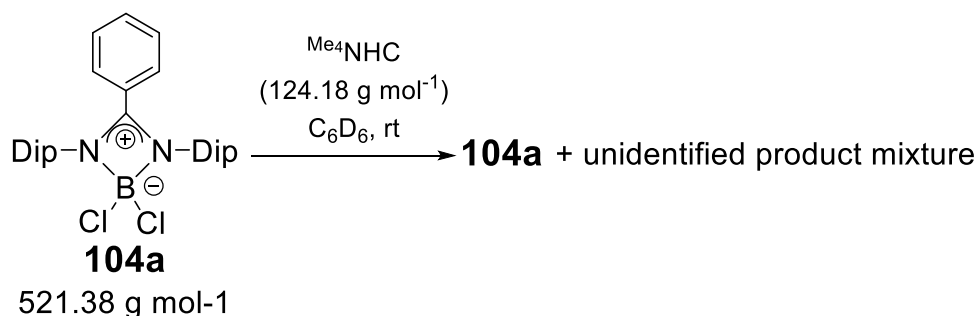


5. Experimental Section

YK217: Borane amidinate complex **104a** (61.0 mg, 0.117 mmol, 1 eq.) is dissolved in C₆D₆ (0.5 mL). The solution is added to Me₄NHC (**33**) (33.4 mg, 0.269 mmol, 2.3 eq.). ¹H NMR spectroscopy indicates an unselective reaction in which the starting material **104a** is nearly fully consumed overnight. The ¹¹B NMR spectrum shows one very broad signal overlapping with the glass peak.

Note: ¹H NMR data were due to signal overlaps beyond interpretation.

¹¹B NMR (96.29 MHz, C₆D₆, 300 K, BF₃-Et₂O): δ = 9.9 (s, minor amounts of starting material), 0.0 (very br s) ppm.



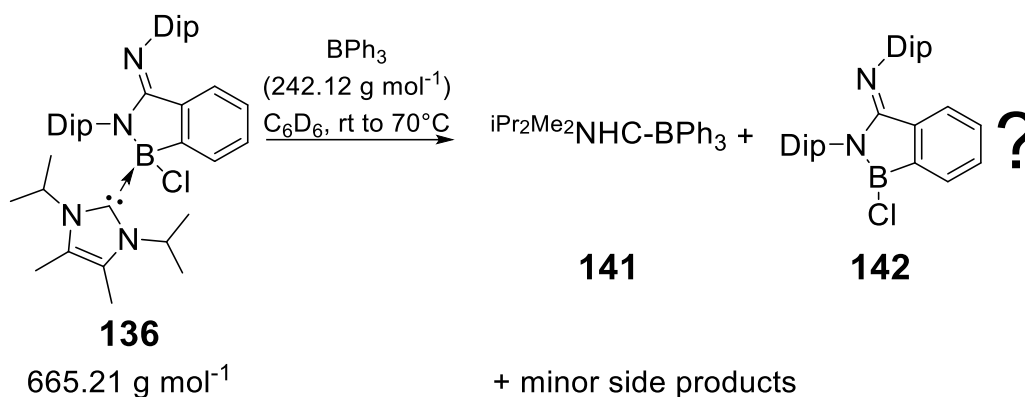
YK219: Borane amidinate complex **104a** (60.0 mg, 0.115 mmol, 1 eq.) is dissolved in C₆D₆ (0.5 mL). The solution is added to Me₄NHC (**139**) (18.5 mg, 0.150 mmol, 1.3 eq.). ¹H NMR spectroscopy indicates an unselective mixture of products and starting material. ¹¹B NMR spectroscopy shows mainly starting material and one very broad resonance.

Note: ¹H NMR data were due to signal overlaps beyond interpretation.

¹¹B NMR (96.29 MHz, C₆D₆, 300 K, BF₃-Et₂O): δ = 9.9 (s, starting material), 0.0 (very br s, unknown product mixture) ppm.

5. Experimental Section

5.5.2 Attempted NHC abstraction from $i\text{Pr}_2\text{Me}_2\text{NHC}$ coordinated (E)-1-chloro-N,2-bis(2,6-diisopropylphenyl)-1,2-dihydro-3H-benzo[c][1,2]azaborol-3-imine **136**

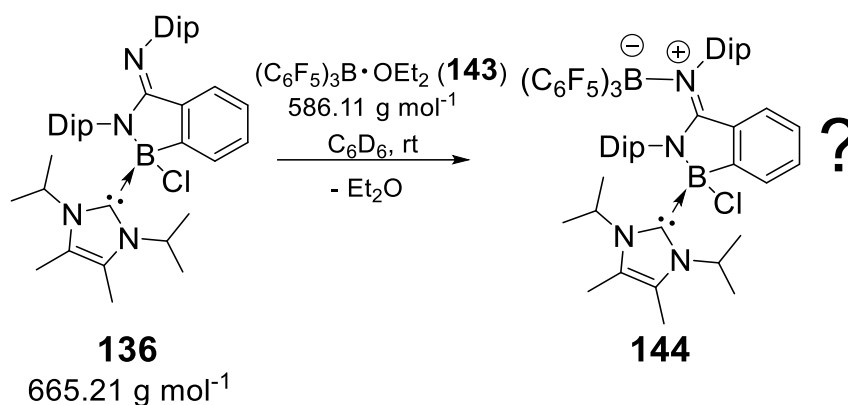


YK228: Triphenyl borane (6.00 mg, 0.025 mmol, 1.1 eq.) and benzo[c][1,2]azaborol-3-imine **136** (15.0 mg, 0.023 mmol, 1 eq.) are mixed as solids and C₆D₆ (0.5 mL) is added. ¹H and ¹¹B NMR spectra indicate no immediate reaction. After heating overnight at 70°C nearly full conversion (according to ¹H and ¹¹B NMR spectra) to proposed **142** and NHC-borane complex **141** is achieved.

Note: Due to signal overlaps in the aryl region only characteristic signals of the main products are given in the ¹H NMR peak list.

¹H NMR (300.13 MHz, C₆D₆, 300 K, TMS): δ = 5.02 (sept, ³J = 7.0 Hz, 2H, NHC-CH(CH₃)₂), 3.21, 3.14 (each sept, each ³J = 6.8 Hz, altogether 4H, Dip-CH(CH₃)₂), 1.52 (s, 6H, NHC-CH₃), 1.28, 1.26 (each d, each ³J = 6.5 Hz, altogether 12H, Dip-CH(CH₃)), 1.06, 0.99 (each d, each ³J = 6.8 Hz, each 6H, Dip-CH(CH₃)₂), 0.69 (d, ³J = 7.0 Hz, 12H, NHC-CH(CH₃)₂) ppm. **¹¹B NMR** (96.29 MHz, C₆D₆, 300 K, BF₃-Et₂O): δ = 57.5 (br s), 43.6 (br s), 0.6 (br s), -8.1 (s, Ph₃B-NHC) ppm.

5. Experimental Section



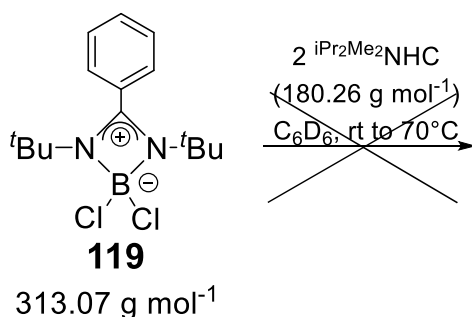
YK229: Benzo[*c*][1,2]azaborol-3-imine **136** (16.0 mg, 0.024 mmol, 1 eq.) is dissolved in C_6D_6 (0.5 mL) and the solution is added to BCF **143** (38.8 mg, 0.066 mmol, 2 eq.). ^1H and ^{11}B NMR spectra show an immediate reaction and full conversion to one uniform product and minor side products. Drying removes Et_2O from the reaction mixture.

Note: Only resonances of the main product are listed below, minor side products are disregarded.

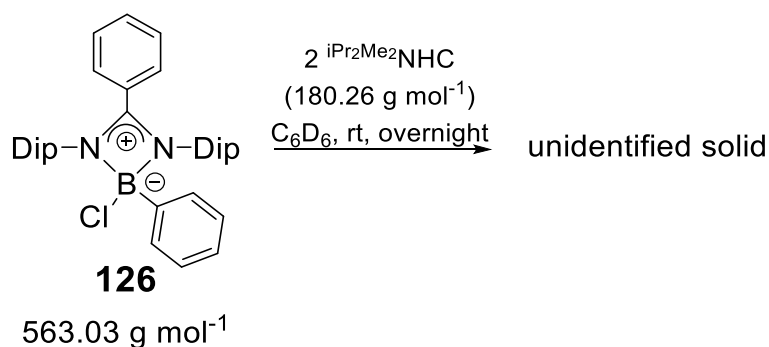
^1H NMR (300.13 MHz, C_6D_6 , 300 K, TMS): $\delta = 7.87$ (d, $^3J = 7.3$ Hz, 1H, Ar-CH), 7.24-7.17 (m, 2H, Ar-CH), 7.15-7.11 (m, 3H, Ar-CH), 7.01 (d, $^3J = 7.5$ Hz, 2H, Ar-CH), 6.74-6.59 (m, 2H, Ar-CH), 4.16 (sept, $^3J = 6.9$ Hz, NHC-CH(CH₃)₂), 2.94, 2.85 (each sept, $^3J = 6.7$ Hz, $^3J = 6.8$ Hz, altogether 4H, Dip-CH(CH₃)₂), 1.76 (s, 6H, NHC-CH₃), 1.14, 1.12 (each d, $^3J = 4.8$ Hz, $^3J = 5.1$ Hz, altogether 12H, CH(CH₃)₂), 1.04, 0.92 (each d, each $^3J = 6.8$ Hz, each 6H, CH(CH₃)₂), 0.88 (d, $^3J = 6.8$ Hz, 3H, CH(CH₃)₂), 0.56, 0.54 (each d, $^3J = 6.7$ Hz, $^3J = 6.3$ Hz, altogether 9H, CH(CH₃)₂) ppm. **^{11}B NMR** (96.29 MHz, C_6D_6 , 300 K, $\text{BF}_3\text{-Et}_2\text{O}$): $\delta = -2.9$ (br s) ppm. **^{19}F NMR** (282.40 MHz, C_6D_6 , 300 K, CFCl_3): $\delta = -131.48$ (d, $^3J = 17.8$ Hz, 6F, $\text{F}_5\text{Ph-}o\text{F}$), -160.75 (br s, 3F, $\text{F}_5\text{Ph-}p\text{F}$), -166.16 (br s, 6F, $\text{F}_5\text{Ph-}m\text{F}$) ppm.

5. Experimental Section

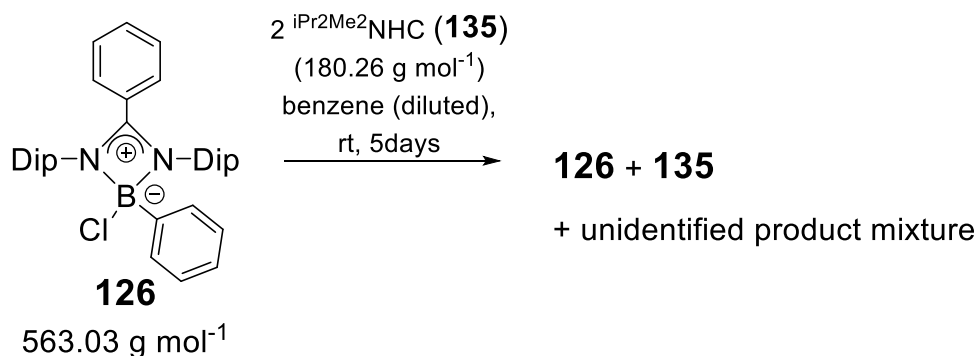
5.5.3 Reactivity of further boryl benzamidinate complexes towards NHCs



YK224: Boron-benzamidinate complex **119** (40.0 mg, 0.128 mmol, 1 eq.) and *i*Pr₂Me₂NHC (**135**) (48.0 mg, 0.268 mmol, 2.1 eq.) are mixed as solids and C₆D₆ (0.5 mL) is added. ¹H and ¹¹B NMR spectra show no reaction, not even after heating to 70°C for two days.



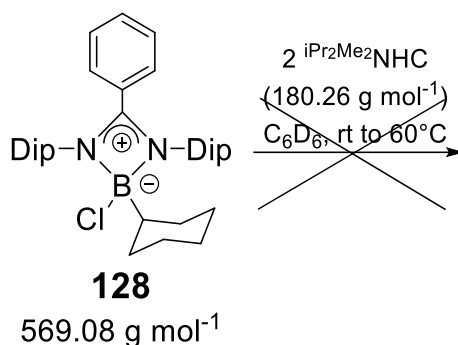
YK223: Boron-benzamidinate complex **126** (60 mg, 0.107 mmol, 1 eq.) and *i*Pr₂Me₂NHC (**135**) (40.0 mg, 0.224 mmol, 2.1 eq.) are mixed as solids and C₆D₆ (0.5 mL) is added. ¹H and ¹¹B NMR spectra show no immediate reaction. Overnight the reaction mixture solidified and no further reaction tracking is possible.



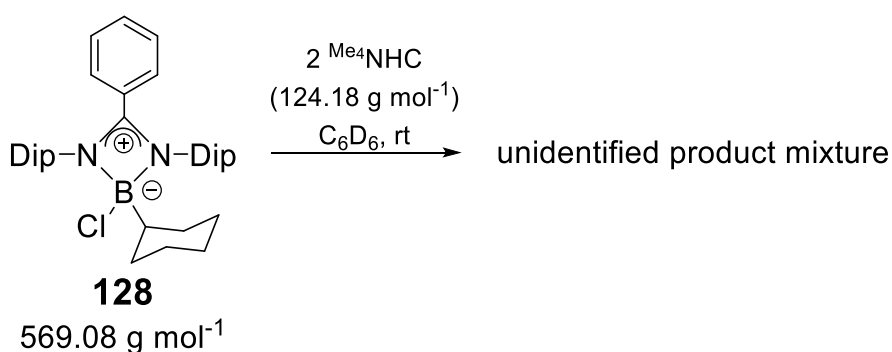
5. Experimental Section

YK223_2: Boron-benzamidinate complex **126** (60 mg, 0.107 mmol, 1 eq.) and $i\text{Pr}_2\text{Me}_2\text{NHC}$ (**135**) (40.0 mg, 0.224 mmol, 2.1 eq.) are mixed as solids and benzene (6 mL) is added until a clear solution is achieved. After 5 days stirring at room temperature only partial conversion is observed *via* ^1H and ^{11}B NMR plus an unidentified mixture of products.

^{11}B NMR (96.29 MHz, C_6D_6 , 300 K, $\text{BF}_3\text{-Et}_2\text{O}$): 12.6 (br s, starting material), 4.3, -4.5 (each br s, unidentified product mixture) ppm.

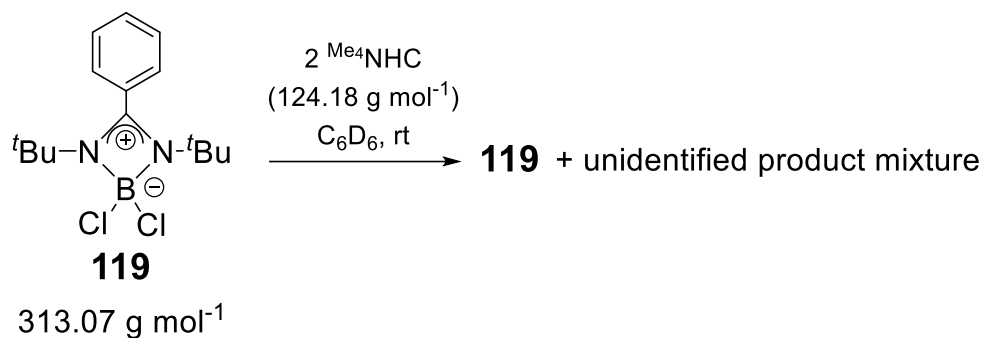


YK211_3: Boron-benzamidinate complex **128** (120 mg, 0.211 mmol, 1 eq.) and $i\text{Pr}_2\text{Me}_2\text{NHC}$ (**135**) (80.0 mg, 0.443 mmol, 2.1 eq.) are mixed as solids and C_6D_6 (0.5 mL) is added. ^1H and ^{11}B NMR spectra show no immediate reaction, not even after heating to 60°C – 70°C for four days (concentration increased after 2 days).



YK221: Boron-benzamidinate complex **128** (60.0 mg, 0.105 mmol, 1 eq.) is dissolved in C_6D_6 (0.5 mL) and the solution is added to $^{\text{Me}}_4\text{NHC}$ (**139**) (27.5 mg, 0.221 mmol, 2.1 eq.). An insoluble, solid mass is formed immediately. No NMR spectrum could be recorded.

5. Experimental Section

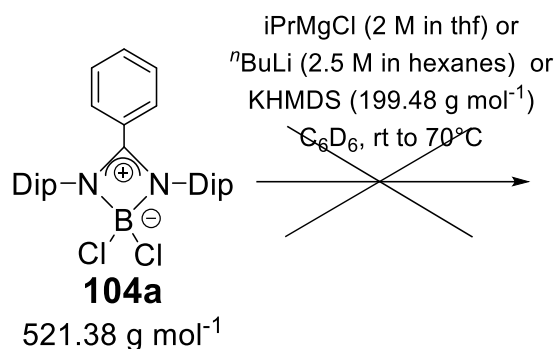


YK225: Me₄NHC (**139**) (40.0 mg, 0.322 mmol, 2.1 eq.) is dissolved in C₆D₆ (0.5 mL) and the solution is added to boron-benzamidinate **119** (48.0 mg, 0.153 mmol, 1 eq.). ¹H and ¹¹B NMR spectra show no immediate reaction. After 2 days at room temperature there's a lot of precipitation. The reaction mixture is filtered and ¹H and ¹¹B NMR spectra show the total consumption of NHC, but leftover starting material and some minor unidentified resonances.

5. Experimental Section

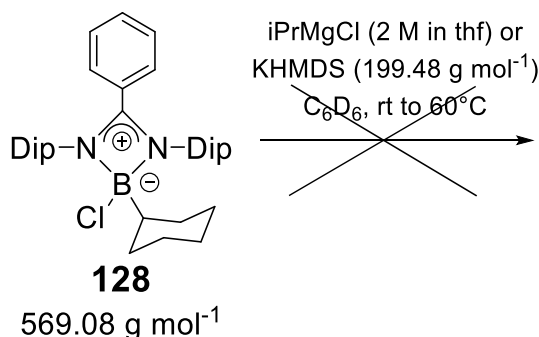
5.6. Reactivity of boryl benzamidates towards metalorganic reagents

5.6.1 Reactivity of (E)-N-(dichloroboryl)-N,N'-bis(2,6-diisopropylphenyl)-benzimidamide **104a** towards metalorganic reagents



YK193/194/213: Boron-benzamidate complex **104a** (YK193: 77.0 mg, 0.148 mmol, 1 eq.; YK194: 35.0 mg, 0.067 mmol, 1 eq.; YK213: 60.0 mg, 0.115 mmol, 1 eq.) is dissolved in C_6D_6 (0.5 mL) and one equivalent of the according metalorganic reagent (YK193: 0.08 mL iPrMgCl in thf (2 M), YK194: 0.03 mL ${}^n\text{BuLi}$ in hexanes (2.5 M), YK213: 23 mg KHMDS) is added at room temperature. ${}^1\text{H}$ and ${}^{11}\text{B}$ NMR spectra show no immediate reaction of the metalorganic reagents with **104a**, not even after heating to 60°C (YK193) or 70°C (YK194), respectively.

5.6.2 Reactivity of (E)-N-(chloro(cyclohexyl)boryl)-N,N'-bis(2,6-diisopropylphenyl)benzimidamide **128** towards metalorganic reagents

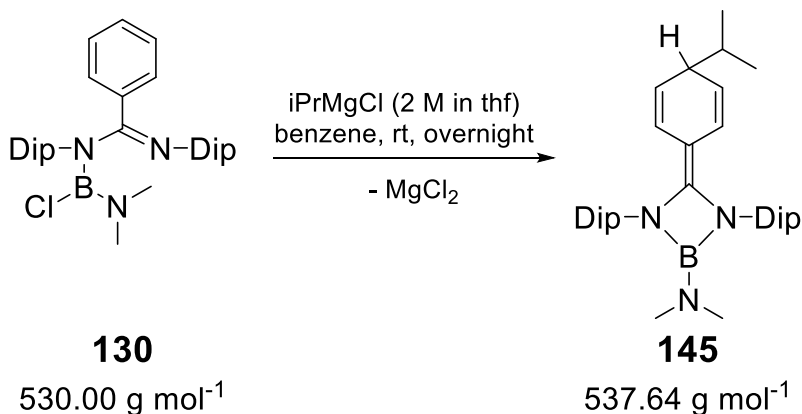


YK210/212 Boron-benzamidate complex **128** (YK210: 60.0 mg, 0.105 mmol, 1 eq.; YK212: 60.0 mg, 0.105 mmol, 1 eq.) is dissolved in C_6D_6 (0.5 mL) and one equivalent of the according metalorganic reagent (YK210: 21 mg KHMDS,

5. Experimental Section

YK212: 0.05 mL iPrMgCl in thf (2 M)) is added at room temperature. ^1H and ^{11}B NMR spectra show no immediate reaction of the metalorganic reagents with **128**, not even after heating to 60°C.

5.6.3 Synthesis of 1,3-bis(2,6-diisopropylphenyl)-4-(4-isopropylcyclohexa-2,5-dien-1-ylidene)-*N,N*-dimethyl-1,3,2-diazaboretidin-2-amine **145**



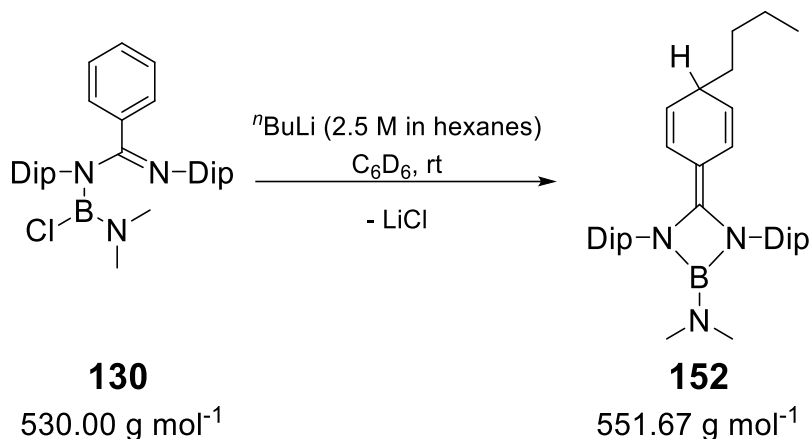
YK201_2: Borane amidinate **130** (192 mg, 0.362 mmol, 1 eq.) is dissolved in benzene (5 mL). Isopropyl magnesiumchloride solution (2 M in thf, 0.18 mL, 0.360 mmol, 1 eq.) is added and stirring is continued overnight. Removal of solvents and volatile components is followed by filtration from hexane. Reducing the filtrate volume gives a pale yellow solution from which 45 mg (23%) of **145** are obtained as colorless crystals at 5°C.

^1H NMR (300.13 MHz, C_6D_6 , 300 K, TMS): $\delta = 7.23\text{-}7.13$ (m, 6H, Dip- CH), 5.93 (dd, $^3\text{J} = 10.3$ Hz, $^4\text{J} = 1.7$ Hz, 2H, cyclohexadiene- CH_{vinyl}), 4.90 (dd, $^3\text{J} = 10.4$ Hz, $^4\text{J} = 4.1$ Hz, 2H, cyclohexadiene- CH_{vinyl}), 3.74, 3.72 (each sept, each $^3\text{J} = 7.0$ Hz, 4H, Dip- $\text{CH}(\text{CH}_3)_2$), 2.86-2.81 (m, 1H, cyclohexadiene- CH), 2.08 (s, 6H, $\text{N}(\text{CH}_3)_2$), 1.42 (dd, $^3\text{J} = 8.1$ Hz, $^4\text{J} = 6.8$ Hz, altogether 13H, $\text{CH}(\text{CH}_3)_2 + \text{Dip-CH}(\text{CH}_3)_2$), 1.31 (dd, $^3\text{J} = 6.9$ Hz, $^4\text{J} = 1.1$ Hz, 12H, Dip- $\text{CH}(\text{CH}_3)_2$), 0.79 (d, $^3\text{J} = 6.8$ Hz, 6H, $\text{CH}(\text{CH}_3)_2$) ppm. **^{11}B NMR** (96.29 MHz, C_6D_6 , 343 K, $\text{BF}_3\text{-Et}_2\text{O}$): $\delta = 24.7$ (s) ppm. **^{13}C NMR{ ^1H }** (75.47 MHz, C_6D_6 , 300 K, TMS): $\delta = 149.6$ (s, $\text{N}\underline{\text{C}}\text{N}$), 147.8, 147.7 (each s, each Dip-Ar- $\underline{\text{C}}_{\text{quart.}}\text{-N}$), 137.1 (s, Dip-Ar- $\underline{\text{C}}_{\text{quart.}}$), 123.7 (br s, Dip- CH), 122.6, 121.6 (each s, each cyclohexadiene- $\underline{\text{C}}_{\text{quart.}}$), 95.1 (s, cyclohexadiene- $\underline{\text{C}}_{\text{quart.}}$), 44.0 (s, cyclohexadiene- $\underline{\text{C}}_{\text{quart.}}$), 36.2 (s, $\text{N}(\underline{\text{C}}\text{H}_3)_2$), 34.3 (s, $\underline{\text{C}}\text{H}(\text{CH}_3)_2$), 29.3, 29.1 (each s,

5. Experimental Section

each Dip- $\underline{\text{C}}\text{H}(\text{CH}_3)_2$, 24.1, 23.9, 23.7, 23.6 (each s, each Dip- $\underline{\text{C}}\text{H}(\underline{\text{C}}\text{H}_3)_2$), 19.0 (s, $\text{CH}(\underline{\text{C}}\text{H}_3)_2$) ppm. **MP:** 145-147°C (stable). **Elemental Analysis:** $\text{C}_{36}\text{H}_{52}\text{BN}_3$ (537.64 g/mol); C 80.15 (calc. 80.42); H 9.49 (calc. 9.75), N 7.87 (calc. 7.82) %.

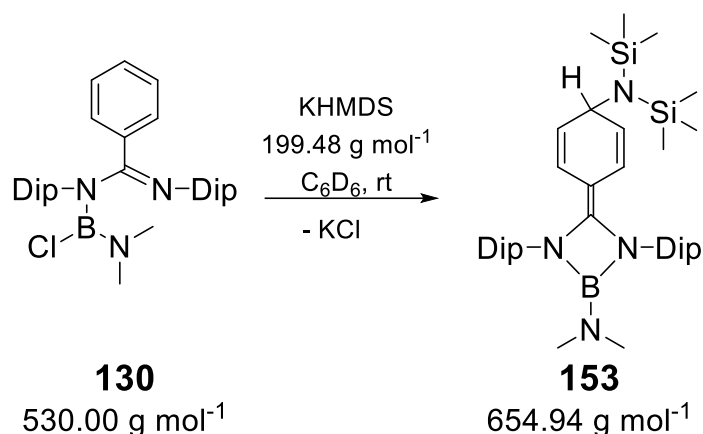
5.6.4 Reactivity of (E)-N-(chloro(dimethylamino)boryl)-N,N'-bis(2,6-diisopropylphenyl)benzimidamide **130** towards metalorganic reagents



YK200: Borane amidinate **130** (51 mg, 0.096 mmol, 1 eq.) is dissolved in C_6D_6 (0.5 mL). *n*-Butyl lithium solution (0.04 mL, 0.10 mmol, 1.04 eq.) is added at room temperature. ^1H and ^{11}B NMR spectra show a quantitative reaction to **152**, analogously to **145**.

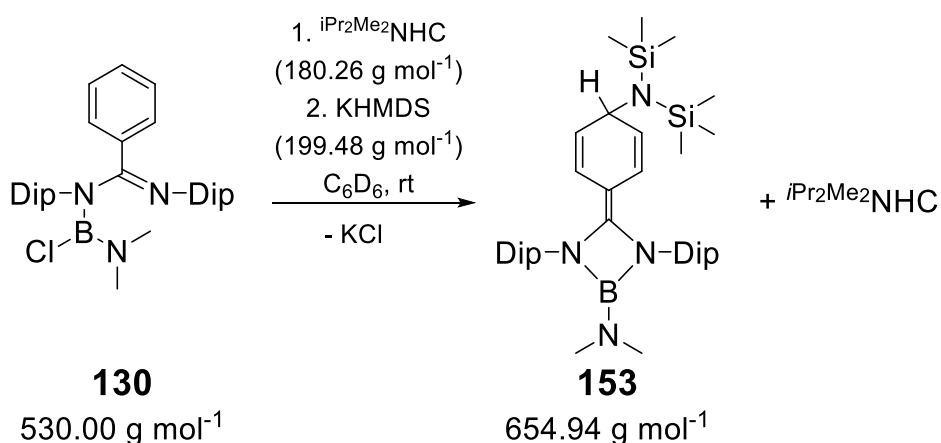
^1H NMR (300.13 MHz, C_6D_6 , 300 K, TMS): δ = 7.21-7.18, 7.15-7.11 (each m, altogether 6H, Dip- $\underline{\text{C}}\text{H}$), 5.88 (dd, $^3\text{J} = 10.3$ Hz, $^4\text{J} = 1.7$ Hz, 2H, cyclohexadiene - $\underline{\text{C}}\text{H}_{\text{vinyl}}$), 4.96 (dd, $^3\text{J} = 10.3$ Hz, $^4\text{J} = 4.0$ Hz, 2H, cyclohexadiene - $\underline{\text{C}}\text{H}_{\text{vinyl}}$), 3.75, 3.73 (each sept, $^3\text{J} = 6.9$ Hz, 4H, Dip- $\underline{\text{C}}\text{H}(\text{CH}_3)_2$), 2.91 (bs, 1H, cyclohexadiene- $\underline{\text{C}}\text{H}$), 2.07 (s, 6H, $\text{N}(\underline{\text{C}}\text{H}_3)_2$), 1.43 (dd, $^3\text{J} = 6.9$, $^4\text{J} = 4.1$ Hz, 12H, Dip- $\underline{\text{C}}\text{H}(\underline{\text{C}}\text{H}_3)_2$), 1.30 (dd, $^3\text{J} = 6.9$ Hz, $^4\text{J} = 1.3$ Hz, 12H, Dip- $\underline{\text{C}}\text{H}(\underline{\text{C}}\text{H}_3)_2$), 1.22-1.10 (m, 6H, *n*Bu- $\underline{\text{C}}\text{H}_2$), 0.81 (t, $^3\text{J} = 7.0$ Hz, 3H, *n*Bu- $\underline{\text{C}}\text{H}_3$) ppm. **^{11}B NMR** (96.29 MHz, C_6D_6 , 343 K, $\text{BF}_3\text{-Et}_2\text{O}$): δ = 24.6 (s) ppm.

5. Experimental Section



YK204: Borane amidinate **130** (50.0 mg, 0.094 mmol, 1 eq.) and KHMDS (18.8 mg, 0.094, 1 eq.) are mixed as solids. C_6D_6 (0.5 mL) is added. ^1H and ^{11}B NMR spectra show a quantitative reaction to **153**, analogously to **145**.

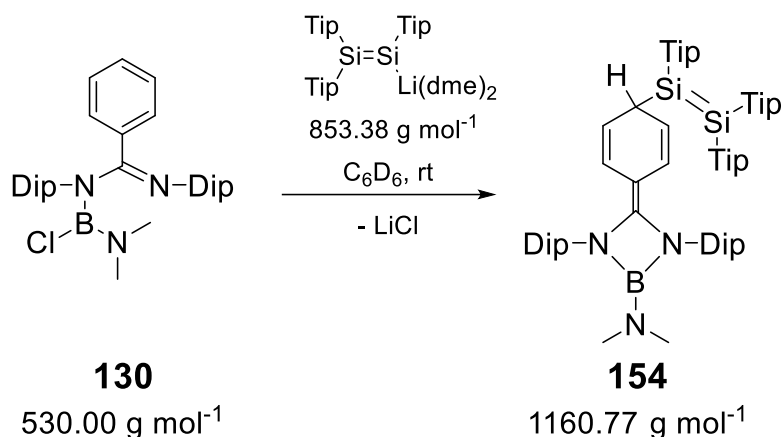
^1H NMR (300.13 MHz, C_6D_6 , 300 K, TMS): $\delta = 7.14\text{-}7.02$ (m, 7H, Dip-CH + C_6D_6), 5.74 (dd, $^3\text{J} = 7.7$ Hz, $^4\text{J} = 1.5$ Hz, 2H, cyclohexadiene-CH_{vinyl}), 4.81 (dd, $^3\text{J} = 7.7$ Hz, $^4\text{J} = 2.7$ Hz, 2H, cyclohexadiene-CH_{vinyl}), 4.37 (sept, $^4\text{J} = 1.4$ Hz, 1H, cyclohexadiene-CH), 3.62, 3.59 (each sept, $^3\text{J} = 5.1$ Hz, 4H, Dip-CH(CH₃)₂), 1.95 (s, 6H, N(CH₃)₂), 1.33 (dd, $^3\text{J} = 11.8$ Hz, $^4\text{J} = 5.2$ Hz, 12H, Dip-CH(CH₃)₂), 1.21 (dd, $^3\text{J} = 7.7$ Hz, $^4\text{J} = 5.1$ Hz, 12H, Dip-CH(CH₃)₂), 0.00 (br s, 18H, N(Si(CH₃)₂)) ppm. ^{11}B NMR (96.29 MHz, C_6D_6 , 343 K, $\text{BF}_3\text{-Et}_2\text{O}$): $\delta = 24.9$ (s) ppm.



YK205: Borane amidinate **130** (50.0 mg, 0.094 mmol, 1 eq.) and $\text{iPr}_2\text{Me}_2\text{NHC}$ (**135**) (16.9 mg, 0.094 mmol, 1 eq.) are dissolved in C_6D_6 (0.5 mL). KHMDS (18.8 mg, 0.094 mmol, 1 eq.) is added. ^1H and ^{11}B NMR spectra indicate full conversion to **153** without participation of NHC.

5. Experimental Section

Note: See above for NMR spectroscopic data of **153**.

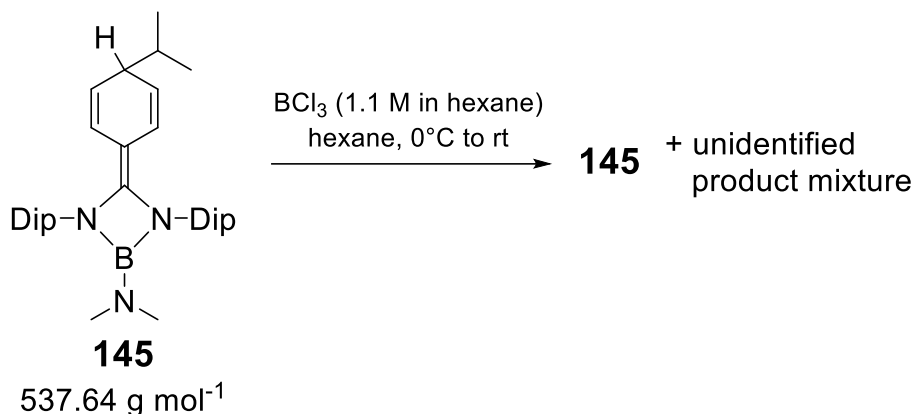


YK209: Borane amidinate **130** (49.7, 0.094 mmol, 1 eq.) and lithium disilenide^{[219], [220]} (80.0 mg, 0.094 mmol, 1 eq.) are mixed as solids and C₆D₆ (0.5 mL) is added. ¹H, ¹¹B and ²⁹Si NMR spectra indicate full conversion to **154** in analogy to **145**.

¹H NMR (300.13 MHz, C₆D₆, 300 K, TMS): δ = 7.12-7.04 (m, 10H, Ar-CH), 6.94 (s, 2H, Ar-CH), 5.58 (dd, ³J = 10.2 Hz, ⁴J = 1.7 Hz, 2H, cyclohexadiene-CH_{vinyl}), 5.23 (dd, ³J = 10.1 Hz, ⁴J = 3.7 Hz, 2H, cyclohexadiene -CH_{vinyl}), 4.04-3.94 (m, 4H, Ar-CH(CH₃)₂), 3.77-3.61 (m, 4H, Ar-CH(CH₃)₂), 3.53 (sept, ³J = 6.9 Hz, 2H, Ar-CH(CH₃)₂), 2.85-2.57 (m, 4H, Ar-CH(CH₃)₂ + cyclohexadiene-CH), 2.04 (s, 6H, N(CH₃)₂), 1.39 (d, ³J = 6.8 Hz, 6H, Ar-CH(CH₃)₂), 1.28-1.22 (m, 30H, Ar-CH(CH₃)₂), 1.18 (d, ³J = 6.7 Hz, 9H, Ar-CH(CH₃)₂), 1.14 (d, ³J = 6.9 Hz, 6H, Ar-CH(CH₃)₂), 1.07 (d, ³J = 6.9 Hz, 12H, Ar-CH(CH₃)₂), 0.93-0.86 (m, 15H, Ar-CH(CH₃)₂) ppm. **¹¹B NMR** (96.29 MHz, C₆D₆, 343 K, BF₃-Et₂O): δ = 26.7 (s) ppm. **²⁹Si NMR** (59.63 MHz, C₆D₆, 300 K, TMS): δ = 75.9, 57.0 ppm.

5. Experimental Section

5.6.5 Reactivity of Diazaboretidine **145** - Attempted Exchange of NMe₂ with Cl



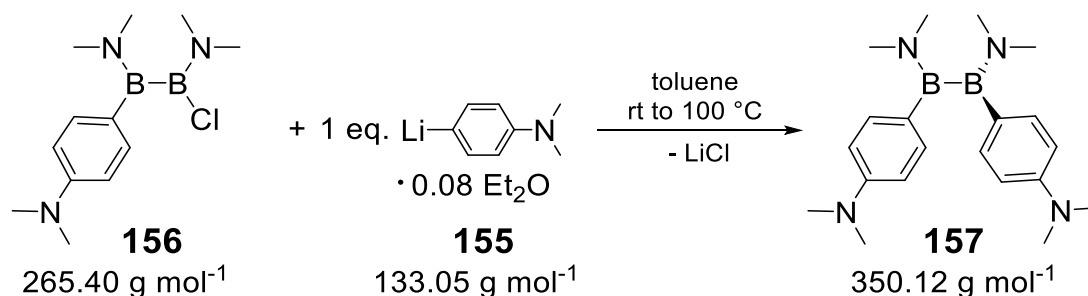
YK214: Diazaboretidine **145** (57 mg, 0.106 mmol, 1 eq.) is dissolved in hexane (4 mL) and cooled to 0°C. BCl₃ solution (1.1 M in hexane, 0.05 mL; 0.053 mmol, 0.5 eq.) is added dropwise *via* syringe. The reaction mixture is allowed to reach room temperature and all volatiles and solvents are removed. ¹¹B NMR spectrum indicates partial conversion to several tetracoordinated boron species.

Note: Due to signal overlaps, apart from distinct resonances of the starting material, the ¹H NMR spectrum is beyond interpretation.

¹¹B NMR (96.29 MHz, C₆D₆, 343 K, BF₃-Et₂O): δ = 24.8 (br s, starting material), 9.9, 8.5, 7.0, 2.8 (unidentified product mixture)

5. Experimental Section

5.7.2 Synthesis of 1,2-bis(dimethylamino)-1,2-bis(para-*N,N*-dimethylaniline) diborane(4) **157**

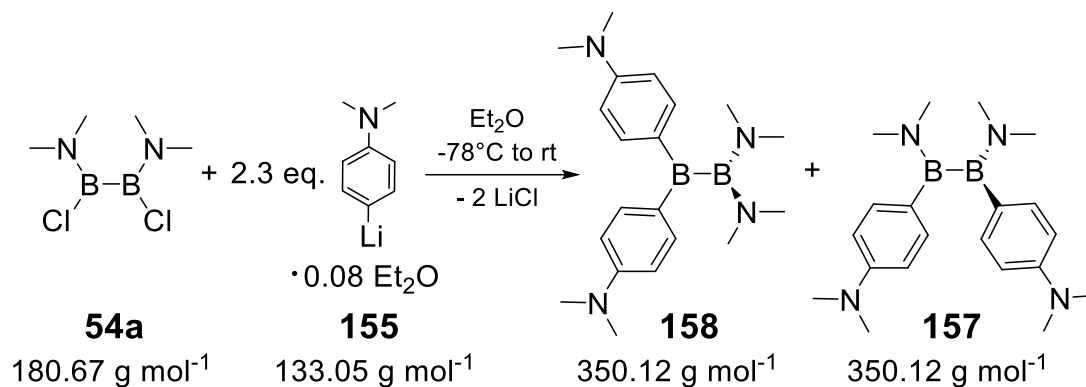


YK123_2: Diborane(4) **156** (500 mg, 1.88 mmol, 1 eq.) is dissolved in Et₂O (25 mL) and cooled to -78 °C (isopropanol/ liquid nitrogen). A solution of 4-(dimethylamino)phenyllithium (250 mg, 1.88 mmol, 1 eq.) in Et₂O (25 mL) is added slowly *via* cannula. The reaction mixture is stirred in the cooling bath for 5 minutes and then allowed to reach room temperature. The solvent is exchanged for toluene and the reaction mixture is heated to 100 °C for one hour. Removal of solvent and volatile species *in vacuo* is followed by filtration from hexane. Reducing the filtrate volume gives a yellow solution from which 212 mg (32%) of diborane(4) **157** are obtained as yellow crystals at 5 °C.

¹H NMR (400.13 MHz, C₆D₆, 300 K, TMS): δ = 7.54 (d, ³J = 8.6 Hz, 4H, Me₂N-PhCH), 6.75 (d, ³J = 8.7 Hz, 4H, Me₂N-PhCH), 2.98 (s, 6H, B-NCH₃), 2.87 (s, 6H, B-NCH₃), 2.58 (s, 12H, (CH₃)₂N-Ph) ppm. **¹¹B NMR** (96.29 MHz, C₆D₆, 300 K, BF₃-Et₂O): δ = 49.4 (br s) ppm. **¹³C NMR** (100.61 MHz, C₆D₆, 300K, TMS): δ = 150.1 (Me₂N-PhC_{quart.}), 134.1 (s, Me₂N-PhCH), 133.4 (br s, Me₂N-PhC_{quart.}-B), 112.8 (s, Me₂N-PhCH), 45.0 (s, B-NCH₃), 40.3 (s, (CH₃)₂N-Ph), 40.1 (s, B-NCH₃) ppm. **UV/Vis** (hexane): λ_{max} = 281 nm (ε = 34910 L mol⁻¹ cm⁻¹). **Elemental analysis:** C₂₀H₃₂B₂N₄ (350.12); C 68.12 (calc. 68.61); H 9.04 (9.21); N 15.57 (16.00) %. **MP:** 130-131 °C (stable).

5. Experimental Section

5.7.3 Isolation of 1,1-bis(dimethylamino)-2,2-bis(para-*N,N*-dimethylaniline) diborane(4) **158**



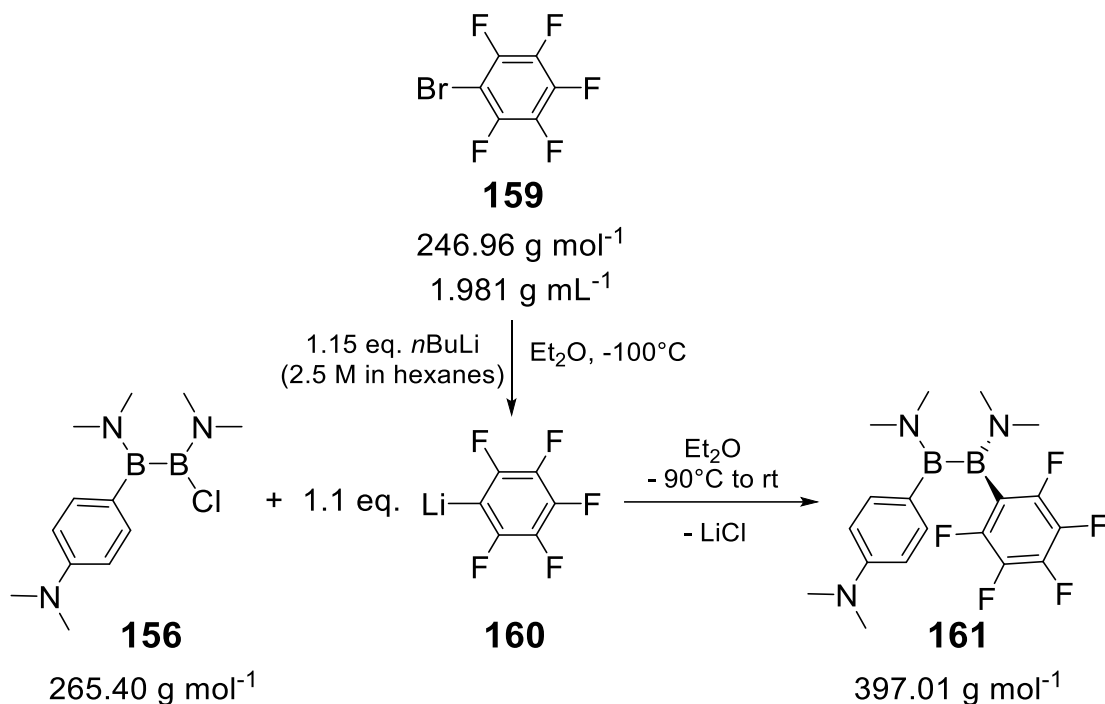
YK118: Diborane(4) **54a** (0.5 mL, 2.99 mmol, 1 eq.) is dissolved in Et₂O (30 mL) and cooled to -78°C (isopropanol/ liquid nitrogen). A solution of 4-(dimethylamino)phenyl lithium (910 mg, 6.84 mmol, 2.3 eq.) in Et₂O (20 mL) is added dropwise through dropping funnel. The reaction mixture is stirred in the cooling bath for 5 minutes and then allowed to reach room temperature. Removal of solvent and volatile species *in vacuo* is followed by filtration from hexane. Reducing the filtrate volume gives a yellow solution from which 1,1-diborane(4) **158** is obtained as yellow crystals at 5°C . ¹H NMR of the mother liquor shows 1,2-diborane(4) **157** as main component.

*Note: Due to a low amount of compound and reproducibility issues **158** is not fully structurally characterized.*

¹H NMR (300.13 MHz, C₆D₆, 300 K, TMS): $\delta = 8.14$ (d, ³J = 8.7 Hz, 4H, Me₂N-PhCH₂), 6.75 (d, ³J = 8.7 Hz, 4H, Me₂N-PhCH₂), 2.82 (s, 12H, B-NCH₃), 2.56 (s, 12H, (CH₃)₂N-Ph) ppm. **¹¹B NMR** (96.29 MHz, C₆D₆, 300 K, BF₃-Et₂O): $\delta = 79.0$ (br s), 38.4 (br, s) ppm.

5. Experimental Section

5.7.4 Synthesis of 1,2-bis(dimethylamino)-1-para-*N,N*-dimethylaniline-2-pentafluorophenyl diborane(4) **161**



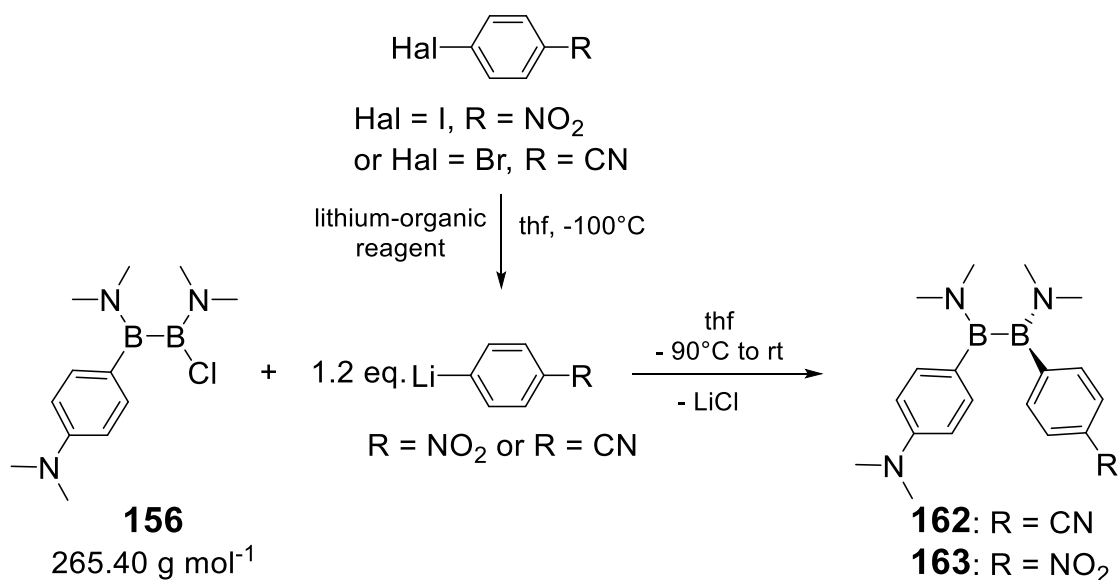
YK115_4: Bromopentafluorobenzene (0.15 mL, 1.18 mmol, 1.1 eq.) is dissolved in Et₂O (10 mL) and cooled to -100°C (ethanol/ liquid nitrogen). *n*Butyl lithium solution in hexanes (0.49 mL, 2.5 M, 1.24 mmol, 1.15 eq.) is added dropwise *via* syringe. Stirring is continued for 15 minutes at -100°C. A precooled solution of diborane(4) **156** (285 mg, 1.07 mmol, 1 eq.) in Et₂O (10 mL) is added *via* cannula. The mixture is stirred for 30 minutes in the cooling bath and is then allowed to reach room temperature. Removal of solvent and volatile species *in vacuo* is followed by filtration from toluene. The solvent is exchanged for *o*-difluorobenzene. Reducing the volume gives a pale-yellow solution from which 253 mg (52%) of diborane(4) **161** (with 0.5 eq. *o*-difluorobenzene) are obtained at -26°C as colorless crystals.

¹H NMR (400.13 MHz, C₆D₆, 300 K, TMS): δ = 7.37 (d, ³J = 8.6 Hz, 4H, Me₂N-Ph_H), 6.71 (d, ³J = 8.7 Hz, 4H, Me₂N-Ph_H), 2.93 (s, 3H, B-NCH₃), 2.80 (s, 3H, B-NCH₃), 2.78 (s, 3H, B-NCH₃), 2.54 (s, 6H, (CH₃)₂N-Ph), 2.43 (s, 3H, B-NCH₃) ppm. **¹¹B NMR** (96.29 MHz, C₆D₆, 300 K, BF₃-Et₂O): δ = 45.8 (br s) ppm. **¹³C NMR** (100.61 MHz, C₆D₆, 300K, TMS): δ = 150.4 (s, Me₂N-Ph_C_{quart.}), 145.3 (dm, ¹J_{C-F} = 237 Hz, F₅Ph_C-F), 140.3 (dm, ¹J_{C-F} = 248 Hz, F₅Ph_C-F), 137.5 (dm, ¹J_{C-F} = 249 Hz, F₅Ph_C-F), 134.0 (s, Me₂N-Ph_C_H), 130.8 (s, Me₂N-Ph_C_{quart.-B}),

5. Experimental Section

112.4 (s, Me₂N-Ph \underline{C} H), 44.7, 43.9, 41.0, 40.4 (each s, each B-N \underline{C} H₃), 40.0 (s, (CH₃)₂N-Ph) ppm. **¹⁹F NMR** (282.40 MHz, C₆D₆, 300 K, CFCl₃): δ = -132.6 (dd, 2F, ³J_{F-F} = 24 Hz, ⁴J_{F-F} = 8 Hz, F₅Ph-*o*E), -156.8 (t, 1F, ³J_{F-F} = 20 Hz, F₅Ph-*p*E), -162.6 (ddd, 2F, ³J_{F-F} = 25 Hz, ³J_{F-F} = 21 Hz, ⁴J_{F-F} = 10 Hz, F₅Ph-*m*E) ppm. **UV/Vis** (Et₂O): λ_{max} = 286 nm (ϵ = 17250 L mol⁻¹ cm⁻¹). **Elemental analysis:** C₁₈H₂₂B₂F₅N₃ (397.01); C 53.96 (calc. 54.46); H 5.48 (5.59); N 10.55 (10.58) %. **MP:** 80-85°C (stable).

5.7.5 Reactivity of 2-chloro-1,2-bis(dimethylamino)-1-para-*N,N*-dimethylaniline diborane(4) **156** towards 4-cyanophenyl lithium and 4-nitrophenyl lithium



General Procedure: The halophenyl derivative (1.2 eq.) is dissolved in thf (4.4 mL/mmol) and cooled to -100°C (ethanol/ liquid nitrogen). Lithium-organic reagent solution (1.25 eq.) is added dropwise *via* syringe. Stirring is continued for 30 minutes at -100°C. A precooled solution of diborane(4) **156** (1 eq.) in thf (5.3 mL/mmol) is added *via* syringe. The mixture is stirred for 30 minutes in the cooling bath and is then allowed to reach room temperature. Solvent and volatile species are removed *in vacuo* and an NMR sample of **162** or **163** is analyzed.

Data for YK114_2: From 500 mg (1.88 mmol) diborane(4) **156**, 411 mg (2.26 mmol) 4-bromobenzonitrile and 1.0 mL (2.37M, 2.37 mmol) *n*-butyl lithium solution in hexanes.

5. Experimental Section

Note: ^1H NMR spectrum could not be evaluated due to signal overlaps.

^{11}B NMR **162** (96.29 MHz, C_6D_6 , 300 K, $\text{BF}_3\text{-Et}_2\text{O}$): $\delta = 47.6$ (br, s), 36.4 (br, s) ppm.

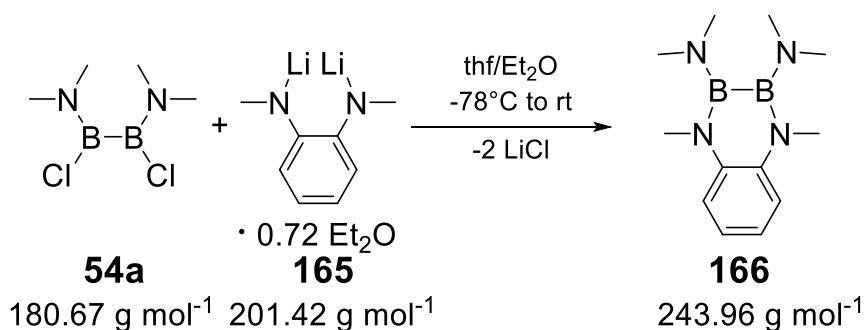
Data for YK121: From 100 mg (0.377 mmol) diborane(4) **156**, 112 mg (0.452 mmol) 4-iodonitrobenzene, 0.25 mL, (1.9 M, 0.471 mmol) phenyllithium solution in dibutylether.

Note: ^1H NMR spectrum could not be evaluated due to signal overlaps.

^{11}B NMR **163** (96.29 MHz, C_6D_6 , 300 K, $\text{BF}_3\text{-Et}_2\text{O}$): $\delta = 48.6$ (br, s), 36.4 (br, s), 1.6 (br, s, unidentified side product) ppm.

5.8. Synthesis of diazadiborinanes

5.8.1 Synthesis of 1,4-dimethyl-2,3-bis(dimethylamino)-1,2,3,4-tetrahydrobenzo[e][1,4,2,3]diazadiborinane **166**

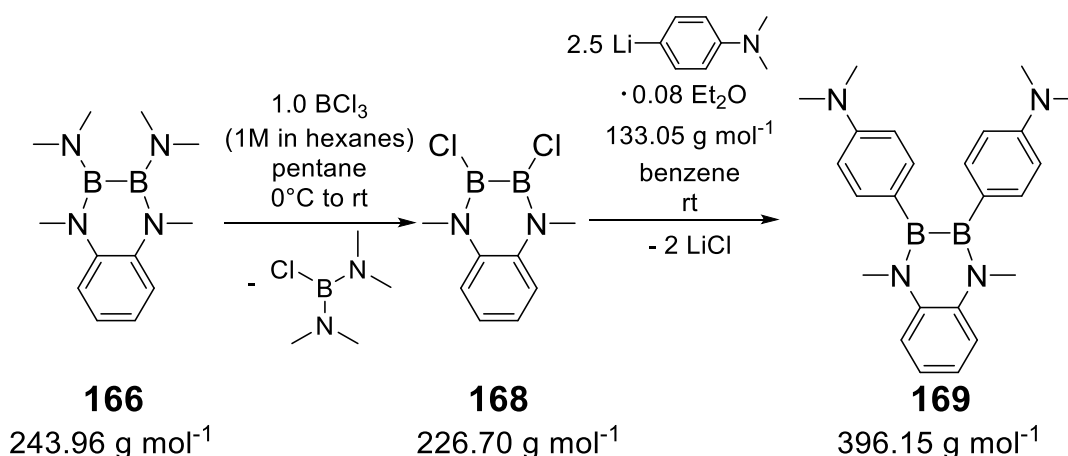


YK150_9: *N,N'*-Dilithio-*N,N'*-dimethyl-1,2-diaminobenzene **165** (3.00 g, 14.9 mmol, 1.05 eq.) is dissolved in thf (250 mL) and cooled to -78°C (isopropanol/ liquid nitrogen). A solution of 1,2-bis(dimethylamino)-dichlorodiborane(4) **54a** (2.6 mL, 15.5 mmol, 1 eq.) in Et_2O (45 mL) is added dropwise *via* dropping funnel over 20 minutes. Stirring is continued in the cooling bath for 1 hour and then allowed to reach room temperature. Stirring is maintained for another hour. Removal of solvent and volatile species *in vacuo* is followed by filtration from hexane. Reducing the filtrate volume gives a yellow solution from which 1.64 g (two fractions, 43%) of cyclic 1,4-diaza-2,3-diborinane **166** are obtained as colorless crystals at room temperature.

5. Experimental Section

¹H NMR (300.13 MHz, C₆D₆, 300K, TMS): δ = 7.14–7.07 (m, 2H, ArH), 7.02–6.96 (m, 2H, ArH), 2.99 (s, 6H, Ar-NCH₃), 2.65 (s, 12H, B-N(CH₃)₂) ppm. **¹¹B NMR** (96.29 MHz, C₆D₆, 300 K, BF₃-Et₂O): δ = 33.7 (s) ppm. **¹³C NMR** (75.47 MHz, C₆D₆, 300K, TMS): δ = 137.6 (s, ArC_{quart.}), 118.6 (s, ArCH), 112.9 (s, ArCH), 42.3 (s, B-N(CH₃)₂), 36.7 (s, Ar-NCH₃) ppm. **UV/Vis** (hexane): λ_{\max} = 314 nm (ϵ = 11830 L mol⁻¹ cm⁻¹), 308 nm (ϵ = 12110 L mol⁻¹ cm⁻¹), 272 nm (ϵ = 9840 L mol⁻¹ cm⁻¹), 234 nm (ϵ = 34860 L mol⁻¹ cm⁻¹). **Elemental analysis**: C₁₂H₂₂B₂N₄ (243.96); C 58.79 (calc. 59.08); H 8.67 (9.09); N 22.78 (22.97) %. **MP**: 135–138°C (stable).

5.8.2 Synthesis of 2,3-bis(para-*N,N*-dimethylaniline)-1,4-dimethyl-1,2,3,4-tetrahydrobenzo[*e*][1,4,2,3]diazadiborinane **169**



YK152_6: Cyclic 1,4-diaza-2,3-diborinane **166** (822 mg, 3.37 mmol, 1 eq.) is dissolved in pentane (120 mL) and cooled to 0°C (ice bath). BCl₃ solution in hexanes (3.5 mL, 1 M, 3.5 mmol, 1.04 eq.) is added *via* syringe. The reaction mixture is stirred in the ice bath for 30 minutes and one hour at room temperature. Removal of solvent and volatile species *in vacuo* afforded the colorless cyclic 1,4-diaza-2,3-diborinane **168** in quantitative yield which is used without further purification.

¹H NMR (400.13 MHz, C₆D₆, 300K, TMS): δ = 6.99–6.95 (m, 2H, ArH), 6.91–6.87 (m, 2H, ArH), 3.05 (s, 6H, Ar-NCH₃) ppm. **¹¹B NMR** (128.38 MHz, C₆D₆, 300 K, BF₃-Et₂O): δ = 40.0 (s) ppm.

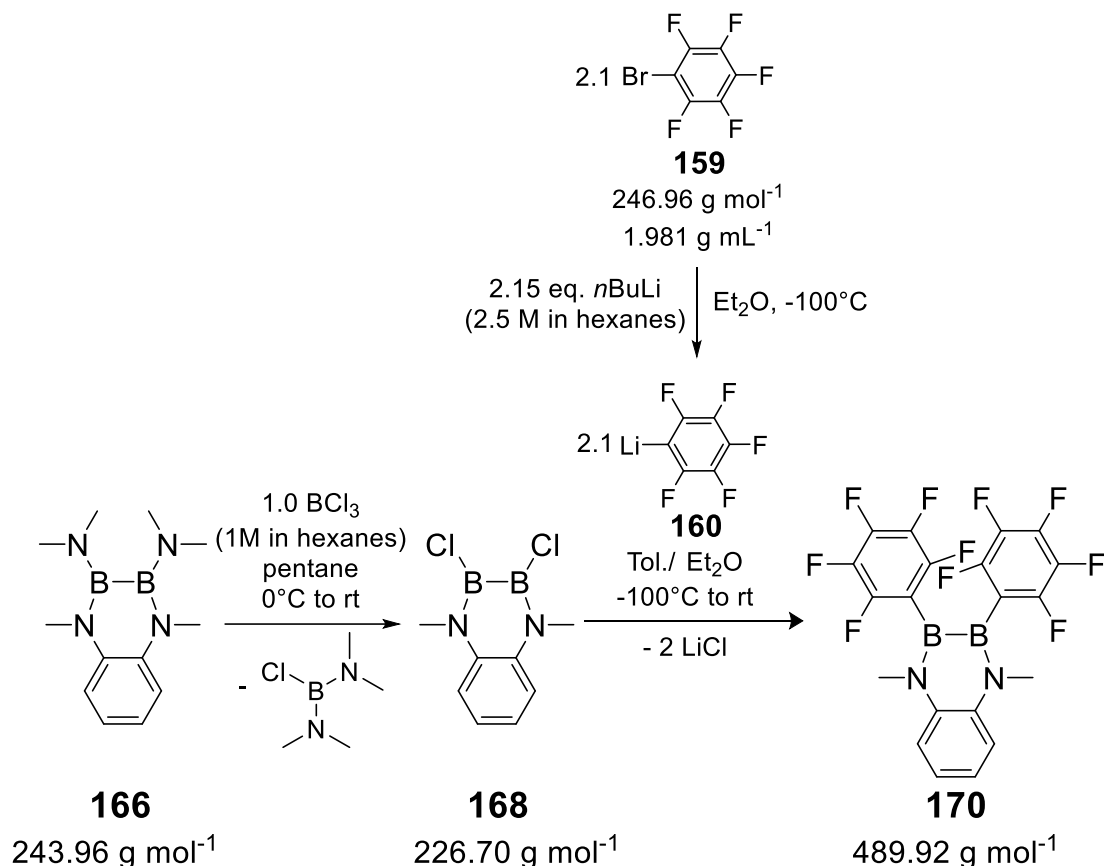
5. Experimental Section

YK154_3: Dichloro cyclic 1,4-diaza-2,3-diborinane **168** (212 mg, 0.939 mmol, 1 eq.) and 4-(dimethylamino)phenyl lithium (312 mg, 2.35 mmol, 2.5 eq.) are mixed as solids and benzene (30 mL) is added at room temperature. Stirring is continued for 1 hour. Removal of solvent and volatile species *in vacuo* is followed by filtration from toluene. Crystals are grown from a yellow solution of the crude product in a mixture of toluene (5 mL) and hexane (10 mL), affording 77 mg (21%) of the desired product **169** at room temperature.

¹H NMR (400.13 MHz, C₆D₆, 300K, TMS): δ = 7.36 (d, ³J = 8.6 Hz, 4H, Me₂N-PhH), 7.35–7.33 (m, 2H, ArH), 7.22–7.18 (m, 2H, ArH), 6.67 (d, ³J = 8.7 Hz, 4H, Me₂N-PhH), 3.40 (s, 6H, Ar-NCH₃), 2.55 (s, 12H, (CH₃)₂N-Ph) ppm. **¹¹B NMR** (128.38 MHz, C₆D₆, 300 K, BF₃-Et₂O): δ = 47.1 (br s) ppm. **¹³C NMR** (100.61 MHz, C₆D₆, 300K, TMS): δ = 150.0 (s, Me₂N-PhC_{quart.}), 138.1 (s, ArC_{quart.}), 134.9 (s, Me₂N-PhCH), 132.2 (br s, Me₂N-PhC_{quart.-B}), 122.0 (s, ArCH), 117.0 (s, ArCH), 112.1 (s, Me₂N-PhCH), 40.1 (s, (CH₃)₂N-Ph), 38.1 (s, Ar-NCH₃) ppm. **UV/Vis** (diethylether): λ_{\max} = 342 nm (ϵ = 35480 L mol⁻¹ cm⁻¹), 261 nm (ϵ = 34650 L mol⁻¹ cm⁻¹), 232 nm (ϵ = 27300 L mol⁻¹ cm⁻¹). **Elemental analysis:** C₂₄H₃₀B₂N₄ (396.15); C 72.69 (calc. 72.77); H 7.58 (7.63); N 13.96 (14.14) %. **MP:** 180-182°C (partially stable).

5. Experimental Section

5.8.3 Synthesis of 2,3-bis(pentafluorophenyl)-1,4-dimethyl-1,2,3,4-tetrahydrobenzo[e][1,4,2,3]diazadiborinane **170**



YK152_6: Cyclic 1,4-diaza-2,3-diborinane **166** (822 mg, 3.37 mmol, 1 eq.) is dissolved in pentane (120 mL) and cooled in an ice bath for 20 minutes. BCl_3 solution in hexanes (3.5 mL, 1 M, 3.5 mmol, 1.04 eq.) is added *via* syringe. The reaction mixture is stirred in the ice bath for 30 minutes and one hour at room temperature. Removal of solvent and volatile species *in vacuo* affords the colorless intermediate **168** in quantitative yield which is used without further purification.

$^1\text{H NMR}$ (400.13 MHz, C_6D_6 , 300K, TMS): $\delta = 6.99\text{--}6.95$ (m, 2H, ArH), $6.91\text{--}6.87$ (m, 2H, ArH), 3.05 (s, 6H, Ar- NCH_3) ppm. $^{11}\text{B NMR}$ (128.38 MHz, C_6D_6 , 300 K, $\text{BF}_3\text{-Et}_2\text{O}$): $\delta = 40.1$ (s) ppm.

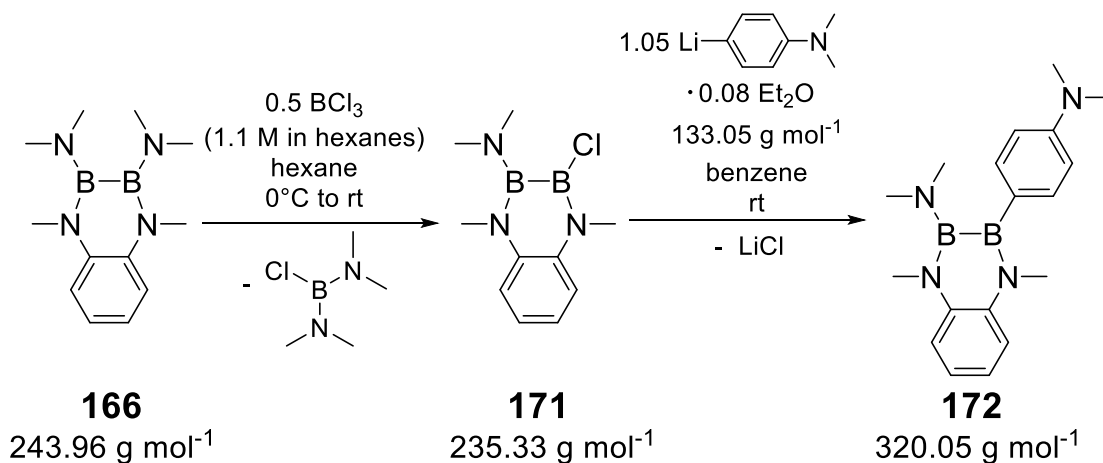
YK163: Bromopentafluorobenzene (degassed, 0.55 mL, 4.41 mmol, 2.1 eq.) is dissolved in Et_2O (50 mL) and cooled to -100°C (ethanol/ liquid nitrogen) for 30 minutes before *n*butyl lithium solution (2.5 M in hexanes, 1.8 mL, 4.50 mmol, 2.15 eq.) is added. The reaction mixture is stirred for 30 minutes at -100°C . Cyclic 1,4-diaza-2,3-diborinane **168** (472 mg, 2.08 mmol, 1 eq.) is dissolved in

5. Experimental Section

toluene (30 mL) and cooled in to -100°C (ethanol/ liquid nitrogen) for 30 minutes. The Diborane-solution is transferred to the anion solution *via* cannula and the reaction mixture is allowed to warm slowly to -60°C . After stirring another hour at room temperature removal of solvent and volatile species *in vacuo* is followed by filtration from toluene. Crystals are grown from a concentrated, colorless solution of the crude product in toluene, affording 269 mg (26%) of the desired cyclic 1,4-diaza-2,3-diborinane **170**.

^1H NMR (400.13 MHz, C_6D_6 , 300K, TMS): $\delta = 7.11$ (s, 4H, ArH), 2.94 (s, 6H, ArNCH₃) ppm. **^{11}B NMR** (96.29 MHz, C_6D_6 , 300 K, $\text{BF}_3\text{-Et}_2\text{O}$): $\delta = 42.2$ (br s) ppm. **^{13}C NMR** (100.61 MHz, C_6D_6 , 300K, TMS): $\delta = 145.8$ (dm, $^1\text{J}_{\text{C-F}} = 239$ Hz, $\text{F}_5\text{PhC-F}$), 141.3 (dm, $^1\text{J}_{\text{C-F}} = 251$ Hz, $\text{F}_5\text{PhC-F}$), 137.6 (dm, $^1\text{J}_{\text{C-F}} = 250$ Hz, $\text{F}_5\text{PhC-F}$), 136.6 (s, ArC_{quart.}), 123.7 (s, ArCH), 117.8 (s, ArCH), 114.9 (br s, $\text{F}_5\text{PhC-B}$) 38.6 (s, Ar-NCH₃) ppm. **^{19}F NMR** (282.40 MHz, C_6D_6 , 300 K, CFCl_3): $\delta = -132.7$ (dd, 4F, $^3\text{J}_{\text{F-F}} = 24$ Hz, $^4\text{J}_{\text{F-F}} = 10$ Hz, $\text{F}_5\text{Ph-oE}$), -153.6 (t, 2F, $^3\text{J}_{\text{F-F}} = 20$ Hz, $\text{F}_5\text{Ph-pE}$), -161.5 (ddd, 4F, $^3\text{J}_{\text{F-F}} = 25$ Hz, $^3\text{J}_{\text{F-F}} = 21$ Hz, $^4\text{J}_{\text{F-F}} = 10$ Hz, $\text{F}_5\text{Ph-mE}$) ppm. **UV/Vis** (diethylether): $\lambda_{\text{max}} = 317$ nm ($\epsilon = 18246$ L mol⁻¹ cm⁻¹), 254 nm ($\epsilon = 13763$ L mol⁻¹ cm⁻¹), 231 nm ($\epsilon = 25011$ L mol⁻¹ cm⁻¹). **Elemental analysis**: $\text{C}_{20}\text{H}_{10}\text{B}_2\text{F}_{10}\text{N}_2$ (489.92); C 48.68 (calc. 49.03); H 2.04 (2.06); N 5.87 (5.72) %. **MP**: $142\text{-}144^{\circ}\text{C}$ (stable).

5.8.4 Synthesis of 1,4-dimethyl-2-dimethylamino-3-para-*N,N*-dimethylaniline-1,2,3,4-tetrahydrobenzo[e][1,4,2,3]diazadiborinane **172**



5. Experimental Section

YK157_6: Cyclic 1,4-diaza-2,3-diborinane **166** (1.64 g, 6.74 mmol, 1 eq.) is dissolved in hexane (120 mL) and cooled to 0°C (ice bath). BCl₃ solution in hexanes (3.0 mL, 1.1 M, 3.3 mmol, 0.49 eq.) is added slowly *via* syringe. The reaction mixture is stirred in the ice bath for 15 minutes and 30 minutes at room temperature. Removal of solvent and volatile species *in vacuo* afforded the colorless, oily intermediate **171**. The crude product is twice dissolved in hexane which is evacuated again for complete removal of chloro bis(dimethylamino)borane. The crude product is used without further purification.

¹H NMR (300.13 MHz, C₆D₆, 300K, TMS): δ = 7.11 (ddd, ³J = 8.5 Hz, ³J = 6.6 Hz, ⁴J = 1.9 Hz, 1H, ArH), 7.01 – 6.93 (m, 3H, ArH), 3.21 (s, 3H, B-NCH₃), 2.85 (s, 3H, B-NCH₃), 2.81 (s, 6H, Ar-NCH₃) ppm. **¹¹B NMR** (96.29 MHz, C₆D₆, 300 K, BF₃-Et₂O): δ = 40.2 (s), 31.8 (s) ppm.

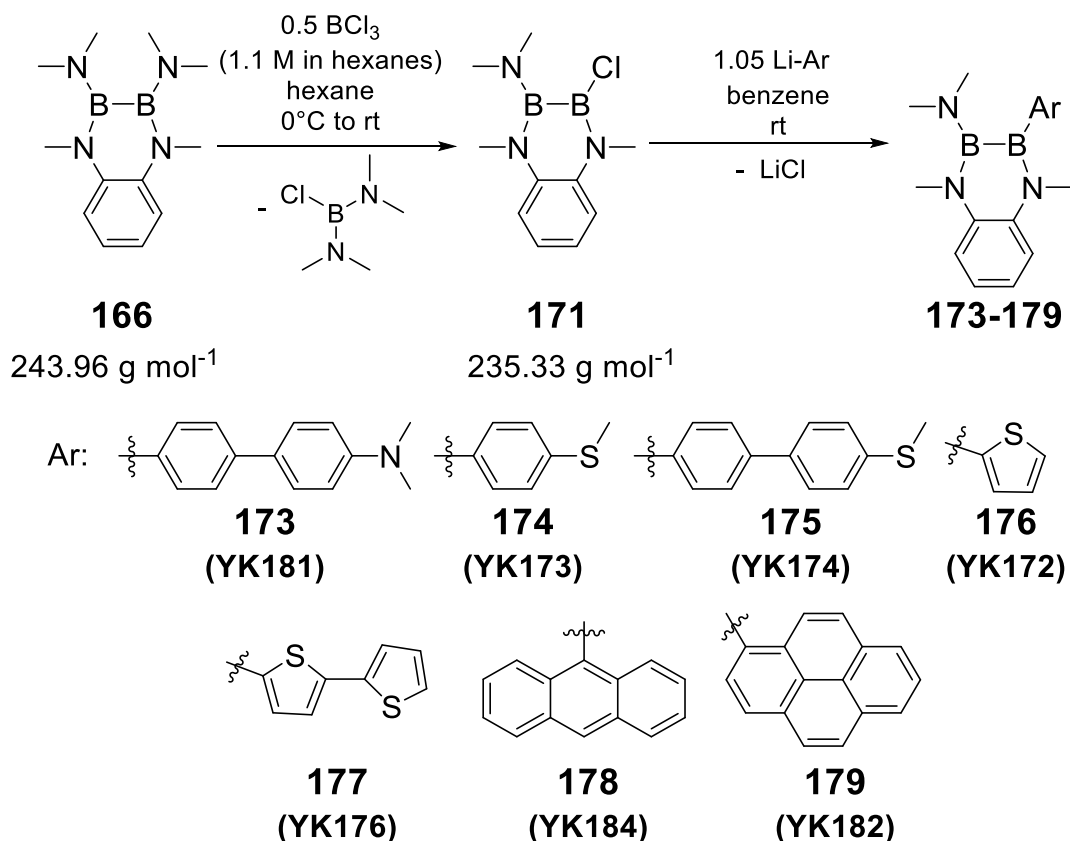
YK158_6: Crude product **171** (6.74 mmol) is dissolved in benzene and filtered. 4-(dimethylamino)phenyl lithium (942 mg, 7.08 mmol, 1.05 eq.) is suspended in benzene (80 mL) and added to the filtrate of **171** at room temperature. Stirring is continued for three hours. Removal of solvent and volatile species *in vacuo* is followed by filtration from hexane. Reducing the filtrate volume gives a yellow solution from which 663 mg (two fractions, 31%) of **172** are obtained as yellow crystals.

¹H NMR (300.13 MHz, C₆D₆, 300K, TMS): δ = 7.28 (d, ³J = 8.7 Hz, 2H, Me₂N-PhH), 7.20 (d, ³J = 7.5 Hz, 2H, ArH), 7.14–7.11 (m, 1H, ArH), 7.04 (ddd, ³J = 8.3 Hz, ³J = 6.9 Hz, ⁴J = 1.7 Hz, 1H, ArH), 6.80 (d, ³J = 8.7 Hz, 2H, Me₂N-PhH), 3.19 (s, 3H, B-NCH₃), 3.05 (s, 3H, B-NCH₃), 2.65 (s, 6H, Ar-NCH₃), 2.60 (s, 6H, (CH₃)₂N-Ph) ppm. **¹¹B NMR** (96.29 MHz, C₆D₆, 300 K, BF₃-Et₂O): δ = 47.2 (br s), 34.0 (br s) ppm. **¹³C NMR** (75.47 MHz, C₆D₆, 300K, TMS): δ = 149.6 (s, Me₂N-PhC_{quart.}), 140.8 (s, ArC_{quart.}), 136.4 (s, ArC_{quart.}), 135.3 (br s, Me₂N-PhC_{quart.}-B), 131.3 (s, Me₂N-PhCH), 122.5 (s, ArCH), 119.0 (s, ArCH), 116.8 (s, ArCH), 115.5 (s, ArCH), 113.1 (s, Me₂N-PhCH), 42.1 (s, Ar-NCH₃), 40.3 (s, (CH₃)₂N-Ph), 38.1 (s, B-N(CH₃)), 37.6 (s, B-NCH₃) ppm. **UV/Vis** (hexane): λ_{\max} = 327 nm (ϵ = 15810 L mol⁻¹ cm⁻¹), 315 nm (ϵ = 14840 L mol⁻¹ cm⁻¹), 243 nm (ϵ = 24880 L mol⁻¹ cm⁻¹), 216 nm

5. Experimental Section

($\epsilon = 34980 \text{ L mol}^{-1} \text{ cm}^{-1}$). **Elemental analysis:** $\text{C}_{18}\text{H}_{26}\text{B}_2\text{N}_4$ (320.05); C 66.98 (calc. 67.55); H 8.19 (8.19); N 17.77 (17.51) %. **MP:** 115-120°C (stable).

5.8.5 Reactivity of 1,4-dimethyl-2-dimethylamino-3-chloro-1,2,3,4-tetrahydrobenzo[e][1,4,2,3]diazadiborinane **171** towards various extended or electron-rich aromatic systems



YK157_6: Cyclic 1,4-diaza-2,3-diborinane **166** (1 eq.) is dissolved in hexane (18 mL/mmol) and cooled to 0°C (ice bath). BCl₃ solution in hexanes (1.1 M, 0.5 eq.) is added slowly *via* syringe. The reaction mixture is stirred in the ice bath for 15 minutes and 30 minutes at room temperature. Removal of solvent and volatile species *in vacuo* afforded the colorless, oily intermediate **171**. The crude product is twice dissolved in hexane which is evacuated again for complete removal of chloro bis(dimethylamino)borane. The crude product is used without further purification.

¹H NMR (300.13 MHz, C₆D₆, 300K, TMS): $\delta = 7.11$ (ddd, ³J = 8.5 Hz, ³J = 6.6 Hz, ⁴J = 1.9 Hz, 1H, ArH), 7.01 – 6.93 (m, 3H, ArH), 3.21 (s, 3H, B-

5. Experimental Section

NCH₃), 2.85 (s, 3H, B-NCH₃), 2.81 (s, 6H, Ar-NCH₃) ppm. **¹¹B NMR** (96.29 MHz, C₆D₆, 300 K, BF₃-Et₂O): δ = 40.2 (s), 31.8 (s) ppm.

General Procedure for reactions with isolated anions (YK172-174 & YK181): Crude product **171** (1 eq.) is dissolved in benzene (12 mL/mmol) and filtered. The corresponding aryl lithium (1.0 eq.) is suspended in benzene (12 mL/mmol) and added to the filtrate of **171** at room temperature. Stirring is continued for three hours. Removal of solvent and volatile species *in vacuo* is followed by filtration from hexane. An NMR sample of the reaction mixture is analyzed.

Data for YK181: From 238 mg (0.976 mmol) Cyclic 1,4-diaza-2,3-diborinane **171** and 199 mg (0.979 mmol) 4'-(dimethylamino)-[1,1'-biphenyl]4-yl lithium.

¹H NMR (400.13 MHz, C₆D₆, 300K, TMS): *Note: Aryl-signals are not listed due to signal overlaps beyond interpretation* δ = 7.79 (d, ³J = 8.0 Hz, 2H, biphenyl-CH), 7.69 (d, ³J = 8.7 Hz, 2H, biphenyl-CH), 7.39 (d, ³J = 8.0 Hz, 2H, biphenyl-CH), 6.69 (d, ³J = 8.8 Hz, 2H, biphenyl-CH), 3.11, 3.05 (each s, each 3H, B-NCH₃), 2.60 (s, 6H, Ar-NCH₃), 2.54 (s, 6H, biphenyl-N(CH₃)₂) ppm. **¹¹B NMR** (96.29 MHz, C₆D₆, 300 K, BF₃-Et₂O): δ = 46.5 (br s), 40.5 (br, s, unidentified side product), 31.8 (br, s) ppm.

Data for YK173: From 307 mg (1.26 mmol) Cyclic 1,4-diaza-2,3-diborinane **171** and 177 mg (1.26 mmol) 4-(methylthio)phenyl lithium.

¹H NMR (400.13 MHz, C₆D₆, 300K, TMS): δ = *Note: Some aryl-signals may not listed due to signal overlaps beyond interpretation* 7.27 (d, ³J = 8.2 Hz, 2H, thioanisole-CH), 7.23-7.18 (m, 2H, Ar-CH), 7.05-7.00 (m, 2H, Ar-CH), 3.02, 3.02 (each s, altogether 6H, B-NCH₃), 2.54 (s, 6H, Ar-NCH₃), 2.07 (s, 6H, thioanisole-CH₃) ppm. **¹¹B NMR** (128.38 MHz, C₆D₆, 300 K, BF₃-Et₂O): δ = 48.7 (br s), 33.5 (br, s) ppm.

Data for YK174: From 307 mg (1.26 mmol) Cyclic 1,4-diaza-2,3-diborinane **171** and 240 mg (1.16 mmol) 4'-(methylthio)-[1,1'-biphenyl]-4-yl lithium.

¹H NMR (400.13 MHz, C₆D₆, 300K, TMS): *Note: Aryl-signals are not listed due to signal overlaps beyond interpretation* δ = 7.62 (d, ³J = 8.2 Hz, 2H, biphenyl-CH), 7.47 (d, ³J = 8.4 Hz, 2H, biphenyl-CH), 7.34 (d, ³J = 8.2 Hz, 2H, biphenyl-

5. Experimental Section

CH), 7.19 (d, $^3J = 8.4$ Hz, 2H, biphenyl-CH), 3.07, 3.05 (each s, each 3H, B-NCH₃), 2.58 (s, 6H, Ar-NCH₃), 2.01 (s, 3H, biphenyl-SCH₃) ppm. **¹¹B NMR** (128.38 MHz, C₆D₆, 300 K, BF₃-Et₂O): $\delta = 48.6$ (br s), 34.7 (br, s) ppm.

Data for YK172: From 308 mg (1.26 mmol) Cyclic 1,4-diaza-2,3-diborinane **171** and 116 mg (1.26 mmol) thiophen-2-yl lithium.

¹H NMR (400.13 MHz, C₆D₆, 300K, TMS): *Note: Some aryl- and thiophene-signals are not listed due to signal overlaps beyond interpretation* $\delta = 7.28$ (dd, $^3J = 4.7$ Hz, $^4J = 0.9$ Hz, 1H, thiophene-CH), 6.89 (dd, $^3J = 3.3$ Hz, $^4J = 0.9$ Hz, 1H, thiophene-CH), 3.09, 2.96 (each s, each 3H, B-NCH₃), 2.55 (s, 6H, Ar-NCH₃) ppm. **¹¹B NMR** (128.38 MHz, C₆D₆, 300 K, BF₃-Et₂O): $\delta = 46.2$ (br s), 33.5 (br, s) ppm.

General Procedure for reactions with previously in solution generated anions (YK176 & YK182 & YK184): To form the aryl lithium the corresponding bromo derivative or bithiophene (1.15 eq.) is dissolved in Et₂O (38 mL/mmol) and cooled to -78°C . *n*-Butyl lithium solution (2.5 M in hexanes, 1.2 eq.) is added and the reaction mixture is stirred one hour in the cooling bath and one hour at room temperature. Crude product **171** (1 eq.) is dissolved in benzene (12 mL/mmol) and filtered. The corresponding aryl lithium is added to the filtrate of **171** at room temperature. Stirring is continued for three hours. Removal of solvent and volatile species *in vacuo* is followed by filtration from hexane. An NMR sample of the reaction mixture is analyzed.

Data for YK176: From 304 mg (1.25 mmol) Cyclic 1,4-diaza-2,3-diborinane **171** and 208 mg (1.25 mmol) bithiophene.

¹H NMR (400.13 MHz, C₆D₆, 300K, TMS): $\delta = 7.22$ (d, $^3J = 3.4$ Hz, 1H, bithiophene-CH), 7.12–7.09 (m, 2H, bithiophene-CH), 7.07–6.95 (m, 4H, Ar-CH), 6.71 (d, $J = 3.2$ Hz, 1H, bithiophene-CH), 6.67 (d, $J = 3.6$ Hz, 1H, bithiophene-CH), 3.12, 2.95 (each s, each 3H, B-NCH₃), 2.58 (s, 6H, Ar-NCH₃) ppm. **¹¹B NMR** (128.38 MHz, C₆D₆, 300 K, BF₃-Et₂O): $\delta = 45.6$ (br s), 33.8 (br, s) ppm.

5. Experimental Section

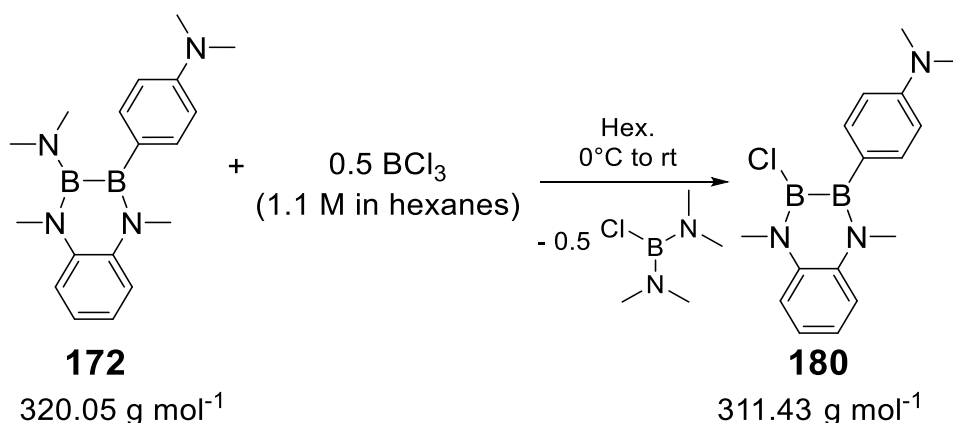
Data for YK184: From 200 mg (0.820 mmol) Cyclic 1,4-diaza-2,3-diborinane **171** and 211 mg (0.861 mmol) 9-bromoanthracene.

¹H NMR (300.13 MHz, C₆D₆, 300K, TMS): δ = 8.16 (s, 1H, anthracene-CH), 7.95 (d, ³J = 8.5 Hz, 2H, anthracene-CH), 7.88 (dd, ³J = 8.6 Hz, ⁴J = 1.1 Hz, 2H, anthracene-CH), 7.80 (dd, ³J = 6.5 Hz, ⁴J = 3.3 Hz, 2H, anthracene-CH), 7.34-7.28 (m, 2H, Ar-CH), 7.27-7.21 (m, 6H (thereof 4H unidentified side product), anthracene-CH) 7.09-7.00 (m, 2H, Ar-CH), 3.07, 2.90 (each s, each 3H, B-NCH₃), 2.18 (s, 6H, Ar-NCH₃) ppm. **¹¹B NMR** (96.28 MHz, C₆D₆, 300 K, BF₃-Et₂O): δ = 47.1 (br s), 33.0 (br, s) ppm.

Data for YK182: From 129 mg (0.529 mmol) Cyclic 1,4-diaza-2,3-diborinane **171** and 149 mg (0.530 mmol) 1-bromopyrene.

¹H NMR (300.13 MHz, C₆D₆, 300K, TMS): *Note: Aryl-signals are not listed due to signal overlaps beyond interpretation* δ = 3.10, 2.98 (each s, each 3H, B-NCH₃), 2.33 (s, 6H, Ar-NCH₃) ppm. **¹¹B NMR** (96.28 MHz, C₆D₆, 300 K, BF₃-Et₂O): δ = 46.9 (br s), 33.2 (br, s) ppm.

5.8.6 Synthesis of 2-chloro-1,4-dimethyl-3-para-*N,N*-dimethylaniline-1,2,3,4-tetrahydrobenzo[e][1,4,2,3]diazadiborinane **180**



YK159_3: Cyclic 1,4-diaza-2,3-diborinane **172** (518 mg, 1.62 mmol, 1 eq.) is dissolved in hexane (40 mL) and cooled to 0°C (ice bath). BCl₃ solution in hexanes (0.74 mL, 1.1 M, 0.814 mmol, 0.5 eq.) is added slowly *via* syringe. Stirring is continued in the ice bath for 40 minutes and 30 minutes at room temperature. Removal of solvent and volatile species *in vacuo* is followed by

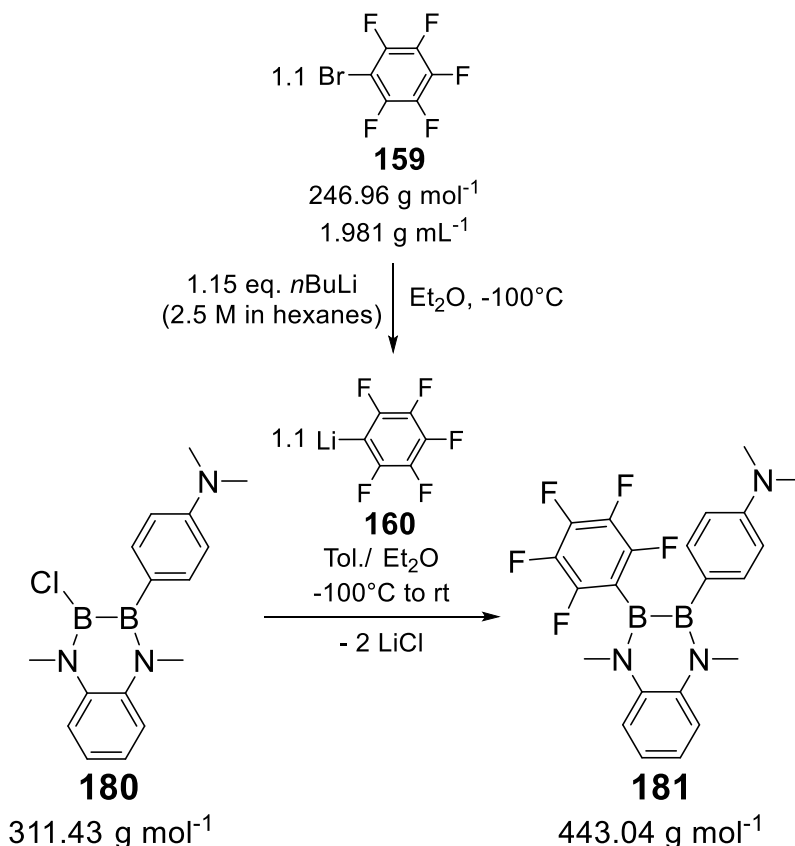
5. Experimental Section

filtration from toluene. Crystals are grown from a colorless solution in a mixture of toluene (3 mL) and hexane (1 mL), affording 256 mg (42%) of the desired **180**.

¹H NMR (300.13 MHz, C₆D₆, 300K, TMS): δ = 7.69 (d, ³J = 8.8 Hz, 2H, Me₂N-PhH), 7.19–7.16 (m, 1H, ArH), 7.14–7.07 (m, 3H, ArH), 6.82 (d, ³J = 8.7 Hz, 2H, Me₂N-PhH), 3.27 (s, 3H, Ar-NCH₃), 3.27 (s, 3H, Ar-NCH₃), 2.60 (s, 6H, (CH₃)₂N-Ph) ppm. **¹¹B NMR** (96.29 MHz, C₆D₆, 300 K, BF₃-Et₂O): δ = 43.2 (br s) ppm. **¹³C NMR** (75.47 MHz, C₆D₆, 300K, TMS): δ = 150.7 (s, Me₂N-PhC_{quart.}), 137.4 (s, ArC_{quart.}), 136.3 (s, ArC_{quart.}), 135.4 (s, Me₂N-PhCH), 129.3 (s, Me₂N-PhC_{quart.-B}), 122.6 (s, ArCH), 122.3 (s, ArCH), 117.3 (s, ArCH), 117.0 (s, ArCH), 112.3 (s, Me₂N-PhCH), 40.1 (s, (CH₃)₂N-Ph), 38.2 (s, Ar-NCH₃), 34.6 (s, Ar-NCH₃) ppm. **UV/Vis** (diethylether): λ_{\max} = 334 nm (ϵ = 21235 L mol⁻¹ cm⁻¹), 255 nm (ϵ = 18680 L mol⁻¹ cm⁻¹), 232 nm (ϵ = 18895 L mol⁻¹ cm⁻¹). **Elemental analysis**: C₁₆H₂₀B₂ClN₃ (311.43); C 61.34 (calc. 61.71); H 6.27 (6.47); N 13.36 (13.49) %. **MP**: 148-153°C (stable).

5. Experimental Section

5.8.7 Synthesis of 1,4-dimethyl-3-para-*N,N*-dimethylaniline-2-pentafluorophenyl-1,2,3,4-tetrahydrobenzo[*e*][1,4,2,3]diazadiborinane **181**



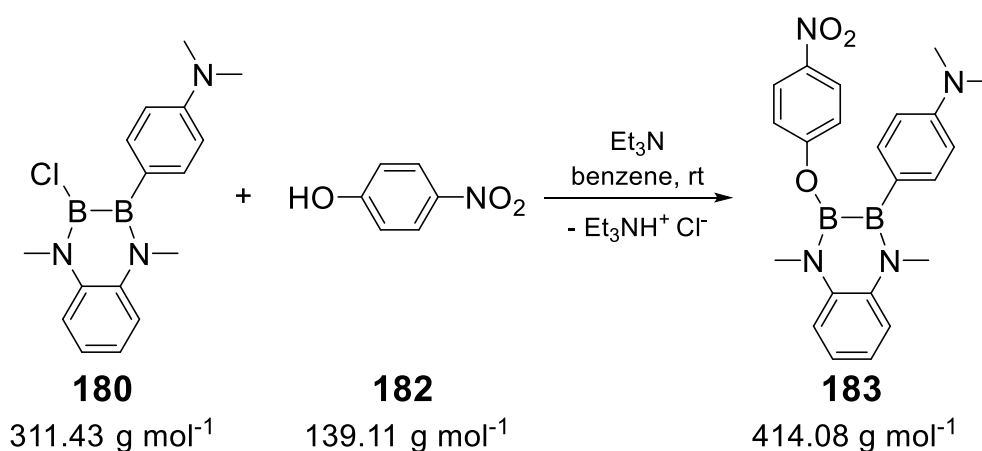
YK162: Bromopentafluorobenzene (degassed, 44 μ L, 0.353 mmol, 1.1 eq.) is dissolved in Et₂O (5 mL) and cooled to -100°C (ethanol/ liquid nitrogen) before *n*butyl lithium solution (2.5 M in hexanes, 0.15 mL, 0.375 mmol, 1.15 eq.) is added. Stirring is continued for 30 minutes at -100°C . **180** (100 mg, 0.321 mmol, 1 eq.) is dissolved in toluene (8 mL) and cooled to -100°C (ethanol/ liquid nitrogen). The cyclic 1,4-diaza-2,3-diborinane-solution (**180**) is transferred to the anion solution *via* cannula and the reaction mixture is allowed to warm slowly to -45°C . After stirring another hour at room temperature removal of solvent and volatile species *in vacuo* is followed by filtration from toluene. Removal of solvent affords 70 mg (49%) as colorless powder of the desired **181**.

¹H NMR (400.13 MHz, C₆D₆, 300K, TMS): δ = 7.26 (d, ³J = 8.6 Hz, 2H, Me₂N-PhH), 7.24–7.18 (m, 3H, ArH), 7.15–7.11 (m, 1H, ArH), 6.59 (d, ³J = 8.6 Hz, 2H, Me₂N-PhH), 3.25, 3.08 (each s, each 3H, Ar-NCH₃), 2.47 (s, 6H, (CH₃)₂N-Ph) ppm. **¹¹B NMR** (128.38 MHz, C₆D₆, 300 K, BF₃-Et₂O): δ = 45.3 ppm. **¹³C NMR**

5. Experimental Section

(100.61 MHz, C₆D₆, 300K, TMS): δ = 149.9 (s, Me₂N-PhC_{quart.}), 145.0 (dm, ¹J_{C-F} = 237 Hz, F₅PhC-F), 140.4 (dm, ¹J_{C-F} = 249 Hz, F₅PhC-F), 137.3 (dm, ¹J_{C-F} = 249 Hz, F₅PhC-F), 137.8 (s, ArC_{quart.}), 135.8 (s, ArC_{quart.}), 133.2 (s, Me₂N-PhCH), 130.0 (s, Me₂N-PhC_{quart.-B}), 123.2, 121.8, 117.1, 116.9 (each s, ArCH), 116.8 (br s, F₅PhC-B), 111.8 (s, Me₂N-PhCH), 39.5 (s, (CH₃)₂N-Ph), 38.3, 37.5 (each s, Ar-NCH₃) ppm. **¹⁹F NMR** (282.40 MHz, C₆D₆, 300 K, CFCl₃): δ = -132.3 (dd, 2F, ³J_{F-F} = 25 Hz, ⁴J_{F-F} = 10 Hz, F₅Ph-oE), -155.8 (t, 1F, ³J_{F-F} = 21 Hz, F₅Ph-pE), -162.3 (ddd, 2F, ³J_{F-F} = 25 Hz, ³J_{F-F} = 21 Hz, ⁴J_{F-F} = 10 Hz, F₅Ph-mE) ppm. **UV/Vis** (hexane): λ_{\max} = 349 nm (ϵ = 16875 L mol⁻¹ cm⁻¹), 313 nm (ϵ = 14960 L mol⁻¹ cm⁻¹), 263 nm (ϵ = 21000 L mol⁻¹ cm⁻¹). **Elemental analysis**: C₂₂H₂₀B₂F₅N₃ (443.04); C 60.58 (calc. 59.64); H 4.78 (4.55); N 9.92 (9.48) %. **MP**: 131-135°C (stable).

5.8.8 Synthesis of 4-(1,4-dimethyl-3-(4-nitrophenoxy)-3,4-dihydrobenzo[e][1,4,2,3]diazadi-borin-2(1H)-yl)-N,N-dimethylaniline **183**



YK165_2: Cyclic 1,4-diaza-2,3-diborinane **180** (185 mg, 0.594 mmol, 1 eq.) is dissolved in benzene (15 mL) and *para*-nitrophenol (82 mg, 0.590 mmol, 1 eq.) is suspended in benzene (15 mL). Triethylamine (0.09 mL, 0.620 mmol, 1.04 eq.) is added to the diborinane solution which is subsequently transferred *via cannula* to the *para*-nitrophenol suspension. The reaction mixture is stirred for 1.5 hours. Removal of solvent is followed by filtration from benzene. Solvent is removed again. Single crystals of **183** suitable for x-ray diffraction were obtained in an NMR-tube from a C₆D₆-solution.

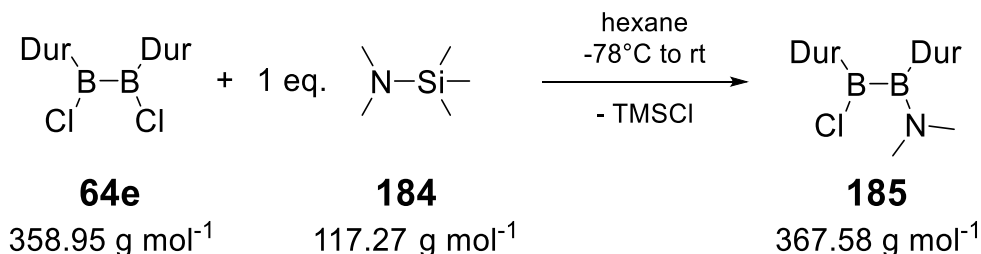
5. Experimental Section

Note: Due to the low solubility of the compound no satisfying signal to noise ratio could be achieved in the ^{13}C NMR spectrum.

^1H NMR (400.13 MHz, C_6D_6 , 300K, TMS): $\delta = 7.62$ (d, $^3J = 9.0$ Hz, 2H, Me₂N-PhH), 7.24-7.20 (m, 3H, ArH), 7.14-7.10 (m, 1H, ArH), 6.64 (d, $^3J = 8.7$ Hz, 2H, Me₂N-PhH), 6.31-6.26 (m, 4H, O₂N-PhH), 3.22, 3.17 (each s, each, 3H, Ar-NCH₃), 2.50 (s, 6H, (CH₃)₂N-Ph) ppm. **^{11}B NMR** (128.38 MHz, C_6D_6 , 300 K, $\text{BF}_3\text{-Et}_2\text{O}$): $\delta = 44.9$ (bs), 33.4 (bs) ppm. **UV/Vis** (Et_2O): $\lambda_{\text{max}} = 316$ nm ($\epsilon = 25100$ L mol⁻¹ cm⁻¹), 259 nm ($\epsilon = 20675$ L mol⁻¹ cm⁻¹), 232 nm ($\epsilon = 26235$ L mol⁻¹ cm⁻¹).

5.9. Synthesis of 1,2-diduryl diboranes(4)

5.9.1 Synthesis of 1-chloro-2-dimethylamino-1,2-(2,3,5,6-tetramethylphenyl) diborane(4) **185**

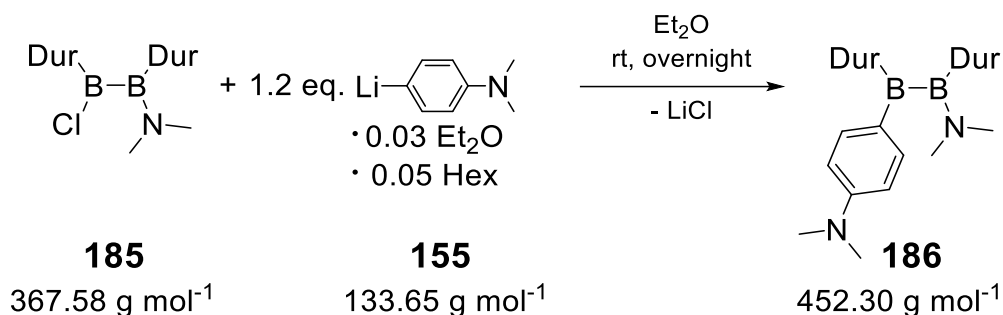


YK185_6: 1,2-Dichlorodiduryl diborane(4) **64e** (500 mg, 1.39 mmol, 1.0 eq.) is dissolved in hexane (30 mL) and cooled to -78°C (isopropanol/ liquid nitrogen). *N,N*-dimethyltrimethylsilylamine (0.223 mL, 1.39 mmol, 1.0 eq.) is added dropwise to the diborane(4)-solution *via* syringe. The reaction mixture is slowly allowed to reach room temperature and stirring is continued for 30 minutes. Removal of solvent and volatile species *in vacuo* is followed by filtration from hexane. Solvent is removed again which gives 422 mg (83%) of diborane(4) **185**, a colorless solid.

$^1\text{H NMR}$ (300.13 MHz, C_6D_6 , 300K, TMS): $\delta = 6.81$ (s, 1H, DurH), 6.79 (s, 1H, DurH), 2.98 (s, 3H, (CH₃)₂N), 2.44 (s, 3H, (CH₃)₂N), 2.06, 2.02, 1.99, 1.83 (each s, each 6H, Dur-CH₃) ppm. **$^{11}\text{B NMR}$** (96.29 MHz, C_6D_6 , 300 K, $\text{BF}_3\text{-Et}_2\text{O}$): $\delta = 87.7$ (br s), 47.2 (br s) ppm. **$^{13}\text{C NMR}$** (100.61 MHz, C_6D_6 , 300K, TMS): $\delta = 145.8$, 143.2 (each s, DurC_{quart.}-B), 134.3, 133.2, 133.2, 131.8 (each s, DurC_{quart.}Me), 131.7, 131.0, (each s, DurCH), 43.3, 40.6 (each s, (CH₃)₂N), 19.7, 19.2, 18.6, 18.6 (each s, Dur-CH₃) ppm. **UV/Vis** (hexane): $\lambda_{\text{max}} = 313$ nm ($\epsilon = 3380 \text{ L mol}^{-1} \text{ cm}^{-1}$). **Elemental analysis:** $\text{C}_{22}\text{H}_{32}\text{B}_2\text{ClN}$ (367.58); C 71.78 (calc. 71.89); H 8.67 (8.78); N 3.51 (3.81) %. **MP:** 123 - 126°C (stable).

5. Experimental Section

5.9.2 Synthesis of 2-dimethylamino-1-para-*N,N*-dimethylaniline-1,2-(2,3,5,6-tetramethylphenyl) diborane(4) **186**

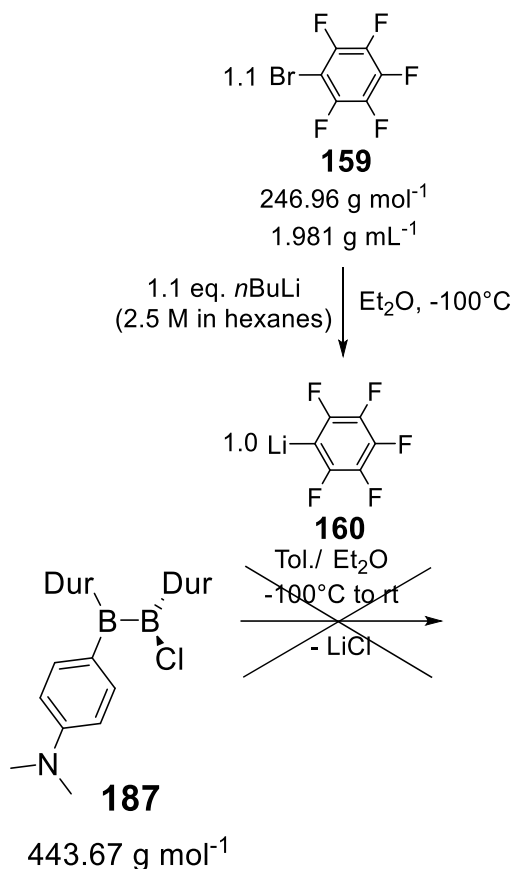


YK187_6: 1-Chloro-2-dimethylamino diduryldiborane(4) **185** (235 mg, 0.639 mmol, 1.0 eq.) and 4-(dimethylamino)phenyllithium (102 mg, 0.767 mmol, 1.2 eq.) are mixed as solids and Et₂O (30 mL) is added. Stirring is continued overnight. Removal of solvent and volatile species *in vacuo* is followed by filtration from hexane. Reducing the filtrate volume gives a yellow solution from which 147 mg (51%) of diborane(4) **186** is obtained as yellow amorphous solid at -78°C.

¹H NMR (300.13 MHz, C₆D₆, 300K, TMS): δ = 8.07 (d, ³J = 7.5 Hz, 2H, Me₂N-PhH), 6.92 (s, 1H, DurH), 6.85 (s, 1H, DurH), 6.53 (d, ³J = 8.8 Hz, 2H, Me₂N-PhH), 3.17, 2.72 (each s, each 3H, (CH₃)₂N), 2.45 (s, 6H, (CH₃)₂N-Ph), 2.17, 2.12 (each s, each 6H, Dur-CH₃), 2.36, 1.76 (each br. s, each 6H, Dur-CH₃) ppm. **¹¹B NMR** (96.29 MHz, C₆D₆, 300 K, BF₃-Et₂O): δ = 87.1 (br s), 53.2 (br. s) ppm. **¹³C NMR** (100.61 MHz, C₆D₆, 300K, TMS): δ = 153.8 (s, Me₂N-PhC_{quart.}), 150.2, 146.5 (each s, DurC_{quart.}-B), 142.6 (s, Me₂N-PhCH), 134.0, 132.5, 132.2, 132.0 (each s, DurC_{quart.}Me), 130.7, (s, Me₂N-PhC_{quart.}-B) 130.1, 129.5, (each s, DurCH), 111.2 (s, Me₂N-PhCH), 45.2, 41.0 (each s, (CH₃)₂N), 39.4 (s, (CH₃)₂N-Ph), 19.9, 19.6, 19.2, 18.5 (each s, Dur-CH₃) ppm. **UV/Vis** (hexane): λ_{max} = 337 nm (ε = 44020 L mol⁻¹ cm⁻¹), 242 nm (ε = 15780 L mol⁻¹ cm⁻¹). **Elemental analysis:** C₃₀H₄₂B₂N₂ (452.30); C 79.39 (calc. 79.67); H 9.20 (9.36); N 5.83 (6.19) %. **MP:** 152-157°C (stable).

5. Experimental Section

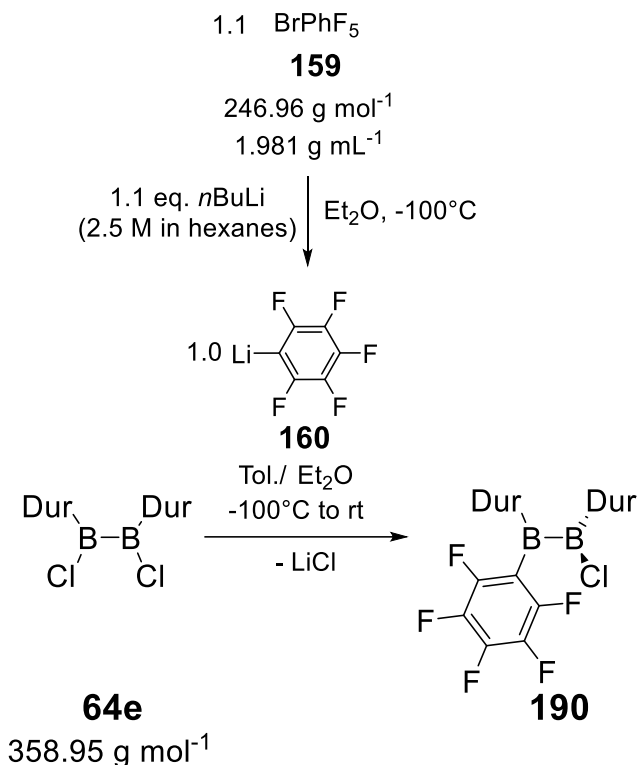
5.9.5 Attempted Synthesis of 1-para-*N,N*-dimethylaniline-2-pentafluorophenyl-1,2-(2,3,5,6-tetramethylphenyl) diborane(4) **189**



YK188_2: Bromopentafluorobenzene (degassed, 0.025 mL, 0.199 mmol, 1.05 eq.) is dissolved in Et₂O (5 mL) and cooled to -100°C (ethanol/ liquid nitrogen) before *n*butyl lithium solution (2.5 M in hexanes, 0.08 mL, 0.208 mmol, 1.1 eq.) is added. Stirring is continued for 45 minutes at -100°C. Diborane(4) **187** (84 mg, 0.189 mmol, 1 eq.) is dissolved in Et₂O (5 mL) and cooled to -100°C (ethanol/ liquid nitrogen). The diborane(4)-solution (**187**) is transferred to the anion solution *via cannula* and the reaction mixture is allowed to warm slowly to room temperature overnight. An NMR sample is analyzed. ¹H and ¹¹B NMR spectra show resonances of the starting material and unidentified decomposition products of the anion.

5. Experimental Section

5.9.6 Synthesis of 2-chloro-1-pentafluorophenyl-1,2-(2,3,5,6-tetramethylphenyl) diborane(4) **190**



YK189_2: Bromopentafluorobenzene (degassed, 0.17 mL, 1.38 mmol, 1.0 eq.) is dissolved in Et₂O (30 mL) and cooled to -100°C (ethanol/ liquid nitrogen) before *n*butyl lithium solution (2.5 M in hexanes, 0.61 mL, 1.52 mmol, 1.1 eq.) is added. Stirring is continued for 30 minutes at -100°C. **64e** (495 mg, 1.38 mmol, 1 eq.) is dissolved in toluene (30 mL) and cooled to -100°C (ethanol/ liquid nitrogen). The diborane(4)-solution (**64e**) is transferred to the anion solution *via cannula* and the reaction mixture is allowed to warm slowly to -45°C. After stirring another hour at room temperature removal of solvent and volatile species *in vacuo* is followed by filtration from hexane. An NMR sample of the crude **190** is analyzed.

¹H NMR (300.13 MHz, C₆D₆, 300K, TMS): δ = 6.84, 6.82 (each s, altogether 2H, DurH), 2.00, 1.98, 1.90, 1.88 (each s, each 6H, Dur-CH₃) ppm. **¹¹B NMR** (96.29 MHz, C₆D₆, 343 K, BF₃-Et₂O): δ = 87.7 (s) ppm. **¹⁹F NMR** (282.40 MHz, C₆D₆, 300 K, CFCl₃): δ = -120.2--120.4 (m, 2F, F₅Ph-oE), -142.5 (tt, 1F, ³J_{F-F} = 21.1 Hz, ⁴J_{F-F} = 8.1 Hz, F₅Ph-pE), -160.7--160.9 (m, 2F, F₅Ph-mF) ppm.

6. Literature

- [1] Boron, *Encyclopedia Britannica*, **2020**,
<https://www.britannica.com/science/boron-chemical-element>,
Accessed 1st February 2021.
- [2] U.S. Geological Survey, *Mineral Commodity Summaries 2021: U.S. Geological Survey*, **2021**.
- [3] R. Thompson, *Pure Appl. Chem.* **1974**, 39, 547–559.
- [4] J. M. Scherer, *Semiconductor Industry: Wafer Fab Exhaust Management*, 1st edition, CRC Press, **2005**.
- [5] T. F. Cooke, *J. Am. Ceram. Soc.* **1991**, 12, 2959–2978.
- [6] D. Pico, C. Wilms, G. Seide, T. Gries, R. Kleinholz, H. Tiesler, *Ullmann's Encycl. Ind. Chem.*, Weinheim, Germany: Wiley-VCH Verlag GmbH & Co. KGaA, **2012**.
- [7] H. G. Pfaender, *Schott Guide to Glass*, Dordrecht : Springer Netherlands : Imprint : Springer, **1996**.
- [8] Y. G. Gogotsi, R. A. Andrievski, *Materials Science of Carbides, Nitrides and Borides*, Dordrecht : Springer Netherlands : Imprint : Springer, **1999**.
- [9] M. M. Balakrishnarajan, P. D. Pancharatna, R. Hoffmann, *New J. Chem.* **2007**, 31, 473–485.
- [10] V. V. Brazhkin, V. L. Solozhenko, *J. Appl. Phys.* **2019**, 125, 130901.
- [11] E. Negishi, M. J. Idacavage, *Formation of Carbon-Carbon and Carbon-Heteroatom Bonds via Organoboranes and Organoborates*, *Org. React.*, **1985**, 33.
- [12] H. C. Brown, *Tetrahedron* **1961**, 12, 117–138.
- [13] The Nobel Prize in Chemistry 1979. NobelPrize.org. Nobel Media AB 2021, <https://www.nobelprize.org/prizes/chemistry/1979/summary/>, Accessed 2nd Feb 2021
- [14] M. A. Légaré, C. Pranckevicius, H. Braunschweig, *Chem. Rev.* **2019**, 119, 8231–8261.

6. Literature

- [15] Y. Su, R. Kinjo, *Chem. Soc. Rev.* **2019**, *48*, 3613–3659.
- [16] Z. Huang, S. Wang, R. D. Dewhurst, N. V. Ignat'ev, M. Finze, H. Braunschweig, *Angew. Chem. Int. Ed.* **2020**, *59*, 8800–8816.
- [17] Z. Huang, S. Wang, R. D. Dewhurst, N. V. Ignat'ev, M. Finze, H. Braunschweig, *Angew. Chem.* **2020**, *132*, 8882–8900.
- [18] E. I. Negishi, *J. Chem. Educ.* **1975**, *52*, 159–165.
- [19] E. C. Neeve, S. J. Geier, I. A. I. Mkhaliid, S. A. Westcott, T. B. Marder, *Chem. Rev.* **2016**, *116*, 9091–9161.
- [20] G. R. Eaton, *J. Chem. Educ.* **1969**, *46*, 547–556.
- [21] B. Wrackmeyer, *Annual Reports on NMR Spectroscopy* **1988**, *20*, 61–203.
- [22] B. Wrackmeyer, *Modern Magnetic Resonance* **2008**, 455–457.
- [23] S. Hermanek, *Chem. Rev.* **1992**, *92*, 325–362.
- [24] B. R. Jefferson, M. F. Lappert, B. Prokai, B. P. Tilley, *J. Chem. Soc. A* **1966**, 1584–1590.
- [25] C. Ergezinger, F. Weller, K. Dehnicke, *Z. Naturforsch. 43b* **1988**, 1621–1627.
- [26] D. J. Brauer, S. Buchheim-Spiegel, H. Bürger, R. Gielen, G. Pawelke, J. Rothe, *Organometallics* **1997**, *16*, 5321–5330.
- [27] M. Findlater, N. J. Hill, A. H. Cowley, *Dalton Trans.* **2008**, 4419–4423.
- [28] C. Jones, D. P. Mills, A. Stasch, W. D. Woodul, *Main Group Chemistry* **2010**, *9*, 23–30.
- [29] M. R. Terry, L. A. Mercado, C. Kelley, G. L. Geoffroy, P. Nombel, N. Lugan, R. Mathieu, R. L. Ostrander, B. E. Owens-Waltermire, A. L. Rheingold, *Organometallics* **1994**, *13*, 843–865.
- [30] P. Blais, T. Chivers, A. Downard, M. Parvez, *Can. J. Chem.* **2000**, *78*, 10–15.
- [31] B. Wrackmeyer, H. E. Maisel, K. Wagner, *Chem. Heterocycl. Compd.*

6. Literature

- 2001**, 37, 1396–1404.
- [32] N. J. Hill, J. A. Moore, M. Findlater, A. H. Cowley, *Chem. Commun.* **2005**, 5462–5464.
- [33] N. J. Hill, M. Findlater, A. H. Cowley, *Dalton Trans.* **2005**, 3229–3234.
- [34] M. Findlater, N. J. Hill, A. H. Cowley, *Polyhedron* **2006**, 25, 983–988.
- [35] Y. Ishida, B. Donnadieu, G. Bertrand, *PNAS* **2006**, 103, 13585–13588.
- [36] G. A. Pierce, N. D. Coombs, D. J. Willock, J. K. Day, A. Stasch, S. Aldridge, *Dalton Trans.* **2007**, 4405–4412.
- [37] H. Braunschweig, R. D. Dewhurst, K. Schwab, K. Wagner, *Acta Cryst. E66* **2010**, o610.
- [38] M. A. Dureen, D. W. Stephan, *J. Am. Chem. Soc.* **2010**, 132, 13559–13568.
- [39] E. W. Y. Wong, D. Dange, L. Fohlmeister, T. J. Hadlington, C. Jones, *Aust. J. Chem.* **2013**, 66, 1144–1154.
- [40] A. R. Cabrera, R. S. Rojas, M. Valderrama, P. Plüss, H. Berke, C. G. Daniliuc, G. Kehr, G. Erker, *Dalton Trans.* **2015**, 44, 19606–19614.
- [41] M. H. Holthausen, M. Colussi, D. W. Stephan, *Chem. Eur. J.* **2015**, 21, 2193–2199.
- [42] A. Antiñolo, F. Carrillo-Hermosilla, R. Fernández-Galán, M. P. Montero-Rama, A. Ramos, E. Villaseñor, R. S. Rojas, A. Rodríguez-Diéguez, *Dalton Trans.* **2016**, 45, 15350–15363.
- [43] A. V. Protchenko, J. Urbano, J. A. B. Abdalla, J. Campos, D. Vidovic, A. D. Schwarz, M. P. Blake, P. Mountford, C. Jones, S. Aldridge, *Angew. Chem. Int. Ed.* **2017**, 56, 15098–15102.
- [44] A. V. Protchenko, J. Urbano, J. A. B. Abdalla, J. Campos, D. Vidovic, A. D. Schwarz, M. P. Blake, P. Mountford, C. Jones, S. Aldridge, *Angew. Chem.* **2017**, 129, 15294–15298.
- [45] A. Ramos, A. Antiñolo, F. Carrillo-Hermosilla, R. Fernández-Galán, M. D. P. Montero-Rama, E. Villaseñor, A. Rodríguez-Diéguez, D. García-Vivó,

6. Literature

- Dalton Trans.* **2017**, *46*, 10281–10299.
- [46] Z. Lu, N. J. Hill, M. Findlater, A. H. Cowley, *Inorg. Chim. Acta* **2007**, *360*, 1316–1322.
- [47] K. L. Bamford, D. W. Stephan, *Dalton Trans.* **2020**, *49*, 17571–17577.
- [48] G. A. Pierce, S. Aldridge, C. Jones, T. Gans-Eichler, A. Stasch, N. D. Coombs, D. J. Willock, *Angew. Chem. Int. Ed.* **2007**, *46*, 2043–2046.
- [49] G. A. Pierce, S. Aldridge, C. Jones, T. Gans-Eichler, A. Stasch, N. D. Coombs, D. J. Willock, *Angew. Chemie* **2007**, *119*, 2089–2092.
- [50] A. J. Arduengo, R. L. Harlow, M. Kline, *J. Am. Chem. Soc.* **1991**, *113*, 361–363.
- [51] S. P. Nolan, *N-Heterocyclic Carbenes: Effective Tools for Organometallic Synthesis*, Wiley-VCH Verlag GmbH & Co. KGaA, **2014**.
- [52] S. Díez-González, *N-Heterocyclic Carbenes: From Laboratory Curiosities to Efficient Synthetic Tools*, 2nd edition, Royal Society Of Chemistry, **2017**.
- [53] P. L. Arnold, I. J. Casely, *Chem. Rev.* **2009**, *109*, 3599–3611.
- [54] D. M. Flanigan, F. Romanov-Michailidis, N. A. White, T. Rovis, *Chem. Rev.* **2015**, *115*, 9307–9387.
- [55] V. Nesterov, D. Reiter, P. Bag, P. Frisch, R. Holzner, A. Porzelt, S. Inoue, *Chem. Rev.* **2018**, *118*, 9678–9842.
- [56] M. Asay, C. Jones, M. Driess, *Chem. Rev.* **2011**, *111*, 354–396.
- [57] C.-S. Wu, M.-D. Su, *J. Comput. Chem.* **2012**, *33*, 103–111.
- [58] C. Jones, P. C. Junk, J. A. Platts, A. Stasch, *J. Am. Chem. Soc.* **2006**, *128*, 2206–2207.
- [59] G. Jin, C. Jones, P. C. Junk, A. Stasch, W. D. Woodul, *New J. Chem.* **2008**, *32*, 835–842.
- [60] C. Jones, P. C. Junk, J. A. Platts, D. Rathmann, A. Stasch, *Dalton Trans.* **2005**, 2497–2499.
- [61] L. Denker, B. Trzaskowski, R. Frank, *Chem. Commun.* **2021**, *57*, 2816–

6. Literature

- 2819.
- [62] Y. Segawa, M. Yamashita, K. Nozaki, *Science* **2006**, *314*, 113–115.
- [63] Y. Segawa, M. Yamashita, K. Nozaki, *Angew. Chem. Int. Ed.* **2007**, *46*, 6710–6713.
- [64] Y. Segawa, M. Yamashita, K. Nozaki, *Angew. Chemie* **2007**, *119*, 6830–6833.
- [65] Y. Segawa, Y. Suzuki, M. Yamashita, K. Nozaki, *J. Am. Chem. Soc.* **2008**, *130*, 16069–16079.
- [66] M. Yamashita, Y. Suzuki, Y. Segawa, K. Nozaki, *Chem. Lett.* **2008**, *37*, 802–803.
- [67] E. S. Schmidt, A. Jockisch, H. Schmidbaur, *J. Am. Chem. Soc.* **1999**, *121*, 9758–9759.
- [68] E. S. Schmidt, A. Schier, H. Schmidbaur, *J. Am. Chem. Soc., Dalton Trans.* **2001**, 505–507.
- [69] R. J. Baker, R. D. Farley, C. Jones, M. Kloth, D. M. Murphy, *J. Am. Chem. Soc., Dalton Trans.* **2002**, 3844–3850.
- [70] R. J. Baker, C. Jones, D. P. Mills, G. A. Pierce, M. Waugh, *Inorg. Chim. Acta* **2008**, *361*, 427–435.
- [71] Y. Liu, S. Li, X. Yang, Q. Li, Y. Xie, H. F. Schaefer, B. Wu, *J. Organomet. Chem.* **2011**, *696*, 1450–1455.
- [72] I. L. Fedushkin, A. N. Lukoyanov, G. K. Fukin, S. Y. Ketkov, M. Hummert, H. Schumann, *Chem. Eur. J.* **2008**, *14*, 8465–8468.
- [73] I. L. Fedushkin, A. N. Lukoyanov, A. N. Tishkina, G. K. Fukin, K. A. Lyssenko, M. Hummert, *Chem. Eur. J.* **2010**, *16*, 7563–7571.
- [74] C. Cui, H. W. Roesky, H. Schmidt, M. Noltemeyer, H. Hao, F. Cimpoesu, *Angew. Chem. Int. Ed.* **2000**, *39*, 4274–4276.
- [75] C. Cui, H. W. Roesky, H. Schmidt, M. Noltemeyer, H. Hao, F. Cimpoesu, *Angew. Chemie* **2000**, *112*, 4444–4446.
- [76] X. Li, X. Cheng, H. Song, C. Cui, *Organometallics* **2007**, *26*, 1039–1043.

6. Literature

- [77] O. Kysliak, H. Görls, R. Kretschmer, *Dalton Trans.* **2020**, 49, 6377–6383.
- [78] N. J. Hardman, B. E. Eichler, P. P. Power, *Chem. Commun.* **2000**, 1991–1992.
- [79] M. S. Hill, P. B. Hitchcock, *Chem. Commun.* **2004**, 1818–1819.
- [80] M. S. Hill, P. B. Hitchcock, R. Pongtavornpinyo, *Angew. Chem. Int. Ed.* **2005**, 44, 4231–4235.
- [81] M. S. Hill, P. B. Hitchcock, R. Pongtavornpinyo, *Angew. Chem.* **2005**, 117, 4303–4307.
- [82] M. S. Hill, P. B. Hitchcock, R. Pongtavornpinyo, *Dalton Trans.* **2005**, 273–277.
- [83] X. Dai, T. H. Warren, *Chem. Commun.* **2001**, 1998–1999.
- [84] Y. Cheng, P. B. Hitchcock, M. F. Lappert, M. Zhou, *Chem. Commun.* **2005**, 752–754.
- [85] Z. J. Tonzetich, A. J. Jiang, R. R. Schrock, P. Müller, *Organometallics* **2007**, 26, 3771–3783.
- [86] M. Reiher, A. Sundermann, *Eur. J. Inorg. Chem.* **2002**, 1854–1863.
- [87] C. Chen, M. Tsai, M. Su, *Organometallics* **2006**, 25, 2766–2773.
- [88] E. Firinci, J. I. Bates, I. M. Riddlestone, N. Phillips, S. Aldridge, *Chem. Commun.* **2013**, 49, 1509–1511.
- [89] P. Bharadwaz, A. K. Phukan, *Inorg. Chem.* **2019**, 58, 5428–5432.
- [90] H. Endemann, *J. Am. Chem. Soc.* **1880**, 2, 366–371.
- [91] G. Urry, T. Wartik, R. E. Moore, H. I. Schlesinger, *J. Am. Chem. Soc.* **1954**, 76, 5293–5298.
- [92] R. J. Brotherton, A. L. McCloskey, *J. Am. Chem. Soc.* **1960**, 82, 6242–6245.
- [93] H. Nöth, W. Meister, *Zeitschrift für Naturforsch. B* **1962**, 17, 714–718.
- [94] W. Nöth, H. ; Schick, H.; Meister, *J. Organomet. Chem.* **1964**, 1, 401–410.

6. Literature

- [95] A. Moezzi, M. M. Olmstead, P. P. Power, *J. Chem. Soc. Dalton Trans.* **1992**, 2429–2434.
- [96] W. Biffar, H. Nöth, H. Pommerening, *Angew. Chem. Int. Ed. Engl.* **1980**, *19*, 56–57.
- [97] W. Biffar, H. Nöth, H. Pommerening, *Angew. Chem.* **1980**, *92*, 63–64.
- [98] R. Hunold, *PhD Thesis, Philipps-University Marburg, Germany* **1988**.
- [99] G. Knörzer, H. Seyffer, H. Pritzkow, W. Siebert, *Z. Naturforsch. B* **1990**, *45*, 985–988.
- [100] A. Moezzi, R. A. Bartlett, P. P. Power, *Angew. Chem. Int. Ed. Engl.* **1992**, *31*, 1082–1083.
- [101] A. Moezzi, R. A. Bartlett, P. P. Power, *Angew. Chemie* **1992**, *104*, 1075–1076.
- [102] P. P. Power, *Inorg. Chim. Acta* **1992**, *198*, 443–447.
- [103] J. Knizek, I. Krossing, H. Nöth, W. Ponikwar, *Eur. J. Inorg. Chem.* **1998**, 505–509.
- [104] H. Hommer, H. Nöth, J. Knizek, W. Ponikwar, H. Schwenk-Kircher, *Eur. J. Inorg. Chem.* **1998**, *2*, 1519–1527.
- [105] A. Rodriguez, G. Fuks, J.-B. Bourg, D. Bourissou, F. S. Tham, G. Bertrand, *Dalton Trans.* **2008**, 4482–4487.
- [106] H. Braunschweig, M. Gross, K. Hammond, M. Friedrich, M. Kraft, A. Oechsner, K. Radacki, S. Stellweg, *Chem. Eur. J.* **2008**, *14*, 8972–8979.
- [107] H. Braunschweig, T. Kupfer, J. Mies, A. Oechsner, *Eur. J. Inorg. Chem.* **2009**, 2844–2850.
- [108] H. Braunschweig, A. Damme, *Acta Crystallogr. E66* **2010**, o3367.
- [109] H. Braunschweig, R. Dörfler, J. Mies, A. Oechsner, *Chem. Eur. J.* **2011**, *17*, 12101–12107.
- [110] S. R. Wang, M. Arrowsmith, J. Böhnke, H. Braunschweig, T. Dellermann, R. D. Dewhurst, H. Kelch, I. Krummenacher, J. D. Mattock, J. H. Müssig, T. Thiess, A. Vargas, J. Zhang, *Angew. Chem. Int. Ed.* **2017**, *56*, 8009–

6. Literature

8013.

- [111] S. R. Wang, M. Arrowsmith, J. Böhnke, H. Braunschweig, T. Dellermann, R. D. Dewhurst, H. Kelch, I. Krummenacher, J. D. Mattock, J. H. Müssig, T. Thiess, A. Vargas, J. Zhang, *Angew. Chem.* **2017**, *129*, 8122–8126.
- [112] A. Rodriguez, F. S. Tham, W. W. Schoeller, G. Bertrand, *Angew. Chem. Int. Ed.* **2004**, *43*, 4876–4880.
- [113] A. Rodriguez, F. S. Tham, W. W. Schoeller, G. Bertrand, *Angew. Chem.* **2004**, *116*, 4984–4988.
- [114] H. Nöth, M. Wagner, *Chem. Ber.* **1991**, *124*, 1963–1972.
- [115] H. Nöth, P. Fritz, *Angew. Chem.* **1961**, *73*, 408.
- [116] R. J. Brotherton, H. M. Manasevit, A. L. McCloskey, *Inorg. Chem.* **1962**, *1*, 749–754.
- [117] A. Moezzi, M. M. Olmstead, P. P. Power, *J. Am. Chem. Soc.* **1992**, *114*, 2715–2717.
- [118] K. Schlüter, A. Berndt, *Angew. Chem. Int. Ed. Engl.* **1980**, *19*, 57–58.
- [119] K. Schlüter, A. Berndt, *Angew. Chem.* **1980**, *92*, 64–65.
- [120] A. Moezzi, M. M. Olmstead, R. A. Bartlett, P. P. Power, *Organometallics* **1992**, *11*, 2383–2388.
- [121] W. J. Grigsby, P. Power, *Chem. Eur. J.* **1997**, *3*, 368–375.
- [122] N. Tsukahara, H. Asakawa, K. H. Lee, Z. Lin, M. Yamashita, *J. Am. Chem. Soc.* **2017**, *139*, 2593–2596.
- [123] F. Ge, X. Tao, C. G. Daniliuc, G. Kehr, G. Erker, *Angew. Chem. Int. Ed.* **2018**, *57*, 14570–14574.
- [124] F. Ge, X. Tao, C. G. Daniliuc, G. Kehr, G. Erker, *Angew. Chem.* **2018**, *130*, 14778–14782.
- [125] B. Riegel, G. Heckmann, H.-D. Hausen, W. Schwarz, H. Binder, E. Fluck, S. Grundei, H. Nöth, M. Schmidt, M. L. McKee, A. Dransfeld, P. v. R. Schleyer, *Z. anorg. allg. Chem.* **1995**, *621*, 1111–1122.

6. Literature

- [126] A. Höfner, B. Ziegler, R. Hunold, P. Willershausen, W. Massa, A. Berndt, *Angew. Chem. Int. Ed. Engl.* **1991**, *30*, 594–596.
- [127] A. Höfner, B. Ziegler, R. Hunold, P. Willershausen, W. Massa, A. Berndt, *Angew. Chem.* **1991**, *103*, 580–582.
- [128] P. Bissinger, H. Braunschweig, A. Damme, R. D. Dewhurst, T. Kupfer, K. Radacki, K. Wagner, *J. Am. Chem. Soc.* **2011**, *133*, 19044–19047.
- [129] H. Braunschweig, A. Damme, J. O. C. Jimenez-Halla, T. Kupfer, K. Radacki, *Angew. Chem. Int. Ed.* **2012**, *51*, 6267–6271.
- [130] H. Braunschweig, A. Damme, J. O. C. Jimenez-Halla, T. Kupfer, K. Radacki, *Angew. Chem.* **2012**, *124*, 6372–6376.
- [131] H. Braunschweig, A. Damme, R. D. Dewhurst, T. Kramer, T. Kupfer, K. Radacki, E. Siedler, A. Trumpp, K. Wagner, C. Werner, *J. Am. Chem. Soc.* **2013**, *135*, 8702–8707.
- [132] N. Arnold, H. Braunschweig, R. D. Dewhurst, F. Hupp, K. Radacki, A. Trumpp, *Chem. Eur. J.* **2016**, *22*, 13927–13934.
- [133] D. Loderer, H. Nöth, H. Pommerening, W. Rattay, H. Schick, *Chem. Ber.* **1994**, *127*, 1605–1611.
- [134] S. Uyanık, H. C. Söyleyici, A. G. Gökçe, E. Fırıncı, O. Burgaz, M. Aygün, Y. Şahin, *Polyhedron* **2017**, *123*, 145–151.
- [135] M. Arrowsmith, H. Braunschweig, K. Radacki, T. Thiess, A. Turkin, *Chem. Eur. J.* **2017**, *23*, 2179–2184.
- [136] X. Xie, M. F. Haddow, S. M. Mansell, N. C. Norman, C. A. Russell, *Dalton Trans.* **2012**, *41*, 2140–2147.
- [137] H. C. Söyleyici, S. Uyanık, R. Sevinçek, E. Fırlıncı, B. Bursalı, O. Burgaz, M. Aygün, Y. Şahin, *Inorg. Chem. Commun.* **2015**, *61*, 214–216.
- [138] T. Thiess, M. Ernst, T. Kupfer, H. Braunschweig, *Chem. Eur. J.* **2020**, *26*, 2967–2972.
- [139] M. A. M. Alibadi, A. S. Batsanov, G. Bramham, J. P. H. Charmant, M. F. Haddow, L. MacKay, S. M. Mansell, J. E. Mcgrady, N. C. Norman, A.

6. Literature

- Roffey, C. A. Russell, *Dalton Trans.* **2009**, 5348–5354.
- [140] X. Xie, C. J. Adams, M. A. M. Al-Ibadi, J. E. McGrady, N. C. Norman, C. A. Russell, *Chem. Commun.* **2013**, 49, 10364–10366.
- [141] P. Bissinger, H. Braunschweig, A. Damme, T. Kupfer, I. Krummenacher, A. Vargas, *Angew. Chem. Int. Ed.* **2014**, 53, 5689–5693.
- [142] P. Bissinger, H. Braunschweig, A. Damme, T. Kupfer, I. Krummenacher, A. Vargas, *Angew. Chem.* **2014**, 126, 5797–5801.
- [143] P. Bissinger, H. Braunschweig, A. Damme, C. Hörl, I. Krummenacher, T. Kupfer, *Angew. Chem. Int. Ed.* **2015**, 54, 359–362.
- [144] P. Bissinger, H. Braunschweig, A. Damme, C. Hörl, I. Krummenacher, T. Kupfer, *Angew. Chem.* **2015**, 127, 366–369.
- [145] A. Hermann, F. Fantuzzi, M. Arrowsmith, T. Zorn, I. Krummenacher, B. Ritschel, K. Radacki, B. Engels, H. Braunschweig, *Angew. Chem. Int. Ed.* **2020**, 59, 15717–15725.
- [146] A. Hermann, F. Fantuzzi, M. Arrowsmith, T. Zorn, I. Krummenacher, B. Ritschel, K. Radacki, B. Engels, H. Braunschweig, *Angew. Chem.* **2020**, 132, 15847–15855.
- [147] R. C. Fischer, P. P. Power, *Chem. Rev.* **2010**, 110, 3877–3923.
- [148] H. Braunschweig, R. D. Dewhurst, *Angew. Chem. Int. Ed.* **2013**, 52, 3574–3583.
- [149] H. Braunschweig, R. D. Dewhurst, *Angew. Chem.* **2013**, 125, 3658–3667.
- [150] H. Braunschweig, R. D. Dewhurst, *Organometallics* **2014**, 33, 6271–6277.
- [151] Y. Su, R. Kinjo, *Coord. Chem. Rev.* **2017**, 352, 346–378.
- [152] M. Arrowsmith, H. Braunschweig, T. E. Stennett, *Angew. Chem. Int. Ed.* **2017**, 56, 96–115.
- [153] M. Arrowsmith, H. Braunschweig, T. E. Stennett, *Angew. Chem.* **2017**, 129, 100–120.
- [154] H. Budy, J. Gilmer, T. Trageser, M. Wagner, *Eur. J. Inorg. Chem.* **2020**, 4148–4162.

6. Literature

- [155] H. Klusik, A. Berndt, *Angew. Chem. Int. Ed. Engl.* **1981**, *20*, 870–871.
- [156] H. Klusik, A. Berndt, *Angew. Chem.* **1981**, *93*, 903–904.
- [157] H. Klusik, A. Berndt, *J. Organomet. Chem.* **1982**, *232*, C21–C23.
- [158] W. J. Grigsby, P. P. Power, *Chem. Commun.* **1996**, 2235–2236.
- [159] H. Asakawa, K. H. Lee, K. Furukawa, Z. Lin, M. Yamashita, *Chem. Eur. J.* **2015**, *21*, 4267–4271.
- [160] S. Akiyama, K. Yamada, M. Yamashita, *Angew. Chem. Int. Ed.* **2019**, *58*, 11806–11810.
- [161] S. Akiyama, K. Yamada, M. Yamashita, *Angew. Chem.* **2019**, *131*, 11932–11936.
- [162] Y. Shiota, M. Kinoshita, T. Noda, K. Okumoto, T. Ohara, *J. Am. Chem. Soc.* **2000**, *122*, 11021–11022.
- [163] H. Doi, M. Kinoshita, K. Okumoto, Y. Shiota, *Chem. Mater.* **2003**, *15*, 1080–1089.
- [164] D. Mutaguchi, K. Okumoto, Y. Ohseido, K. Moriwaki, Y. Shiota, *Org. Electron.* **2003**, *4*, 49–59.
- [165] W. L. Jia, D. R. Bai, T. McCormick, Q. De Liu, M. Motala, R. Y. Wang, C. Seward, Y. Tao, S. Wang, *Chem. Eur. J.* **2004**, *10*, 994–1006.
- [166] W. L. Jia, X. D. Feng, D. R. Bai, Z. H. Lu, S. Wang, G. Vamvounis, *Chem. Mater.* **2005**, *17*, 164–170.
- [167] W. L. Jia, M. J. Moran, Y. Y. Yuan, Z. H. Lu, S. Wang, *J. Mater. Chem.* **2005**, *15*, 3326–3333.
- [168] F. Li, W. Jia, S. Wang, Y. Zhao, Z. H. Lu, *J. Appl. Phys.* **2008**, *103*, 034509.
- [169] Z. Chen, X. K. Liu, C. J. Zheng, J. Ye, C. L. Liu, F. Li, X. M. Ou, C. S. Lee, X. H. Zhang, *Chem. Mater.* **2015**, *27*, 5206–5211.
- [170] G. Turkoglu, M. E. Cinar, T. Ozturk, *Molecules* **2017**, *22*, 1522–1545.
- [171] J. C. Doty, B. Babb, P. J. Grisdale, M. Glogowski, J. L. R. Williams, *J.*

6. Literature

Organomet. Chem. **1972**, *38*, 229–236.

- [172] W. Kaim, A. Schulz, *Angew. Chem. Int. Ed. Engl.* **1984**, *23*, 615–616.
- [173] W. Kaim, A. Schulz, *Angew. Chem.* **1984**, *96*, 611–612.
- [174] Z. Yuan, N. J. Taylor, T. B. Marder, I. D. Williams, S. K. Kurtz, L.-T. Cheng, *J. Chem. Soc., Chem. Commun.* **1990**, 1489–1492.
- [175] Z. Yuan, N. J. Taylor, R. Ramachandran, T. B. Marder, *Appl. Organomet. Chem.* **1996**, *10*, 305–316.
- [176] Z. Yuan, J. C. Collings, N. J. Taylor, T. B. Marder, C. Jardin, J. F. Halet, *J. Solid State Chem.* **2000**, *154*, 5–12.
- [177] M. Charlot, L. Porrès, C. D. Entwistle, A. Beeby, T. B. Marder, M. Blanchard-Desce, *Phys. Chem. Chem. Phys.* **2005**, *7*, 600–606.
- [178] Z. Yuan, C. D. Entwistle, J. C. Collings, D. Albesa-Jové, A. S. Batsanov, J. A. K. Howard, N. J. Taylor, H. M. Kaiser, D. E. Kaufmann, S. Y. Poon, W.-Y. Wong, C. Jardin, S. Fathallah, A. Boucekkine, J.-F. Halet, T. B. Marder, *Chem. Eur. J.* **2006**, *12*, 2758–2771.
- [179] J. C. Collings, S. Y. Poon, C. Le Droumaguet, M. Charlot, C. Katan, L. O. Pålsson, A. Beeby, J. A. Mosely, H. M. Kaiser, D. Kaufmann, W. Y. Wong, M. Blanchard-Desce, T. B. Marder, *Chem. Eur. J.* **2009**, *15*, 198–208.
- [180] C. D. Entwistle, J. C. Collings, A. Steffen, L. O. Pålsson, A. Beeby, D. Albesa-Jové, J. M. Burke, A. S. Batsanov, J. A. K. Howard, J. A. Mosely, S. Y. Poon, W. Y. Wong, F. Ibersiene, S. Fathallah, A. Boucekkine, J. F. Halet, T. B. Marder, *J. Mater. Chem.* **2009**, *19*, 7532–7544.
- [181] Y. Chen, D. Cao, S. Wang, C. Zhang, Z. Liu, *J. Mol. Struct.* **2010**, *969*, 182–186.
- [182] J. Ohshita, Y. Tominaga, D. Tanaka, Y. Ooyama, T. Mizumo, N. Kobayashi, H. Higashimura, *Dalton Trans.* **2013**, *42*, 3646–3652.
- [183] L. Ji, R. M. Edkins, L. J. Sewell, A. Beeby, A. S. Batsanov, K. Fucke, M. Drafz, J. A. K. Howard, O. Moutounet, F. Ibersiene, A. Boucekkine, E. Furet, Z. Liu, J. F. Halet, C. Katan, T. B. Marder, *Chem. Eur. J.* **2014**, *20*,

6. Literature

13618–13635.

- [184] L. Ji, R. M. Edkins, A. Lorbach, I. Krummenacher, C. Brückner, A. Eichhorn, H. Braunschweig, B. Engels, P. J. Low, T. B. Marder, *J. Am. Chem. Soc.* **2015**, *137*, 6750–6753.
- [185] B. Chen, G. Feng, B. He, C. Goh, S. Xu, G. Ramos-Ortiz, L. Aparicio-Ixta, J. Zhou, L. Ng, Z. Zhao, B. Liu, B. Z. Tang, *Small* **2016**, *12*, 782–792.
- [186] G. Turkoglu, M. E. Cinar, T. Ozturk, *Eur. J. Org. Chem.* **2017**, 4552–4561.
- [187] J. Merz, J. Fink, A. Friedrich, I. Krummenacher, H. H. Al Mamari, S. Lorenzen, M. Haehnel, A. Eichhorn, M. Moos, M. Holzapfel, H. Braunschweig, C. Lambert, A. Steffen, L. Ji, T. B. Marder, *Chem. Eur. J.* **2017**, *23*, 13164–13180.
- [188] J. He, F. Rauch, A. Friedrich, D. Sieh, T. Ribbeck, I. Krummenacher, H. Braunschweig, M. Finze, T. B. Marder, *Chem. Eur. J.* **2019**, *25*, 13777–13784.
- [189] J. Merz, M. Dietz, Y. Vonhausen, F. Wöber, A. Friedrich, D. Sieh, I. Krummenacher, H. Braunschweig, M. Moos, M. Holzapfel, C. Lambert, T. B. Marder, *Chem. Eur. J.* **2020**, *26*, 438–453.
- [190] M. P. Coles, R. F. Jordan, *J. Am. Chem. Soc.* **1997**, *119*, 8125–8126.
- [191] Y. Lei, F. Chen, Y. Luo, P. Xu, Y. Wang, Y. Zhang, *Inorg. Chim. Acta* **2011**, *368*, 179–186.
- [192] D. O. Meléndez, J. A. Castro-Osma, A. Lara-Sánchez, R. S. Rojas, A. Otero, *J. Polym. Sci. Part A Polym. Chem.* **2017**, *55*, 2397–2407.
- [193] J. Grundy, M. P. Coles, P. B. Hitchcock, *J. Organomet. Chem.* **2002**, *662*, 178–187.
- [194] R. T. Boéré, V. Klassen, G. Wolmershäuser, *J. Chem. Soc., Dalton Trans.* **1998**, 4147–4154.
- [195] C. Loh, S. Seupel, H. Görls, S. Kriek, M. Westerhausen, *Eur. J. Inorg. Chem.* **2014**, 1312–1321.
- [196] J. Barker, M. Kilner, *Coord. Chem. Rev.* **1994**, *133*, 219–300.

6. Literature

- [197] M. L. Cole, A. J. Davies, C. Jones, P. C. Junk, *New J. Chem.* **2005**, *29*, 1404–1408.
- [198] C. Jones, P. C. Junk, J. A. Platts, D. Rathmann, A. Stasch, *Dalton Trans.* **2005**, 2497–2499.
- [199] P. C. Junk, M. L. Cole, *Chem. Commun.* **2007**, 1579–1590.
- [200] F. T. Edelmann, *Adv. Organomet. Chem.* **2008**, *57*, 183–352.
- [201] A. Stasch, C. Jones, *Dalton Trans.* **2011**, *40*, 5659–5672.
- [202] C. S. Wu, M.-D. Su, *J. Comput. Chem.* **2012**, *33*, 103–111.
- [203] S. Muthaiah, D. C. H. Do, R. Ganguly, D. Vidović, *Organometallics* **2013**, *32*, 6718–6724.
- [204] M. Hejda, A. Lyčka, R. Jambor, A. Růžička, L. Dostál, *Dalton Trans.* **2013**, *42*, 6417–6428.
- [205] M. Hejda, A. Lyčka, R. Jambor, A. Růžička, L. Dostál, *Dalton Trans.* **2014**, *43*, 12678–12688.
- [206] A. Sidiropoulos, A. Stasch, C. Jones, *Main Group Met. Chem.* **2019**, *42*, 121–124.
- [207] M.-T. Chen, K.-M. Wu, C.-T. Chen, *Eur. J. Inorg. Chem.* **2012**, 720–726.
- [208] H. Cui, J. Zhang, C. Cui, *Organometallics* **2013**, *32*, 1–4.
- [209] A. Jana, V. Huch, H. S. Rzepa, D. Scheschkewitz, *Angew. Chem. Int. Ed.* **2015**, *54*, 289–292.
- [210] A. Jana, V. Huch, H. S. Rzepa, D. Scheschkewitz, *Angew. Chem.* **2015**, *127*, 291–295.
- [211] D. Reiter, R. Holzner, A. Porzelt, P. J. Altmann, P. Frisch, S. Inoue, *J. Am. Chem. Soc.* **2019**, *141*, 13536–13546.
- [212] D. Dhara, S. Das, P. Kalita, A. Maiti, S. K. Pati, D. Scheschkewitz, V. Chandrasekhar, A. Jana, *Dalton Trans.* **2020**, *49*, 993–997.
- [213] D. Reiter, P. Frisch, D. Wendel, F. M. Hörmann, S. Inoue, *Dalton Trans.* **2020**, *49*, 7060–7068.

6. Literature

- [214] M. Reuman, A. I. Meyers, *Tetrahedron* **1985**, *41*, 837–860.
- [215] T. G. Gant, A. I. Meyers, *Tetrahedron* **1994**, *50*, 2297–2360.
- [216] A. I. Meyers, *J. Heterocycl. Chem.* **1998**, *35*, 991–1002.
- [217] F. L. Ortiz, M. J. Iglesias, I. Fernández, C. M. A. Sánchez, G. R. Gómez, *Chem. Rev.* **2007**, *107*, 1580–1691.
- [218] W. C. Wertjes, E. H. Southgate, D. Sarlah, *Chem. Soc. Rev.* **2018**, *47*, 7996–8017.
- [219] D. Scheschkewitz, *Angew. Chem. Int. Ed.* **2004**, *43*, 2965–2967.
- [220] D. Scheschkewitz, *Angew. Chem.* **2004**, *116*, 3025–3028.
- [221] K. Anton, H. Fußstetter, H. Nöth, *Chem. Ber.* **1984**, *117*, 2542–2546.
- [222] P. Y. Chavant, M. Vaultier, *J. Organomet. Chem.* **1993**, *455*, 37–46.
- [223] C. D. Entwistle, T. B. Marder, *Angew. Chem. Int. Ed.* **2002**, *41*, 2927–2931.
- [224] C. D. Entwistle, T. B. Marder, *Angew. Chem.* **2002**, *114*, 3051–3056.
- [225] C. D. Entwistle, T. B. Marder, *Chem. Mater.* **2004**, *16*, 4574–4585.
- [226] S. Yamaguchi, A. Wakamiya, *Pure Appl. Chem.* **2006**, *78*, 1413–1424.
- [227] F. Jäkle, *Coord. Chem. Rev.* **2006**, *250*, 1107–1121.
- [228] Y. Ren, F. Jäkle, *Dalton Trans.* **2016**, *45*, 13996–14007.
- [229] L. Ji, S. Griesbeck, T. B. Marder, *Chem. Sci.* **2017**, *8*, 846–863.
- [230] S. Y. Li, Z. B. Sun, C. H. Zhao, *Inorg. Chem.* **2017**, *56*, 8705–8717.
- [231] T. W. Hudnall, C. W. Chiu, F. P. Gabbaï, *Acc. Chem. Res.* **2009**, *42*, 388–397.
- [232] C. R. Wade, A. E. J. Broomsgrove, S. Aldridge, F. P. Gabbaï, *Chem. Rev.* **2010**, *110*, 3958–3984.
- [233] F. Jäkle, *Chem. Rev.* **2010**, *110*, 3985–4022.
- [234] Z. M. Hudson, S. Wang, *Acc. Chem. Res.* **2009**, *42*, 1584–1596.

6. Literature

- [235] S. Griesbeck, Z. Zhang, M. Gutmann, T. Lühmann, R. M. Edkins, G. Clermont, A. N. Lazar, M. Haehnel, K. Edkins, A. Eichhorn, M. Blanchard-Desce, L. Meinel, T. B. Marder, *Chem. Eur. J.* **2016**, *22*, 14701–14706.
- [236] S. Griesbeck, M. Ferger, C. Czernetzi, C. Wang, R. Bertermann, A. Friedrich, M. Haehnel, D. Sieh, M. Taki, S. Yamaguchi, T. B. Marder, *Chem. Eur. J.* **2019**, *25*, 7679–7688.
- [237] S. Griesbeck, E. Michail, C. Wang, H. Ogasawara, S. Lorenzen, L. Gerstner, T. Zang, J. Nitsch, Y. Sato, R. Bertermann, M. Taki, C. Lambert, S. Yamaguchi, T. B. Marder *Chem. Sci.* **2019**, *10*, 5405–5422.
- [238] S. Griesbeck, E. Michail, F. Rauch, H. Ogasawara, C. Wang, Y. Sato, R. M. Edkins, Z. Zhang, M. Taki, C. Lambert, S. Yamaguchi, T. B. Marder, *Chem. Eur. J.* **2019**, *25*, 13164–13175.
- [239] Ž. Ban, S. Griesbeck, S. Tomić, J. Nitsch, T. B. Marder, I. Piantanida, *Chem. Eur. J.* **2020**, *26*, 2195–2203.
- [240] O. Kwon, S. Barlow, S. A. Odom, L. Beverina, N. J. Thompson, E. Zojer, J. L. Brédas, S. R. Marder, *J. Phys. Chem. A* **2005**, *109*, 9346–9352.
- [241] C. Branger, M. Lequan, R. M. Lequan, M. Barzoukas, A. Fort, *J. Mater. Chem.* **1996**, *6*, 555–558.
- [242] S. Bin Zhao, P. Wucher, Z. M. Hudson, T. M. McCormick, X.-Y. Liu, S. Wang, X.-D. Feng, Z.-H. Lu, *Organometallics* **2008**, *27*, 6446–6456.
- [243] A. G. Crawford, A. D. Dwyer, Z. Liu, A. Steffen, A. Beeby, L.-O. Pålsson, D. J. Tozer, T. B. Marder, *J. Am. Chem. Soc.* **2011**, *133*, 13349–13362.
- [244] A. G. Crawford, Z. Liu, I. A. I. Mkhaliid, M.-H. Thibault, N. Schwarz, G. Alcaraz, A. Steffen, J. C. Collings, A. S. Batsanov, J. A. K. Howard, T. B. Marder, *Chem. Eur. J.* **2012**, *18*, 5022–5035.
- [245] Z. Zhang, R. M. Edkins, J. Nitsch, K. Fucke, A. Eichhorn, A. Steffen, Y. Wang, T. B. Marder, *Chem. Eur. J.* **2015**, *21*, 177–190.
- [246] R. Kurata, A. Ito, M. Gon, K. Tanaka, Y. Chujo, *J. Org. Chem.* **2017**, *82*, 5111–5121.
- [247] N. Yuan, W. Wang, Y. Fang, J. Zuo, Y. Zhao, G. Tan, X. Wang,

6. Literature

Organometallics **2017**, *36*, 2498–2501.

- [248] L. Ji, I. Krummenacher, A. Friedrich, A. Lorbach, M. Haehnel, K. Edkins, H. Braunschweig, T. B. Marder, *J. Org. Chem.* **2018**, *83*, 3599–3606.
- [249] H. Xiang, J. Cheng, X. Ma, X. Zhou, J. J. Chruma, *Chem. Soc. Rev.* **2013**, *42*, 6128–6185.
- [250] L. Yuan, W. Lin, K. Zheng, L. He, W. Huang, *Chem. Soc. Rev.* **2013**, *42*, 622–661.
- [251] Z. Guo, S. Park, J. Yoon, I. Shin, *Chem. Soc. Rev.* **2014**, *43*, 16–29.
- [252] A. Barbieri, E. Bandini, F. Monti, V. K. Praveen, N. Armaroli, (2017) *The Rise of Near-Infrared Emitters: Organic Dyes, Porphyrinoids, and Transition Metal Complexes*. In: Armaroli N., Bolink H. (eds) *Photoluminescent Materials and Electroluminescent Devices*. Topics in Current Chemistry Collections. Springer, Cham.
- [253] T. E. Stennett, P. Bissinger, S. Griesbeck, S. Ullrich, I. Krummenacher, M. Auth, A. Sperlich, M. Stolte, K. Radacki, C.-J. Yao, F. Würthner, A. Steffen, T. B. Marder, H. Braunschweig, *Angew. Chem. Int. Ed.* **2019**, *58*, 6449–6454.
- [254] T. E. Stennett, P. Bissinger, S. Griesbeck, S. Ullrich, I. Krummenacher, M. Auth, A. Sperlich, M. Stolte, K. Radacki, C. Yao, F. Würthner, A. Steffen, T. B. Marder, H. Braunschweig, *Angew. Chem.* **2019**, *131*, 6516–6521.
- [255] Z. Zhang, R. M. Edkins, J. Nitsch, K. Fucke, A. Steffen, L. E. Longobardi, D. W. Stephan, C. Lambert, T. B. Marder, *Chem. Sci.* **2015**, *6*, 308–321.
- [256] A. Sundararaman, K. Venkatasubbaiah, M. Victor, L. N. Zakharov, A. L. Rheingold, F. Jäkle, *J. Am. Chem. Soc.* **2006**, *128*, 16554–16565.
- [257] A. Rodriguez, G. Fuks, J.-B. Bourg, D. Bourissou, F. S. Tham, G. Bertrand *Dalton Trans.* **2008**, 4482–4487.
- [258] J. de Jong, D. Heijnen, H. Helbert, B. L. Feringa, *Chem. Commun.* **2019**, *55*, 2908–2911.
- [259] M. E. Peover, B. S. White, *Electrochim. Acta* **1966**, *11*, 1061–1067.

6. Literature

- [260] T. Mizoguchi, R. N. Adams, *J. Am. Chem. Soc.* **1962**, *84*, 2058–2061.
- [261] H. Yang, D. O. Wipf, A. J. Bard, *J. Electroanal. Chem.* **1992**, *331*, 913–924.
- [262] N. Arnold, H. Braunschweig, A. Damme, R. D. Dewhurst, L. Pentecost, K. Radacki, S. Stellwag-Konertz, T. Thiess, A. Trumpp, A. Vargas, *Chem. Commun.* **2016**, *52*, 4898–4901.
- [263] P. L. Coe, R. Stephens, J. C. Tatlow, *J. Chem. Soc.* **1962**, 3227–3231.
- [264] W. E. Parham, R. M. Piccirilli, *J. Org. Chem.* **1976**, *41*, 1268–1269.
- [265] H. A. Brune, B. Stapp, G. Schmidtberg, *J. Organomet. Chem.* **1986**, *307*, 129–137.
- [266] D. Tian, J. Jiang, H. Hu, J. Zhang, C. Cui, *J. Am. Chem. Soc.* **2012**, *134*, 14666–14669.
- [267] L. Weber, J. Halama, L. Böhling, A. Brockhinke, A. Chrostowska, C. Darrigan, A. Dargelos, H. G. Stammler, B. Neumann, *Eur. J. Inorg. Chem.* **2013**, 4268–4279.
- [268] L. Weber, J. Halama, K. Hanke, L. Böhling, A. Brockhinke, H.-G. Stammler, B. Neumann, M. A. Fox, *Dalton Trans.* **2014**, *43*, 3347–3363.
- [269] L. Weber, D. Eickhoff, A. Chrostowska, C. Darrigan, H.-G. Stammler, B. Neumann, *Chemistry of Heterocyclic Compounds* **2017**, *53*, 54–65.
- [270] L. Weber, *Coord. Chem. Rev.* **2008**, *252*, 1–31.
- [271] L. Weber, L. Böhling, *Coord. Chem. Rev.* **2015**, *284*, 236–275.
- [272] J. C. del Valle, J. Catalán, *Phys. Chem. Chem. Phys.* **2019**, *21*, 10061–10069.
- [273] C. Präsang, Y. Sahin, M. Hofmann, G. Geiseler, W. Massa, A. Berndt, *Eur. J. Inorg. Chem.* **2004**, 3063–3073.
- [274] B. Valeur, M. N. Berberan-Santos, *Molecular Fluorescence*, Wiley-VCH Weinheim, **2013**.
- [275] S. Kundu, S. Sinhababu, V. Chandrasekhar, H. W. Roesky, *Chem. Sci.* **2019**, *10*, 4727–4741.

6. Literature

- [276] P. J. Bailey, A. J. Blake, M. Kryszczuk, S. Parsons, D. Reed, *J. Chem. Soc., Chem. Commun.* **1995**, 1647–1648.
- [277] A. L. Brazeau, M. M. Hänninen, H. M. Tuononen, N. D. Jones, P. J. Ragoona, *J. Am. Chem. Soc.* **2012**, *134*, 5398–5414.
- [278] M. Nutz, B. Borthakur, R. D. Dewhurst, A. Deißberger, T. Dellermann, M. Schäfer, I. Krummenacher, A. K. Phukan, H. Braunschweig, *Angew. Chem. Int. Ed.* **2017**, *56*, 7975–7979.
- [279] M. Nutz, B. Borthakur, R. D. Dewhurst, A. Deißberger, T. Dellermann, M. Schäfer, I. Krummenacher, A. K. Phukan, H. Braunschweig, *Angew. Chem.* **2017**, *129*, 8084–8089.
- [280] N. M. Obeid, L. Klemmer, D. Maus, M. Zimmer, J. Jeck, I. Bejan, A. J. P. White, V. Huch, G. Jung, D. Scheschkewitz, *Dalton Trans.* **2017**, *46*, 8839–8848.
- [281] N. Kuhn, T. Kratz, *Synthesis.* **1993**, 561–562.
- [282] Y. Soltani, L. C. Wilkins, R. L. Melen, *Angew. Chem. Int. Ed.* **2017**, *56*, 11995–11999.
- [283] Y. Soltani, L. C. Wilkins, R. L. Melen, *Angew. Chem.* **2017**, *129*, 12157–12161.
- [284] D. Oesch, N. W. Luedtke, *Chem. Commun.* **2015**, *51*, 12641–12644.
- [285] A. Ulman, *Acc. Chem. Res.* **2001**, *34*, 855–863.
- [286] G. J. Moxey, F. Ortu, L. G. Sidley, H. N. Strandberg, A. J. Blake, W. Lewis, D. L. Kays, *Dalton Trans.* **2014**, *43*, 4838–4846.
- [287] C. A. Nijhuis, E. Jellema, T. J. J. Sciarone, A. Meetsma, P. H. M. Budzelaar, B. Hessen, *Eur. J. Inorg. Chem.* **2005**, 2089–2099.
- [288] R. Soundararajan, D. S. Matteson, *Organometallics* **1995**, *14*, 4157–4166.
- [289] M. J. G. Lesley, N. C. Norman, C. R. Rice, D. W. Norman, R. T. Baker, *Inorganic Syntheses*, **2004**, *34*, 1-48.
- [290] A. J. Kendall, L. N. Zakharov, D. R. Tyler, *J. Inorg. Organomet. Polym.*

6. Literature

2016, 26, 1313–1319.

[291] S. Gendler, A. L. Zelikoff, J. Kopilov, I. Goldberg, M. Kol, *J. Am. Chem. Soc.* **2008**, 130, 2144–2145.

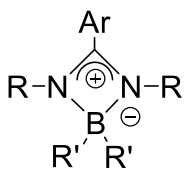
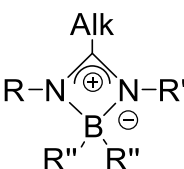
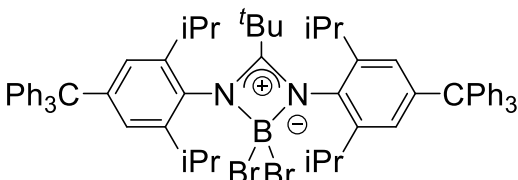
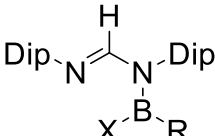
[292] V. Taberner, T. Cuenca, M. E. G. Mosquera, C. R. de Arellano, *Polyhedron* **2009**, 28, 2545–2554.

[293] H. Nöth, H. Pommerening, *Chem. Ber.* **1986**, 119, 2261–2271.

7. Appendix

7.1 Overview of numbered compounds

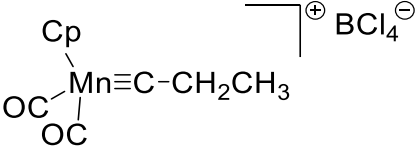
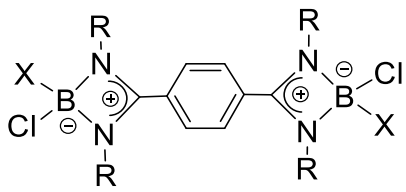
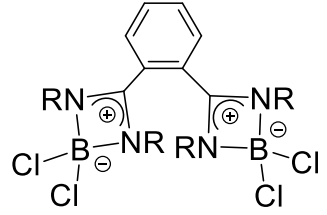
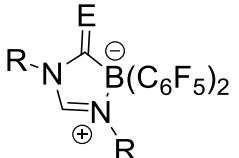
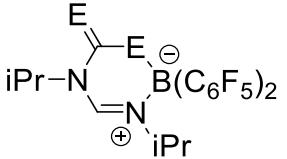
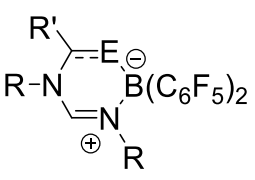
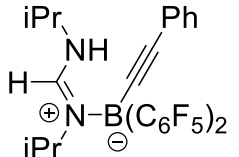
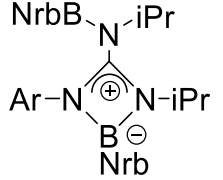
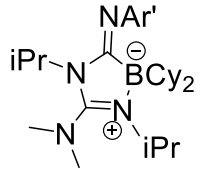
Table 5. Numbered compounds (introduction).

Compound	Number
	<p>1a: Ar = Ph, R = SiMe₃, R' = Br; 1b: Ar = Ph, R = SiMe₃, R' = Cl; 1c: Ar = Ph, R = Cy, R' = Cl; 1d: Ar = Ph, R = iPr, R' = Br; 1e: Ar = C₆F₅, R = ^tBu, R' = C₆F₅; 1f: Ar = C₆F₅, R = iPr, R' = C₆F₅; 1g: Ar = C₆F₅, R = SiMe₃, R' = C₆F₅; 1h: Ar = C₆F₅, R = Dip, R' = C₆F₅; 1i: Ar = Mes*, R = Cy, R' = Cl;</p>
	<p>3a: Alk = Me, R = R' = Cy, BR''₂ = BCl₂; 3b: Alk = Me, R = R' = iPr, BR''₂ = BCl₂; 3c: Alk = Me, R = Dip, R' = C₆F₅, BR''₂ = B(C₆F₅)₂; 3d: Alk = Me, R = Dip, R' = <i>p</i>-Ph-CN, BR''₂ = B(C₆F₅)₂; 3e: Alk = ⁿBu, R = R' = ^tBu, BR''₂ = BCIPh; 3f: Alk = ⁿBu, R = R' = Cy, BR''₂ = BCIPh; 3g: Alk = ^tBu, R = R' = Cy, BR''₂ = BCIPh; 3h: Alk = ^tBu, R = R' = 2,6-diisopropyl-4-tritylphenyl, BR''₂ = BBr₂</p>
	4
	5a: R = NiPr ₂ , X = Br; 5b: R = Ph, X = Cl;

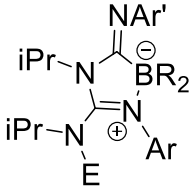
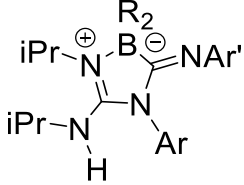
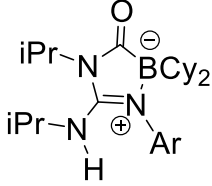
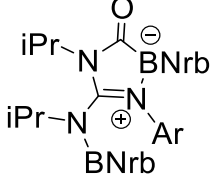
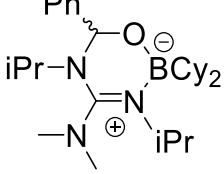
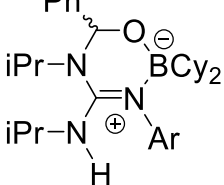
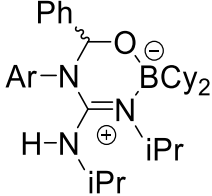
7. Appendix

	6a: R = <i>i</i> Pr; 6b: R = <i>t</i> Bu;
	7
	8
	9a: R = Me; 9b: R = SnMe ₃
	2 a: R = Me, R' = <i>i</i> Pr, R'' = CF ₃ ; 2b: R = Me, R' = Cy, R'' = CF ₃ ; 2c: R = Me, R' = Ph, R'' = CF ₃ ; 2d: R = Me, R' = <i>p</i> -Tol, R'' = CF ₃ ; 2e: R = Me, R' = <i>p</i> -MeO-Ph, R'' = CF ₃ ; 2f: R = Me, R' = Dip, R'' = Br; 2g: R = Me, R' = <i>i</i> Pr, R'' = Nrb; 2h: R = Me, R' = Cy, R'' = Nrb; 2i: R = Me, R' = <i>i</i> Pr, R'' = Cy; 2j: R = Me, R' = Cy, R'' = Cy; 2k: R = Me, R' = Dip, R'' = Cy; 2l: R = Ph, R' = Mes, R'' = Cl; 2m: R = Ph, R' = Dip, R'' = Cl; 2n: R = SiMe ₃ , R' = Cy, R'' = Cl; 2o: R = <i>i</i> Pr, R' = Dip, R'' = Br; 2p: R = Cy, R' = Dip, R'' = Br; 2q: R = <i>i</i> Pr, R' = Cy, R'' = Cl; 2r: R = Cy, R' = Cy, R'' = Cl;
	10a: R = <i>i</i> Pr, R' = H, R'' = <i>i</i> Pr, R''' = Ph; 10b: R = <i>i</i> Pr, R' = H, R'' = <i>i</i> Pr, R''' = <i>p</i> -Tol; 10c: R = <i>i</i> Pr, R' = H, R'' = <i>i</i> Pr, R''' = <i>p</i> -

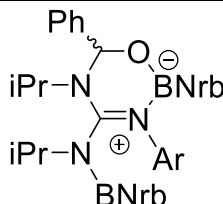
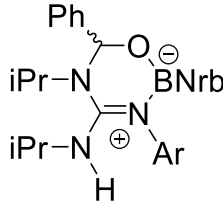
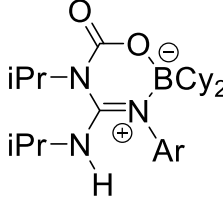
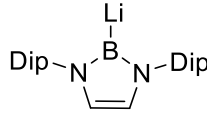
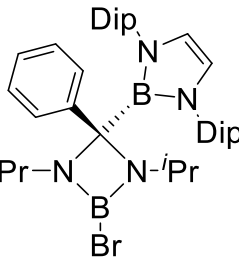
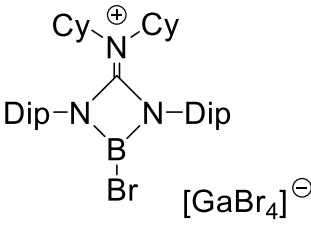
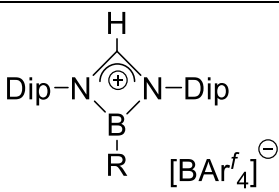
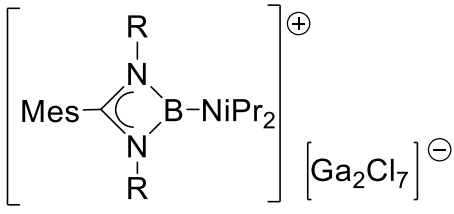
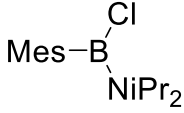

7. Appendix

	<p>^tBu-Ph; 10d: R = iPr, R' = BCy₂, R'' = iPr, R''' = <i>p</i>-^tBu-Ph.</p>
	11
	<p>12a: X = Cl, R = SiMe₃; 12b: X = Ph, R = SiMe₃; 12c: X = Cl, R = Cy; 12d: X = Ph, R = Cy;</p>
	13 : R = SiMe ₃
	<p>14a: R = iPr, E = O; 14b: R = ^tBu, E = O; 14c: R = iPr, E = N^tBu; 14d: R = ^tBu, E = N^tBu;</p>
	15a : E = O; 15b : E = NiPr
	<p>16a: saturated C-E bond, R = iPr, R' = Ph, E = O; 16b: saturated C-E bond, R = ^tBu, R' = Ph, E = O; 16c: C-E double bond, R = iPr, R' = Me, E = N.</p>
	17
	18
	<p>19a: Ar' = 2,6-Me₂-Ph; 19b: Ar' = 4-OMe-Ph</p>

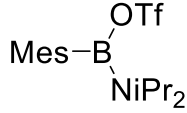
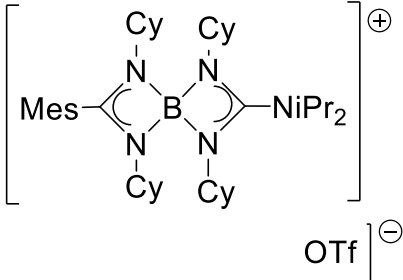
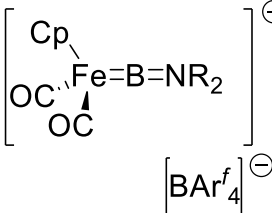
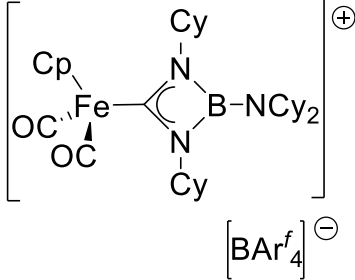
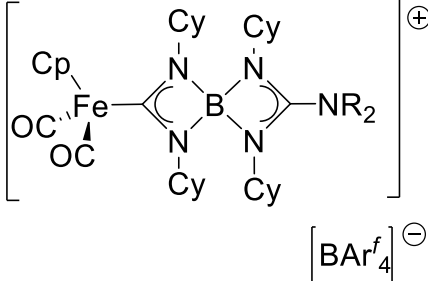
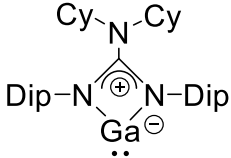
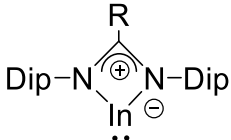
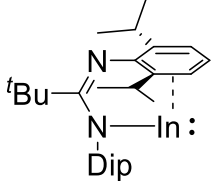
7. Appendix

	<p>20a: Ar' = 2,6-Me₂-Ph, BR₂ = BCy₂, Ar = Ph-<i>p</i>-^tBu, E = H; 20b: Ar' = 4-OMe-Ph, BR₂ = BCy₂, Ar = Ph-<i>p</i>-^tBu, E = H; 20c: Ar' = 2,6-Me₂-Ph, BR₂ = BCy₂, Ar = Ph-<i>p</i>-^tBu, E = BCy₂; 20d: Ar' = 4-OMe-Ph, BR₂ = BCy₂, Ar = Ph-<i>p</i>-^tBu, E = BCy₂; 20e: Ar' = 2,6-Me₂-Ph, BR₂ = BNrb, Ar = Ph-<i>p</i>-Me, E = BNrb; 20f: Ar' = 4-OMe-Ph, BR₂ = BNrb, Ar = Ph-<i>p</i>-Me, E = BNrb</p>
	<p>21a: Ar' = 2,6-Me₂-Ph, BR₂ = BCy₂, Ar = Ph-<i>p</i>-^tBu, E = H; 21b: Ar' = 4-OMe-Ph, BR₂ = BCy₂, Ar = Ph-<i>p</i>-^tBu, E = H;</p>
	<p>22a: Ar = Ph-<i>p</i>-^tBu</p>
	<p>22b: Ar = Ph-<i>p</i>-Me</p>
	<p>23</p>
	<p>24a Ar = Ph-<i>p</i>-^tBu</p>
	<p>25 Ar = Ph-<i>p</i>-^tBu</p>

7. Appendix

	24b Ar = Ph- <i>p</i> -Me
	26 Ar = Ph- <i>p</i> -Me
	27 Ar = Ph- <i>p</i> - ^t Bu
	28
	29
	30
	31a : R = NiPr ₂ ; 31b : R = Ph
	32a (R = Cy) and 32b (R = iPr)
	33
	34a (R = Cy) and 34b (R = iPr)

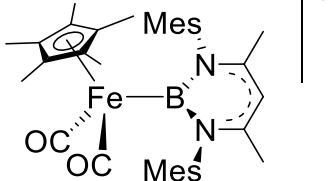
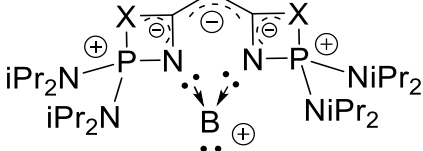
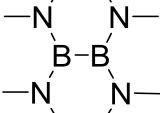
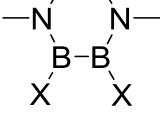
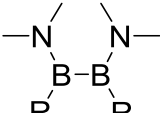
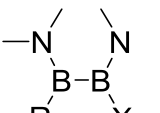
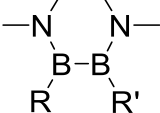
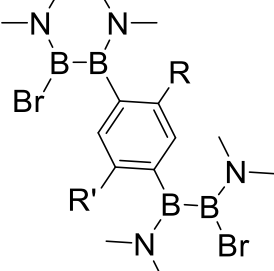
7. Appendix

	35
	36
	37a (R = Cy) and 37b (R = iPr)
	38
	39a (R = Cy) and 39b (R = iPr)
	40
	41a: R = NCy ₂ ; 41b: R = 2,6-dimethylpiperidine
	41c

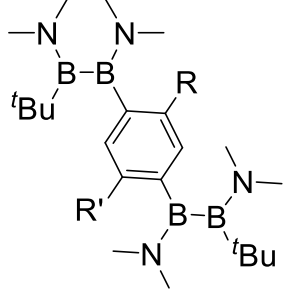
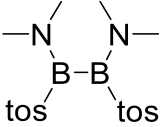
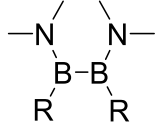
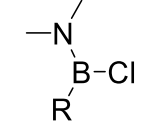
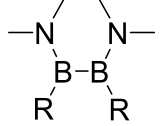

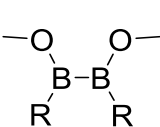
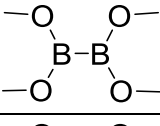
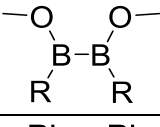
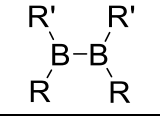
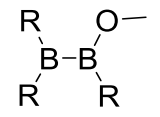
7. Appendix

	<p>42a: R = ^tBu; 42b: R = NCy₂; 42c: R = NiPr₂; 42d: R = 2,6-dimethylpiperidine</p>
	<p>43a: E = Ga; 43b: E = In; 43c: E = Tl</p>
	<p>44a: saturated backbone, Ar = Dip; 44b: saturated backbone, Ar = Mes; 44c: unsaturated backbone, Ar = Dip; 44d: unsaturated backbone, Ar = Mes; 44e: phenyl fused backbone, Ar = Dip; 44f: phenyl fused backbone, Ar = Mes</p>
	<p>45a: R = ^tBu, R' = H; 45b: R = Dip, R' = H; 45c: R = Dip, R' = Me; 45d: R = 2,6-(di-4-tert-butylphenyl)phenyl, R' = Me</p>
	<p>46</p>
	<p>47a: R = Me; 47b: R = ^tBu</p>
	<p>48</p>
	<p>49a: R = Me, Ar = Ar' = Dip; 49b: R = Me, Ar = Dip, Ar' = 2-methoxyphenyl; 49c: R = CF₃, Ar = Ar' = Dip</p>
	<p>50a: R = Me, R' = 2,6-dimethylphenyl, R'' = H; 50b: R = Ph, R' = SiMe₃, R'' = H; 50c: R = H, R' = Dip, R'' = Ph; 50d: R = Me, R' = Dip, R'' = H; 50e: R = Me, R' = 2,6-difluorophenyl, R'' = H</p>

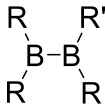
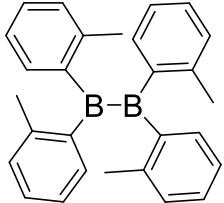
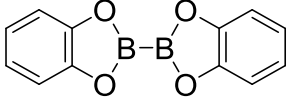
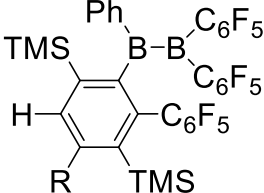
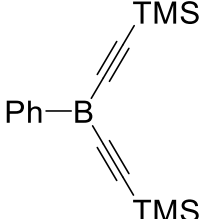
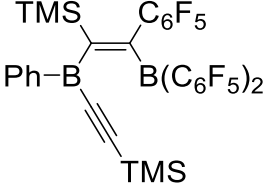
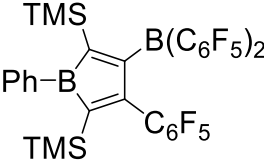
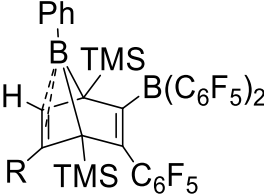
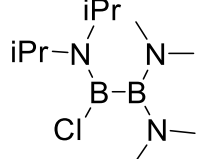
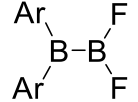
7. Appendix

	<p>51</p>
	<p>52a (X = CMe) and 52b (X = N)</p>
	<p>53</p>
	<p>54a (X = Cl) and 54b (X = Br)</p>
	<p>55a: R = ⁿBu, 55b: R = ^tBu, 55c: R = allyl, 55d: R = Ph, 55e: R = Mes, 55f: R = 1-ind, 55g: R = Cp, 55h: R = flu, 55i: R = Tip, 55j: R = An, 55k: R = Dur, 55l: R = 4-^tbutyl-2,6-dimethylphenyl, 55m: R = 2,5-di-^tbutylphenyl,</p>
	<p>56a: R = ^tBu, X = Cl, 56b: R = allyl, X = Cl, 56c: R = Mes, X = Br, 56d: R = 1-ind, X = Cl, 56e: R = ^tBu, X = Br, 56f: R = Cp, X = Br, 56g: R = flu, X = Br, 56h: R = octaflu, X = Br,</p>
	<p>57a: R = ^tBu, R' = Ph, 57b: R = ^tBu, R' = Npth, 57c: R = flu, R' = Cp, 57d: R = octaflu, R' = Cp, 57e: R = Mes, R' = Ph</p>
	<p>58a: R = R' = H, 58b: R = Me, R' = H, 58c: R = R' = Me</p>

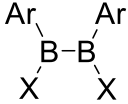
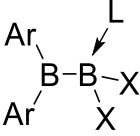
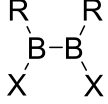
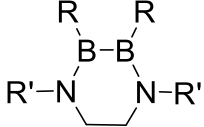
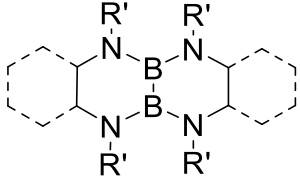
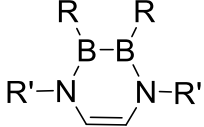
7. Appendix

	<p>59a: R = R' = H, 59b: R = Me, R' = H, 59c: R = R' = Me</p>
	<p>60</p>
	<p>61: R = CC-Ph</p>
	<p>62a: R = ^tBu, 62b: R = Ph, 62c: R = Et</p>
	<p>63: R = Et</p>
	<p>64a: R = ^tBu, X = Cl; 64b: R = ^tBu, X = Br; 64c: R = Mes, X = Cl, 64d: R = Mes, X = Br; 64e: R = Dur, X = Cl; 64f: R = Dur, X = Br; 64g: R = 4-^tbutyl-2,6-dimethylphenyl, X = Cl; 64h: R = 2,5-di-^tbutylphenyl, X = Cl;</p>
	<p>65a: R = Mes; 65b: R = Dur; 65c: R = 4-^tbutyl-2,6-dimethylphenyl; 65d: R = 2,5-di-^tbutylphenyl.</p>
	<p>66</p>
	<p>67a: R = ^tBu; 67b: R = Mes</p>
	<p>68: R = ^tBu, R' = CH₂^tBu</p>
	<p>69a: R = ^tBu; 69b: R = Mes; 69c: R = 2,6-Mes₂-Ph;</p>

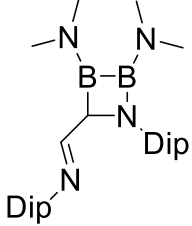
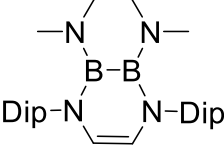
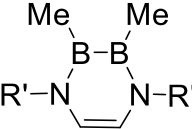
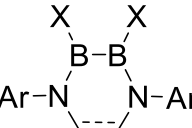
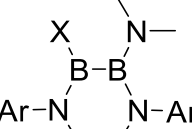
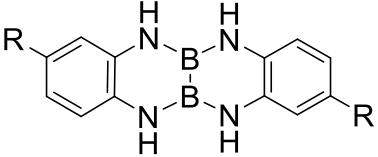
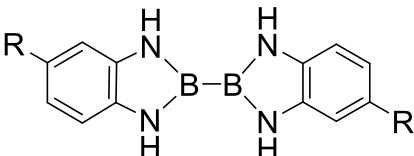
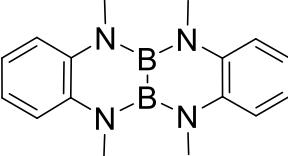
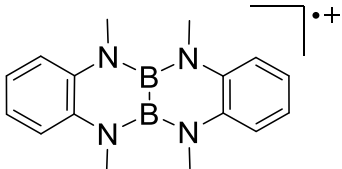
7. Appendix

	<p>70a: R = ^tBu, R' = CH₂^tBu; 70b: R = ^tBu, R' = Me; 70c: R = Mes, R' = CH₂SiMe₃; 70d: R = Mes, R' = Ph.</p>
	<p>71</p>
	<p>72</p>
	<p>73a: R = nPr, 73b: R = Ph</p>
	<p>74</p>
	<p>75</p>
	<p>76</p>
	<p>77a: R = nPr, 77b: R = Ph</p>
	<p>78</p>
	<p>79a: Ar = Mes, 79b: Ar = Dur</p>

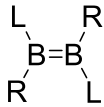
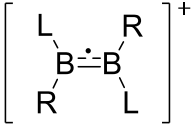
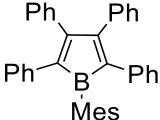
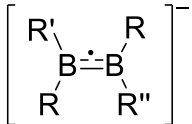
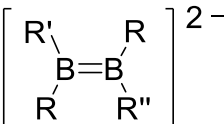
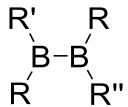
7. Appendix

	80: Ar = Mes, X = I
	81a: Ar = Mes, X = Cl, L = SIMes, 81b: Ar = Mes, X = Br, L = PEt ₃ , 81c: Ar = Mes, X = Br, L = PCy ₂ Me, 81d: Ar = Mes, X = Cl, L = PEt ₃ , 81e: Ar = Mes, X = I, L = PEt ₃ , 81f: Ar = Mes, X = Cl, L = PCy ₂ Me, 81g: Ar = Mes, X = I, L = PCy ₂ Me, 81h: Ar = Mes, X = Br, L = SIMes, 81i: Ar = Mes, X = Cl, L = IDip, 81j: Ar = Mes, X = Cl, L = CAAC ^{Me} , 81k: Ar = Mes, X = Br, L = CAAC ^{Me} , 81l: Ar = Dur, X = Cl, L = CAAC ^{Me} , 81m: Ar = Dur, X = Br, L = CAAC ^{Me}
	82: R = NEt ₂ , X = Br;
	83a: R = NMe ₂ , R' = Me; 83b: R = NEt ₂ , R' = Me; 83c: R = NMe ₂ , R' = Mes; 83d: R = NMe ₂ , R' = Dip; 83e: R = NMe ₂ , R' = 2,6-dimethylphenyl; 83f: R = NMe ₂ , R' = 2,4-dimethylphenyl; 83g: R = NMe ₂ , R' = benzyl; 83h: R = NMe ₂ , R' = <i>p</i> -tolyl; 83i: R = Mes, R' = <i>p</i> -tolyl;
	84a: R' = 2,6-dimethylphenyl; 84b: R' = 2,4-dimethylphenyl; 84c: R' = <i>p</i> -tolyl; 84d: cyclohexyl-backbone, R' = H.
	85a: R = NMe ₂ , R' = 2,4-dimethylphenyl; 85b: R = NMe ₂ , R' = Mes; 85c: R = NMe ₂ , R' = 2,6-dimethylphenyl; 85d: R = NMe ₂ , R' = <i>p</i> -tolyl; 85e: R = Mes, R' = <i>p</i> -tolyl; 85f: R = Dur, R' = <i>p</i> -tolyl; 85g: R = NMe ₂ , R' = tBu

7. Appendix

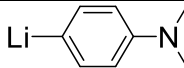
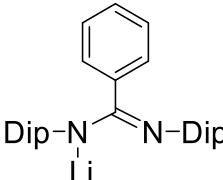
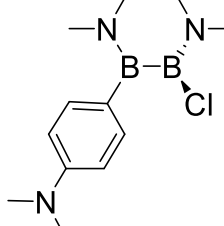
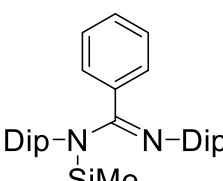
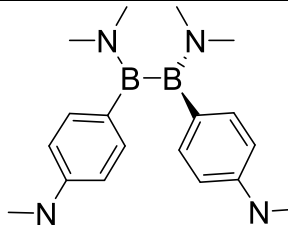
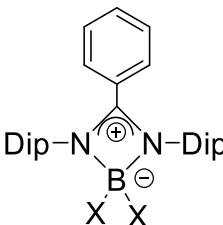
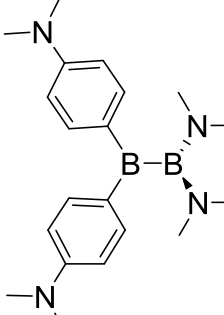
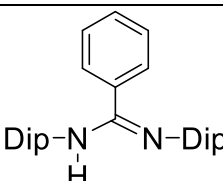
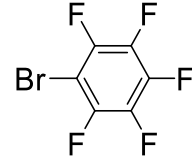
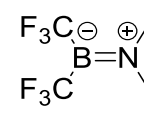
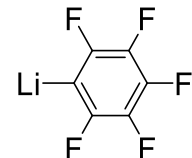
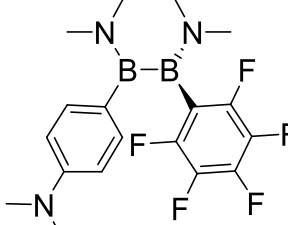
	86
	87
	88a: R' = Mes; 88b: R' = 2,6-dimethylphenyl
	89a: Ar = Mes, X = H; 89b: Ar = Mes, X = Cl; 89c: Ar = Mes, X = Br; 89d: Ar = Mes, X = I; 89e: Ar = 2,6-dimethylphenyl, X = Cl; 89f: Ar = 2,6-dimethylphenyl, X = Br; 89g: Ar = <i>p</i> -tolyl, X = Cl; 89h: Ar = <i>p</i> -tolyl, X = Br
	90a: Ar = Mes, X = H; 90b: Ar = Mes, X = Cl; 90c: Ar = Mes, X = Br; 90d: Ar = 2,6-dimethylphenyl, X = Cl; 90e: Ar = 2,6-dimethylphenyl, X = Br; 90f: Ar = <i>p</i> -tolyl, X = Cl; 90g: Ar = <i>p</i> -tolyl, X = Br
	91a: R = H; 91b: R = Me; 91c: R = ^t Bu
	92a: R = H; 92b: R = Me
	93
	94

7. Appendix

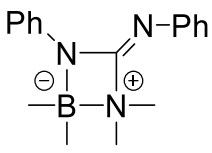
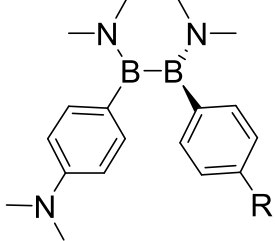
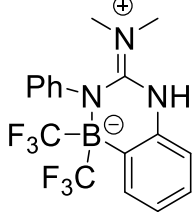
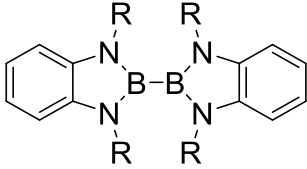
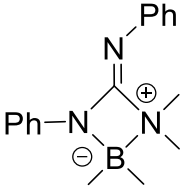
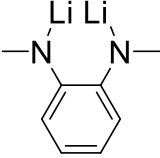
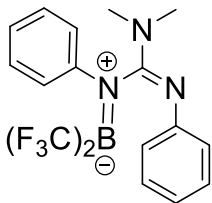
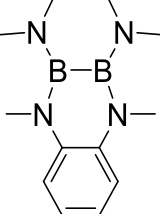
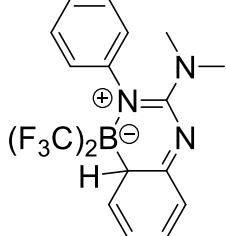
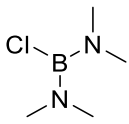
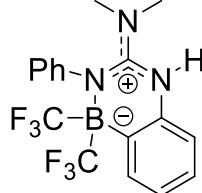
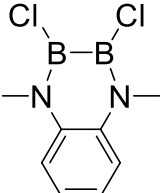
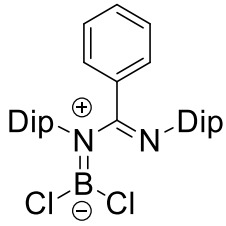
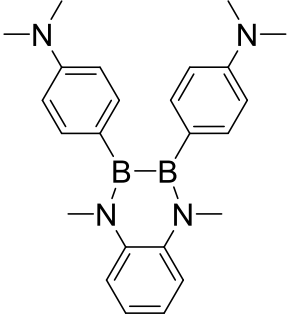
	<p>95a: R = Dur, L = IMe; 95b: R = Mes, L = PEt₃; 95c: R = iPr, L = liPr; 95d: R = 4,4-dimethylpent-2-en-2-yl, L = liPr;</p>
	<p>96a: R = Dur, L = IMe; 96b: R = Mes, L = PEt₃; 96c: R = iPr, L = liPr; 96d: R = 4,4-dimethylpent-2-en-2-yl, L = liPr</p>
	<p>97</p>
	<p>98a: R = R' = R'' = CH₂C(CH₃); 98b: R = R' = R'' = CH₂C(CD₃); 98c: R = R' = R'' = C(CH₃), 98d: R = OMe, R' = R'' = Mes; 98e: R = R' = Mes, R'' = Ph; 98f: RR'B = pinB, R = R'' = Mes;</p>
	<p>99a: R = R' = Mes, R'' = Ph; 99b: R = NMe₂, R' = R'' = Ph; 99c: R = R' = R'' = o-tol</p>
	<p>100a: R = R' = R'' = CH₂C(CH₃); 100b: R = R' = R'' = CH₂C(CD₃); 100c: R = R' = R'' = C(CH₃); 100d: RR'B = pinB, R = R'' = Mes</p>

7. Appendix

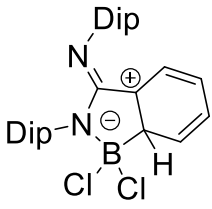
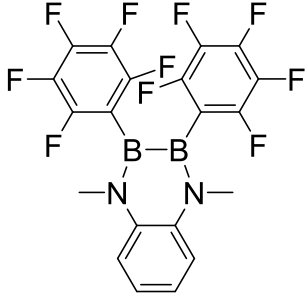
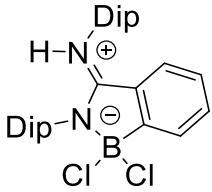
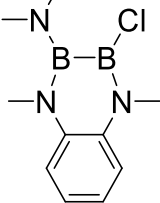
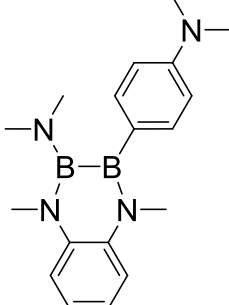
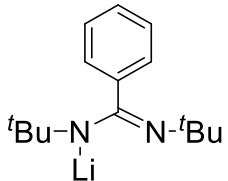
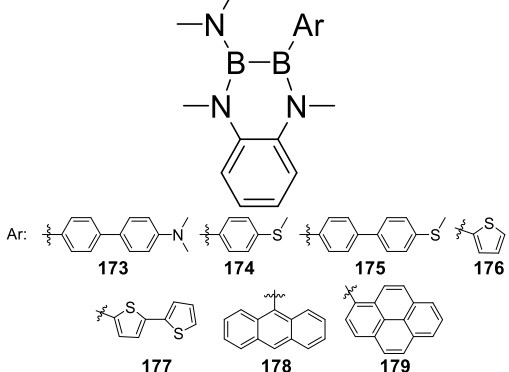
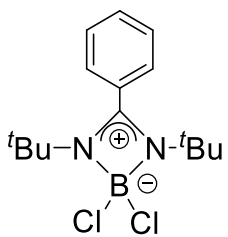
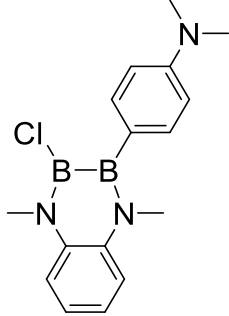
Table 6. Numbered Compounds (Results and Discussion, Conclusion and Outlook, Experimental Section)

Compound	Number	Compound	Number
Dip-N≡N-Dip	101		155
	102		156
	103		157
	104a: X = Cl, 104b: X = Br		158
	105		159
	106		160
Ph-N=C=N-Ph	107		161

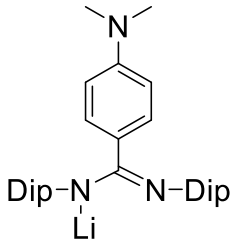
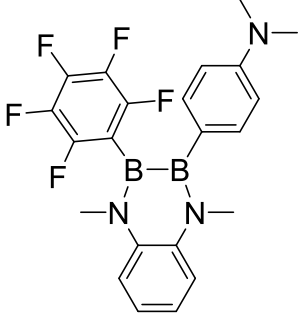
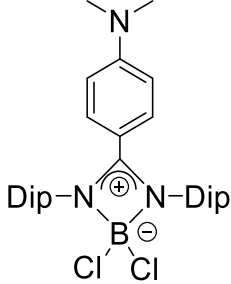
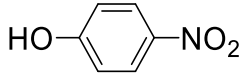
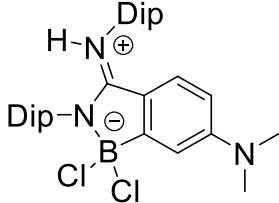
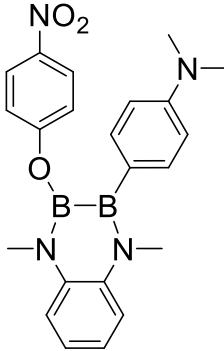
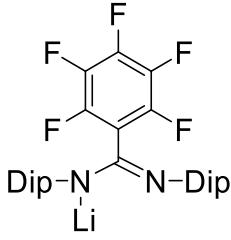
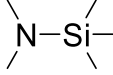
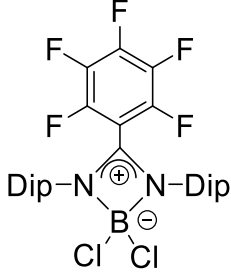
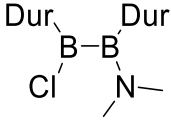
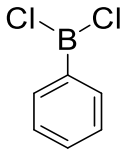
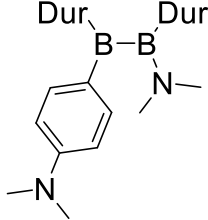
7. Appendix

	108		162: R = CN 163: R = NO ₂
	109		164: R = Me
	110		165
	111		166
	112		167
	113		168
	114		169

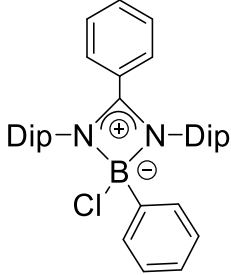
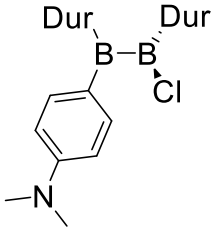
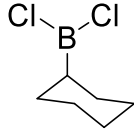
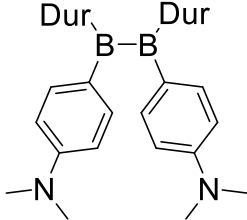
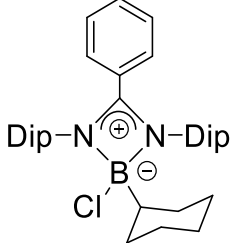
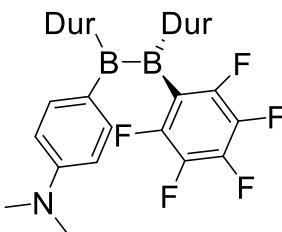
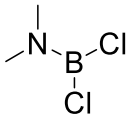
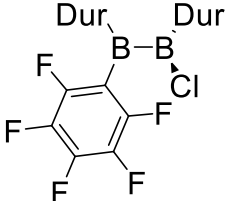
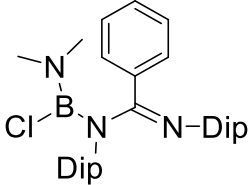
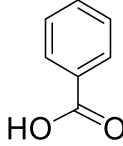
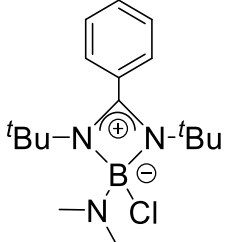
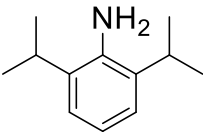
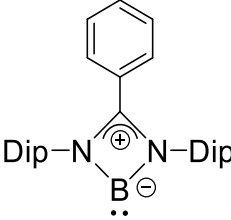
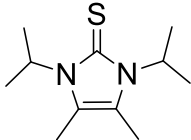
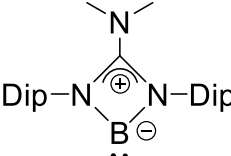
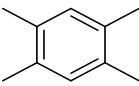
7. Appendix

	115		170
	116		171
${}^t\text{Bu}-\text{N}=\text{N}-{}^t\text{Bu}$	117		172
	118		173-179
	119		180

7. Appendix

 <p>Dip-N Li</p>	120		181
 <p>Dip-N[⊕] N-Dip B[⊖] Cl Cl</p>	121		182
 <p>Dip H-N[⊕] Dip-N[⊖] B[⊖] Cl Cl</p>	122		183
 <p>Dip-N Li</p>	123		184
 <p>Dip-N[⊕] N-Dip B[⊖] Cl Cl</p>	124		185
	125		186

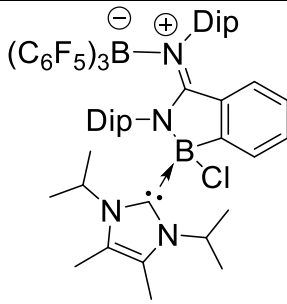
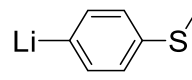
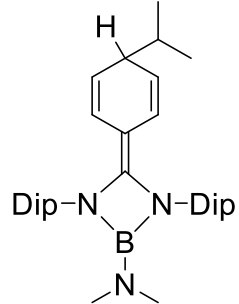
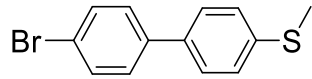
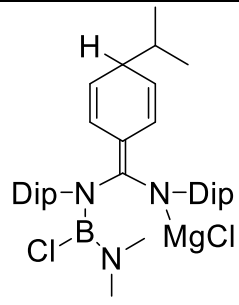
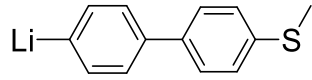
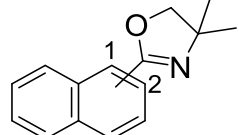
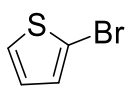
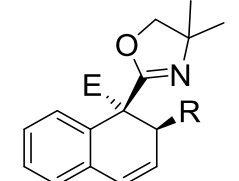
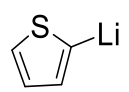
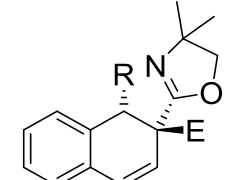
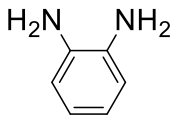
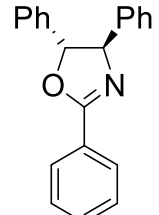
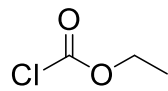
7. Appendix

	126		187
	127		188
	128		189
	129		190
	130		191
	131		192
	132		193
	133		194

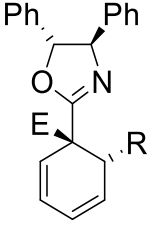
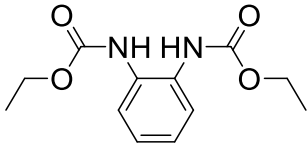
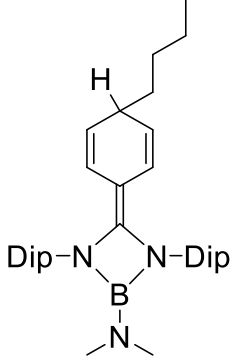
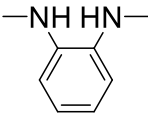
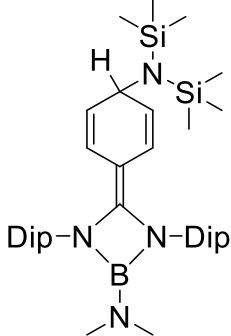
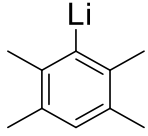
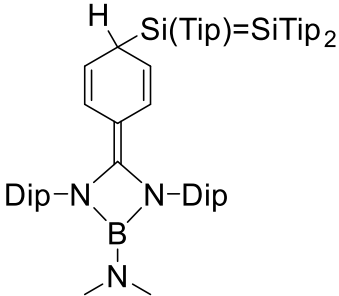
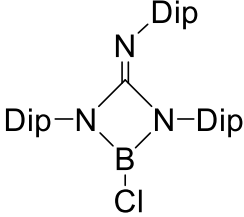
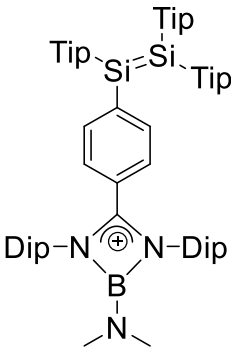
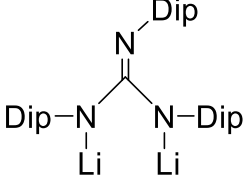
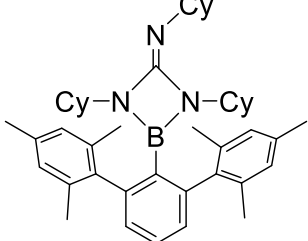
7. Appendix

	134		195
iPr_2Me_2NHC	135		196
	136	BCl_3	197
	137	Bu_3SiH	198
	138	Me_2NH	199
Me_4NHC	139	$(Me_2N)_3B$	200
BPh_3	140		201
$iPr_2Me_2NHC-BPh_3$	141		202
	142		203
$(C_6F_5)_3B \cdot OEt_2$	143		204

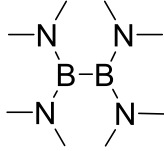
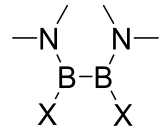
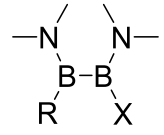
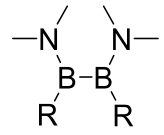
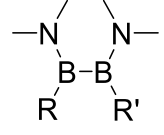
7. Appendix

	144		205
	145		206
	146		207
	147		208
	148		209
	149		210
	150		211

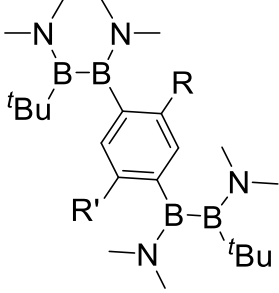
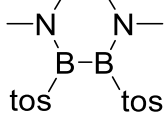
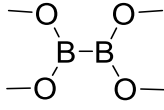
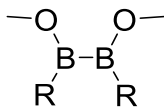
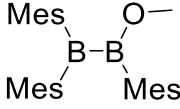
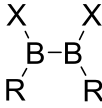
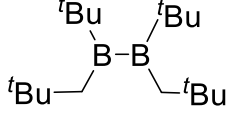
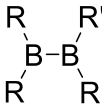
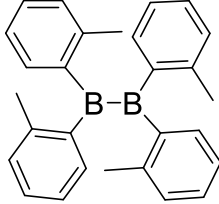
7. Appendix

	151		212
	152		213
	153		214
	154		215
	218		216
			217

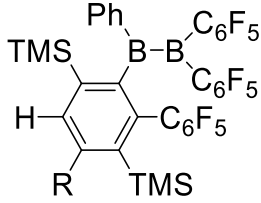
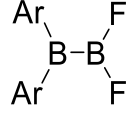
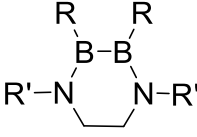
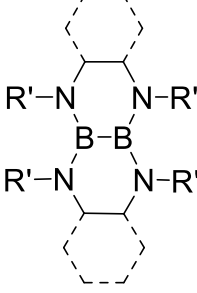
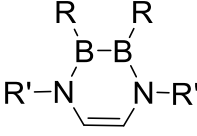
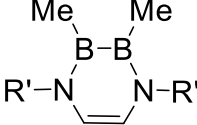
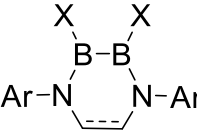
7.2 ^{11}B NMR signals of diboranes(4)Table 7. Reviewed diboranes(4) and their ^{11}B NMR chemical shifts.

Diborane	^{11}B NMR chemical shifts [ppm]
	36.6 ^[293]
	X = Cl: 37.5 ^[293] X = Br: 38.0 ^[293]
	R = allyl, X = Cl: 43.3 (only one signal, which is often observed for monochlorinated diboranes(4)) ^[99] R = Mes, X = Br: 47.4, 41.4 ^[95] R = 3-ind, X = Cl: 43.6 ^[103] R = ^t Bu, X = Br: 49.4, 42.3 ^[105] R = Cp, X = Br: 41.0 ^[106] R = flu, X = Br: 43.0 ^[106] R = Octaflu, X = Br: 42 ^[109]
	R = ⁿ Bu: 52.1 ^[114] R = ^t Bu: 54.6 ^[98] R = allyl: 49.9 ^[99] R = Ph: 49.3 ^[95] R = Mes: 55 ^[98] / 50.2 ^[95] R = 1-ind: 48.6 ^[103] R = flu: 47.5 ^[114] / 48.1 ^[107] R = Tip: 55 ^[98] / 49.6 ^[108] R = An: 52.1 ^[110,111] R = Dur: 50 ^[98] R = 4- ^t Bu-2,6-Me ₂ -Ph: 50 ^[98] R = 2,5- ^t Bu ₂ -Ph: 56 ^[98] R = CC-Ph: 37.1 ^[114]
	R = ^t Bu, R' = Ph: 53.0, 50.4 ^[105] R = flu, R' = Cp: 47.4 ^[106] R = octaflu, R' = Cp: 48 ^[109]

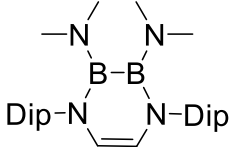
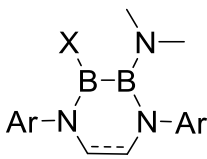
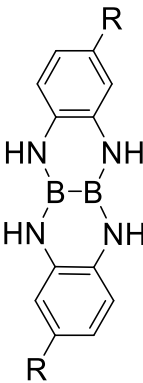
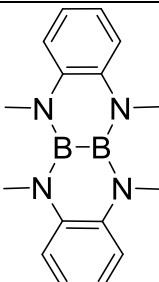
7. Appendix

	<p>R = R' = H: 44^[112,113] R = H, R' = Me: 43.8^[105] R = R' = Me: 51.6^[105]</p>
	30.4 ^[114]
	31.2 ^[120]
	<p>R = Mes: 62^[98]/ 61^[120] R = Dur: 61^[98] R = 4-<i>t</i>-butyl-2,6-dimethylphenyl: 59^[98] R = 2,5-<i>t</i>Bu₂-Ph: 62^[98]</p>
	98, 59 ^[117]
	<p>R = <i>t</i>Bu, X = Cl: 85^[98] R = Mes, X = Cl: 85^[98] R = Mes, X = Br: 86^[104] R = Dur, X = Cl: 87^[98] R = 4-<i>t</i>-butyl-2,6-dimethylphenyl, X = Cl: 85^[98]</p>
	103 ^[118,119]
	<p>R = <i>t</i>Bu, R' = CH₂<i>t</i>Bu: 104^[118,119] R = Mes, R' = CH₂SiMe₃: 100^[120] R = Mes, R' = Ph: 99^[117,120]</p>
	89 ^[122]

7. Appendix

	<p>R = nPr: 84.1, 74.3^[123,124] R = Ph: 85.6^[123,124]</p>
	<p>Ar = Dur: 82, 29^[126,127] Ar = Mes: similar to Dur^[126,127]</p>
	<p>R = NMe₂, R' = Me: 34.9^[133] R = NEt₂, R' = Me: 35.1^[133] R = NMe₂, R' = Mes: 33.4^[135], 34^[134] R = NMe₂, R' = Dip: 33^[134] R = NMe₂, R' = 2,6-dimethylphenyl: 37^[134] R = NMe₂, R' = 2,4-dimethylphenyl: 34^[134] R = NMe₂, R' = benzyl: 37^[134] R = NMe₂, R' = <i>p</i>-tolyl: 35^[134] R = Mes, R' = <i>p</i>-tolyl: 47^[134]</p>
	<p>R' = 2,6-dimethylphenyl: 37^[134] R' = 2,4-dimethylphenyl: 34^[134] R' = <i>p</i>-tolyl: 34^[134] cyclohexyl-backbone, R' = H: 30.7^[136]</p>
	<p>R = NMe₂, R' = 2,4-dimethylphenyl: 32^[137] R = NMe₂, R' = Mes: 34.1^[135] R = NMe₂, R' = 2,6-dimethylphenyl: 33.5^[138] R = NMe₂, R' = <i>p</i>-tolyl: 34.1^[138] R = Mes, R' = <i>p</i>-tolyl: 48^[137] R = Dur, R' = <i>p</i>-tolyl: 47^[137] R = NMe₂, R' = <i>t</i>Bu: 36.7^[138]</p>
	<p>R' = Mes: 49.0^[138] R' = 2,6-dimethylphenyl: 40.5^[138]</p>
	<p>Ar = Mes, X = H, sat: 44.0^[135] Ar = Mes, X = H, unsat: 45.1^[135] Ar = Mes, X = Cl, unsat.: 40.9^[138]</p>

7. Appendix

	<p>Ar = Mes, X = Br, unsat.: 42.0^[138]</p> <p>Ar = Mes, X = I, unsat.: 41.4^[138]</p> <p>Ar = 2,6-dimethylphenyl, X = Cl, unsat.: 40.5^[138]</p> <p>Ar = 2,6-dimethylphenyl, X = Br, unsat.: 41.4^[138]</p> <p>Ar = <i>p</i>-tolyl, X = Cl, unsat.: 40.5^[138]</p> <p>Ar = <i>p</i>-tolyl, X = Br, unsat.: 41.1^[138]</p>
	33.8 ^[138]
	<p>Ar = Mes, X = H, sat: 45.8, 30.5^[135]</p> <p>Ar = Mes, X = H, unsat: 45.3, 31.7^[135]</p> <p>Ar = Mes, X = Cl, unsat.: 41.1, 30.7^[138]</p> <p>Ar = Mes, X = Br, unsat.: 40.7, 31.1^[138]</p> <p>Ar = 2,6-dimethylphenyl, X = Cl, unsat.: 40.7, 30.4^[138]</p> <p>Ar = 2,6-dimethylphenyl, X = Br, unsat.: 40.4, 31.0^[138]</p> <p>Ar = <i>p</i>-tolyl, X = Cl, unsat.: 40.6, 31.6^[138]</p> <p>Ar = <i>p</i>-tolyl, X = Br, unsat.: 40.1, 32.0^[138]</p>
	<p>R = H: 33.4^[139]</p> <p>R = Me: 32.7^[139]</p> <p>R = ^tBu: 33.0^[136]</p>
	34.2 ^[140]

7.3 Crude product ^1H NMR spectra of reactions between 91 and various aryl lithium compounds

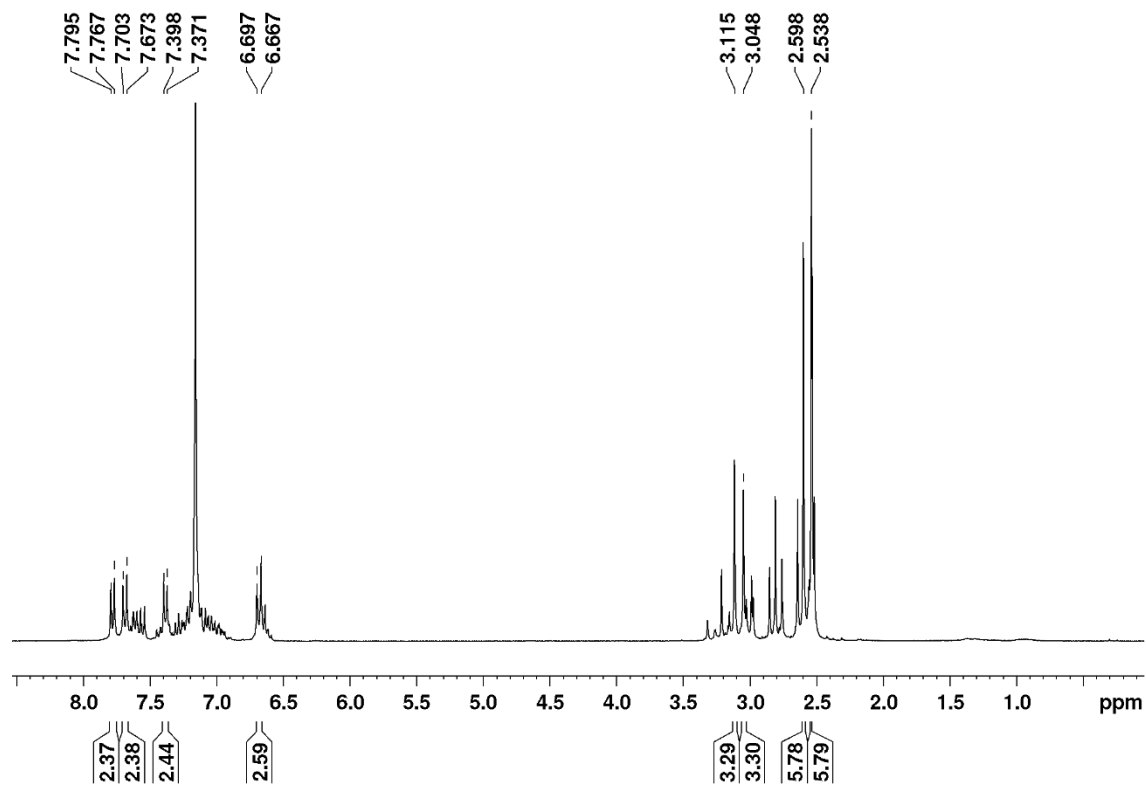


Figure 92. ^1H NMR spectrum of YK181. Selected resonances of anticipated product 93 marked and integrated.

7. Appendix

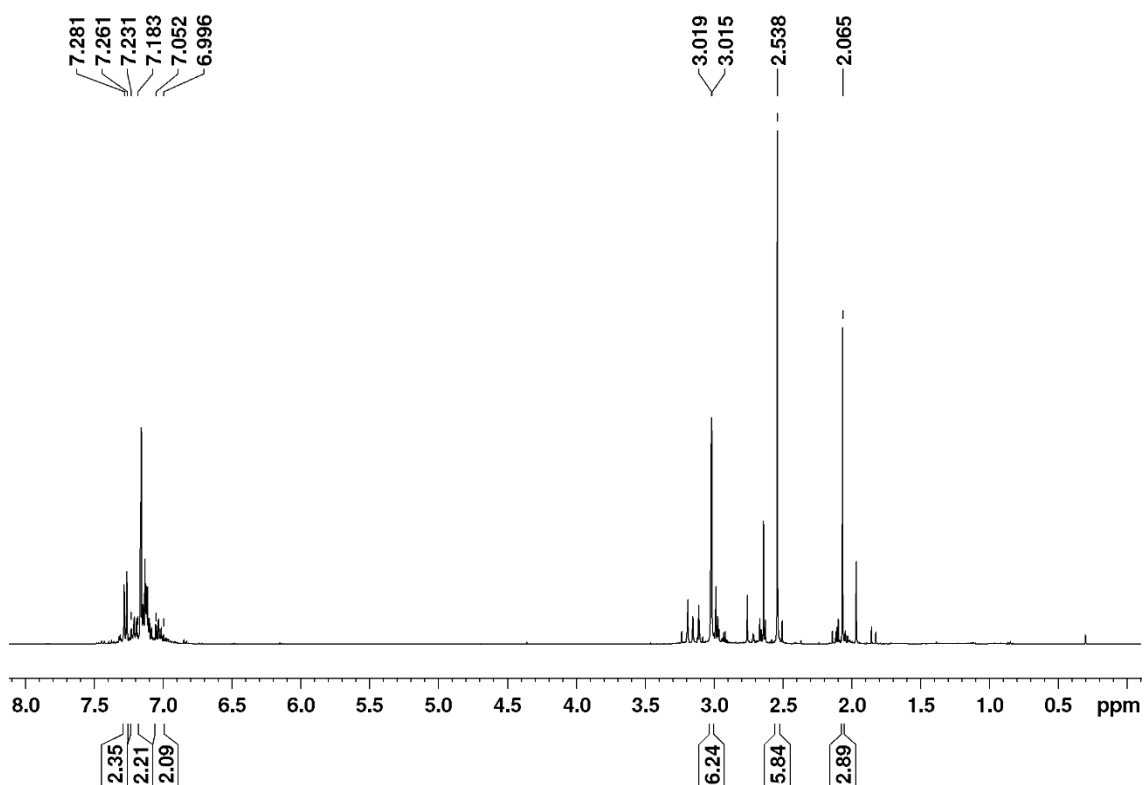


Figure 93. ¹H NMR spectrum of YK173. Selected resonances of anticipated product **94** marked and integrated.

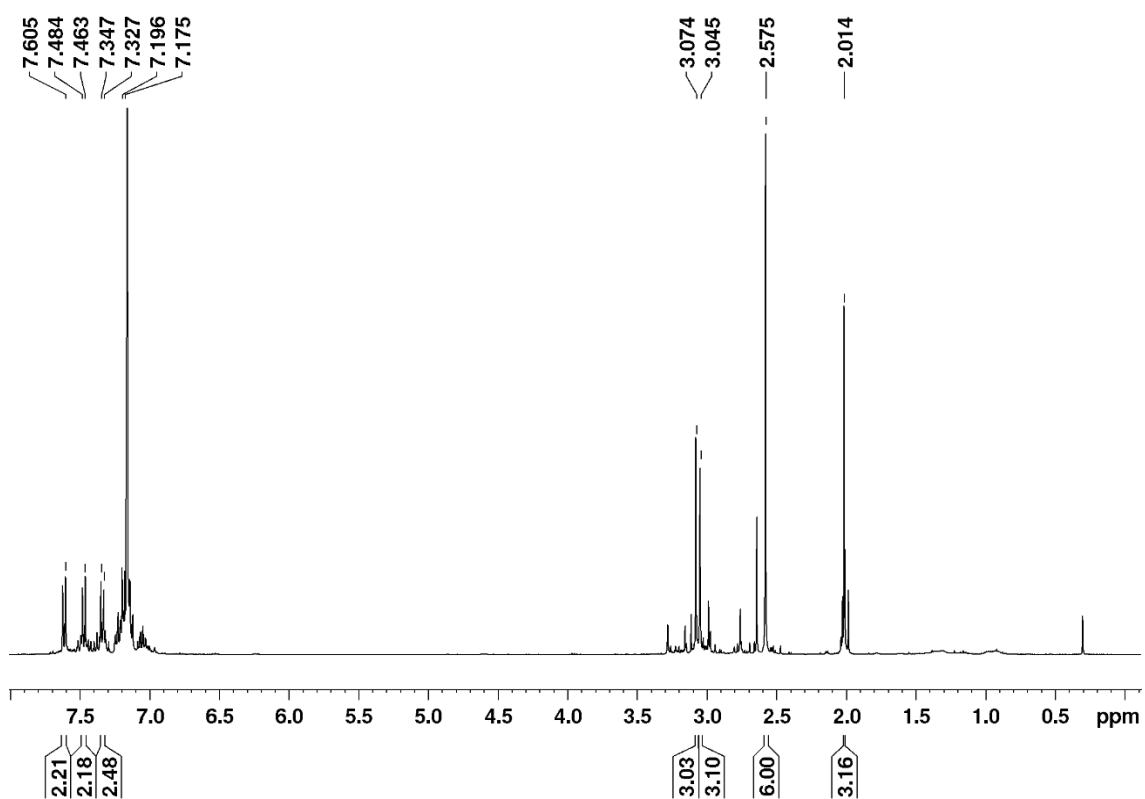


Figure 94. ¹H NMR spectrum of YK174. Selected resonances of anticipated product **95** marked and integrated.

7. Appendix

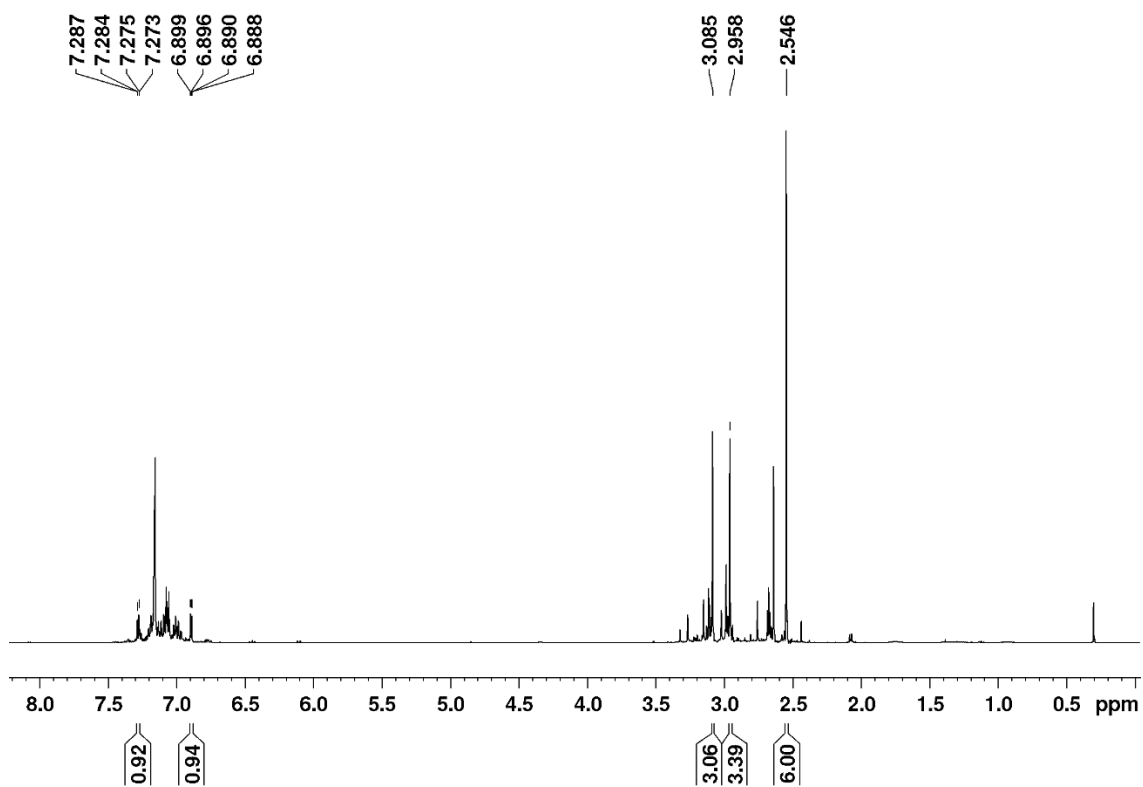


Figure 95. ¹H NMR spectrum of YK172. Selected resonances of anticipated product **96** marked and integrated.

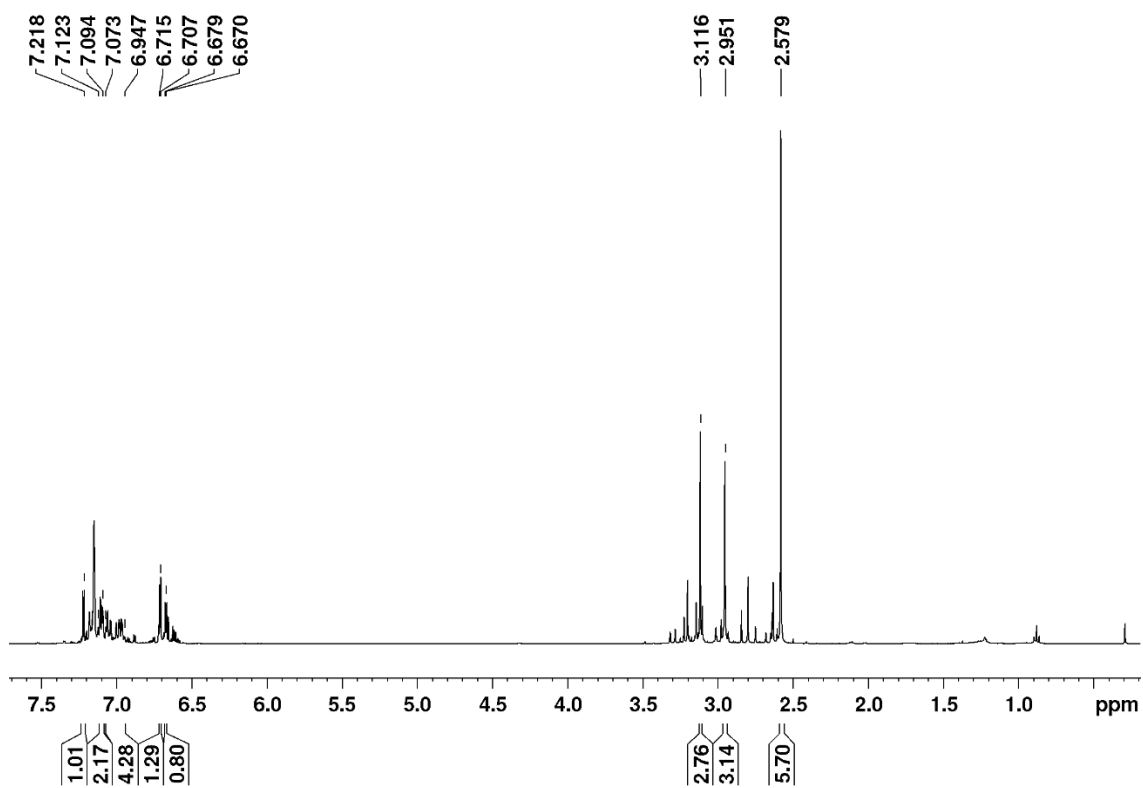


Figure 96. ¹H NMR spectrum of YK176. Selected resonances of anticipated product **97** marked and integrated.

7. Appendix

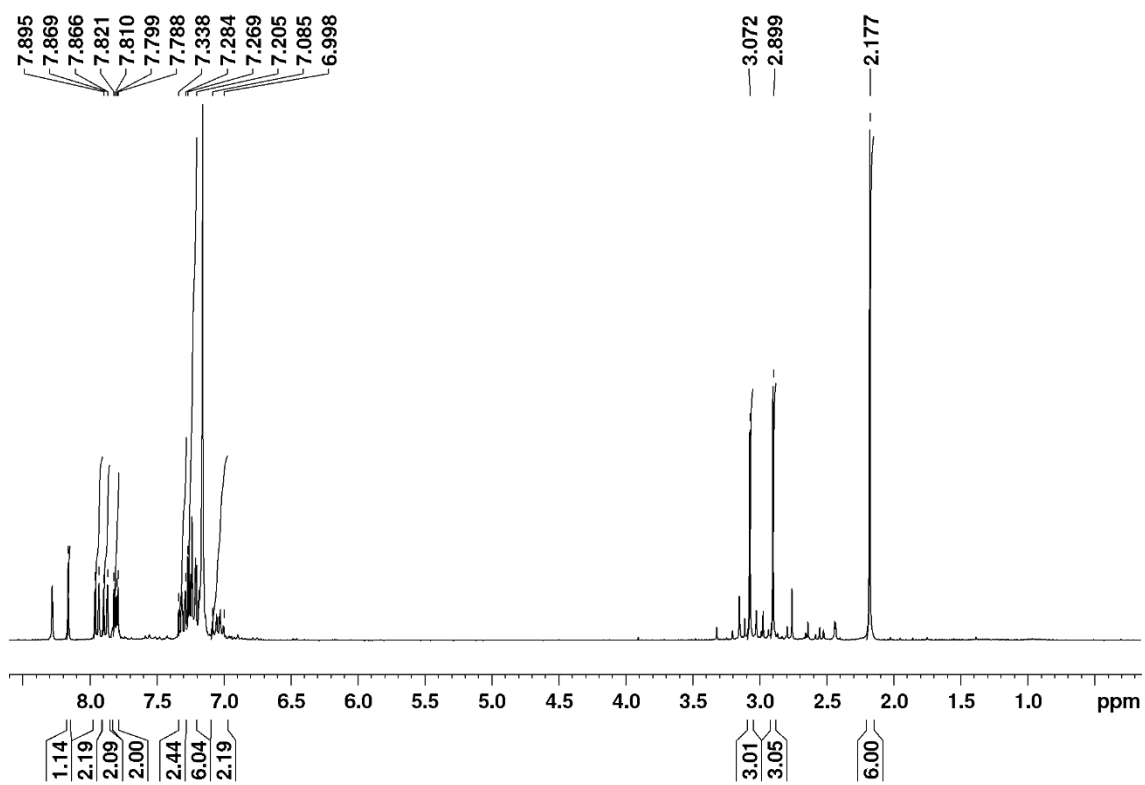


Figure 97. ¹H NMR spectrum of YK184. Selected resonances of anticipated product **98** marked and integrated.

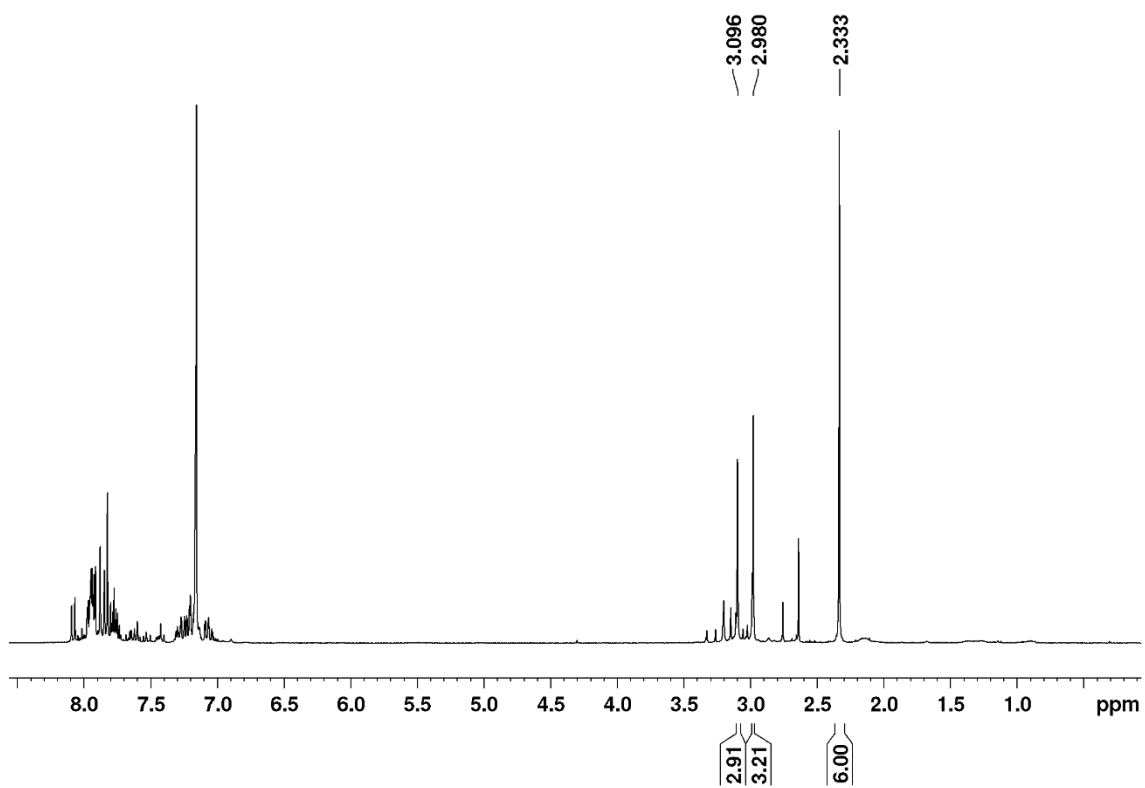


Figure 98. ¹H NMR spectrum of YK182. Selected resonances of anticipated product **99** marked and integrated.

7.4 UV-vis Spectra and ϵ determination

7.4.1 2-chloro-1,2-bis(dimethylamino)-1-para-*N,N*-dimethylaniline diborane(4) **156**

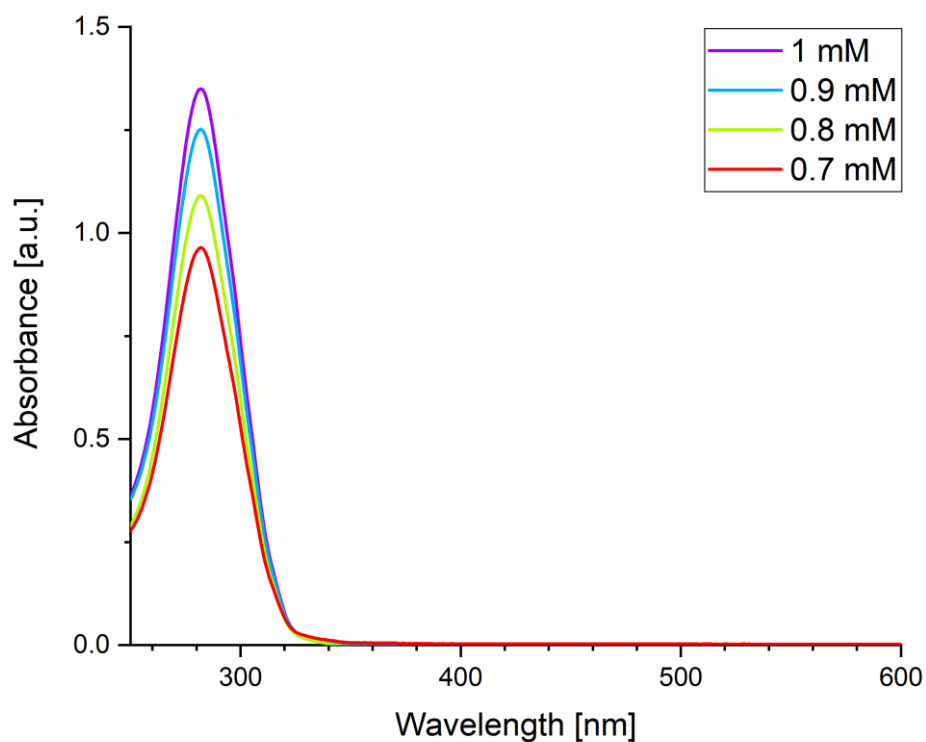


Figure 99. UV/Vis spectra of 1,2-bis(dimethylamino) diborane(4) **156** in hexane at different concentrations (0.7 mM – 1 mM).

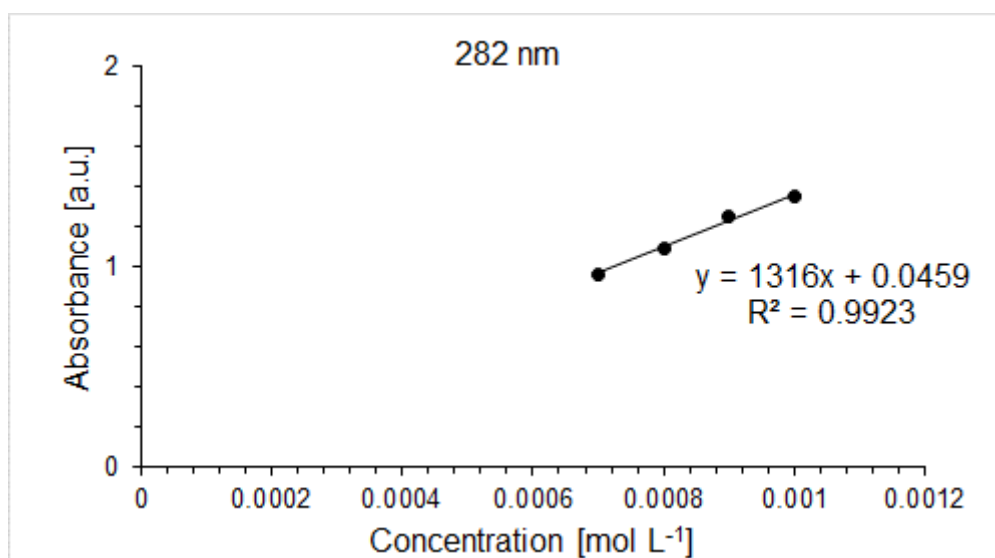


Figure 100. Determination of ϵ ($13200 \text{ M}^{-1} \text{ cm}^{-1}$) by linear regression of absorbance ($\lambda = 282 \text{ nm}$) of **156** against concentration.

7.4.2 1,2-bis(dimethylamino)-1,2-bis(para-*N,N*-dimethylaniline) diborane(4)

157

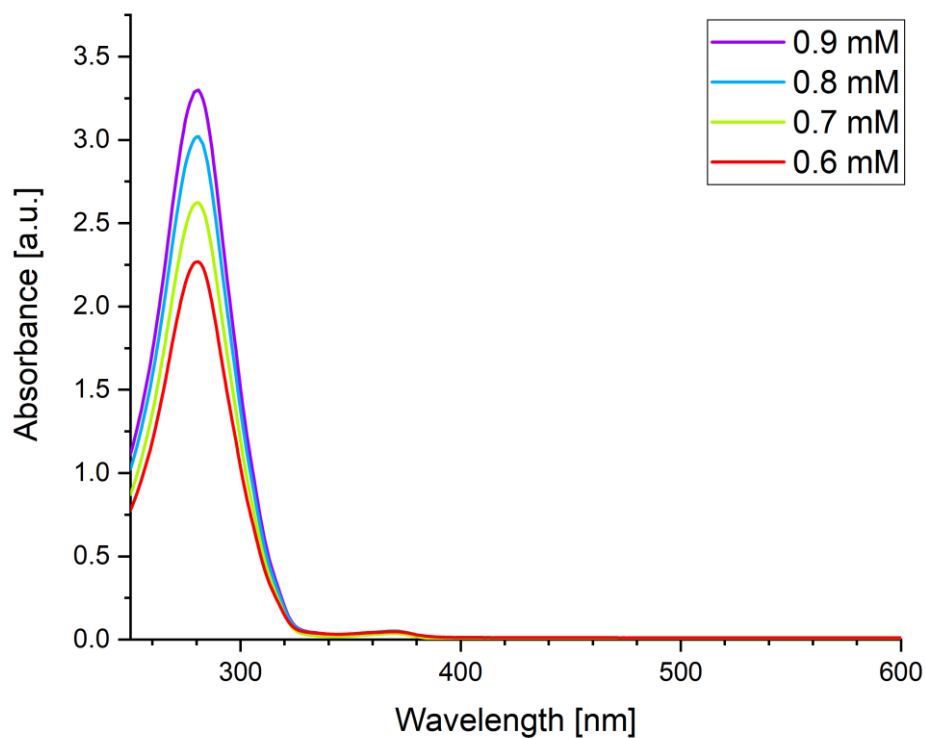


Figure 101. UV/Vis spectra of 1,2-bis(dimethylamino) diborane(4) **157** in hexane at different concentrations (0.6 mM – 0.9 mM).

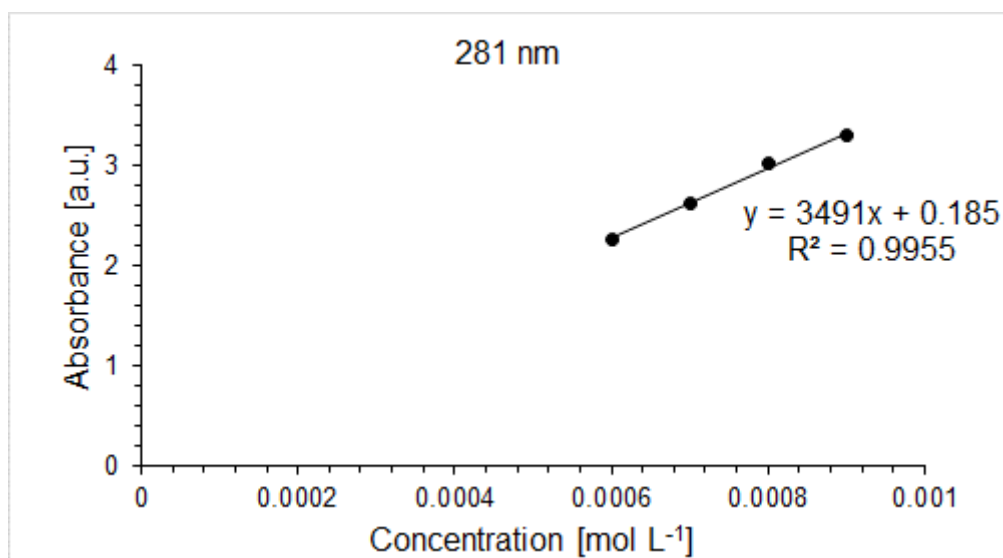


Figure 102. Determination of ϵ (34900 M⁻¹ cm⁻¹) by linear regression of absorbance ($\lambda = 281$ nm) of **157** against concentration.

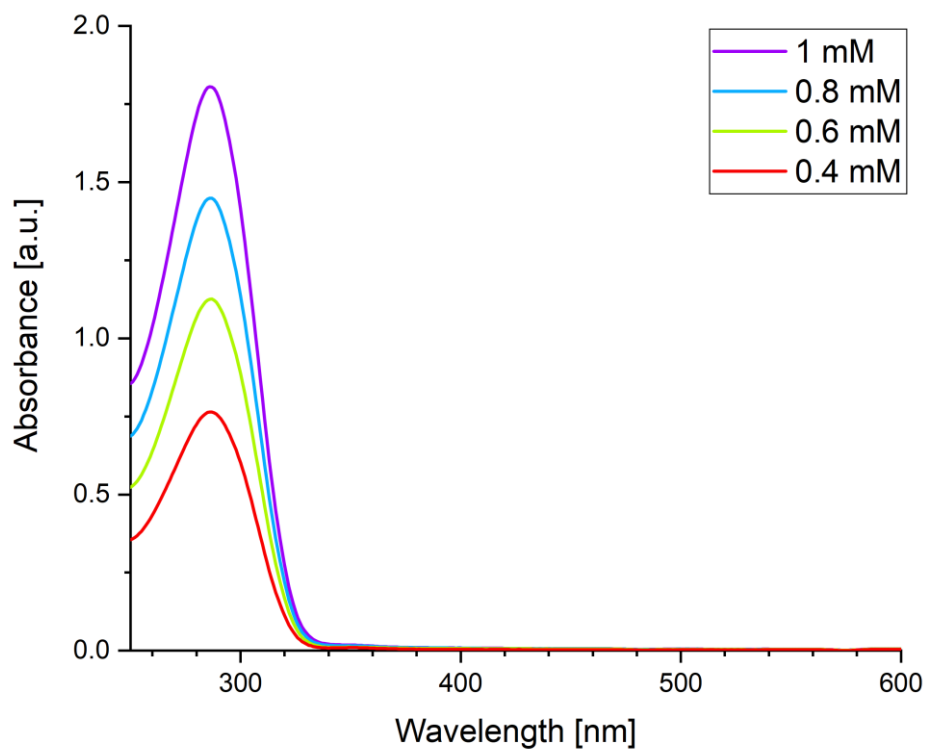
7.4.3 1,2-bis(dimethylamino)-1-para-*N,N*-dimethylaniline-2-pentafluorophenyl diborane(4) 161

Figure 103. UV/Vis spectra of 1,2-bis(dimethylamino) diborane(4) **161** in diethylether at different concentrations (0.4 mM – 1 mM).

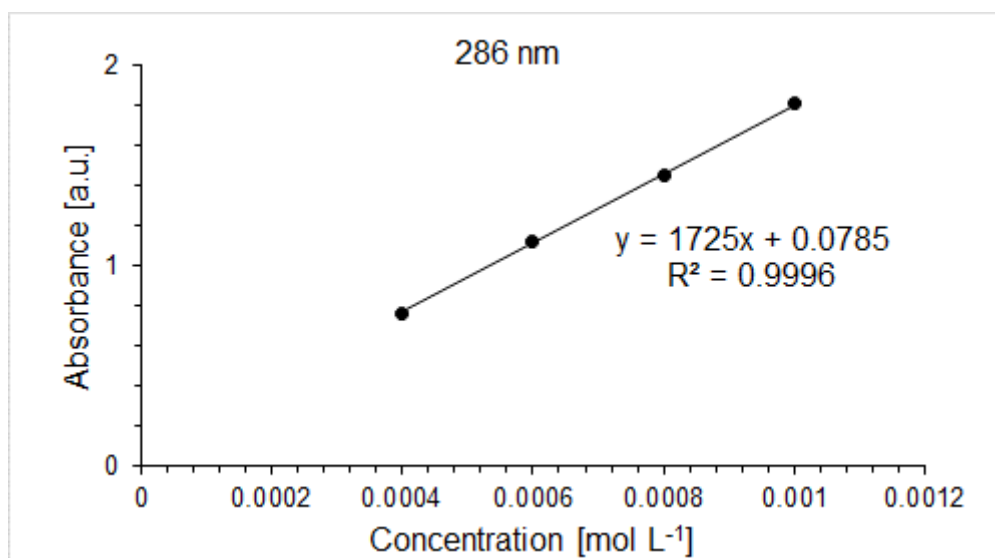


Figure 104. Determination of ϵ ($17300 \text{ M}^{-1} \text{ cm}^{-1}$) by linear regression of absorbance ($\lambda = 286 \text{ nm}$) of **161** against concentration.

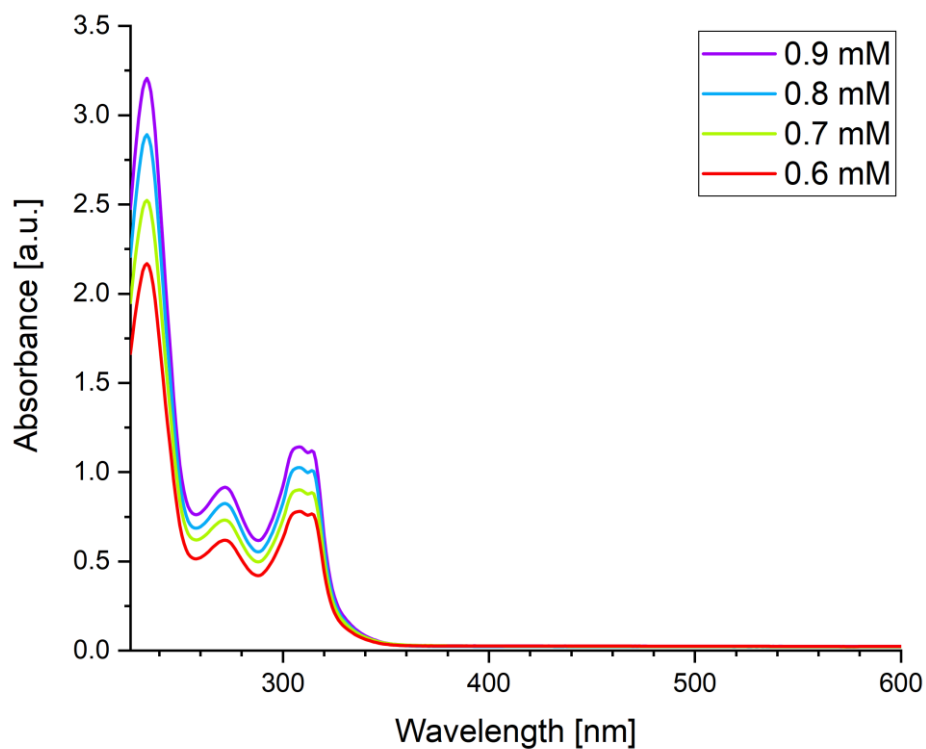
7.4.4 1,4-dimethyl-2,3-bis(dimethylamino)-1,2,3,4-tetrahydrobenzo[e]-[1,4,2,3]diazadiborinane 166

Figure 105. UV/Vis spectra of cyclic 1,4-diaza-2,3-diborinane **166** in hexane at different concentrations (0.6 mM – 0.9 mM).

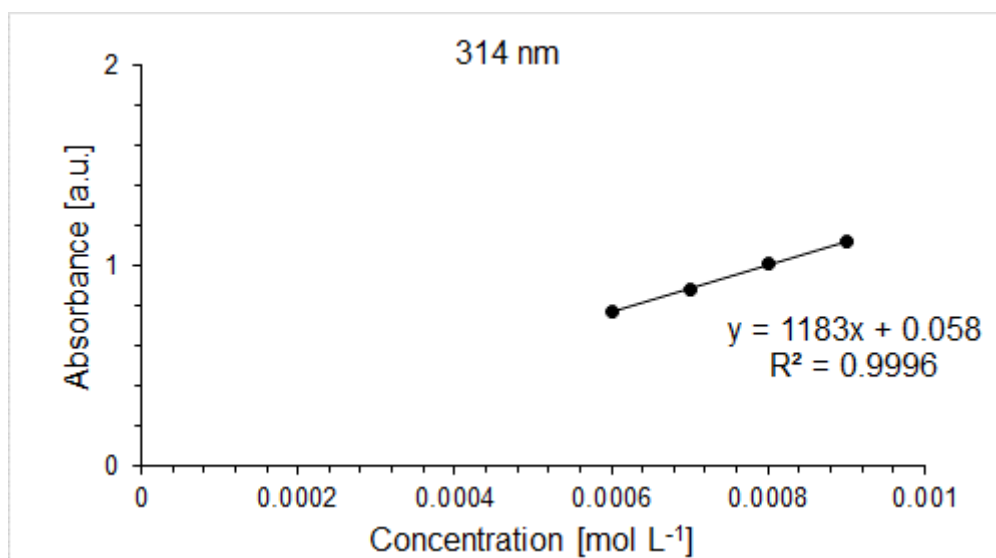


Figure 106. Determination of ϵ ($11800 \text{ M}^{-1} \text{ cm}^{-1}$) by linear regression of absorbance ($\lambda = 314 \text{ nm}$) of **166** against concentration.

7. Appendix

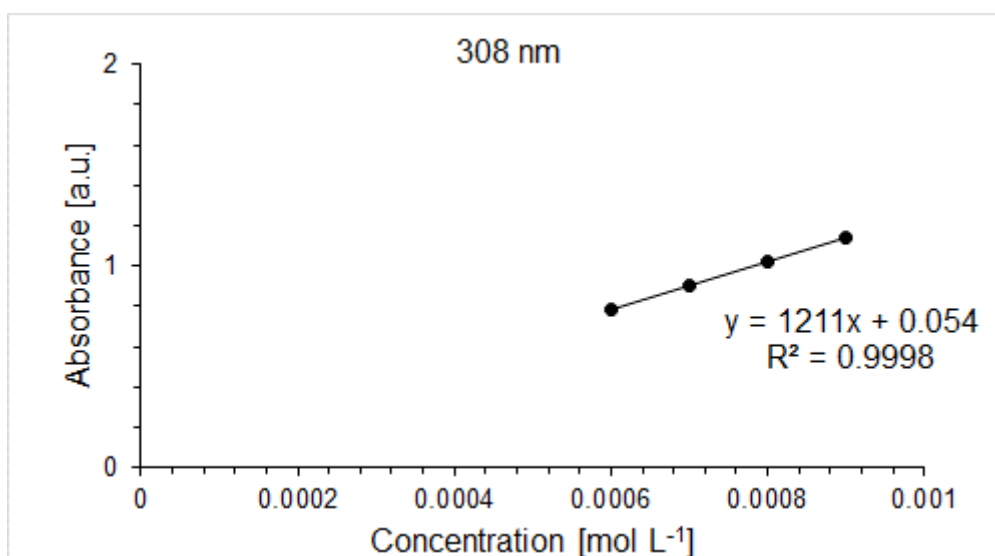


Figure 107. Determination of ϵ ($12100 \text{ M}^{-1} \text{ cm}^{-1}$) by linear regression of absorbance ($\lambda = 308 \text{ nm}$) of **166** against concentration.

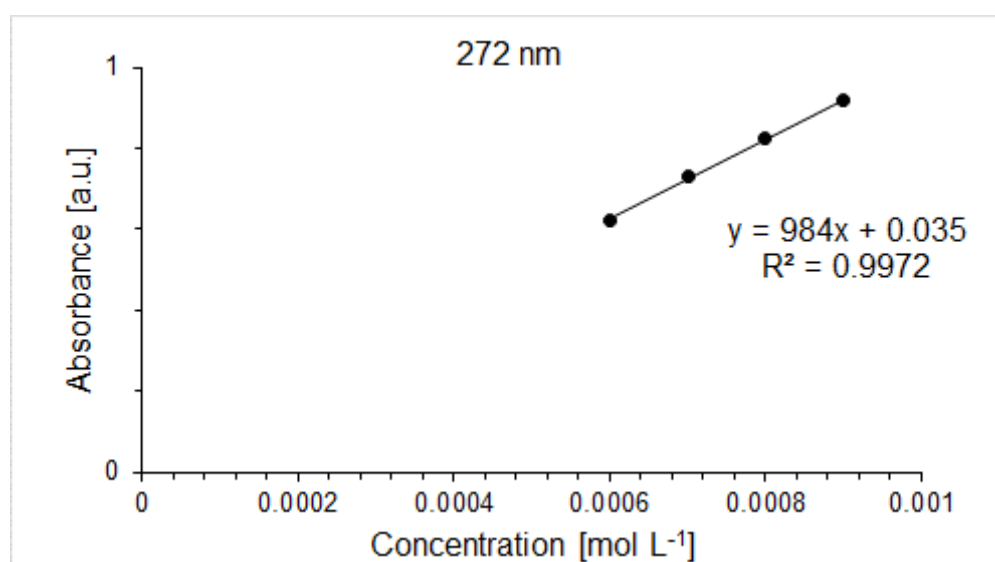


Figure 108. Determination of ϵ ($9840 \text{ M}^{-1} \text{ cm}^{-1}$) by linear regression of absorbance ($\lambda = 272 \text{ nm}$) of **166** against concentration.

7. Appendix

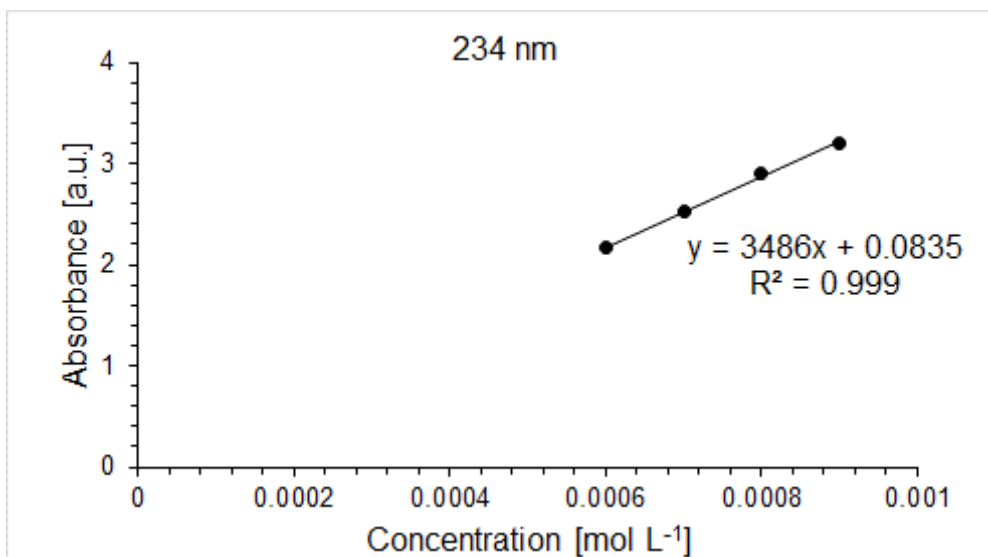


Figure 109. Determination of ϵ ($34900 \text{ M}^{-1} \text{ cm}^{-1}$) by linear regression of absorbance ($\lambda = 234 \text{ nm}$) of **166** against concentration.

7.4.5 2,3-bis(para-*N,N*-dimethylaniline)-1,4-dimethyl-1,2,3,4-tetrahydrobenzo[*e*][1,4,2,3]diazadiborinane **169**

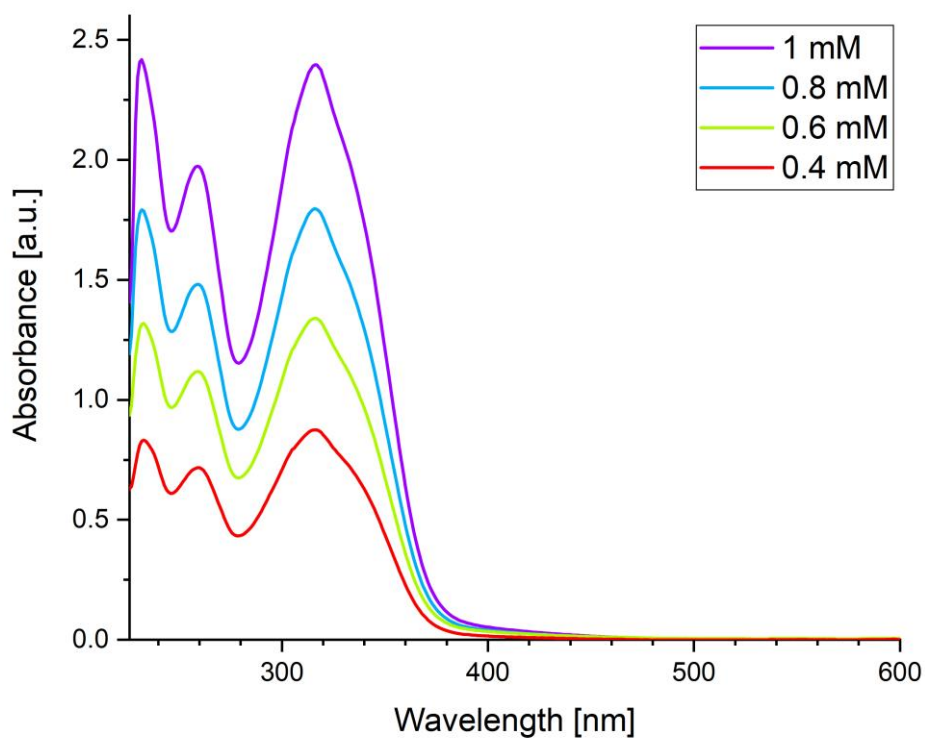


Figure 110. UV/Vis spectra of cyclic 1,4-diaza-2,3-diborinane **169** in diethylether at different concentrations (0.4 mM – 1 mM).

7. Appendix

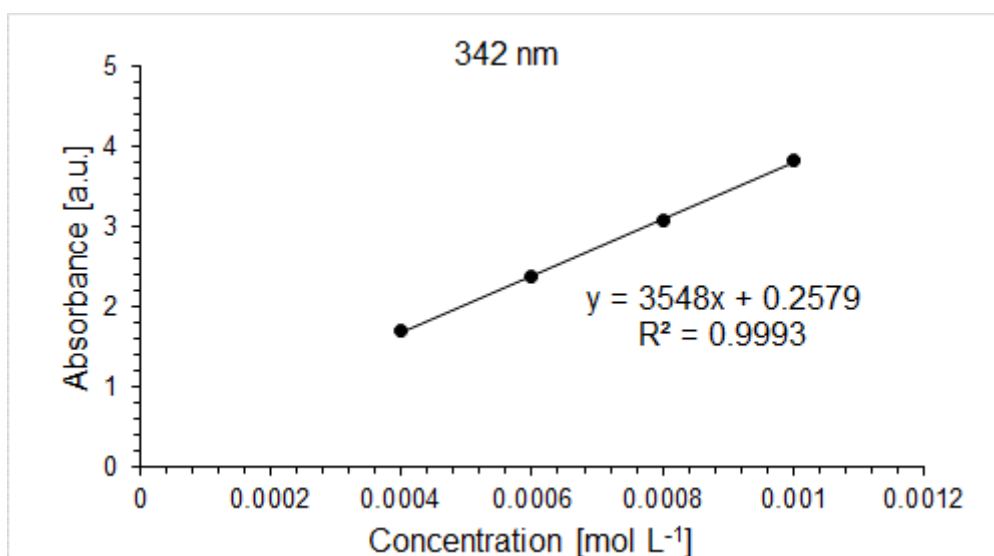


Figure 111. Determination of ϵ ($35500 \text{ M}^{-1} \text{ cm}^{-1}$) by linear regression of absorbance ($\lambda = 342 \text{ nm}$) of **169** against concentration.

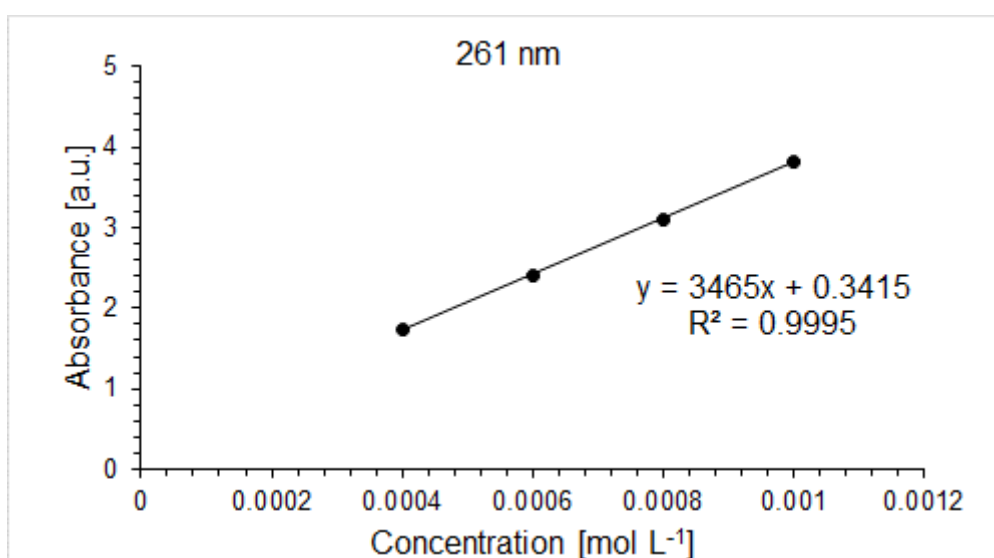


Figure 112. Determination of ϵ ($34700 \text{ M}^{-1} \text{ cm}^{-1}$) by linear regression of absorbance ($\lambda = 261 \text{ nm}$) of **169** against concentration.

7. Appendix

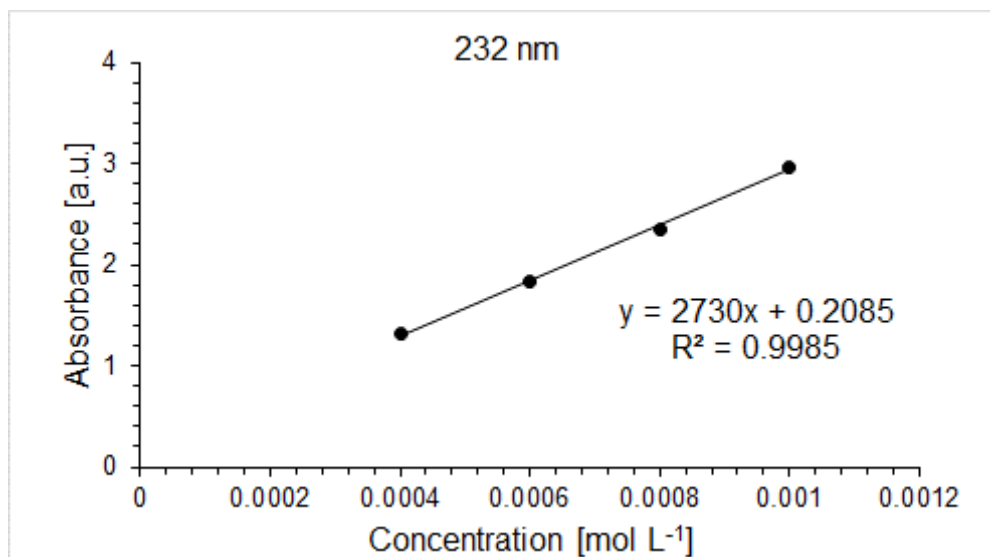


Figure 113. Determination of ϵ ($27300 \text{ M}^{-1} \text{ cm}^{-1}$) by linear regression of absorbance ($\lambda = 232 \text{ nm}$) of **169** against concentration.

7.4.6 2,3-bis(pentafluorophenyl)-1,4-dimethyl-1,2,3,4-tetrahydrobenzo[e]-[1,4,2,3]diazadiborinane **170**

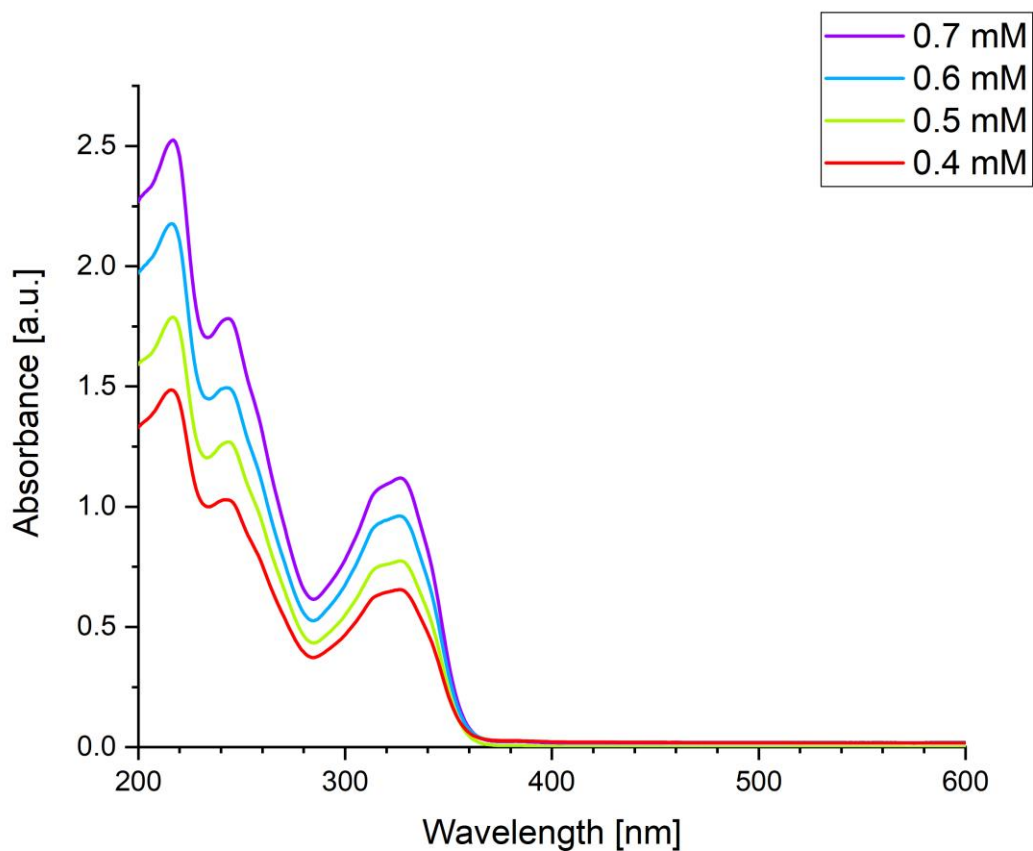


Figure 114. UV/Vis spectra of cyclic 1,4-diaza-2,3-diborinane **170** in diethylether at different concentrations (0.4 mM – 0.7 mM).

7. Appendix

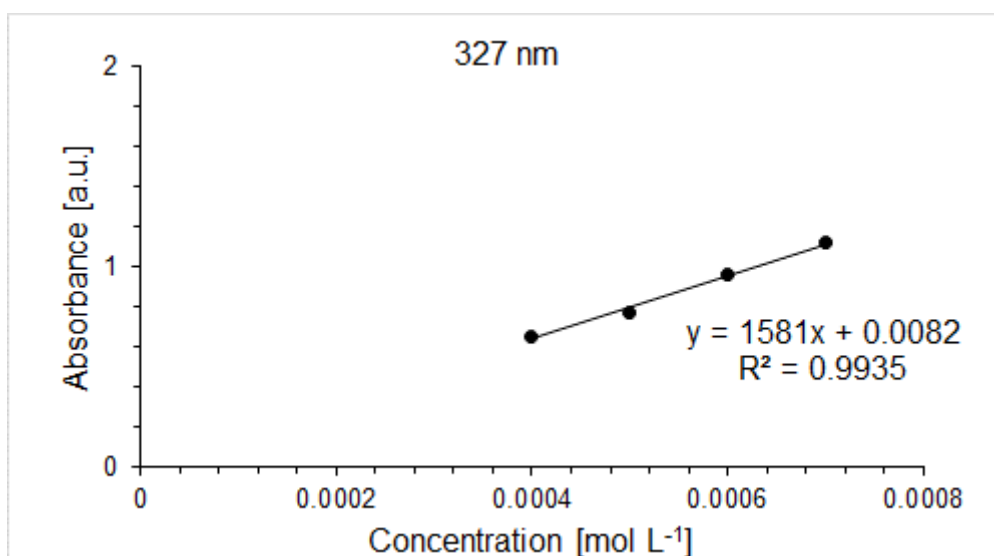


Figure 115. Determination of ϵ ($15800 \text{ M}^{-1} \text{ cm}^{-1}$) by linear regression of absorbance ($\lambda = 327 \text{ nm}$) of **170** against concentration.

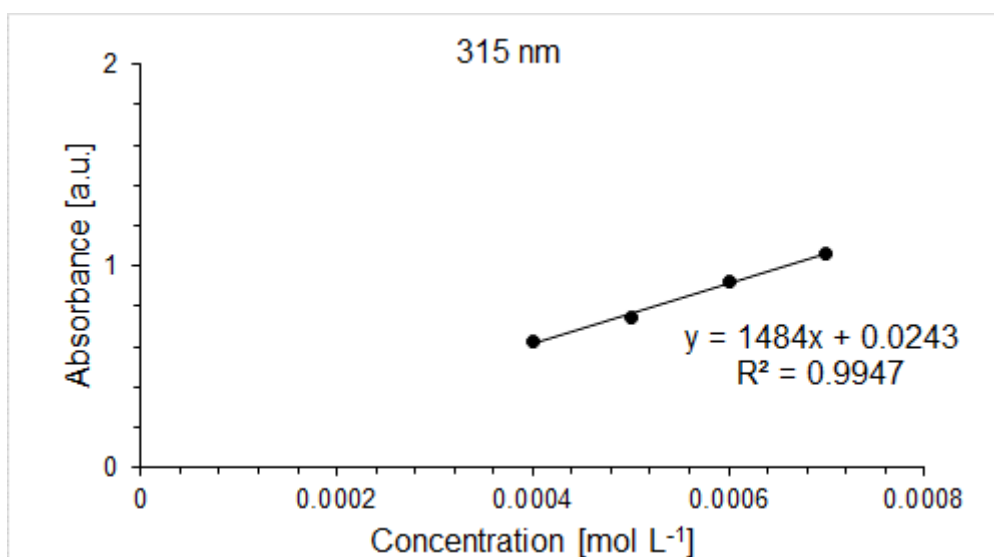


Figure 116. Determination of ϵ ($14800 \text{ M}^{-1} \text{ cm}^{-1}$) by linear regression of absorbance ($\lambda = 315 \text{ nm}$) of **170** against concentration.

7. Appendix

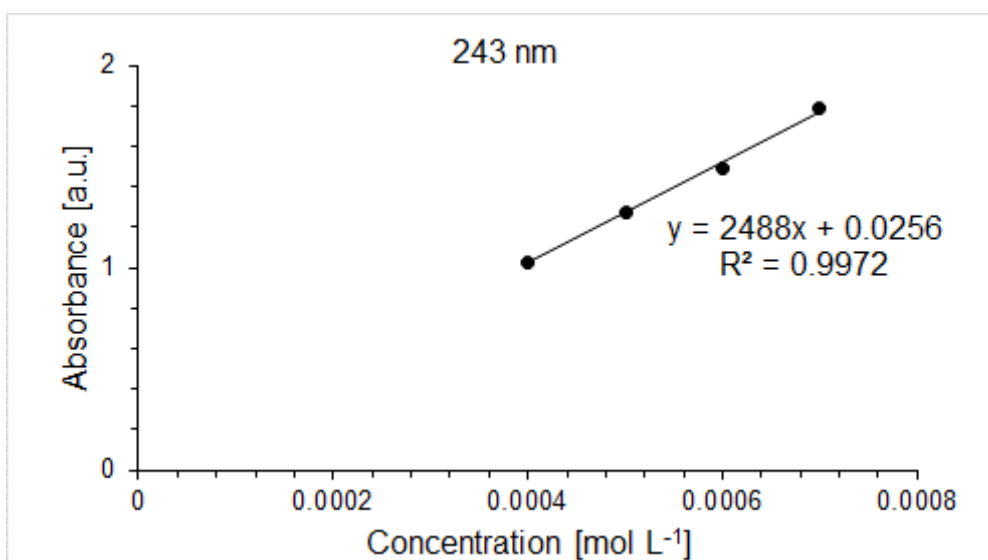


Figure 117. Determination of ϵ ($24900 \text{ M}^{-1} \text{ cm}^{-1}$) by linear regression of absorbance ($\lambda = 243 \text{ nm}$) of **170** against concentration.

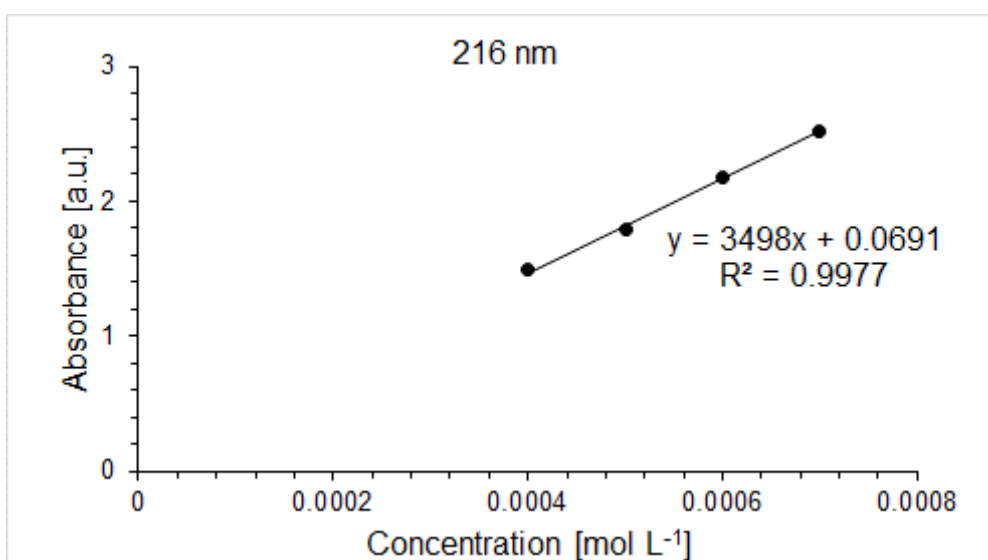


Figure 118. Determination of ϵ ($35000 \text{ M}^{-1} \text{ cm}^{-1}$) by linear regression of absorbance ($\lambda = 216 \text{ nm}$) of **170** against concentration.

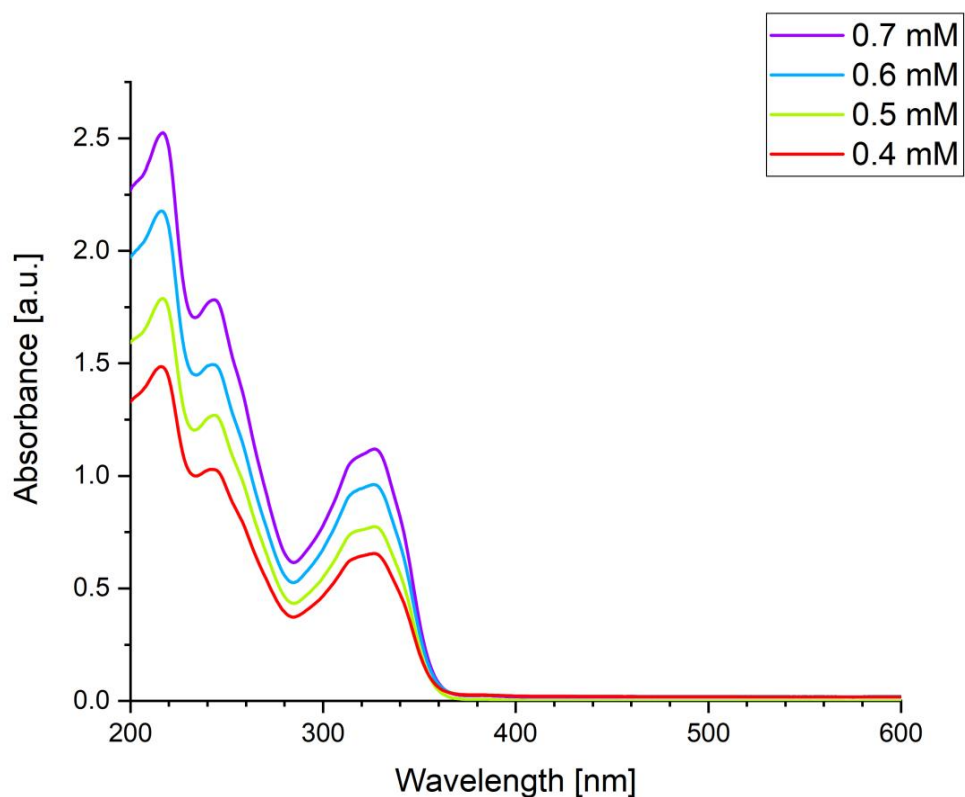
7.4.7 1,4-dimethyl-2-dimethylamino-3-para-*N,N*-dimethylaniline-1,2,3,4-tetrahydrobenzo[e][1,4,2,3]diazadiborinane 172

Figure 119. UV/Vis spectra of cyclic 1,4-diaza-2,3-diborinane **172** in hexane at different concentrations (0.4 mM – 0.7 mM).

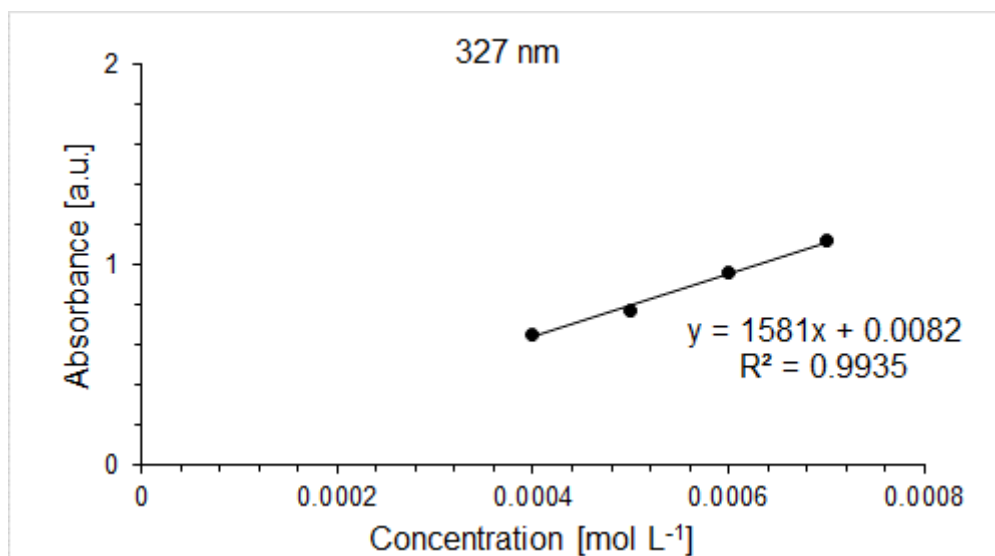


Figure 120. Determination of ϵ (15800 M⁻¹ cm⁻¹) by linear regression of absorbance ($\lambda = 327$ nm) of **172** against concentration.

7. Appendix

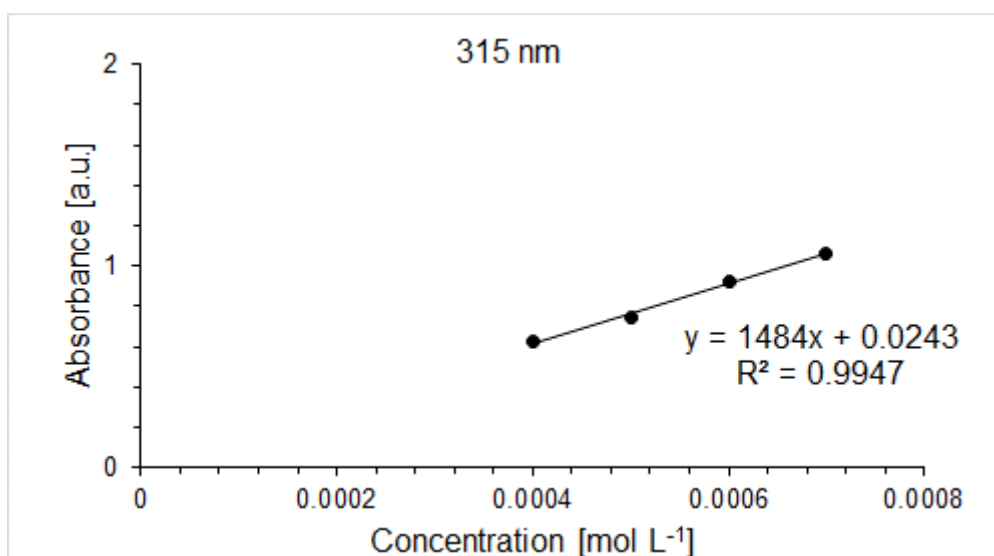


Figure 121. Determination of ϵ ($14800 \text{ M}^{-1} \text{ cm}^{-1}$) by linear regression of absorbance ($\lambda = 315 \text{ nm}$) of **172** against concentration.

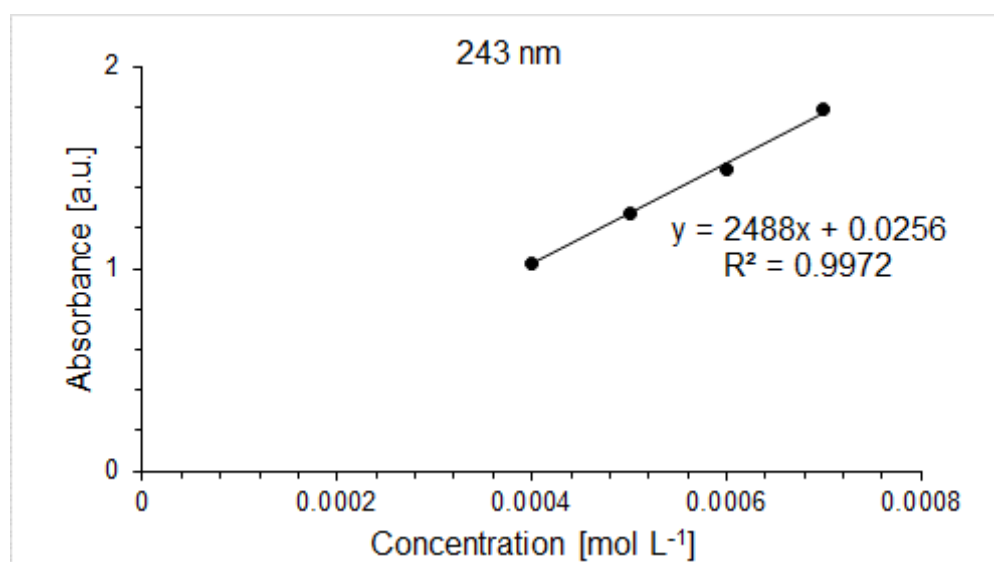


Figure 122. Determination of ϵ ($24900 \text{ M}^{-1} \text{ cm}^{-1}$) by linear regression of absorbance ($\lambda = 243 \text{ nm}$) of **172** against concentration.

7. Appendix

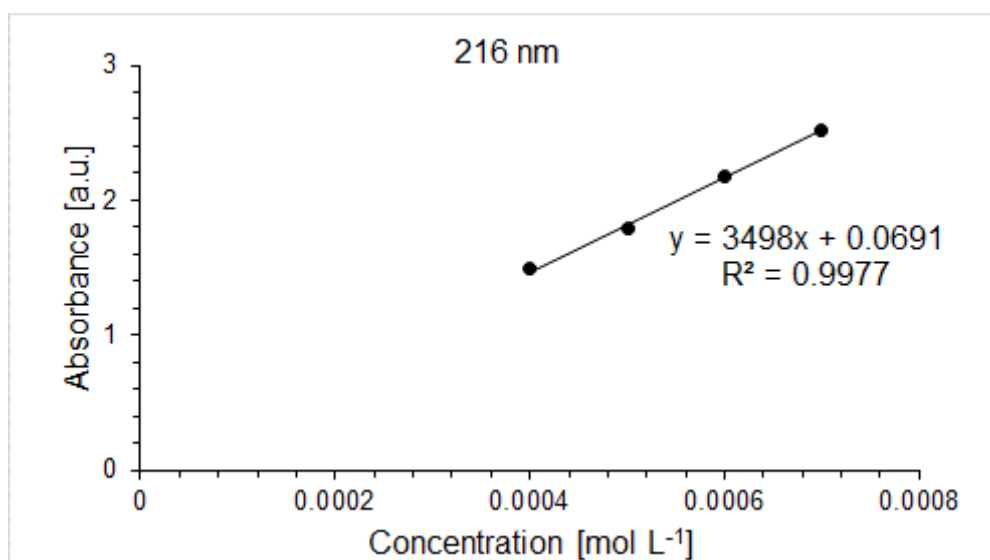


Figure 123. Determination of ϵ ($35000 \text{ M}^{-1} \text{ cm}^{-1}$) by linear regression of absorbance ($\lambda = 216 \text{ nm}$) of **172** against concentration.

7.4.8 2-chloro-1,4-dimethyl-3-para-*N,N*-dimethylaniline-1,2,3,4-tetrahydrobenzo[e][1,4,2,3]diazadiborinane **180**

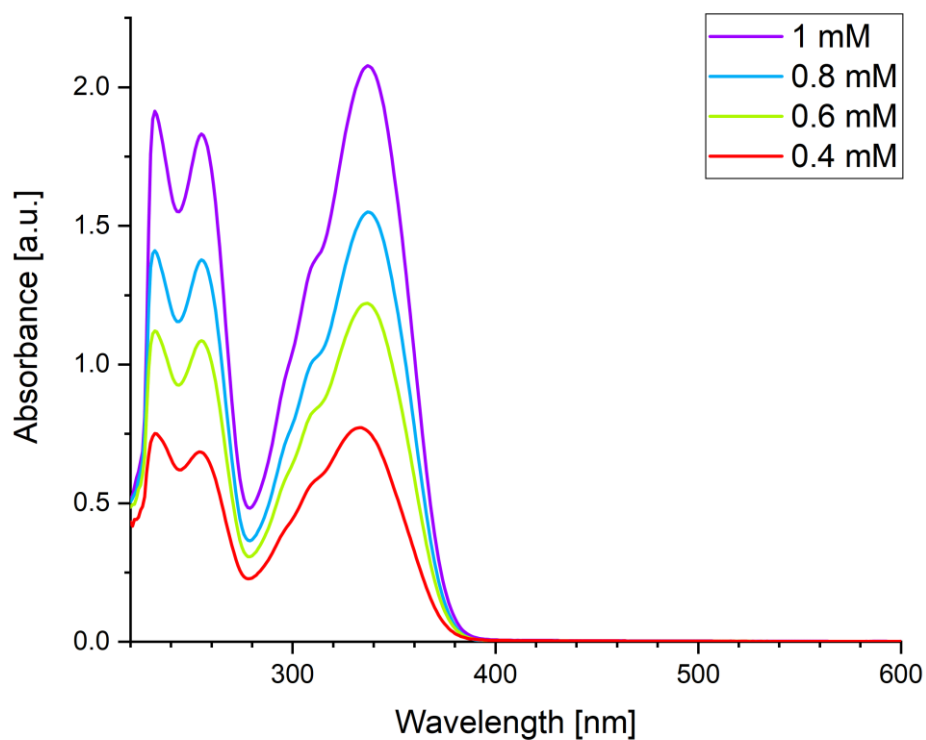


Figure 124. UV/Vis spectra of cyclic 1,4-diaza-2,3-diborinane **180** in diethylether at different concentrations (0.4 mM – 1 mM).

7. Appendix

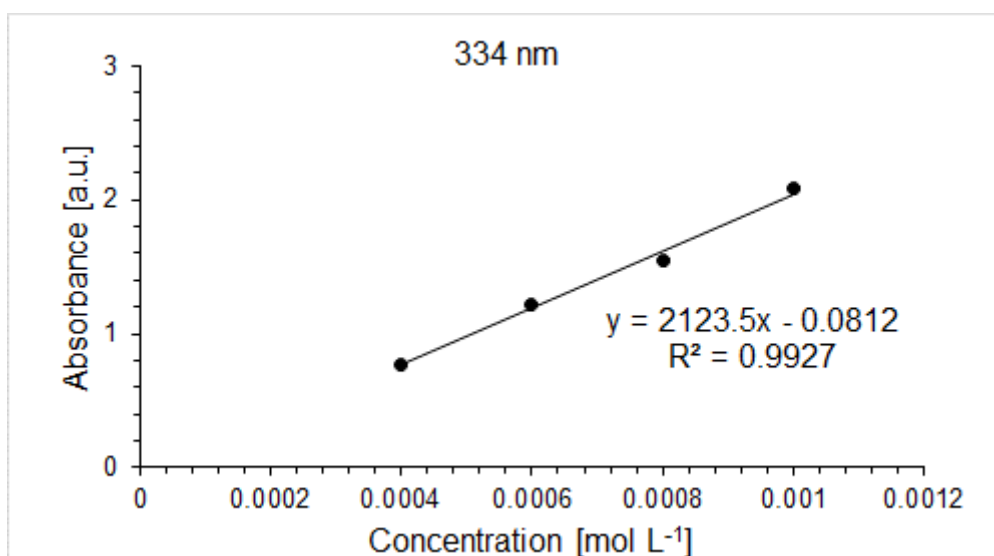


Figure 125. Determination of ϵ ($21200 \text{ M}^{-1} \text{ cm}^{-1}$) by linear regression of absorbance ($\lambda = 334 \text{ nm}$) of **180** against concentration.

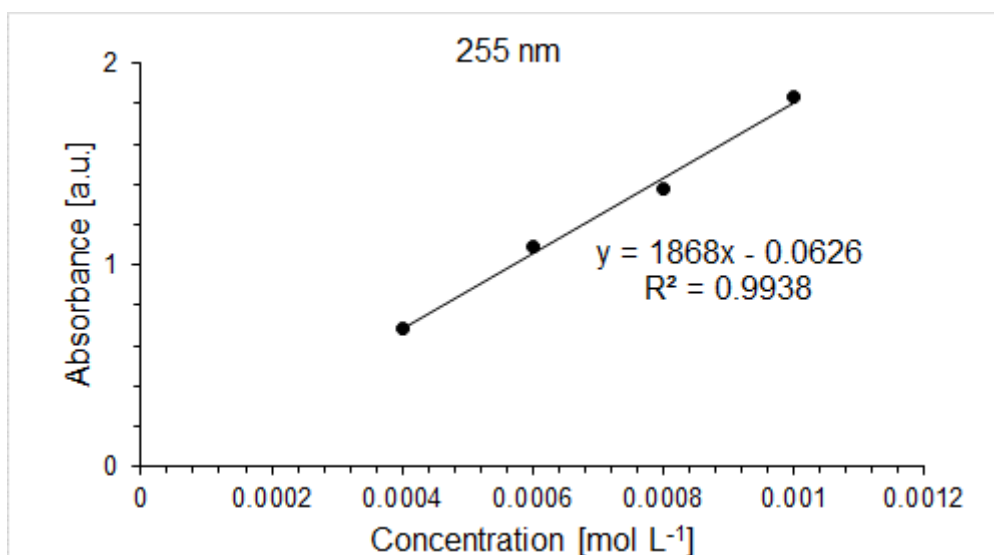


Figure 126. Determination of ϵ ($18700 \text{ M}^{-1} \text{ cm}^{-1}$) by linear regression of absorbance ($\lambda = 255 \text{ nm}$) of **180** against concentration.

7. Appendix

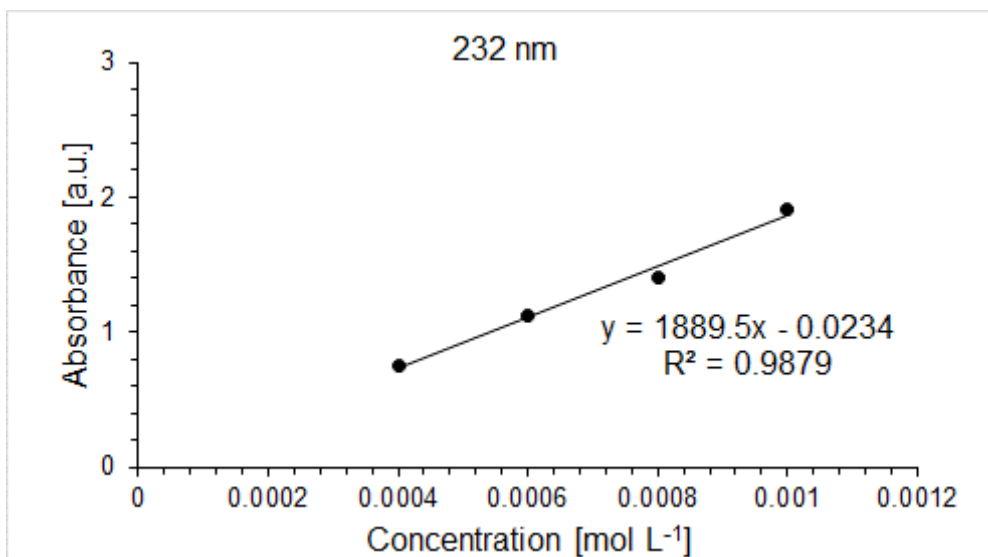


Figure 127. Determination of ϵ ($18900 \text{ M}^{-1} \text{ cm}^{-1}$) by linear regression of absorbance ($\lambda = 232 \text{ nm}$) of **180** against concentration.

7.4.9 1,4-dimethyl-3-para-*N,N*-dimethylaniline-2-pentafluorophenyl-1,2,3,4-tetrahydrobenzo[*e*][1,4,2,3]diazadiborinane **181**

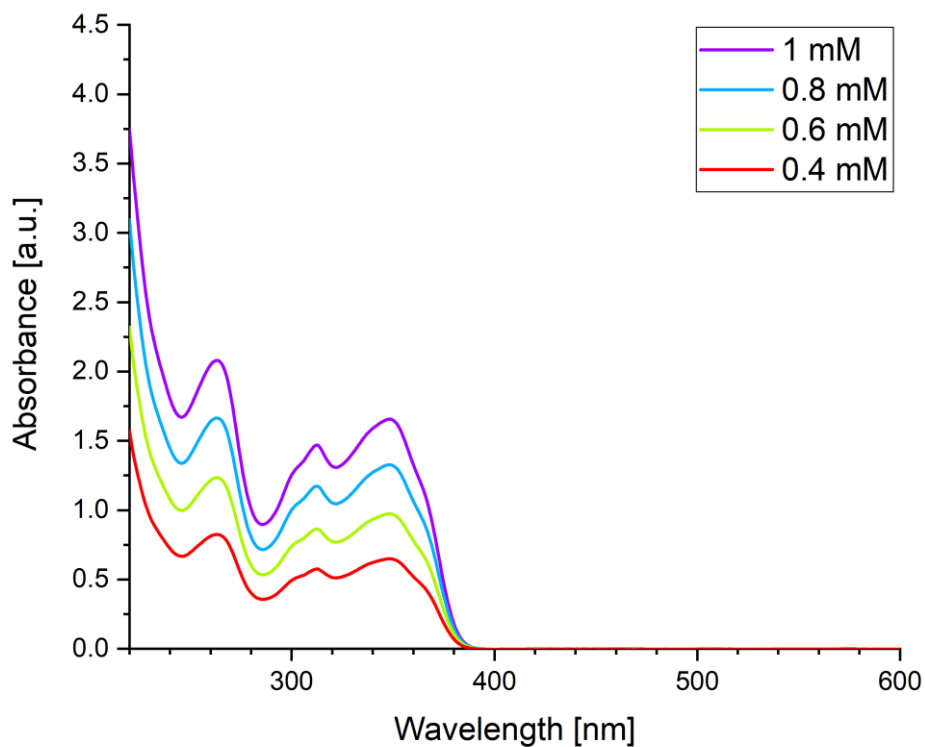


Figure 128. UV/Vis spectra of cyclic 1,4-diaza-2,3-diborinane **181** in hexane at different concentrations (0.4 mM – 1 mM).

7. Appendix

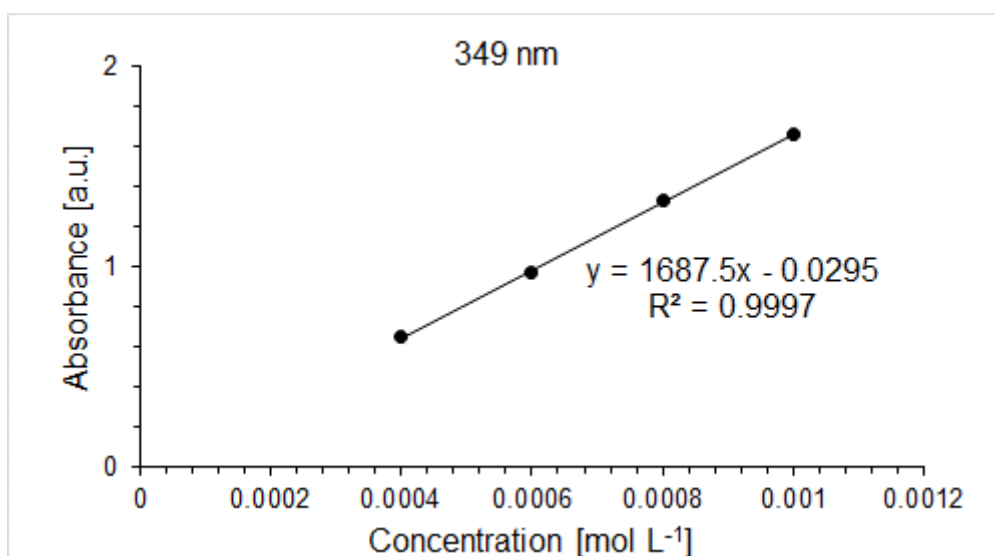


Figure 129. Determination of ϵ ($16900 \text{ M}^{-1} \text{ cm}^{-1}$) by linear regression of absorbance ($\lambda = 349 \text{ nm}$) of **181** against concentration.

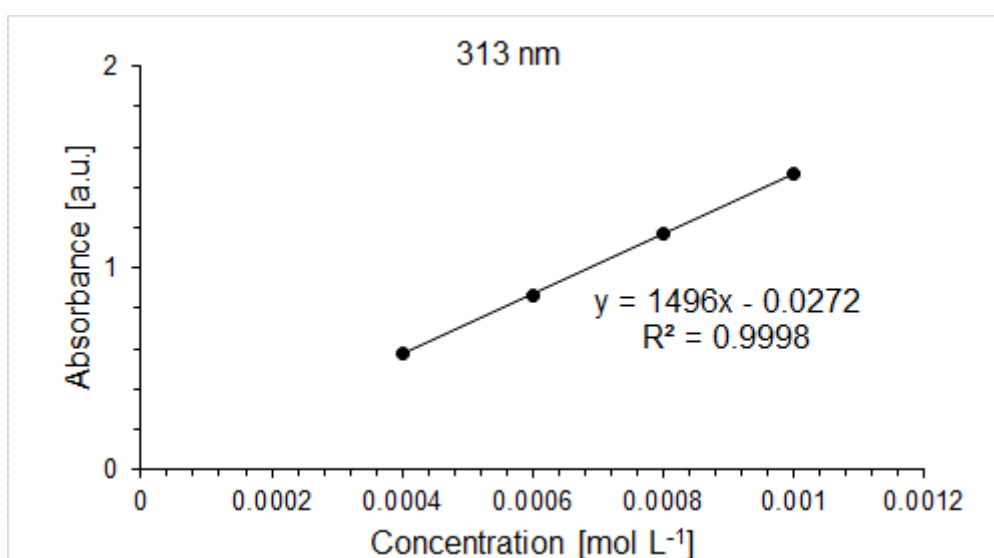


Figure 130. Determination of ϵ ($15000 \text{ M}^{-1} \text{ cm}^{-1}$) by linear regression of absorbance ($\lambda = 313 \text{ nm}$) of **181** against concentration.

7. Appendix

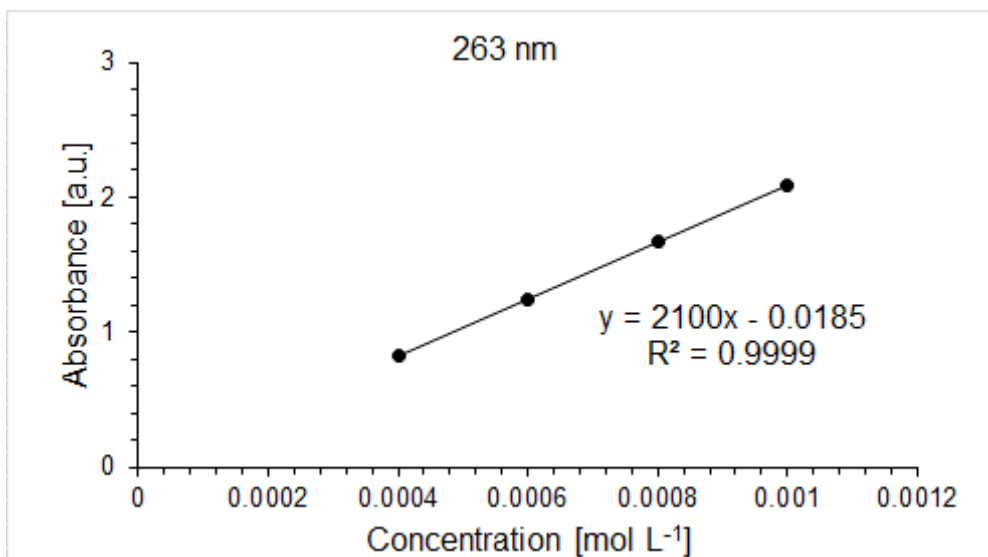


Figure 131. Determination of ϵ ($21000 \text{ M}^{-1} \text{ cm}^{-1}$) by linear regression of absorbance ($\lambda = 263 \text{ nm}$) of **181** against concentration.

7.4.10 4-(1,4-dimethyl-3-(4-nitrophenoxy)-3,4-dihydrobenzo[e]-[1,4,2,3]diazadi-borinin-2(1H)-yl)-N,N-dimethylaniline **183**

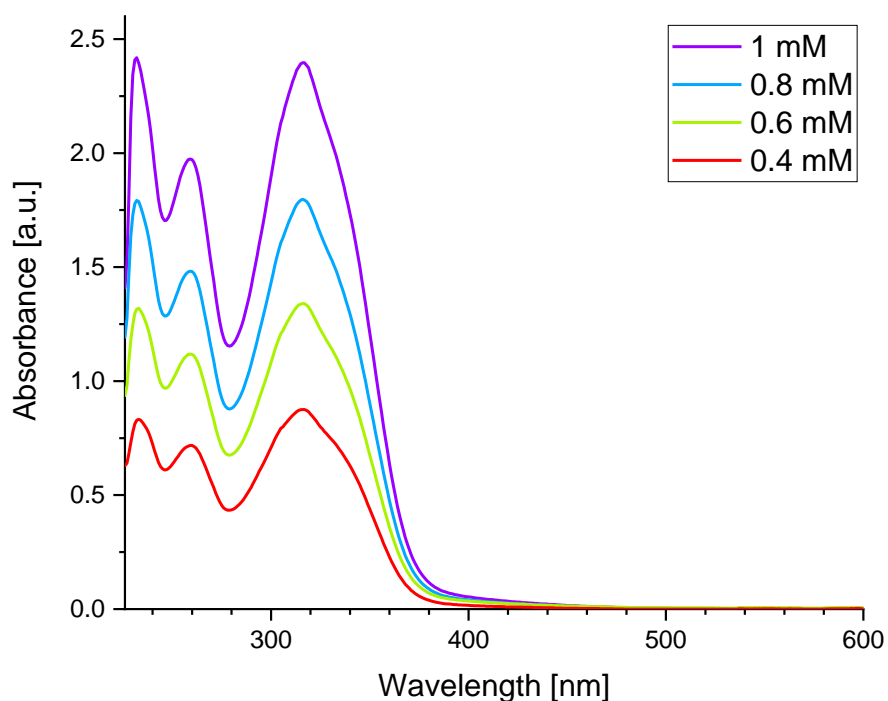


Figure 132. UV/Vis spectra of cyclic 1,4-diaza-2,3-diborinane **183** in diethylether at different concentrations (0.4 mM – 1 mM).

7. Appendix

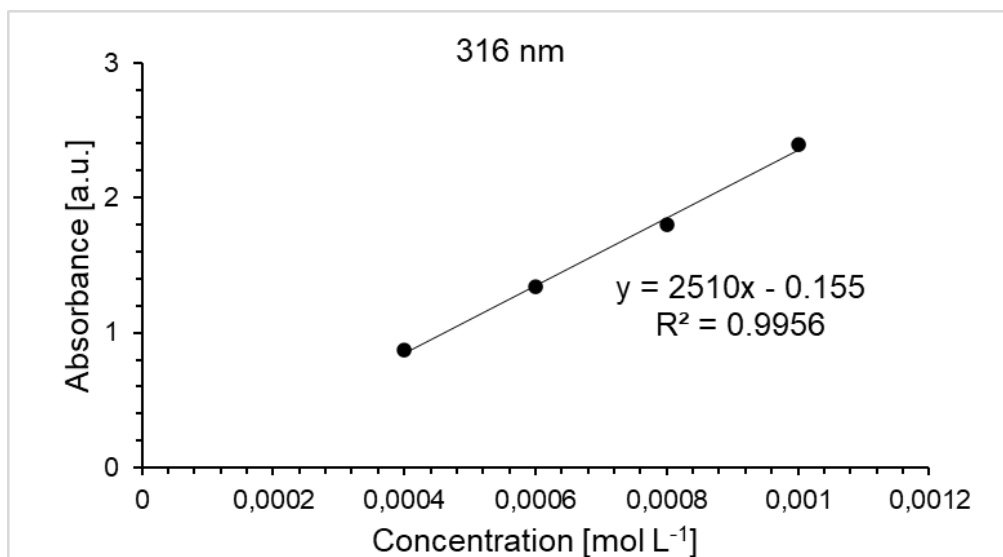


Figure 133. Determination of ϵ ($25100 \text{ M}^{-1} \text{ cm}^{-1}$) by linear regression of absorbance ($\lambda = 316 \text{ nm}$) of **183** against concentration.

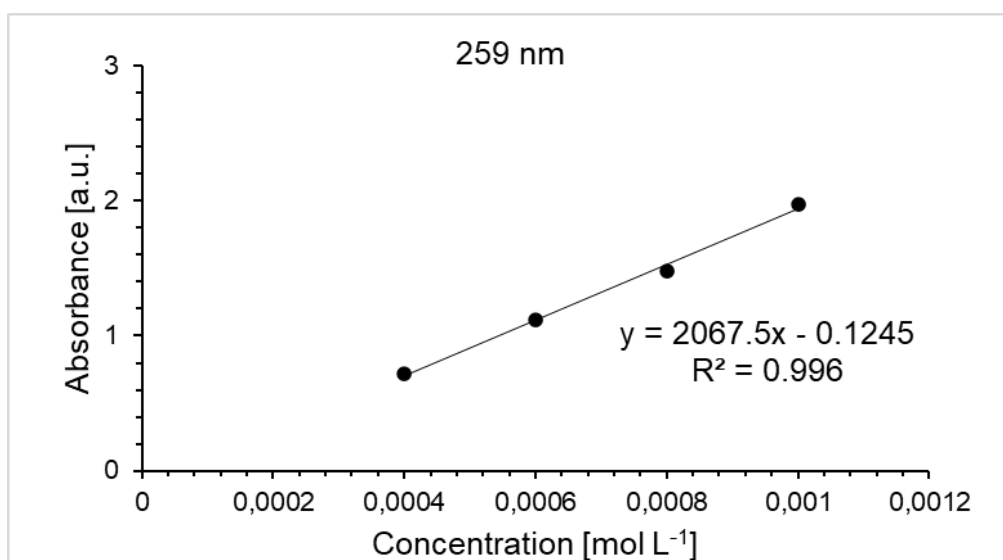


Figure 134. Determination of ϵ ($20700 \text{ M}^{-1} \text{ cm}^{-1}$) by linear regression of absorbance ($\lambda = 259 \text{ nm}$) of **183** against concentration.

7. Appendix

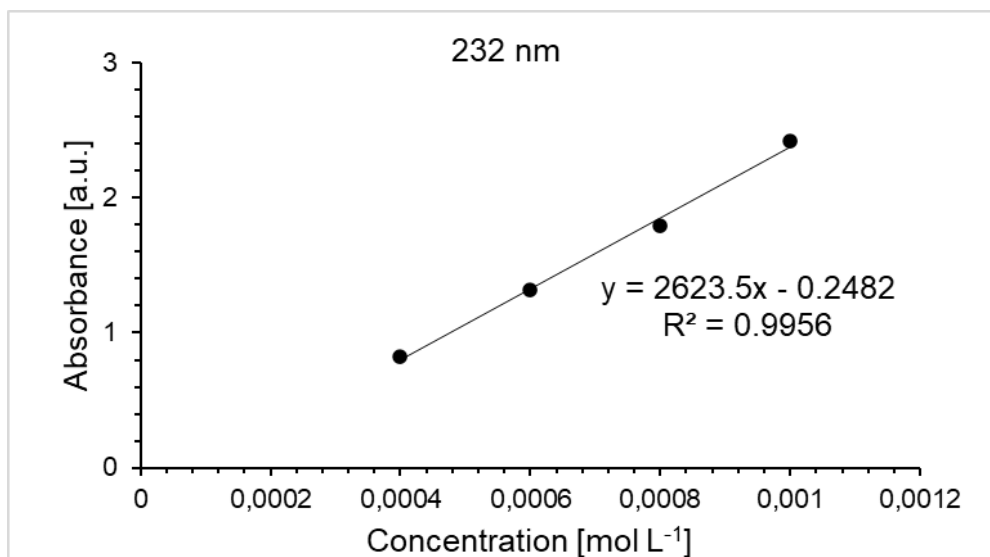


Figure 135. Determination of ϵ ($26200 \text{ M}^{-1} \text{ cm}^{-1}$) by linear regression of absorbance ($\lambda = 232 \text{ nm}$) of **183** against concentration.

7.4.11 1-chloro-2-dimethylamino-1,2-(2,3,5,6-tetramethylphenyl) diborane(4) **185**

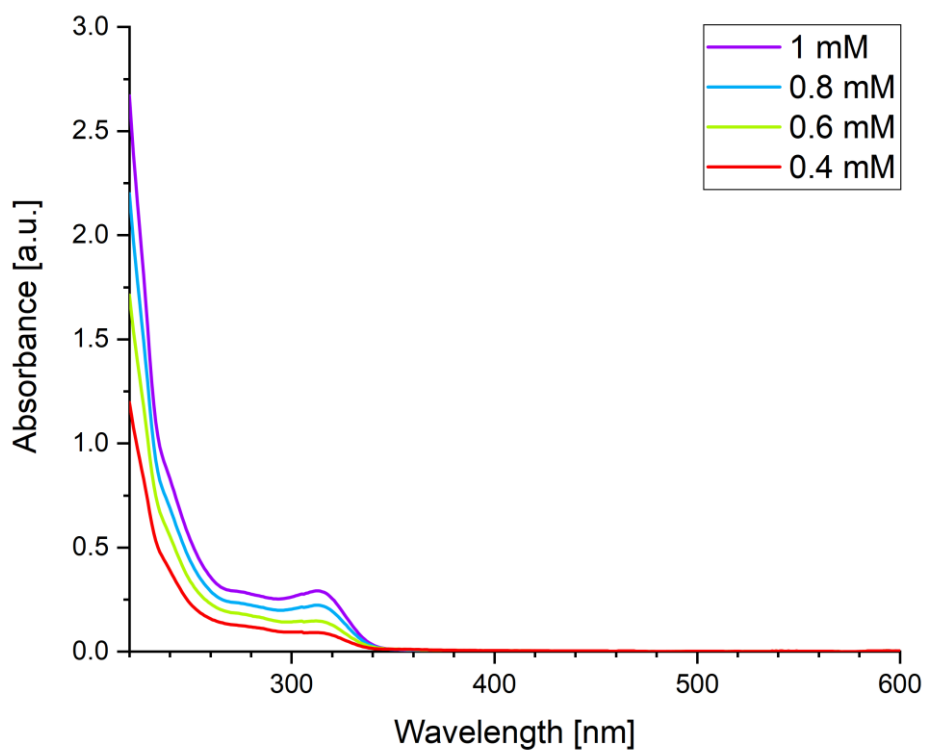


Figure 136. UV/Vis spectra of 1,2-diduryl diborane(4) **185** in hexane at different concentrations (0.4 mM – 1 mM).

7. Appendix

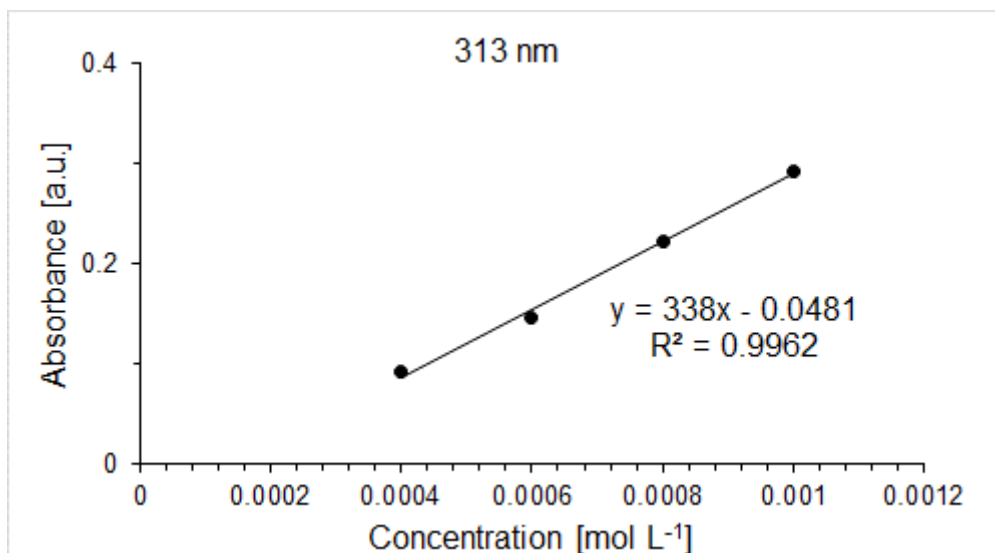


Figure 137. Determination of ϵ ($3380 \text{ M}^{-1} \text{ cm}^{-1}$) by linear regression of absorbance ($\lambda = 313 \text{ nm}$) of **185** against concentration.

7.4.12 2-dimethylamino-1-para-*N,N*-dimethylaniline-1,2-(2,3,5,6-tetramethylphenyl) diborane(4) **186**

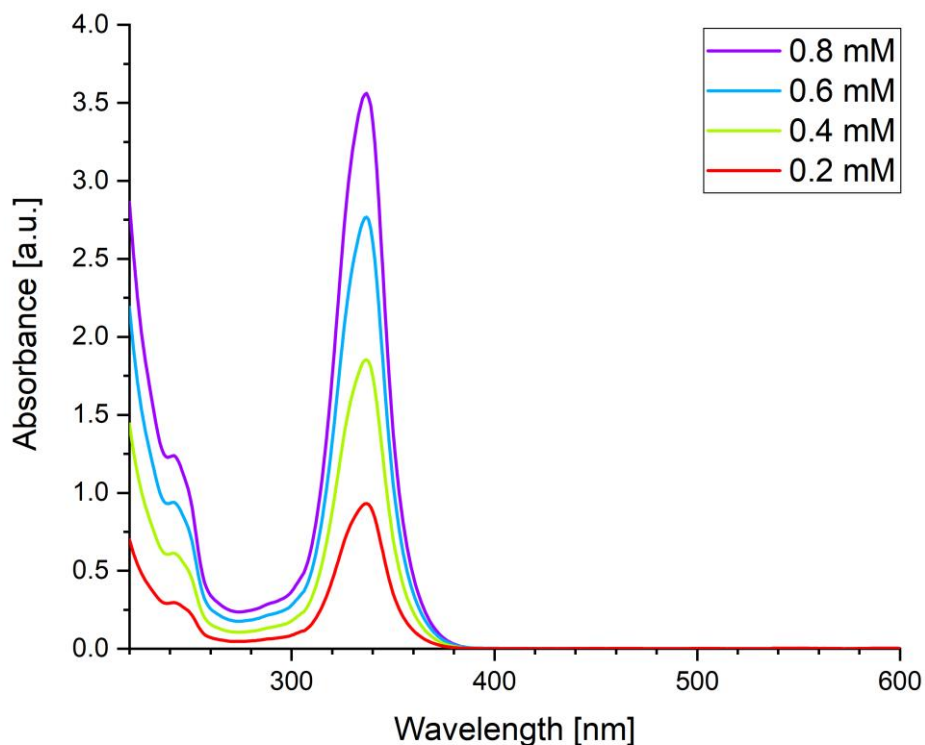


Figure 138. UV/Vis spectra of 1,2-diduryl diborane(4) **186** in hexane at different concentrations (0.2 mM – 0.8 mM).

7. Appendix

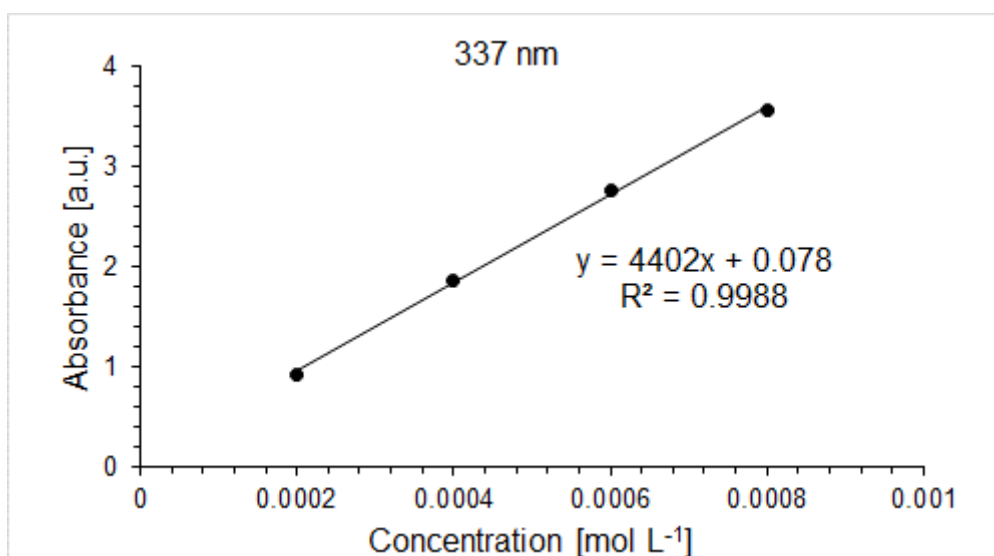


Figure 139. Determination of ϵ ($44000 \text{ M}^{-1} \text{ cm}^{-1}$) by linear regression of absorbance ($\lambda = 337 \text{ nm}$) of **186** against concentration.

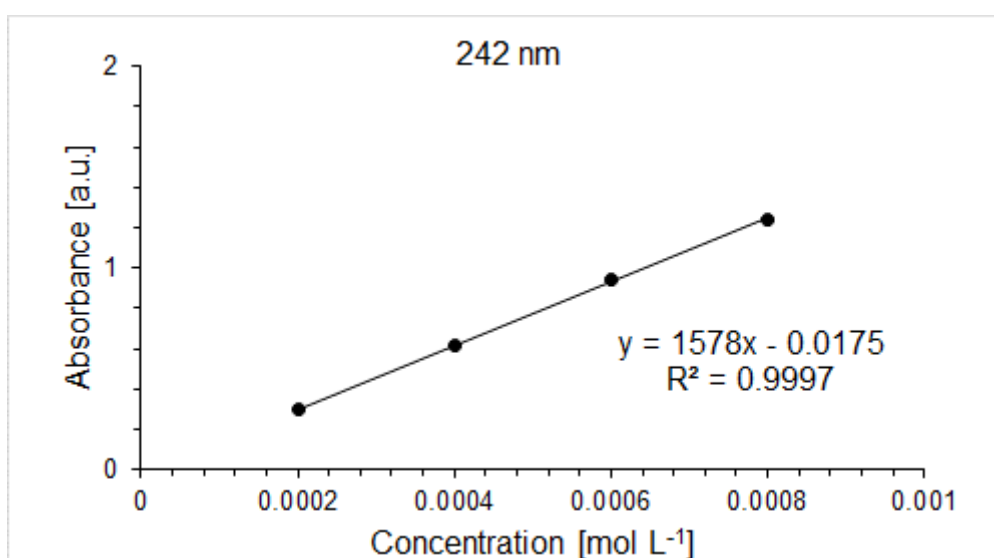


Figure 140. Determination of ϵ ($15800 \text{ M}^{-1} \text{ cm}^{-1}$) by linear regression of absorbance ($\lambda = 242 \text{ nm}$) of **186** against concentration.

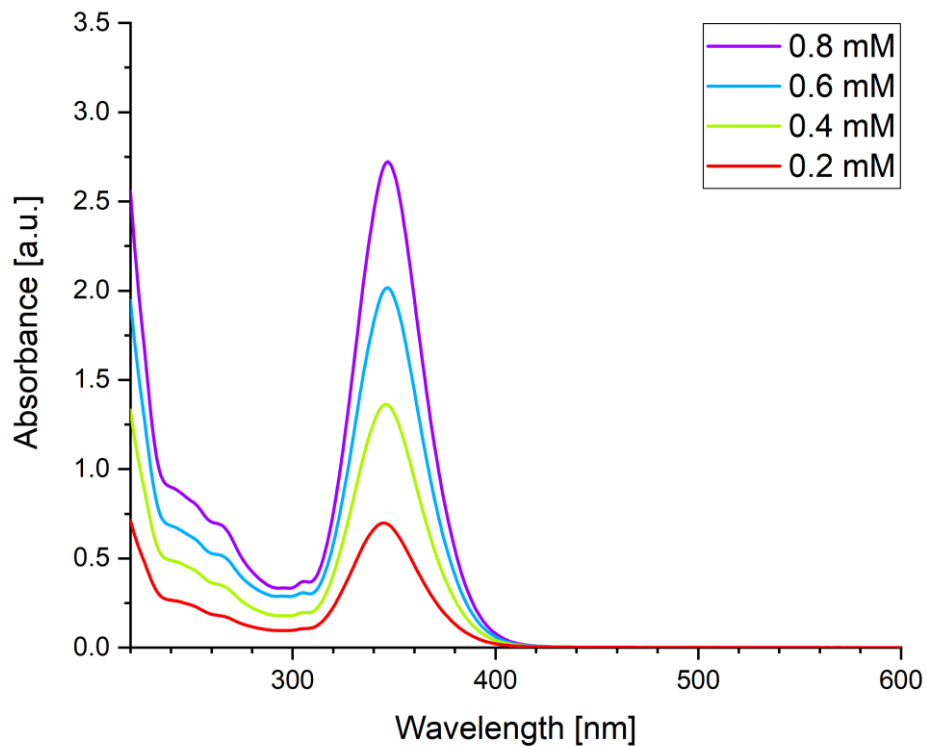
7.4.13 2-chloro-1-*para*-*N,N*-dimethylaniline-1,2-(2,3,5,6-tetramethylphenyl) diborane(4) 187

Figure 141. UV/Vis spectra of 1,2-diduryl diborane(4) **187** in hexane at different concentrations (0.2 mM – 0.8 mM).

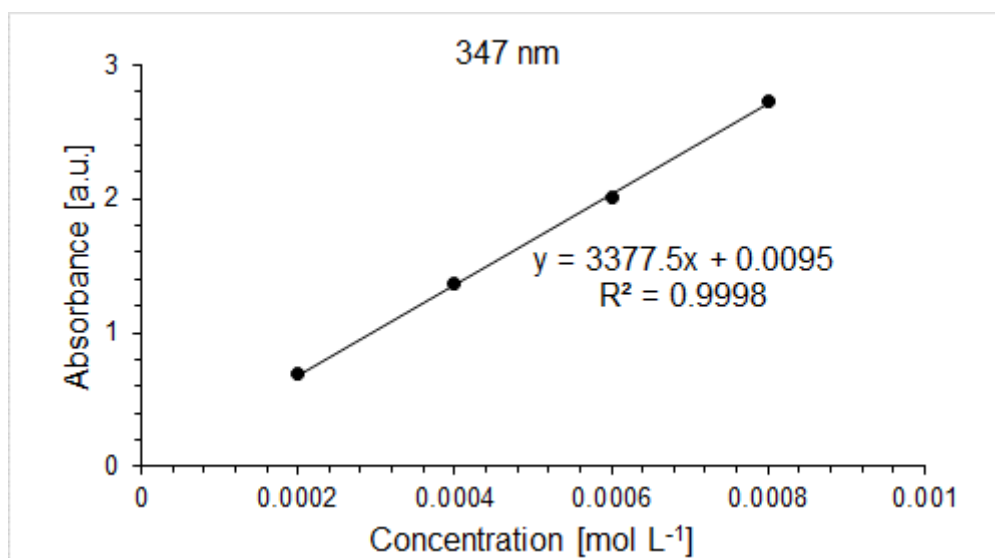


Figure 142. Determination of ϵ ($33800 \text{ M}^{-1} \text{ cm}^{-1}$) by linear regression of absorbance ($\lambda = 347 \text{ nm}$) of **187** against concentration.

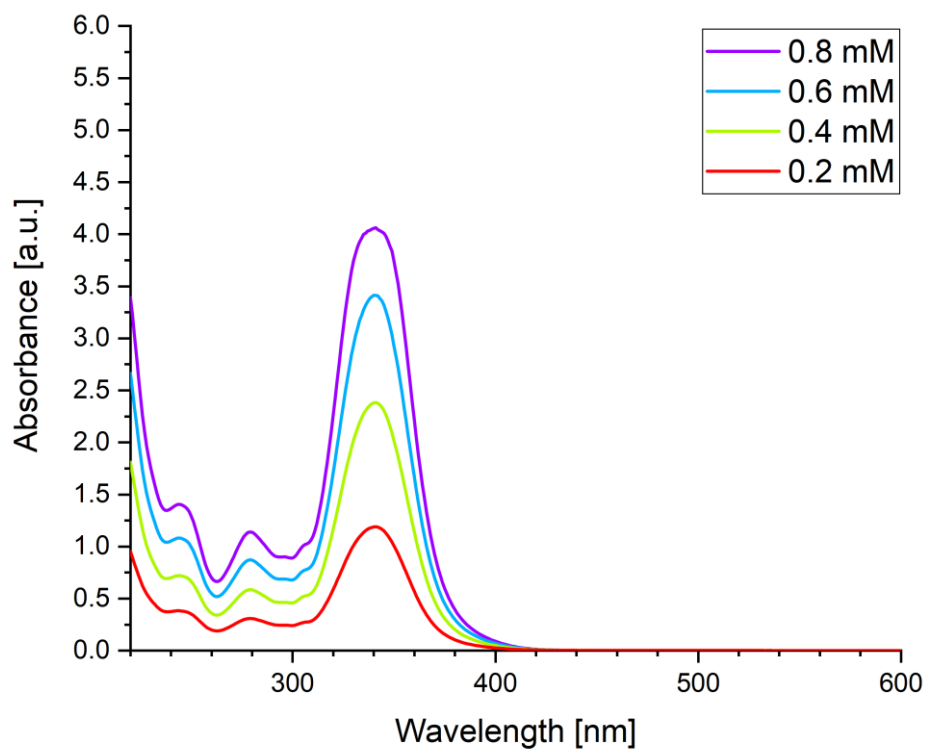
7.4.14 1,2-para-*N,N*-dimethylaniline-1,2-(2,3,5,6-tetramethylphenyl) diborane(4) 188

Figure 143. UV/Vis spectra of 1,2-diduryl diborane(4) **188** in hexane at different concentrations (0.2 mM – 0.8 mM).

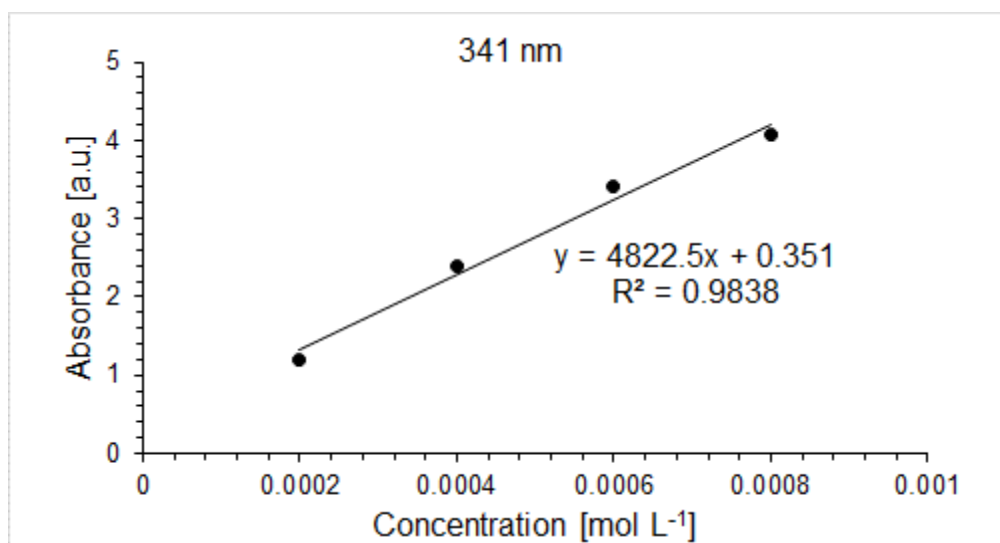


Figure 144. Determination of ϵ ($48200 \text{ M}^{-1} \text{ cm}^{-1}$) by linear regression of absorbance ($\lambda = 341 \text{ nm}$) of **188** against concentration.

7. Appendix

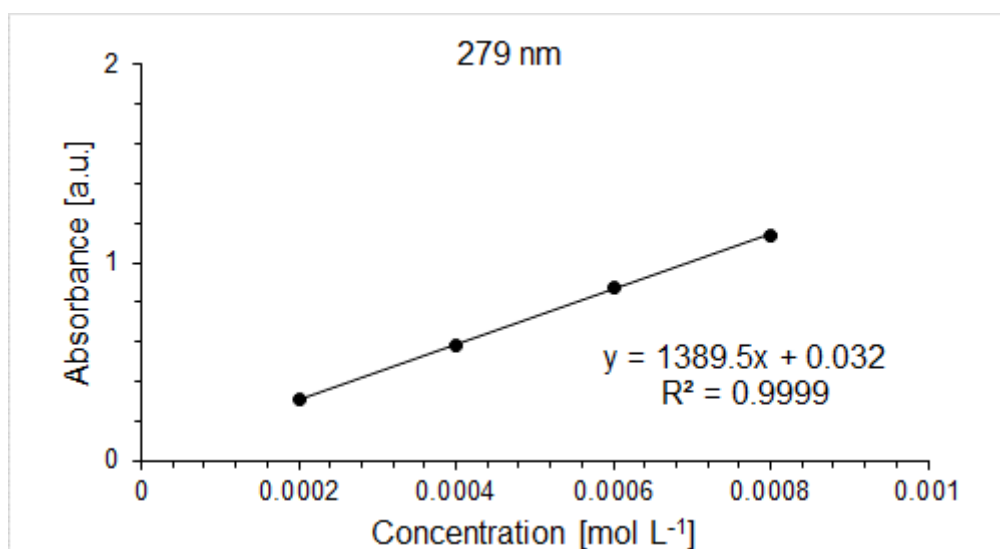


Figure 145. Determination of ϵ ($13900 \text{ M}^{-1} \text{ cm}^{-1}$) by linear regression of absorbance ($\lambda = 279 \text{ nm}$) of **188** against concentration.

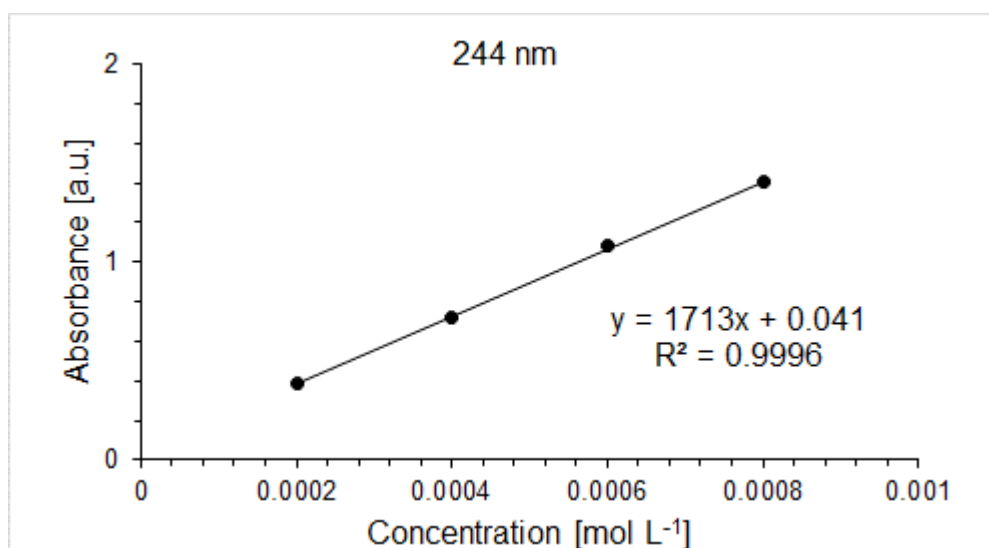


Figure 146. Determination of ϵ ($17100 \text{ M}^{-1} \text{ cm}^{-1}$) by linear regression of absorbance ($\lambda = 244 \text{ nm}$) of **188** against concentration.

7. Appendix

7.5 Crystal data and structure refinement

7.5.1 (E)-N,N'-bis(2,6-diisopropylphenyl)-N-(trimethylsilyl)benzimidamide

103

Identification code	sh3831	
Empirical formula	C ₃₄ H ₄₈ N ₂ Si	
Formula weight	512.83	
Temperature	152(2) K	
Wavelength	0.71073 Å	
Crystal system	Monoclinic	
Space group	P2 ₁	
Unit cell dimensions	a = 12.1798(5) Å	α = 90°.
	b = 14.4172(7) Å	β = 104.6193(15)°.
	c = 18.5891(7) Å	γ = 90°.
Volume	3158.5(2) Å ³	
Z	4	
Density (calculated)	1.078 Mg/m ³	
Absorption coefficient	0.098 mm ⁻¹	
F(000)	1120	
Crystal size	0.229 x 0.227 x 0.044 mm ³	
Theta range for data collection	1.132 to 26.786°.	
Index ranges	-15 ≤ h ≤ 15, -18 ≤ k ≤ 18, -23 ≤ l ≤ 23	
Reflections collected	38933	
Independent reflections	13447 [R(int) = 0.0415]	
Completeness to theta = 25.242°	100.0 %	
Absorption correction	Semi-empirical from equivalents	
Max. and min. transmission	0.7454 and 0.7071	
Refinement method	Full-matrix least-squares on F ²	
Data / restraints / parameters	13447 / 1 / 689	
Goodness-of-fit on F ²	1.023	
Final R indices [I > 2σ(I)]	R1 = 0.0464, wR2 = 0.0872	
R indices (all data)	R1 = 0.0725, wR2 = 0.0970	
Absolute structure parameter	-0.05(5)	
Extinction coefficient	n/a	
Largest diff. peak and hole	0.191 and -0.224 e.Å ⁻³	

7. Appendix

7.5.2 (E)-N-(dichloroboryl)-N,N'-bis(2,6-diisopropylphenyl)-benzimidamide 104a

Identification code	sh3848a
Empirical formula	C ₃₁ H ₃₉ B Cl ₂ N ₂
Formula weight	521.35
Temperature	293(2) K
Wavelength	0.71073 Å
Crystal system	Trigonal
Space group	P ₃ ₁ 21
Unit cell dimensions	a = 14.597(2) Å α = 90°. b = 14.597(2) Å β = 90°. c = 12.0020(15) Å γ = 120°.
Volume	2214.7(7) Å ³
Z	3
Density (calculated)	1.173 Mg/m ³
Absorption coefficient	0.241 mm ⁻¹
F(000)	834
Crystal size	0.815 x 0.681 x 0.158 mm ³
Theta range for data collection	1.611 to 26.785°.
Index ranges	-18 ≤ h ≤ 18, -18 ≤ k ≤ 17, -15 ≤ l ≤ 15
Reflections collected	34470
Independent reflections	3132 [R(int) = 0.1334]
Completeness to theta = 25.242°	100.0 %
Absorption correction	Semi-empirical from equivalents
Max. and min. transmission	0.7454 and 0.6757
Refinement method	Full-matrix least-squares on F ²
Data / restraints / parameters	3132 / 0 / 170
Goodness-of-fit on F ²	1.003
Final R indices [I > 2σ(I)]	R1 = 0.0936, wR2 = 0.2162
R indices (all data)	R1 = 0.1458, wR2 = 0.2431
Absolute structure parameter	0.0(3)
Extinction coefficient	n/a
Largest diff. peak and hole	1.777 and -0.649 e.Å ⁻³

7. Appendix

7.5.3 (E)-N,N'-di-tert-butyl-N-(dichloro-boryl)benzimidamide 119

Identification code	sh4371_a	
Empirical formula	C ₁₅ H ₂₃ B Cl ₂ N ₂	
Formula weight	313.06	
Temperature	140(2) K	
Wavelength	0.71073 Å	
Crystal system	Monoclinic	
Space group	C2/c	
Unit cell dimensions	a = 14.2713(5) Å	α = 90°.
	b = 10.6734(4) Å	β = 116.7160(10)°.
	c = 12.4297(4) Å	γ = 90°.
Volume	1691.21(10) Å ³	
Z	4	
Density (calculated)	1.230 Mg/m ³	
Absorption coefficient	0.376 mm ⁻¹	
F(000)	664	
Crystal size	0.371 x 0.222 x 0.072 mm ³	
Theta range for data collection	2.489 to 31.536°.	
Index ranges	-20 ≤ h ≤ 20, -15 ≤ k ≤ 15, -18 ≤ l ≤ 18	
Reflections collected	17930	
Independent reflections	2821 [R(int) = 0.0250]	
Completeness to theta = 25.242°	99.9 %	
Absorption correction	Semi-empirical from equivalents	
Max. and min. transmission	0.7462 and 0.7098	
Refinement method	Full-matrix least-squares on F ²	
Data / restraints / parameters	2821 / 0 / 96	
Goodness-of-fit on F ²	1.024	
Final R indices [I > 2σ(I)]	R1 = 0.0278, wR2 = 0.0712	
R indices (all data)	R1 = 0.0321, wR2 = 0.0747	
Extinction coefficient	n/a	
Largest diff. peak and hole	0.385 and -0.236 e.Å ⁻³	

7. Appendix

7.5.4 (E)-*N*-(dichloroboryl)-*N,N'*-bis(2,6-diisopropylphenyl)-2,3,4,5,6-pentafluorobenzimidamide 124

Identification code	sh4305	
Empirical formula	C ₃₂ H ₃₆ B Cl ₄ F ₅ N ₂	
Formula weight	696.24	
Temperature	132(2) K	
Wavelength	0.71073 Å	
Crystal system	Monoclinic	
Space group	P2 ₁ /c	
Unit cell dimensions	a = 20.5392(4) Å	α = 90°.
	b = 9.9043(2) Å	β = 104.4440(10)°.
	c = 17.4491(4) Å	γ = 90°.
Volume	3437.41(13) Å ³	
Z	4	
Density (calculated)	1.345 Mg/m ³	
Absorption coefficient	0.396 mm ⁻¹	
F(000)	1440	
Crystal size	0.196 x 0.156 x 0.124 mm ³	
Theta range for data collection	1.024 to 31.564°.	
Index ranges	-29 ≤ h ≤ 30, -14 ≤ k ≤ 11, -23 ≤ l ≤ 25	
Reflections collected	34020	
Independent reflections	11480 [R(int) = 0.0452]	
Completeness to theta = 25.242°	100.0 %	
Absorption correction	Semi-empirical from equivalents	
Max. and min. transmission	0.7462 and 0.7186	
Refinement method	Full-matrix least-squares on F ²	
Data / restraints / parameters	11480 / 0 / 533	
Goodness-of-fit on F ²	1.028	
Final R indices [I > 2σ(I)]	R1 = 0.0550, wR2 = 0.1301	
R indices (all data)	R1 = 0.0935, wR2 = 0.1507	
Extinction coefficient	n/a	
Largest diff. peak and hole	1.093 and -1.009 e.Å ⁻³	

7. Appendix

7.5.5 (E)-N-(chloro(phenyl)boryl)-N,N'-bis(2,6-diisopropyl-phenyl)benzimidamide 126

Identification code	sh4366_a	
Empirical formula	C75 H90 B2 Cl4 N4	
Formula weight	1210.92	
Temperature	140(2) K	
Wavelength	0.71073 Å	
Crystal system	Triclinic	
Space group	P-1	
Unit cell dimensions	a = 9.2911(3) Å	$\alpha = 105.6750(10)^\circ$.
	b = 18.0422(6) Å	$\beta = 91.6910(10)^\circ$.
	c = 21.1328(7) Å	$\gamma = 96.6650(10)^\circ$.
Volume	3380.86(19) Å ³	
Z	2	
Density (calculated)	1.190 Mg/m ³	
Absorption coefficient	0.220 mm ⁻¹	
F(000)	1292	
Crystal size	0.408 x 0.150 x 0.040 mm ³	
Theta range for data collection	2.006 to 26.773°.	
Index ranges	-11 ≤ h ≤ 11, -22 ≤ k ≤ 22, -26 ≤ l ≤ 26	
Reflections collected	66482	
Independent reflections	14359 [R(int) = 0.0670]	
Completeness to theta = 25.242°	100.0 %	
Absorption correction	Semi-empirical from equivalents	
Max. and min. transmission	0.7454 and 0.6951	
Refinement method	Full-matrix least-squares on F ²	
Data / restraints / parameters	14359 / 0 / 766	
Goodness-of-fit on F ²	1.029	
Final R indices [I > 2σ(I)]	R1 = 0.0486, wR2 = 0.1030	
R indices (all data)	R1 = 0.0723, wR2 = 0.1160	
Extinction coefficient	n/a	
Largest diff. peak and hole	0.442 and -0.353 e.Å ⁻³	

7. Appendix

7.5.6 (E)-N-(chloro(cyclohexyl)boryl)-N,N'-bis(2,6-diisopropylphenyl)-benzimidamide 128

Identification code	4319_a	
Empirical formula	C ₉₅ H ₁₂₄ B ₂ Cl ₂ N ₄	
Formula weight	1414.49	
Temperature	133(2) K	
Wavelength	0.71073 Å	
Crystal system	Monoclinic	
Space group	P2 ₁ /n	
Unit cell dimensions	a = 10.5754(2) Å	α = 90°.
	b = 17.7377(3) Å	β = 100.7670(10)°.
	c = 23.0932(5) Å	γ = 90°.
Volume	4255.63(14) Å ³	
Z	2	
Density (calculated)	1.104 Mg/m ³	
Absorption coefficient	0.123 mm ⁻¹	
F(000)	1532	
Crystal size	0.484 x 0.137 x 0.038 mm ³	
Theta range for data collection	1.998 to 29.596°.	
Index ranges	-14 ≤ h ≤ 14, -24 ≤ k ≤ 18, -32 ≤ l ≤ 32	
Reflections collected	64722	
Independent reflections	11954 [R(int) = 0.0463]	
Completeness to theta = 25.242°	100.0 %	
Absorption correction	Semi-empirical from equivalents	
Max. and min. transmission	0.7459 and 0.7235	
Refinement method	Full-matrix least-squares on F ²	
Data / restraints / parameters	11954 / 389 / 533	
Goodness-of-fit on F ²	1.040	
Final R indices [I > 2σ(I)]	R1 = 0.0516, wR2 = 0.1344	
R indices (all data)	R1 = 0.0697, wR2 = 0.1488	
Extinction coefficient	n/a	
Largest diff. peak and hole	0.915 and -0.431 e.Å ⁻³	

7. Appendix

7.5.7. (E)-N-(chloro(dimethylamino)boryl)-N,N'-bis(2,6-diisopropylphenyl)-benzimidamide 130

Identification code	sh4281_a	
Empirical formula	C ₃₃ H ₄₅ B Cl N ₃	
Formula weight	529.98	
Temperature	140(2) K	
Wavelength	0.71073 Å	
Crystal system	Monoclinic	
Space group	P2 ₁ /c	
Unit cell dimensions	a = 10.0506(2) Å	α = 90°.
	b = 19.1730(3) Å	β = 100.9870(10)°.
	c = 16.4603(2) Å	γ = 90°.
Volume	3113.76(9) Å ³	
Z	4	
Density (calculated)	1.131 Mg/m ³	
Absorption coefficient	0.148 mm ⁻¹	
F(000)	1144	
Crystal size	0.218 x 0.217 x 0.064 mm ³	
Theta range for data collection	2.322 to 28.717°.	
Index ranges	-13 ≤ h ≤ 13, -25 ≤ k ≤ 25, -22 ≤ l ≤ 19	
Reflections collected	40403	
Independent reflections	8032 [R(int) = 0.0369]	
Completeness to theta = 25.242°	99.6 %	
Absorption correction	Semi-empirical from equivalents	
Max. and min. transmission	0.7458 and 0.7227	
Refinement method	Full-matrix least-squares on F ²	
Data / restraints / parameters	8032 / 0 / 353	
Goodness-of-fit on F ²	1.026	
Final R indices [I > 2σ(I)]	R1 = 0.0397, wR2 = 0.0978	
R indices (all data)	R1 = 0.0505, wR2 = 0.1050	
Extinction coefficient	n/a	
Largest diff. peak and hole	0.311 and -0.315 e.Å ⁻³	

7. Appendix

7.5.8 (E)-N,N'-di-*tert*-butyl-N-(chloro(dimethylamino)-boryl)benzimidamide

131

Identification code	4419_a	
Empirical formula	C ₁₇ H ₂₉ B Cl N ₃	
Formula weight	321.69	
Temperature	132(2) K	
Wavelength	0.71073 Å	
Crystal system	Monoclinic	
Space group	P2 ₁ /c	
Unit cell dimensions	a = 9.4984(3) Å	α = 90°.
	b = 24.1359(7) Å	β = 107.221(2)°.
	c = 8.6311(3) Å	γ = 90°.
Volume	1889.99(11) Å ³	
Z	4	
Density (calculated)	1.131 Mg/m ³	
Absorption coefficient	0.203 mm ⁻¹	
F(000)	696	
Crystal size	0.281 x 0.216 x 0.210 mm ³	
Theta range for data collection	1.687 to 27.944°.	
Index ranges	-12 ≤ h ≤ 12, -31 ≤ k ≤ 31, -11 ≤ l ≤ 11	
Reflections collected	30056	
Independent reflections	4533 [R(int) = 0.0411]	
Completeness to theta = 25.242°	100.0 %	
Absorption correction	Semi-empirical from equivalents	
Max. and min. transmission	0.7456 and 0.7051	
Refinement method	Full-matrix least-squares on F ²	
Data / restraints / parameters	4533 / 48 / 238	
Goodness-of-fit on F ²	1.021	
Final R indices [I > 2σ(I)]	R1 = 0.0455, wR2 = 0.1050	
R indices (all data)	R1 = 0.0657, wR2 = 0.1152	
Extinction coefficient	n/a	
Largest diff. peak and hole	0.251 and -0.305 e.Å ⁻³	

7. Appendix

7.5.9 Benzazaborole 136

Identification code	sh3997
Empirical formula	C ₄₂ H ₅₈ B Cl N ₄ , 2(C ₆ H ₆)
Formula weight	821.40
Temperature	152(2) K
Wavelength	0.71073 Å
Crystal system	Orthorhombic
Space group	P2 ₁ 2 ₁ 2 ₁
Unit cell dimensions	a = 9.3594(3) Å α = 90°. b = 19.4142(6) Å β = 90°. c = 26.6113(8) Å γ = 90°.
Volume	4835.4(3) Å ³
Z	4
Density (calculated)	1.128 Mg/m ³
Absorption coefficient	0.118 mm ⁻¹
F(000)	1776
Crystal size	0.265 x 0.148 x 0.078 mm ³
Theta range for data collection	1.298 to 27.198°.
Index ranges	-12 ≤ h ≤ 12, -24 ≤ k ≤ 24, -34 ≤ l ≤ 34
Reflections collected	65119
Independent reflections	10751 [R(int) = 0.0655]
Completeness to theta = 25.242°	100.0 %
Absorption correction	Semi-empirical from equivalents
Max. and min. transmission	0.7455 and 0.6804
Refinement method	Full-matrix least-squares on F ²
Data / restraints / parameters	10751 / 32 / 526
Goodness-of-fit on F ²	1.033
Final R indices [I > 2σ(I)]	R1 = 0.0457, wR2 = 0.0904
R indices (all data)	R1 = 0.0711, wR2 = 0.1002
Absolute structure parameter	0.04(3)
Extinction coefficient	n/a
Largest diff. peak and hole	0.194 and -0.227 e.Å ⁻³

7. Appendix

7.5.10 Diazaboretidine 145

Identification code	stru4304_a
Empirical formula	C ₃₆ H ₅₂ B ₃ N ₃
Formula weight	537.61
Temperature	153(2) K
Wavelength	0.71073 Å
Crystal system	Monoclinic
Space group	P2 ₁ /n
Unit cell dimensions	a = 9.3442(4) Å α = 90°. b = 19.0647(8) Å β = 103.9200(10)°. c = 18.9802(6) Å γ = 90°.
Volume	3281.9(2) Å ³
Z	4
Density (calculated)	1.088 Mg/m ³
Absorption coefficient	0.062 mm ⁻¹
F(000)	1176
Crystal size	0.408 x 0.320 x 0.130 mm ³
Theta range for data collection	2.136 to 29.601°.
Index ranges	-12 ≤ h ≤ 11, -25 ≤ k ≤ 26, -22 ≤ l ≤ 26
Reflections collected	42250
Independent reflections	9189 [R(int) = 0.0304]
Completeness to theta = 25.242°	99.9 %
Absorption correction	Semi-empirical from equivalents
Max. and min. transmission	0.7459 and 0.6935
Refinement method	Full-matrix least-squares on F ²
Data / restraints / parameters	9189 / 0 / 373
Goodness-of-fit on F ²	1.039
Final R indices [I > 2σ(I)]	R1 = 0.0444, wR2 = 0.1164
R indices (all data)	R1 = 0.0529, wR2 = 0.1232
Extinction coefficient	n/a
Largest diff. peak and hole	0.348 and -0.307 e.Å ⁻³

7. Appendix

7.5.11 2-chloro-1,2-bis(dimethylamino)-1-para-*N,N*-dimethylaniline diborane(4) 156

Identification code	sh3916	
Empirical formula	C ₁₂ H ₂₂ B ₂ Cl N ₃	
Formula weight	265.39	
Temperature	152(2) K	
Wavelength	0.71073 Å	
Crystal system	Triclinic	
Space group	P-1	
Unit cell dimensions	a = 6.6512(2) Å	α = 88.905(2)°.
	b = 8.9583(3) Å	β = 76.1371(18)°.
	c = 13.6050(5) Å	γ = 71.3537(17)°.
Volume	744.25(4) Å ³	
Z	2	
Density (calculated)	1.184 Mg/m ³	
Absorption coefficient	0.242 mm ⁻¹	
F(000)	284	
Crystal size	0.480 x 0.477 x 0.236 mm ³	
Theta range for data collection	1.545 to 31.510°.	
Index ranges	-9<=h<=9, -13<=k<=13, -19<=l<=19	
Reflections collected	18569	
Independent reflections	4904 [R(int) = 0.0198]	
Completeness to theta = 25.242°	99.9 %	
Absorption correction	Semi-empirical from equivalents	
Max. and min. transmission	0.7462 and 0.7169	
Refinement method	Full-matrix least-squares on F ²	
Data / restraints / parameters	4904 / 0 / 251	
Goodness-of-fit on F ²	1.045	
Final R indices [I>2σ(I)]	R1 = 0.0377, wR2 = 0.1024	
R indices (all data)	R1 = 0.0462, wR2 = 0.1087	
Extinction coefficient	n/a	
Largest diff. peak and hole	0.557 and -0.213 e.Å ⁻³	

7. Appendix

7.5.12 1,2-bis(dimethylamino)-1,2-bis(para-*N,N*-dimethylaniline) diborane(4) 157

Identification code	sh3946a	
Empirical formula	C ₂₀ H ₃₂ B ₂ N ₄	
Formula weight	350.11	
Temperature	142(2) K	
Wavelength	0.71073 Å	
Crystal system	Monoclinic	
Space group	P2 ₁ /n	
Unit cell dimensions	a = 9.9230(3) Å	α = 90°.
	b = 13.6830(5) Å	β = 105.8506(17)°.
	c = 15.8473(6) Å	γ = 90°.
Volume	2069.88(13) Å ³	
Z	4	
Density (calculated)	1.124 Mg/m ³	
Absorption coefficient	0.066 mm ⁻¹	
F(000)	760	
Crystal size	0.311 x 0.261 x 0.248 mm ³	
Theta range for data collection	2.000 to 28.095°.	
Index ranges	-13 ≤ h ≤ 12, -18 ≤ k ≤ 18, 0 ≤ l ≤ 20	
Reflections collected	9736	
Independent reflections	4993 [R(int) = 0.0502]	
Completeness to theta = 25.242°	100.0 %	
Absorption correction	Semi-empirical from equivalents	
Max. and min. transmission	0.7456 and 0.6989	
Refinement method	Full-matrix least-squares on F ²	
Data / restraints / parameters	4993 / 0 / 355	
Goodness-of-fit on F ²	1.074	
Final R indices [I > 2σ(I)]	R1 = 0.0658, wR2 = 0.1499	
R indices (all data)	R1 = 0.1045, wR2 = 0.1648	
Extinction coefficient	n/a	
Largest diff. peak and hole	0.301 and -0.220 e.Å ⁻³	

7. Appendix

7.5.13 1,1-bis(dimethylamino)-2,2-bis(para-*N,N*-dimethyl-aniline) diborane(4) 158

Identification code	sh3926	
Empirical formula	C ₂₀ H ₃₂ B ₂ N ₄	
Formula weight	350.11	
Temperature	152(2) K	
Wavelength	0.71073 Å	
Crystal system	Monoclinic	
Space group	P2 ₁ /c	
Unit cell dimensions	a = 16.5745(5) Å	α = 90°.
	b = 8.7883(2) Å	β = 114.5348(11)°.
	c = 15.7010(4) Å	γ = 90°.
Volume	2080.54(10) Å ³	
Z	4	
Density (calculated)	1.118 Mg/m ³	
Absorption coefficient	0.066 mm ⁻¹	
F(000)	760	
Crystal size	0.687 x 0.591 x 0.134 mm ³	
Theta range for data collection	1.350 to 27.436°.	
Index ranges	-21 ≤ h ≤ 21, -11 ≤ k ≤ 11, -20 ≤ l ≤ 20	
Reflections collected	17438	
Independent reflections	4749 [R(int) = 0.0245]	
Completeness to theta = 25.242°	100.0 %	
Absorption correction	Semi-empirical from equivalents	
Max. and min. transmission	0.7455 and 0.7000	
Refinement method	Full-matrix least-squares on F ²	
Data / restraints / parameters	4749 / 0 / 363	
Goodness-of-fit on F ²	1.026	
Final R indices [I > 2σ(I)]	R1 = 0.0420, wR2 = 0.1009	
R indices (all data)	R1 = 0.0600, wR2 = 0.1111	
Extinction coefficient	n/a	
Largest diff. peak and hole	0.330 and -0.179 e.Å ⁻³	

7. Appendix

7.5.14 1,2-bis(dimethylamino)-1-para-*N,N*-dimethylaniline-2-pentafluorophenyl diborane(4) 161

Identification code	sh4014	
Empirical formula	C ₁₈ H ₂₄ B ₂ F ₅ N ₃ , C ₆ H ₄ F ₂	
Formula weight	511.10	
Temperature	152(2) K	
Wavelength	0.71073 Å	
Crystal system	Triclinic	
Space group	P-1	
Unit cell dimensions	a = 9.9891(4) Å	α = 98.949(2)°.
	b = 11.1868(4) Å	β = 106.2579(16)°.
	c = 12.4828(5) Å	γ = 104.6579(17)°.
Volume	1256.46(9) Å ³	
Z	2	
Density (calculated)	1.351 Mg/m ³	
Absorption coefficient	0.115 mm ⁻¹	
F(000)	528	
Crystal size	0.642 x 0.368 x 0.234 mm ³	
Theta range for data collection	1.752 to 33.192°.	
Index ranges	-15 ≤ h ≤ 15, -17 ≤ k ≤ 17, -19 ≤ l ≤ 19	
Reflections collected	35832	
Independent reflections	9593 [R(int) = 0.0211]	
Completeness to theta = 25.242°	100.0 %	
Absorption correction	Semi-empirical from equivalents	
Max. and min. transmission	0.7465 and 0.6966	
Refinement method	Full-matrix least-squares on F ²	
Data / restraints / parameters	9593 / 0 / 429	
Goodness-of-fit on F ²	1.033	
Final R indices [I > 2σ(I)]	R1 = 0.0469, wR2 = 0.1281	
R indices (all data)	R1 = 0.0644, wR2 = 0.1412	
Extinction coefficient	n/a	
Largest diff. peak and hole	0.396 and -0.355 e.Å ⁻³	

7. Appendix

7.5.15 1,4-dimethyl-2,3-bis(dimethylamino)-1,2,3,4-tetrahydrobenzo[e]-[1,4,2,3]diazadiborinane 166

Identification code	sh4018	
Empirical formula	C ₁₂ H ₂₂ B ₂ N ₄	
Formula weight	243.95	
Temperature	152(2) K	
Wavelength	0.71073 Å	
Crystal system	Orthorhombic	
Space group	Pbca	
Unit cell dimensions	a = 15.3904(6) Å	α = 90°.
	b = 9.3258(3) Å	β = 90°.
	c = 19.5845(8) Å	γ = 90°.
Volume	2810.92(18) Å ³	
Z	8	
Density (calculated)	1.153 Mg/m ³	
Absorption coefficient	0.069 mm ⁻¹	
F(000)	1056	
Crystal size	0.490 x 0.384 x 0.088 mm ³	
Theta range for data collection	2.080 to 30.372°.	
Index ranges	-21 ≤ h ≤ 21, -13 ≤ k ≤ 13, -27 ≤ l ≤ 27	
Reflections collected	30484	
Independent reflections	4242 [R(int) = 0.0443]	
Completeness to theta = 25.242°	100.0 %	
Absorption correction	Semi-empirical from equivalents	
Max. and min. transmission	0.7460 and 0.7179	
Refinement method	Full-matrix least-squares on F ²	
Data / restraints / parameters	4242 / 0 / 251	
Goodness-of-fit on F ²	1.014	
Final R indices [I > 2σ(I)]	R1 = 0.0462, wR2 = 0.1151	
R indices (all data)	R1 = 0.0750, wR2 = 0.1345	
Extinction coefficient	n/a	
Largest diff. peak and hole	0.434 and -0.196 e.Å ⁻³	

Least-squares planes (x,y,z in crystal coordinates) and deviations from them

(* indicates atom used to define plane)

$$8.2525 (0.0053) x + 7.8699 (0.0021) y + 0.3563 (0.0089) z = 8.1139 (0.0027)$$

* -0.2622 (0.0007) B1

* 0.1009 (0.0007) N3

7. Appendix

* 0.0956 (0.0007) C1

* -0.0992 (0.0007) C6

* -0.0941 (0.0007) N4

* 0.2590 (0.0007) B2

Rms deviation of fitted atoms = 0.1702

7.5.16 2,3-bis(para-*N,N*-dimethylaniline)-1,4-dimethyl-1,2,3,4-tetrahydrobenzo[e][1,4,2,3]diazadiborinane 169

Identification code	sh4057	
Empirical formula	C ₂₄ H ₃₀ B ₂ N ₄	
Formula weight	396.14	
Temperature	142(2) K	
Wavelength	0.71073 Å	
Crystal system	Monoclinic	
Space group	P2 ₁ /n	
Unit cell dimensions	a = 17.3573(9) Å	α = 90°.
	b = 9.3269(4) Å	β = 103.508(3)°.
	c = 27.8586(12) Å	γ = 90°.
Volume	4385.3(4) Å ³	
Z	8	
Density (calculated)	1.200 Mg/m ³	
Absorption coefficient	0.070 mm ⁻¹	
F(000)	1696	
Crystal size	0.569 x 0.166 x 0.034 mm ³	
Theta range for data collection	1.264 to 27.250°.	
Index ranges	-22 ≤ h ≤ 22, -11 ≤ k ≤ 11, -35 ≤ l ≤ 35	
Reflections collected	38124	
Independent reflections	9720 [R(int) = 0.0745]	
Completeness to theta = 25.242°	100.0 %	
Absorption correction	Semi-empirical from equivalents	
Max. and min. transmission	0.7455 and 0.6860	
Refinement method	Full-matrix least-squares on F ²	
Data / restraints / parameters	9720 / 9 / 779	
Goodness-of-fit on F ²	1.002	
Final R indices [I > 2σ(I)]	R1 = 0.0577, wR2 = 0.1162	
R indices (all data)	R1 = 0.1405, wR2 = 0.1487	
Extinction coefficient	n/a	
Largest diff. peak and hole	0.212 and -0.200 e.Å ⁻³	

7. Appendix

Least-squares planes (x,y,z in crystal coordinates) and deviations from them

(* indicates atom used to define plane)

$$14.7391 (0.0086) x + 4.8344 (0.0072) y - 8.2713 (0.0238) z = 3.1509 (0.0131)$$

$$* -0.0394 (0.0016) \text{ B1}$$

$$* 0.0545 (0.0015) \text{ N1}$$

$$* -0.0254 (0.0016) \text{ C1}$$

$$* -0.0169 (0.0016) \text{ C6}$$

$$* 0.0273 (0.0016) \text{ N2}$$

$$* -0.0001 (0.0017) \text{ B2}$$

Rms deviation of fitted atoms = 0.0322

7.5.17 2,3-bis(pentafluorophenyl)-1,4-dimethyl-1,2,3,4-tetrahydrobenzo[e]- [1,4,2,3]diazadiborinane 170

Identification code	sh4141
Empirical formula	C ₂₀ H ₁₀ B ₂ F ₁₀ N ₂ , 0.5 (C ₇ H ₈)
Formula weight	535.99
Temperature	142(2) K
Wavelength	0.71073 Å
Crystal system	Monoclinic
Space group	P2 ₁ /n
Unit cell dimensions	a = 12.3016(6) Å α = 90°. b = 7.1478(4) Å β = 103.302(3)°. c = 26.3120(13) Å γ = 90°.
Volume	2251.5(2) Å ³
Z	4
Density (calculated)	1.581 Mg/m ³
Absorption coefficient	0.150 mm ⁻¹
F(000)	1076
Crystal size	0.362 x 0.242 x 0.038 mm ³
Theta range for data collection	1.591 to 32.733°.
Index ranges	-18 ≤ h ≤ 18, -10 ≤ k ≤ 10, -40 ≤ l ≤ 40
Reflections collected	159504
Independent reflections	8302 [R(int) = 0.0428]
Completeness to theta = 25.242°	100.0 %
Absorption correction	Semi-empirical from equivalents
Max. and min. transmission	0.7464 and 0.7190
Refinement method	Full-matrix least-squares on F ²
Data / restraints / parameters	8302 / 122 / 373

7. Appendix

Goodness-of-fit on F^2	1.028
Final R indices [$I > 2\sigma(I)$]	$R1 = 0.0504$, $wR2 = 0.1291$
R indices (all data)	$R1 = 0.0854$, $wR2 = 0.1521$
Extinction coefficient	n/a
Largest diff. peak and hole	0.418 and -0.448 e. \AA^{-3}

Least-squares planes (x,y,z in crystal coordinates) and deviations from them

(* indicates atom used to define plane)

$$2.0546 (0.0064) x + 7.0343 (0.0008) y + 0.5298 (0.0151) z = 3.0696 (0.0063)$$

$$* 0.0091 (0.0010) \text{ B1}$$

$$* 0.0111 (0.0009) \text{ N2}$$

$$* -0.0257 (0.0010) \text{ C1}$$

$$* 0.0174 (0.0009) \text{ C6}$$

$$* 0.0050 (0.0009) \text{ N1}$$

$$* -0.0169 (0.0010) \text{ B2}$$

$$\text{Rms deviation of fitted atoms} = 0.0157$$

7.5.18 1,4-dimethyl-2-dimethylamino-3-para-*N,N*-dimethylaniline-1,2,3,4-tetrahydrobenzo[e][1,4,2,3]diazadiborinane 172

Identification code	sh4097
Empirical formula	$\text{C}_{18} \text{H}_{26} \text{B}_2 \text{N}_4$
Formula weight	320.05
Temperature	122(2) K
Wavelength	0.71073 \AA
Crystal system	Orthorhombic
Space group	Pbca
Unit cell dimensions	$a = 15.5600(18) \text{\AA}$ $\alpha = 90^\circ$. $b = 9.8859(12) \text{\AA}$ $\beta = 90^\circ$. $c = 23.262(3) \text{\AA}$ $\gamma = 90^\circ$.
Volume	$3578.3(7) \text{\AA}^3$
Z	8
Density (calculated)	1.188 Mg/m^3
Absorption coefficient	0.070 mm^{-1}
F(000)	1376
Crystal size	0.436 x 0.108 x 0.095 mm^3
Theta range for data collection	1.751 to 27.987 $^\circ$.
Index ranges	$-20 \leq h \leq 20$, $-12 \leq k \leq 13$, $-30 \leq l \leq 30$

7. Appendix

Reflections collected	49592
Independent reflections	4290 [R(int) = 0.1287]
Completeness to theta = 25.242°	100.0 %
Absorption correction	Semi-empirical from equivalents
Max. and min. transmission	0.7456 and 0.6974
Refinement method	Full-matrix least-squares on F ²
Data / restraints / parameters	4290 / 0 / 322
Goodness-of-fit on F ²	1.001
Final R indices [I>2sigma(I)]	R1 = 0.0526, wR2 = 0.1027
R indices (all data)	R1 = 0.1232, wR2 = 0.1333
Extinction coefficient	0.0019(3)
Largest diff. peak and hole	0.244 and -0.219 e.Å ⁻³

Least-squares planes (x,y,z in crystal coordinates) and deviations from them

(* indicates atom used to define plane)

$$- 1.7918 (0.0123) x + 9.3541 (0.0028) y + 7.0340 (0.0165) z = 6.2063 (0.0054)$$

$$* 0.0792 (0.0013) C1$$

$$* -0.0167 (0.0014) C6$$

$$* -0.0965 (0.0013) N2$$

$$* 0.1321 (0.0014) B2$$

$$* -0.0735 (0.0014) B1$$

$$* -0.0245 (0.0013) N1$$

$$\text{Rms deviation of fitted atoms} = 0.0809$$

7. Appendix

7.5.19 2-chloro-1,4-dimethyl-3-para-*N,N*-dimethylaniline-1,2,3,4-tetrahydro-benzo[e][1,4,2,3]diazadiborinane 180

Identification code	sh4119	
Empirical formula	C ₁₆ H ₂₀ B ₂ Cl N ₃	
Formula weight	311.42	
Temperature	152(2) K	
Wavelength	0.71073 Å	
Crystal system	Monoclinic	
Space group	C2/c	
Unit cell dimensions	a = 18.2273(4) Å	α = 90°.
	b = 10.1084(3) Å	β = 103.5829(14)°.
	c = 17.4910(4) Å	γ = 90°.
Volume	3132.56(14) Å ³	
Z	8	
Density (calculated)	1.321 Mg/m ³	
Absorption coefficient	0.242 mm ⁻¹	
F(000)	1312	
Crystal size	0.404 x 0.174 x 0.068 mm ³	
Theta range for data collection	2.299 to 28.091°.	
Index ranges	-24 ≤ h ≤ 24, -13 ≤ k ≤ 13, -23 ≤ l ≤ 23	
Reflections collected	30693	
Independent reflections	3800 [R(int) = 0.0398]	
Completeness to theta = 25.242°	100.0 %	
Absorption correction	Semi-empirical from equivalents	
Max. and min. transmission	0.7456 and 0.7215	
Refinement method	Full-matrix least-squares on F ²	
Data / restraints / parameters	3800 / 0 / 279	
Goodness-of-fit on F ²	1.026	
Final R indices [I > 2σ(I)]	R1 = 0.0331, wR2 = 0.0828	
R indices (all data)	R1 = 0.0431, wR2 = 0.0892	
Extinction coefficient	n/a	
Largest diff. peak and hole	0.363 and -0.296 e.Å ⁻³	

Least-squares planes (x,y,z in crystal coordinates) and deviations from them

(* indicates atom used to define plane)

18.0908 (0.0013) x - 1.2212 (0.0052) y - 3.7719 (0.0075) z = 5.9765 (0.0026)

* -0.0313 (0.0008) N1

* 0.0144 (0.0008) C1

7. Appendix

* 0.0191 (0.0008) C2

* -0.0343 (0.0008) N2

* 0.0173 (0.0009) B2

* 0.0148 (0.0009) B1

Rms deviation of fitted atoms = 0.0233

7.5.20 1,4-dimethyl-3-para-*N,N*-dimethylaniline-2-pentafluorophenyl-1,2,3,4-tetrahydrobenzo[*e*][1,4,2,3]diazadiborinane 181

Identification code	sh4231	
Empirical formula	C ₂₂ H ₂₀ B ₂ F ₅ N ₃	
Formula weight	443.03	
Temperature	142(2) K	
Wavelength	0.71073 Å	
Crystal system	Triclinic	
Space group	P-1	
Unit cell dimensions	a = 7.5473(4) Å	α = 85.5787(14)°
	b = 11.8469(6) Å	β = 83.1875(15)°
	c = 12.0590(6) Å	γ = 73.6504(13)°
Volume	1026.23(9) Å ³	
Z	2	
Density (calculated)	1.434 Mg/m ³	
Absorption coefficient	0.116 mm ⁻¹	
F(000)	456	
Crystal size	0.367 x 0.267 x 0.214 mm ³	
Theta range for data collection	1.702 to 32.666°	
Index ranges	-11 ≤ h ≤ 10, -17 ≤ k ≤ 17, -18 ≤ l ≤ 18	
Reflections collected	26914	
Independent reflections	7508 [R(int) = 0.0269]	
Completeness to theta = 25.242°	100.0 %	
Absorption correction	Semi-empirical from equivalents	
Max. and min. transmission	0.7464 and 0.7282	
Refinement method	Full-matrix least-squares on F ²	
Data / restraints / parameters	7508 / 0 / 369	
Goodness-of-fit on F ²	1.037	
Final R indices [I > 2σ(I)]	R1 = 0.0437, wR2 = 0.1169	
R indices (all data)	R1 = 0.0604, wR2 = 0.1290	
Extinction coefficient	n/a	
Largest diff. peak and hole	0.524 and -0.227 e.Å ⁻³	

7. Appendix

Least-squares planes (x,y,z in crystal coordinates) and deviations from them

(* indicates atom used to define plane)

$$4.8397 (0.0022) x + 10.6656 (0.0019) y + 3.2628 (0.0045) z = 11.9169 (0.0011)$$

$$* -0.0517 (0.0007) \text{ B1}$$

$$* 0.0375 (0.0006) \text{ N1}$$

$$* 0.0087 (0.0007) \text{ C1}$$

$$* -0.0353 (0.0007) \text{ C6}$$

$$* 0.0134 (0.0007) \text{ N2}$$

$$* 0.0274 (0.0007) \text{ B2}$$

Rms deviation of fitted atoms = 0.0325

7.5.21 4-(1,4-dimethyl-3-(4-nitrophenoxy)-3,4-dihydrobenzo[e]-[1,4,2,3]diazadi-borinin-2(1H)-yl)-N,N-dimethylaniline 183

Identification code	sh4165cu	
Empirical formula	C22 H24 B2 N4 O3	
Formula weight	414.07	
Temperature	133(2) K	
Wavelength	1.54178 Å	
Crystal system	Monoclinic	
Space group	C2/c	
Unit cell dimensions	a = 20.8395(13) Å	$\alpha = 90^\circ$.
	b = 8.0681(4) Å	$\beta = 100.638(3)^\circ$.
	c = 25.2970(14) Å	$\gamma = 90^\circ$.
Volume	4180.2(4) Å ³	
Z	8	
Density (calculated)	1.316 Mg/m ³	
Absorption coefficient	0.704 mm ⁻¹	
F(000)	1744	
Crystal size	0.146 x 0.093 x 0.026 mm ³	
Theta range for data collection	3.555 to 80.353°.	
Index ranges	-24<=h<=26, -10<=k<=10, -32<=l<=30	
Reflections collected	33809	
Independent reflections	4519 [R(int) = 0.0280]	
Completeness to theta = 67.679°	99.6 %	
Absorption correction	Semi-empirical from equivalents	
Max. and min. transmission	0.7543 and 0.6877	
Refinement method	Full-matrix least-squares on F ²	
Data / restraints / parameters	4519 / 0 / 376	

7. Appendix

Goodness-of-fit on F^2	1.054
Final R indices [$I > 2\sigma(I)$]	$R1 = 0.0340$, $wR2 = 0.0920$
R indices (all data)	$R1 = 0.0360$, $wR2 = 0.0940$
Extinction coefficient	n/a
Largest diff. peak and hole	0.387 and -0.221 e. \AA^{-3}

Least-squares planes (x,y,z in crystal coordinates) and deviations from them (* indicates atom used to define plane)

$$- 12.2911 (0.0064) x - 4.8171 (0.0025) y + 16.2733 (0.0067) z = 2.9636 (0.0028)$$

$$* 0.0137 (0.0007) \text{ B1}$$

$$* -0.0275 (0.0006) \text{ N1}$$

$$* 0.0161 (0.0006) \text{ C1}$$

$$* 0.0094 (0.0006) \text{ C6}$$

$$* -0.0220 (0.0006) \text{ N2}$$

$$* 0.0103 (0.0007) \text{ B2}$$

$$\text{Rms deviation of fitted atoms} = 0.0177$$

7. Appendix

7.5.22 1-chloro-2-dimethylamino-1,2-(2,3,5,6-tetramethylphenyl) diborane(4) 185

Identification code	sh4205	
Empirical formula	C ₂₂ H ₃₂ B ₂ Cl N	
Formula weight	367.55	
Temperature	132(2) K	
Wavelength	0.71073 Å	
Crystal system	Triclinic	
Space group	P-1	
Unit cell dimensions	a = 7.6201(4) Å	α = 78.8383(11)°.
	b = 16.4202(8) Å	β = 84.5323(12)°.
	c = 17.8783(8) Å	γ = 89.4860(12)°.
Volume	2184.59(18) Å ³	
Z	4	
Density (calculated)	1.118 Mg/m ³	
Absorption coefficient	0.180 mm ⁻¹	
F(000)	792	
Crystal size	0.403 x 0.398 x 0.118 mm ³	
Theta range for data collection	1.166 to 30.512°.	
Index ranges	-10 ≤ h ≤ 10, -23 ≤ k ≤ 23, -25 ≤ l ≤ 25	
Reflections collected	36547	
Independent reflections	13280 [R(int) = 0.0289]	
Completeness to theta = 25.242°	100.0 %	
Absorption correction	Semi-empirical from equivalents	
Max. and min. transmission	0.7461 and 0.6851	
Refinement method	Full-matrix least-squares on F ²	
Data / restraints / parameters	13280 / 0 / 715	
Goodness-of-fit on F ²	1.034	
Final R indices [I > 2σ(I)]	R1 = 0.0463, wR2 = 0.1162	
R indices (all data)	R1 = 0.0693, wR2 = 0.1293	
Extinction coefficient	n/a	
Largest diff. peak and hole	0.462 and -0.460 e.Å ⁻³	

7. Appendix

7.5.23 2-chloro-1-*para*-*N,N*-dimethylaniline-1,2-(2,3,5,6-tetramethylphenyl) diborane(4) 187

Identification code	sh4233	
Empirical formula	C ₂₈ H ₃₆ B ₂ Cl N, 0.5(C ₇ H ₈)	
Formula weight	489.71	
Temperature	142(2) K	
Wavelength	0.71073 Å	
Crystal system	Monoclinic	
Space group	P2 ₁ /n	
Unit cell dimensions	a = 8.8269(3) Å	α = 90°.
	b = 38.5769(17) Å	β = 99.129(3)°.
	c = 17.0725(8) Å	γ = 90°.
Volume	5739.8(4) Å ³	
Z	8	
Density (calculated)	1.133 Mg/m ³	
Absorption coefficient	0.153 mm ⁻¹	
F(000)	2104	
Crystal size	0.305 x 0.200 x 0.090 mm ³	
Theta range for data collection	1.318 to 27.150°.	
Index ranges	-10 ≤ h ≤ 11, -49 ≤ k ≤ 49, -21 ≤ l ≤ 21	
Reflections collected	53793	
Independent reflections	12686 [R(int) = 0.0625]	
Completeness to theta = 25.242°	100.0 %	
Absorption correction	Semi-empirical from equivalents	
Max. and min. transmission	0.7455 and 0.7013	
Refinement method	Full-matrix least-squares on F ²	
Data / restraints / parameters	12686 / 0 / 672	
Goodness-of-fit on F ²	1.016	
Final R indices [I > 2σ(I)]	R1 = 0.0514, wR2 = 0.1064	
R indices (all data)	R1 = 0.0970, wR2 = 0.1236	
Extinction coefficient	n/a	
Largest diff. peak and hole	0.256 and -0.295 e.Å ⁻³	